UNIVERSITY OF SOUTHAMPTON

FACULTY OF ENGINEERING, SCIENCE AND MATHEMATICS

School of Geography

Hydrodynamics and Sedimentary Structures of Antidunes in Gravel and Sand Mixtures

by

Richard Breakspear

Thesis for the degree of Doctor of Philosophy

October 2008

UNIVERSITY OF SOUTHAMPTON

ABSTRACT

FACULTY OF ENGINEERING, SCIENCE & MATHEMATICS
SCHOOL OF GEOGRAPHY

Doctor of Philosophy

HYDRODYNAMICS AND SEDIMENTARY STRUCTURES OF ANTIDUNES IN GRAVEL AND SAND MIXTURES

by Richard Breakspear

This thesis firstly reviews the current literature available on antidune bedforms and their hydrodynamic environment, alongside recent studies of the turbulence environments associated with bedforms in unidirectional flow. Based on this understanding, three suites of experiments were designed and conducted to elucidate turbulent flow structure within the standing waves above antidunes and to record the sedimentary response of a loose mobile bed that constituted the antidunes. The first suite of experiments used Acoustic Doppler Velocimetry (ADV) to quantify and characterise the flow structure above fixed bedforms and this was supported by a second suite of experiments that used high-speed video to visualise flow structure. Finally, in the third suite of experiments a loose bed of sediment was allowed to deform into antidunes beneath standing waves and the resultant sedimentary structures were recorded and related to the growth and decay of both standing waves and antidune form. Taken together these data have been interpreted in order to identify and elucidate the bulk-flow, turbulent environment of the flow field above antidunes and the sedimentary structures that characterise the preserved antidune bedding.

The ADV experiments have shown that a coherent and organised spatial pattern of turbulence exists above antidune bedforms. Initially, when antidune amplitude is small, turbulent stresses are relatively equally distributed along the entire bed boundary layer, however as antidune amplitude increases there is a progressive concentration of turbulent stresses. Turbulence becomes increasingly concentrated in the near-bed region within the trough between upstream and downstream contiguous antidunes and on the upstream flank of the antidune immediately downstream. Velocities in the trough region drop significantly below the mean velocity elsewhere over antidune bedforms. A clear distinction can be drawn between sand and gravel antidunes, with gravel antidunes having comparatively much lower velocities in the trough region, and turbulence stresses (ejections, sweeps, turbulence Intensity, TKE and Reynolds Stress) an order of magnitude higher than for sand bedforms. Further, experiments over a porous gravel bed indicate levels of near bed turbulence higher than over a gravel-surfaced concrete bedform without interstitial flow. High-speed photography and interpretation of streak images further supports this ADV data.

It is proposed that antidunes break when turbulence reaches an ‘intensity’ that constitutes a threshold above which rapid erosion occurs in the trough causing a pronounced increase in turbulent ejections laden with sediment and consequent rapid deposition on the downstream antidune flank. Flow then stalls over the downstream antidune; the standing wave collapses and erodes much of the bed. In terms of distinctive sedimentary structure, three types of bedding were observed in sediment sections taken after mobile bed runs where antidunes had been active. Type I bedding is formed by the erosion of the bed and marks the lowest surface formed by antidune downcutting during active migration or collapse. Type II bedding is formed by turbulent sweeps during antidune growth and migration. However the contrasts in sediment size and type that mark bedding are dependent on the heterogeneity of bed sediment. A third type of downstream dipping, bipartite planar bedding was observed to form under an upstream migrating standing wave. The preservation of a suite of sedimentologic features produced by a period of antidune activity is however dependent on the degree of downcutting and erosion during standing wave collapse.

Table of Contents

List of Tables

List of Figures

List of Plates

List of Boxes

List of Equations

DECLARATION OF AUTHORSHIP

I, ……., [please print name]

declare that the thesis entitled [enter title]

……

……

and the work presented in the thesis are both my own, and have been generated by me as the result of my own original research. I confirm that:

- this work was done wholly or mainly while in candidature for a research degree at this University;
- where any part of this thesis has previously been submitted for a degree or any other qualification at this University or any other institution, this has been clearly stated;
- where I have consulted the published work of others, this is always clearly attributed;
- where I have quoted from the work of others, the source is always given. With the exception of such quotations, this thesis is entirely my own work;
- I have acknowledged all main sources of help;
- where the thesis is based on work done by myself jointly with others, I have made clear exactly what was done by others and what I have contributed myself;
- none of this work has been published before submission, **or** [delete as appropriate] parts of this work have been published as: [please list references]

Signed: ……..

Date:…….

Acknowledgements:

Professor Paul Carling (PhD supervisor) for PhD funding, and all the advice discussion and support. A big thanks to all the staff at the School of Geography, University of Southampton that helped support the completion of this PhD. My long suffering (then) girlfriend, Emma Stace for all the help and support, and encouragement along the way – and especially for being the one to accompany me for Health and Safety reasons at the very cold and draughty flume facility during weekend runs. I'm sure all the 'cute' bunnies outside weren't that much of a consolation. My parents for all their support and additional financial assistance. Stuart McLelland (School of Geography, Hull University) provided the loan of the Nortek NDV used in these experiments. Travis Mason (Channel Coastal Observatory, National Oceanographic Centre) provided a valuable introduction to the Matlab software package. Jon Williams (School of Earth, Ocean and Environmental Sciences, Plymouth University) provided valuable assistance with the spectral processing of ADV data in Matlab, Atle Lohrmann of Nortek kindly checked some sample ADV data for quality and consistency. Andy Vowles provided photographical assistance. Les Whitcombe helped with the initial set-up (read heavy re-engineering) of the flume facility, assisted by the staff at the University's Automobile Design and Advisory Unit who (perhaps unfortunately) shared a building with the flume facility, but regardless helped modify the flume with the aid of acetylene welding torches and a forklift truck. Artur Radecki-Pawlik kindly translated a Polish scientific paper. Duncan Kitts and Sergey Krasnoshchekov provided much appreciated support in manning the sediment hopper refill marathon during the mobile bed experiments. I'm sure shifting over one tonne of sediment in nearly 100 hundred buckets in twenty minutes was not what they expected from my 'Help Wanted' email. Finally thanks to the numerous people who helped in whatever small way, who I have not mentioned here.

Nomenclature

b	Transverse wavelength of TDAs (Kennedy, 1961)
c	Celerity
d	Depth
d_m	Mean depth
D	Grain size
D_*	Grain roughness height
D_{50}	Median grain size
F	ADV accuracy
Fr	Froude number
Fr_{den}	Densiometric Froude Number
f_R	ADV frequency
g	Acceleration due to gravity
h	Height
H	Hole Size
k	Wavenumber
L	Length Scale
N	Newtons
n	Manning's 'n' roughness value
P	Turbulence Production
R	Boundary Layer Correlation Coefficient
Re	Reynolds Number
Re*	Grain Reynolds Number
TI	Turbulence Intensity
u_*	Shear velocity
$\overline{U}$	Mean streamwise velocity
Uc	Convective velocity
U^2	Normal Stress
u'	Instantaneous deviation of U (streamwise) velocity
u_i	Instantaneous u velocity
$\lvert u'v' \rvert$	Instantaneous u' and v' velocity deviation
$\overline{V}$	Mean vertical velocity
V^2	Normal Stress
v'	Instantaneous deviation of V (vertical) velocity
v_i	Instantaneous v velocity
$\overline{W}$	Mean spanwise velocity
W^2	Normal Stress
w'	Instantaneous deviation of W (spanwise) velocity
w_i	Instantaneous w velocity
Y	Vertical length scale
θ	Shields Number
λ	Wavelength
μ	Kinematic viscosity
π	Pi
ρ	Density
τ_R	Time Averaged Reynolds Stress
σ_g	Sediment sorting coefficient

1 Introduction

This study was undertaken in order to increase the understanding of the hydrodynamics and sedimentary structures associated with antidune bedforms which, compared with lower stage (ripples and dunes) and transitional (USPB) bedforms, have received relatively little attention. A through literature review (Chapter 2) has been carried out to detail the current understanding of these bedforms and to collate together the diverse pool of literature relating to upper regime flow and specifically antidunes.

Antidunes deposits are thought to be a relatively rare phenomena in the sedimentological record, because the sedimentary structures formed by antidunes are frequently destroyed by subsequent reworking, before burial and eventual diagenesis. Preservation in the rock record is therefore thought to be rare. However preservation does occur in some environments, typically in highly aggrading situations, such as glacial outwash fans formed by Jökulhlaups (Russell *et al*., 2002 and 2003; Russell, 2005; and Duller *et al*., In press), desert outwash fans (Blair, 1999 and 2000), fluvial deposits associated with steep streams draining areas of recently deposited pyroclastics (Clifton, 1990), and through rapid flow cut-off (Alexander and Fielding, 1997). The identification of these bedforms, allows the inference of a high-energy environment with supercritical (shallow, fast) flow. Field geologists frequently identify antidune deposits at outcrop (see Table 2.7 and Table 2.10), and these inferences would be aided by detailed laboratory studies. Nelson *et al*. (1993) have stressed the need for an increased understanding of bedform process in order to inform palaeoflood and palaeoenvironmental interpretation of exposures in the geological record.

This thesis seeks to redress this situation by studying the hydraulic climate responsible for the formation of antidune sedimentary structures in sand/gravel mixtures. These experiments under controlled conditions have been designed to provide valuable quantitative data on the antidune regime bulk flow, turbulence, sediment transport, dynamics and sediment transport. The mapping of spatial and temporal patterns in the organisation of the turbulence environment has allowed detailed sedimentological inferences to be made. Acoustic Doppler Velocimetry (ADV) over fixed bedforms, (Chapter 4); High-Speed photography over fixed forms, (Chapter 5); and

mobile bed experiments, (Chapter 6) of freely-forming, time-varying antidunes, followed by subsequent sediment sectioning and interpretation have been used to progressively investigate antidune regime flow. Importantly this thesis focuses on gravelly antidunes, as opposed to the sand antidunes investigated by previous researchers (Kennedy, 1961; Middleton, 1965; Yagishita and Taira, 1989; Yokokawa *et al*., 2000 and Alexander *et al*., 2001). The results are interpreted, and conclusions drawn with the twin purposes of aiding our understanding of these bedforms and their turbulent environment, and increasing the veracity of field interpretation of inferred antidune sedimentary structures. Results detail the key properties of the flow profile above antidunes, and indicate that the formation of antidune sedimentary structures is strongly linked to the properties of the turbulent flow above. A synthesis of the experimental data obtained has allowed useful tools to be prepared for the field geologist to aid the identification and interpretation of antidunes in the ancient sedimentary record.

2 Literature Review

2.1 Introduction

This section introduces the main principles and theories of fluvial hydraulics necessary to underpin the hydrodynamic study of antidunes. Secondly, an assessment and evaluation of the literature is provided so as to identify areas that require investigation. These subject areas are then addressed by defining aims and hypotheses, which through this study, will contribute to advancing the present state of knowledge.

The Froude number (Fr) defines the ratio of inertial to gravitational forces:

$$Fr = \frac{\overline{U}}{\sqrt{gd}}$$ **Eq. 2.1 Froude Number**

where, Fr is the Froude number (dimensionless), $\overline{U}$ is the mean velocity (in m/s), g is acceleration due to gravity (in N/kg) and d is the depth (in m). It delineates flows into two regimes:

Fr < 1 subcritical flow: gravitational force dominates
Fr = 1 critical flow
Fr > 1 supercritical flow; inertial force dominates

The celerity of a shallow water wave is given by:

$$c = \sqrt{gd}$$ **Eq. 2.2 Celerity**

where c is celerity (m/s)

For Fr < 1; c < U: water surface waves migrate downstream.
At Fr = 1; c = U: water surface waves are stationary.
For Fr > 1; c > U: water surface waves migrate upstream.

Antidunes are a class of bedforms that develop at the transition between subcritical and supercritical flow, typically between Fr: 0.84 – 1.77 (Kennedy, 1963; Southard and Boguchwal, 1990) and usually, at their

steepest, they are approximately in-phase with and beneath a standing wave. During some parts of the growth phase they can be out of phase with the water surface and downstream migrating, (Kennedy, 1963 and 1969; Reynolds 1965; Engelund and Hansen, 1966; Allen, 1969b), these downstream migrating antidunes are described below, but are not treated in any detail within this work.

In supercritical flow, a water surface wave associated with an antidune is relatively stable such that it tends to be persistent in its location as it grows in steepness, although eventually it may break upstream-wards causing a hydraulic jump to occur for a short period of time. In subcritical flow water surface waves over labile bedforms are less persistent as they can dissipate upstream into the trough between bedforms.

Antidunes are but one of many bedforms that are produced by the interaction of granular materials with a flow. Features analogous to antidunes occur in many geophysical flows resulting in a variety of sedimentological structures and morphological expression within exposures. Whilst, recent studies (Bridge and Best, 1988; Best and Bridge, 1992; Gyr and Müller, 1996; Nelson *et al*., 1993; Nelson *et al.,* 1995) have explained the turbulent interactions responsible for the ripple, dune and the Upper Stage Plane Bed (USPB) regime; the antidune regime is still comparatively ill-understood. This study aims to clarify the sedimentology and hydrodynamics of the antidune regime.

The morphologies of various bedforms and their sedimentary structures are characteristic of the flow that formed them; thus, with correct inference, palaeohydraulic interpretations can be drawn from examples of sedimentary structures within the sedimentary record. However, through multiple controlling variables such as velocity, flow depth, sediment size, particle density, fluid density and viscosity (Allen, 1984), a wide variety of bedforms result, making clear, absolute interpretations difficult. The occurrence of some transitional bedforms, such as those between dunes and antidunes and lack of a detailed understanding of the turbulent flow fields above bedforms also can lead to confused interpretations. Knowledge of the exact formulative turbulence mechanisms and maintenance, the internal structures and grain fabric characteristics (size, orientation) of antidunes should allow patterns that are (and are not) characteristic of antidunes to be

identified. This knowledge would give the field geologist better interpretational information: thus contemporary examples, whether studied in the field or flume are the key to interpreting past examples recorded within the geological record. Near supercritical and supercritical flows necessary for upper regime bedforms are rarer than subcritical flows; but importantly they are associated with geomorphologically importantly conditions: i.e. perturbed environments and short-duration, high-magnitude events. Thus, the inference of antidune structures in ancient deposits indicates a specific palaeo-sedimentological environment: shallow, high-velocity flow. For example, Pierson and Scott (1985); Clifton (1990) and Simon and Hardison (1994) observed critical and supercritical flows with antidunes associated with the sediment-laden (post Mount St. Helens eruption) Toutle River. Their data suggest that supercritical flow is common, with antidune bedforms and standing waves commonly occurring. Clifton, (1990) inferred structures identified in Pleistocene deposits as being produced by antidunes, suggesting past volcanic induced perturbations to the Toutle River system.

Because the types of deposit produced by antidunes are poorly understood and synthesised, erroneous interpretation may be common. Quite possibly antidune structures are misclassified as non-antidune structures, and non-antidune structures as antidune structures. General unawareness among researchers of the antidunes as a moderately common feature in the sedimentological record may thus contribute to the lack of identification (Fielding, 2006). Araya and Masuda, (2001, p11) state the starting point for this PhD thesis:

> **"*The classification of antidune geometries is so insufficient that the processes and mechanisms of the formation of sedimentary structures have been poorly understood. Detailed descriptions and analysis of the bedforms and the resultant deposits should be conducted based on a more established classification from experimental or hydraulic approaches.*"**

This literature review is divided into three sections to approach this problem. Firstly the hydrodynamics and sedimentology of fluvial bedforms

neighbouring the antidune regime are discussed, secondly potential flow theory and turbulence theories associated with bedform formation are discussed. Finally flume, field and geological studies and examples are reviewed to identify what is considered to be flow characteristics and bedforms associated with antidunes.

2.2 Bedform Formation

Here a brief outline of the characteristics of a range of alluvial bedforms (including antidunes) is provided. Bedforms produce specific sedimentary structures which relate to the prevailing flow conditions. Sedimentary structures consist of laminations produced by grain segregations that delineate packets of sediment. The primary sedimentary structures produced by a bedform are truncated by the next bedform that passes over their deposits, producing a more complicated outcrop on examination. Some non-antidune structures can be erroneously interpreted as being of an antidune origin; others are of interest as indications of environments transitional or equivalent to antidune flow: they provide context to the antidune regime of flow. Lower Stage Plane Bed (LSPB) and ripples, which occur at low shear stresses before the dune stage, are omitted for brevity, whilst dunes, USPB, Downstream Migrating Antidunes (DMAs) and Upstream Migrating Antidunes (UMAs) are discussed.

Allen (1984) considered that "*the sequence of bed configurations is related to the changing conditions imposed upon the bed*". With increasing Fr then, the idealised bedform transitions in a range of sediments are:

for sands:

LSPBs → ripples → dunes → USPBs → UMAs → chute and pool

for fine to medium gravel:

No movement → LSPBs → dunes → DMAs → UMAs → USPB and chute and pool

for coarse gravel too coarse to form dunes:

No movement → LSPBs → UMAs → USPB and chute and pool

Figure 2.1 illustrates how these sequences differ with grain size; the transitions can be imprecise (Carling, 1999), in response to U, d and sediment size, the variables considered most important in delimiting stability fields in Southard's (1971) and Ashley's (1990) meta-analysis of field and flume data.

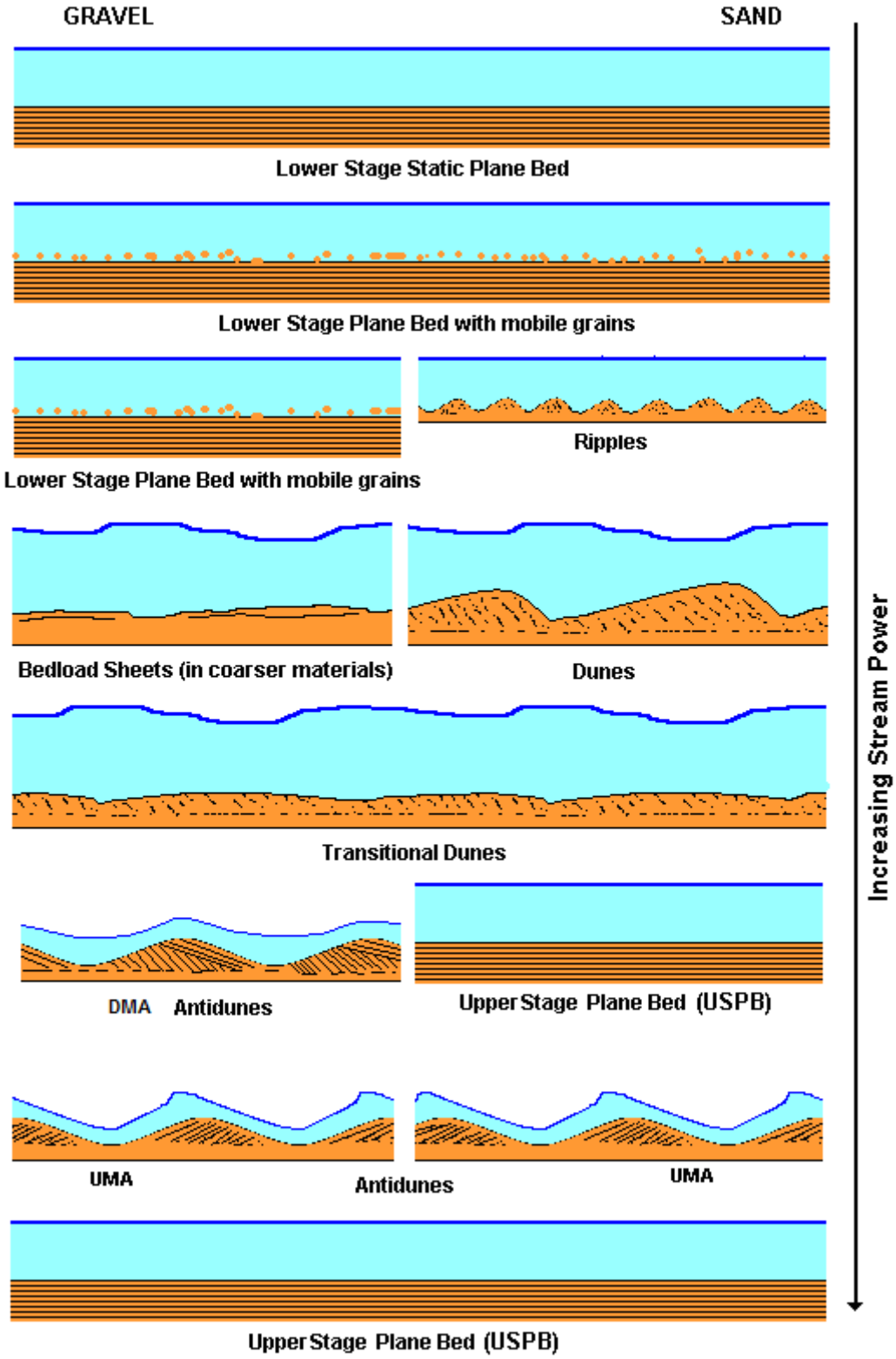

Figure 2.1 Potential Sequence of Bedform Transformations

The sequence of bedforms is complicated; primarily velocity, depth and grain size control bedform dynamics (flow left to right). The bed configurations possible around the transition from subcritical to supercritical are complicated, in some cases dunes may morph into DMAs creating hybrid bed features as changing flow conditions alter the patterns of sediment deposition. In other cases antidunes may not form and USPB will persist.

2.2 Bedform Types

2.2.1 Dunes

The key features of dunes are detailed in Table 2.1 below:

Table 2.1 Key Features and Observations on Dunes from the Literature

Flow	Subcritical flow. θ (Shields Number) > 0.1 lower for two dimensional dunes, higher for three dimensional. Maximum amplitude at θ > 0.25 (Fr = ~ 0.75), begin to reduce in amplitude when θ > 0.3 (Fr = 0.84): Simons *et al.* (1961); Guy *et al*. (1966); Carling (1999). Water surface waves are out-of-phase with the bed wave: Figure 2.1 (becoming more in phase as Fr increases). Separation zone in lee of dune is important sedimentologically, in the formation of sedimentary structures.
Scale	Wavelength (λ) = 0.6 – 100m (Jackson, 1976); scale with flow depth, incipient dunes overlap into ripple size (Carling, 1999). Size also scales with dimensionless shear stress (Bridge, 2003). Dune median sediment size (D_{50}): from 0.15mm, but up to 60mm if mixture is heterogeneous enough (Carling, 1999). Maximum dimensions in centre of dune stability field, dimensions decrease above this point: transitional (LeClair, 2002).
Types	Asymmetric, long shallow sloping upstream face, sharp downstream face set at the angle of repose. Large separation zone plays important role in sediment transport and as a roughness agent (Best and Kostaschuk, 2002; Maddux *et al*. 2003). Two dimensional (Plate 2.1 a) – straight/sinuous crested. Venditti *et al*. (2005) suggest that once 2D forms progression to 3D dunes is inevitable with time, due to the amplification of defects in the bedform crestlines. Three dimensional – catenary/lunate crests (Plate 2.1 b) – complex profile – friction coefficient 50% more than for two dimensional dunes due to secondary flow circulation around non-continuous crest, which also reduces macroturbulence as flow separation is reduced (Maddux *et al*. 2003).
Exceptions	Low angle dunes formed in less powerful flows/suspended sediment dominated environments may lack permanent separation zones (Best and Kostaschuk, 2002).
Sedimentary structures	Straight and sinuous dunes produce planar cross bedding. Catenary and lunate dunes produce trough cross bedding. Low angle dune deposits can superficially resemble the laminae produced in DMAs.

Plate 2.1 Types of Dune

A: sinuous crested dunes in fine gravel at Hills Flats, Oldbury-on-Severn, Gloucestershire (tidal flow, dominant flow from right). B: lunate dunes in sand - fine granules at Airy Point, Bideford, Devon (tidal flow, dominant flow from right), (λ of the above dunes is 5m and amplitude 0.25m).

The subcritical flow above dunes responds to a rise in bed level by increasing in velocity, and becoming shallower; as the bed level drops, velocity decreases and the flow becomes deeper (Figure 2.2). The bulk flow causes erosion of sediment from the crest and deposition downstream producing an asymmetrical profile.

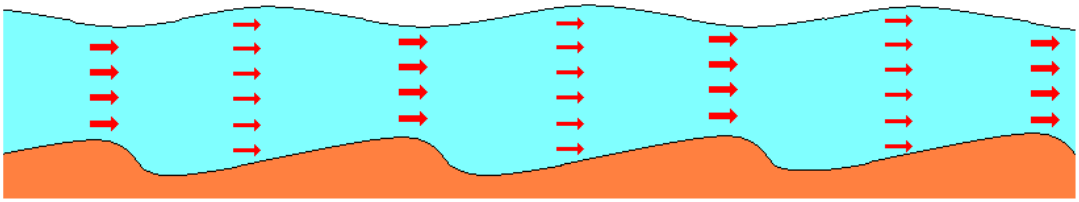

Figure 2.2 Bed Level and Water Level Phasing

Out of phase bed and water surface waves occur in the dune phase causing flow constriction; flow accelerates over crests and decelerates over troughs. At higher Fr, near the dune transition to antidunes the waves may become almost in phase.

In the dune regime bedding forms from foresets on the lee of the dune, deposition occurs by the settling out of finer grains from suspension and the intermittent avalanching of dense/coarse grains down the lee by turbulent sweeps - these laminations marking individual foresets (Figure 2.3).

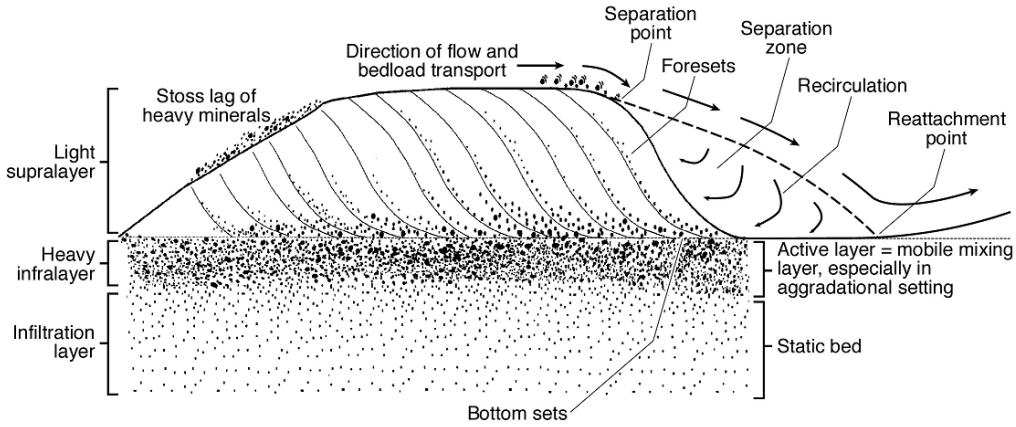

Figure 2.3 Sediment Sorting by Transport

Sediment sorting over dunes is responsible for the grain size segregation that produces dune sedimentary structures. Turbulence over the crest of the dune and the separation zone are key agents: the increased momentum entering the boundary layer allows coarser/denser grains to move. A bottom-set deposit forms where dense/coarse particles avalanching down the lee accumulate at the bottom of the foresets. When a large percentage of clasts are immobile, partial transport occurs: less-mobile particles are left as a 'heavy-infralayer', (vertical scale exaggerated, dune length: 2-5m and amplitude 0.25m), see further review in Carling and Breakspear (2006).

Turbulent flow enhances grain sorting, segregating differing grains which enhance bedding patterns; this is illustrated in Figure 2.4. The frequency of these turbulent events modulates deposition and erosion; controlling the rate of dune growth, migration and wavelength (Best, 1993). Gravel dunes have less pronounced bedding, as fine grains are not available to give contrast to foresets.

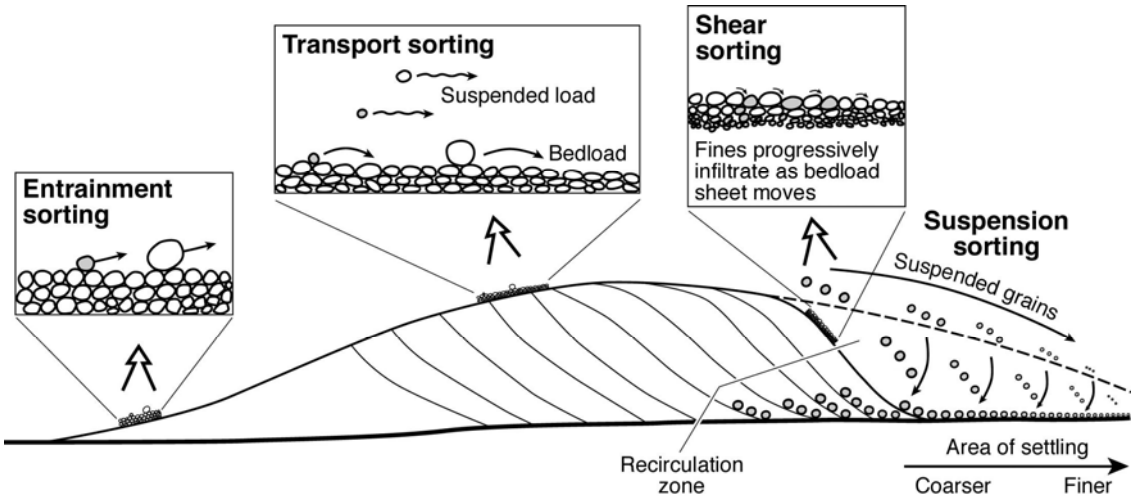

Figure 2.4 Sediment Sorting by Bedforms

Sediment is sorted by these processes over dunes: this is well established in the literature (see review in Carling and Breakspear, 2006). Over antidunes similar

processes of sorting must occur to produce the laminations characteristic of antidunes; albeit the faster velocities and rapid sedimentation may reduce the effectiveness of sorting, (vertical scale exaggerated, dune length 2-5m and amplitude 0.25m).

In coarser gravels bedforms become muted; instead the dune phase is represented by bedload sheets (Carling, 1999), which are low amplitude incipient dunes with dune like spacing. Bedload sheets have limited amplitudes as insufficient grains are in motion; no assessment of flow separation is available, but their low-amplitude likely limits its development (*sensu* Best and Kostaschuk's (2002) low-amplitude dunes). In granular to gravel sized material the USPB stage is omitted (Carling, 1999), because grains are too heavy for the high levels of suspension required to modify the turbulence structure, which is required for USPB formation (Bridge and Best, 1988). At the dune: antidune transition a complex mixture of dune and DMA forms may occur (Kennedy, 1961; Carling, 1999). In this high shear stress/high Fr flow symmetrical gravel dunes are still present as washed out structures within upper regime flow (Garde and Ranga-Raju, 1977; Kostaschuk and Villard, 1996) and asymmetrical humpback and convex duneforms (Saunderson and Lockett, 1983; Bridge and Best 1988). Middleton (1965) thought the grain size controlled the symmetry of transitional forms; coarser dunes stay asymmetrical, whilst finer sand dunes become symmetrical. Chakraborty and Bose (1992) documented an exposure indicative of the transition from dunes to Upper Stage Plane Bed (USPB). In this exposure, concave upwards foresets formed by dune bedforms transform via sigmoidal sets (laminations increasingly convex up) to parallel horizontal laminations. Different exposures indicated that this process can occur both laterally and vertically, Chakraborty and Bose postulate that high-levels of suspended sedimentation are essential to ensuring deposit preservation.

2.2.2 Upper Stage Plane Bed (USPB)

The key features of USPBs are detailed in Table 2.2.

Table 2.2 Key Features and Observations on USPBs from the Literature

Flow	Supercritical: Fr 0.8 > 1.3 (Bridge and Best 1997)
Scale	Maximum bedform amplitudes of several grains (0.75 – 11mm Best and Bridge, 1992), therefore, USPB offers only skin resistance to the flow. Do not scale with velocity like antidunes Best and Bridge (1992) found no agreement with Kennedys' (1963) equation $U^2 = \frac{g\lambda}{2\pi}$
Formation	Low amplitude bedwaves. Variously interpreted to be washed out dunes or DMAs or even a bedform themselves (Cheel, 1990). Role of turbulence not completely clear.
Transition Exceptions	Between lower regime and upper regime is indicated by the out of phase (Best and Bridge, 1992) and in phase (Cheel, 1990) miniature bedforms observed in flume experiments. Wren *et al*. (2005) investigated the flow above low-amplitude transitional USPB-antidune forms.
Sedimentary structures	Parallel laminations, characterised by Coarsening Upwards or Fining Upwards sediment and heavy mineral sheets (Cheel and Middleton, (1986) - see Figure 2.5. Laminations potentially produced by muted bedforms (Paola *et al*. 1989; Best and Bridge, 1992) with no flow separation, and/or suppressed turbulence - ejections and sweeps - (Cheel and Middleton, 1986; Best and Bridge, 1992; Bridge and Best, 1997). In section laminations are distinguishable from antidune deposits by their lateral extensiveness and much shallower angles of dip (Cotter and Graham, 1991).

Best and Bridge's (1992) laminae (Figure 2.5), which formed in flows where the Fr was supercritical were produced by extremely low amplitude long wavelength bedforms out of phase with water surface waves, thus flow accelerated over the crest and decelerated over the trough, which is dune-like behaviour characteristic of lower stage Fr < 1 bedforms or even DMAs. Cheel (1990) describes bedwaves that are in-phase with the water surface waves: an antidune like behaviour characteristic of the upper flow regime.

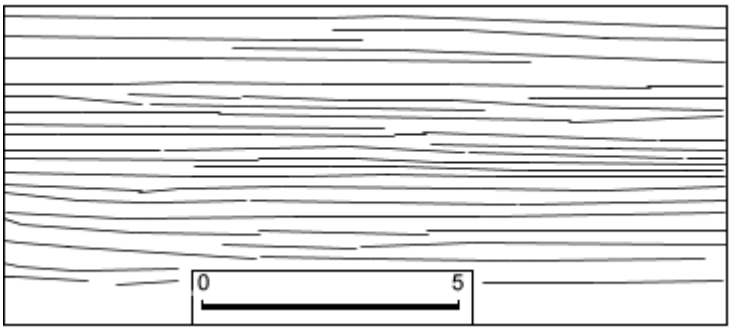

Figure 2.5 USPB Lamination

USPB laminations: thin horizontal laminae marked by variations in grain size, formed due to grain segregation by low-amplitude bedforms (redrawn from Best and Bridge, 1992). Flow into picture, scale in centimetres.

It is thought the increase in suspended load at the onset of the USPB regime (> 10% by volume in the near-bed zone: Allen and Leeder, 1980) suppresses turbulent structures at the bed (Bridge and Best, 1988), thus observed bedforms are muted in amplitude. Turbulence in the USPB regime

forms the parallel laminations characteristic of USPBs via grain segregation (Cheel, 1990) over low-amplitude long wavelength bedforms (McBride *et al.*, 1975; Best and Bridge, 1988; Paola *et al*., 1989; Bridge, 2003). Turbulent ejections and sweeps act over these bedforms to produce FU and CU (Fining Upwards and Coarsening Upwards, respectively) sequences; as the scale of these bedforms is similar to that of turbulence no foreset sorting occurs and planar laminae result (Paola *et al*., 1989). Sweeps produce CUs through dispersive sorting; ejections produce FUs through fallout of suspended grains. The smooth bed surface of FU sequences effectively 'glaze' (Paola *et al*., 1989; Bridge and Best, 1988) the bed, subduing turbulence for a time; coarser particles move over the bedform to be deposited in the trough (McBride *et al*., 1975). Thus, the muted bedforms (downstream migrating: Bridge and Best, 1988; upstream migrating: Cheel, 1990) relate to the DMA and UMA stages of bedforms respectively and are USPBs due to turbulence suppression by suspended sediment. With increasing grain size the USPB stability field decreases in width and eventually disappears, at which point dunes transform into antidunes with no intervening USPB. Bridge and Best (1988) and Best (1993) indicate that this is perhaps due to the reduced levels of suspended sediment, which over sand USPB act to reduce near-bed turbulence and hence bedform development.

Simons *et al*. (1961) and Kennedy (1961) considered USPB quite rare, noting (in the fine sands used in their flume studies) that with appropriate disturbances antidunes formed. Kennedy thought many of Gilbert's (1914) USPB beds would have been antidunes if disturbed, Gilbert having expended great care avoiding disturbances to the flow. Disturbances cause local accumulations of sediment to occur which when amplified forming larger bedwaves which then change the flow structure, amplifying into antidunes.

2.2.3 Antidunes

Gilbert (1914) suggested the term antidune to describe an upstream moving bedform observed in the upper flow regime, although named by Gilbert, 'antidunes' were previously observed by other researchers, (e.g. Cornish, 1899 and Owens, 1908). Kennedy (1961) included all in-phase bedforms as antidune forms (with increasing Fr):

- DMAs: asymmetric, dune-like transitional forms.
- DMAs: symmetric antidune like forms.
- Stationary Antidunes.
- UMAs with non-breaking standing waves.
- UMAs with breaking standing waves.

Antidunes can occur as two or Three Dimensional Antidunes (TDAs) depending on the hydrodynamic climate, two dimensional forms are discussed here, followed by TDAs. Kennedy's convention is followed herein, Figure 2.6 details the occurrence of the above forms; Figure 2.7 illustrates the hydrodynamics of antidunes; Table 2.3 provides the essential properties of antidunes and Figure 2.8 shows the types of sedimentary structures produced by antidune forms. An antidune is a bedform, and not a sedimentary structure (Araya and Masuda, 2001), and the term refers specifically to the sediment mound underneath a standing wave, (Figure 2.7) herein. Detailed papers on antidunes have been published by: Kennedy (1961), (1963) and (1969); Middleton (1965); Shaw and Kellarhals (1977); Alexander and Fielding (1997); Carling (1999); Alexander *et al.* (2001); Carling and Shvidchenko (2002), Wren *et al.* (2005) and Fielding (2006).

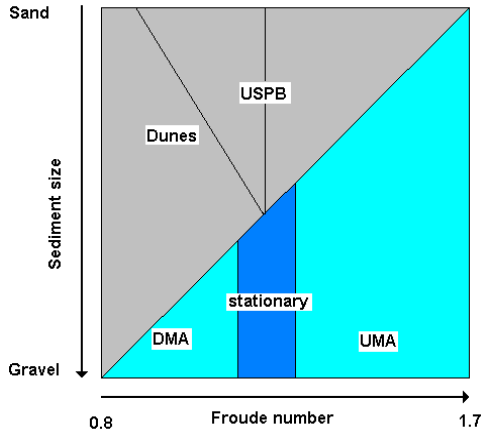

Figure 2.6 Indicative Framework for Bedform Formation and Transition

Diagrammatic representation of the sequence of bedforms with increasing Fr related to sediment size. The dependence of multiple routes through bedform types with increasing Fr on sediment size is shown. Dunes and USPB occur in the grey area, antidunes in the blue area. Stationary antidunes occur around Fr = 1, the USPB zone is divided into two: on the left low-amplitude downstream migrating forms occur; on the right low-amplitude upstream migrating forms occur. Importantly there are three forms of antidunes which may occur in gravel. Diagram based on Kennedy, (1963).

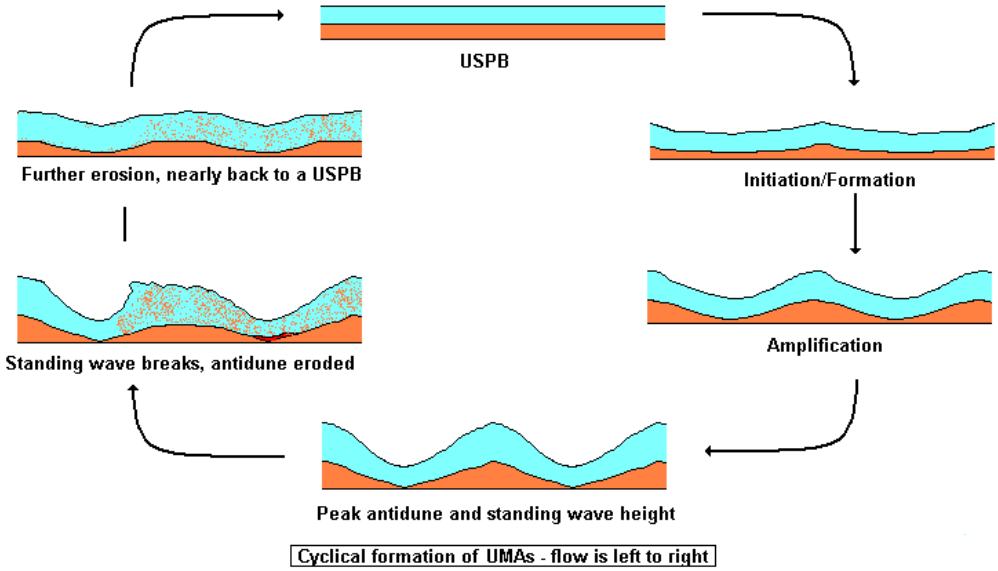

Figure 2.7 Upstream Migrating Antidune Growth Cycle

Suggested cycle of UMA growth and formation in sand; this process is well understood and has been observed by many researchers (e.g. Middleton, 1965; Allen, 1969a). However, the pattern for gravel forms is much less well understood.

Table 2.3 Essential Features of Antidune Bedforms.

Flow	Near critical to supercritical flow: Fr > 0.84 (Kennedy, 1961) < 1.7 (Gradowczyk, 1968). Fr is important, related to c.
Scale	Antidune wavelengths scale with the flow depth and the Fr: $\lambda = 2\pi dFr$ (Allen, 1969b). Alluvial antidunes have been found with λ between 0.1 and 30.5m and h: 0.01 – 1.5m (Kennedy, 1961; Simons and Richardson, 1971).
Formation	Supercritical flow – water surface waves in phase with bed waves: affect their shape (Bridge, 2003). Occur in trains of 3 - 12 individual antidunes (Kennedy, 1961; Alexander and Fielding, 1997), because of this and their sinusoidal symmetry, the appellation 'sinusbed' was also used by Gilbert (1914) and others. Whilst, individual antidunes may migrate upstream, overall a train of antidunes moves downstream, (Kennedy, 1961; Allen, 1985). Scour from flow over a UMA causes new UMAs to establish downstream; USPB is re-established behind the upstream-most UMA (Kennedy, 1961). Standing waves above periodically break; these hydraulic jumps were termed 'whitecaps' by Gilbert, and 'combing' by Kennedy. Breaking periodicity ranging from ten seconds for beach runnels, to several minutes for river antidunes (Clifton *et al*., 1972; Allen, 1984).
Transition Exceptions	From USPBs in sand straight to UMA forms generally without the DMA phase. From dunes in gravels (see Figure 2.21), complex interplay of forms morphologically dune like or transitional DMAs. At Fr > 1.7 antidunes become muted and USPB reappears in gravel or chute-and-pool in sand.

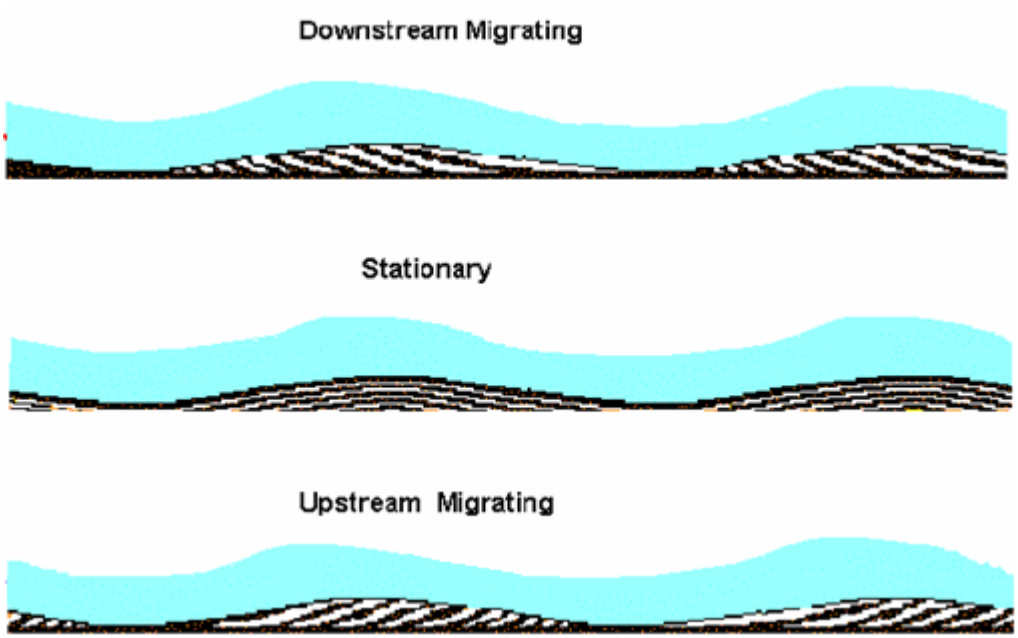

Figure 2.8 Types of Antidune Bedding

Types of antidune bedding, formed during the building stages of antidune growth. These deposits will be modified upon the breaking of the standing wave.

Antidune Flow Dynamics

Compared to equilibrium dunes the amplitude of antidunes tends to be relatively low, due to the much higher flow velocities required to form larger antidunes. Kennedy (1961) gave the equation:

$$\lambda = 2\pi d_m$$

Eq. 2.3 Antidune Wavelength

where d_m is mean water depth (in m), to describe the spacing of antidunes. Kennedy (1961); Simons *et al.* (1961); Allen (1984); Chanson (2000) and Bridge (2003) consider that the critical height for the breaking of an antidunes standing wave is approximately 0.15λ. At this point the height of the antidune amplitude equals the water depth in the trough; on breaking the standing wave may be up to two times the height of the antidune (Figure 2.9). As the perturbation velocity (the movement of the antidune) is resisted by gravity (Kennedy, 1961) the standing wave breaks.

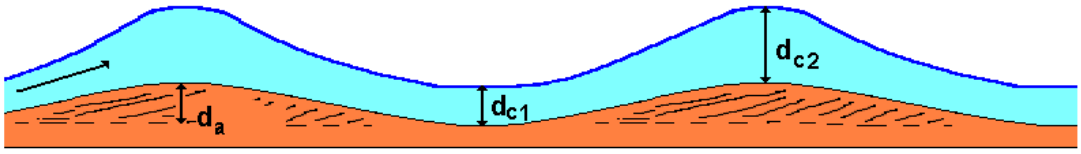

Figure 2.9 Critical Condition for Hydraulic Jump Formation

The critical condition, above which a hydraulic jump forms. At breaking point the relation $d_a = d_{c1}$ and $2d_a = d_{c2}$ holds, (scaled to Kennedy's (1963) $\lambda = 2\pi d_m$).

Flow above antidunes is hydraulically efficient (until the standing waves break), with Manning's 'n' roughness values of 0.01 – 0.013 the flow resistance is 10% of the typical values for dunes, and only 10-15% more than for USPB (Kennedy, 1961; Yalin, 1972). Allen (1966) and Hand *et al.* (1969) considered that if streamlines are parallel to the bed/water surface, skin drag will be the major roughness element for antidunes. However as Mehrotra (1983) observed, for UMAs form drag (drag associated with decelerating flow) will occur upstream of the bedform. This may provide a turbulent environment conducive to sediment erosion, with deposition occurring immediately downstream on the adjacent antidune flank – producing upstream migration.

Behaviour of Antidunes

The standing wave above an antidune is an undular hydraulic jump that forms a classic hydraulic jump on breaking. Undular hydraulic jumps (Fr = 1 to 2) are particularly unsteady and oscillatory since the standing wave can disperse (Gilbert, 1914). Antidunes are extremely dynamic in sand; UMAs (Figure 2.7 and Plate 2.2) rapidly grow from an USPB (Kennedy, 1961). As the antidune grows, flow increasingly accelerates into the trough and decelerates up towards the crest, increasing the magnitudes of erosion in the trough and deposition over the crestal region, the increasingly adverse pressure gradient on the upstream flank of UMAs (Kennedy, 1961) impedes the supercritical flow. Eventually the flow 'stalls' (Kennedy, 1969; Clifton, 1990); and water stored in the steepened standing wave cannot dissipate upstream against the flow when $c < Fr$. Eventually energy is dissipated as an upstream breaking hydraulic jump occurs and the flow may become briefly subcritical; this destroys the antidune in a burst of rapid chaotic sediment entrainment and returns the bed to a USPB state, the process of amplification of the standing wave and the rebuilding of the antidune can then restart (Figure 2.1). Kennedy (1961); Simons *et al.* (1961); Middleton (1965); Allen (1984) and Kubo and Yokokawa (2001) thought a separation zone to progressively form at the bed on the upstream side of a UMA just before the

standing wave breaks. This zone is not a classic separation zone as reported for dunes, but a momentary feature associated with the UMAs breaking standing wave. Suspended sediment is not considered to be required for antidune formation (Parker, 1975); bedload alone is responsible in gravel.

Plate 2.2 Sandy UMAs

Sandy (UMA) antidunes beneath standing waves in Three Cliffs Bay, Pembrokeshire. Flow bottom-left to top-right, note the regular form on the standing waves above the antidunes, (standing wave λ approximately 1 metre).

Breaking of a standing wave often causes standing waves immediately downstream to break (Foley, 1977); upstream standing waves will not break, as surface waves cannot propagate upstream in supercritical flow (Allen, 1984). The release of water previously in these standing waves causes periodic bores of water to occur (Kennedy, 1961; Foley, 1977, Grachev, 1980; Langford and Bracken, 1987).

DMAs occur in gravel and coarse sands when antidunes form directly from the dune stage (Carling, 1999); at higher Fr DMAs may transform to UMAs (Figure 2.7). Fukuoka (1982) found dune-like separation zones associated with DMAs, where grain avalanching occurred. The standing wave associated with DMAs is clear but less pronounced than for UMAs, with the deepest flow occurring over the trough, whilst DMAs appear to be more stable, with less periodic breaking.

The Dune: Antidune Transition

Data on the complex transition between dunes and antidunes is limited, and further research is required (Carling, 1999); Figure 2.10:

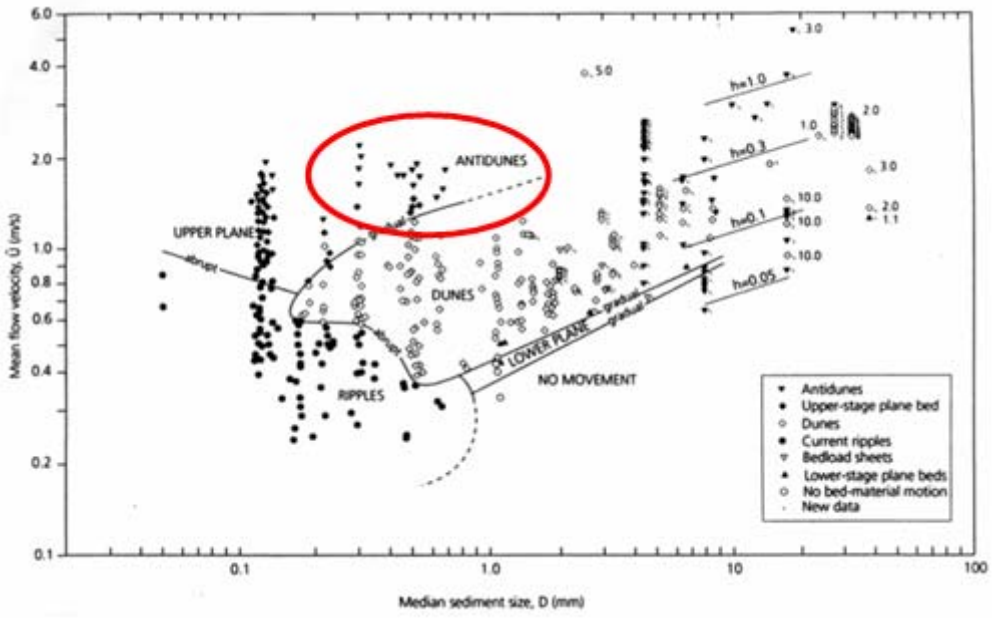

Figure 2.10 Bedform Transition Boundaries Delineated by $\overline{U}$ and D_{50}

Based on experimental data, bedform transitions can be delineated according to $\overline{U}$ and D_{50}. Due to limited data, the dune: antidune transition (highlighted in red) is one of the least clear transitions. Data is especially limited for the transition in coarser sediment, which are less easily mobilised in laboratory flumes. Diagram from Carling (1999).

In some flows, dunes and antidunes may coexist (Kennedy, 1961; Best, 1993; Carling and Shvidchenko, 2002); because as sediment coarsens bedform adjustments increasingly lag changing flow conditions (Engelund and Hansen, 1966; Carling, 1999). Where the relative depth (d_R):

$$d_R = \left(\frac{d_m}{D_{50}} \right)$$ **Eq. 2.1 Relative Depth**

is less than 100 (d_R is dimensionless) or D_{50} is > 2 to 3mm, no intervening USPB occurs (Carling (1999) and Wieprecht (2000) respectively). DMAs resemble dunes because they are a transitional form where Fr = 0.84 to 1 (Carling and Shvidchenko, 2002); dunes develop directly into an antidune form (Kennedy, 1961), as the dune is eroded into a more symmetrical shape by the flow, and antidune deposits form on a washed-out dune base (they have a dune core). Thus, Carling (1999) stated '*the morphological distinction*

alone is no use'. This complex transitory state occurs as the water surface wave is not yet completely in-phase with the bed wave (since at Fr < 1: Fr < c) the undular hydraulic jump dissipates. To the author's knowledge there are only limited studies of the behaviour of the standing wave above DMAs (Fukouka, 1982) or stationary antidunes. Carling and Shvidchenko (2002) showed that the dune: antidune transition occurs at lower Fr as the relative depth decreases; transitional bedforms having been reported for Fr: of 0.5 - 1.8. Shaw and Kellerhals (1977); Whittaker and Jaeggi (1982); Alexander and Fielding (1997) and Carling (1999) find that antidunes in coarse sediments under shallow flows may be of relatively low amplitude. Therefore, the Fr and the sediment size are the most important controls on the type and morphology of the antidune that forms.

Three-Dimensional Antidunes

Kennedy (1961) also considered TDAs, these form beneath three-dimensional standing waves, often termed 'rooster tails', which form due to a superposition of the normal translational surface water wave and an additional transverse surface water wave (Plate 2.3). Kennedy (1961) found that TDAs tend to form in coarser sand than two-dimensional antidunes. Ohtsu *et al.* (2003) found the three-dimensionality in flumes to be due to lateral shock waves occurring above Fr >1.2; especially in narrow flumes, where at the flume wall flow becomes temporarily subcritical. TDAs are also seen in rivers due to reflection from channel banks (Robillard, 1965 and Robillard and Kennedy, 1967), when zones of retarded flow are pulled away from the channel boundaries, intersecting to form the peaks of TDAs. In the case of TDAs, λ is also shorter, but since TDAs are due to a superposition of two waves the standing waves are taller (Kennedy, 1963); since c equals the water velocity these water waves are stationary. Kennedy (1963) states the following equation for TDAs:

$$U^2 = \frac{g\lambda}{2\pi}\sqrt{1+\lambda/b^2}$$ **Eq. 2.5 Velocity Wavelength Relationship for TDAs**

where b = transverse λ (in m) of TDAs, in addition to Kennedy's studies, Araya and Masuda (2001) consider these three dimensional antidunes to be particularly common in conditions of high-suspended sediment fallout.

However, there is much less literature available for three-dimensional antidunes.

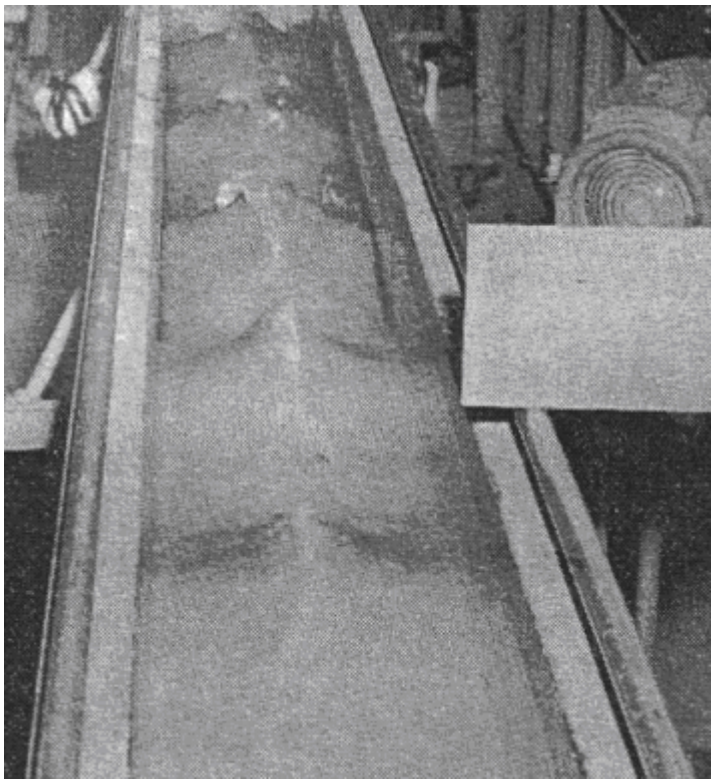

Plate 2.3 Three Dimensional Antidunes

Three Dimensional Antidunes (TDAs) in Kennedy's flume experiments. These forms are produced due to an additional transverse wave caused here by flume sidewall effects (taken from Kennedy, 1961) and by reflection from channel banks in rivers.

2.2.4 Cut-off of Bedform Formation in Coarse Material

When the bedstock is sufficiently coarse, at sediment sorting values (σ_g) above 2.3 antidunes will not form, instead an armour layer forms (Wilcock, 1993); the shear stress required to move coarser sediment is infrequent, when it does occur entrainment removes finer sediment suitable for bedform formation. Wilcock (1993) defines the sorting coefficient (σ_g) by:

$$\sigma_g = \left(\frac{D_{84}}{D_{16}} \right)^{\frac{1}{2}}$$

Eq. 2.6 Sediment Sorting Coefficient

2.2.5 Other Bedforms Associated with Antidune Regime Flow

Chute-and-Pool, Transverse Ribs (TRs) and Step-and-Pool forms have been linked by some researchers to the antidune regime of flow, and details are presented in Table 2.4. These bedforms are associated with the extreme end of upper regime flow.

Table 2.4 Antidune Equivalent Bedforms

Details, conditions and explanations for three types of bedforms that occur above the upper limits of labile antidunes.

Feature	Chute-and-pool	Transverse rib	Step-and-pool
Figure	Figure 2.11.	Figure 2.12.	Figure 2.13.
U **or** Fr	Velocities above antidune regime. Values: Gradowczyk, (1968); Alexander *et al*. (2001).	Antidune regime velocities, but sediment is non-labile. Allen, (1983) suggested flow depth proportional to clast size in the transverse rib.	Antidune regime velocities, but sediment is non-labile. Heterogeneous sediment with extreme coarse clasts essential (Chin, 1999). Particles > D_{50} must be mobile.
Sediment size	Generally limited to fine sands due to high velocities needed to mobilise sufficient sediment. Often temporary, short lived due to rapid removal of sediment and reductions in slope or flow velocity.	In steep, coarser grained systems (Rust and Gostin (1981); Best, 1993; Leeder, 1999) with high clast size to depth ratios and brief, shallow-depth high-energy flows (Koster, 1978; Lunt and Bridge, 2004). Sediments are too coarse and heterogeneous to move as classic labile bedforms: transverse ribs are composed of less mobile material coarser than the true bed material (Whitaker and Jaeggi, 1982). a-b plane of particle parallel to flow, and upstream imbricated (McDonald and Day, 1978). Not true bedwaves by Kennedy's terms.	Occur in steep coarse-grained channels, slopes of 2.5 - 25° are typical (Whittaker and Jaeggi, 1982). Extreme (D_{90}) clast sizes required. Antidunes > transverse-ribs > step-and-pool as a continuum, with increasing sediment size and slope (Chin, 1999). Not true bedwaves by Kennedy's terms. Pools are subcritical, steps are supercritical, the degree of supercritical flow is stage dependent (Wooldridge and Hicken, 2002), who also suggest ~20 years to develop.
Feature morphology and deposits	Backset deposits may superficially resemble antidune backsets. Grains 'Plastered' in place by flow (Jopling and Richardson (1966), thus grain orientations/imbrications are highly-variable compared to antidunes. Fralick (1999) describes a preserved chute-and-pool deposit with sets resembling those of antidunes. Again investigation showed a clear difference: the steep backset beds with particles inclined at high-angles indicating a chute-and-pool origin.	Transverse ridges of coarse clasts are deposited under the crests of standing waves, the zone of minimum bed shear stress in antidune regime flow. Sand drape between features is deposited by waning flow. Consist of "*regularly spaced pebble, cobble or boulder ridges orientated transverse to the flow*" (McDonald and Banerjee, 1971), no more than a few particles high (Shaw and Kellerhals, 1977). Rice *et al*. (2002) postulate an antidune origin for TR features observed on imagery of flood deposits on Mars.	Transverse ridges of (~D_{90}) clasts (Chin, 1989). Shear stress is greatest in pools, thus eroded sediment collects at steps under a hydraulic jump where shear stress is lower, clasts interlock (Chin, 1999). Whitaker and Jaeggi, 1983; Grant and Mizuyama, 1992; Billi *et al.,* 1998; Chin, 1999; Chartrand and Whiting (2000); Lenzi (2001) found step and pool λ and flows to correlate with that expected for antidune regime flow.
Formation	At high Fr antidunes change to chute and pool bedforms, with a permanent hydraulic jump (Alexander *et al.* (2001). Shallow, supercritical flow	Transverse ribs are a form of antidune (Allen, 1985; Best, 1993 and Leeder, 1999). Clear particle-size to λ relationship exists (Bridge, 2003); also influenced by slope (McDonald and Banerjee	Antidune regime flow has been proposed for their formation (Whittaker and Jaeggi, 1982; Koster, 1978); Grant *et al*. (1990); Lenzi (2001). Whittaker and Jaeggi (1982) thought antidune theory only

	on steep sloping sections of bed terminating in a pool with hydraulic jump to subcritical flow, and deposition of backset laminae.	(1971); the λ decreasing as sediment coarsens. McDonald and Day, 1978; Allen, 1983: upstream migrating hydraulic jumps responsible for their formation. Gustavson (1974) and Koster (1978) proposed since hydraulic jumps are rare in rivers with transverse ribs that these features form under standing waves. Boothroyd and Ashley (1975); Whittaker and Jaeggi (1982); Allen (1984) and (Best, 1993) considering them an antidune form. Gustavson (1974); Rust and Gostlin (1981): stone cells due to inference pattern of shock waves (like Kennedy's 3D antidunes). "checkerboard pattern of stone mounds" – each under a rooster tail.	explained initial 'clastic antidunes' (*sensu* transverse ribs). Develop into step and pool through surface coarsening and larger clasts (D_{90}) blocking their migration, fixing their position (Chin, 1999). Whilst Zimmermann and Church (2001); Lee and Ferguson (2002) and Curran and Wilcock (2005) dispute the antidune hypothesis. Instead, Curran and Wilcock (2005) propose that rather than the coupling of bed and surface water waves, the accelerated flow below a step is thought to prohibit deposition in its immediate vicinity. The next step therefore accumulated further downstream outside of this zone.

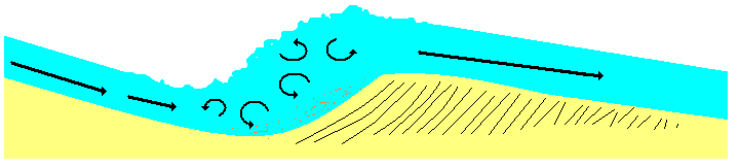

Figure 2.11 Chute and Pool Bedform

The deposition of backset laminae occurs beneath a hydraulic jump in the pool section.

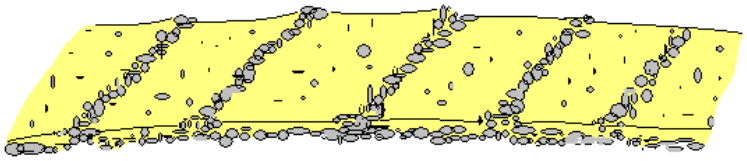

Figure 2.12 Transverse Ribs

Diagrammatic representation of TRs, the finer sand layer in-between TRs is a waning flow deposit.

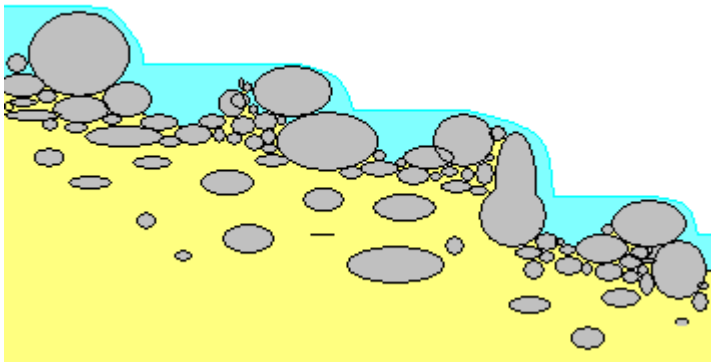

Figure 2.13 Step and Pool Bedforms

Diagrammatic representation of a step-pool reach

2.2.6 Interstitial Flow Through Bedforms

Bedforms consist of discrete particles, and are permeable such that pressure gradients drive an interstitial flow through the bed, this flow being proportional to the inter-particle pore size. The ingress or egress of this flow from the bed alters turbulence dynamics and increases flow separation (Ho and Gelhar, 1983); and reduces boundary layer thickness, thus increasing near bed velocities and shear stresses (Prinos, 1995). Momentum that would be imparted on the bed surface continues with the flow as it passes into the bed, hence modifying sediment transport, compared to the no interstitial-flow case. Simons *et al.* (1961) thought this flow an important influence on bedform formation; Allan and Frostick (1999) have confirmed its influence on the entrainment of openwork gravels. Wilcock *et al.* (2001) observed the critical transition of increased gravel transport with increased sand content occurs when the threshold between a framework and matrix supported bed is crossed - this suggests reduced flow through the bed increases near bed shear stress. In antidune regime flow for gravel forms, where the flow impinges on the permeable surface, this effect could affect flow-bed interactions, influencing bedform formation and stability. However there have been no studies of this effect with respect to antidunes.

2.3 Theories of Formation

2.3.1 Potential Flow Theory

Potential Flow Theory (PFT) was initially proposed by Anderson (1953) and advanced by Kennedy (1963 and 1969); Engelund and Hansen (1966); Hayashi (1970); Nakagawa and Tsujimoto (1980); Richards (1980); Engelund and Fredsøe (1982); Coleman and Fenton (2000) and Colombini (2004). Deigaard (2006) developed a numerical model to specifically to investigate the cyclic formation and collapse of antidune bedforms. PFT analyses the '*inherent instability of the sediment-water interface*' and '*considers the character of potential flow above a fixed undular bed*', (Carling and Shvidchenko, 2002). It is a stability analysis of the effect of bulk flow

parameters (Fr and wavenumber, k) and sediment transport on the spacing, λ and speed of collective sediment waves (Anderson, 1953). PFTs give an insight into the bedform mechanics occurring, but do not elucidate the detailed physical processes that occur at the bed-flow interface, such as turbulence. PFT has been used for geological interpretations of the flow above bedforms (Carling and Shvidchenko, 2002); as it has been shown to accurately predict the occurrence of stable bedform from bulk flow data (Anderson, 1953; Kennedy, 1963 and 1969; Engelund and Hansen (1966); Carling and Shvidchenko, 2002). Figure 2.14 shows the delineation of theoretical bedform-existence regimes by PFT and a general fit with experimentally-derived data.

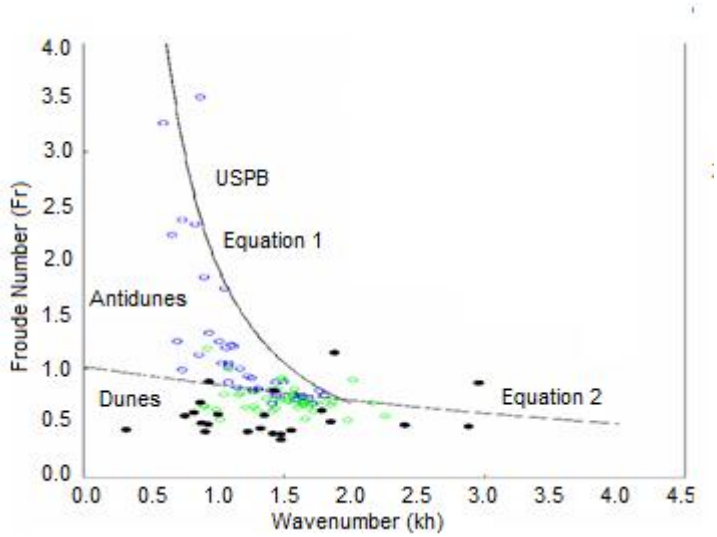

Figure 2.14 Delineation Between Dune and Antidune Regimes

Equations 2.14 and 2.15 can be used to broadly delineate the dune and antidune regimes, providing a broad framework to compare with available data. Dunes are shown in black, transitional forms in green and upstream migrating or stationary antidunes in blue (Diagram: P. Carling, unpublished).

The equations that distinguish these stages (after Anderson, 1953; Kennedy, 1963 and Reynolds, 1965) are:

$$\textbf{Equation 1} = \sqrt{\frac{\tan d(kd)}{kd}} \qquad \textbf{Eq. 2.7 PFT Equation 1, Figure 2.14}$$

Where k = the wavenumber (in m^{-1})

$$\textbf{Equation 2} = \sqrt{\frac{1}{(kd)\tan d(kd)}} \qquad \textbf{Eq. 2.8 PFT Equation 2, Figure 2.14}$$

PFTs can produce asymmetrical dune forms, plane bed and symmetrical antidune forms all with appropriate water surface waves, developing from a plane bed with increasing velocity and sediment transport. Bedforms can be shown to move downstream and/or upstream for the appropriate flow conditions. Bedforms form in response to initial flow perturbations of periodical wavelengths acting on a plane bed, defined by $\lambda = 2\pi \frac{U^2}{g}$ (Lamb, 1932), initiated by a bed irregularity, the dominant λ of bedform is considered to be that which grows the fastest.

In PFT, the Sediment Transport Rate (STR) is related to the flows lowest streamline adjacent to the bed, the STR changes in relationship to any change in the near bed flow further affecting the near bed flow and these adjustments jointly lead to a change in the downstream bed elevation. The STR does not adjust instantaneously to changes in flow stresses at the bed, so a lag term (δ), is included in PFT analysis. The term is justified as being due to turbulence associated with bedforms causing a temporal lag for grains to fall-out, be entrained and taken into suspension, thus maximum instantaneous sediment transport is never reached (Parker, 1975; Allen, 1984 and Engelund and Fredsøe, 1982). The lag is important in defining bedform stability and the direction of movement in the case of antidunes (Kennedy, 1963 and 1969; Parker, 1975; Allen, 1984). Kennedy (1963 and 1969) suggested that as the height of the bedform crest increased, increasing shear stresses above the crest induce greater sediment transport and thus limit further increases in h. Huang and Chiang (2001) clarified the limiting factor on bedform growth: at low flow, skin drag is dominant, but at high flow, form drag (not accounted for in PFT) becomes dominant due to the increasing pressure gradient exerted by steepening bedforms; sediment transport is then suppressed.

Kennedy (1963 and 1969) found that PFT could not completely explain the occurrence of antidunes because antidune dynamics and sediment transport were too complex. Similarly Fredsøe (1974) noted the poor correlation between predictions of dune dimensions derived from PFT with mature dune dimensions: PFT only predicts initiating dunes accurately. PFT does not explicitly account for turbulence or the detail of local physical

processes, as a mechanism for bedform formation, but relies on bulk flow parameters alone (Reynolds, 1965; Engelund and Hansen, 1966; Carling and Shvidchenko, 2002). The dismissal of flow separation as a second order effect rather than a cause of bedforms is a particular limitation of PFT (Leeder, 1983), indeed Nelson *et al.* (1995) consider PFT to be more of a qualitative framework than a predictor. The author concurs with Leeder (1983) and Nelson *et al*. (1995) that whilst PFT may provide a qualitative framework, a true understanding of the variety of bedforms and transitions between requires investigation and understanding of the changing feedbacks between mobile beds, bulk flow properties and turbulence.

2.3.2 Turbulence

As a moving fluid shears internally or across a boundary, turbulent eddies develop and through momentum and vorticity act to entrain, lift and transport mass as fluid and as sediment move away from the boundary into the main flow (Grass and Mansour-Tehrani, 1996). When examined statistically, these turbulent eddies can be seen to exhibit coherence in their spatial and temporal organisation. Over a hydraulically smooth boundary a near-continuous arrangement of flow parallel high and low speed streaks are present which as the outer flow layer advects past are extended into hairpin vortices (Smith, 1996; Bridge, 2003). Yalin (1992), Buffin-Bélanger *et al.*. (2000), Roy and Buffin-Bélanger (2001), Roy *et al*. (2004) and Paiement-Paradis *et al*. (2003) also thought these streaks to be present in gravel bed rivers. The ends of these vortices propagate out of the viscous boundary layer as ejections into the outer flow profile, advecting with the flow. A sweep of high-speed fluid from the outer wall layer flows in behind the near-bed ejection. The inner and outer wall layers then re-establish; this process is cyclic but non-periodic and occurs intermittently over the wall layer (Smith, 1996). Vortices shed into the outer flow ultimately dissipate; such that turbulent anisotropy decreases away from the boundary layer. However, occasional, larger coherent flow structures do upwell to the water surface, forming ‘boils’. These event periods are relatively short, but provide the bed stresses responsible for size selective sediment transport (Grass, 1970;

Williams *et al.,* 1989; Bridge and Best, 1992) and hence the characteristics of depositional units (Best, 1993).

However, in flows with a Reynolds Number (Re, dimensionless) > 4000 (i.e. which would include the turbulent antidune regime), turbulence becomes less structured (Leeder, 1983). When the roughness elements size is well in excess of any laminar sub-layer thickness that could exist, streaks do not exist (Smith, 1996). Instead, vortex production occurs through shedding of Kelvin-Helmholtz vortices when the wall layer is truncated by individual roughness elements – clasts, or ripple/dune crests - and rolls-up (Figure 2.15 and Figure 2.16). The Grain Reynolds number (Re*, dimensionless) is defined as:

$$Re* = \frac{u* D}{\mu}$$ **Eq. 2.9 Grain Reynolds Number**

where u_* is the shear velocity (m/s), D is the particle size (m) and μ is the kinematic viscosity (m^2/s); Re* can be used to define these transitions, when Re* < 5, particles are hidden in the near-bed viscous layer; Re* = 5 to 70 is transitional and at Re* >70 particles protrude through the viscous layer and interact strongly with the flow. Rougher boundaries shed more vortices, and can produce higher amplitude ejections and sweeps (Smith, 1996; Bridge, 2003). The turbulent flow structure in high-velocity flows with high suspended sediment loads has not been clarified, but is considered (Best, 1993) to be 'suppressed'.

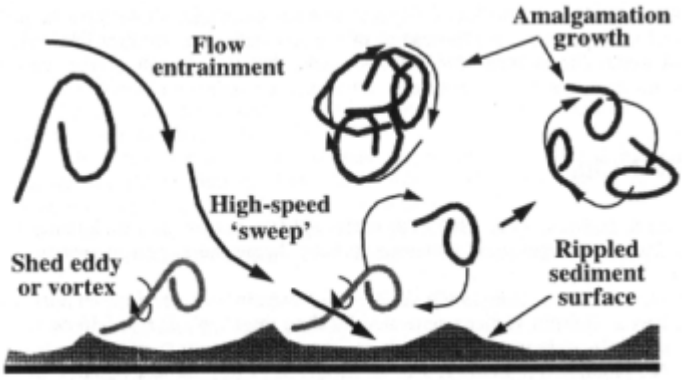

Figure 2.15 Turbulent Structure Development - Bedforms

Turbulent structures associated with ripples and dune bedforms are produced as Kelvin-Helmholtz vortices shed from the shear layer between the main flow and downstream separation zone (reproduced from Smith, 1996). Importantly this occurs in deep flows, where water surface wave: bed wave phase is not important.

As bedforms develop turbulence production changes, instead of the uplift of wall-layer streaks, Kelvin-Helmholtz vortices are produced at the shear layer between the main flow and separated flow. Bedforms then start to control their surrounding turbulent environment; this in turn controls sediment transport over downstream bedforms and thus their growth.

In this thesis the following symbology is used:

- Instantaneous downstream-ward (x) velocity - u_i
- Instantaneous vertical (y) velocity - v_i
- Instantaneous lateral (z) velocity - w_i

By calculating the respective means ($\overline{U}$, $\overline{V}$ and $\overline{W}$) of a data set, the velocity deviations: u', v' and w' can be derived from Eq. 2.10, 2.11 and 2.12 respectively:

$$u' = u_i - \overline{U} \qquad \text{Eq. 2.10 Definition of } u'$$

$$v' = v_i - \overline{V} \qquad \text{Eq. 2.11 Definition of } v'$$

$$w' = w_i - \overline{W} \qquad \text{Eq. 2.12 Definition of } w'$$

Units for instantaneous velocities, instantaneous velocity deviations and mean velocities are m/s.

Quadrant Analysis (Section 3.3.2) can be used to examine and statistically assess the instantaneous velocity deviations and their sedimentological importance. Taken together, these instantaneous velocity deviations $|u'v'|$, form the time averaged Reynolds Stress (τ_R, m^2/s^2). The instantaneous velocity deviations u' and v' can be used to define four types of turbulent event: ejections, sweeps, outward interactions and inward interactions. Ejection events ($u'<0, v'>0$) have a small positive contribution to τ_R, and may suspend particles into the flow as the faster flow above particles reduces pressure and creates dynamic lift (Dittrich *et al.*, 1996). Sweep events ($u'>0, v'<0$) are the main agent mobilising particles in repose on the bed (Hogg *et al.*, 1996; Lapointe, 1992; Grass, 1982). During sweeps, high-speed fluid enters the boundary layer, having a large positive contribution to τ_R, thus they are responsible for the majority of bedload

particle motions even though they occur for a fraction of the time (Grass, 1971; Best, 1993; Williams, 1996 and Hogg *et al.*, 1996). These infrequent, high-magnitude sweeps/outward-interactions provide large contributions to τ_R in excess of critical for a longer period (Cantwell, 1981; Lapointe, 1992; Lapointe *et al.*, 1996). Inward interactions ($u'<0, v'<0$) contribute negatively to τ_R, and do not move sediment (Bennett and Bridge, 1995); because fluid is decelerating at the wall.

Outward interactions ($u'>0, v>0'$) contribute positively to τ_R, and suspend large amounts of sediment as for ejections (Bennett and Bridge, 1995; Nelson *et al.*, 1995; Le Couturier *et al.*, 2000) due to high instantaneous velocities moving away from the bed. In addition to the u' and v' components, Heathershaw and Thorne (1985); Williams *et al.* (1989); Clifford and French (1993); suggest the importance of the normal stresses (U^2; V^2 and even W^2) in initiating coarse sediment motion, with high values increasing the drag force. Where a boundary layer develops in skimming flow, ejections/sweeps dominate (Papanicolaou, 2000), but with larger bedforms (Bennett and Best, 1995; Le Couturier *et al.*, 2000) and larger clasts the occurrence of outward and inward interactions increases (Bennett and Best, 1995; Papanicolaou, 2000). Thus, for complex beds sediment transport cannot be calculated from the bed shear stress approach because events important sedimentologically contribute negatively to the bed shear stress (Le Couturier *et al.*, 2000).

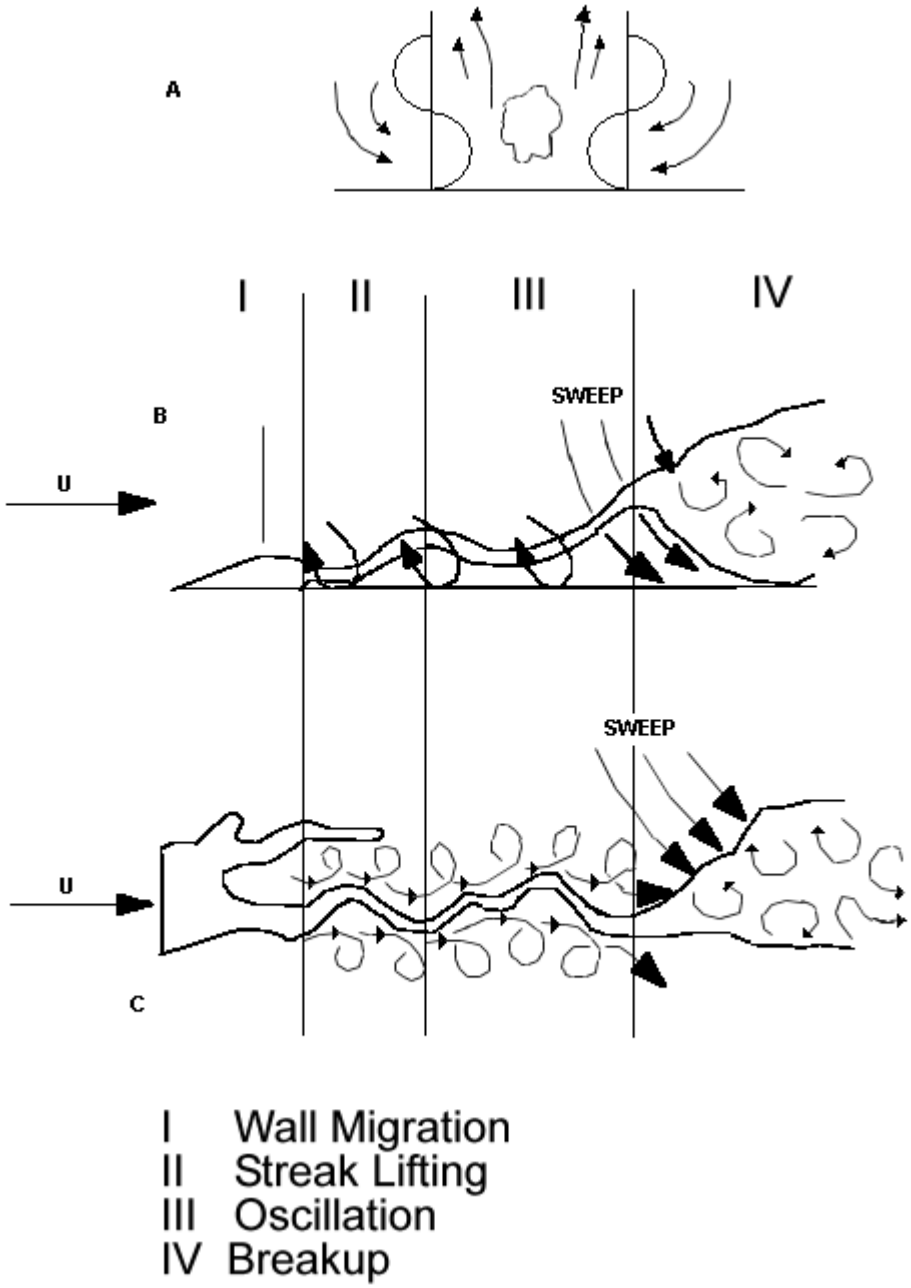

Figure 2.16 Three-Dimensional Structure of Turbulence

A: downstream view, B: side on view, C: view from above. This figure illustrates how the burst-sweep cycle is three-dimensional; sweeps involve sideways as well as vertical turbulent components. The additional stress provided by the w' component is thought (Williams, 1996) to be particularly important in mobilising coarser less mobile sediments (redrawn from Williams, 1996).

Turbulent flow theories account for the development of bedforms from bed defects and turbulent interactions at the flow boundary (Raudkivi and Witte, 1990; Best and Bridge, 1992; Best, 1993). Figure 2.17 shows a sequence of low/high-speed streaks and horseshoe vortices, Best and Bridge (1992) thought these the cause of initial bed defects causing sediment to

accumulate and produce a local flow disturbance. Separated flow downstream of the defect allows more grains to accumulate, whilst at a reattachment point turbulent flow again impinges on the bed, mobilising grains, which creates another defect downstream as reattachment-turbulence subsides (Raudkivi, 1966). Once the boundary layer becomes disturbed the spatial change in STR allows these defects to form spontaneously over the bed and propagate into bedforms. This scenario must hold for antidunes forming from plane bed (the case in coarser sediments) as they are regular periodic perturbations of the bed surface; initially even in this rough flow periodic turbulent structures must form from interactions with the wall layer alone. As incipient bedforms form and grow they modify the three-dimensional flow field causing the distribution of turbulent events in the flow to become increasingly fixed to the bedform geometry. Once turbulent events become fixed, they exert increasing control on the local sediment transport rate and allow further increases in bedform amplitude (Jackson, 1976; Leeder, 1983; Müller and Gyr, 1996; Le Couturier *et al*., 2000). Importantly, as bedforms grow and cause periodic disruptions to the boundary layer, a significant spatial variation in the magnitude and duration of turbulent events becomes possible. Therefore, once bedforms have formed turbulence no longer scales directly to the shear velocity (Nelson *et al*., 1995). For example, in the case of dunes, Bennett and Best (1995) show how the macroturbulence associated with the separation zone controls developed dune geometry, rather than the classic boundary layer ejection-sweep model. Understanding these turbulent structures is key to understanding sediment transport and therefore bedform sedimentology. As the general characteristics of the turbulent flow structure associated with initial defects, ripples, dunes and USPBs are now well established (Bridge and Best, 1988; Best and Bridge, 1992; Bridge and Best, 1997; Müller and Gyr, 1996; Nelson *et al*., 1993; Nelson *et al.,* 1995), understanding these provides the basis for developing an understanding of antidune regime turbulence and sedimentology.

For dunes Nelson *et al*. (1993) and Nelson *et al.* (1995) observe that vortices are shed at the crest where the developed boundary layer ends, and the separation zone begins. High-magnitude turbulent events occur where the

separation zone reattaches, here high-velocity fluid comes close to the bed where the boundary layer is reforming, entraining large quantities of sediment. This turbulence controls sediment transport and enforces dune stability and morphology (Nelson *et al*., 1993 and Nelson *et al.,* 1995); crest exposure to high velocity flow limits further vertical growth. For sand dunes, Bennett and Best (1995) found the largest magnitude turbulence events were concentrated within the separation zone, at the reattachment point and along the shear layer between the main flow and the separation zone. Outward interactions were associated with the separation zone and its reattachment points, taking sediment away from the trough and the lower leeside of the dune. Inward interactions were also associated with flow reattachment. Ejections were mainly associated with the separation zone and the near-bed boundary layer on the dune's stoss side. At the crest ejection events were observed to move away from the bed towards the water surface where they appeared as turbulent 'boils'. The more infrequent, larger-magnitude ejections appear responsible for transporting coarser grains over dune crests to produce laminations in dune foresets. Bennett and Bridge (1995) found sweeps associated with the reattachment point; where they move sediment out of the trough, up the stoss side of the next contiguous dune downstream.

In the dune regime, the largest turbulent events are associated with the separation zone and its reattachment point, the high levels of turbulence mobilising large quantities of sediment. McLean *et al.* (1994) emphasise that it is this detailed structure of turbulence in the near-bed zone that is responsible for initiating sediment motion and mediating deposition. Turbulence associated with the separation zone is two to three times larger than that associated with a non-separated flow (Bridge, 2003); further, turbulence is always closely associated with the decelerations and accelerations of the flow over bedforms (Best and Kostachuk, 2002). In higher velocity flows, Bridge and Best (1988) found the turbulence associated with asymmetrical and humpbacked dunes to have reduced downstream and upward directed components: this is presumably the closest analogy to antidune regime flow.

In the USPB regime turbulence is thought to be muted (Best 1993), with no secondary vortices forming (Boyer and Roy, 1991), preventing the feedback between increasingly fixed turbulence and sediment transport

required for the development of large scale bedforms. However, turbulence is responsible for producing the parting laminations and the lamina characteristic of USPB.

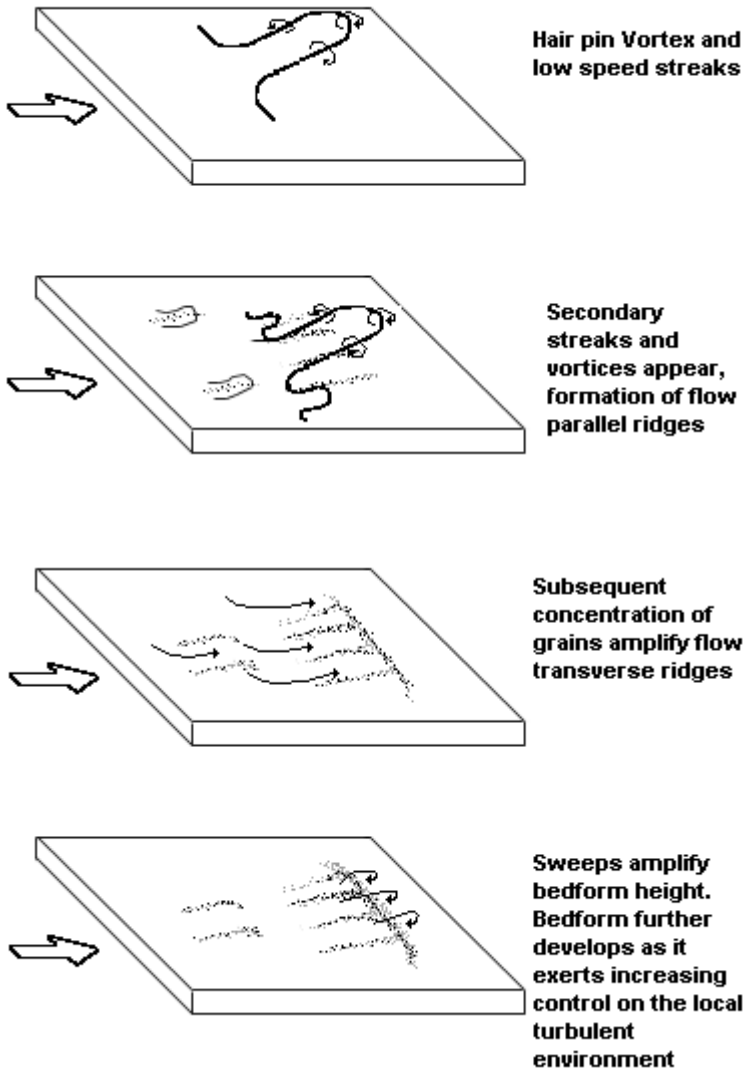

Figure 2.17 Turbulence Induced Bedform Formation

Variation in bed shear stresses associated with the formation and ejection of turbulent vortices allows mobile sediment to concentrate into discrete ridges, this being the initiation of ripple bedforms (redrawn from Best and Bridge, 1992).

There has been no detailed examination of the turbulence structure over antidunes. Referring to breaking UMAs in fine sands, Jackson (1976) states: "*the remarkable energetic large-scale turbulence of breaking antidunes must overwhelm the less vigorous turbulent structure of bursting. The burst cycle is probably neither recognisable in, nor relevant to such flows*". However, the turbulent structure associated with non-breaking gravel

DMAs at lower Fr in deeper flows (transitional from dunes) should display more order. The studies of Saunderson and Lockett (1983) and Bridge and Best (1988) on transitional dune forms suggest a more ordered structure similar to that associated with dunes, but with crucial modifications due to the higher Fr. At the dune: antidune transition, bed and water waves are slightly out of phase and dune and DMA forms may coexist. This mixture of different bedform λ produces adjusting flow cells resulting in instability of form (Carling and Shvidchenko, 2002) and symmetrical forms more so than asymmetric forms (Kennedy, 1961; Simons *et al.,* 1961) fluctuating between dune and DMA flow patterns. The bedforms within this transitional phase are not well adjusted to these flow cells (Klaven and Kopaliani, 1974; Carling and Shvidchenko, 2002); flow cells above DMAs averaging 122% (between 95% - 149%) of the bedform λ. For such shallow flows Roy *et al.* (1996) stated that turbulence anisotropy decreases rapidly away from the boundary, this is expected to be the case for antidunes with turbulence production concentrated near the bed and eddies being rapidly advected. For antidunes, higher turbulence intensities should be associated with the retarded flow and depositional areas. In the antidune regime the lack of a large and temporally stable separation zone (in contrast to equilibrium dunes) and in-phase water-surface and bed-waves may mean vortices are not shed from the crests in the manner observed for ripples and dunes (Figure 2.15). In such fully developed turbulent flow it is likely that the formation of turbulent events will be poorly defined, especially in sand antidunes with high suspended sediment levels.

2.4 Palaeohydraulics: Antidunes in the Flume, Field and Geological Record

2.4.1 Introduction

The extremely turbid and dynamic flow associated with antidunes has meant a thorough understanding of turbulence, sediment transport and preserved sedimentary structures has eluded researchers. This lack of certainty has proven particularly problematic when interpreting and identifying ancient antidune deposits in the geologic record. Preservation of antidune

sedimentary structures (and sometimes the morphology) is possible, if waning flow is practically instantaneous due to rapid flow diversion or a rapid fall of the flood peak (Shaw and Kellerhals, 1977; Alexander and Fielding, 1997) such as may occur in pro-glacial environments (Brennand, 1994; Russell and Arnott, 2003; Duller *et al*., in press) under which conditions rapid sedimentation (Jopling and Richardson, 1966) can lead to antidune structures being preserved as no subsequent reworking occurs. Cyclic migration and formation of antidunes results in sets of deposits which are specific to antidunes, these deposits consist of inclined lenses and draped laminae, specific to the hydrodynamic climate in which they formed (Allen, 1984); Table 2.5.

Table 2.5 Bedforms and Laminae Examined by Authors

This table details the five main laminae types typically associated with antidune bedforms in the literature. It is intended to provide a guide to the laminae typically ascribed to each bedform; however the actual sedimentary structures in field and flume deposits will be more complex.

Bedform and Laminae	Interpretations	Researchers
Bedform Downstream Migrating Antidune **Typical Laminae** Downstream low-angled inclined bedding (Figure 2.8 a). Complete laminae approximately 0.5 times the λ of the antidune.	Deposited on the downstream face of an antidune. Limited observations suggest this is the rarest form of antidune. Uncertainty remains as to whether these are distinct antidune bedforms, or a transitional form (perhaps over a dune core) in response to increasing Fr of the flow.	Middleton (1965); Reinheck and Singh (1973); Barwis and Hayes (1985); Langford and Bracken (1987); Clifton (1990) and Alexander and Fielding (1997).
Bedform Stationary Antidune **Typical Laminae** Parallel but gently undulating lamination in vertical section (Figure 2.8 b).	These forms are thought to be associated with in-phase non-breaking stationary standing waves. Growth occurs through progressive deposition of convex laminations on the antidunes crest that thin out on the flanks (Allen, 1985). The preservation potential of parallel but undular bedding may be higher due to the non-breaking standing waves.	Kennedy (1961); Reinheck and Singh (1973); Collinson and Thompson (1982); Allen (1985); Cheel (1990).
Bedform Upstream Migrating Antidune **Typical Laminae** Upstream dipping low-angled bedding of lenses (Figure 2.8 c). Complete laminae approximately 0.5 times the λ of the antidune. May include some downstream-dipping sets.	Deposited on the upstream face of an antidune, length of laminae preserved dependent on aggradation rate and the degree of erosion caused by the breaking standing wave. Downstream dipping sets deposited by temporary shift downstream of the standing wave, or during wave breaking (Alexander et al., 2001).	Kennedy (1961); Middleton (1965); Reinheck and Singh (1973); Hand (1974); Allen (1982); Barwis and Hayes (1985); Langford and Bracken (1987); Yagishita and Taira (1989); Cheel (1990); Clifton (1990); Alexander *et al.* (2001).
Bedform Upstream Migrating Antidune (with violently breaking standing wave). **Typical Laminae** Sand-gravel couplets (and finer	Laminae thought to form when the standing wave above the antidune breaks violently. This erodes and suspends the sediment within the antidune bedform. Couplets then form due to the rapid redeposition of	Blair (1987); Clifton (1990); Blair and McPherson (1999); Blair (1999); Blair (2000); Moscariello *et al*. (2002); Russell and Arnott (2003)

gravel-coarse gravel couplets)	coarser sediment, followed by deposition of finer sediment.	
Bedform Transverse ribs **Typical sedimentary structures** Ridges (ribs) of clasts aligned transverse to the direction of flow. A sand drape, deposited during waning flow is often present inbetween ribs.	Thought to be a bedform produced by antidune regime flow over a coarser, clastic bed.	Boothroyd (1970); Blair and McPherson (1999);

Yokokawa *et al.* (2000) stated that antidune deposits should be concordant and overlain onto an erosional surface; while Clifton (1990) found that they may also be truncated by an upper erosional surface. Where antidune deposits are not truncated, the length of laminae are thought to provide an indication of antidune λ (Kennedy, 1963; Barwis and Hayes, 1985; Langford and Bracken, 1987; Alexander *et al*., 2001), thus providing a useful palaeoflow indicator.

2.4.2 Flume Based Antidune Studies

Flume studies of bedforms to date have concentrated on lower regime bedforms (ripples and dunes); with few flume studies of upper regime bedforms, the majority concerned with upper stage plane beds (USPBs) (such as: Best and Bridge, 1992). The few previous studies of antidunes have almost entirely consisted of studies of their formation in fine to medium sand and have concentrated on the upstream migrating antidune (UMA) form in fine sand; a summary of these antidune morphologies is shown in Table 2.6.

Alexander *et al.* (2001), focused on the internal structures of antidunes in non-aggrading and (for the first time) aggrading conditions; rapidly buried antidune structures were preserved (Figure 2.18). Yagishita and Taira (1989) detailed the grain orientation/fabric of antidune internal structures. Yokokawa *et al.* (2000) and Alexander *et al*. (2001) stated the following features as characteristic features of antidune sedimentary structures in fine sands (nomenclature is from Alexander *et al.* 2001):

1. Concave upwards, shallow, symmetrical lenses;
2. Convex upwards, symmetrical lenses;
3. Erosional surface at base of lenses, overlain by concordant laminae;

4. Interior of lenses is structureless; and
5. Upstream dipping foreset structures are rare.

Based on the comparison of various previous authors' antidune deposits and interpretations, Figure 2.18 and Figure 2.19 have been developed to synthesise the variety of sedimentary structures which have been postulated or observed to have an antidune origin. Key features in these diagrams include lenticular lenses of sediment defined by Type I and Type II laminae, which are explained further in Figure 2.24.

Table 2.6 Antidune Morphologies from the Literature

Summary of antidune morphologies from the literature (* indicates values not stated). The wide variation in amplitude and λ is evident, as is the small average grain size used for these experiments. **†** = transition dune forms.

	Bedform λ	Bedform Amplitude	Indicated U (m/s)	Fr	Sediment size /details
Alexander *et al.* (2001)	0.76 - 1.14 m	0.07 m	1.3	1.5	0.42 mm D_{50}
Cheel (1990)	0.065 m	0.0026 m	0.8	0.67	0.19 mm D_{50}
Foley (1977) and Foley (1978)	~0.35 m	-	0.8	-	0.28 mm D_{50} sand + 0.7 - 1.0 cm pebbles.
Gilbert (1914)	-	-	0.6 – 1.2	0.8 -3.2	Gilbert 1914: dip of backset proportional and antidune h proportional to standing wave h. D_{50} 0.3 to 0.5 mm.
Hand (1974)	-	-	-	-	Supercritical density currents - observed same pattern of antidune growth and breaking as Middleton (1965).
Hunzicker (1930)	~0.3 m	~0.017 m	0.37 - 0.72	1.2 - 1.3	Basic study. Many dimensions not reported (sand D_{50} = 0.25 mm).
Jopling and Richardson (1966)	-	-	1.14	>1	0.3 mm D_{50}
Kennedy (1961)	~1 m	~0.1 m	0.8 -1.4	0.8 - 2.4	0.233 mm D_{50} and 0.534 mm D_{50}
Kubo and Yokokawa (2001)	0.4 - 1 m	0.01 - 0.02 m	0.84	1.3	'fine' sand*
McBride *et al.* (1975)	2 - 8 m	0.03 -0.06 m	0.4	1 - 1.4	0.19 mm - 0.78mm D_{50}. Downstream migrating in-phase waves: formed USPB planar laminations.
McDonald and Day (1978)	0.13 - 0.34 m	0.031 – 0.04m	0.9	0.45 - 2	Transverse ribs. 5.2 mm and 9.6 mm D_{50} for pebbles + coarse sand mixture.
McDonald and Vincent (1972)	0.91	0.049	0.88	(Pipe flow)	0.47mm D_{50} [Pressure wave - analogous to antidunes]
Middleton (1965)	1 - 2 m	0.05 m	~1.3	1.1 -1.7	0.19 mm D_{50}
Moss *et al.* (1980)	0.01 – 0.2m	0.001 – 0.05m	-	> 1	D_{50} = 0.43mm. Observed upstream migration in faster velocity flow over steeper slopes, and downstream migration in lower velocity flows over shallower slopes. Styles not discrete, continuum.

Table 2.6 (continued)

	Bedform λ	Bedform Amplitude	Indicated U (m/s)	Fr	Sediment size /details
Saunderson and Lockett (1983)†	0.9m	0.1m	0.96-1.27	0.8 - 1.1	0.5 mm D_{50}
Shaw and Kellarhals (1977)	~0.25 m*	~0.025 m*	0.75 - 0.96	0.9 - 1.3	8 mm D_{50}
Simons, Richardson and Albertson (1961); Simons and Richardson (1963); Simons, Richardson and Nordin (1965)	1.5 - 3.0 m	0.09 - 0.15 m	1.18 1.51 m/s	1 - 1.3	0.27 mm D_{50} and 0.45 mm D_{50}
Wren *et al*. (2005)	-	mm's	1.33m/s	1.1	Fine sand. Bedforms interpreted as a transition phase between USPB and antidunes.
Yagishita and Taira (1989)	0.6 -0.7 m	0.03 m	0.9 - 1.08	1.66 - 1.76	1.00 mm D_{50} No structures preserved, grain imbrication analysis undertaken, the antidunes had upstream imbrication on both faces (this would only be expected on the upstream side of a dune, with fallout deposits from suspended sediment on lee side of dune).
Yokokawa *et al*. (2000)	0.4-1 m	0.01 - 0.02 m	0.84	1.3	0.18 mm Lens like cross-stratification, thought to be indicative of high sediment supply.

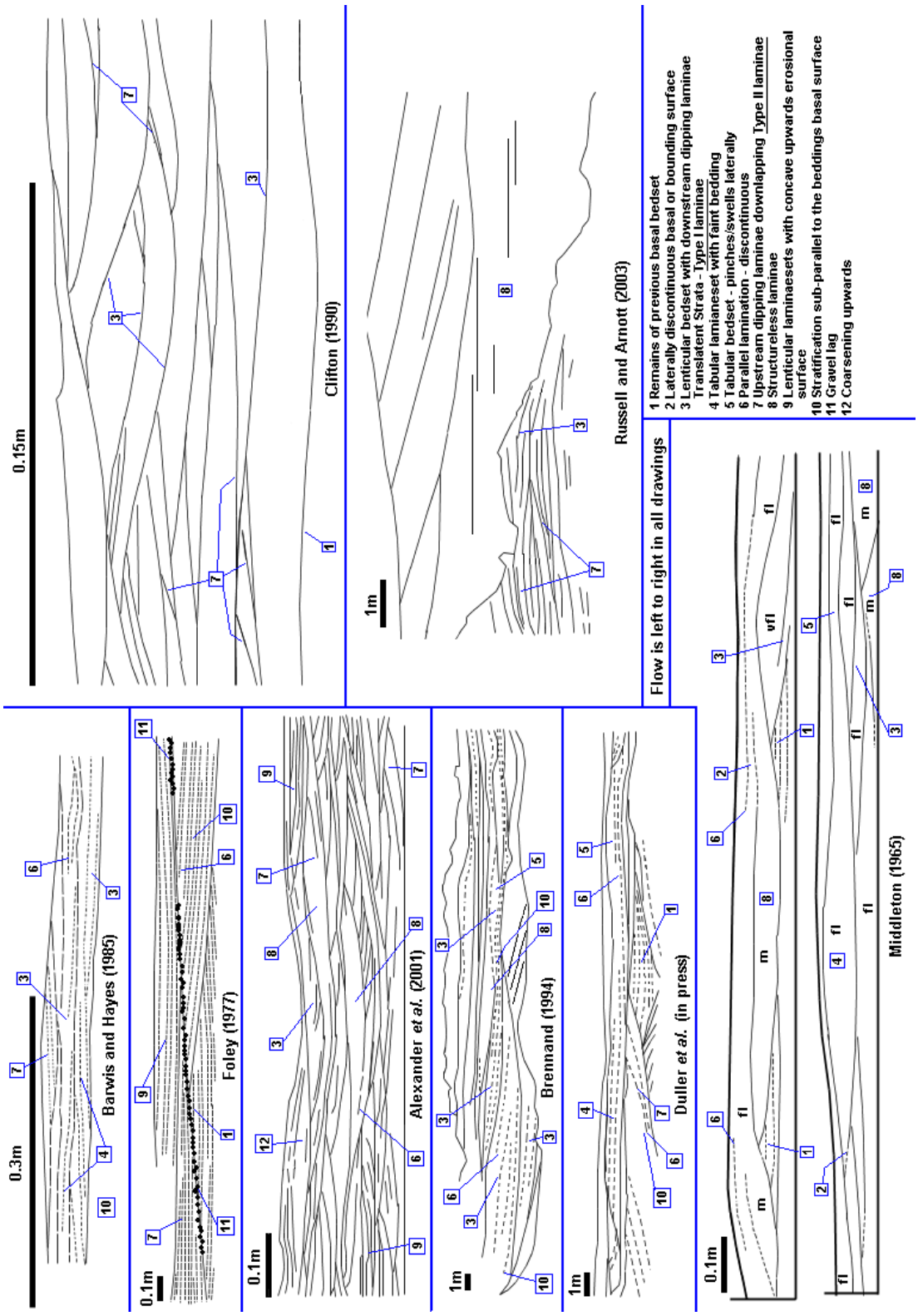

Figure 2.18 Antidune Laminae 1 (after Duller *et al*., in press)

Structures associated with antidunes in fine to medium sand (Middleton, 1965; Foley, 1977; Barwis and Hayes, 1985; Clifton, 1990; Alexander *et al*., 2001; Russell and Arnott, 2003) and coarse sediment (Brennand, 1994 and Duller *et al*., in press). Dimensions as indicated by respective scale bars. Further details of these examples are contained in Table 2.6, 2.7 and 2.10.

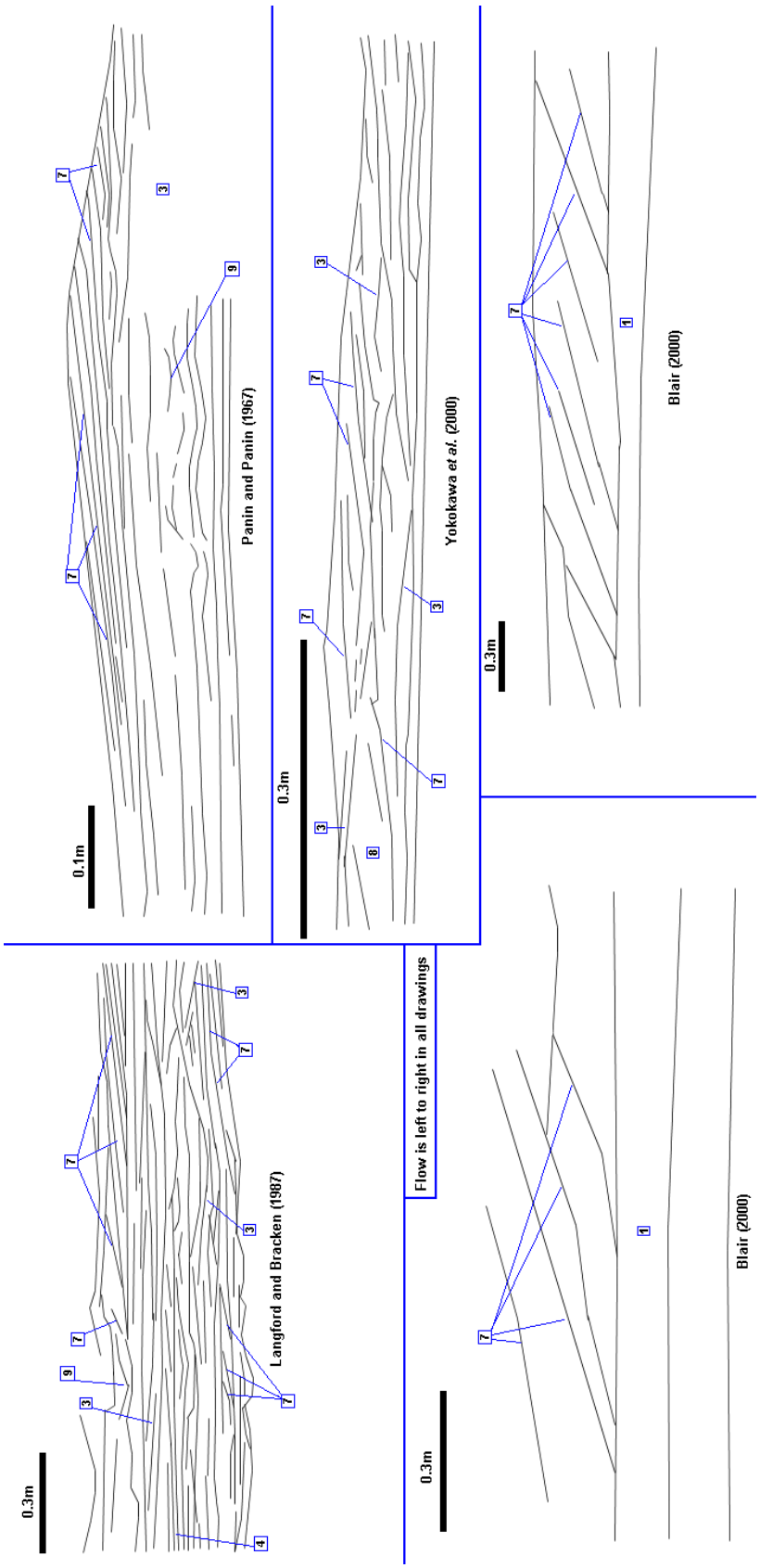

Figure 2.19 Antidune Laminae 2

Structures associated with antidunes in fine to medium sand (Langford and Bracken, 1987; Panin and Panin, 1967; Yokokawa *et al*. 2000) and coarse sediment (Blair, 2000). Dimensions as indicated by respective scale bars, key on Figure 2.18. Further details of these examples are contained in Table 2.6, 2.7 and 2.10.

The lenses in Middleton's (1965) and Yokokawa *et al.'s* (2000) antidune deposits (Figure 2.18) were massive with faint laminations, because of the homogenous fine sand used and rapid rates of suspended sediment deposition. Whilst, the medium sand used by Alexander *et al.* (2001) meant that laminations were more easily observed. Any laminations were associated with grain size variations and heavy minerals; Cheel (1984) in particular found heavy minerals segregated at the crest. High angle *a*-b plane imbrication (at angles steeper than the depositional slope) is a common characteristic that was observed by: Kennedy (1961); Allen (1966); Langford and Bracken (1987); Yagishita and Taira (1989); Yagishita (1994) and Fay (2002). Grains are often imbricated at up to 20 - 40° from the horizontal (high-angle imbrication) on UMAs due to the grain-to-grain collisions during rapid deposition in an impinging[1] flow (Yagishita and Taira, 1989); whilst on low-amplitude antidunes Cheel (1990) found imbrication at 13 - 14°. It is not known if this range of imbrication holds for DMAs where grain avalanching may be important. Foley (1977) experimentally produced dropout armour lenses.

Middleton (1965), Yokokawa *et al.* (2000), Cheel (1990) and Alexander *et al*. (2001) found symmetrical lenticular cross-bedded structures (laminations) deposited at between 10° and 20° on the upstream or downstream flanks of the antidunes, whilst rarer convex upwards deposits occurred under standing waves (see Figure 2.18 for more detail).

Preferential preservation of the laminae from larger antidunes occurs because of the deeper scouring associated with larger antidunes (Kennedy, 1961; Foley, 1978; Alexander *et al*., 2001). Alexander *et al.* (2001) found it impossible to distinguish between antidunes from aggrading and non-aggrading conditions. Cheel (1990) proposed that with increasing flow strength sedimentary structures in fine sand change in the sequence shown in Figure 2.20; his '*Antidune Backset Cross-Laminae'* partially resemble the deposits found by Alexander *et al.* (2001) shown in Figure 2.18.

Jopling and Richardson (1966) studied a sediment-laden shooting-flow terminating in a hydraulic jump. Upstream laminae of the kind produced by UMAs was produced upstream of a tabular deposit, with dune-like foresets

[1] Yagishita and Taira use this word to describe the flow that is impacting forcefully on the upstream face of antidunes in their experiments.

forming on the downstream flank, whilst antidunes forming on top of the tabular unit left deposits consisting of: "*symmetrical shaped undular bedding, with or without pockets of backset bedding*".

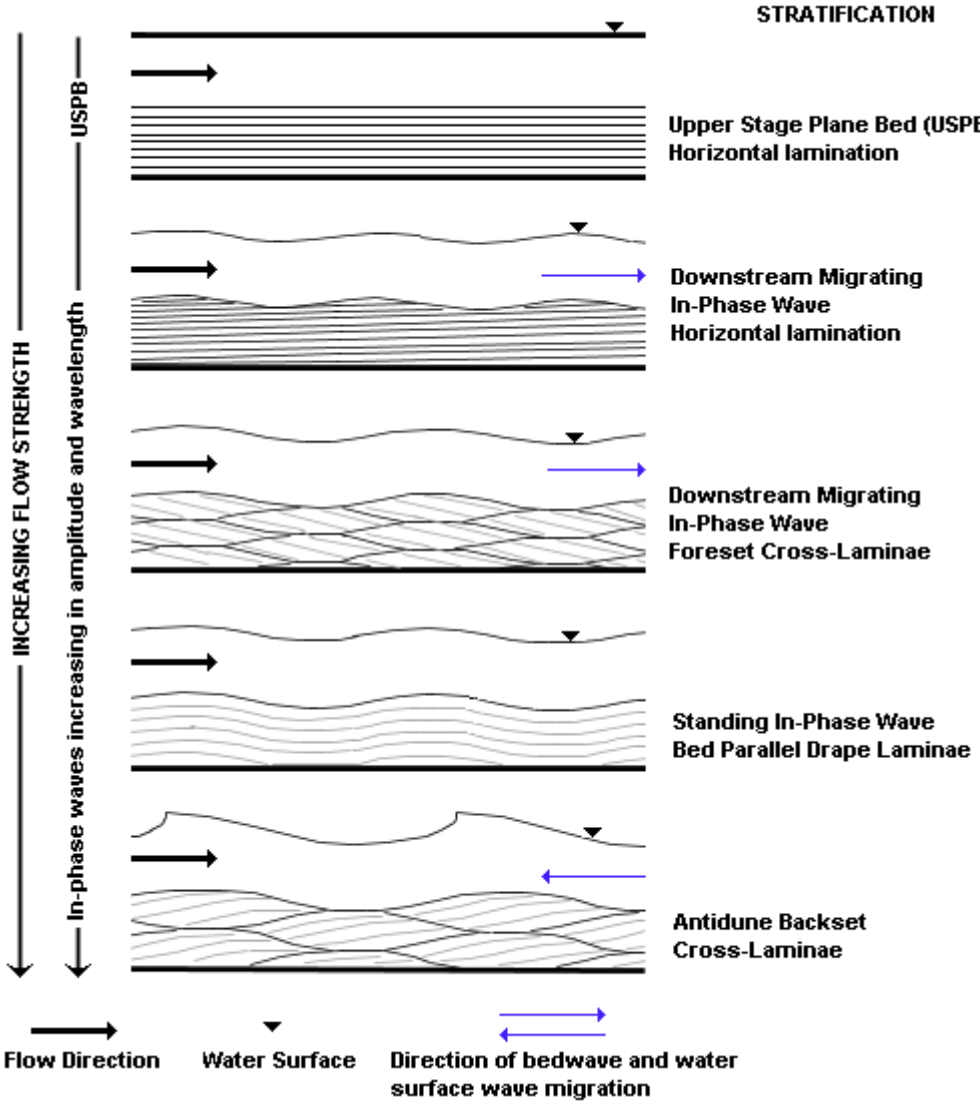

Figure 2.20 Cheel (1990) Bedform Sequence

Cheel (1990) proposed this sequence of bedform deposits with increasing flow strength from USPB to antidune. The relation of sedimentary structures to bedforms is clear. In contrast, Paola *et al*. (1989) thought low-amplitude bedforms were required to form USPB lamination. Diagram redrawn from Cheel, 1990).

In a conduit flume, McDonald and Vincent (1972) observed low amplitude bed waves, with parallel laminations; they proposed tentatively that these could be a type of antidune deposit, related to the upstream movement of pressure waves in the closed conduit, as antidunes are not considered able to form without a free surface. The only flume study that utilised coarser sediments (D_{50} = 8 mm) was that by Shaw and Kellerhals (1977), who

concluded that the equations for sand antidunes were equally applicable to gravel forms, but gave no sedimentological details. Saunderson and Lockett (1983) produced convex and humpback dunes with sigmoidal cross bedding (Figure 2.21); these had bedding transitional between that expected for dunes and antidunes. The convex symmetrical dunes were "*dynamically similar to in-phase waves"*; whilst the humpback dunes were *"on the edge of the in-phase wave stability field".* Thus, these are transitional (non-equilibrium) DMA forms forming before the USPB stage in sediment that was too coarse to form the USPB stage immediately, but at higher shear stresses may form USPB and/or UMAs. The deposits on the back of the humpback dune look superficially similar to those found in a DMA by Alexander and Fielding (1997) which was also a non-equilibrium form, forming during the waning flow stage.

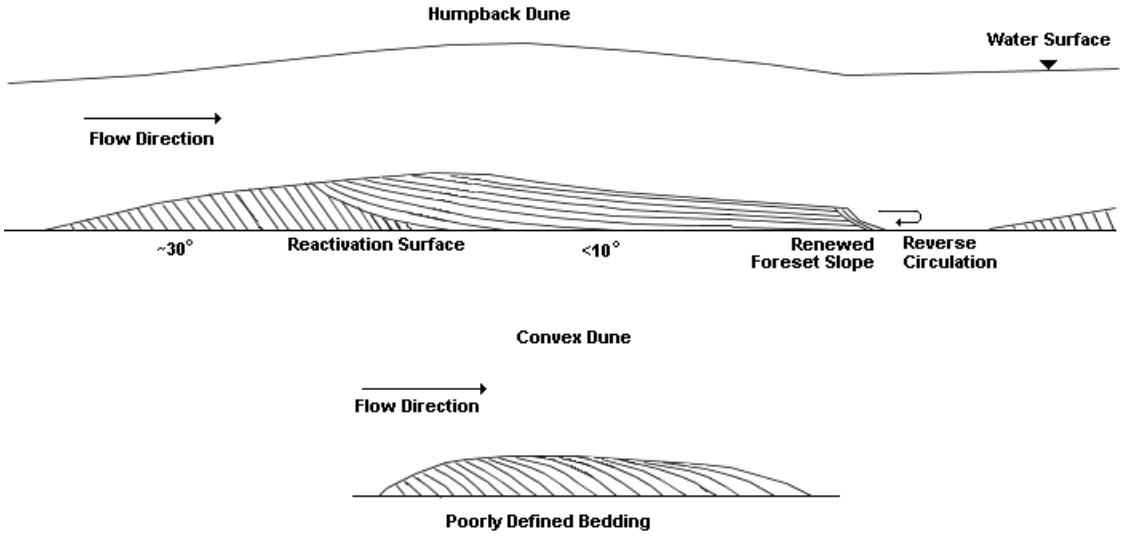

Figure 2.21 Transitional Dunes

Transitional dunes (redrawn from Saunderson and Lockett, 1983). The humpback dunes *"distinctive, low angle topset bedding, merging into steep foreset beds, and into bottomset beds smoothly"* is transitional between that expected for dunes and antidunes. Note the low angle deposits and the near in-phase bed and water surface waves, (Top dune is 2m long, 0.15m tall, bottom dune 0.75m long and 0.15m tall).

2.4.3 Present Day Field Examples

Table 2.7 outlines antidunes examined in the field, summarising the morphologies. Shaw and Kellerhals (1977) provided an examination of symmetrical gravel antidunes they believed formed under stationary standing waves (Plate 2.4). Shaw and Kellerhals found equations relating antidune λ

to velocity appropriate for these forms. Shaw and Kellerhals postulated that the differences between their antidunes which were formed in coarse sediment and had relatively simple internal structures and antidunes formed in finer sediments, was due to the much higher Re^* for coarse bedload particles in shallow antidune regime flow.

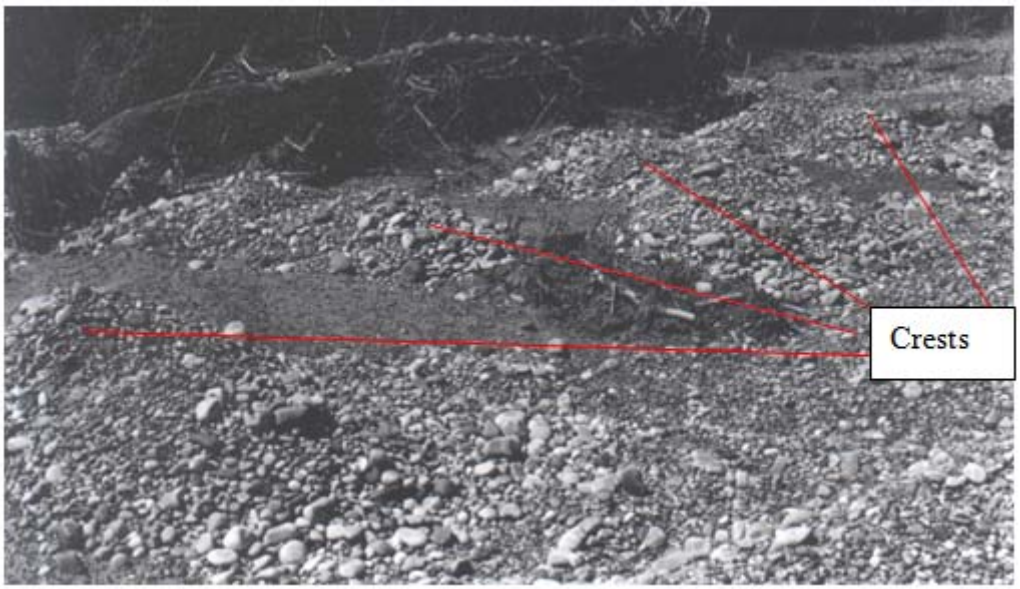

Plate 2.4 Mounds Inferred to be Antidunes North –Saskatchewan River, Canada

Shaw and Kellerhals (1977) antidunes in the North Saskatchewan River, Canada. Antidunes appear as mounds of gravel between the top right and bottom left of the photo. These antidunes apparently formed under stationary standing waves in a flood (photo: from unpublished original: courtesy J. Shaw), forms are approximately 0.5m tall and λ is 3m.

Table 2.7 Morphologies of Field Antidunes

Morphologies of inferred antidunes examined in the field in the present.

Study	λ (m)	h (m)	Morphology	Est. velocity (m/s)	Est Fr	Sediment (mm)	Comments
Alexander and Fielding (1997)	8 - 19	0.25 -1	Asymmetrical. Steep stoss (6° - 16°), shallow lee.	4.4	0.8 - 1	Coarse sand and gravel, clasts up to 0.1m in diameter.	Grain orientations observed match those of Cheel (1984); Yagishita and Taira (1989) and Cheel (1990).
Barwis and Hayes (1985)	0.4 - 1.15	0.005 - 0.02	Laminae ~0.25m long	-	-	Fine beach sand.	Low-angle cross laminae formed by antidune migration. Change from upslope dips to downstream dips down fan (change in antidune migration direction – UMA, stationary, DMA).
Blair (1987)	-	-	Slope = 2.5°. Deposits 0.2m thick, 1-3m wide and 4-5m long (perhaps TDAs).	3 - 6	1.4 - 2.8	Sand/gravel	
Blair and McPherson (1999)	-	-	Couplet sets 0.1 - 1 m thick	-	-	Sandy cobble to pebbly-gravel.	Sand-gravel couplets: upslope dipping low angle cross-bed deposits due to antidune migration and planar bedded produced by antidune washout (clasts: a-b plane transverse to flow, and a-b plane dipping upstream). Change from upstream dip to downstream dip as move down fan (as per Barwis and Hayes, 1985). Standing waves dissipate gradually, hence preservation Less common lenticules of gravel in sinuous ridges - transverse ribs - low sediment supply conditions.
Blair (1999)	5-25	0.2 - 0.6	Gravel couplets 1 - 5 m long and sandy couplets up to 10 m long. Up to 0.25m thick. Backsets dip upstream 5° - 28°, beds 1 - 3 m long and up to 0.4 m thick.	3 - 6.2	1.6	Sand - pebble range.	Rhythmic gravelly and sandy planar couplets. Coarse and fine couplet sequences. Early-phase backset (Facies B) -beds or washout-phase sheetflood couplets (Facies A), depending on erosional intensity.
Blair (2000)	-	0.07 - 0.4	Mainly planar sand-gravel couplets. Backsets 5° - 24°.	-	-	Sand to pebble range.	

Table 2.7 (continued)

Study	λ (m)	*h* (m)	Morphology	Est. velocity (m/s)	Est. Fr	Sediment (mm)	Comments
Boothroyd (1970)	-	-	-	-	-	Gravel/pebble	Flow transverse pebble strips atop bars.
Clifton (1990)	-	-	Inverse grading, low angle down and upstream dipping cross stratification (0.01-0.05m thick and less than 15°).	-	-	-	Bank exposures of Holocene era, fluvially reworked volcanic sediment.
Clifton (1990)	0.2 - 3	0.009 - 0.15	Inversely graded lenticular laminae, dips up and downstream. Dips 5 - 10°	0.75 - 2.66	0.9 - 3.49	Fine sand (D_{50} = ~0.25)	Antidunes produced in beach runnels
Duller *et al*. (in press)	24-96	-	Lenticular and tabular bedsets, thickest at mid-point (dip <5˚). Tapered dip by up to 10˚., some exclusively upstream. Laminations mostly concave up. Rare convex up interpreted as whole antidunes.	6-12	1	Sandy gravel grade. Laminations faint, deposits often massive with limited visible laminations.	Antidunes sedimentary structures found in 1918 jökulhlaup depositionary sequence in Iceland. Generally interpreted as DMAs, with some sedimentary structures identified as UMAs and chute-and-pool. Tabular/lenticular laminations typically 5 – 0.6m thick (λ - thickness ratios: 0.01-0.060). Regular/irregular laminations typically 0.05 – 0.6m thick (λ - thickness ratios: 0.09-0.011 and 0.11+ respectively). Erosive base dip at 20-30˚ up or downstream – with clasts conc. above. Flow depth estimated as between 5 and 19m.
Fahnestock (1963)	2.5	0.3	-	2.5	1.45	Sandy to gravel with pebbles	Several examples of antidunes observed, including some three-dimensional antidunes. Sedimentary structures not examined.
Foley (1977) and Foley (1978)	0.27-0.92	-	-	-	-	Sand. Large clasts layers associated with dropout armour under standing waves above antidunes.	Dropout armour - size of equates well with maximum transportable sizes at peak flow. Hence lenses as a quantitative hydrodynamic indicator.

Table 2.7 (continued)

Study	λ (m)	h (m)	Morphology	Est. velocity (m/s)	Est. Fr	Sediment (mm)	Comments
Harms and Fahnestock (1965)	-	-	-	-	-	D_{50} = 0.21	Antidunes on point bars. Some low angle to near planar bedding
Kjær *et al*. (2004)	-	-	-	-	-	Sandy gravel	Planar to low-angle cross-bedding sand facies interbedded with fine gravel. Icelandic outwash deposits, interpreted as antidune deposits.
Langford and Bracken (1987)	0.7 - 1.2	0.04	laminae sets 0.02 - 0.03 m thick and 0.3 - 0.9 m long	-	1 - 1.7	Fine sand (D_{50} = 0.15)	Antidunes forming in sand on fast moving riffle-pool mesoforms.
McDonald and Banerjee (1971)	0.15 m - 2.26	-	Transverse Ribs.	-	-	Pebbly sand.	Notes other controls on spacing - slope, suspended sediment concentration.
McDonald and Day (1978)	0.25 - 2.25	-	Transverse Ribs.	-	-	Pebbly sand.	Clasts a-plane transverse to flow, a-b plane dips upstream. Sand to pebbly gravel. Spacing increases with pebble size.
Nordin (1963)	3.04 - 6.1	0.61 - 0.91	-	-	-	D_{50} = 0.03 - 0.15	Fine to medium sand (0.002 to 0.5 mm)
Panin and Panin (1967)	0.5 - 1.2	0.02 – 0.06	Asymmetric shaped, steeper lee (2°- 5°) slope compared to stoss (5° - 9°). Upstream dipping laminae (3°	-	-	D_{50} = 0.07 - 0.25	Laminae high-lighted by concentrations of darker minerals.
Russell *et al*. (2002) and Russell *et al*. (2003)	40-100	0.5-2	Large flow traverse bedforms. Upstream dipping cross-stratified with poorly sorted sediment.	-	-	Coarse sand to gravel with pebbles and some boulders.	Antidunes on an Icelandic outwash plain, Jökulhlaup origin. Bedform size decreasing down slope, with largest clasts being found on the bedform crest.

Table 2.7 (continued)

Study	λ (m)	h (m)	Morphology	Est. velocity (m/s)	Est. Fr	Sediment (mm)	Comments
Shaw and Kellerhals (1977)	2 - 3	0.2	Regular trains of gravel mounds.	1.76	-	Lag cover of large unsorted clasts at base and peaks. Inner core of well sorted openwork gravel with sand matrix.	Mounds formed during overland flow, interpreted as antidunes. Preservation could be accounted for by rapid flow cut-off during waning flood stage.
Yagishita (1995)	0.15 - 0.6	0.065	-	0.44 - 1.5	1.3 - 2.4	Fine sand (D_{50} = 0.29)	Antidunes in a beach runnel, three dimensional.
Zieliński (1982)	1.5	0.4	Flow transverse forms. Grow and decay with pulsing flow into reservoir.	1 – 1.5	>1	D_{50} = 0.2.5 ('waste' fines from gravel plant)	Upstream dipping (< 10˚)

Alexander and Fielding (1997) examined (asymmetrical) DMA deposits (Figure 2.22), akin to the *'downstream-migrating in-phase wave foreset cross laminae'* phase in Cheel (1990): Figure 2.20. Similar low-angle DMA deposits were found by Duller *et al*. (in press) in an Icelandic jökulhlaup depositionary sequence (see Figure 2.18). In the Burdekin DMAs, cross-sets were located on the lee side and lenses consisted of sandy-gravel with erosive bases (Figure 2.22); these may represent dunes truncated and deflated by supercritical flows (Pickering *et al*., 2001). Alexander and Fielding (1997) found an accumulation of large clasts lacking strong grain orientation on the crest of antidunes (contrary to the flanks); this was also observed by Foley (1977) and Shaw and Kellerhals (1977) and was attributed to the local flow pattern. It was suggested that deposition of clasts by saltation or from suspension by turbulence associated with the standing wave was responsible for the observed clast orientations at the crest (see Plates 2.5 and 2.6). The strong flow over the antidunes upstream face produces well orientated clasts on the stoss compared to the lee; deposition upon these antidunes was thought to be continuous with grain avalanching not being important. The coarse surface lag is a characteristic of gravel antidunes due to the high transport capacity at the Fr appropriate for their formation (Shaw and Kellerhals, 1977; Alexander and Fielding, 1997): see Plate 2.6. Together, Alexander and Fielding (1997) thought the characteristics above were distinct evidence to distinguish antidunes from dune deposits.

Plate 2.5 Mounds Inferred to be Antidunes in the Burdekin River, Australia

Alexander and Fielding's (1997) DMA in the Burdekin River, Australia (flow from left to right). Note the low amplitude of the antidunes and the segregation of clasts near to the crest (Photo courtesy of C. Fielding), yellow notebook (~0.25m) for scale, dimensions in Table 2.7.

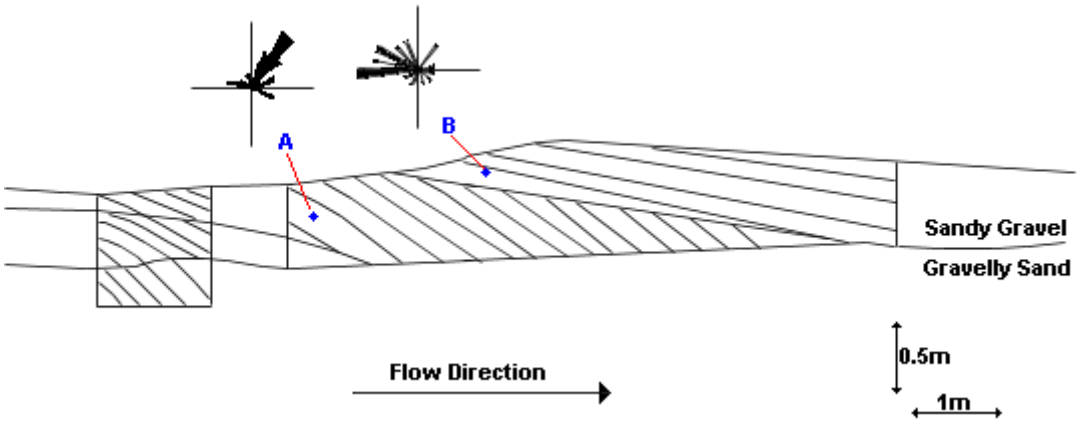

Figure 2.22 Burdekin Bedform Cross-Bedding

Cross-section of low-angle cross-bedded structures from DMAs, the rose diagrams show the observable variation pebble a-b plane dip between the (antidune) low-angle cross bedding in the sandy gravel and the (dune) cross-bedding in the steeper cross-bedded gravely sand (redrawn from Alexander and Fielding, 1997).

Plate 2.6 Burdekin Bedform Clast Size Variation

Observable variation in clast size and orientation between the lee, crest and stoss of the antidune (taken from Alexander and Fielding, 1997). The clasts exposed at the surface vary along cross-section, large clasts occur on the stoss particularly on the crest, but were rarer on the lee slope. Clasts were orientated with a-b plane parallel to the flow on the stoss, with a-b plane transverse to the flow just before the crest, a chaotic organisation at the crest and limited a-b plane flow parallel alignment on the lee side. Pictures approximately 1 metre wide, flow bottom to top of each image, shoes are a British size 5.

Duller *et al*. (in press) interpreted the variety of up and downstream dipping laminations in jökulhlaup deposits as representing stationary to quasi-upstream migrating antidunes, noting that upstream migrating antidunes would be expected to produce solely upstream dipping laminations. Foley (1977) details '*dropout armours*' - discontinuous gravel lenses (see Figure 2.18), one clast thick within the low-angle bedding of antidune deposits, formed by the transport of gravel over a sand bed surface

in antidune phase. The gravel clasts tended to slow and accumulate at the antidune crests and stoss sides, subsequent destruction of antidunes burying them. Any fractions of the lenses not reworked by subsequent antidunes are preserved in the sedimentological record. Foley argued that the determination of the maximum Shields criterion for individual clasts allowed production of a palaeoflow estimation. Foley *et al.* (1978) showed antidunes were responsible for much of the scour occurring in desert arroyo floods, the deepest scour corresponding to the largest antidunes.

Langford and Bracken (1987) noted that breaking standing waves persisted above antidunes in Medano Creek, the antidunes were not destroyed immediately: they thought wash-out to be associated with the release of a 'slug' of water stored in the standing waves, rather than by the actual turbulent breaking of individual standing waves themselves. Blair (1987) examined deposits from a dam burst where aerial photos had shown standing and breaking waves. Antidune inferred deposits consisted of gravel-sand couplets indicative of a very rapid rate of sedimentation in order for sand structure preservation. Since an increase in bed roughness occurs on deposition (due to bedform formation), Blair thought that only minor velocity variations were required for deposition in these high-suspended sediment flows. Gilbert (1914), Simons and Richardson (1966), Langford and Bracken (1987), Blair and McPherson (1994), and Blair (1999) found these couplets associated with antidunes. Whilst Moscariello *et al*. (2002) found similar couplet features in alluvial fans, and inferred their formation via the violent breaking of antidunes. Blair (1999) considered there to be three types of standing wave breaking each producing different sedimentary structures:

1) Standing wave dissipates, bed flattens, antidune low-angle upstream dipping laminae truncated, but preserved (rare);
2) Moderate washout: standing wave breaks, slight erosion and infilling of troughs occur, laminations preserved;
3) Violent washout: antidune oversteepens, standing wave breaks. All fine material eroded and suspended to leave a gravel deposit; deposition of sand then completes gravel-sand couplet formation;

4) Process repeats.

Blair, (1999 and 2000) attributed more symmetrical deposition (i.e. on lee as well as stoss) to higher sediment concentrations. Further, better preservation of antidune sedimentary structures was found under areas that had experienced deeper flows, as evidenced by deeper beds of more steeply dipping deposits (in deeper flows antidunes have a greater amplitude, thus their foreset deposits have a steeper dip). If this is the case, the perceived lack of preservation of antidune structures in flume studies, and the limited findings of flume studies that have been undertaken may mask potentially greater preservation of antidune sedimentary structures in the field where the availability of deeper flows and much higher continuous sediment concentrations provide much better preservation potential. Blair (2000) provided two mechanisms for the production of sedimentary structures by antidunes, one by dissipation of standing waves and one by violent breaking (shown in Figure 2.23), importantly these produce very different types of sedimentary structures.

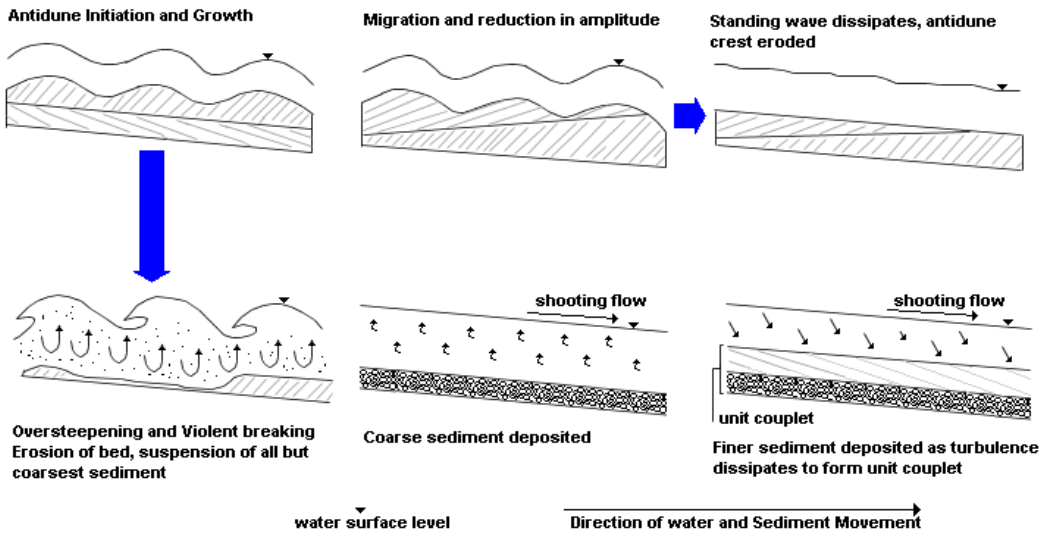

Figure 2.23 Standing Wave Breaking and Sedimentation

The top row of diagrams show the sedimentary structures resulting from less violent dissipation of the standing wave and erosion of antidune crests. The lower row of diagrams show the formation of sedimentary structures due to violent breaking of the standing wave, completely destroying the antidunes below, sediment being redeposited as a unit couplet of coarse and fine grained laminae (redrawn from Blair, 2000).

The antidune structures of Schwartz (1982), Barwis and Hayes (1985), Langford and Bracken (1987) and Clifton (1990) (Table 2.7, Figure 2.18 and Figure 2.19) were morphologically the same as those of Alexander *et al*. (2001), with heavy minerals (Davis Jnr, 1985; Barwis and Hayes, 1985; Clifton, 1990) and grain size differences marking lenses. The suites of deposits (Figure 2.18) as described by Barwis and Hayes (1985), Langford and Bracken (1987) and Clifton (1990) changed from upstream dipping backsets to downstream dipping foresets. Deposits consisted of sub-horizontal sets of lenses, changing from low-angle foreset to backset beds downslope, which these authors inferred to relate to the decreasing Fr of the flow above. The deposits were therefore interpreted as representing a transformation from UMA to DMA forms. Hunzicker (1930) and Clifton (1990) found heavy minerals concentrated in the trough and coarser/lighter particles at the crest of antidunes. Concentrations of heavy dark minerals being the material that commonly defines laminae boundaries in upper regime flow (Cheel, 1984). Clifton (1990) produced in-situ deposits in beach runnels under aggrading conditions, noting that due to the upsection climb of the bed the upstream dipping laminae (Figure 2.18) exhibited clearer Type I and Type II laminae than those formed under equilibrium sediment supply conditions. During the examination of larger scale Pleistocene and present day deposits in the Toutle River, Clifton (1990) found sedimentary structures similar to those produced artificially in beach runnels. Both the beach runnel and Toutle River deposits contained Type I and Type II (Figure 2.24; Table 2.8) laminae.

Table 2.8 Clifton (1990) Laminae Types

Type I are formed by strong scour on standing wave collapse, producing lag deposits (the laminae boundary), and so are more common. Type II is often rare or absent as these relate to lenses forming on migrating antidunes, sorting is not always possible with rapid deposition or homogenous sediment mixtures.

Type	Definition
Type I:	Eroded into the underlying sediment; contain heavy minerals, inversely grade into coarser lighter sediment, lenticular to tabular in appearance. Sigmoidal deposits dip downstream at 5–15° depending on amount of aggradation; deposits between two type I laminae formed at the same time. These were also observed by Langford and Bracken (1987).
Type II:	Rarer, downlap onto Type I at base, truncated by Type I at top (where antidune upstream flank contacts erosional surface form last set). Heavy minerals delineate lamina, dip at 5-20°.

Type II laminae were more common in beach deposits, and comparatively rare in the Toutle River deposits, which broadly resembled USPB laminations. Clifton observed that the rate of aggradation controlled the degree of truncation by later antidunes (Figure 2.24).

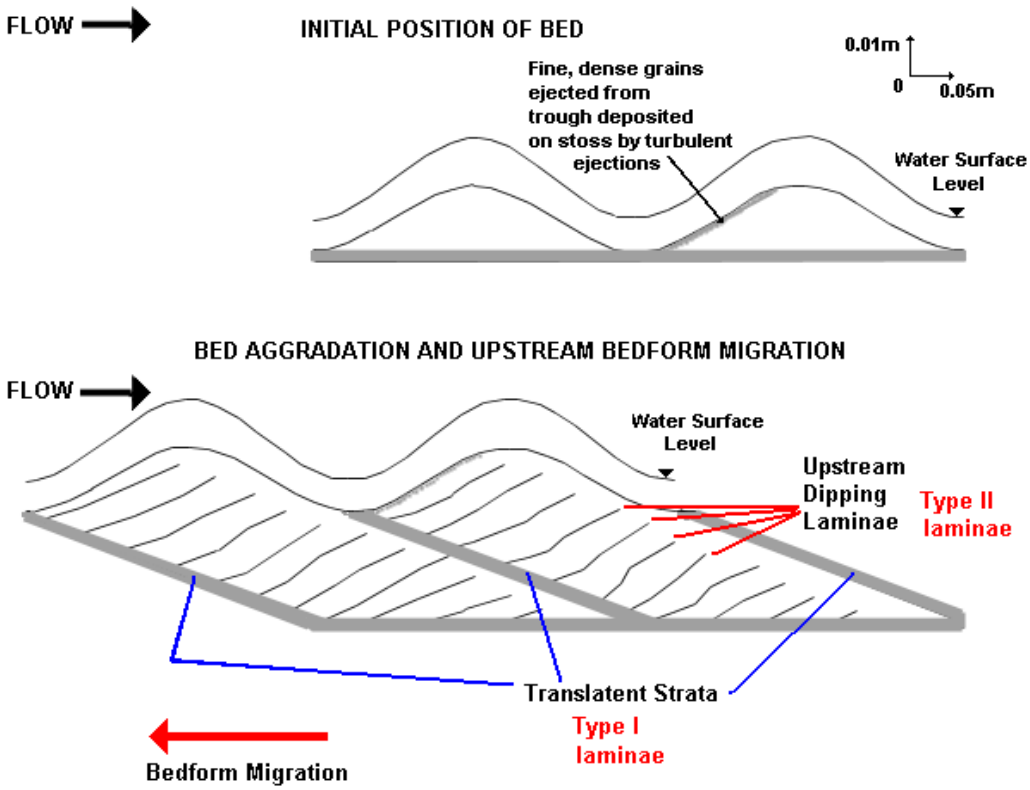

Figure 2.24 Clifton's Translatent Strata

This diagram shows the model produced by Clifton (1990) to illustrate the production of translatent strata by the upstream migration of antidunes under aggrading conditions. Type I laminae are formed by the upstream migration of the trough between antidunes, with the rarer Type II forming due to intermittent sediment sorting processes. The angle of climb due to bed aggradation and the antidune λ define the shape of laminae.

Clifton suggests Barwis and Hayes' (1985), Langford and Bracken's (1987) and his Toutle River deposits that lack Type II laminae are the more common form. Clifton thought these are associated with antidunes developed beneath less powerfully breaking standing waves; deposits with Type II laminae then are related to more powerful flow, where sediment can be sorted to clearly mark Type II laminae. These low-angle deposits (Type-I laminae) being overlooked in other literature, which primarily identifies upstream dipping cross-sets as antidune produced bedding. Thus, according to Clifton (1990) there are three types of deposit associated with antidunes:

1. Deposits containing Type I but no Type II laminae;
2. Deposits containing both Type I and Type II laminae;
3. Bipartite gravel-sand couplets.

However, the distinction between deposit types 1 and 2 may be more of a product of limited definition due to homogenous sediment than differing physical process. Further, as observed by Alexander *et al*. (2001) downstream dipping laminae are common amongst the upstream dipping laminae of antidune deposits. The mixture of upstream dipping and downstream dipping laminae is a key criterion for identifying antidune deposits.

Due to the large roughness elements associated with coarse gravel and very shallow braided rivers, large antidunes are uncommon; rather antidunes may occur as transverse ribs, where the bulk flow conditions are appropriate to their formation. Ashworth *et al*. (1994) and Grant (1997) suggest that channel hydraulics and bed configuration in braided rivers act to keep the average Fr below critical for most of the time. Grant (1997) thought antidunes a bed response to supercritical flow which, eventually causes an unstable hydraulic jump to 'brake' the flow, dissipating energy, the bore released by breaking standing waves reinstating subcritical conditions.

2.4.4 Antidunes in the Geological Record

Identification of structures deposited by antidune regime flow in the geological record is a speculative and reasoned supposition based on a limited knowledge of present day antidune deposits in the field and laboratory flumes. A lack of experimental investigation and knowledge of these structures in coarser sediments and their associated hydrodynamic behaviour means that only limited inferences from coarse-grained outcrops is possible at present. Alexander and Fielding (1997) postulated that gravel antidune deposits allow identification of an antidune origin and provide a useful tool for interpreting palaeoflow conditions.

Hand *et al.* (1969) considered three reasons for the lack of antidunes in the geological record. All of the explanations presented in Table 2.9 partly

explain the absence of deposits; Hand *et al*. (1969) thought experimental evidence and identified field deposits show preservation occurs and lend credence to case 'c'. Fielding (2006) considered antidunes to be moderately to well represented in the geological record, but with their recorded frequency being hampered by limited guides (i.e. detailed field and flume interpretations) to identification. Duller *et al*. (in press) echo this point, and further note that the scale of some bedforms (λ: 24 – 96m), may preclude their identification without sufficiently extensive exposures. Detailed examination of the literature provides many examples of putative antidunes, indeed whilst not as common as other bedforms; many papers interpret deposits in the geological record as antidune sedimentary structures. Key papers are summarised in Table 2.10.

Table 2.9 Reasons for the Rarity of Antidune Deposits

The key arguments for the rarity of identified antidune sedimentary structures in the geological record.

CASE	REASON	AGREEMENTS
a)	Antidune deposits are rare in the stratigraphic record.	Collinson and Thompson (1982); Yagishita and Taira (1989).
b)	Antidunes do not produce distinct structures capable of preservation.	Rust and Gibling (1990); Twenhofel (1950); Einsele (2000).
c)	A lack of clarity as to what antidune deposits in the geological record should look like: antidune structures have thus been misinterpreted or overlooked at outcrop.	Hand *et al*. (1969); Allen (1985); Alexander and Fielding (1997); Yagishita (2004); Fielding (2006); Duller *et al*. (in press).

Table 2.10 Sedimentary Structures Interpreted as Being Produced by Antidune Bedforms

This table contains the key morphological features of sedimentary structures interpreted in the literature as being produced by antidunes, or antidune-like bedforms. A broader discussion of these is provided in the main text. DT: Deposit Type; T = Turbidite, Ti = Tsunamite, F = Fluvial, P = Pyroclastic density flow, O = Outwash fan, W = Washover fan.

Study	DT	λ (m)	h (m)	Sedimentary Structures	Sediment
Barwis and Tankard (1983)	W	-	-	Low-angle planar cross bed set. Antidunes as "trains of regularly spaced lenses of well sorted medium to coarse sand". Some barely visible backset bedding. Antidunes in Pleistocene washover deposits. Similar to Barwis and Hayes (1985).	Fine sand.
Barwis and Hayes (1985)	W	0.6	0.03 - 0.04	Examined backset bedding lenses in three different exposures.	Fine grained sand, and coarse sand - fine granules.
Bartsch-Winkler and Schmoll (1984)	Tidal	-	-	Lenticular sequences and intervening wavy or parallel laminations. All severely contorted by subsequent geological processes.	Tidal silt
Beeson, Self and McPherson (1984)	P	0.8 - 2	-	Pyroclastic flow. – speed 30 - 100 m/s, flow density 1.0 - 1.2kg/lm^3. Large scale internal stratification. Sigmoidal upflow migrating bedforms.	Fine to granule volcanoclastic.
Bornhold and Prior (1990)	Delta	50-120	2-5	Transverse symmetrical bedforms in deltaic depositional sequence. Formed after large flood due to glacial lake draining. Imaged by sonar.	Sand to gravel.
Boudon and Lajoie (1989)	P	-	-	Antidunes present as low-angle foreset and backset laminae and sinusoidal wave-like undulations	Fine to granule volcanoclastic.
Brown and Branney (2004)	P	9	0.4	Low –angle cross-stratified, dipping downstream at ~10°.	Fine to granule volcanoclastic.
Brennand (1994)	G	12	1	Deposits stacked and offset. Lenticular geometry. Sandy in-phase waves with some low-angled beds dipping up or downstream. Inverse or normal bedding. Larger clasts concentrated on bedding planes.	'diffusely graded sand/granules' and 'imbricate, polymodal, matrix rich gravel'
Cassidy *et al.* (2003)	G	-	-	Identified low-angle upstream dipping deposits in glacial outwash sediments. Interpreted larger scale buried features as forming under a hydraulic jump under high sediment concentration during flood peak. Smaller scale structures dipping upstream at shallower angles represent antidune bedforms. Formed during sediment working in shallow supercritical waning flows.	Glacial outwash – fine sand, gravel grading up to boulder size.
Cole (1991)	P	1	0.5	'Regressive' – (upstream migrating) structures similar to those described by Schminke *et al.* (1973) and Fisher and Waters (1970). Upstream migrating and downstream migrating bedforms in same sedimentary sequences – evidence for bedform origin	Fine to granule volcanoclastic.

Table 2.10 (continued)

Study	DT	λ (m)	*h* (m)	Sedimentary Structures	Sediment
Cole and Scarpati (1993)	P	6	1.5	Upstream dipping (~35˚), inverse graded layers, bedding 0.4 – 0.8m thick. Superficially similar to antidune bedding, however, interpreted as having a chute-and-pool style depositional origin. Strong erosive base to lowest backsets.	Fine to granule volcanoclastic.
Collinson (1966)	F	-	-	Generally horizontal but are often mutually erosive in a gentle way to give a rather lenticular bedding pattern. Similar to Middleton (1965).	Coarse sand - granule-fine gravel.
Crowe and Fisher (1973)	P	-	-	Antidunes present as low-angle foreset and backset laminae and sinusoidal wave-like undulations.	Fine to granule volcanoclastic.
Fielding and Webb (1996)	F	-	-	Postulated antidune origin from undulating, convex-up bedding, and upstream inclined, and low angle crossbedding.	Fine sand.
Fisher and Waters (1969); Fisher and Waters (1970)	P	1 - 2	0.05 - 0.2	Slope of lenses between 1-5 and up to 15 degrees. Undular deposits more likely to be composed of finer sediments. Laminae deposition all over antidune form, preferentially on upstream side.	Silt - sand.
Fisher (1990)	P	1.3	0.1	Antidunes present as low-angle foreset and backset laminae and sinusoidal wave-like undulations.	D_{50} = 0.25 mm.
Fralick (1999)	F	-	-	Inferred 0.65 m/s and 0.01m depth from reconstruction. Laminae preferentially thicker on upstream stoss side of antidune.	Coarse grained sandstones.
Gevrek and Kazanci (2000)	P	-	-	Antidunes present as low-angle foreset and backset laminae and sinusoidal wave-like undulations.	Fine to granule volcanoclastic.
Giannetti and De Casa (2000)	P	-	-	Antidunes present as low-angle foreset and backset laminae and sinusoidal wave-like undulations.	Fine to granule volcanoclastic.
Hand *et al*. (1969)	O	0.63	0.065	Wave's side slope at 22° (excluding palaeoslope).	D_{50} = 2.1 mm granular conglomerate
Hand *et al*. (1972)	T	0.64	-	Postulated to occur at base of density current.	Medium to coarse sand.

Table 2.10 (continued)

Study	DT	λ	*h*	Sedimentary Structures	Sediment
Hornung *et al.* (2007)	F	2 – 10m	0.2 – 1 m	Gentle, sub-horizontal up or downstream dipping laminations. Antidunes stacked. Interpreted as migrating antidunes, which with waning flow, grade into 3D dunes. Associated with sediment laden jets aggressing from beneath grounded ice.	Fine sand to coarse gravel.
Lee (2004)	O	90-105m	1.4-2.6m	Giant antidunes close to passes in the lake system, huge currents capable of producing large bedforms. Upcurrent slope steepest. Detailed sedimentary structures not given.	Coarse gravel to cobble sized.
Leys (1983)	P	Up to 15 m	Up to 4 m	Lee-side beds deposited at less than the angle of repose, abundant stoss-side beds. Mainly downflow crest migration.	Pyroclastic material - generally sand to fine gravel sized. Antidunes present as low-angle foreset and backset laminae and sinusoidal wave-like undulations.
Lister (1981)	O	-	-	Three layers: lower horizontally bedded unit, then middle low angled upstream dipping cross-strata, and then upper massive structureless unit truncating the middle unit	Coarse gravel to cobble sized.
Mack *et al.* (1996)	F	4 - 5 m	0.2 - 0.5 m	Symmetric or nearly symmetrical bedforms. Upstream and downstream dipping laminae (< 15°)	Pumice: gravel sized, up to 0.3m Ø - long axis of clasts parallel to dip of laminae. Deposition in response to dammed river outburst flood.
Manville *et al.* (2002)	P	-	0.2 - 0.6 m	Clasts imbricated at 22 - 45° angles	Deposits consisted of dome shaped packages with steep upstream stoss sides; accumulated around a core of coarser lithic pumice gravel (also found by Shaw and Kellerhals, 1977 and Alexander and Fielding, 1997).
Mattson and Alvarez (1973)	P	2 - 4.5 m	0.1 - 0.3 m	Symmetrical and asymmetrical forms. Wavy laminae, indicating deposition over whole bedform, preferentially on upstream side.	Pyroclastic material - generally sand to fine gravel sized.

Table 2.10 (continued)

Study	DT	λ (m)	*h* (m)	Sedimentary Structures	Sediment
McConnico and Bassett (2004)	T	-	-	Backstacking deposits. Coarse grained antidunes forming due to standing waves associated with slump blocks.	Gravel.
McCracken (1969)	T	-	-	Asymmetric dune-shaped wedges of graded granular coarse sand with backset lamination dipping upcurrent. Imbrication in a downstream direction.	Graded granular coarse sand.
Migeon *et al*. (2001)	T	1000 - 2000	~10 - 30	Backset deposits on upstream prograding bedforms, undular parallel laminations.	Mud, silt and sand sized material.
Morris *et al*. (1998)	T	400	2	Transverse, grading to V shaped bedforms interpreted as antidunes forming in a thinning turbidity current near the abyssal plain.	-Mud, silt and sand sized material.
Nakayama and Yoshikawa (1997)	F	-	-	Antidune cross-bedding, fining upwards sequences. Erosive bases to sets common.	Coarse volcanic ash and tuffaceous sand.
Pickering *et al*. (2001)	T	100	3	Backfilling sandy macroforms as channel fill in a submarine channel.	-
Power (1961)	O	-	-	Material orientated parallel to the backset and fining top-to-bottom. High angle - 20°	Fine-to-granular conglomerates.
Russell (2005)	G	-	-	Steep upstream dipping beds (20 – 30˚) associated with localised supercritical flow around grounded ice blocks. Stratification subdued, but marked by some limited orientation of clasts.	Glacial outwash – fine sand, gravel grading up to boulder size.
Russell and Arnott (2003)	G	0.3 - 0.4	-	Low angle cross-stratification. Dips of less than 10°. In-phase waves in undular of weak hydraulic jump. Laminae, 0.02 – 0.03m thick.	Medium sand.
Rust and Gibling (1990)	F	0.5 - 1.1	0.05 - 0.1	Three-dimensional antidunes. Mounds slope at up to 20°, more commonly < 10°.	0.3 mm sand.

Table 2.10 (continued)

Study	DT	λ (m)	*h* (m)	Sedimentary Structures	Sediment
Schminke *et al*. (1973)	P	2 - 3	~0.2	Steep stoss sides and low-dipping lee sides.	Fine sand to fine gravel
Segschneider *et al*. (2002)	P	2	0.8	Dome-like, low angle cross-laminated beds which dip upstream. Stoss side steeper than lee. Coarser clasts on the stoss side compared to lee side. Interpreted as deposits of UMAs.	Sand or pebbly sand.
Walker (1967)	T	0.4 - 0.6	0.02 -0.04	Laminae 1-2 mm thick. Low-amplitude wavy profiles. Consistent grain imbrication, shortening λ downstream. Crests transverse to palaeoflow direction.	0.07 mm fine sand.
Wunderlich (1972)	W	-	-	Long lenses of antidune stratification. Lenses up to 0.02 m thick.	Sand, 0.05 to 0.5mm.
Wynn *et al*. (2002)	T	800	6	Backset deposits on upstream prograding bedforms.	Coarse grained
Yagishita (1994)	T	0.4 - 1.4 .	-	Gently dipping 'in-phase wave drape laminae' (Cheel, 1990). Grain fabric indicates antidune origin.	Well-imbricated pebbly sandstone.

Mack *et al.* (1996) inferred an antidune origin, rather than dune origin for pumiceous deposits formed around a volcanically dammed river, based on the erosional bases to deposits and the presence of upstream or downstream dipping low-angle laminae. Manville *et al.* (2002) again inferred an antidune origin for pumiceous deposits associated with the resedimentation of volcanic materials, preserved due to high-sedimentation rates.

Gorrell and Shaw (1991); Brenand (1994); Delaney (2002), Russell and Arnott (2003) and Hornung *et al*. (2007) identify upper regime deposits in subaqueous glacial outflow deposits (details in Table 2.7), appearing in the stratigraphic record as rare suites of high-energy lithofacies, such as Russell and Arnott's structures, shown herein in Figure 2.18. The energy lost by the egress and expansion of pressurised subglacial flow reduced sediment transport capacity and caused a rapid deposition of sediment. In this zone, Brennand (1994) and Russell and Arnott (2003) found bipartite-gravel couplets; inferred to represent the washout of antidunes by Blair (1987). McDonald and Vincent (1972) found similar gravel antidune backsets and inferred formation in open conduit flow on an esker.

Alternatively to the glacier margin and open conduit theory Brennand (1994) observed that antidunes should be able to exist at a density interface, such as that suggested by Hand (1974) for turbidites. McDonald and Vincent (1972) produced antidune-like bedforms in a pressurised flume, providing a further option of antidunes forming due to pressure waves in a closed conduit without a free-surface. However, theory suggests that antidune deposits do not form in closed circuit tunnels or pipes without free-surfaces (Yalin, 1972; McDonald and Vincent, 1972; Engelund and Fredsøe, 1982). It is difficult to reconcile McDonald and Vincent's findings with theory without a more detailed investigation of the flow above these bedforms. Perhaps investigation would show areas of 'dead flow' in the upper region of the flow above the intervening troughs. These regions of dead flow could support a hypothesis that flow oscillates vertically in a sinusoidal fashion along the pressurised flume, allowing bedforms to form in the corresponding areas of 'dead flow' along the flume bed. In sub-glacial conditions this could be achieved by the flow eroding into the ice roof of the conduit. Whilst

producing morphologically similar deposits, without the free surface it would though appear that these bedforms would not be subject to destruction by a breaking standing wave.

Sedimentation of pyroclastic density flows may produce bedforms, the sedimentary structures of which resemble fluvial deposits. Such deposits were identified by Fisher and Waters (1969), Fisher and Waters (1970), Crowe and Fisher (1973), Mattson and Alvarez (1973), Schminke *et al.* (1973), Leys (1983), Beeson *et al*. (1984), Rowley *et al*. (1985), Boudon and Lajoie (1989), Charland and Lajoie (1989), Fisher (1990), Cole (1991), Cole and Scarpati (1993), Gevrek and Kazanci (2000), Giannetti and De Casa (2000) and Segschneider *et al*. (2002), details in Table 2.10. In all of these cases antidunes were present as low-angle foreset and backset laminae and sinusoidal wave-like undulations. Schminke *et al.* (1973) observed four bedform structures in Pleistocene deposits; rapid deposition from a high-speed aerial sediment-laden mixture (a base-surge) was inferred:

- dunes;
- plane bed;
- antidunes (Figure 2.25); and
- chute and pool.

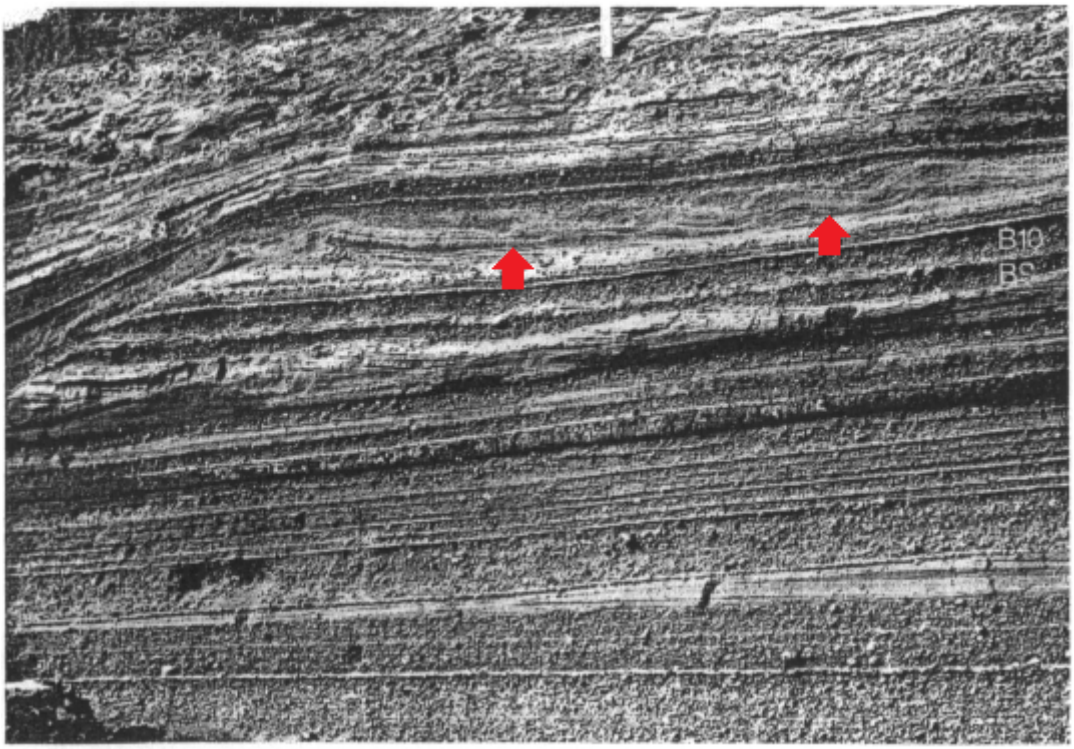

Figure 2.25 Inferred Antidune Deposits - Volcanoclastic

Pyroclastic USPB and antidune deposits (taken from: Schminke *et al.,* 1973). Flow left to right, photo shows approximately a 6.5m width of exposure. Arrows indicate antidune structures with upstream dipping laminae. See Table 2.10 for further details.

Allen (1984) argued that the depositional style (upstream or downstream accreting) of pyroclastic bedforms relates to the wetness of the tephra. Wetness controls the balance between tephra sticking to the upstream face of the bedform and causing upstream bedform progradation and deposition in the lee, causing downstream progradation. Further differences in between pyroclastic forms and sub-aqueous forms relate to the compressibility of air-sediment suspensions compared to water-sediment suspensions. This wetness control would fit with observations of Cole (1991) who observed upstream and downstream migrating forms adjacent to each other in the same strata. The author considers that whilst pyroclastic bedforms commonly appear morphologically similar to subaqueous forms, it is difficult to further develop this comparison on account of their very different formative processes. Charland and Lajoie (1989) postulated that stationary long-wavelength antidune forms were responsible for the long-wavelength undulating parallel laminations observed in pyroclastic flow deposits in Martinique. A similar process to turbidite flows is suggested, with antidunes

forming at the interface between the bed and a dense moving suspension of volcanoclastic particles.

Rust and Gibling (1990) identified three-dimensional antidunes (‘*radially symmetric mounds’*), superficially resembling HCS/SCS, but forming definitively in a fluvial environment with current lineation indicating upper flow regime. Concordant strata indicate these forms were stationary, accounting for their preservation. Hand *et al.* (1969) inferred 19 symmetrical undulations of varying amplitudes in outwash fan deposits to be antidunes (Figure 2.26); no clear internal structures are evident. Shorter amplitude waves are present with sand drapes in the troughs which Hand *et al.* (1969) considered evidence of breaking antidunes; infilled by rapid deposition.

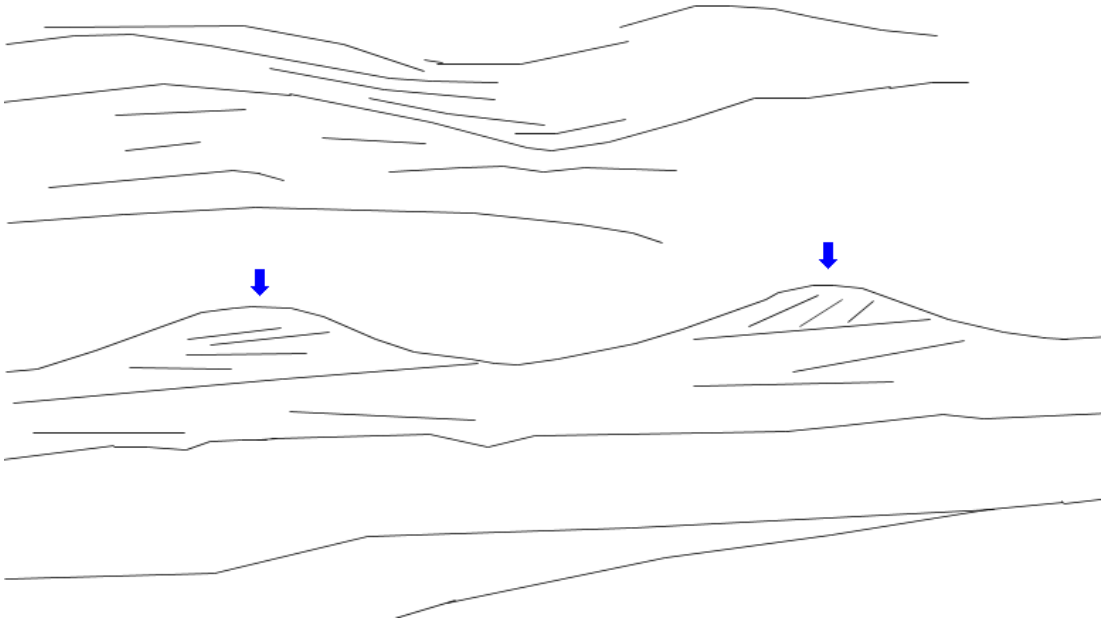

Figure 2.26 Inferred Antidune Deposits – Outwash Fan

Hand *et al.’s* (1969) antidunes, the wavy sinusoidal shape and lack of internal structures are apparent. Preferential erosion of the exposure has removed the overlaying exposure. Arrows indicate two bedforms, with λ: 0.69m. Upstream dipping laminae can be seen beneath these. Redrawn from Hand *et al*. (1969).

Hand *et al.* (1969) conducted a palaeohydraulic analysis of the antidunes by estimating $\overline{U}$ from Eq. 2.13 (Kennedy, 1961) and a modification of the Darcy-Weisbach equation.

$$\overline{U} = \frac{g/\lambda}{2\pi}$$

Eq. 2.13 Equation used in palaeohydraulic reconstruction by Hand *et al*. (1969)

As antidune standing waves break when the λ: d ratios are greater than 0.142 (Kennedy, 1961), only a narrow range of depths were possible; Hand *et al.'s* (1969) resulting estimate supported an antidune origin for these deposits.

Turbidites form during the redistribution of sediment on the continental margins to deeper parts of the ocean bed. During deposition a denser, concentrated bottom layer containing coarser sediments settles out from a less dense upper layer (silt/clay) of the turbidity current (Prave and Duke, 1990 and Falk and Dorsey, 1998). Deformation of this layer by the less dense flow above may produce bedforms; with antidune-like bedforms potentially forming if the flow is supercritical (Prave and Duke, 1990; Wynn *et al*., 2002). Prave (1990) stated the following relationship for turbidite bedform λ.

$$\frac{\lambda}{d} = \Delta\rho$$

Eq. 2.14 Turbidite Bedform Wavelength

Where ρ is density (kg/m^3). This equation describes the relationship between the densities of the two layers of the turbidity current, λ and fluid depth. The densiometric Froude number (Fr_{den}) – Eq. 2.15 is used for turbidity currents; it includes a term for the extra density of the turbidity current (Fr_{den} is dimensionless).

$$Fr_{den} = \sqrt{\frac{U^2}{(\Delta\rho - \rho)gd}}$$

Eq. 2.15 Densiometric Froude Number

Falk and Dorsey (1998) suggest that dispersive grain pressure acts to keep suspended sediment levels high. Hand *et al*. (1972) state that 'antidune' structures cannot form in flows where Fr_{den} is less than critical, but do not state if the Fr = >0.84 threshold applies.

Inferred antidune depositional structures occur frequently in the turbidite literature: Collinson (1966); Walker (1967), Skipper (1971), Hand *et al*. (1969), Hand *et al*. (1972), Normark *et al.* (1980), Bartsch-Winkler and Schmoll (1984), Galli (1990), Pickering (1995), Rissetti (1997), Wynn *et al*.

2000; Wynn *et al.* (2002), McConnico and Bassett (2004), Fildani *et al*. (2006) details in Table 2.10. Thus, if correct this implies that turbidites readily preserve antidune structures due to high-magnitude deposition events. Gravel waves have been observed in the marine environment and an antidune origin has been inferred (i.e. Fox *et al*., 1968, Malinverno *et al*., 1988, Bornhold and Prior, 1990, Hughes-Clarke *et al*., 1990, Nemec, 1990; Piper and Kontopoulos, 1994, Morris *et al*., 1998, Massari and D'Alessandro, 2000, Pickering *et al*., 2001), details in Table 2.10. Because the internal structures are poorly known classification is difficult, identification of the deposits internal structures would help identify the depositional mechanism. Wynn *et al*. (2002) and Migeon *et al*. (2001) identified backset deposits on upstream prograding bedforms to corroborate antidune regime flow as the formative mechanism. Inferred antidune deposits forming in silt/sand sediment have been observed to have a more symmetrical morphology and migrate upstream, whilst wave forms in gravel were more variable (Normark *et al.,* 1980 and Wynn *et al.*, 2002); suggesting that as for on land, antidune morphology becomes more complicated with DMA and dune-like forms occurring as sediment size increases.

Yagishita (1994) inferred an antidune origin for well-imbricated pebbly sandstone with gently dipping in-phase wave drapes. Further, it is thought that a lack of distinctive fore/back set deposits is common in turbidites; instead wave drapes vary in their symmetry to give upstream or downstream-wards growth. Yagashita inferred that because there was no finer mud layers inbetween these layers, deposition must have occurred as one continuous event characterised by rapid burial. Walker (1967) examined similar turbidite deposits, and from the low-amplitude wavy profile and consistent grain orientations and decreasing amplitude downstream inferred an antidune origin. Morris *et al.* (1998) observed a downslope decrease in λ of transversely-orientated straight-crested long- λ antidune-like bed features from density currents; they suggested changing sediment concentrations, flow thickness and current velocity were responsible. Inferred erosional antidunes cut into the sea-bed have been identified by Pickering (1995): for storm return flow and by Shiki and Yamazaki (1996) and Massari and D'Alessandro (2000) in tsunamites.

There is considerable uncertainty with regard to the inferred antidune origin of some turbidite structures, due to the difficulty in observing formative events and depositional processes. Additionally, exposed turbidite deposits often have limited ancillary evidence of the depositional palaeoenvironment. Prave and Duke (1990) consider that other methods of formation: reflections, currents, tsunamis, tides thermo-haline and internal waves are not likely causes as the λ produced by these would be less akin to the observed ones, which fit well with an inferred antidune hypothesis. Whilst Hand *et al*. (1972) and Skipper (1971) observed single set cross-stratification, and suggested that this was deposited by antidunes. Later reinterpretation by Prave and Duke (1990) suggested the deposits formed by reflections in a confined turbidite flow indicating the difficulty of correct classification. This later conclusion was reached in spite of the use of palaeoflow indicators that suggested a unidirectional flow. Araya and Masuda (2001) considered that the examination of grain orientations could have provided insights that would have improved the veracity of identification. Similarly, Kubo and Nakajima (2002) observed what appeared to be upstream migrating bedforms in Fr < 0.84 flow however, these proved not to be antidunes but to have formed via sediment deposition upstream of flow obstacles. Therefore great care should be taken when interpreting deposits such as McConnico and Bassett's (2004) backset beds, which were interpreted as antidunes forming over slump blocks. Further, Wynn and Stow (2002) and Kubo and Nakajima (2002) find that within the marine environment conditions necessary for the formation of upper-flow-regime deposits are rare outside of turbidity current depositional events. Therefore turbidite morphologies and internal structures observed may have intervening superimposed lower-flow-regime influences.

At outcrop, tempestite deposits such as Hummocky Cross Stratification (HCS) or Swaley Cross stratification (SCS) deposits superficially resemble those of antidunes (Masuda *et al.*, 1993; Yokokawa *et al.,* 2000; Alexander *et al.,* 2001; Yagishita *et al*., 2004); especially to turbidite antidune deposits due to other similarities, such as grain size and type (Einsele and Seilacher, 1991; Massari, 1996). Detailed examination of outcrops is required, based on grain fabric interpretation to assess a deposits origin accurately (Yagishita *et al*., 2004); clarification would allow more accurate

palaeohydraulic reconstructions. HCS and SCS are shown in Figure 2.27a and Figure 2.27b, respectively; they are antidune 'mimics' superficially resembling antidunes despite the different hydraulic conditions of formation. Importantly, HCS and SCS are three-dimensional, with exposures at section taken 90° appearing similar to each other (as shown in Figure 2.27). As noted by Alexander *et al*. (2001), exposures of antidune deposits as a product of unidirectional flow exposures appear very different in flow parallel and flow transverse section; this is a key diagnostic criterion.

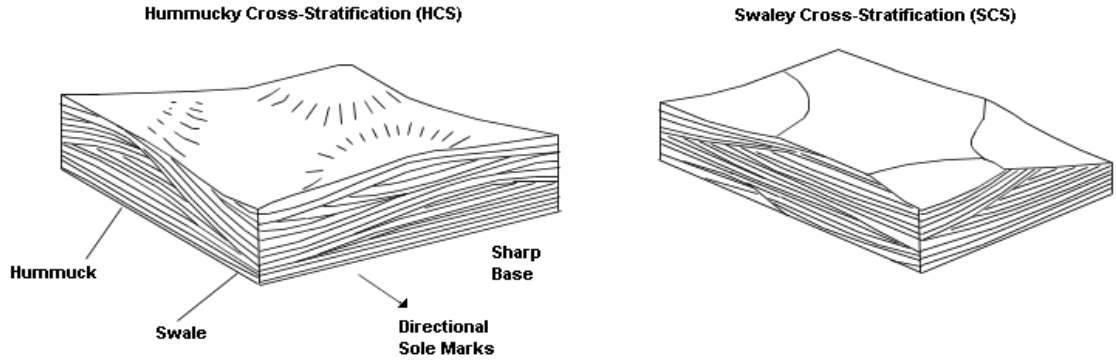

Figure 2.27 HCS and SCS Deposits

Diagram on the left shows Hummucky Cross stratification (HCS), and diagram on the right Swaley Cross Stratification (SCS) both formed by sedimentation under storm waves. These deposits form at the storm wave base due to current and wave action. In cross-section exposures may exhibit similarities to antidune cross-bedding (redrawn from: Leeder, 1999). Scale: sides of section ~10m in length.

Yagishita (1994) thought many supposed HCS and SCS deposits could be unidirectional antidune deposits, with interpretational difficulties caused by the faintness of the inferred antidunes lamination and its limited preservation potential. Table 2.11 outlines the misinterpretations and criteria for positive identification associated with the interpretation of supposed antidune structures.

Table 2.11 Antidune Misinterpretations

This table details common confusions when interpreting structures in the sedimentary record. Key distinguishing features are high-lighted, multiple positives providing for best identification.

Feature	Characteristic features	Authors
Antidunes	Antidune deposits show clear differences in flow parallel and flow transverse section – unlike HCS/SCS (2). (2) observed from detailed experiments that antidune deposits can be characterised as: "…primarily lenticular laminaesets with concave-upward erosional bases (troughs)". Specifically, laminaesets may be upstream dipping (growth and upstream migration of antidune and standing wave); fill the trough region symmetrically (wave-breaking); with some distinctive downstream dipping laminae (migration of asymmetrical bedwaves after wave breaking). Concordant laminae without truncations are not associated with HCS/SCS (5) – good indication of turbidite antidune origin (5, 12). Evidence of supercritical unidirectional palaeoflows (1, 2). Grain imbrication consistent with antidunes (1). Can be similar to HCS/SCS, but bimodal (up/downstream) grain imbrication with a-b plane flow parallel is characteristic of antidunes (3, 13). 30° grain imbrication typical (4). Evidence of rapid vertical aggradation (12) USPB-indicating parallel-lamination lends additional support (1). Shorter, more regular λ (12) than HCS/SCS deposits (3); but not useful on its own (5). Antidune less asymmetrical (12). Compatible λ /h ratios suggest an antidune origin for deposits (12); downstream decreasing also (13, 14)	1 - Araya and Masuda (2001) 2 - Alexander *et al.* (2001) 3 - Yokokawa *et al*. (2000) 4 – Yagishita and Taira (1989) 5 – Yagishita (1994) 6 - Rust and Gibling (1990), per comm. with Cheel. 7 - Barwis and Hayes (1985). 8 - Alexander and Fielding (1997). 9 - Yagishita and Taira (1989) 10 - Fralick (1999) 11 – Pickering and Hiscott (1988) 12 - Prave and Duke (1990) 13 – Walker (1967) 14 – Morris *et al*. (1998) 15 – Masuda *et al*. (1993) 16 – Jopling and Richardson (1966)
HCS/SCS	Common confusion with antidune deposits (2, 3, 7, 11 and 15). 15° grain imbrication typical (4). Truncations - cyclic variation in grain imbrication between truncations due to back-and-fourth wave/current motion distinguish laminae form those of antidunes (6). Unlike antidune deposits, HCS and SCS deposits are 3D, therefore exposures at 90° will show similar patterns of lamination (2).	
Bars	Cross-sets can resemble antidune cross-sets. Vectorial indicators of palaeoflow direction and of upper flow regime required to distinguish (8).	
Dunes	Low angle toe-sets of dunes resemble the characteristic low-angle deposits of antidunes (9).	
Chute and Pool	Characteristic isolated sets of upstream-dipping high-angled inclined strata (2). Backsets resemble those of antidunes, despite permanently breaking standing wave, high-angle grain imbrication (10) Highly variable grain orientation and imbrication angles (16).	
Refelected Turbiditty Currents	Undulating surface – associated with the sedimentary structures produced by reflected turbidity currents,(11).	
Tsumiinites	Undulating surface – associated with the sedimentary structures produced by tsumiinite (11).	

2.5 Discussion of Literature Reviewed

In the text below, the expected characteristics of antidune sedimentary structures are summarised from the consideration of the literature reviewed above (Section 2.4). Latterly these suppositions are investigated using flume experiments of the deposition of sediment beneath experimentally induced

standing waves (Chapter 6). DMAs are characterised by low-angle downstream sloping deposits (Figure 2.22), these form in the zone of net deposition on the downstream side of the antidune. It is unclear whether DMAs are a distinct bedform, or a hybrid transitional forming over a dune core. Observations of DMAs generally come from field examples with a paucity of evidence of DMAs forming from a flat bed in flume experiments. Stationary antidunes are characterised by undular surface-parallel horizontal laminae forming consistently over the whole antidune (Figure 2.20). UMAs are characterised by very low angle downstream dipping laminae (Type I laminae) and low-angle upstream sloping deposits (Type II laminae) these form in the zone of net deposition on the upstream side of the antidune (examples in Figure 2.24).

Bulk flow defines the type of sedimentary structure; with local turbulent flow providing the mechanism for its specific definition. Some degree of turbulence or sediment sorting must occur during antidune growth and migration because antidune deposits contain Type II (internal) laminae as well as Type I (erosional). Due to their spatial frequency Type II must form during the growth phase, rather than forming due to destructive processes. Turbulence is a common mechanism for the grain segregation that defines sedimentary structures (Allen, 1984). However, kinematic sorting in low-amplitude bedwaves passing over bedforms (Carling and Breakspear, 2006) can also effectively segregate different grain sizes and densities. The origin of antidune laminae is unclear (Bridge, 2003); Barwis and Hayes (1985) suggested shear sorting, whilst Alexander *et al*. (2001) suggested low-amplitude bedwaves form the laminations. Bridge and Best (1988, 1997) thought the turbulence scale too small to form laminations in USPB; instead turbulence acting over low-amplitude bedwaves was suggested. Over dunes turbulence provides the excess shear stress required to move coarse/heavy mineral grains over the crest and create foreset laminations (Best, 1993). Cheel (1984) described a similar process of turbulent sorting over low-amplitude bedwaves, producing USPB laminations. DMAs, stationary and UMAs each produce distinct styles of bedding therefore the associated processes must differ to some degree. The two types of laminae observed for UMA bedding suggest the faint laminae (Type II) are produced during the

growth stage, and the more common laminae (Type I) are produced erosively as the antidune trough migrates upstream with UMA migration (Figure 2.24). Standing wave breaking may also produce Type I laminae by truncating underlying antidune deposits. Therefore, sediment transport and/or turbulent processes similar to those observed above dunes and USPBs must be responsible for the Type II laminae. Over antidune bedforms there is a continuous movement of bedload, either as a carpet of particles moving in traction or as low-amplitude bedwaves. Kinematic sorting (Carling and Breakspear, 2006) in this layer may segregate grains, potentially if these segregated grains are deposited *en masse* on a downstream antidune, they could be the origin of Type II laminae. Larger, less-dense (silicate) grains that project out of the boundary layer would be moved out of the trough region, towards the antidune crest. The finer, denser grains remain in place until turbulent motions disrupt the boundary layer and shear them from the bed surface; preferential deposition of these occurs in areas of lower turbulence downstream, creating laminae boundaries. As deposition is rapid there will be limited time for this sorting to occur, which perhaps explains the poor definition of Type II deposits (low-angle antidune bedding) compared to Type I (truncation and scour by subsequent bedform) observed by Clifton (1990), (see Table 2.8 and Figure 2.24). Turbulent ejections and sweeps from the trough may be an additional supporting mechanism for laminae formation.

On gravel antidunes similar processes will potentially occur, with the lower amount of fines and the trapping and blocking of fines by the coarser surface topography perhaps acting to reduce grain segregation. Thus, the differentiation of deposits will be poorer; but some structure will be given by size-sorting, orientation and imbrication of gravel clasts. Gravel antidunes mark a transition from sand antidunes, where the majority of grains are equally mobile and may all participate in bedform formation, to one with oversize clasts in which bedforms are discontinuous, muted (antidunes occur as transverse ribs) or do not form and armouring occurs instead.

In terms of location of deposition, the laminae associated with DMA are similar to those for dunes, supporting the notion that they are transitional features. Further, the pronounced bedding style of DMAs (see Alexander

and Fielding, 1997) would not be expected of grains deposited in a separation zone (i.e. dune cross-bedding). In DMAs the lack of a separation zone, and instead an area of near-bed retarded flow that produces strong grain orientation on the bed is thus the most likely mechanism. Laminae will then be able to form from low-amplitude bedwaves passing over and from turbulent motions moving the denser heavy mineral fraction of the bedload over the crest, as for dunes, but with subsequent sorting and orientating as they form low-angle antidune cross bedding. For stationary antidunes the water surface and bed wave are tightly in phase, and laminations are contiguous over the whole antidune. A similar mechanism to the shear sorting of grains by turbulent events in the boundary layer in a manner similar to that for USPBs (*sensu* Bridge and Best, 1988 and 1997) is thought logical. UMA deposits represent a transitional process towards chute-and-pool bedforms, where the rapid excavation of sediment in the trough region is deposited on the adjacent downstream antidune flank. The transition to chute and pool forms occurring when the Fr of the flow is sufficient to support a permanently breaking hydraulic jump. For the flow over UMAs, the Fr is such that a breaking standing wave is rapidly dissipated (Kennedy, 1969). The volume of material eroded, and subsequent immediate excess deposition downstream means that the antidune grows upstreamwards. Additionally sediment may be transported by low-amplitude bedwaves and turbulent sweeps. These bedwaves and turbulent motions then allow a degree of sediment sorting and produce distinguishable laminae (see Figure 2.28). These processes therefore explain the formation of classic low-angle antidune sedimentary structures - Clifton's Type II laminae.

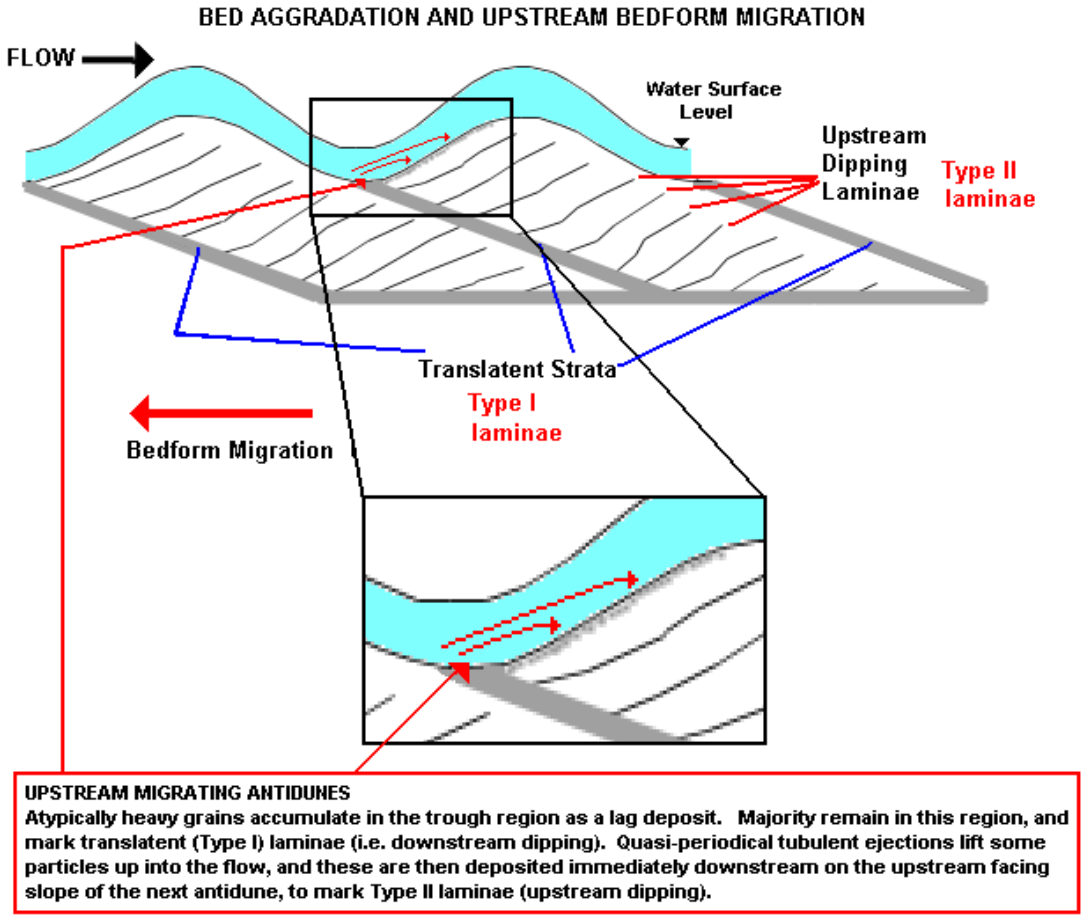

Figure 2.28 Hypothesised Formation of Type I and Type II Laminae

Type I laminae form through standing wave migration, scouring and then deposition due to coarser/heavier atypical particles being left as a lag deposit. However, Type II forms due to quasi-periodical turbulent fluctuations in the flow which move atypical sediment particles from the trough region onto the accumulating side of the antidune. These particles delineate Type II laminae.

Type I antidune laminae occurs due to extensive antidune migration and aggradation, as well as from repeated standing wave building and breaking. The breaking of the standing wave truncates the deposits of an antidune, by the wholesale erosion of large portions of the antidune. This process frequently leaves deposits representing just the toes of these sets; although in highly aggrading settings whole laminae are more frequently preserved (Clifton, 1990; Blair, 1999), see Figure 2.18 and Figure 2.19. When a standing wave breaks, eroded sediment is rapidly deposited on the bed downstream; on downstream antidunes either as low angle downstream dipping laminae or low angle upstream dipping laminae or in-situ as plane bed. Since the breaking of one standing wave often causes downstream

standing waves to break the formation of antidune laminae entirely by this mechanism alone seems suspect. It is thought that the upstream-dipping laminae that form during antidune growth must form due to a continuous sediment sorting process rather than the sorting of sediment released though erosion of an antidune by the collapse of a standing wave.

This cyclic growth and collapse process is variously described in the antidune literature as the main formative process for antidune sedimentary structures, and is well illustrated by Alexander *et al.'s* (2001) flume photos and Yokokawa *et al.'s* (2000) observations (which are illustrated in Figure 2.29 with stills from experiments carried out as part of this thesis). It may be the case that for gravel antidunes in the field (which tend to exist in deeper flows and may exhibit greater stability) turbulent sorting during antidune building is a more important method of producing the grain size variations which distinguish between individual upstream dipping low-angle laminae (Type II laminae).

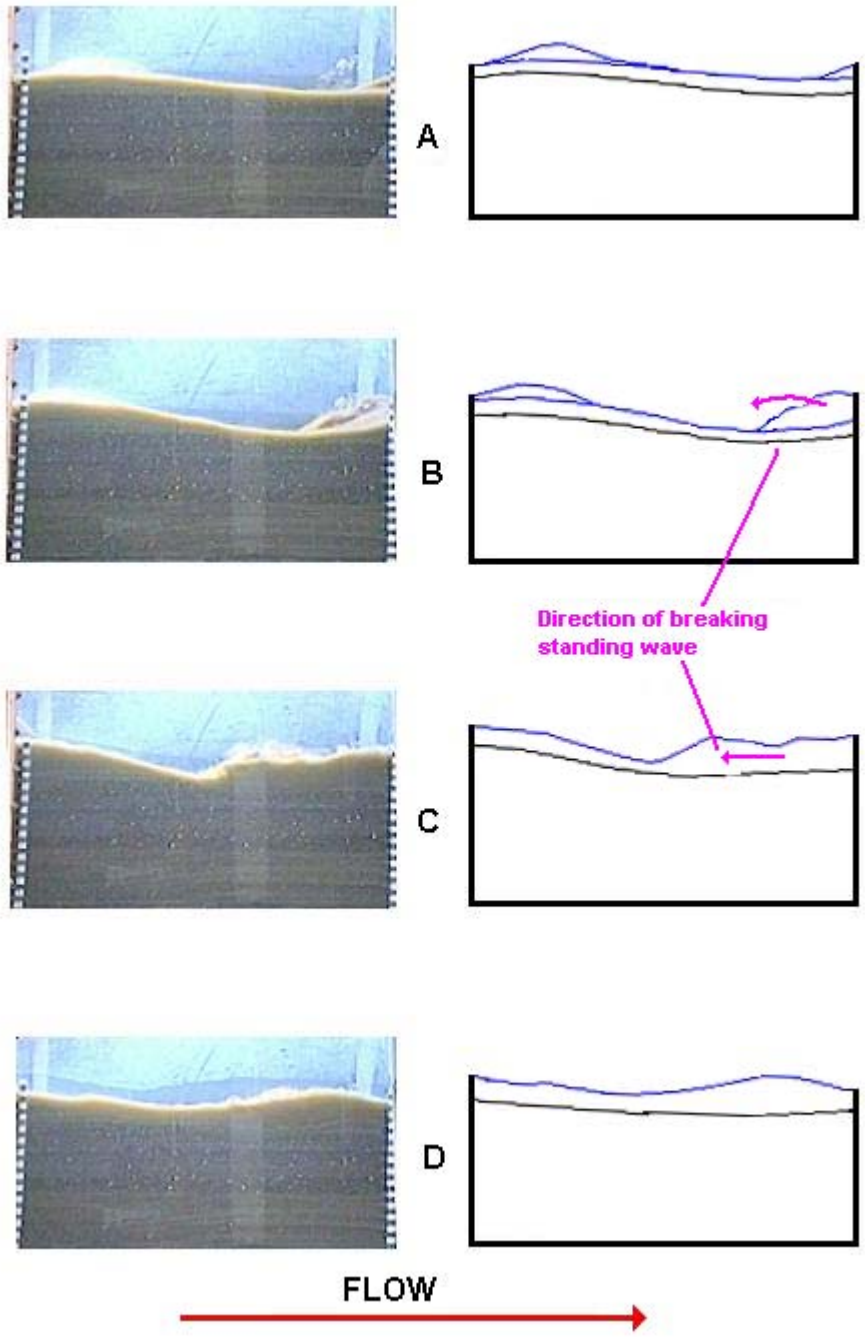

Figure 2.29 Antidune Growth and Formation

Sequence of images showing the antidune growth and formation cycle. This shows Yokokawa *et al*.'s stage 1 in 2.29A and 2.29B, Yokokawa *et al*.'s stages 2, 3 and 4 in 2.29C and Yokokawa *et al*.'s stage 5 in 2.29D (flow left to right).

Yokokawa *et al*. (2000) observations:

1. *Before the standing wave breaks, a concave upwards erosional surface is formed by the upstream migrating antidune. Deposition*

occurs on the upstream side of the antidune (that is in the downstream side of the lenticular hollow);

2. *The standing wave breaks and a highly concentrated sediment suspension associated with the breaking wave migrates upstream;*
3. *Turbulent eddies sustain suspended sediment of the clouds existing in the lenticular hollows;*
4. *Suspended sediment falls into the lenticular hollow and aggrades the bed surface, small scale oscillations occur due to eddies just above surface and rework the surface;*
5. *The bed surface aggrades continuously as eddies diminish;*

After step 5, antidune bedforms may then reform, and the cycle may repeat. Based on the literature examined, Figure 2.30 shows the bedding types thought to be formed by antidune migration, growth and collapse. This thesis now further investigates the bulk flow structure, spatial organisation of turbulence and sedimentology.

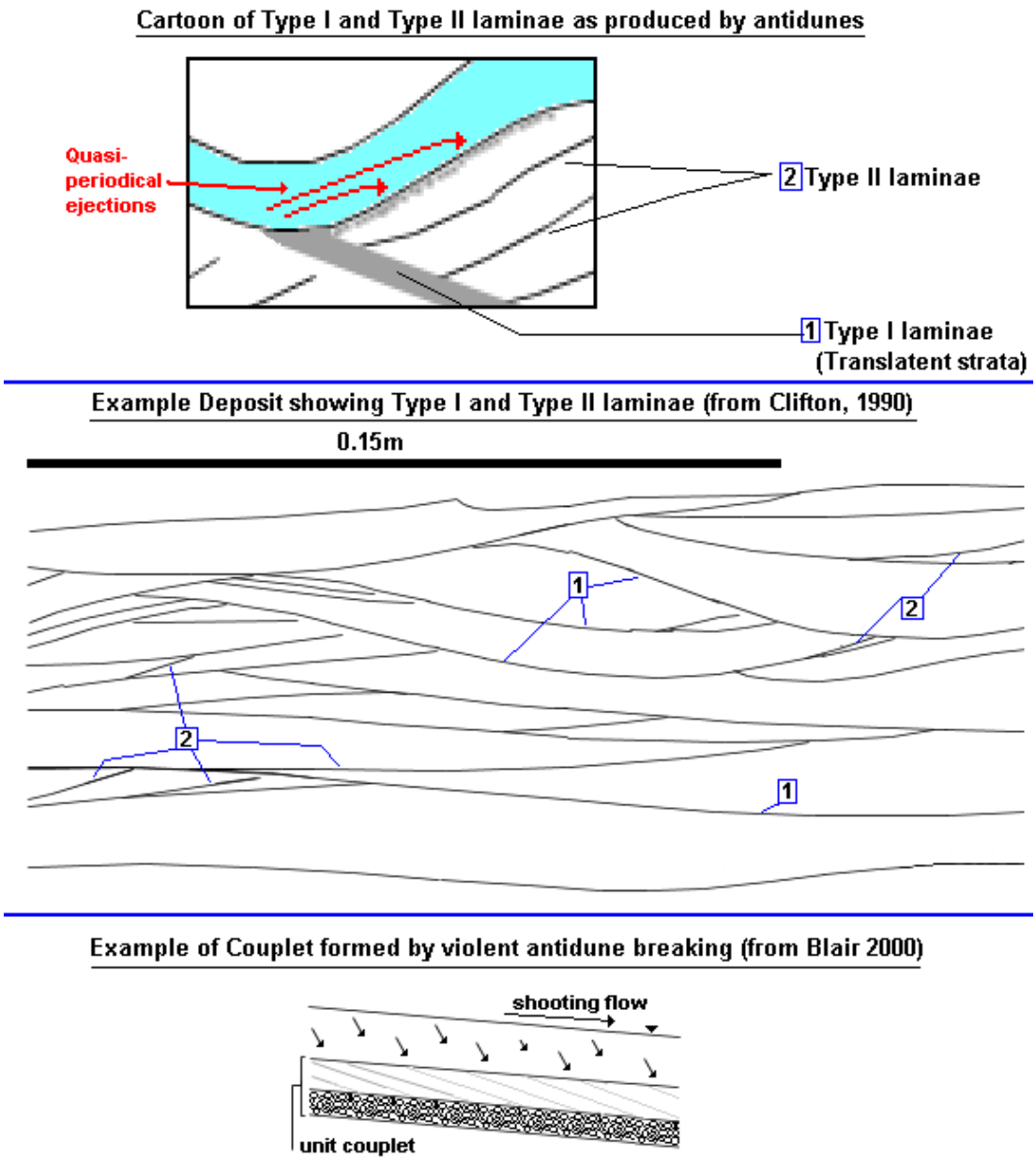

Figure 2.30 Hypothesised Antidune Bedding Types

Based on the literature surveyed it is proposed that antidunes produce Type I and Type II laminae, and in more violent washout unit couplets pairs of coarse and fine material.

2.6 Outcomes of Literature Review

- Antidune deposits are perhaps more frequent than commonly thought.
- There is a need for investigation into antidune initiation, growth and collapse and the turbulent structure of the associated flow. There are

no specific details in the literature of the flow structure when the standing wave above an antidune begins to break.

- There are no detailed investigations of antidune development in coarser materials (D_{50} > 1 mm), although it is known that the structure of turbulent flow above lower-stage gravel bedforms differs markedly from that above sand forms. Thus, the hydrodynamics of the flow above antidunes is not quantitatively (or even qualitatively) understood. The morphological differences between dunes, UMAs and DMAs are ill-defined and definitions of conditions of formation for gravel antidunes are lacking.
- There are no detailed examinations of the morphologies, laminae and grain properties of gravel antidunes in relation to the sediment mixture. The relation of these lamination styles to the three-dimensional geometry of antidunes and antidune migration, wave growth and breaking is still not resolved.
- Investigation of the affects of aggradation and degradation on antidune development and the related stratigraphy in gravel mixtures is yet to be undertaken. During aggradation, erosion of crests and infilling of troughs should produce a specific set of deposits. Verification of the type of deposits associated with the washout of gravel antidunes is required. The preservation of structures associated with the development of antidunes within gravel deposits should have a greater potential (in contrast to sand), due to the presence of coarser less-mobile particles.
- If sedimentary deposits containing antidune internal structures can be produced and examined in the flume, the interpretation of antidune internal structures in the geological record can then be clarified. Thus, there will be a clear distinction of the type of deposit that represents antidune regime flow and so deposits formed in fast, shallow supercritical flow can be identified with veracity. This will reduce confusion with other depositional processes such as HCS and SCS, reflected turbidity currents and lower regime dune deposits.
- Investigation into the transition flows at critical Fr where DMAs form is necessary, this has been examined from the dune side of the

transition, but not with specific focus to DMAs. The question remains as to whether DMAs are bedforms in their own right, or rather a hybrid, transitional non-equilibrium feature.

- Models relating bulk flow properties to antidune geometry have not advance beyond the pioneering work of Kennedy (1961, 1963 and 1969), in contrast to the state of affairs with dune morphology. More advanced models, perhaps incorporated sedimentological variables such as grain size, grain sorting and bed porosity would prove very useful.

2.6.2 Aims and Hypotheses

From this literature review, these **aims** can be set out:

1. Collect quantitative flow data for UMA flow. This data should be of sufficient spatial-density and for time periods sufficient to highlight periodical turbulent events in the flow as well as providing bulk flow parameters.
2. Over UMAs, examine flow: bed interactions to gain an understanding of how the flow interacts with the bed and detail any areas of retarded flow.
3. Differentiate the standing-wave flow structure over UMAs from that occurring in the dune and/or USPB regime: clarify how turbulence is produced in antidune flow; Detail the macroturbulent structure of the flow. Explain how the flow structure produces the stratigraphy and other sedimentological attributes of antidunes.
4. Produce UMA deposits in a sand-granule-fine gravel mixture. Examine how the lenses and laminations of antidunes (including distinctive sets) are produced and the style of imbrication that results.

Specific **hypotheses** set out are:

1. The flow above UMA will present specific turbulent coherent flow structures with characteristics amenable to statistical treatment and description.

2. Loose bed experiments will show that the turbulent flow patterns will mediate the erosional and depositional behaviour and the stratigraphy produced by UMAs. UMAs represent conditions where maximum flow velocities entrain into suspension much more sediment than can be supported at the lowest velocities over an antidune. Deposition will occur under the decelerating flow on the upstream flank. Certain turbulent events will periodically move coarser and heavy mineral grains out of a retarded flow zone to form the laminations.
3. Antidune laminae are not (at least not solely) produced by antidune standing-waves breaking.
4. The imbrication and morphological characteristics of UMA deposits will be distinctive although definition will be poor in the gravel mixtures used.

3 Methodology

3.1 Flume Setup and Hydraulic Modelling

3.1.1 Chilworth Flume

The small Chilworth flume is a purpose built research facility with transparent perspex and glass sides and a steel base. It has a working length of 6.5 m, a width of 0.4 m and a depth of 0.4 m. The flume is equipped with an electrically driven centrifugal pump, the pump capacity being 100 l/s, providing a maximum flow capacity of 0.08 m^3/s. The pump is nonadjustable, flow adjustment being made via a restricting valve in the recirculating pipe that delivers the water to the flume. An attached calibrated ultrasonic (Flow-Tronic 'FLO-SONIC') flow meter records the inlet pipe discharge to an accuracy of +/- 1 l/s. This meter and the flow control valve were used to set the discharge for each experiment run. The slope of the flume can be adjusted up to -1.5° (slope: 0.02). The sump tank holds approximately 5 m^3 of water.

Water is pumped from the sump tank via the flow control valve, up to a header tank attached to the flume, entering the flume via a flow-straightening grill. This arrangement worked well for the range of velocities used, allowing Fr of between 0.1 and 2 to be produced. Water exiting the flume passes over a series of baffles and through a gravel trap, where separation of entrained sediment from the flow occurs, water then collects in the sump tank before being recirculated.

The Nortek Acoustic Doppler Velocimeter (ADV) and Electromagnetic Flow Meter (ECM) were mounted to a movable instrument carriage which slid along guide rails along the top of the flume walls. A tiltable mounting pole attached beneath the carriage, allowed the ADV probe to be positioned parallel to the undulating bed. At the end of the mounting pole an adjustable clamp was used to hold the ADV probe within the flow, whilst allowing rotation through 360° to focus on each survey point. The carriage could be locked into position throughout each experiment. Figure 3.1 shows a technical drawing of the flume.

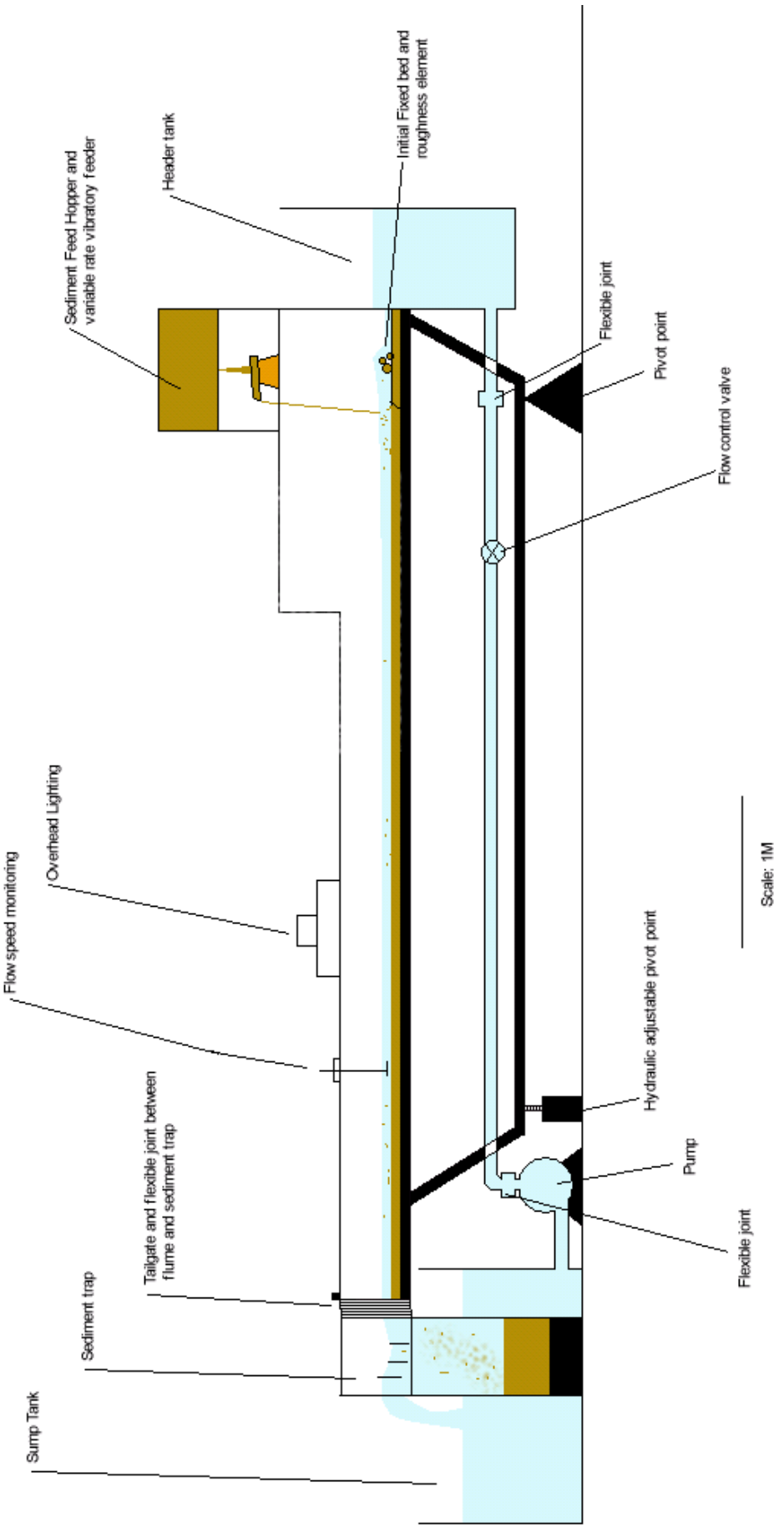

Figure 3.1 Experimental Flume

3.1.2 Flume Considerations

Paphitis and Collins (2001) stated that artificial channels can be adjusted to meet certain experimental requirements: thus *"the application of hydraulic theories will produce, therefore, results representative of natural conditions; hence, they are reasonably accurate for simulating and characterising natural environmental conditions."* However, in order to evaluate the results from flume experiments it is necessary to understand the limiting conditions and the controls on experimental data collected using them.

3.1.3 Flume Structure

Drag occurs at all of the boundaries of a flume, not just the bed. In flume experiments the decelerating effects and associated disturbance caused by the flume sidewalls to the turbulent flow structure may extend well into the flow due to the low width-depth ratio. Williams (1970) found this effect to be most pronounced at flows of low Re and/or deeper than 0.1 m, its effect being less important at higher Re flows; a channel width 3 to 5 times the depth being recommended (for this investigation, the flume width was approximately 4 times the depth). Due to the high velocities in these experiments (1.0 – 2.0 m/s) and the flow disruption caused by antidune structures forming and breaking in the bed it was thought that this consideration would be less important. However, for the ADV and high-speed camera investigations above a fixed undular bed, a strong side-to-side (spanwise) flow component was noted (a problem detailed by Nezu and Nakagawa, 1993), which appeared to be related to the deceleration of near wall flow to subcritical velocities (as per Ohtsu et al., 2003). However, for the mobile bed experiments, flume sidewall effects on the flow structure appeared to be less extensive. This was likely related to differences in flow depths, with flows being ~0.05 m deep for the mobile bed, against 0.07 – 0.15 m for the fixed bedforms and the presence (or not) of a deformable bed. Indeed, Kennedy (1961) noted that any three-dimensional aspect of antidunes and their standing waves tended to be greatest away from the

sidewalls, in the centre of the flume, apparently due to the decelerating effects at the wall, and spanwise flow induced by it.

3.1.4 Location Effects

All ADV measurements were obtained along the flume centreline, to minimise sidewall effects on the flow profile. The central portion of the flume, starting 2.5 m downstream of the flume inlet and exit was used to minimise inlet and outlet disturbances to the flow. For the velocities used in these experiments, Williams (1970) found a distance of 6.6m down the flume was required to establish a stable boundary layer and developed flow structure. However, in view of the high relative roughness (the flow was approximately 0.07 – 0.15 m deep for ADV experiments and 0.05 m for the mobile bed experiments) and the form roughness associated with the antidunes, and the additional roughness temporarily occurring on breaking of the standing waves, conducting the measurements closer to the flume entrance was considered satisfactory.

3.1.5 Temperature Effects

Temperature affects the density, kinematic viscosity of water and speed of sound in water. Hubbell and Ali (1961) established through experiment that lower temperatures produced higher shear stresses and hence higher sediment transport rates. The Nortek ADV 'water temperature' setting was adjusted when necessary during the measurements of turbulent flow structure above a fixed bed because, in the extreme, the water temperature changed between 13 °C and 23 °C through summer days. Mobile bed experiments were of relatively short duration during which no variations in temperature occurred.

3.1.6 Recirculating and Non-Recirculating Flumes

The experimental flume used for these experiments could not recirculate sediment. As the investigations were focused on the sedimentary structures formed by dynamically forming antidune bedforms, a non-recirculating flume was considered to be suitable. A recirculating flume with

the ability to recirculate the quantities of coarse sediment required was not available.

3.1.7 Hydraulic Modelling

The modelling of fluvial processes with a hydraulic flume provides a means to elucidate the exact nature of fluvial processes; Peakall *et al*. (1996) states that:

"the relationships between fluvial processes and form are often extremely difficult to quantify using conventional field and numerical techniques. Physical modelling offers a complementary technique to these methods and may be used to simulate complex processes and feedbacks in many geomorphic phenomena. Depending on the temporal/spatial scale of a particular research problem, physical models may be either 1:1 replicas of the field prototype, scale with Froude number only, have distorted scales or serve as unscaled experimental analogues that attempt to reproduce some properties of the prototype".

Thus physical modelling has several advantages over other methods: i.e. mathematical models, where only conditions specified are included. Peakall *et al*. (1996) states that through physical modelling it is possible to observe the formative processes in a reduced time-frame with controlled and manageable laboratory conditions, further it is possible to include *'physical variables, not known a priori with non-linear affects'*. Indeed Bridge and Best (1988), stated:

"It is our view that progress towards a generalized bedform theory can only come with detailed knowledge of the interaction between turbulent flow, sediment transport and bedforms gained from experimental studies over real, moving bedforms under controlled conditions. Experimental conditions close to the stability limits of particular bedforms are expected to yield crucial information"

The bedforms in this study can be taken as 1:1 equivalents (analogues) of prototype bedforms which could form outside of the laboratory or, as scaled representative model examples of antidunes, which can be used to understand the flow structures that exist above larger antidunes in natural flows. In the 1:1 scale case, it can be considered that in terms of similitude the prototype and model antidune are geometrically, kinematically and dynamically equivalent. Scale issues between prototype and model are limited, because antidune λ is proportionate to the flow depth and velocity (Kennedy, 1963 & 1969), Eq. 3.1 and Eq. 3.2. In the case of comparison with larger field examples, geometric similitude is achieved because the model shape was appropriately scaled, and kinematic, as the streamlines over the scaled bedform will be similar. However, full dynamic similitude (ratio of forces) is not achieved as sediment size, and sediment and fluid densities will be relatively different. Although, given the highly turbulent (high Re) flow and dynamic nature of standing wave growth and collapse, this lack of full similitude will be relatively less important as the main characteristics of antidune regime flow are captured. For D > 0.002 m Yalin (1972) found water waves, fluid resistance and sediment transport to be Fr similar at a first approximation.

3.2 Experimental Setup

At present there is no technique for directly monitoring the flow above antidunes whilst they are simultaneously forming and collapsing on a mobile bed as the hydrodynamic environment is far too dynamic. In these experiments, measurement of the hydrodynamics of the flow above several fixed self-similar antidune profiles provided an opportunity to evaluate the hydrodynamics of antidunes that have formed in mobile sediment by analogy. No existing turbulence study of dunes or USPB bedforms can elucidate on the detail of flow over antidunes, because the rapid cyclic deformation, creation and destruction of undulations in the bed is a characteristic unique to antidune regime flow. The turbulent structures associated with antidunes are unique due to the progressive building and collapse of a mobile bed, and these turbulent structures change rapidly in time and space.

Therefore, in order to best investigate the hydrodynamics of antidunes, three sets of experiments were designed.

1. ADV measurements over fixed antidune bedforms;
2. High-speed camera measurements over fixed antidune bedforms; and
3. Aggrading mobile bed runs to preserve antidune produced sedimentary structures.

The fixed antidune bedforms of various amplitudes provided a relatively constant hydrodynamic climate for the collection by ADV and high-speed camera of quality repeatable flow measurements, without complications from bedform migration and sediment transport (Best and Kostachuk, 2002).

3.2.1 Fixed Bed Experiments

The fixed antidune bed was composed of a series of fixed λ cast concrete antidune bed inserts over which measurements were taken. The λ was predicted according to Kennedy's (1963 and 1969), Reynold's (1965) and Parker's (1975) equations which relate antidune λ and maximum stable amplitude:

$$\lambda = 2\pi h \qquad \textbf{Eq. 3.1 Antidune Wavelength 1}$$

$$\lambda = 2\pi \frac{U^2}{g} \qquad \textbf{Eq. 3.2 Antidune Wavelength 2}$$

Using the solutions to these equations an antidune with a λ of 0.66 m and maximum amplitude of 0.105 m was selected as the model. This size was chosen to ensure that:

1. the whole antidune λ was fully visible in each flume side panels, between the metal frame, important for high-speed video work;
2. flow depth was sufficient to immerse the ADV probe; and
3. the volume of flow above the bedforms could be contained by the flume sump without surging.

According to Eq. 3.1 and Eq. 3.2 this bedform would typically occur under a flow of mean velocity 1 m/s with depth 0.105 m, giving a mean Fr of 1. In

practice (Chapter 4 and 5) it was found that flow velocities over the various amplitudes at water depths of between 0.07 and 0.15 m varied between 0.7 and 1.9 m/s. It is thought that this occurs as the predictive equations do not take full account of the dynamic nature of the full flow profile above an actual antidune bedform due to skin roughness and perhaps the lack of a mobile bed. Additionally, Eq. 3.1 and Eq. 3.2 are simplifications based on empirical observations and Potential Flow Theory.

Four amplitudes of two-dimensional bedform inserts were produced, these were:

1. 0.100 m;
2. 0.075 m;
3. 0.050 m; and
4. 0.025 m.

These amplitudes represented frozen 'snapshots' of the development of an antidune from initial plane bed to full height. These amplitudes were produced as three different types of artificial bedform:

1. Concrete bedform, gravel surfaced;
2. Concrete bedform, sand surfaced; and
3. Openwork fixed-gravel bedform.

These sand and gravel surfaced bedforms are shown in Plates 3.1 and 3.2. The surfacing was produced by coating the top surface of the concrete inserts with varnish, and then with either medium silver sand (D_{16} = 160 μm, D_{50} = 274 μm, D_{84} = 360 μm), or fine gravel (D_{16} = 0.47 mm, D_{50} = 1.7 mm, D_{84} = 6.18 mm), (as per the method used by Nelson *et al*., 1993) to give the smooth casts a representative surface roughness. Trials to induce deposition of grains from high velocity water flow onto the inserts and then latterly to fix the grains proved unsuccessful. Consequently, it was not possible to reproduce water-lain natural grain orientations including any imbrication, but the surface grain coating should have produced a similar effect on the flow as a naturally imbricated roughness element would have with the same grain

size distribution. Natural grains sizes were used, the bedforms being 1:1 scale model: prototype, a scaling ratio not possible for dune studies (such as Best and Kostaschuk, 2002). As an approximation to indicate comparative d_R, the gravel used (D_{50} 1.7 mm) for these antidunes with a 0.1m deep flow would scale to give a sediment D_{50} of 1.7 cm for prototype antidunes forming under a 1 m deep flow, a realistic supposition.

For the 0.1 m amplitude antidune bedforms establishing and sustaining supercritical flow proved very difficult, when established the standing wave quickly broke. An amplitude of 0.1 m is, according to Eq. 3.1 and Eq. 3.2 for a 0.66 m λ antidune bedform, the upper stability limit. The same type of flow instability was found above the 0.075 m amplitude openwork gravel antidune. Therefore, ADV measurements and high-speed camera work were only conducted over eight different antidune bedforms (see Table 3.1).

Plate 3.1 Concrete Antidune Bedform Inserts

Concrete antidune bedforms surfaced with sand and gravel. Top left to bottom right: 0.025 m λ sand, 0.050 m λ sand and 0.075 m λ sand; 0.025 m λ gravel, 0.050 m λ gravel and 0.075 m λ gravel (sand covering appears very faintly).

Plate 3.2 Openwork Fixed-Gravel Inserts

Table 3.1 Types of Antidune Bedform Investigated in this thesis

Antidune Amplitude	Gravel Skin	Sand Skin	Openwork-Gravel
0.025 m	SW stable, investigated	SW stable, investigated	SW stable, investigated
0.050 m	SW stable, investigated	SW stable, investigated	SW stable, investigated
0.075 m	SW stable, investigated	SW stable, investigated	SW unstable
0.100 m	SW unstable	SW unstable	SW unstable

Where SW is Standing Wave.

This type of hydrodynamic investigation of the flow above fixed bedforms has been undertaken for dunes by (Raudkivi, 1966; Nelson *et al*., 1993; McLean *et al*., 1994; Bennett and Bridge, 1995; Bennett and Best, 1995; Best and Kostaschuk, 2002; and Maddux *et al*., 2003).

These forms had the effect of representing various stages of growth of an antidune but provided a controlled, fixed bed above which reproducible hydrodynamic measurements readily could be taken from fixed points in the flow that could be re-occupied for subsequent measurements. Thus, it was possible to acquire the "*detailed, reproducible time averaged flow and turbulence measurements*" (Bennett and Bridge, 1995), needed to

characterise the hydrodynamic climate. These forms do not migrate, and are two-dimensional (their profile following a sine wave) and as such the fixed bed does not replicate mobile antidunes exactly as there is no migration, no suspended or bed load and no interstitial flow (McLean *et al*., 1994; Bennett and Best, 1995; Best and Kostaschuk, 2002). The runs carried out using openwork gravel antidune bedform shapes (Plate 3.2) partially address this by allowing the effect of interstitial flow to be investigated. Thus three sets of inserts (sand skin roughness, gravel skin roughness, gravel matrix) that could quickly be moved in and out of the flume were produced. Putty and foam were used to seal the small joints between sections and the flume walls to provide a continuous six- λ surface and to prevent exchange of water between the stream flow and the water filled 'dead' space beneath the inserts (Figure 3.2 and Plate 3.3). The joints between the inserts were sealed flat and flush (joint width typically 0.5 cm), to ensure that the bed surface was effectively continuous with no abrupt lips which could cause artefacts in the collected ADV data.

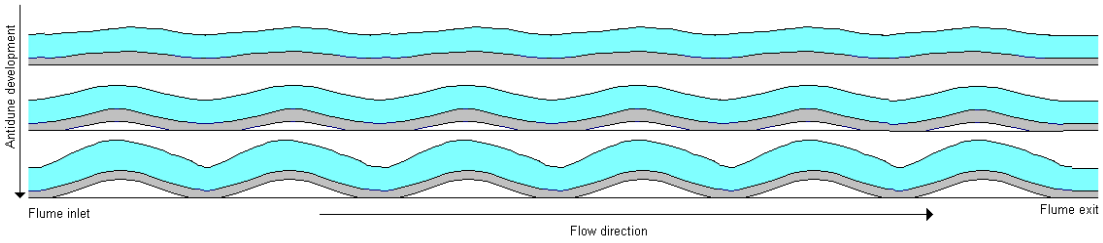

Figure 3.2 Schematic of Antidune Inserts in-Flume

Plate 3.3 Concrete Inserts in-Flume

Water depth was measured by a graduated tape on the flume walls and by point-gauge. The flume discharge was determined by an in-situ ultrasonic flow meter (calibrated with an Electromagnetic Current Meter), and the water temperature monitored.

The flumes flow control valve was set to give the desired discharge for each set of antidune bedforms (details in Tables 3.4 – 3.9 and Tables 3.11 – 3.12). For each fixed-bed run the flume pump was turned on with the valve at this setting, this meant a rapid inflow of water into the flume occurred, establishing the required supercritical flow above the antidune forms. The flume was then left to run for 20 minutes to allow the system to settle, and any entrained/trapped air to dissipate. After each set of measurements were taken, the pumps were turned off allowing the flume to rapidly drain, and the next set of bedforms to be installed into the flume.

3.3 Acoustic Doppler Velocimetry

Taylor's *'frozen turbulence'* approximation (Batchelor, 1960) assumes that since turbulent structures and events advect with the flow, by measuring turbulence continuously for short periods at different locations, a picture of the whole flow can be constructed. Together the data points in a transect provide time-averaged information on the characteristics of turbulence in a slice of flow. Therefore a regular grid of measurement points was used to position the ADV probe at multiple locations along the flume centreline above each antidune form. 22 vertical profiles were taken, every 0.031 m, starting at the crest of one antidune form and working downstream-wards through the intervening trough up to the crest of the downstream antidune bedform. Multiple flow measurements were taken in each vertical profile, as detailed in Table 3.2. By obtaining time series measurements at each point in the transect allows the typical temporal velocity variations at each point to be captured. Statistics calculated for each point in the flow transect can be plotted together, allowing spatial patterns to be identified.

Table 3.2 ADV Probe Measurement Locations in the Vertical Flow Profile

Antidune Type	ADV	Number of vertical Measurements	
Gravel 0.025 m Amplitude	100 Hz/25 Hz	7	0.5, 1, 2, 3, 4, 5, 6 cm from bed
Gravel 0.050 m Amplitude	100 Hz/25 Hz	8	0.5, 1, 2, 3, 4, 5, 6, 7 cm from bed
Gravel 0.075 m Amplitude	100 Hz/25 Hz	8	0.5, 1, 2, 3, 4, 5, 6, 7 cm from bed
Sand 0.025 m Amplitude	25 Hz	6	0.5, 1, 2, 3, 4, 5 cm from bed
Sand 0.050 m Amplitude	25 Hz	6	0.5, 1, 2, 3, 4, 5 cm from bed
Sand 0.075 m Amplitude	25 Hz	6	0.5, 1, 2, 3, 4, 5 cm from bed
Openwork Gravel 0.025 m Amplitude	25 Hz	7	0.5, 1, 2, 3, 4, 5, 6 cm from bed
Openwork Gravel 0.050 m Amplitude	25 Hz	7	0.5, 1, 2, 3, 4, 5, 6 cm from bed

In this experiment ADV measurements were made using a Nortek Doppler velocimeter, operating at both 100 Hz and 25 Hz, due to the limited availability of the specialised controller needed to run the probe at 100 Hz. Previous investigations of antidune regime flow such as Wren *et al*. (2005) used a 25 Hz ADV in experiments with a mean flow of 1.3 m/s. A complete set of ADV measurements being collected at 25 Hz for all eight of the antidunes in Table 3.2, 100 Hz measurements were only collected for the three gravel surfaced antidune forms. Therefore in total 11 suites of ADV measurements were collected.

The ADV used was a Nortek NDV, with a 90˚ sideways mounted probe. The probe consists of a central transmit transducer, and three receiving transducers set 120˚ apart, with a maximum radius of 0.025 m (see Plate 3.4). Receiving tranducers are angled at 30˚, focusing on the sampling volume which is located 0.050 m from the probe. Probe velocity range was set to +/- 2.5 m/s and the sample volume to 9 mm^3. These settings were in line with the Nortek's recommendations and were the most appropriate for measurement in the shallow, highly turbulent flow – the small measurement volume minimising the occurrence of Doppler broadening and the velocity range chosen to prevent aliasing. At 100 Hz the covariance of the data is minimised allowing data quality to be kept high (Lane *et al.*, 1998), however data recorded at 25 Hz appeared satisfactory. In both cases the ADV is sampling at rates faster than 25 Hz or 100 Hz, averaging samples to the

respective output frequency. Since the speed of sound in water is temperature dependent the temperature was monitored, and the probe's controller software settings adjusted throughout each experiment cycle. The ADV probe used had a sideways looking head (90° to stem) and was mounted on a flexible cable, allowing the flexibility of probe location and orientation to obtain the sample volumes required to investigate the flow profile.

ADVs sense the velocities remotely, as the head is set away from the sample volume being measured, thus the flow is not affected by the disturbances associated with the immersed probe head. In terms of accuracy, Nortek quote the instrument as being accurate to +/- 0.5% of the true velocity, whilst Voulgaris and Trowbridge (1998) consider a (Sontek) ADV to be accurate to within 1% of the true mean flow velocity value (at all flow speeds); and for the $|u'v'|$ differences to be again approximately negligible within 1% of the value obtained by LDV. Appropriate filtering of collected data is required to remove noise associated with phase shifts (Doppler noise); scatter motions, velocity gradients, aerated flow and boundary interference (Lane *et al*., 1998 and Voulgaris and Trowbridge, 1998). However, apparent noise and low-correlation may be symptomatic of high levels of shear and small scale turbulence (Goring and Nikora, 2002; Wahl, 2003; Strom and Panaicolaou, 2007). Only frequencies below the Nyquist frequency (the frequency of measurement divided by two) will be reliably recorded (Lohrmann *et al*., 1994). Therefore for the data collection rates of 100 Hz and 25 Hz used here thresholds are 50 Hz and 12.5 Hz respectively, for data above these frequencies aliasing may occur.

3.3.1 ADV Setup for Antidune Hydrodynamics

Previous work has used ADV to investigate the velocity profile of shallow flows, such as that by Ferro (2003) where the roughness height (D_*) was of the same order of magnitude as d. In these experiments the ADV probe stem was mounted horizontally beneath a movable trolley fixed to the flume guide-rails, with the probe head looking sideways. As well as adjusting the depth of the probe, the ADV probe stem could then be rotated to place

the measurement volume at the required height above the bed, the spanwise position of the measurement volume then being adjusted so that all measurement volumes fell on the same vertical transect along the centre of the flume, as shown in Figure 3.3 and Plate 3.4. The slope of the horizontal probe mounting was adjusted, to keep the probe stem parallel to the bed and flow. Correction for probe orientation was included in the ADV data pre-processing stage.

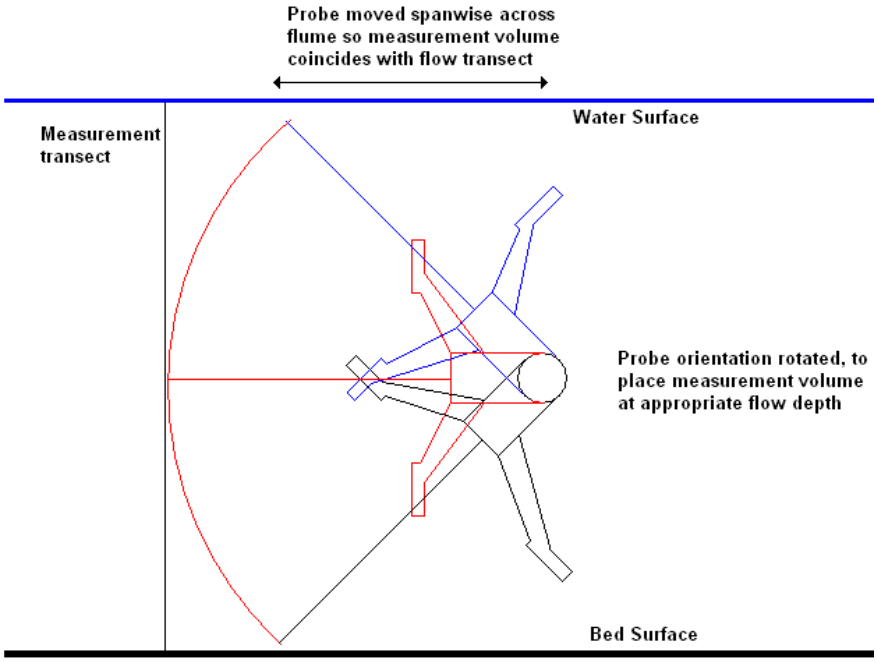

Figure 3.3 ADV Probe Head Orientation

Placement and orientation of sideways looking ADV. Flow direction is into page.

Plate 3.4 ADV Probe Head In-Flume

Flow left to right

Data were collected for 180 seconds at each location in the flow transects (giving at 100 Hz, 18,000 measurements per record; and at 25 Hz, 4,500 measurements per record); a record length that is compatible with the suggestions of Buffin-Bélanger and Roy (2005). A longer record length ensures there are a large number of data points once data has been filtered, reducing the risk of bias in the data. Chanson *et al*. (2005) consider that for high levels of accuracy, 5,000 data points are the minimum for first and second order statistical moments (mean, rms), and 50,000 for higher statistical moments (skew, τ_R, TKE). In this thesis, due to the large number of data points to be collected in each flow profile a record length of 180 seconds was the maximum practical record length.

3.3.2 ADV Data Analysis

Collected data was analysed using WinADV[2] (Wahl, 2000) and bespoke MatLab routines.

[2] http://www.usbr.gov/pmts/hydraulics_lab/twahl/winadv/

Pre-Processing

Pre-processing was performed to remove noise from the ADV data (low correlation, low Signal-to-Noise-Ratio and data spikes) and to correct for the orientation of the ADV. Filtering was used to remove inappropriate data and instrument/measurement noise. Recommendations for the removal of data based on correlation coefficient vary from excluding data with a correlation coefficient (COR) below 0.7 (Lane *et al.*, 1998 and Ferro, 2003), 0.6 (McLelland and Nicholas, 2000) and 0.5 (Nicholas, 2005; Strom and Papanicolaou, 2007) and 0.4 (Martin *et al.*, 2002). Whilst low correlations may represent poor quality data (air bubble/debris in flow), low correlations are also produced by highly turbulent flow; therefore user discretion is required in the filtering of data. Potentially, increased temporal resolution, such as a higher frequency ADV instrument (i.e. 100 Hz compared to 25 Hz) will provide for greater discrimination, although Doppler noise will be increased. For the Signal to Noise Ratio (SNR) it is recommended to remove data with a SNR below 15 Db (McLelland and Nicholas, 2000). Above 20 Db, SNR has little effect on data quality (Gordon, 2000). For this thesis, typical SNR values were between 35 and 40 Db and data with a SNR below 30 was removed. In terms of COR, where more then 70% of the data remained, data with an average COR below 0.7 was removed. Where filtering based on average correlation coefficient left less than 70% of data, the correlation coefficient used was reduced until around 70% of original data remained in the output file (following the method of Martin *et al.*, 2002; Strom and Papanicolaou, 2007). Similar levels of data exclusion were found to be required by Wilcox and Wohl (2007) for ADV measurements of a highly turbulent step-pool system.

Table 3.3 gives an indication of the filtering performed based on average COR thresholds, used to give an output file with at least 70% of data remaining. The poorest quality data shown in Table 3.3 occurred in the trough region between antidune bedforms, due to the high level of turbulence in the region (see Section 4). As Strom and Papanicolaou (2007) stated, there is a need to include this lower quality data for completeness in order to describe flow properties in all regions of the flow profile.

Table 3.3 Proportion of Files with >70% Data Remaining at Various Average CORs

	COR >0.7	COR >0.6	COR >0.5	COR >0.4
Gravel 100 Hz	84.0%	94.1%	99.6%	100%
Gravel 25 Hz	40.9%	71.1%	89.0%	100%
Open-gravel 25 Hz	49.0%	64.0%	78.9%	100%
Sand 25 Hz	99.2%	100%	100%	100%

In addition to filtering based on SNR and COR, a Phase-Space threshold despiking filter (Nikora and Goring, 1998; Wahl, 2000; Goring and Nikora, 2002 and Wahl, 2003) was utilised for all data files. This despiking method removes data spikes caused by aliasing, and requires no user calibration in order to detect spikes. Limited data was removed by filtering based on average SNR and the phase-threshold despiking filter, almost all data discarded were removed by filtering based on the average COR. For the production of turbulence statistics, data removed from the signal were replaced with 'NaN' flags, to avoid biasing the data with interpolated data points. For spectral analysis, no data was removed from the signal in order to undertake a Fast Fourier Transform, output frequency data being averaged. García *et al*. (2005) introduced the parameter 'F', to numerically describe an ADVs ability to accurately measure instantaneous velocities. García *et al*. suggested that ideally values of F > 20.

$$F = \frac{Lf_R}{U_C} \qquad \textbf{Eq. 3.3 ADV ability to measure turbulent flow}$$

where, L = length scale (m), f_R = ADV frequency (Hz), and U_C = convective velocity (m/s). Calculations with the experimental parameters in this thesis (L = 0.15 to 0.2 m, f_R = 100 Hz, and U_C =1.4 to 1.7m/s), gives values for F between 8.8 and 14.3. Reference to Garcia *et al*.'s ADV performance curves indicates that these values of F correspond to an underestimation of second moment statistics by between 15 – 20% and fourth moment by 30 – 50% respectively. At 25 Hz, F values are between 3 and 3.6, giving underestimates of between 30 and 60% for second and fourth order moments respectively.

Further calculations were undertaken to investigate the distribution and patterns in turbulence in the flow profile over the antidune bedforms. The

equations described and used by Best and Kostachuck (2002) in their investigation of turbulence over low-angle dunes are used here for the antidune turbulence environment.

Basic Investigations

The mean velocity, Root Mean Square and Skew were calculated for the x (U), y (V) and z (W) velocity components of each ADV time series as per Eq. 3.4 – 3.6. Units for these three variables are m/s.

$$\overline{U} = \frac{1}{n}\sum_{i=1}^{n} u_i \qquad \textbf{Eq. 3.4 Mean Velocity}$$

$$U_{rms} = \left[\frac{1}{n}\sum_{i=1}^{n}\left(u_i - \overline{U}\right)\right]^{0.5} \qquad \textbf{Eq. 3.5 Root Mean Square}$$

$$U_{Skew} = \frac{1}{n}\sum_{i=1}^{n}\left(\frac{u_i - \overline{U}}{U_{rms}}\right)^3 \qquad \textbf{Eq. 3.6 Skew}$$

Where n is total number of measurements and $u' = u_i - \overline{U}$. A value of skew of 0 means a distribution is normal, whilst negative values indicate it is skewed to the left (small magnitude $|u'v'|$ fluctuations) and positive values skewed to the right (large magnitude $|u'v'|$ fluctuations).

From the ADV time series at each point in the flow transects, the Turbulent Kinetic Energy (TKE, m^2/s^2) was calculated using Eq. 3.7; and τ_R (m^2/s^2) from Equations 3.8 and 3.9. The TKE method has been found to give more precise estimates of the bed shear stress, particularly on coarser grained beds; as it is also derived from all three *u', v'* and *w'* components available from ADV data (Sukhodolov *et al*., 1998; Thompson *et al*., 2003).

$$TKE = \frac{u'^2 + v'^2 + w'^2}{2} \qquad \textbf{Eq. 3.7 Turbulent Kinetic Energy}$$

$$-\overline{u'v'} = \frac{1}{n}\sum_{i=1}^{n}\left(u_i - \overline{U}\right)\left(v_i - \overline{V}\right) \qquad \textbf{Eq. 3.8 Time Averaged Reynolds Stress 1}$$

$$\tau_R = -\rho\overline{u'v'}$$ **Eq. 3.9 Time Averaged Reynolds Stress 2**

Turbulence Production (P, dimensionless), a measure of the location and rate of turbulence production, was estimated from Eq. 3.10.

$$P = \overline{-u'v'}\frac{\partial \overline{U}}{\partial Y}$$ **Eq. 3.10 Turbulence Production**

The Boundary Layer Correlation Coefficient (R, dimensionless) is a measure of the intensity and thickness of the boundary layer, was calculated from Eq. 3.11. A value of 0.4 is typical of flow over flat bed boundaries (Hinze, 1975), McLean *et al*. (1994) and Best and Kostachuk (2002) found values of between 0.3 and 0.5 over low-angle dunes. Lower values are due to increased flow unsteadiness (Nelson *et al*., 1993 and McLean *et al*., 1994).

$$R = \frac{\overline{u'v'}}{\left[\left(\overline{u'}\right)^2\left(\overline{v'}\right)^2\right]^{0.5}}$$ **Eq. 3.11 Boundary Layer Correlation Coefficient**

Likewise, the Turbulence Intensity (TI, dimensionless), a measure of the size of turbulent fluctuations in the flow, was calculated from Eq. 3.12.

$$TI = \frac{U_{rms}}{\overline{U}}$$ **Eq. 3.12 Turbulence Intensity**

Line plots of the normalised $\overline{U}$ (dimensionless) at each vertical measurement elevation were produced using Eq. 3.13

$$Normalised\ \overline{U} = \frac{\overline{U}}{\overline{U}_{surface}}$$ **Eq. 3.13 Normalised $\overline{U}$**

Quadrant Analysis

Quadrant Analysis (Kline *et al.*, 1967; Wilmarth and Lu, 1972; Lu and Wilmarth, 1973; Nezu and Nakagawa, 1993; McLean *et al.,* 1994; Nelson *et al*., 1995 and Best, 1996) is a technique to investigate the turbulent flow structure. Instantaneous *u'* and *v'* flow deviations from the velocity record are subdivided into four types of turbulent events: Outward interactions, ejections, inward interactions and sweeps, where:

- outward interaction: $u' > 0$, $v' > 0$ Quadrant 1
- ejection: $u' < 0$, $v' > 0$ Quadrant 2
- inward interaction: $u' < 0$, $v' < 0$ Quadrant 3
- sweep: $u' > 0$, $v' < 0$ Quadrant 4

The technique has been successfully utilised by Nelson *et al*. (1995); Bennett and Best, (1995) and Best and Kostaschuk (2002) in the investigation of the turbulent flow profile above fluvial bedforms. McLean *et al*. (1994) and Williams (1996) investigated the importance of these temporal events in sediment transport. Following the method of Best and Kostaschuk (2002) quadrant analysis of 180 second long segments of the ADV data was undertaken. Figure 3.4 shows how quadrant analysis delineates $|u'v'|$ stresses into five zones – key $|u'v'|$ events in each of the four quadrants above the line defined by Eq. 3.14, plus smaller less intense $|u'v'|$ events below the line defined by Eq. 3.14. The hole size (H_o) was determined according to Eq. 3.15 in order to investigate the distribution of the more intense events in each quadrant.

$$|u'v'| = H_\circ |u'v'| \qquad \textbf{Eq. 3.14 Quadrant Analysis - Hole Size}$$

$$H_o = \frac{|u'v'|}{\left[(U_{rms})(V_{rms})\right]} \qquad \textbf{Eq. 3.15 Quadrant Analysis - Hole Size}$$

A Hole Size of 2 was found to be appropriate, typically leading to 97 – 99% of events being excluded. The mean $|u'v'|$ values of events above the threshold defined by the hole size were also computed.

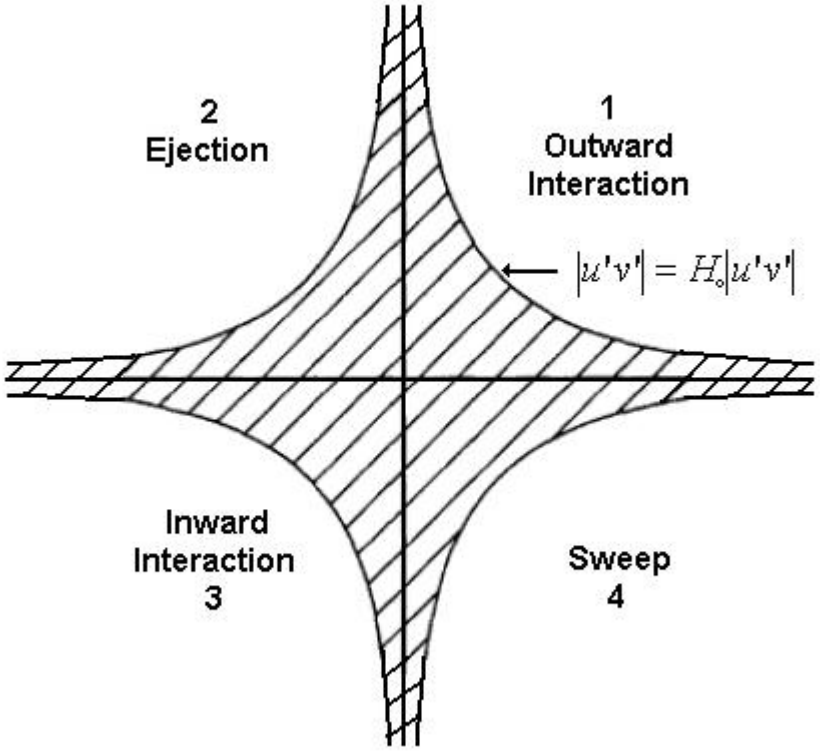

Figure 3.4 Quadrant Analysis

Output Data Visualisation

Visualisation of the large volume of output data post processing was undertaken using MatLab v14. Values obtained for each location in the flow transect were interpolated to provide a continuous flow slice indicating spatial and temporal properties of turbulence across the antidune bedforms.

Spectral Analysis

Spectral analysis provides a means of investigating the dominant periodicity of turbulent events in a velocity time series. A Fast Fourier Transform was used to convert the raw data time signal into the frequency domain. A forty point moving average filter was used in MatLab to process the output frequency data. These data were then plotted against the -5/3 dissipation rate, suggested by Kolmogorov's (1941) theory on the dissipation of turbulence as the rate by which turbulent eddies decay.

Four runs were conducted, the summary details for which are shown in Tables 3.4 - 3.7.

Table 3.4 Experimental Conditions Gravel Surfaced Bedforms 100 Hz

Condition	**Value**		
Temperature	13 ➔ 21˚C		
Flume Bed Slope	1.5˚ or 0.0167 constant during the run		
Amplitude of antidune bedform inserts.	**0.025 m** (trough / crest)	**0.050 m** (trough / crest)	**0.075 m** (trough / crest)
Q **(m^3/s)**	0.066	0.066	0.066
U **(m/s)**	1.7 / 1.7	1.5 / 1.6	1.2 / 1.4
d **(m)**	0.1 / 0.1	0.11 / 0.11	0.12 / 0.13
Fr	1.71 / 1.71	1.44 / 1.62	1.11 / 1.29

Table 3.5 Experimental Conditions Gravel Surfaced Bedforms 25 Hz

Condition	**Value**		
Temperature	13 ➔19˚C		
Flume Bed Slope	1.5˚ or 0.0167 constant during the run		
Amplitude of antidune bedform inserts.	**0.025 m** (trough / crest)	**0.050 m** (trough / crest)	**0.075 m** (trough / crest)
Q **(m^3/s)**	0.066	0.066	0.066
U **(m/s)**	1.7 /1.7	1.2 / 1.3	1.1/ 1.4
d **(m)**	0.1 / 0.1	0.11 / 0.11	0.12 / 0.12
Fr	1.71 / 1.71	1.15 / 1.25	1.01 / 1.29

Table 3.6 Experimental Conditions Sand Surfaced Bedforms 25 Hz

Condition	**Value**		
Temperature	13 ➔ 20˚C		
Flume Bed Slope	1˚ or 0.0111 constant during the run		
Amplitude of antidune bedform inserts.	**0.025 m** (trough / crest)	**0.050 m** (trough / crest)	**0.075 m** (trough / crest)
Q **(m^3/s)**	0.062	0.062	0.062
U **(m/s)**	1.85 / 1.95	1.6 / 1.7	1.5 / 1.6
d **(m)**	0.085 / 0.085	0.09 / 0.08	0.1 / 0.1
Fr	2.03 / 2.13	1.70 / 1.91	1.51 / 1.61

Table 3.7 Experimental Conditions Open-Gravel Bedforms 25 Hz

Condition	**Value**		
Temperature	13 ➔ 20˚C		
Flume Bed Slope	1.5˚ or 0.0167 constant during the run		
Amplitude of antidune bedform inserts.	**0.025 m** (trough / crest)	**0.050 m** (trough / crest)	
Q **(m^3/s)**	0.066	0.066	
U **(m/s)**	1.8 / 1.8	1.2 / 1.4	
d **(m)**	0.1 / 0.1	0.115 / 0.115	

Fr	1.81 / 1.81	1.12 / 1.32	

The conditions detailed in Tables 3.4 – 3.7 were kept constant for each of the set of bedform inserts used in each of the four experiments. Flow conditions were checked regularly to ensure that the chosen control conditions did not drift.

3.4 Particle Tracking and High-Speed Camera Analysis

3.4.1 Introduction

To provide a complementary analysis to the data obtained through ADV, the second set of experiments used a high-speed camera to obtain high-frequency images of tracer laden flow over antidunes bedforms. Flow visualisation provides a means for obtaining non-intrusive, high-frequency information on the flow structure, which unlike the point measurements obtained from ADV data, provide instantaneous impressions of the entire flow field (Merzkirch, 1974).

Each frame collected represents a frozen image of a set of particles suspended in the flow at any one point in time, the movement of these particles from frame to frame showing the movement of the flow; thus turbulent structures can be elucidated from these motions. In this process the assumption is that these particles can accurately represent the two dimensional structure of the flow (Merzkirch, 1974). However, particles suspended in the flow are exposed to drag so will not follow the flow exactly. The seeding density needs to be sufficient and constant, to allow for consistent particle detection.

3.4.2 Camera, Hardware and Software Specifications

A high-speed PhotonFocus™ MV-D752 CMOS (Complementary Metal Oxide Semiconductor) camera with a global shutter (all pixels sensed and shuttered synchronously) was used to obtain images of the flow. CMOS cameras have high quantum efficiency with low system noise and are highly

sensitive to optical radiation thus being less sensitive to exposure time, a crucial factor in high speed imaging. The camera was capable of recording images at a maximum speed of 350fps (752 X 582 pixels, 0.438 megapixels), and had adjustable exposure times, producing monochrome images at an 8-bit greyscale resolution. Images were stored directly to a connected computer's hard disc via the cameras digital interface Cameralink™, to a Silicon Software 64-bit PCI card MicroEnable™ III XXL framegrabber; this set up allowed data rates of up to 200 MB/s, the software recorded video files as *.avi, the maximum file size being limited to 4GB by the hardware. The Photon Focus camera software and Silicon Software's 'MicroDisplay' were used to control the basic camera settings, and control the image acquisition process respectively.

3.4.3 Theory of High Speed Imaging

By taking a series of frames that record the positions of suspended neutrally-buoyant highly-reflective tracer particles in quick succession, the movement of particles between frames can be observed. The velocity of particles can be calculated by measuring the distance moved compared to the time (exposure time + gap between exposures) between successive frames. Ideally, sufficient particles should be captured in each frame, the majority of which should remain in the next frame, and out-of-plane motion would ideally be minimal. Bias may occur as the highest velocity particles will have the lowest exposure due to the distance moved in a given frame, additionally these particles will preferentially leave each frame, preventing the identification of successive particle positions (Smit and Lim, 2000).

3.4.4 Specific Setup for this Flume

The entire flume was blacked out using hardboard and black HDPE sheeting. A movable enclosure held a 2000 W halogen light box over the flume, a light guide allowed a tight 0.04 m X 0.005 m strip of light down into and along the centre of the flume; whilst the camera was mounted adjustably alongside the flume. This light curtain was sufficient to illuminate a thin strip of particles within the Field-Of-View (FOV), balancing the need to keep enough particles in the light curtain against obtaining messy images showing

particles moving out of the x-y plane in a wide swathe of the flume. Data was collected at 50 fps (particle streak stills) and 200 fps (high-speed video image analysis) which represented a trade-off between the image frequency versus exposure time and file size. Five spatially overlapping videos were taken of flow over each antidune, since the camera FOV only covered one quarter of the antidune λ.

The maximum lens speed was used, maximising exposure and minimising the field of depth; allowing more critical focusing of the camera (Smit and Lim, 2000). The shutter speed was set so that particles being tracked moved minimally between frames; although the illumination intensity ultimately limits the shutter speed. The camera was trialled to assess which settings provided the optimum image quality (highest range of DNs) with the flume and lighting setup. The CMOS sensor attaches most significance to the radiances detected in the centre of the pixel, with a bell-shaped distribution giving less sensitivity at the edges when the pixel's DN is assigned. Minimising the pixel size means the tracer particle will be wholly over at least one pixel at a particular moment in time. Thus the maximum FOV is determined by the size of the particles to be visualised. Since the pliolite used as tracer had a D_{50} of 0.5 mm, the FOV was set so each pixel was approximately one third of the size (0.167 mm) of the particles to be detected; the FOV used (0.1400 m by 0.1084 m) gave a pixel size of 0.186 mm.

3.4.5 Image Processing

Slow-motion playback of the recorded images allowed observation and closer understanding of the structures in the flow. From these images, it was then possible to deduce how the turbulent structure of the flow evolved as the antidune bed inserts were changed, increasing in size. Sets of frames that show turbulent events in particular detail have been included in the results section as a visual record.

The 'OSS Video Decompiler' program was used to break down the *.avi video files into individual *.bmp images. Further data analysis was then undertaken in MatLab v14. Images were pre-processed by masking areas of the frames representing the bed and the water surface and air above. A

critical pixel brightness was used to threshold the frames, thereby classifying all brighter pixels as representing highly-reflective tracer particles. This produced binary images that more clearly showed the tracking particles (brightness DN = 255) against a black (brightness DN = 0) background.

These images were then processed using the 'Matlab Particle Tracking Code'[3] developed by Daniel Blair and Eric Dufresne, based on the IDL particle tracking algorithm developed by John Crocker and Eric Weeks. These scripts identify the location and size of the tracking particles for each binary image. A search radius was then set, the script then identifies particle pairs by classifying the closest bright spot within the search radius in the subsequent image in the subsequent image. If no particles are present in the search radius, no particle pair is identified. Based on the displacement between each position in the particle pair, a vector can be obtained, and based on the frame exposure time and time between frames a velocity calculated.

The velocity of the particle-pair vector was then plotted at the vector midpoint. As detected particle pairs were irregularly spaced, data were gridded in MatLab to produce a contoured flow slice displaying detected flow velocities. The five contoured flow slices were stitched together in Matlab to form a contoured slice of flow over the whole antidune bedform. Two runs were conducted, the summary details for which are shown in Tables 3.8 and 3.9. The conditions detailed in Tables 3.8 and 3.9 were kept constant for each of the three bed configurations (0.025, 0.050 and 0.075 m amplitude antidunes) used in the gravel and sand experiments respectively. Flow conditions were checked after each exchange between the different concrete bed inserts to ensure that the chosen control conditions had not drifted. The enclosure of the entire flume in blackout materials for this experiment precluded the continuous recording of the experiment on standard video equipment. Likewise continuous measurement was not possible with intrusive instruments (ECM or ADV) which would have disrupted the flow and thus measurements.

[3] http://physics.georgetown.edu/matlab/

Table 3.8 Experimental Conditions Gravel Surfaced Bedforms

Condition	Value
Temperature	13 ➔ 18˚C
Flume Bed Slope	1.5˚ or 0.0167 constant during the run
Q **(m^3/s)**	0.066 m^3/s
U **(m/s)**	See Table 3.4
d **(m)**	
Fr	
Bed	0.025, 0.050 and 0.075 m amplitude concrete inserts (gravel surfaced)

Table 3.9 Experimental Conditions Sand Surfaced Bedforms

Condition	Value
Temperature	13 ➔18˚C
Flume Bed Slope	1˚ or 0.0111 constant during the run
Q **(m^3/s)**	0.062 m^3/s
U **(m/s)**	See Table 3.6
d **(m)**	
Fr	
Bed	0.025, 0.050 and 0.075 m amplitude concrete inserts (sand surfaced)

3.5 Mobile Bed Experiments

The third set of experiments used a mobile sand-gravel bed, and investigated the formation antidune sedimentary structures.

3.5.1 Sediment Characteristics

Sediment was collected from a field site in the Severn Estuary, Gloucestershire, UK. This sediment consisted of platey, rounded oblate, red shale particles in the granule to small gravel size range; density 1.93 g/cm^3. The sediment was washed in a 500 μm sieve to remove the majority of the muddy finer fractions, and passed through a 1cm sieve to remove coarser particles. 1 mm diameter quartz granules and washed silver sand were added to augment the finer grain size range, to produce a sediment mixture that would readily produce bedforms and highlight internal structures. Trials showed that this mixture was fully mobile, and readily formed antidune bedforms allowing new data to be collected on antidune sedimentary

structures in coarse sediment. The presence of platey granule-gravel sized particles meant that it was possible to examine particle orientation, including variations in imbrication angle. Two sediment mixtures were used in the two mobile bed runs, details of sieve analyses are displayed below in Table 3.10, and Plate 3.5 shows the typical grain sizes present.

Plate 3.5 Gravel Sediment

Table 3.10 Sediment Characteristics

Sediment Mix 1		Sediment Mix 2	
D_{90}	3.32 mm	**D90**	2.76 mm
D_{50}	1.21 mm	**D50**	1.06 mm
D_{10}	0.36 mm	**D10**	0.31 mm
SD	1.49 mm	**SD**	1.32 mm

† sediment was bimodal in distribution

During each run well-mixed air-dried sediment was continually fed into the flume at a constant rate via a sediment hopper and a (Eriez '46C') vibratory feeder. Two assistants continually filled the sediment feed hopper throughout each flume-run, using pre-filled buckets which were emptied into the hopper one by one from an elevated walkway. According to the manufacturer, the feed rate can be set between 0 and 3.8 kg/s and is fully adjustable via a graduated control. A calibration was performed using the chosen sediment to determine the actual feed-rate for the experiments. For

the first experiment the feed rate was 0.8 kg/s, whilst for the second the feed rate was initially 0.8 kg/s increasing to 1.1 kg/s. A sediment feed shoot ensured the sediment entered the water over a small strip of flume 0.5 m downstream of the inlet grill.

Sediment mixture homogeneity was ensured by removing all sediment from the flume, air-drying and then re-mixing the entire sediment stock after each run. On inspection after each run, preferential deposition of sand near the flume entrance, and larger gravel particles near the flume exit was observed. This process was thought to relate to the greater exposure of the larger, more prominent gravel particles, and hence greater transport rate. The feeder set up was similar to that used by Williams (1970) and Ashmore (1982); the rate of input was balanced with the output, through initial trial runs, so that for measurement runs it could be strictly controlled. The light coloured fine sand contrasted the red colour of the fine gravel which helped delineate bedding and laminations. In addition, handfuls of very dark grey silicon carbide (density = 3.2 g/cm^3) were added to the flume during runs to help highlight sedimentary structures during periods of bed aggradation. A manually-controlled, vertically aligned, tailgate plate held the bed sediment filament in place. This plate was raised in steps of 0.01 m every 1 minute, allowing the bed to gradually aggrade, sediment not retained in the flume collecting in the sediment trap within the sump. Sediment volumes within the flume were measured volumetrically once the flume was drained. As Wilcock (2000) found, it was particularly difficult to measure the height of the bed surface along the centre-line of the flume rapidly and precisely during the experimental runs, especially to a good accuracy when there is a high discharge, a problem compounded by the dynamic nature of antidune bedforms.

Water depth and bed elevation adjacent to the perspex side wall was interpolated latterly from camera stills and video footage of the experiments and markings made on the side of the flume during flume runs. Velocity was calculated using two methods, the discharge-area method, since the flume discharge was constant throughout the experiment. Secondly, velocity was calculated from the movement of particles apparent in consecutive video stills

of the flow since it is extremely difficult to continuously measure the velocity of the sediment laden flow over the rapidly aggrading bed in the flume through the experiment. As particles tracked between video frames were adjacent to the wall, estimated velocities will be a slight underestimate of velocities in the centre of the flume, but they are considered to be representative. For Run 2, the discharge-area method was not found to be suitable since the apparent discharge had changed over the run, the reasons for which were unclear. It is thought that the increased head the pump was pumping to as the bed aggraded and the increased volume of water stored in the header tank above the bed and in interstitial spaces in the aggrading bed reduced the head of water in the sump tank above the recirculating pump.

For each run the flume pump was turned on and the flow control valve gradually opened to the desired flow rate (Tables 3.11 and 3.12). At the end of the flume run the control valve was rapidly closed (preventing rapid draining of the flume by reverse flow to the sump) and the flume pump turned off.

A VHS video was recorded of the second run which was later digitised to DVD format. 'Auto Gordian Knot' software was used to convert the DVD video file to an .avi file, which was de-interleaved into .jpeg stills using 'OSS Video Decompiler'. No video was recorded of the first run, although multiple still images were taken. A software program called 'Exif.7.19' was used to extract the Exif image information imbedded in each digital photo, information which includes the exact moment of image capture (rather than the time of file creation). 'Picassa' was used to manually adjust the stills to improve brightness and contrast to aid interpretation. Comparison of this time with the level of sediment against the scale markers attached to the flume side allowed the rate of sediment aggradation to be obtained.

3.5.2 Sectioning of Labile Bed Sedimentary Structures

After each of the labile bed experiments the flume was left to drain for 5 days, until excess water had completely drained from the sediment. Sediment sections were carefully excavated in the damp sediment to leave a clean edge, to which trays containing polyurethane foam were applied as successfully used by Skipper *et al.* (1998) and Carling *et al.* (2005). The

excavated areas were then backfilled to hold the trays in place, as the foam expanded, and set. After two days the trays were carefully removed to reveal the peels of the sedimentary sections. The resulting peels appear very successful in capturing the sedimentary structures and the interface between USPB and antidune structures preserved in the flume. Plate 3.6 shows the process of producing these polyurethane peels.

For Run 1 the flume was sectioned both lengthways and spanwise after the first run, as per Alexander *et al*. (2001) had found the spanwise sections did give some information on the three-dimensionality of structures and show the effects of flume width. However, on analysis it was felt that the transverse sections showed relatively little, and by interrupting a continuous flow parallel section, reduced its value. Therefore in Run 2, a continuous flow parallel section was excavated with no transverse sections. Figures 3.5 and 3.6 show the location of the peels taken in each run. In Run 1 an additional peel was taken (Peel 5) after the original set (Peels 1 – 4) as the sedimentary structures in Peel 2 continued upstream. Peel 5 overlaps with Peel 2 and continues upstream until the truncation by flow-transverse peel 1. After Run 2, Peels 2 and 3 were initially taken. Peel 3 is not examined in this thesis (openwork USPB at downstream end of flume). Peel 2 was taken as a long section to reveal a large continuous stretch of sedimentary structures from the section of the flume with antidune activity. Upon removal Peel 2 showed that the sedimentary structures continued upstream, so Peel 1 was taken (sedimentary structures in the upper part of the flume were not visible during the experiment due to the sides at the top end of the flume being opaque. Unfortunately damage (sediment section collapse) occurred to a 0.04 m section between Peels 1 and 2 in preparation for the taking of Peel 2.

High definition photographs of these sections were taken under several types of studio lighting with a 10 megapixel digital SLR camera to produce images capable of demonstrating the gross structures preserved, internal structures, grain sizes and sorting, grain packing and support, imbrication angle (protractor and inclinometer for angle of dip of the clasts a-b plane) and heavy or light mineral inclusion.

Serif PhotoPlus 6.0 was then used to draw interpretation and annotations of the peels on top of the photographs. Annotations were drawn

to show sedimentary structures, their dimensions and the internal characteristics of sedimentary packages, based on a manual examination of the sedimentary peels.

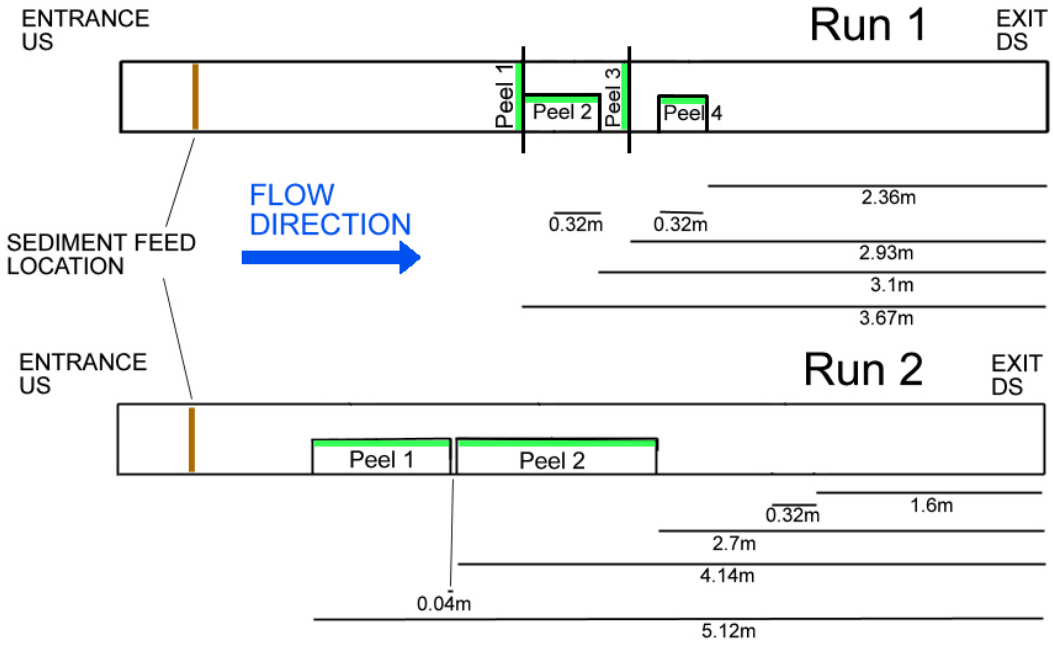

Figure 3.5 Plan View of Sediment Peel Locations in Flume

The distances indicate the distance from the downstream end of the flume to the location of individual sediment sections.

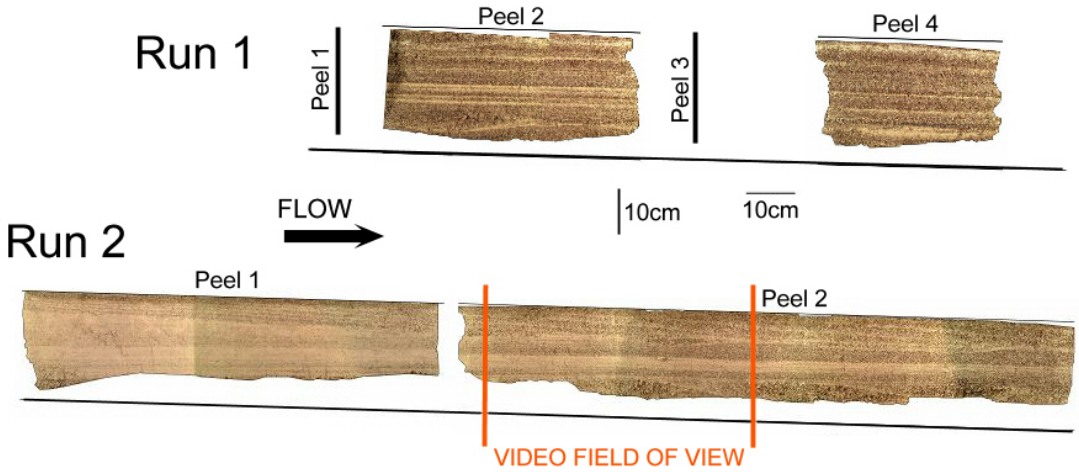

Figure 3.6 Composite View of Peels from Run 1 and Run 2.

As the timing, flow characteristics and bedform behaviour that produced these sedimentary sections was observed and photographed, a direct comparison between process and deposit was obtainable. Thus, providing

information that will guide the palaeohydraulic interpretation of possible antidunes structures in field outcrops.

Plate 3.6 Sediment Sectioning Techniques

Clockwise from top left: excavated sections; polyurethane foam trays placed and backfilled; re-excavation to reveal trays; end result.

Details and summary details of the two runs are shown in Tables 3.11 and 3.12.

Table 3.11 Experimental Conditions During Run 1

Condition	Value
Temperature	13 ➔ 18˚C
Sediment Feed Rate	0.4 litres/second
Average Aggradation Rate	0.18 mm/second
Tailgate Raising	0.01 m per minute
Flume Bed Slope	1.5˚ or 0.0167 constant during the run
Q **(m^3/s)**	0.011 m^3/s
U **(m/s)**	0.66 m/s
d **(m)**	0.043 m
Fr	1.59

Bed	Low (0.025 m) amplitude concrete antidune bedforms inserts, gravel surfaced
Time length of Exp.	17 minutes
Sediment mix	Run 1 Mixture (Table 3.10)

Table 3.12 Experimental Conditions During Run 2[4]

Condition	Value
Temperature	13 ➔19˚C
Sediment Feed Rate	First 20 minutes: 0.4 litres/second, then 0.57 litres/second.
Average Aggradation Rate	0.17 mm/second
Tailgate Raising	0.01 m per minute
Flume Bed Slope	1.5˚ or 0.0167 constant during the run
Q **(m^3/s)**	0.011 m^3/s ➔ 0.007 ➔ 0.006
U **(m/s)**	0.9 m/s ➔ 0.7 m/s ➔ 0.8 m/s
d **(m)**	0.035 m ➔ 0.025 m ➔ 0.02 m
Fr	1.6 ➔ 1.35 ➔ 1.75
Bed	Low (0.025 m) amplitude concrete antidune bedforms inserts, gravel surfaced.
Time length of Exp.	24 minutes 21 seconds
Sediment mix	Run 2 Mixture (Table 3.10)

[4] The multiple values for Run conditions are taken at 6, 14 and 21 ½ minutes, which represent the middle of the 1st period of antidune activity, the middle of the intervening USPB stage and the middle of the 2nd period of antidune activity. Figures 6.3 and 6.4 give more detail of variations during the run.

4 ADV Investigation of Antidune Regime Flow – Results and Interpretation

4.1 Spatial Characteristics of Turbulence Over Gravel Antidune Bedforms (ADV 100 Hz)

The flow conditions, methods and techniques used in these experiments are outlined in the Methodology (**Chapter 3**). The upstream end of the flow slices presented in this section were located 2.67 m downstream of the flume entrance and the downstream end of the flow slices being 3.17m from the downstream end of the flume (the bedform insert λ being 0.66 m). The red line above each flow slice represents the water surface as measured with a point gauge, whilst the blue line is a smoothed water surface.

The bedform inserts in section 4.1 and 4.4 are the gravel surfaced concrete inserts detailed in Chapter 3. The bedform inserts in section 4.2 are the openwork-gravel inserts detailed in Chapter 3. The bedform inserts in section 4.3 are the sand surfaced concrete inserts detailed in Chapter 3.

4.1.1 $\overline{U}$, U_{rms} and U_{skew} for 0.025, 0.050 and 0.075 m Amplitude Gravel Antidune Bedforms

With increasing amplitude, significant changes can be seen in the distribution of $\overline{U}$ values over the gravel surfaced antidune bedforms. Over 0.025 m amplitude forms (Figure 4.1) velocities are in the region of 1.7 – 1.8 m/s for the majority of the flow profile. A thin boundary layer is present near the bed, with velocities at the crests drop to 1.6 m/s, in the trough velocities drop as low as 1.3 m/s (0.75 of $\overline{U}$ in the upper parts of the flow). These retarded velocities are notably skewed downstream of the trough onto the upstream facing flank of the downstream antidune. Over 0.050 m amplitude forms (Figure 4.2) velocities are in the region of 1.45 – 1.65 m/s for the majority of the flow profile. Only a poorly developed boundary layer is present near the bed, velocities at the crests drop to 1.4 m/s. However, in the trough velocities drop as low as 0.8 m/s (0.52 of $\overline{U}$ in the upper parts of

the flow). Again, a skew is evident downstream of the trough onto the upstream facing flank of the downstream antidune. Over 0.075 m amplitude forms (Figure 4.3) velocities are in the region of 1.2 – 1.5 m/s for the majority of the flow profile. Again a poorly developed boundary layer is present near the bed and velocities at the crests drop to 1.3 m/s. However, in the trough velocities drop as low as 0.6 m/s (0.44 of $\overline{U}$ in the upper parts of the flow). Again, for the lowest velocities a skew is evident downstream of the trough onto the upstream facing flank of the downstream antidune. However, the area of retarded flow can be seen developing earlier on the downslope of the upstream antidune, and on the downstream antidune, high velocities occur directly adjacent to the crest. Towards the bed, and at the trough, the increasing divergence from velocities in the upper flow profile can be seen in the respective normalised velocity plots in Figures 4.4a, 4.5a and 4.6a. For all three amplitudes (Figures 4.1 – 4.3) the highest U_{rms} values occur adjacent to the bed due to the variability of instantaneous velocities, the effect being strongest in the trough between antidunes. These high rms values are indicative of generally retarded flow near the bed (i.e. between 0.75 and 0.44 of the mean flow speed), interjected with periods of intermittent high speed turbulent motions. Similarly, for all three amplitudes the U_{skew} negative, meaning that whilst velocities are in general high, there is a notable amount of lower instantaneous velocities.

For all three amplitudes, the lowest skew is present nearest the water surface (low friction, always high instantaneous velocities). Initially, a low skewness occurs adjacent to the bed (high friction, always small instantaneous velocities), more negative skewness being present in the mid flow profile. A cross-over effect can be seen developing for the 0.050 m, and then 0.075 m antidunes, as the most negative skew moves from the mid-flow profile on the upstream antidune flank, to the bed on the downstream antidune. This is interpreted as being caused by the exposure of the downstream antidunes upstream facing flank to high velocity flow, the negative skew being caused by intermittent low instantaneous velocities attributable to the roughness of the adjacent bed. The line plots of $\overline{U}$, U_{rms} and U_{skew}, in Figure 4.7 – 4.9 further illustrate these trends.

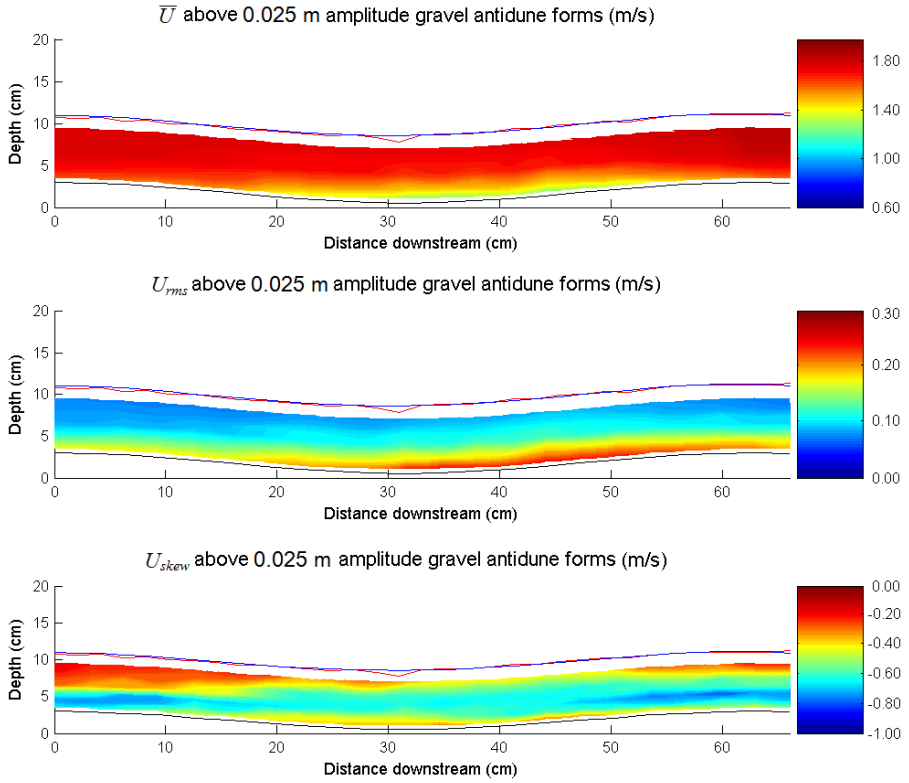

Figure 4.1 $\overline{U}$, U_{rms} and U_{skew} above a 0.025 m Amplitude Gravel Antidune Bedform (ADV: 100 Hz)

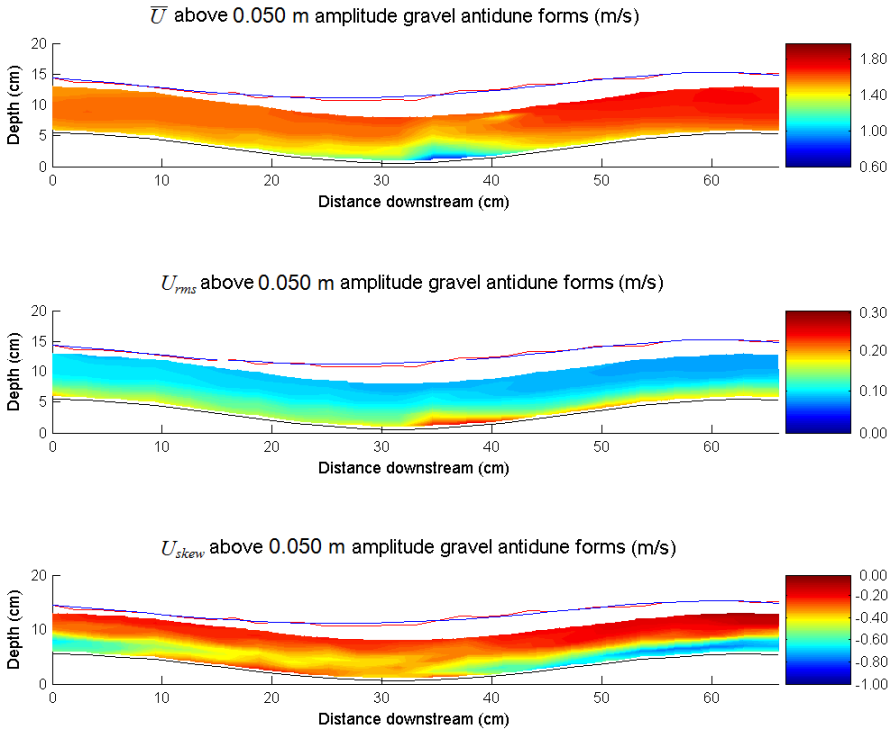

Figure 4.2 $\overline{U}$, U_{rms} and U_{skew} above a 0.050 m Amplitude Gravel Antidune Bedform (ADV: 100 Hz)

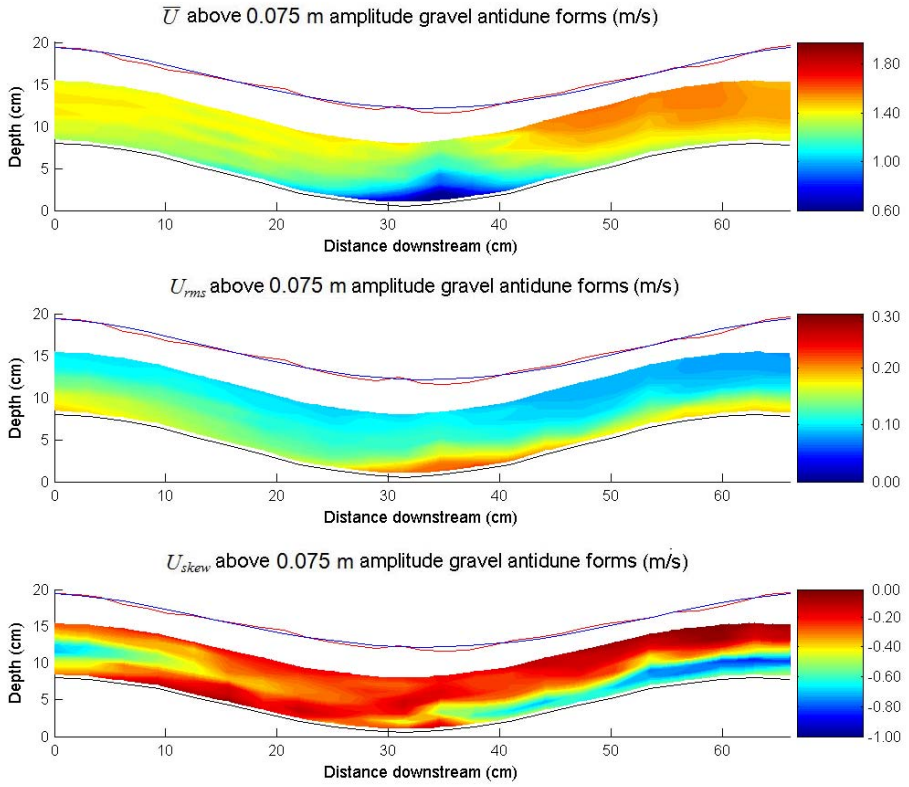

Figure 4.3 $\overline{U}$, U_{rms} and U_{skew} above a 0.075 m Amplitude Gravel Antidune Bedform (ADV: 100 Hz)

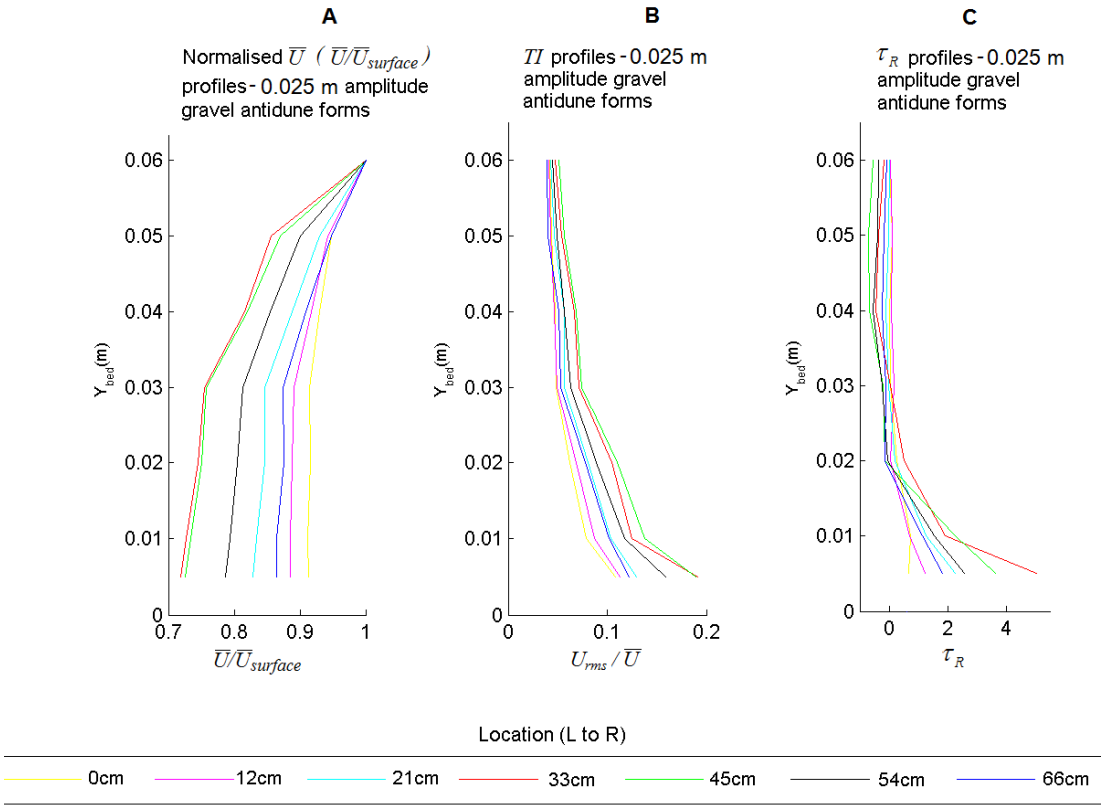

Figure 4.4 $\overline{U}$ *(normalised)*, TI and τ_R Profiles for Flow above a 0.025 m Amplitude Gravel Antidune Bedform (ADV: 100 Hz)

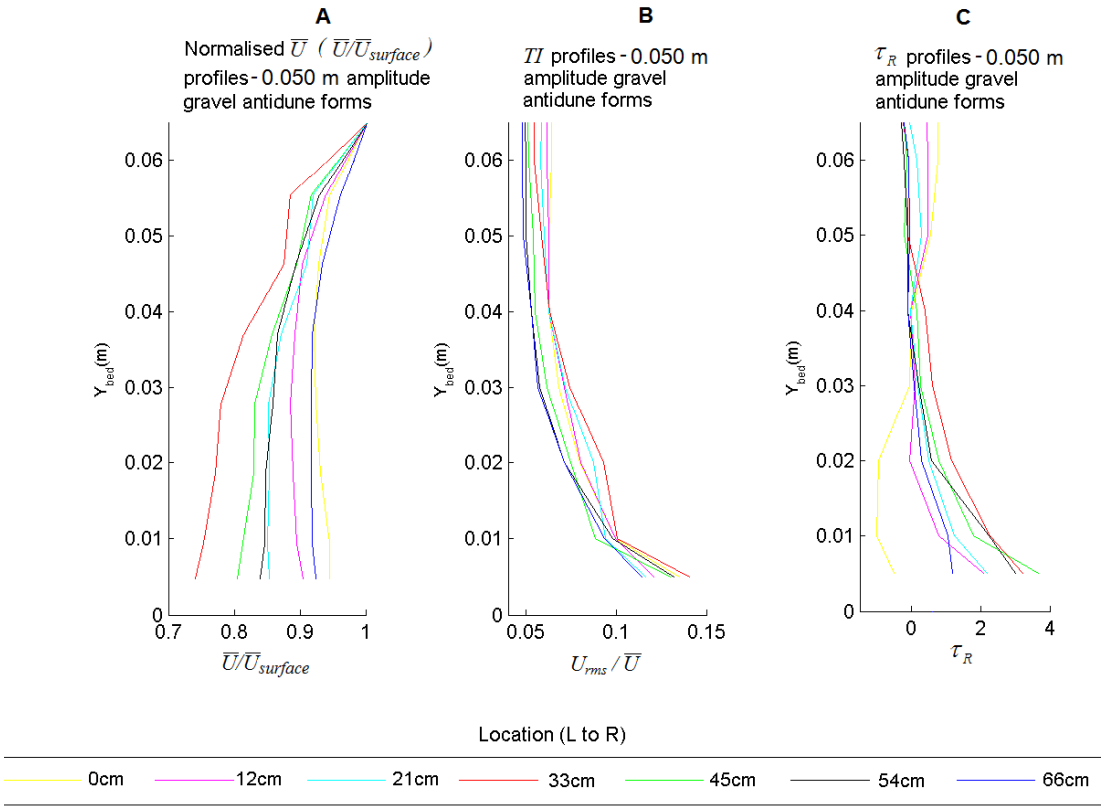

Figure 4.5 $\overline{U}$ *(normalised)*, TI and τ_R Profiles for Flow above a 0.050 m Amplitude Gravel Antidune Bedform (ADV: 100 Hz)

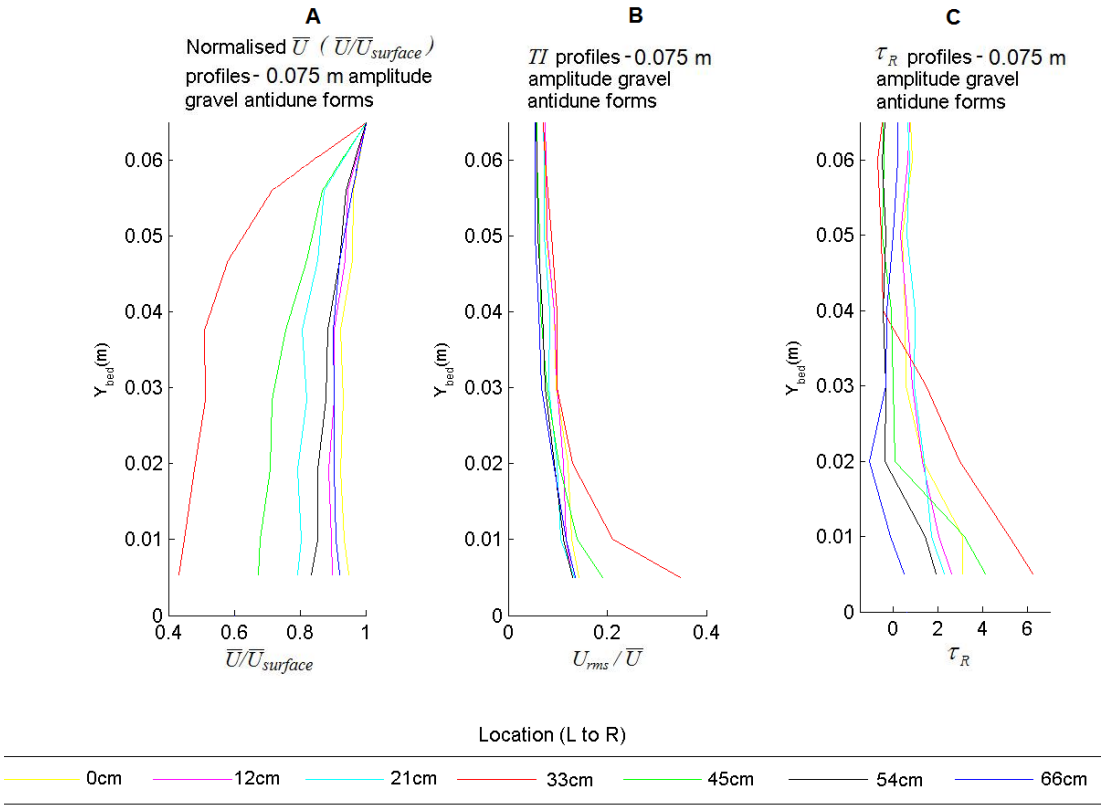

Figure 4.6 $\overline{U}$ *(normalised)*, TI and τ_R Profiles for Flow above a 0.075 m Amplitude Gravel Antidune Bedform (ADV: 100 Hz)

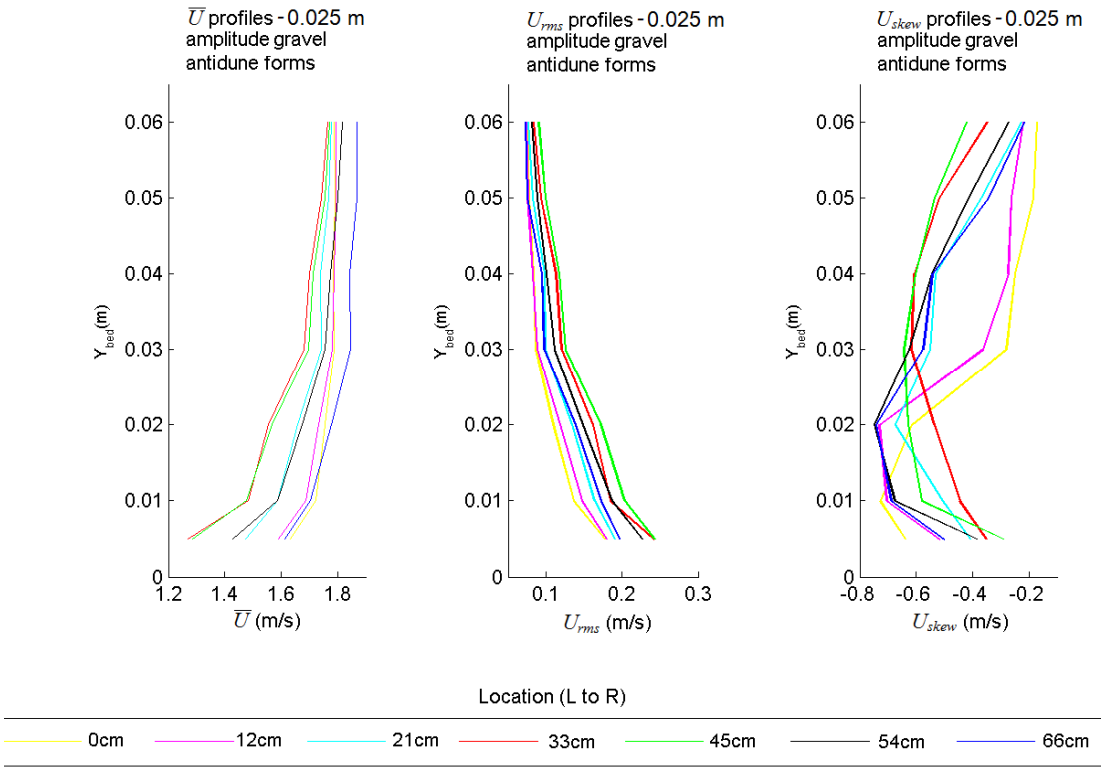

Figure 4.7 Profiles of $\overline{U}$, U_{rms} and U_{skew} for Flow above a 0.025 m Amplitude Gravel Antidune Bedform (ADV: 100 Hz)

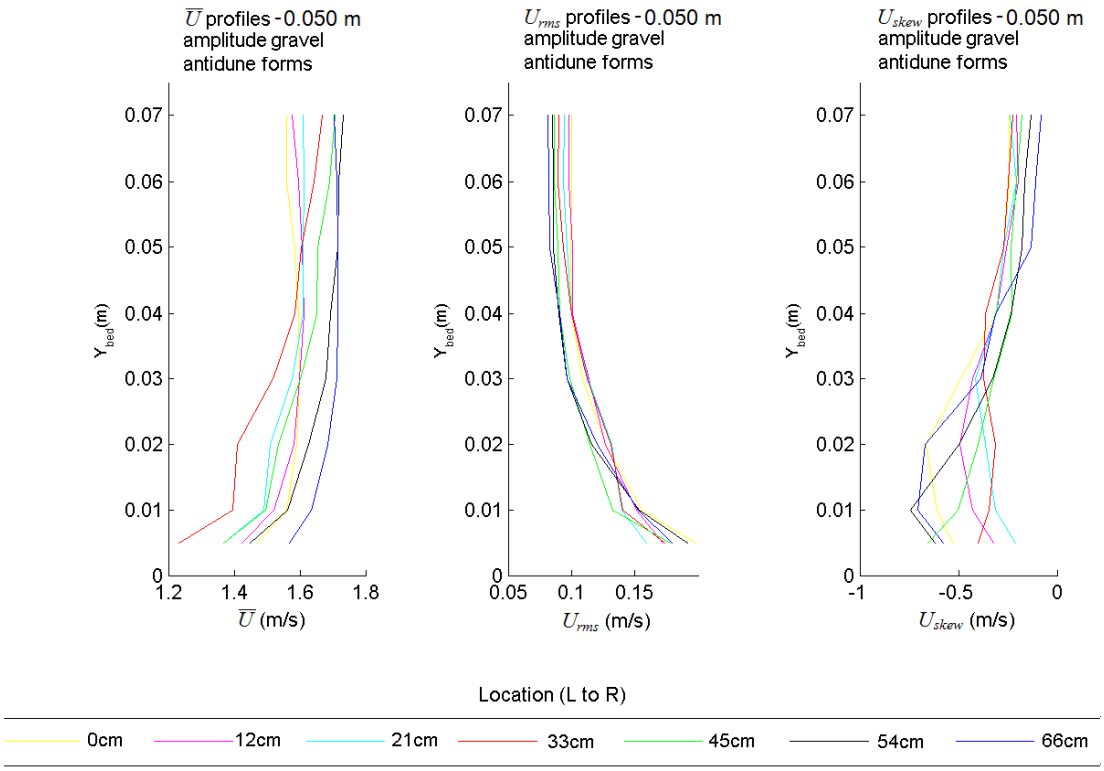

Figure 4.8 Profiles of $\overline{U}$, U_{rms} and U_{skew} for Flow above a 0.050 m Amplitude Gravel Antidune Bedform (ADV: 100 Hz)

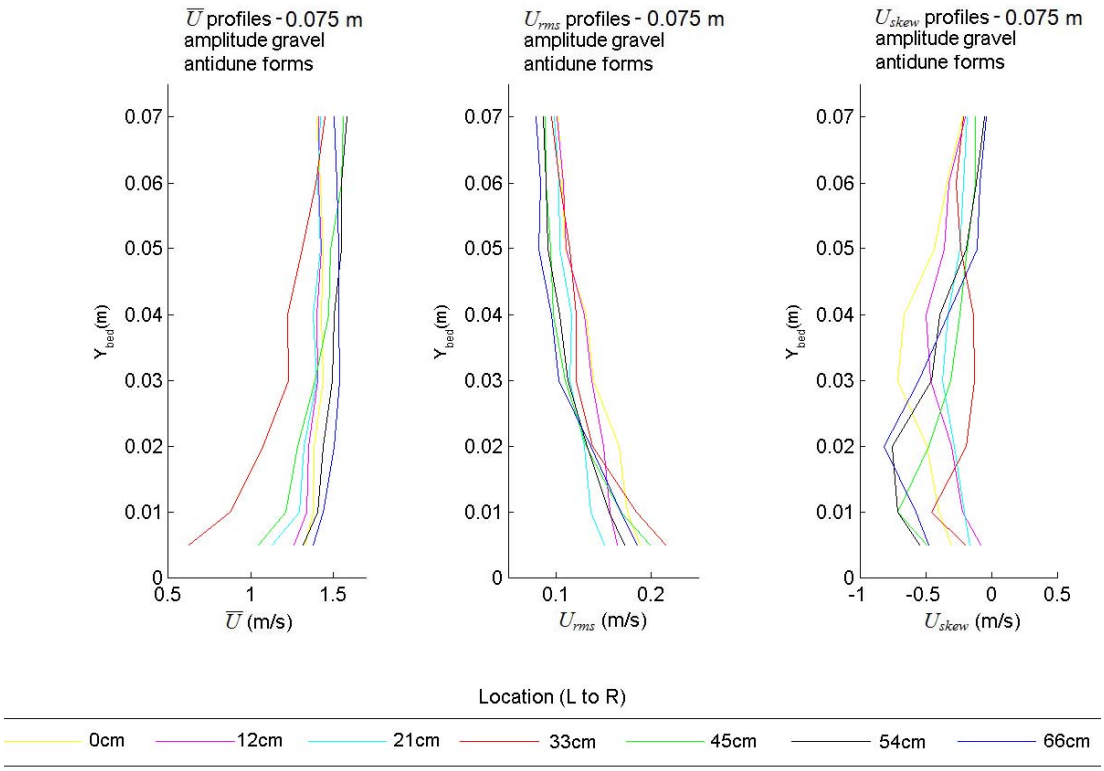

Figure 4.9 Profiles of $\overline{U}$, U_{rms} and U_{skew} for Flow above a 0.075 m Amplitude Gravel Antidune Bedform (ADV: 100 Hz)

4.1.2 $\overline{V}$, V_{rms} and V_{skew} for 0.025, 0.050 and 0.075 m Amplitude Gravel Antidune Bedforms

For the vertical velocity element, (Figures 4.10 – 4.12) $\overline{V}$ tends towards positive (away from the bed) in the flow profile above the bed of the upstream antidunes crest and downstream flank, and in the upper flow profile above the downstream antidunes crest. Velocity tends towards negative (towards the bed) in the upper flow profile above the upstream antidunes flank and trough. As the amplitude increases, $\overline{V}$ values become increasingly negative in the upper flow profile on the downstream flank of the upstream antidune, and positive adjacent to the bed. On the upstream facing flank and crest of the downstream antidune $\overline{V}$ tends towards 0; this is interpreted as high velocity flow passing over the crest of the upstream antidune, and descending onto the mid flank of the downstream antidune. As for U_{rms} previously, it is thought that V_{rms} is highest near the bed, due to the variability of instantaneous velocities in the boundary layer above the antidune bedforms. Likewise, V_{skew} tends to be negatively skewed in the lower flow profile and positively skewed in the upper flow profile. This indicates the

occurrence of generally high instantaneous velocities in the upper flow profile with occasional very high instantaneous velocities, and generally high instantaneous velocities with some very low instantaneous velocities in the lower flow profile. The line plots of $\overline{V}$, V_{rms} and V_{skew}, in Figure 4.13 – 4.15 further illustrate these trends. The change from more vertically symmetric, to vertically asymmetric flow profiles can be seen toward the trough region, profiles which become increasingly asymmetric as the antidune amplitude increases.

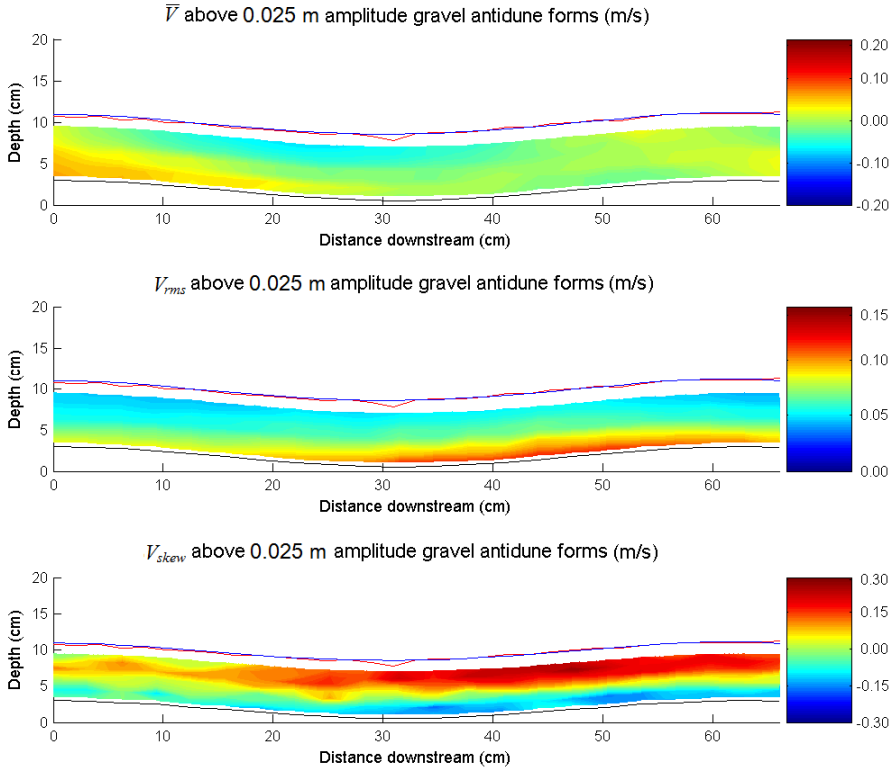

Figure 4.10 $\overline{V}$, V_{rms} and V_{skew} above a 0.025 m Amplitude Gravel Antidune Bedform (ADV: 100 Hz)

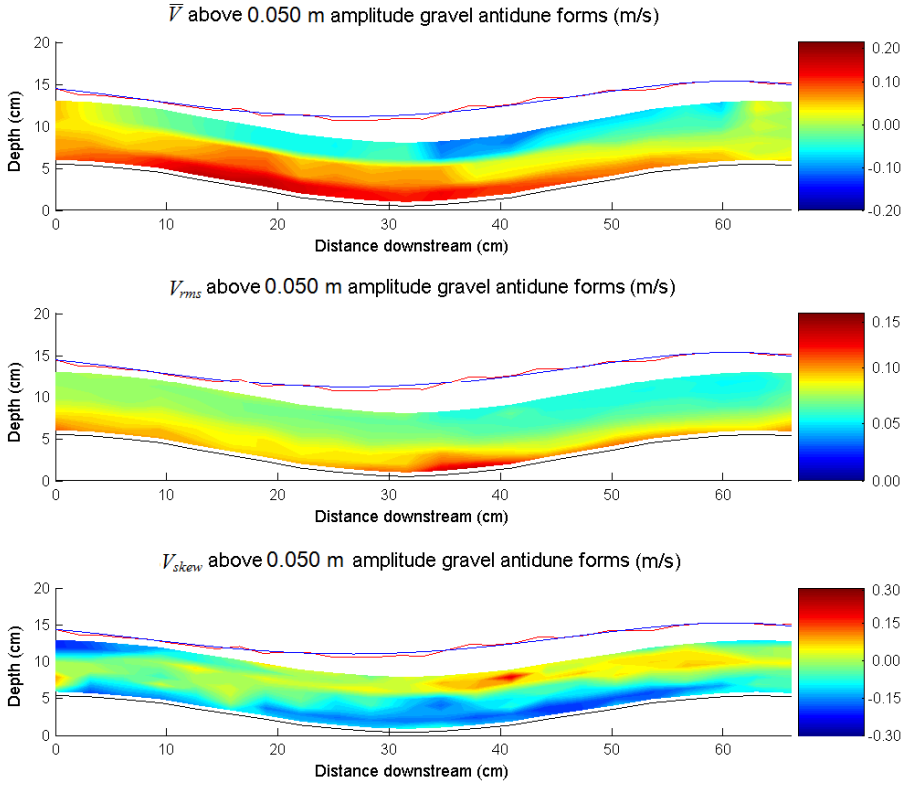

Figure 4.11 $\overline{V}$, V_{rms} and V_{skew} above a 0.050 m Amplitude Gravel Antidune Bedform (ADV: 100 Hz)

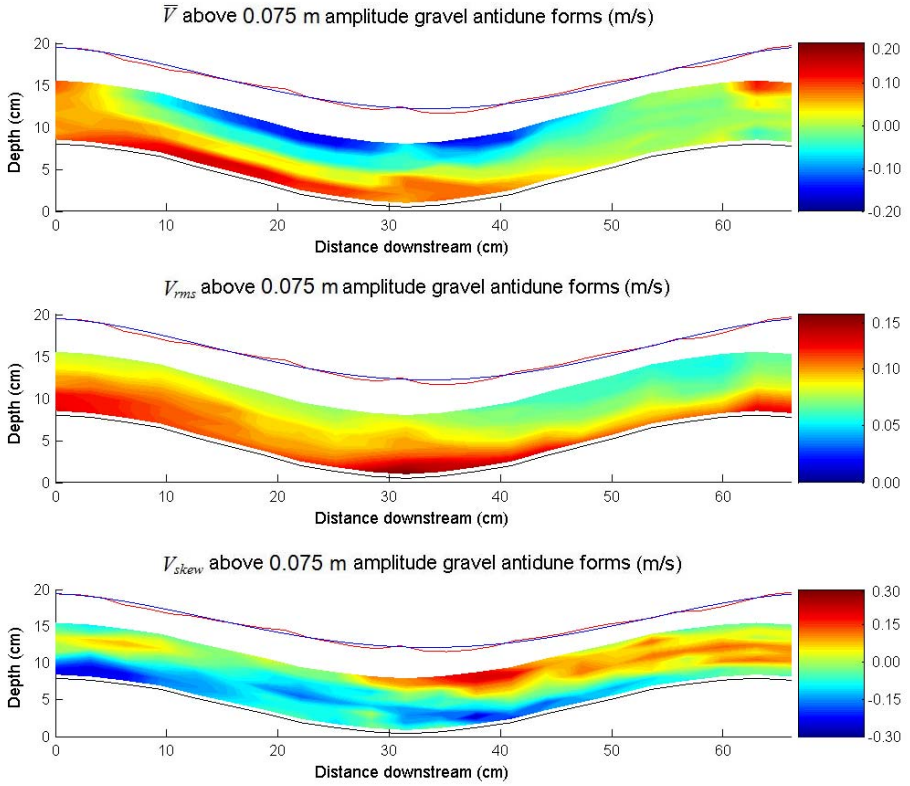

Figure 4.12 $\overline{V}$, V_{rms} and V_{skew} above a 0.075 m Amplitude Gravel Antidune Bedform (ADV: 100 Hz)

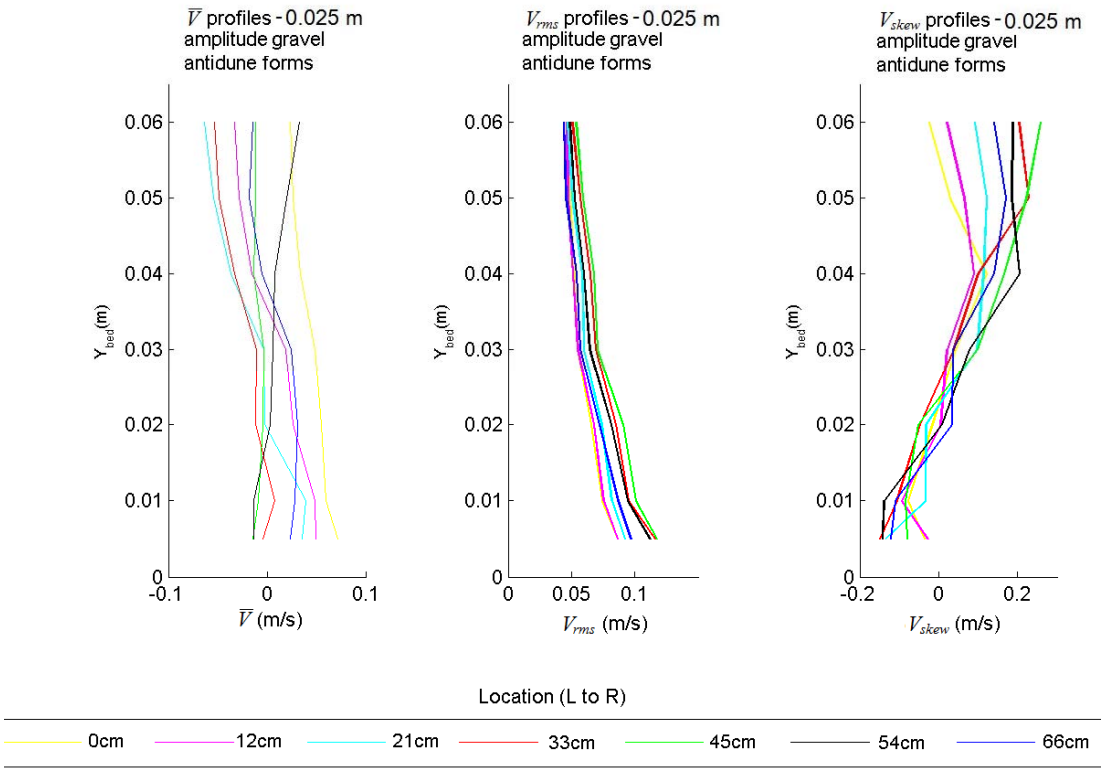

Figure 4.13 Profiles of $\overline{V}$, V_{rms} and V_{skew} for Flow above a 0.025 m Amplitude Gravel Antidune Bedform (ADV: 100 Hz)

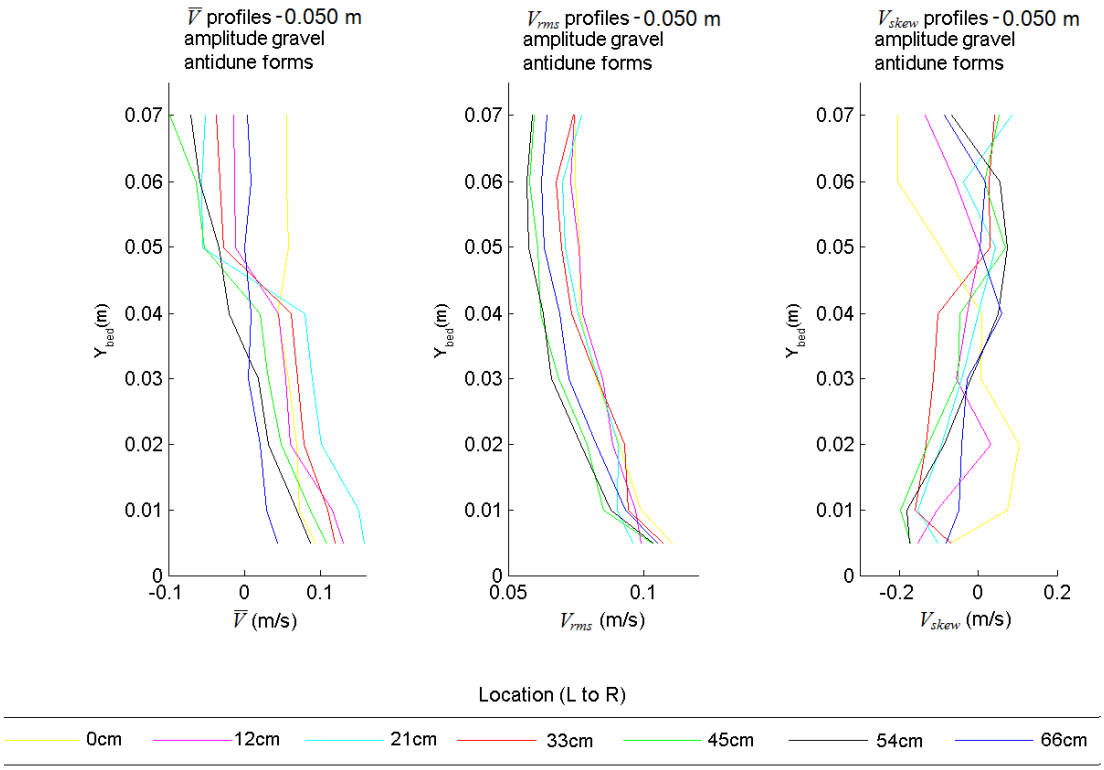

Figure 4.14 Profiles of $\overline{V}$, V_{rms} and V_{skew} for Flow above a 0.050 m Amplitude Gravel Antidune Bedform (ADV: 100 Hz)

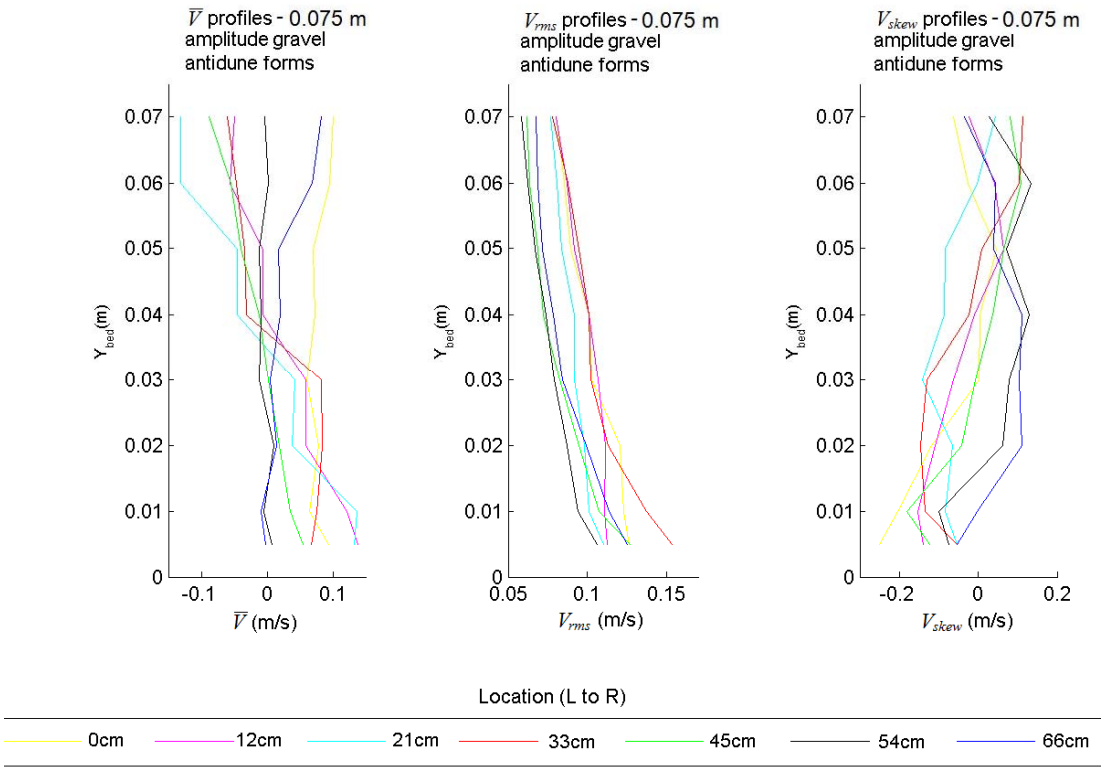

Figure 4.15 Profiles of $\overline{V}$, V_{rms} and V_{skew} for Flow above a 0.075 m Amplitude Gravel Antidune Bedform (ADV: 100 Hz)

4.1.3 $\overline{W}$, W_{rms} and W_{skew} for 0.025, 0.050 and 0.075 m Amplitude Gravel Antidune Bedforms

In terms of $\overline{W}$ (Figures 4.16 – 4.18) there is a clear, oscillating side to side secondary flow element in the flume, giving blocks of positive and negative $\overline{W}$. W_{rms} values are highest at the bed (especially in the trough), and W_{skew} values most negatively skewed at the bed, due to the retarding of flow in the boundary layer, and the lack of friction near the water surface.

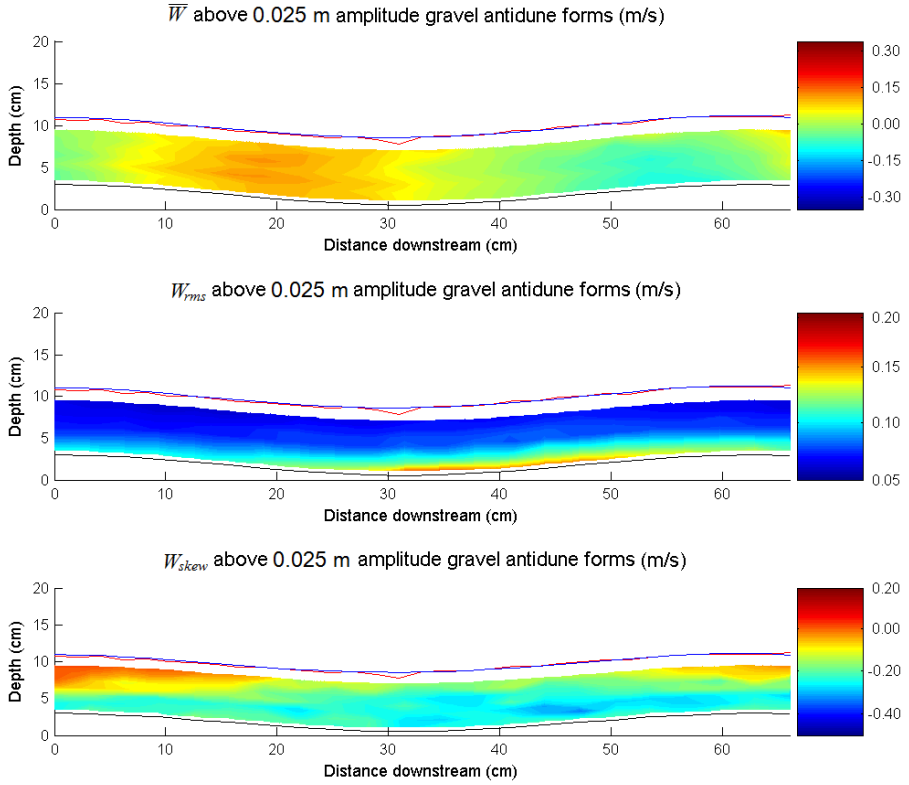

Figure 4.16 $\overline{W}$, W_{rms} and W_{skew} above a 0.025 m Amplitude Gravel Antidune Bedform (ADV: 100 Hz)

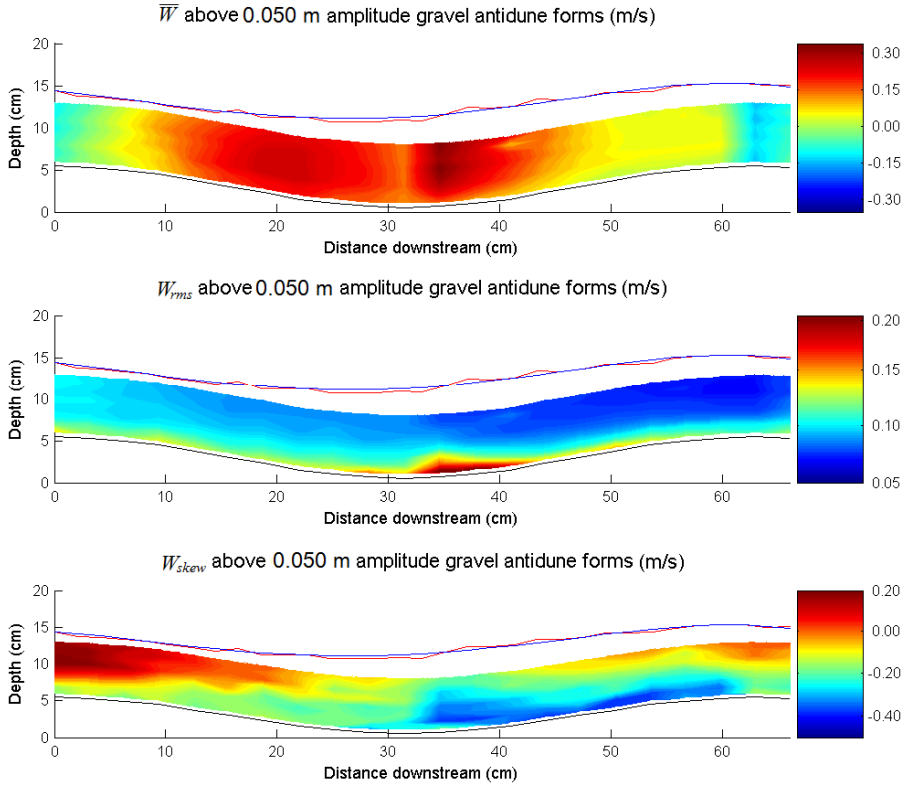

Figure 4.17 $\overline{W}$, W_{rms} and W_{skew} above a 0.050 m Amplitude Gravel Antidune Bedform (ADV: 100 Hz)

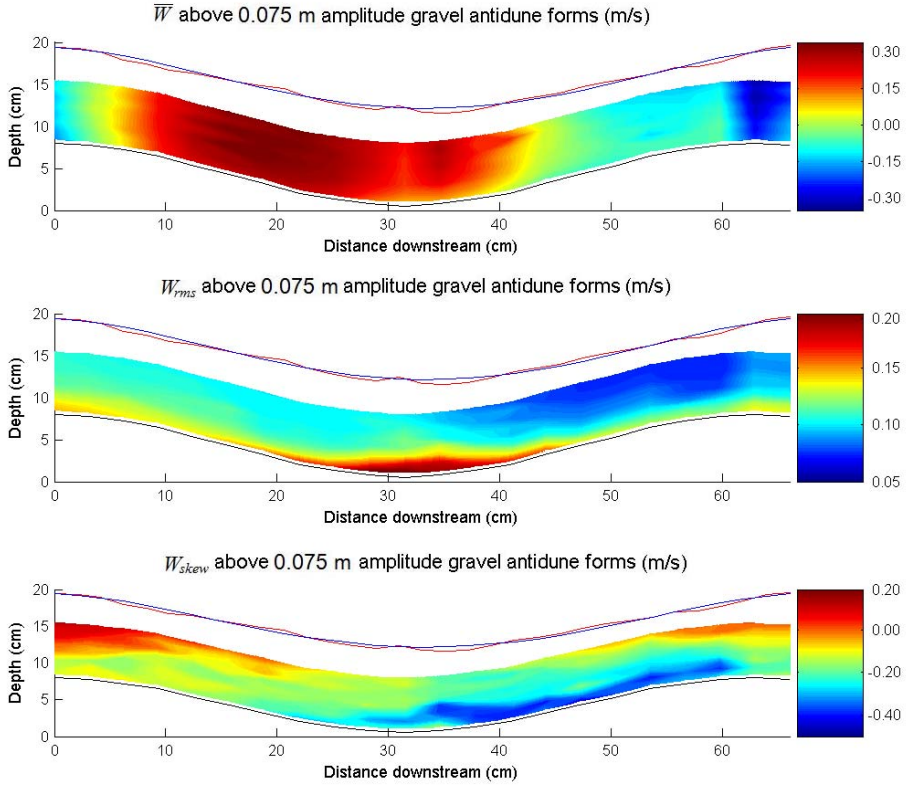

Figure 4.18 $\overline{W}$, W_{rms} and W_{skew} above a 0.075 m Amplitude Gravel Antidune Bedform (ADV: 100 Hz)

4.1.4 TKE and τ_R for 0.025, 0.050 and 0.075 m Amplitude Gravel Antidune Bedforms

Plots of TKE and τ_R (Figures 4.19 – 4.21) show close agreement, and indicate stresses are highest adjacent to the bed, especially on the upstream facing flank of the downstream antidune. An increase in TKE and τ_R can be seen with increasing amplitude, as well as the increasing concentration of stress in the trough region. The increases in τ_R towards the bed and particularly at the trough can be seen in the respective line plots in Figures 4.4c, 4.5c and 4.6c. The change from more vertically symmetric, to vertically asymmetric flow profiles can be seen toward the trough region, profiles which become increasingly asymmetric as antidune amplitude increases.

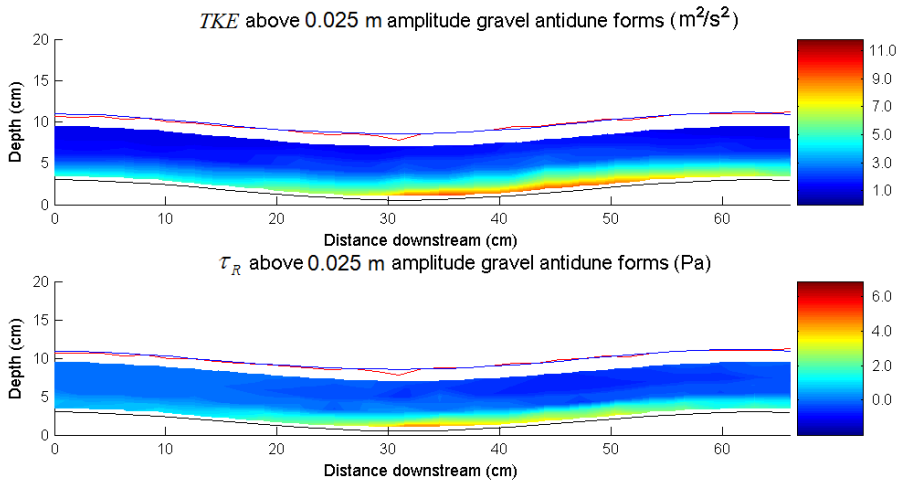

Figure 4.19 TKE **and** τ_R **above a 0.025 m Amplitude Gravel Antidune Bedform (ADV: 100 Hz)**

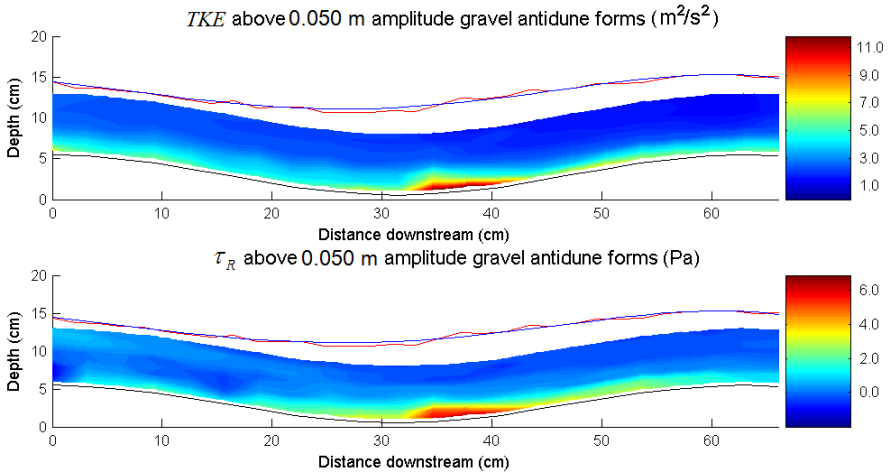

Figure 4.20 TKE **and** τ_R **above a 0.050 m Amplitude Gravel Antidune Bedform (ADV: 100 Hz)**

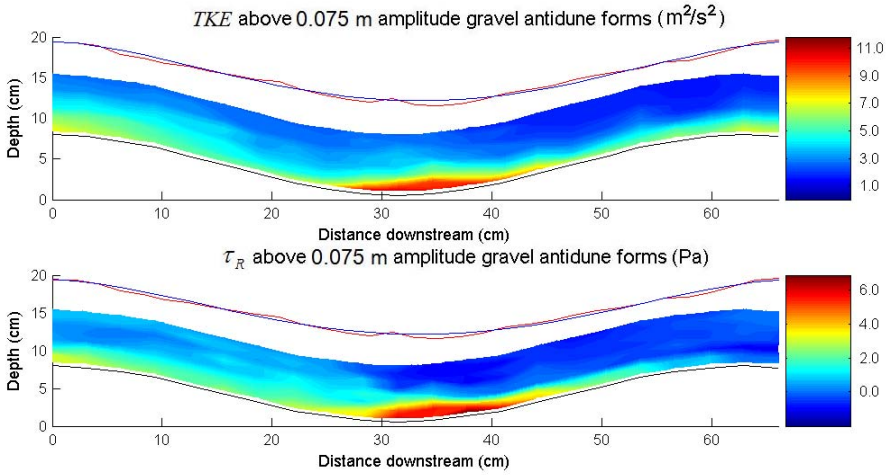

Figure 4.21 TKE **and** τ_R **above a 0.075 m Amplitude Gravel Antidune Bedform (ADV: 100 Hz)**

4.1.5 Quadrant Analysis – Gravel Antidune Bedforms 100 Hz

Proportion of Time Events above a Hole Size of 2 for 0.025, 0.050 and 0.075 m Amplitude Gravel Antidune Bedforms

Quadrant Analysis (Figures 4.22 – 4.24) shows that the for all quadrants, the most events above the hole size occur in the upper parts of the flow. This is perhaps due to the effects of water surface level fluctuations and the in-phase nature of the water surface and bed; however these events in the upper flow are important in suspension transport, rather than in sediment transport along the bed. There are though significant events of sedimentological importance adjacent to the bed occurring for between 0.5% and 3% of the velocity record.

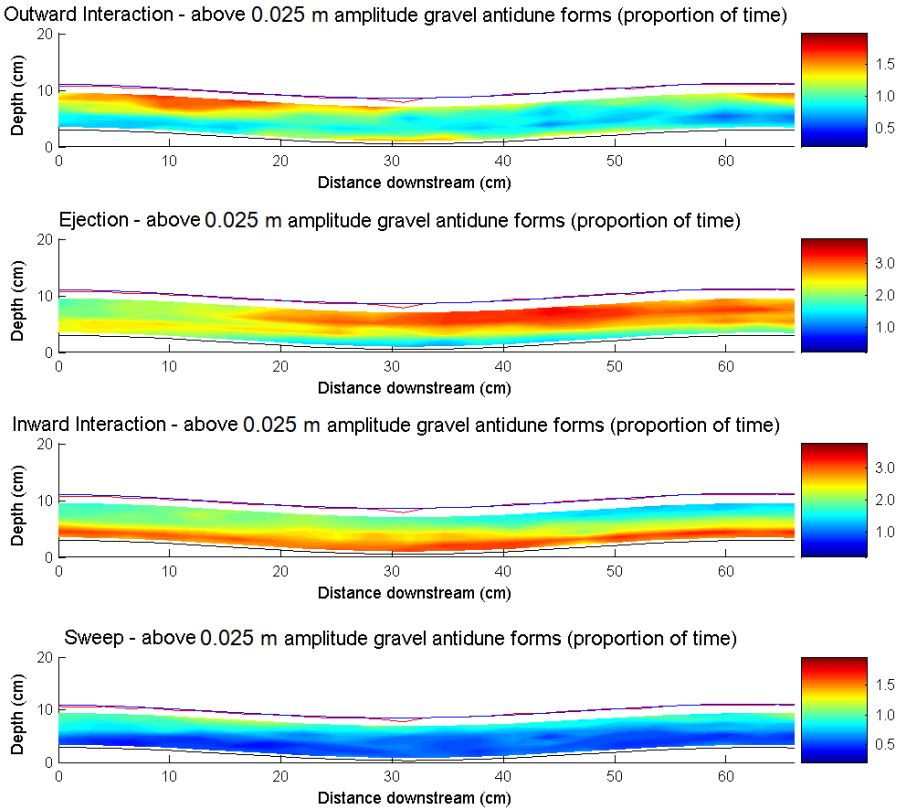

Figure 4.22 Quadrant Analysis of Turbulence above a 0.025 m Amplitude Gravel Antidune Bedform (ADV: 100 Hz, Proportion of Time Events above Hole Size = 2)

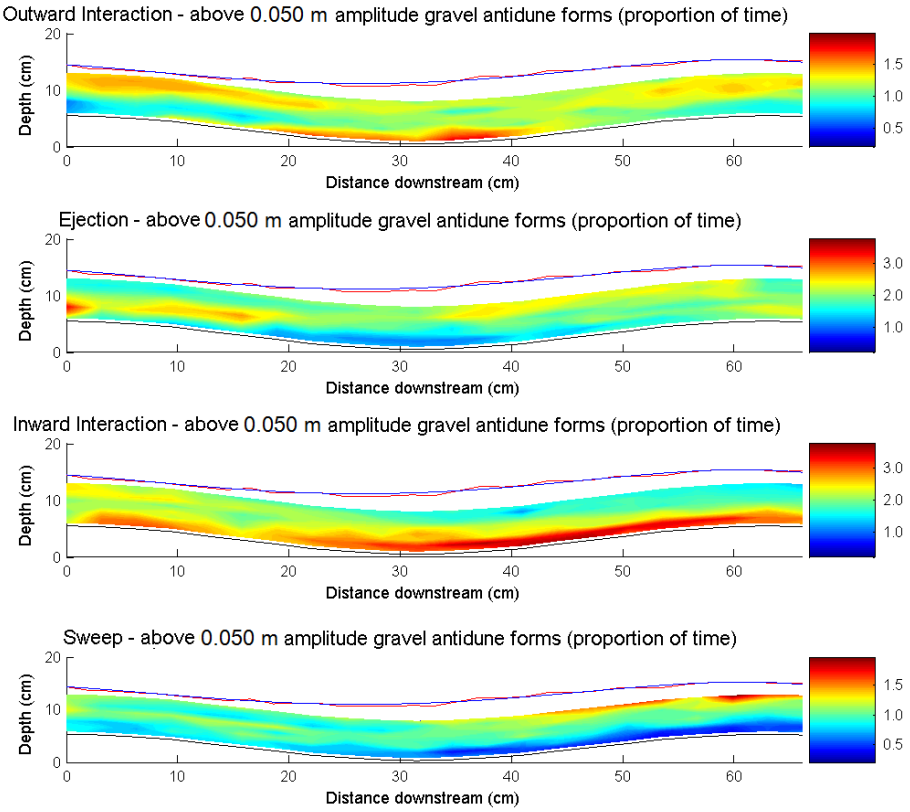

Figure 4.23 Quadrant Analysis of Turbulence above a 0.050 m Amplitude Gravel Antidune Bedform (ADV: 100 Hz, Proportion of Time Events above Hole Size = 2)

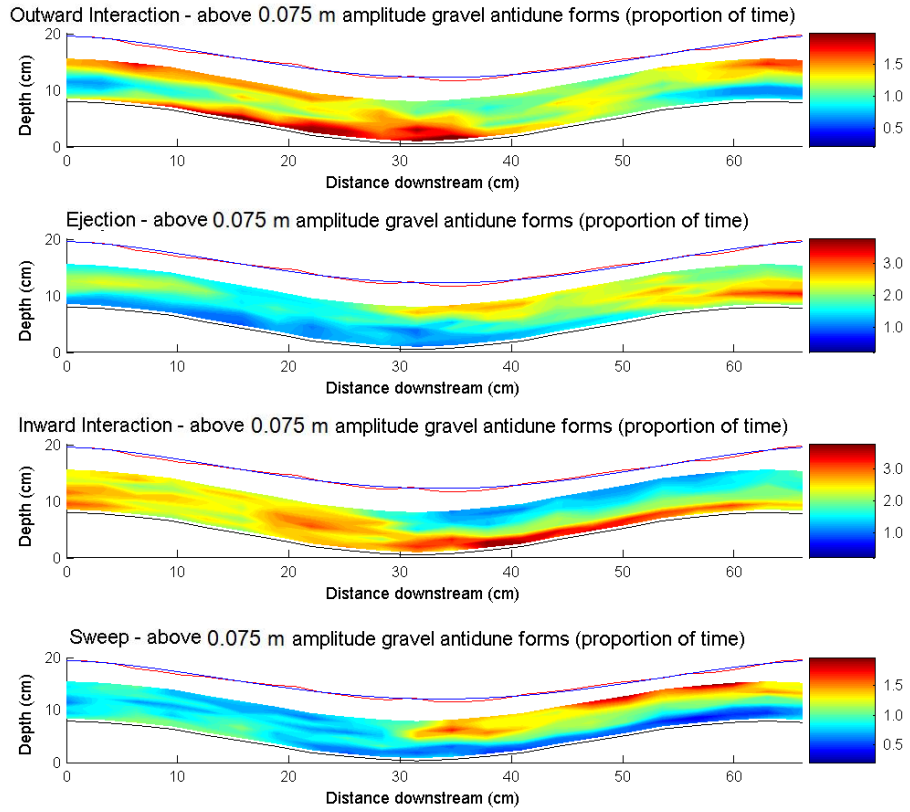

Figure 4.24 Quadrant Analysis of Turbulence above a 0.075 m Amplitude Gravel Antidune Bedform (ADV: 100 Hz, Proportion of Time Events above Hole Size = 2)

Mean Stress for Events above a Hole Size of 2 for 0.025, 0.050 and 0.075 m Amplitude Gravel Antidune Bedforms

Investigation of the average $|u'v'|$ stresses (Figures 4.25 – 4.27) during these events indicates that the highest $|u'v'|$ stresses occur adjacent to the bed. The distribution of stresses is for the 0.025 m amplitude relatively even, along the entire boundary layer, however for all quadrants it becomes increasingly concentrated in the trough region as antidune amplitude increases. In particular, $|u'v'|$ values during ejections increase from -0.08 m/s in the boundary layer of 0.025 m amplitude antidunes, to -0.1 m/s in the trough region of 0.050 m and 0.075 m amplitude antidunes. Likewise for sweeps, $|u'v'|$ values increase from -0.08 m/s in the boundary layer of 0.025 m amplitude antidunes, to -0.095 m/s in the trough region of 0.050 m and 0.075 m amplitude antidunes.

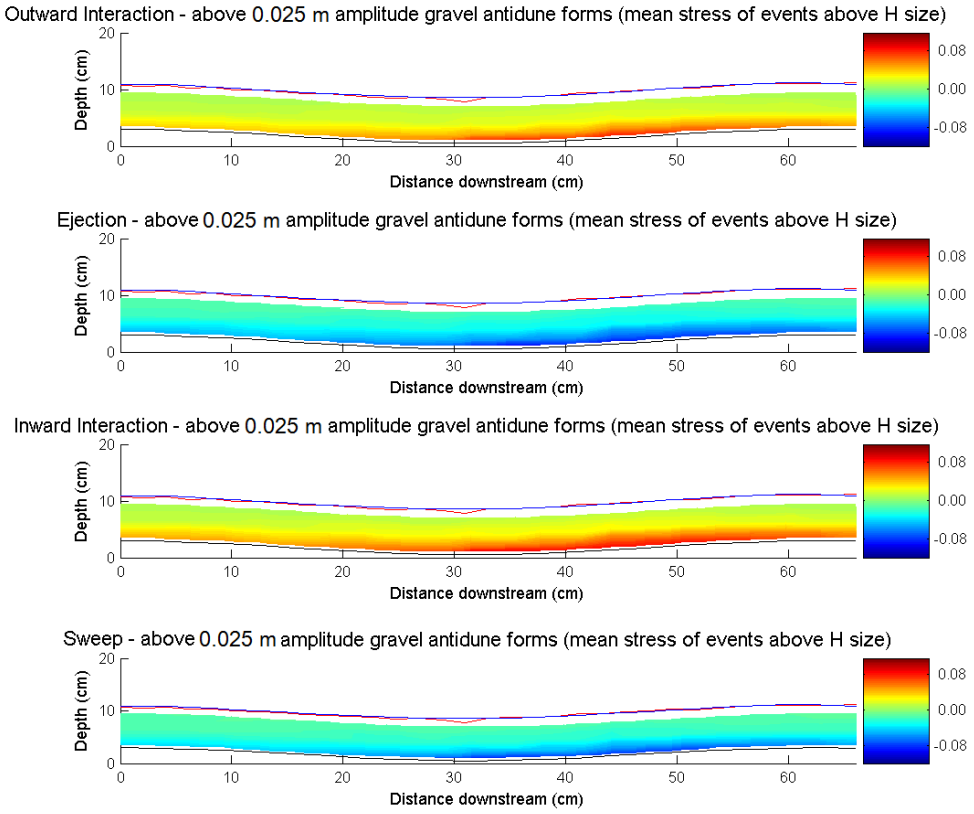

Figure 4.25 Quadrant Analysis of Turbulence above a 0.025 m Amplitude Gravel Antidune Bedform (ADV: 100 Hz, Mean Stress for Events above Hole Size = 2)

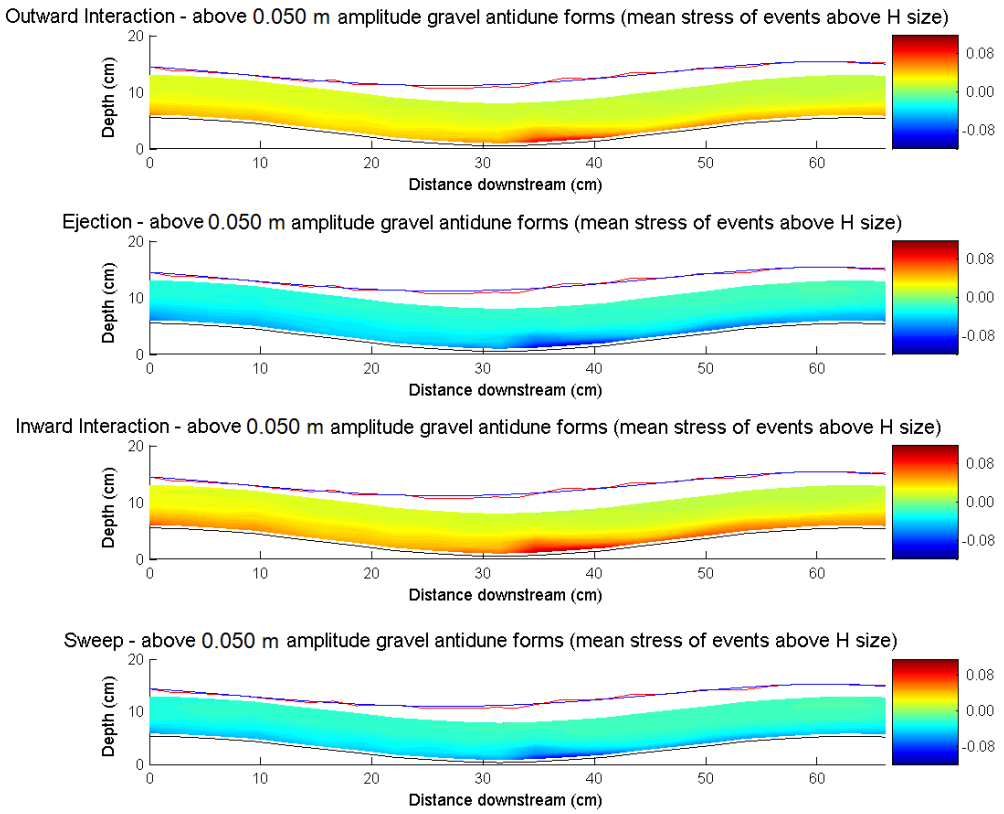

Figure 4.26 Quadrant Analysis of Turbulence above a 0.050 m Amplitude Gravel Antidune Bedform (ADV: 100 Hz, Mean Stress for Events above Hole Size = 2)

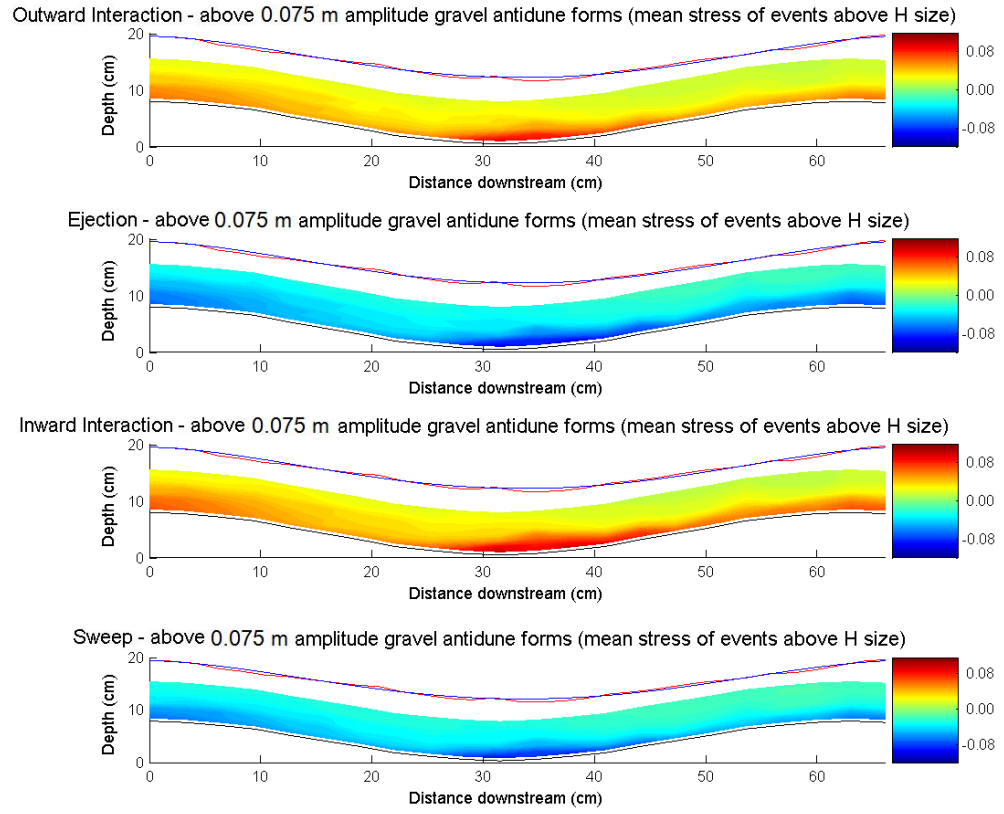

Figure 4.27 Quadrant Analysis of Turbulence above a 0.075 m Amplitude Gravel Antidune Bedform (ADV: 100 Hz, Mean Stress for Events above Hole Size = 2)

4.1.6 P, R and TI for 0.025, 0.050 and 0.075 m Amplitude Gravel Antidune Bedforms

Plots of P, R and TI (Figures 4.28 – 4.30), support the above results and interpretations. P is concentrated in the trough between each antidune bedform, maximum values, remaining at similar levels for 0.025 m, 0.050 m and 0.075 m amplitude antidunes. R, a measure of the presence and integrity of any boundary layer, is relatively evenly distributed (R is 0.15) over 0.025 m antidunes, indicating a constant thin semi-developed boundary layer, although this value is perhaps on the low side, values of 0.3 – 0.5 having been found previously. However, with increasing antidune amplitude the highest values of R occur in the trough region. As for P, TI is highest in the trough between each antidune for all three amplitudes of bedform. Values of TI increase from 0.19, to 0.28 and the 0.5 with increasing antidune amplitude; indicating the increasingly turbulent hydrodynamic environment as antidunes steepen. The increases in TI towards the bed, and particularly at the trough can be seen in the respective line plots in Figures 4.4b, 4.5b and 4.6b.

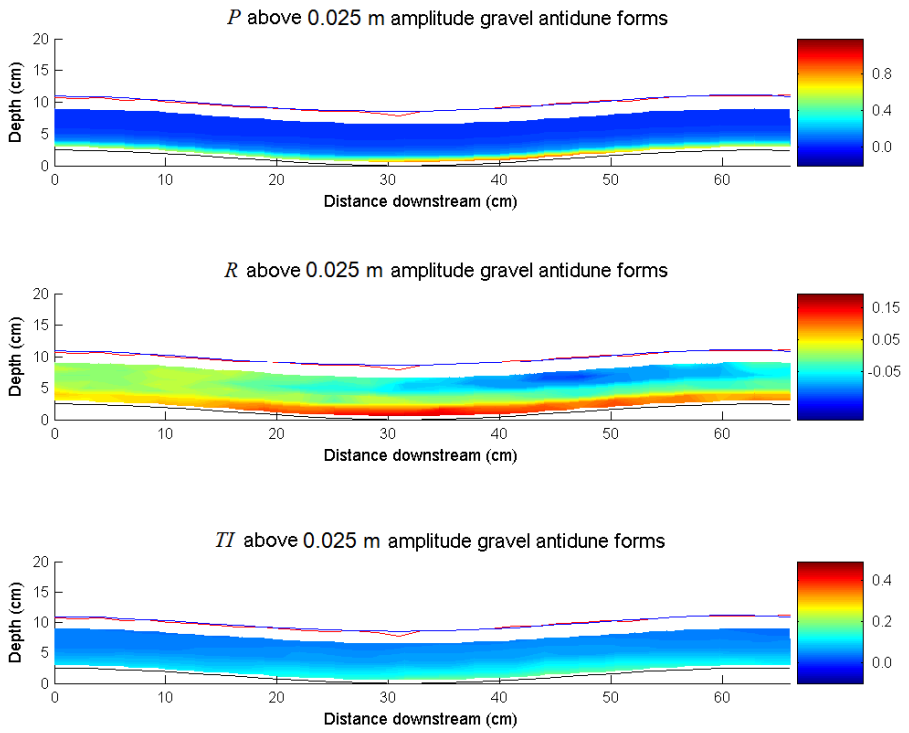

Figure 4.28 P, R and TI above a 0.025 m Amplitude Gravel Antidune Bedform (ADV: 100 Hz)

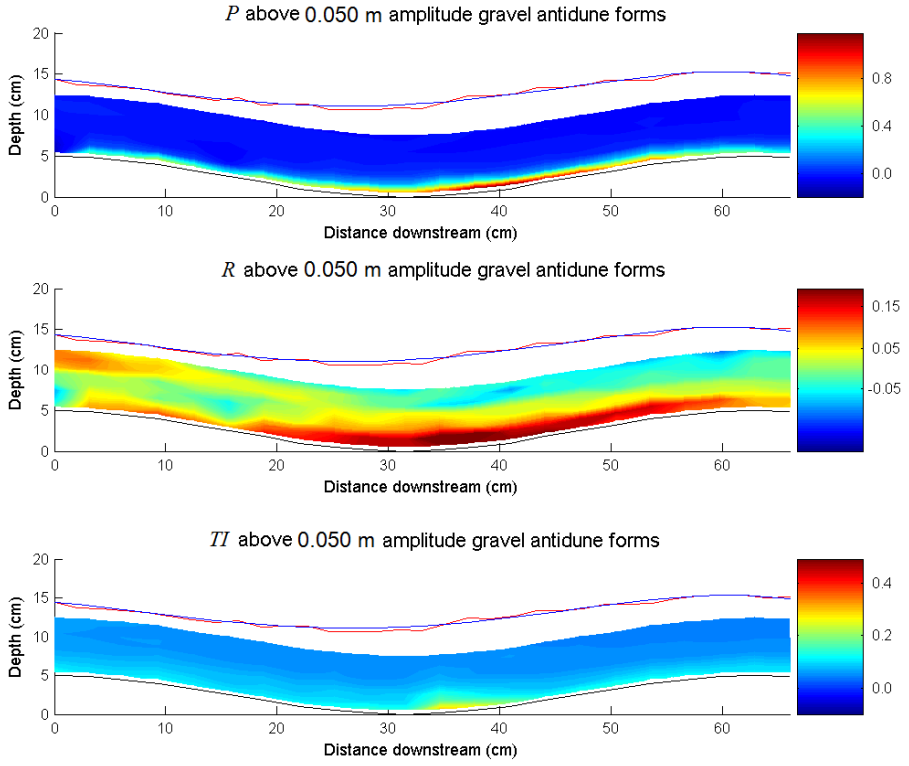

Figure 4.29 P, R and TI above a 0.050 m Amplitude Gravel Antidune Bedform (ADV: 100 Hz)

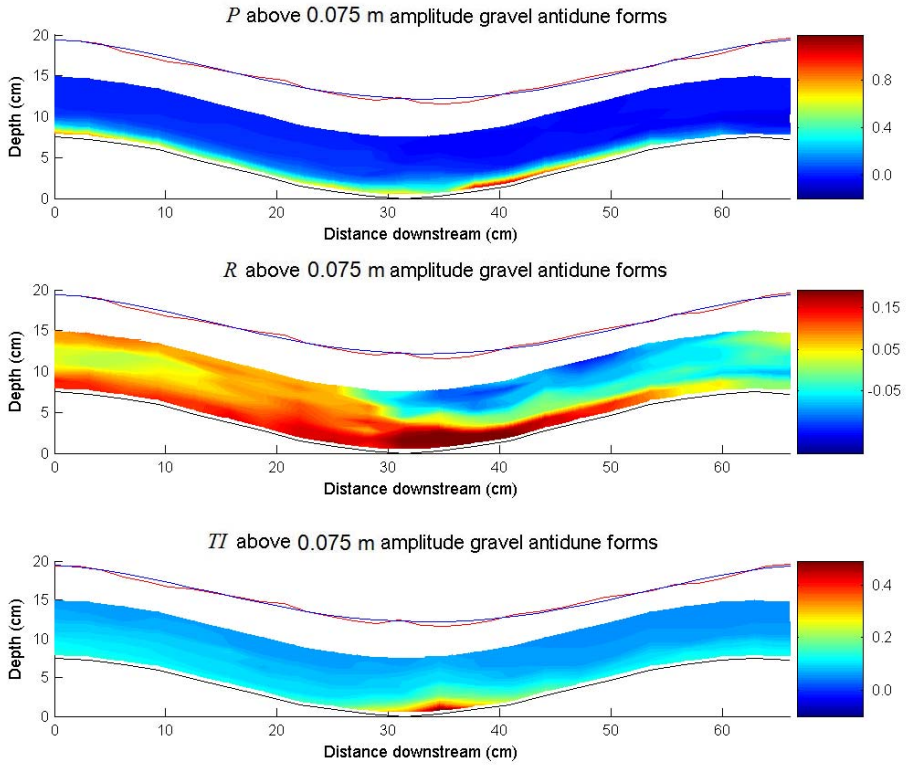

Figure 4.30 P, R and TI above a 0.075 m Amplitude Gravel Antidune Bedform (ADV: 100 Hz)

Summary – Turbulence Structure over Gravel Surfaced Antidunes

100 Hz ADV investigations show that the most intense turbulence occurs in the trough region. In this lower trough region there is a marked reduction in $\overline{U}$ values, and a corresponding increase in U_{rms} and V_{rms}. This difference in values of $\overline{U}$ between the lower trough and upper parts of the flow increases ($\overline{U}$ values in the lower trough being 75%, 52% and 44% of the $\overline{U}$ values in the flow profile above for 0.025, 0.050 and 0.075 m amplitude forms respectively) as antidune amplitude increases. In the region between the downstream end of the trough and lower slope of the downstream antidune, values of turbulent stresses increase progressively[1]: TI [0.17, 0.27 and 0.5], τ_R [4.5, 6 and 6.5], and TKE [9, 11.5 and 11], whilst Q2 (ejections) and Q4 (sweeps) become increasingly spatially concentrated into this region. The magnitude of these values increases as the antidune amplitude increases. It is postulated that the intense turbulence associated with steepening antidunes, may lead to rapid erosion in the trough, steepening the downstream bedform which in turn causes the standing wave to collapse.

[1]Numbers in square brackets refer to values for 0.025, 0.050 and 0.075 m amplitude antidune bedforms respectively.

Box 4.1 Summary of Flow Profile and Turbulence over Gravel Surfaced Antidunes (100Hz)

4.2 Spatial Characteristics of Turbulence over Openwork-Gravel Antidune Bedforms (ADV 25 Hz)

4.2.1 $\overline{U}$, U_{rms} and U_{skew} for 0.025 and 0.050 m Amplitude Openwork-Gravel Antidune Bedforms

With increasing amplitude, significant changes can be seen in the distribution of $\overline{U}$ values over the gravel surfaced antidune bedforms. Over 0.025 m amplitude forms (Figure 4.31) velocities are in the region of 1.7 – 1.8 m/s for the majority of the flow profile. A thin boundary layer is present near the bed, velocities at the crests drop to 1.65 m/s and 1.5 m/s (upstream/downstream crests respectively), in the trough velocities drop as low as 1.3 m/s (0.74 of $\overline{U}$ in the upper parts of the flow). Again, these retarded velocities are notably skewed downstream of the trough onto the

upstream facing flank of the downstream antidune. Over 0.050 m amplitude forms (Figure 4.32) velocities are in the region of 1.2 – 1.5 m/s for the majority of the flow profile. Only a poorly developed boundary layer is present near the bed, velocities at the crests drop to 1.25 m/s. However, in the trough velocities drop as low as 0.5 m/s (0.37 of $\overline{U}$ in the upper parts of the flow). Again, a skew is evident downstream of the trough onto the upstream facing flank of the downstream antidune. Towards the bed, and at the trough, the increasing divergence from velocities in the upper parts of the flow can be seen in the respective normalised velocity plots in Figures 4.33a – 4.34a. As for the gravel surfaced antidune bedform inserts, for all amplitudes of openwork gravel antidune bedform insert (Figures 4.31 – 4.32) the highest U_{rms} values occur adjacent to the bed. Similarly, for both amplitudes U_{skew} is mostly negative, with the lowest skewness occurring at the surface and bed, and the highest values in the middle parts of the flow. Initially, a low skewness occurs adjacent to the bed (high friction, always small instantaneous velocities), more negative skewness being present in the middle parts of the flow. For the 0.050 m amplitude form, a positive skew develops in a small region on the lower upstream facing flank of the downstream antidune – this has been interpreted as the hollow bed allowing higher instantaneous velocities to occur nearer the bed. The line plots of $\overline{U}$, U_{rms} and U_{skew}, in Figures 4.35 – 4.36 further illustrate these trends.

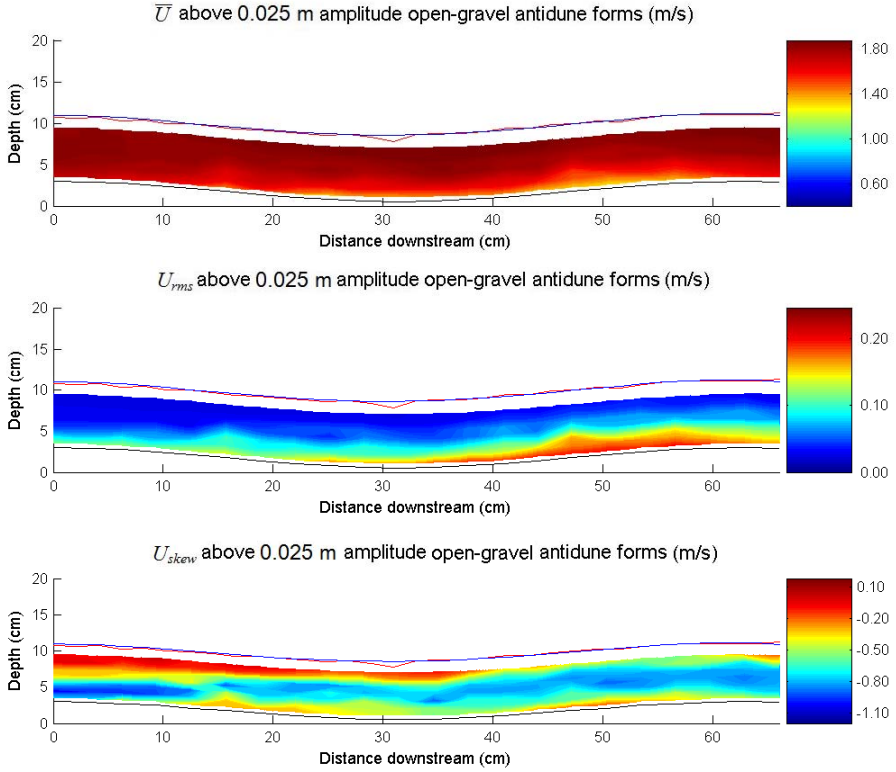

Figure 4.31 $\overline{U}$, U_{rms} and U_{skew} above a 0.025 m Amplitude Openwork-Gravel Antidune Bedform (ADV: 25 Hz)

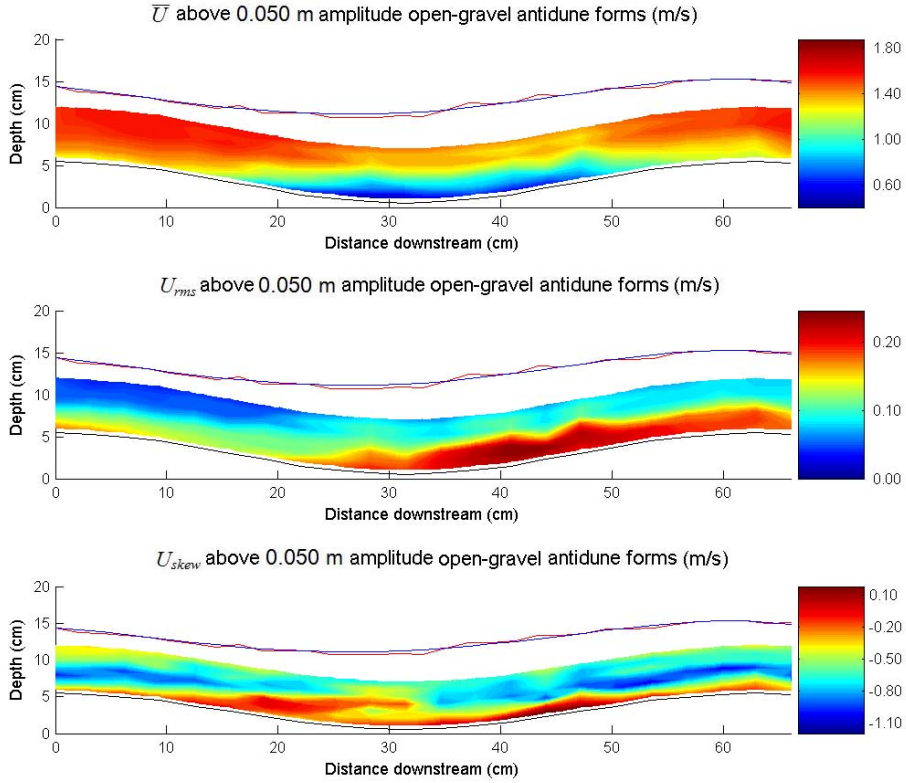

Figure 4.32 $\overline{U}$, U_{rms} and U_{skew} above a 0.050 m Amplitude Openwork-Gravel Antidune Bedform (ADV: 25 Hz)

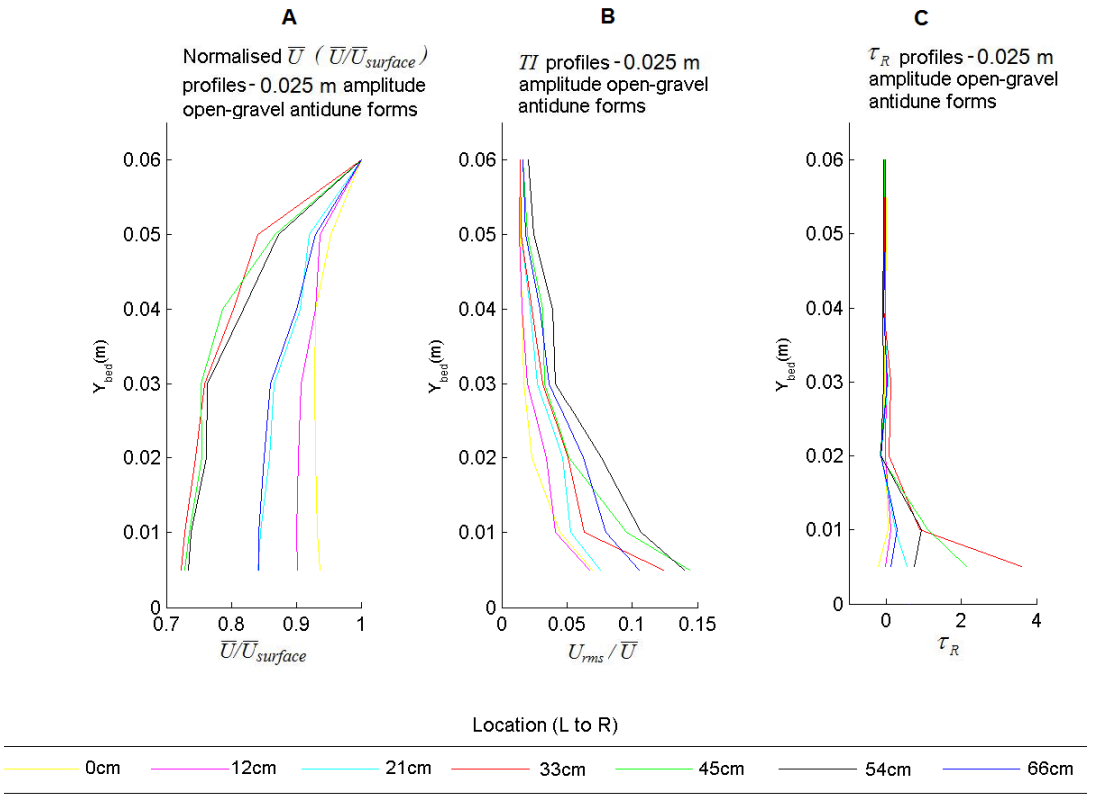

Figure 4.33 $\overline{U}$ *(normalised)*, TI and τ_R Profiles for Flow above a 0.025 m Amplitude Openwork-Gravel Antidune Bedform (ADV: 25 Hz)

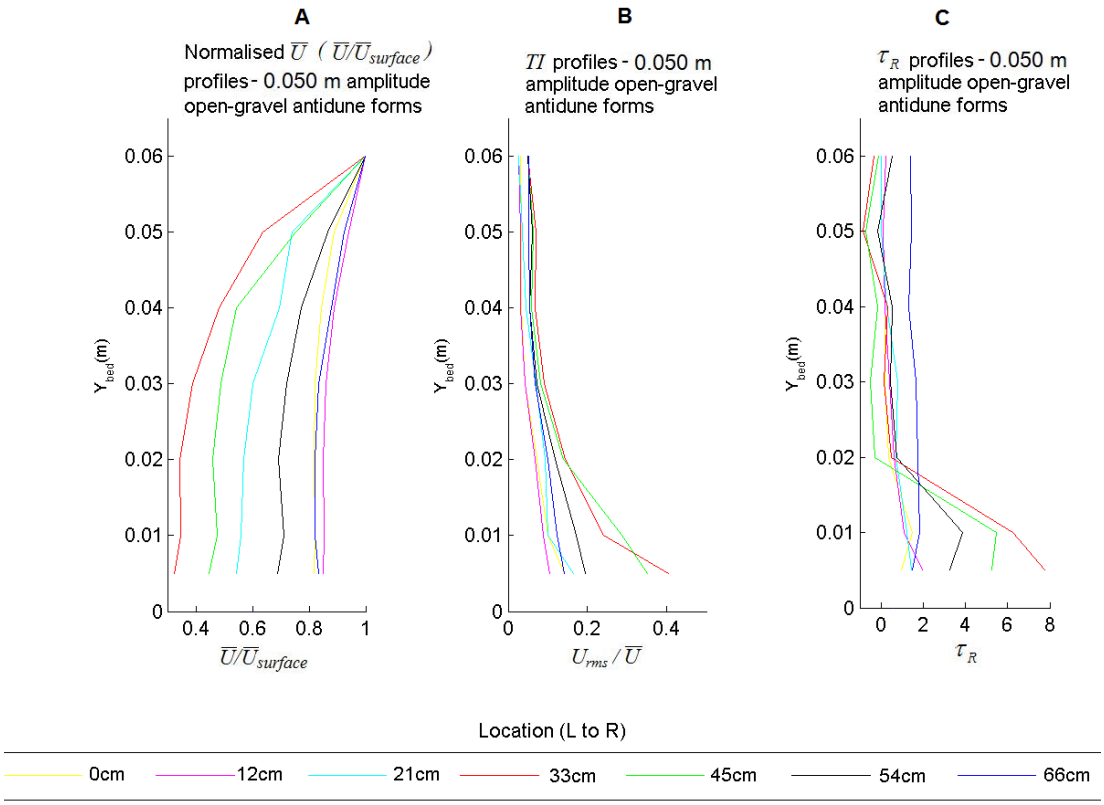

Figure 4.34 $\overline{U}$ *(normalised)*, TI and τ_R Profiles for flow above a 0.050 m Amplitude Openwork-Gravel Antidune Bedform (ADV: 25 Hz)

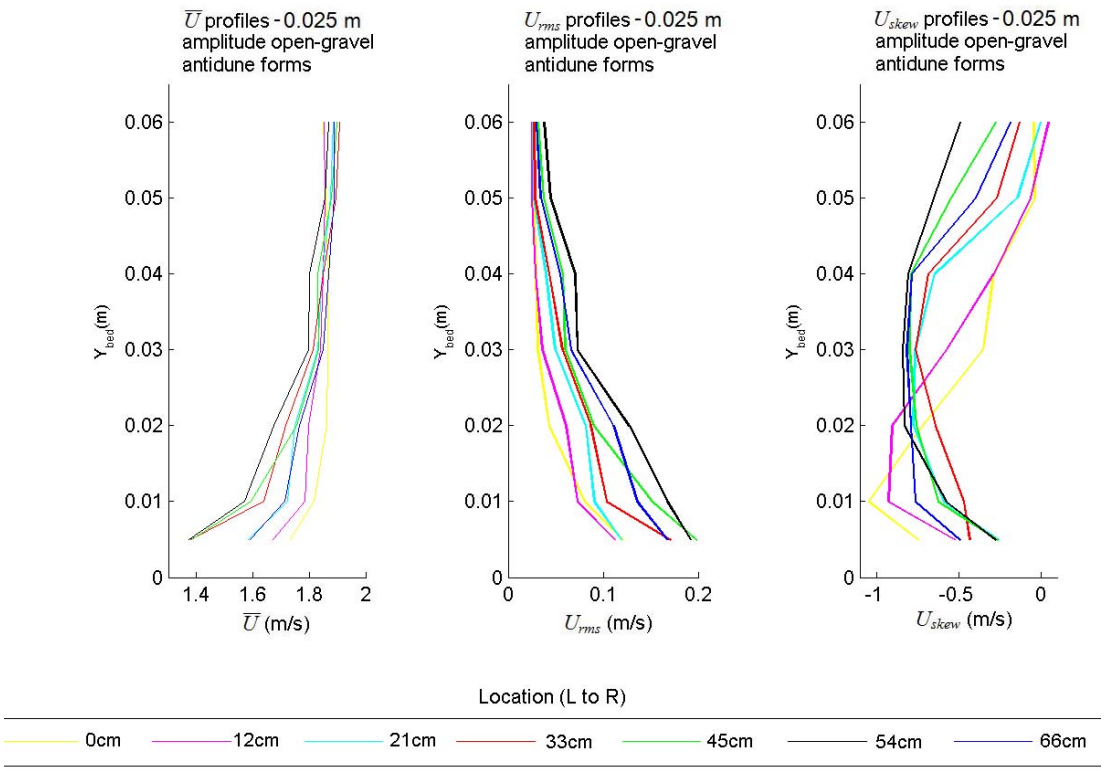

Figure 4.35 Profiles of $\overline{U}$, U_{rms} and U_{skew} for Flow above a 0.025 m Amplitude Openwork-Gravel Antidune Bedform (ADV: 25 Hz)

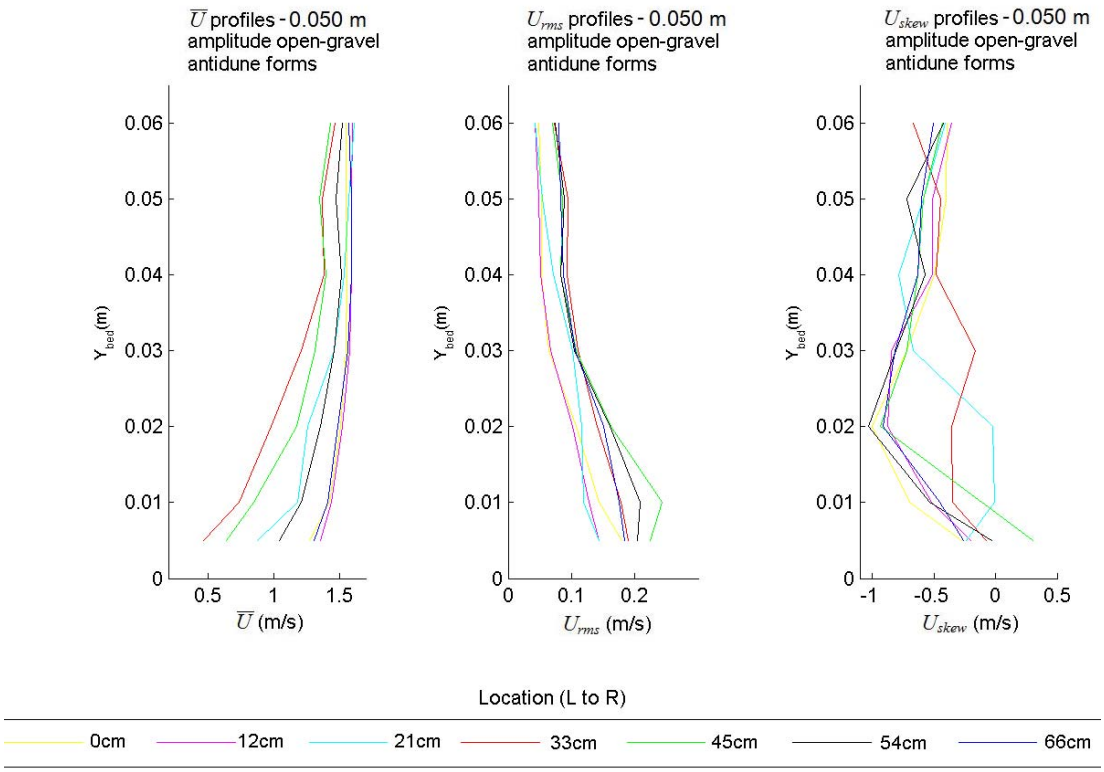

Figure 4.36 Profiles of $\overline{U}$, U_{rms} and U_{skew} for Flow above a 0.050 m Amplitude Openwork-Gravel Antidune Bedform (ADV: 25 Hz)

4.2.2 $\overline{V}$, V_{rms} and V_{skew} for 0.025 and 0.050 m Amplitude Openwork-Gravel Antidune Bedforms

For the vertical velocity element, (Figures 4.37 – 4.38) $\overline{V}$ tends towards positive (away from the bed) in the flow profile above the bed of the upstream antidunes crest and downstream flank, and in the upper parts of the flow above the downstream antidunes upstream facing flank. Velocity tends towards negative (towards the bed) in the upper parts of the flow above the upstream antidunes flank and trough. As the amplitude increases, $\overline{V}$ values become increasingly negative in the upper parts of the flow on the downstream flank of the upstream antidune, and positive adjacent to the bed. Reasons for the very low $\overline{V}$ values above the upstream crest and very high $\overline{V}$ values above the downstream crest are unclear. As for U_{rms}, V_{rms} is highest near the bed, due to the variability of instantaneous velocities in the boundary layer above the antidune bedforms. Likewise, V_{skew} tends to be negatively skewed in the lower parts of the flow and positively skewed in the upper parts of the flow. This indicates the occurrence of generally high instantaneous velocities in the upper parts of the flow with occasional very high instantaneous velocities, and generally high instantaneous velocities with some very low instantaneous velocities in the lower part of the flow. The line plots of $\overline{V}$, V_{rms} and V_{skew}, in Figures 4.39 – 4.40 further illustrate these trends. The change from more vertically symmetric, to vertically asymmetric flow can be seen toward the trough region, the flow becoming increasingly vertically asymmetric as antidune amplitude increases.

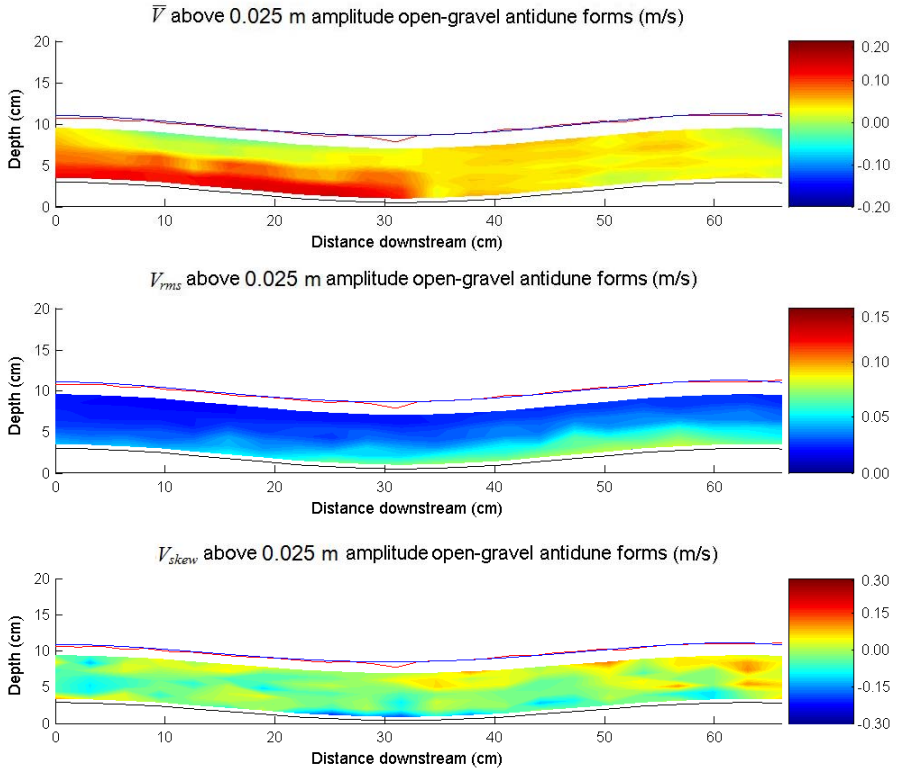

Figure 4.37 $\overline{V}$, V_{rms} and V_{skew} above a 0.025 m Amplitude Openwork-Gravel Antidune Bedform (ADV: 25 Hz)

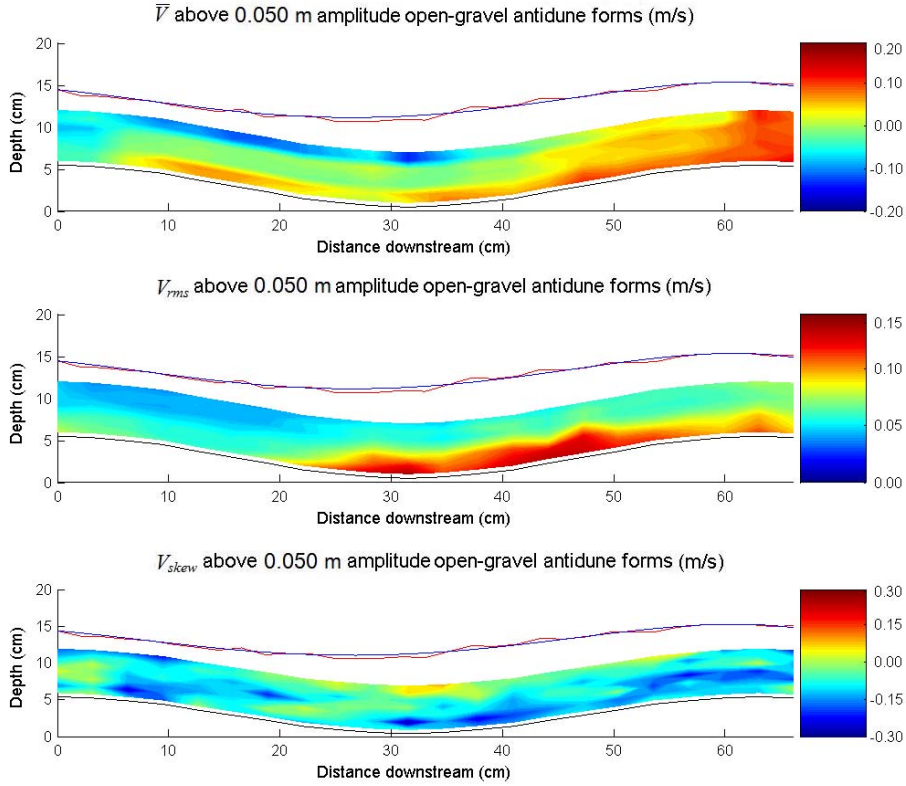

Figure 4.38 $\overline{V}$, V_{rms} and V_{skew} above a 0.050 m Amplitude Openwork-Gravel Antidune Bedform (ADV: 25 Hz)

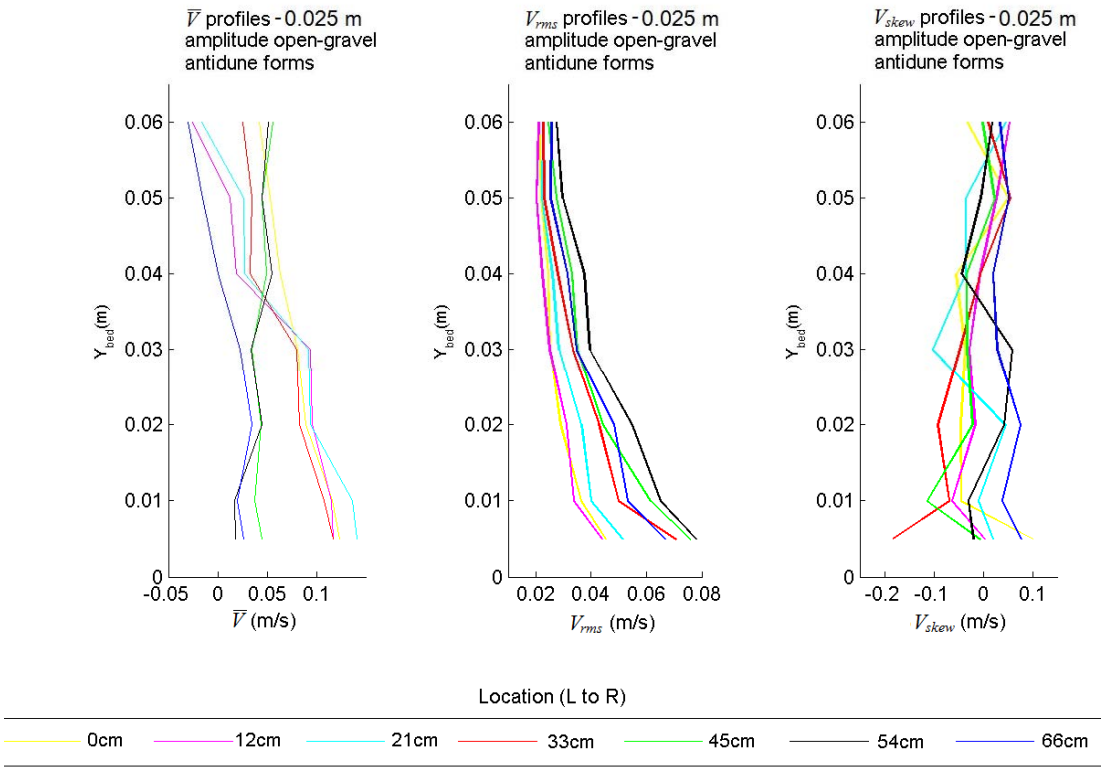

Figure 4.39 Profiles of $\overline{V}$, V_{rms} and V_{skew} for Flow above a 0.025 m Amplitude Openwork-Gravel Antidune Bedform (ADV: 25 Hz)

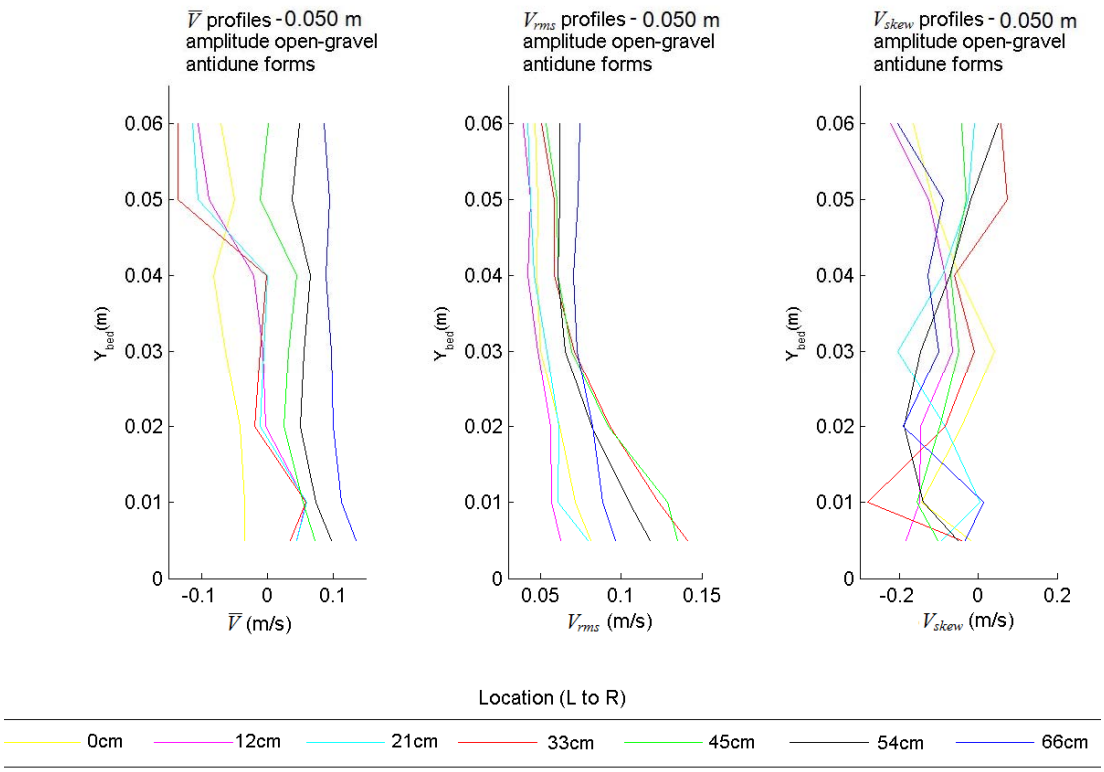

Figure 4.40 Profiles of $\overline{V}$, V_{rms} and V_{skew} for Flow above a 0.050 m Amplitude Openwork-Gravel Antidune Bedform (ADV: 25 Hz)

4.2.3 $\overline{W}$, W_{rms} and W_{skew} for 0.025 and 0.050 m Amplitude Openwork-Gravel Antidune Bedforms

In terms of $\overline{W}$ (Figures 4.41 - 4.42) there is a clear, oscillating side to side secondary flow element in the flume, giving blocks of positive and negative $\overline{W}$. As for gravel surface antidune bedform inserts W_{rms} values are highest at the bed - especially in the trough, and W_{skew} values most negatively skewed at the bed, due to the retarding of flow in the boundary layer, and the lack of friction near the water surface.

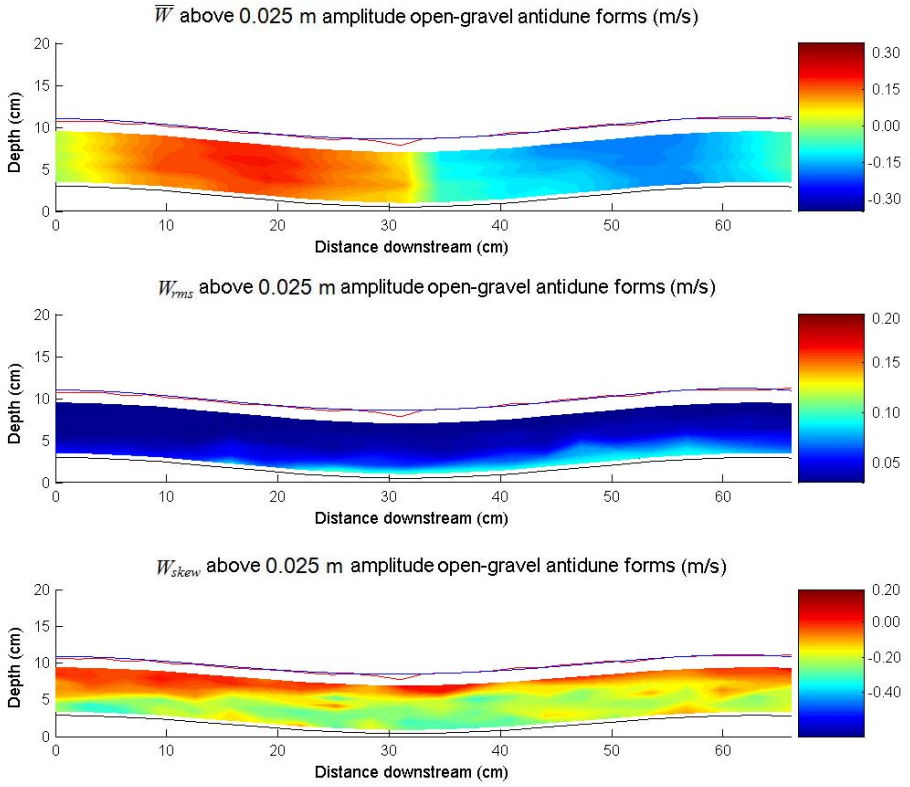

Figure 4.41 $\overline{W}$, W_{rms} and W_{skew} above a 0.025 m Amplitude Openwork-Gravel Antidune Bedform (ADV: 25 Hz)

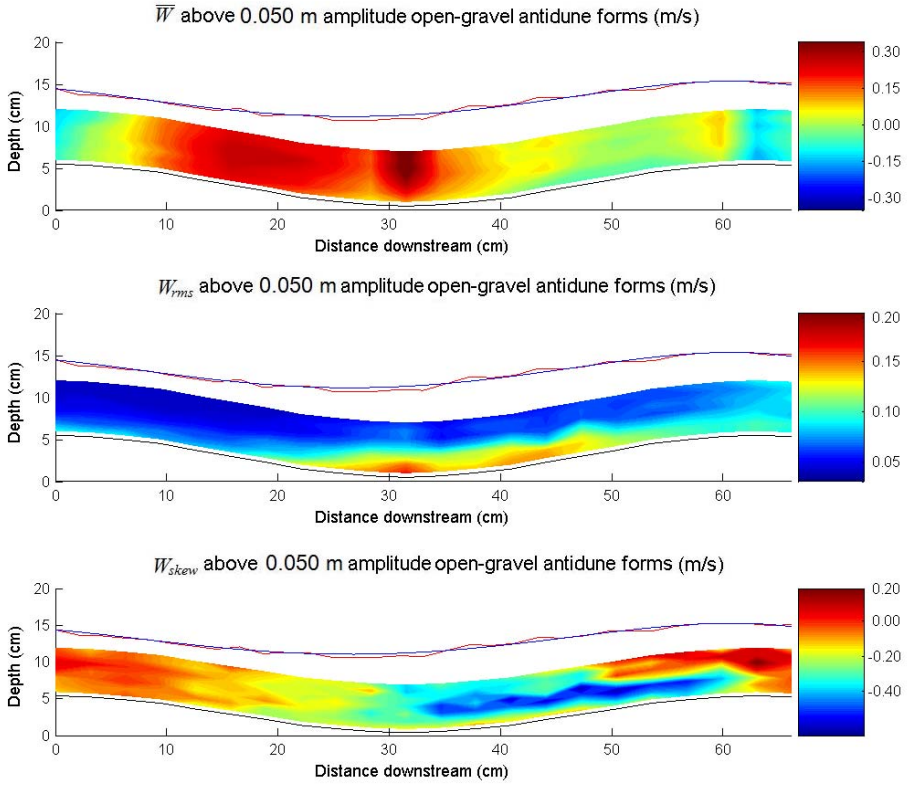

Figure 4.42 $\overline{W}$, W_{rms} and W_{skew} above a 0.050 m Amplitude Openwork-Gravel Antidune Bedform (ADV: 25 Hz)

4.2.4 TKE and τ_R for 0.025 and 0.050 m Amplitude Openwork-Gravel Antidune Bedforms

Plots of TKE and τ_R (Figures 4.43 – 4.44) show close agreement, and indicate stresses are highest adjacent to the bed, especially on the upstream facing flank of the downstream antidune. An increase in TKE and τ_R can be seen with increasing amplitude, as well as the increasing concentration of stress in the trough region. The increases in τ_R towards the bed and particularly at the trough can be seen in the respective line plots in Figures 4.33c– 4.34c. The change from more vertically symmetric, to vertically asymmetric flow can be seen toward the trough region, flow becoming increasingly vertically asymmetric as antidune amplitude increases.

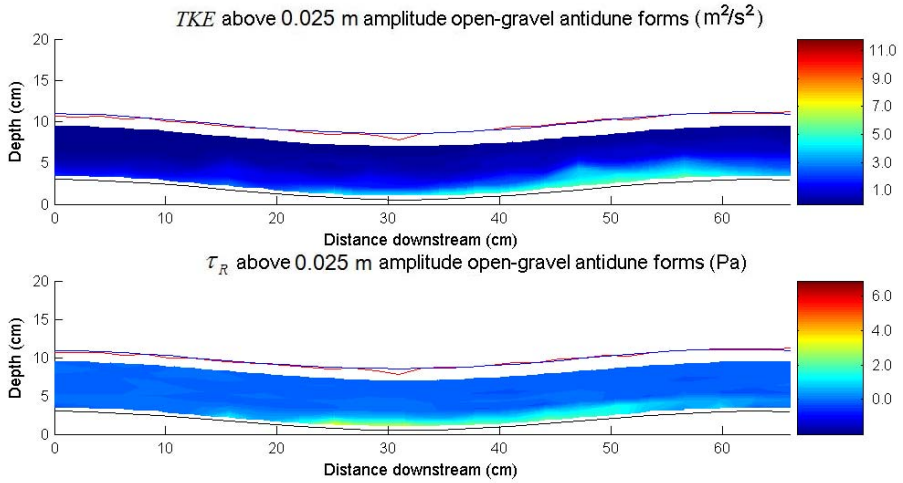

Figure 4.43 TKE **and** τ_R **above a 0.025 m Amplitude Openwork-Gravel Antidune Bedform (ADV: 25 Hz)**

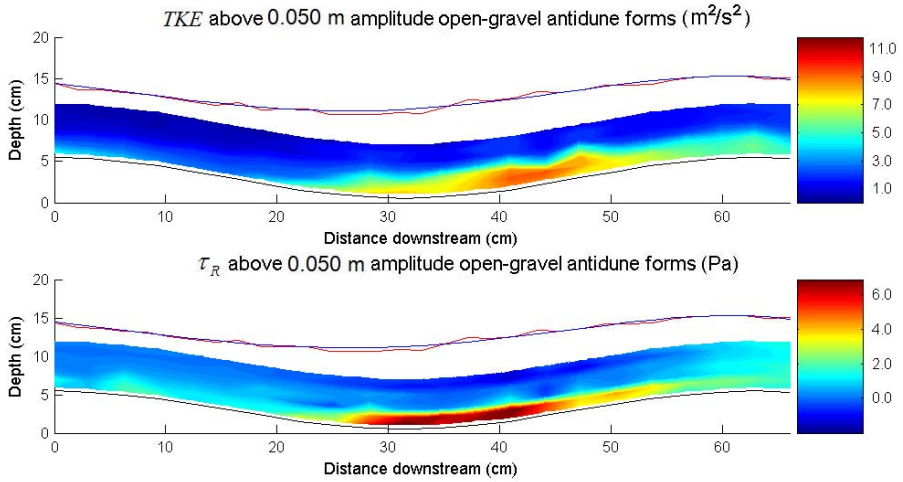

Figure 4.44 TKE **and** τ_R **above a 0.050 m Amplitude Openwork-Gravel Antidune Bedform (ADV: 25 Hz)**

4.2.5 Quadrant Analysis – Openwork-Gravel Antidune Bedforms 25 Hz

Proportion of Time Events above a Hole Size of 2 for 0.025, 0.050 m Amplitude Openwork-Gravel Antidune Bedforms

Quadrant Analysis (Figures 4.45 – 4.46) shows that for all quadrants, the most events above the hole size occur in the upper parts of the flow. Significant events of sedimentological importance occur adjacent to the bed for between 0.5% and 4% of the velocity record.

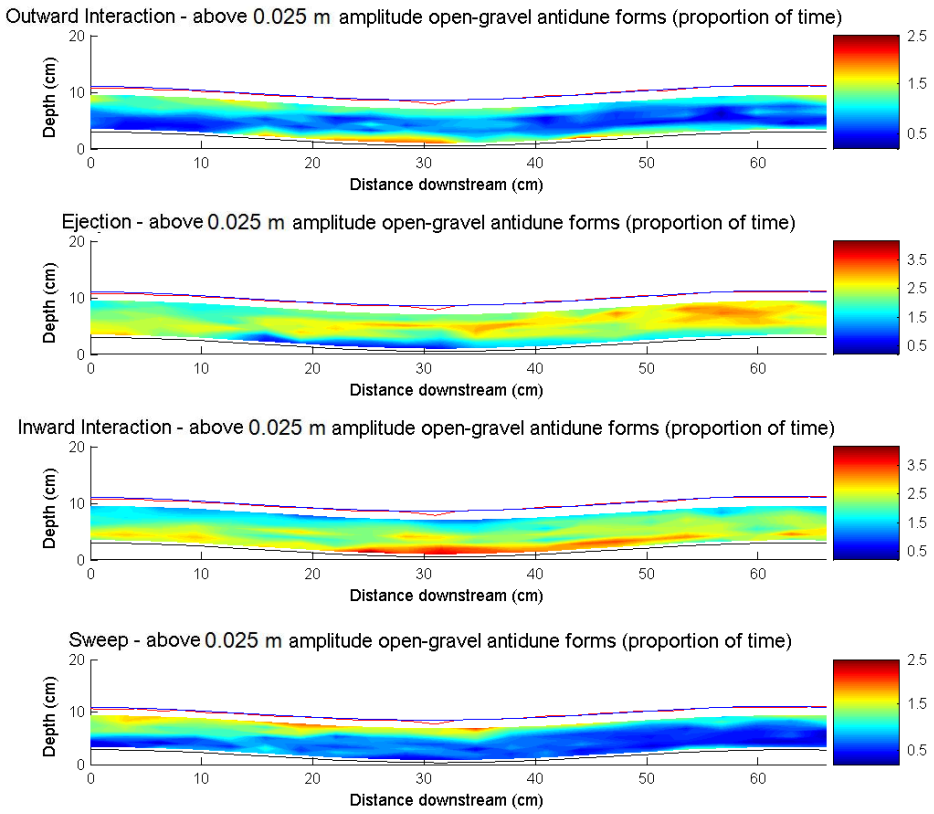

Figure 4.45 Quadrant Analysis of Turbulence above a 0.025 m Amplitude Openwork-Gravel Antidune Bedform (ADV: 25 Hz, Proportion of Time Events above Hole Size = 2)

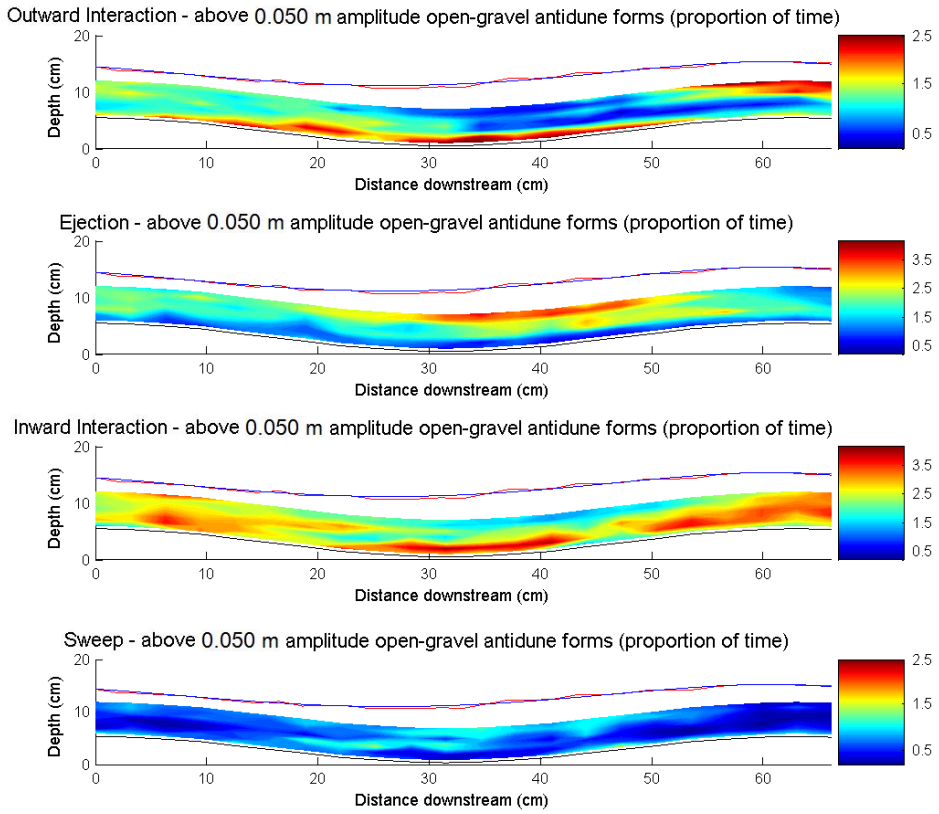

Figure 4.46 Quadrant Analysis of Turbulence above a 0.050 m Amplitude Openwork-Gravel Antidune Bedform (ADV: 25 Hz, Proportion of Time Events above Hole Size = 2)

Mean Stress for Events above a Hole Size of 2 for 0.025, 0.050 m Amplitude Gravel Antidune Bedforms

Investigation of the average $|u'v'|$ stresses (Figures 4.47 – 4.48) during these events indicates that the highest $|u'v'|$ stresses occur adjacent to the bed. The distribution of stresses is for the 0.025 m amplitude spread along the majority of the boundary layer, however for all quadrants it becomes increasingly concentrated and intense in the trough region as antidune amplitude increases. In particular, $|u'v'|$ values during ejections increase from -0.05 m/s in the boundary layer of 0.025 m amplitude antidunes, to -0.085 m/s in the trough region of 0.050 m amplitude antidunes. Likewise for sweeps, $|u'v'|$ values increase from -0.045 m/s in the boundary layer of 0.025 m amplitude antidunes, to -0.085 m/s in the trough region of 0.050 m amplitude antidunes.

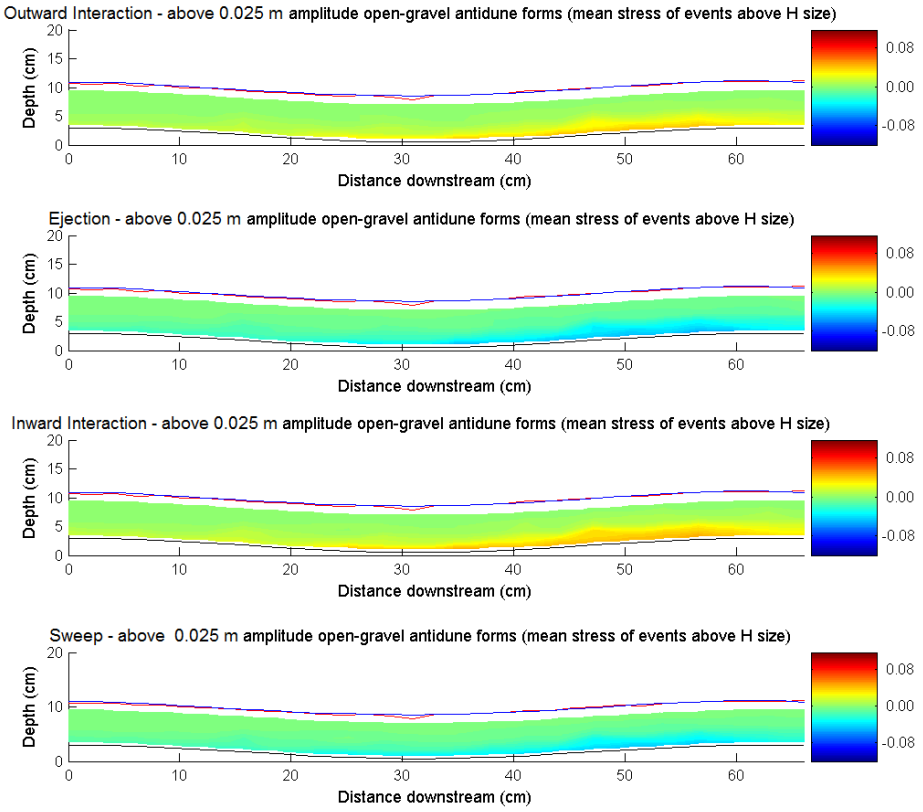

Figure 4.47 Quadrant Analysis of Turbulence above a 0.025 m Amplitude Openwork-Gravel Antidune Bedform (ADV: 25 Hz, Mean Stress for Events above Hole Size = 2)

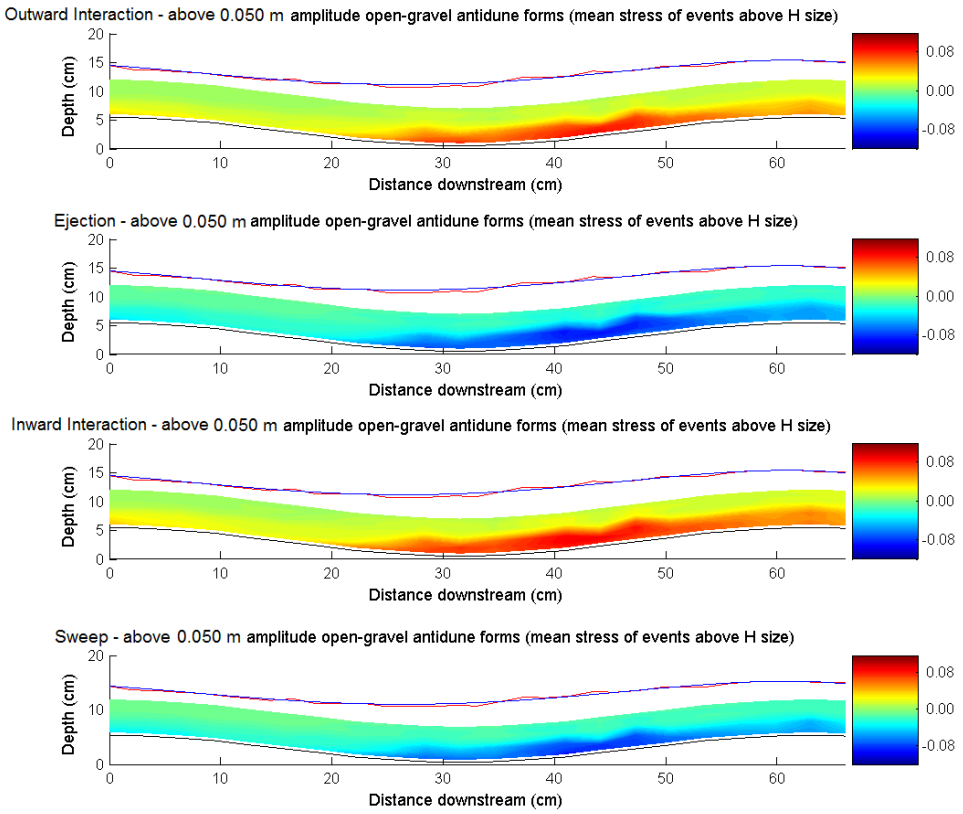

Figure 4.48 Quadrant Analysis of Turbulence above a 0.050 m Amplitude Openwork-Gravel Antidune Bedform (ADV: 25 Hz, Mean Stress for Events above Hole Size = 2)

4.2.6 P, R and TI for 0.025 and 0.050 m Amplitude Openwork-Gravel Antidune Bedforms

Plots of P, R and TI (Figures 4.49 – 4.50), support the above results and interpretations. P is concentrated in the trough between each antidune bedform, maximum values, remaining at similar levels (0.9) for 0.025 m and 0.050 m amplitude antidunes. The highest values of R (0.2 to 0.3), a measure of the presence and integrity of any boundary layer, occur primarily in the trough region and at the bed on the upstream facing flank of the downstream antidune for 0.025 m antidunes, perhaps due to flow egressing from the bed on the downstream face of the upstream antidune bedform. For the 0.050 m antidune amplitude, high values of R occur primarily in the trough region. As for $\overline{V}$ (Figure 4.38), reasons for the values above each crest are unclear. As for P, TI is highest in the trough between each antidune for all three amplitudes of bedform. Values of TI increase from 0.14 to 0.39 with increasing antidune amplitude. The increases in TI towards the bed, and

particularly at the trough can be seen in the respective line plots in Figures 4.33b – 4.34b.

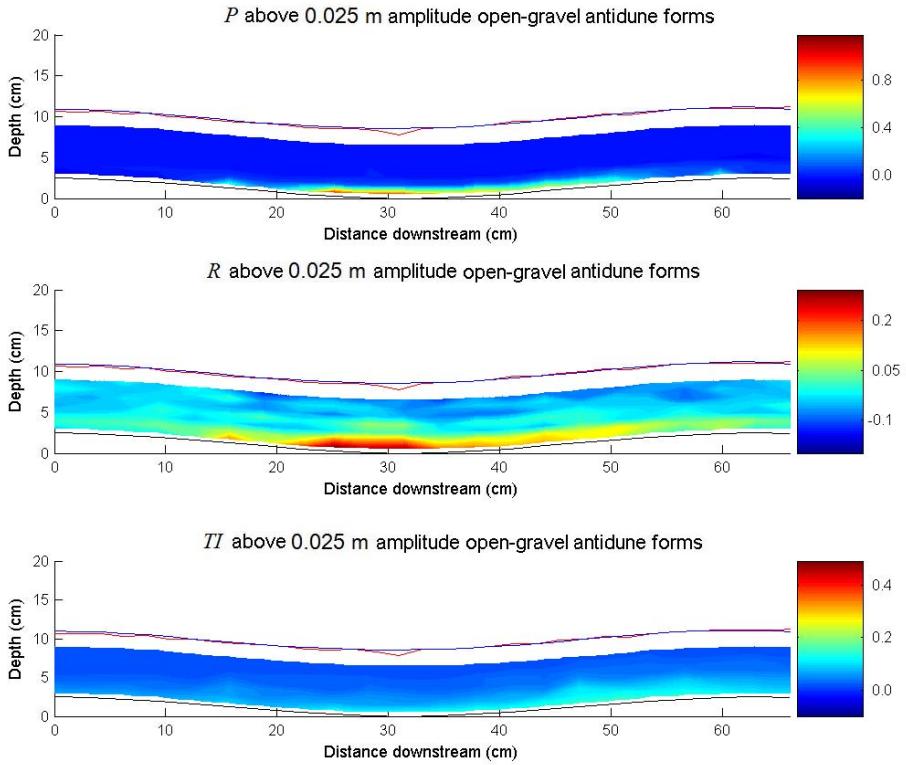

Figure 4.49 P, R and TI above a 0.025 m Amplitude Openwork-Gravel Antidune Bedform (ADV: 25 Hz)

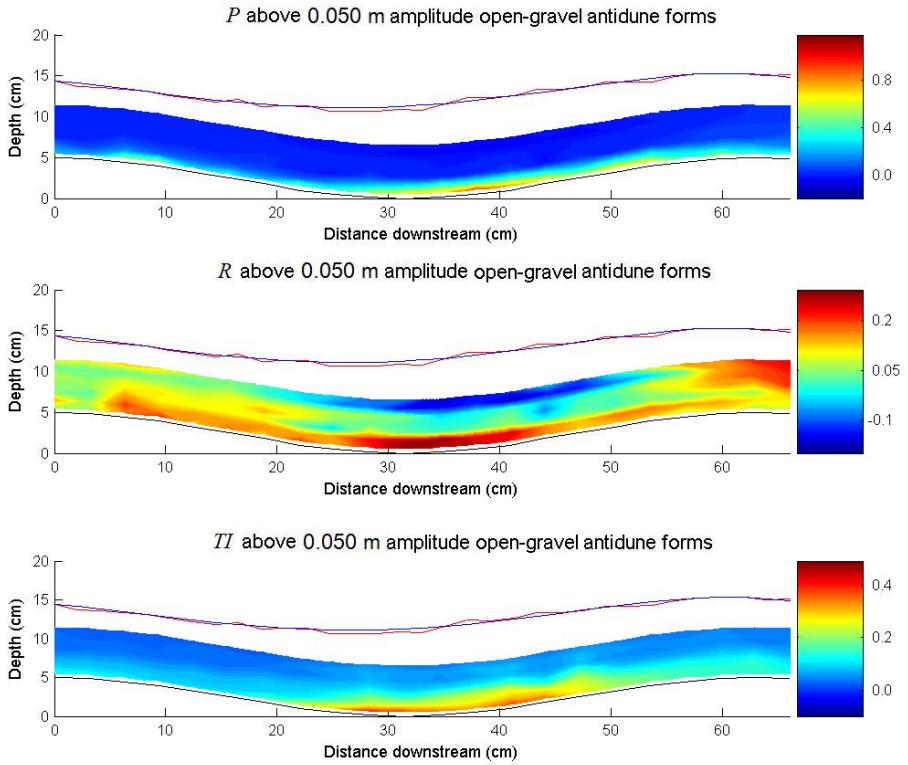

Figure 4.50 P, R and TI above a 0.050 m Amplitude Openwork-Gravel Antidune Bedform (ADV: 25 Hz)

There are no graphs for 0.075 m amplitude openwork-gravel antidune bedforms as flow above these forms was not stable.

Summary – Turbulence Structure over Openwork-Gravel Antidunes

25 Hz ADV investigations show that the most intense turbulence occurs in the trough region. In this lower trough region there is a marked reduction in values of $\overline{U}$, and a corresponding increase in U_{rms} and V_{rms}. This difference in $\overline{U}$ velocity between the lower trough and upper parts of the flow increases ($\overline{U}$ in the lower trough being 74% and 37% of $\overline{U}$ in the flow above for 0.025 and 0.050 m amplitude forms respectively) as antidune amplitude increases. In the region between the downstream end of the trough and lower slope of the downstream antidune, values of turbulent stresses increase progressively[1]: TI [0.14 and 0.37], τ_R [3 and 7], and TKE [5 and 9], whilst Q2 (ejections) and Q4 (sweeps) become increasingly spatially concentrated into this region. The magnitude of these values increases as the antidune amplitude increases. It is postulated that the intense turbulence associated with steepening antidunes, may lead to rapid erosion in the trough, steepening the downstream bedform, which causes the standing wave to collapse. Compared to solid gravel surfaced antidune forms (see Box 4.1), the values for

turbulence statistics over openwork-gravel antidune bedforms are very similar. However, given that the 25 Hz ADV used to measure flow over openwork-gravel antidune bedforms will have underestimated these turbulence statistics (see discussion in Section 3.3.1 and Box 4.4 which compares solid gravel surface antidune measurements at 100 Hz and 25 Hz), it is thought that turbulence is infact more intense (up to 60%) over open-gravel forms. This is discussed further in Section 7.1.2.

[1]Numbers in square brackets refer to values for 0.025 and 0.050 m amplitude antidune bedforms respectively.

Box 4.2 Summary of Flow Profile and Turbulence over Openwork-Gravel Antidunes (25 Hz)

4.3 Spatial Characteristics of Turbulence over Sand Antidune Bedforms (ADV 25 Hz)

4.3.1 $\overline{U}$, U_{rms} and U_{skew} for 0.025, 0.050 and 0.075 m Amplitude Sand Antidune Bedforms

With increasing amplitude, significant changes can be seen in the distribution of $\overline{U}$ over the sand surfaced antidune bedforms. Over 0.025 m amplitude forms (Figure 4.51) velocities are in the region of 1.85 – 1.94 m/s for the majority of the flow. A thin boundary layer is present near the bed, velocities at the crests drop to 1.87 m/s and 1.91 m/s (upstream/downstream crests respectively), in the trough velocities only drop to 1.8 m/s (0.95 of $\overline{U}$ in the upper parts of the flow). No notable skewing of velocities occurs, downstream of the trough onto the upstream facing flank of the downstream antidune. Over 0.050 m amplitude forms (Figure 4.52) velocities are in the region of 1.6 – 1.72 m/s for the majority of the flow. Only a poorly developed boundary layer is present near the bed, velocities at the crests drop to 1.65 m/s and 1.68 m/s (upstream/downstream crests respectively). However, in the trough velocities drop as low as 1.52 m/s (0.92 of $\overline{U}$ in the upper parts of the flow). Again, no notable skewing of velocities occurs, downstream of the trough onto the upstream facing flank of the downstream antidune. Over 0.075 m amplitude forms (Figure 4.53) velocities are in the region of 1.54 – 1.7 m/s for the majority of the flow. Only a poorly developed boundary layer is present near the bed, velocities at the crests drop to 1.53 m/s and 1.68 m/s (upstream/downstream crests respectively). However, in the trough velocities drop as low as 1.27 m/s (0.78 of $\overline{U}$ in the upper parts of the flow).

Again, no notable skewing of velocities occurs, downstream of the trough onto the upstream facing flank of the downstream antidune. Towards the bed, and at the trough, the increasing divergence from velocities in the upper flow can be seen in the respective normalised velocity plots in Figures 4.54a, 4.55a and 4.56a. As for gravel surface antidune bedform inserts and the openwork gravel antidune bedform inserts, for all amplitudes (Figures 4.51 – 4.53) the highest U_{rms} values occur adjacent to the bed. For all amplitudes U_{skew} is negative, with the lowest (most negative) skewness

occurring at the bed, and the highest (nearest zero) values near the water surface. This is interpreted, as an indication of high velocity flow occurring throughout the flow, almost until the bed where some lower instantaneous velocities increase the negativity of skew. The most extreme skews appear above the beds on the bedform crests. The line plots of $\overline{U}$, U_{rms} and U_{skew}, in Figures 4.57 – 4.59 further illustrate these trends.

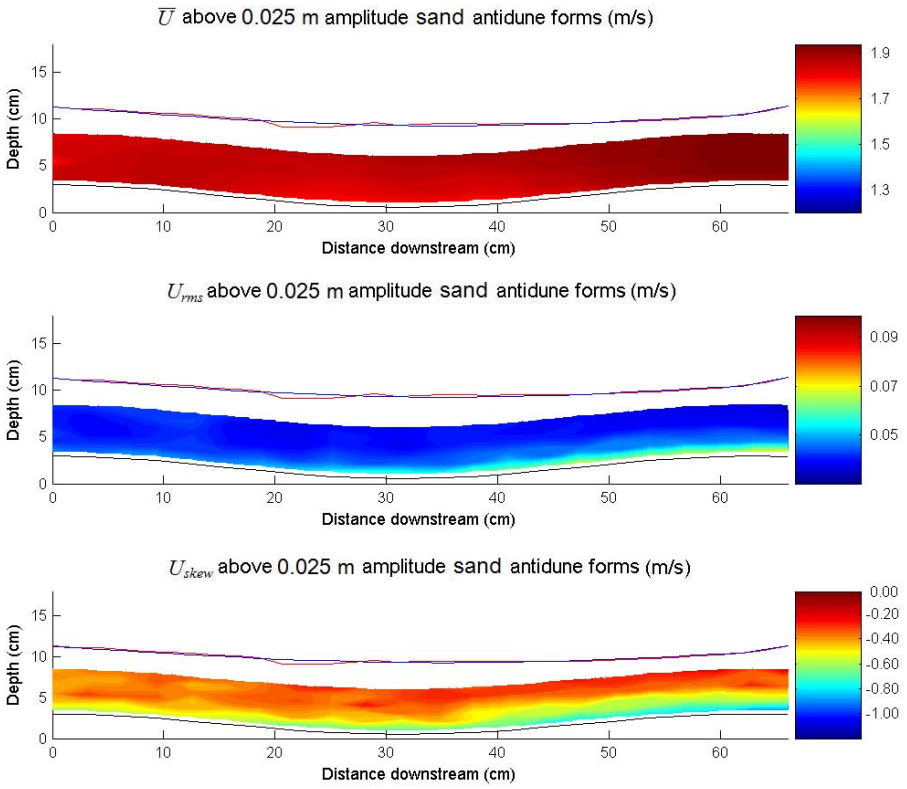

Figure 4.51 $\overline{U}$, U_{rms} and U_{skew} above a 0.025 m Amplitude Sand Antidune Bedform (ADV: 25 Hz)

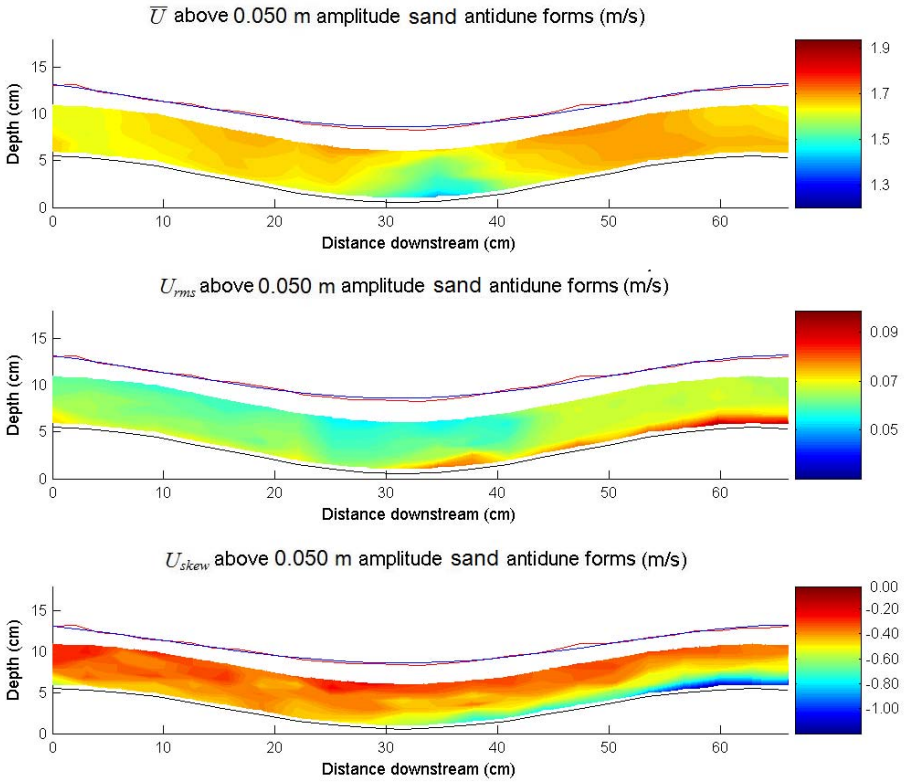

Figure 4.52 $\overline{U}$, U_{rms} and U_{skew} above a 0.050 m Amplitude Sand Antidune Bedform (ADV: 25 Hz)

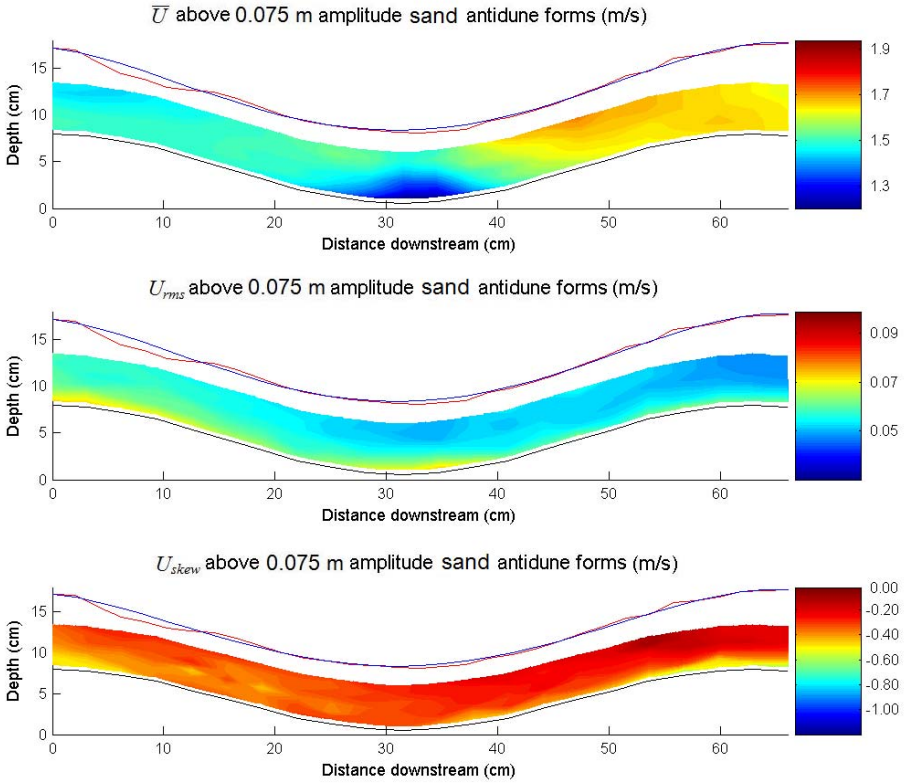

Figure 4.53 $\overline{U}$, U_{rms} and U_{skew} above a 0.075 m Amplitude Sand Antidune Bedform (ADV: 25 Hz)

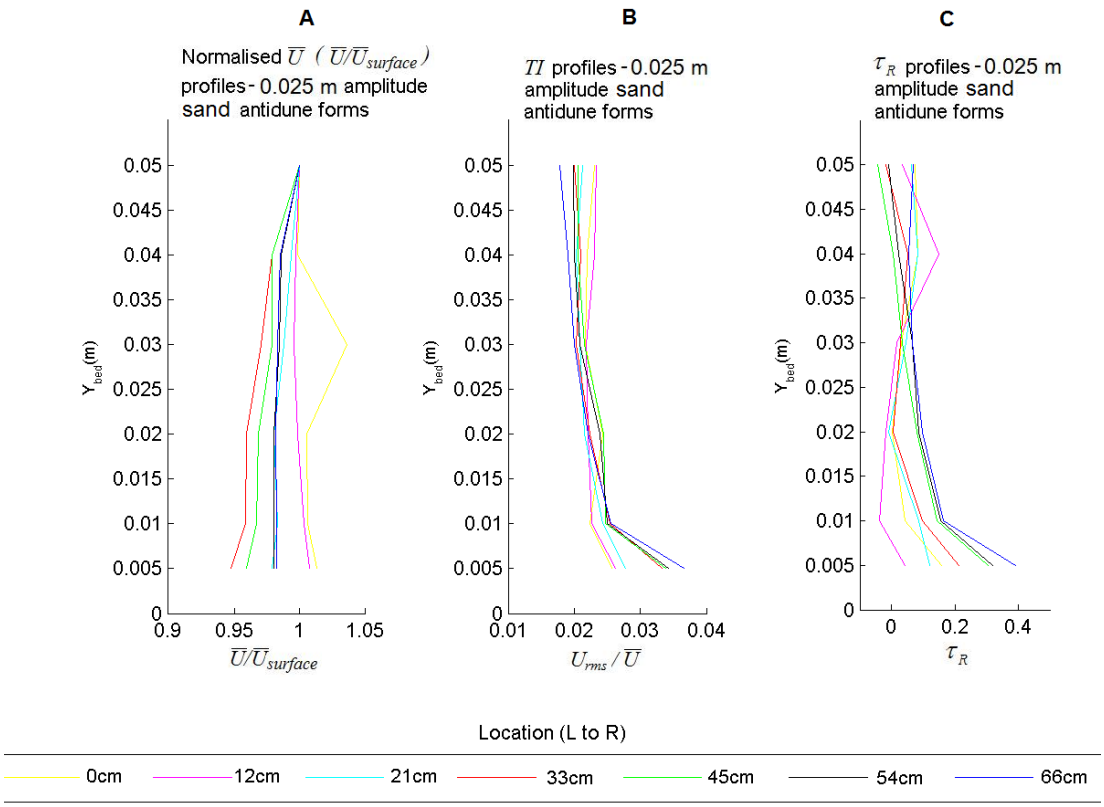

Figure 4.54 $\overline{U}$ *(normalised)*, TI and τ_R Profiles for Flow above a 0.025 m Amplitude Sand Antidune Bedform (ADV: 25 Hz)

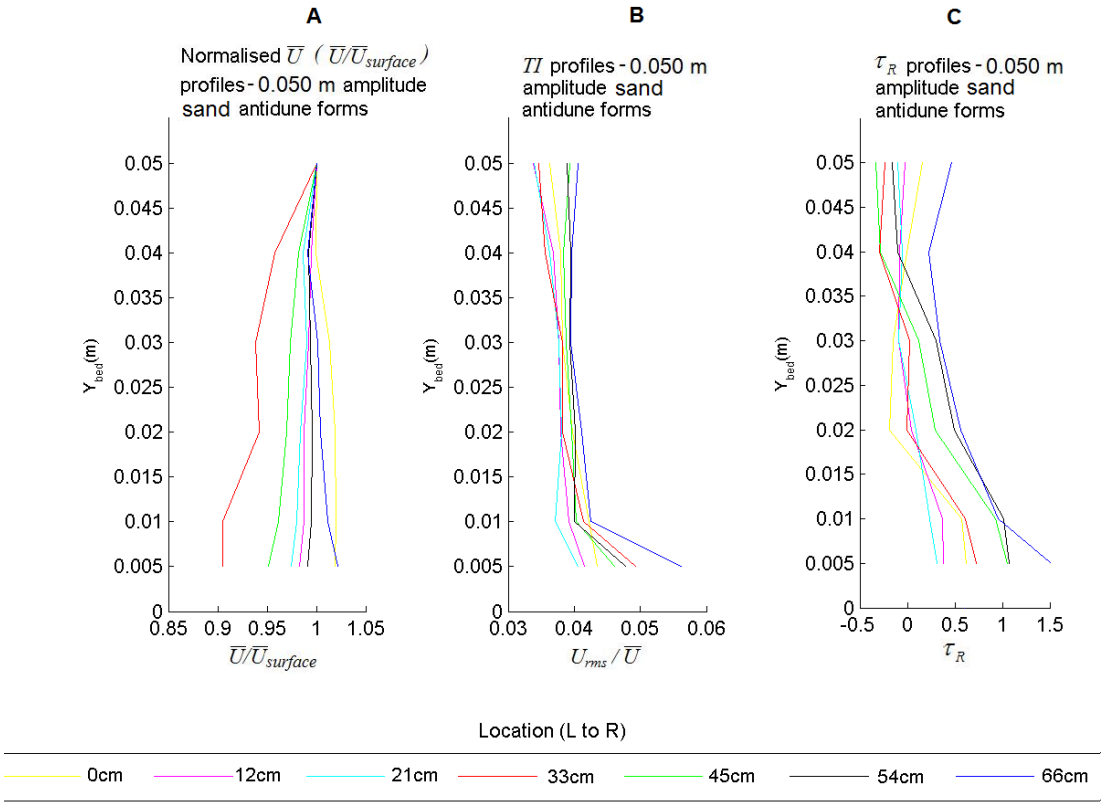

Figure 4.55 $\overline{U}$ *(normalised)*, TI and τ_R Profiles for Flow above a 0.050 m Amplitude Sand Antidune Bedform (ADV: 25 Hz)

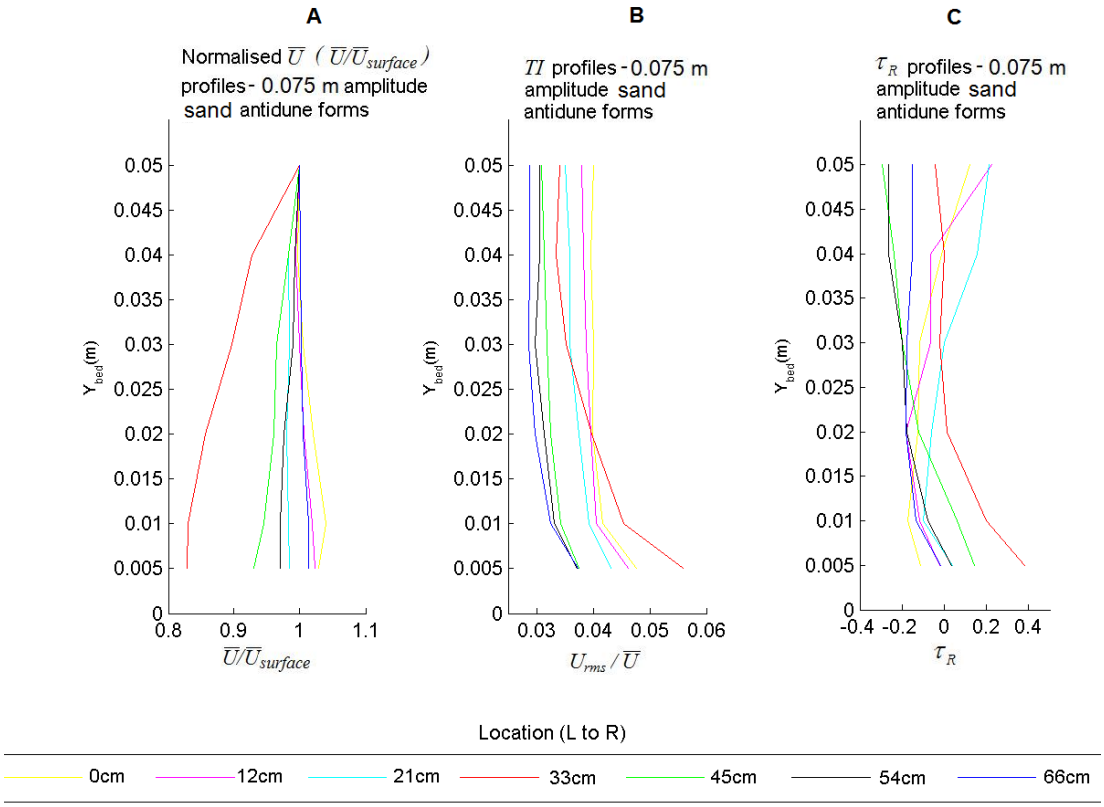

Figure 4.56 $\overline{U}$ *(normalised)*, TI and τ_R Profiles for Flow above a 0.075 m Amplitude Sand Antidune Bedform (ADV: 25 Hz)

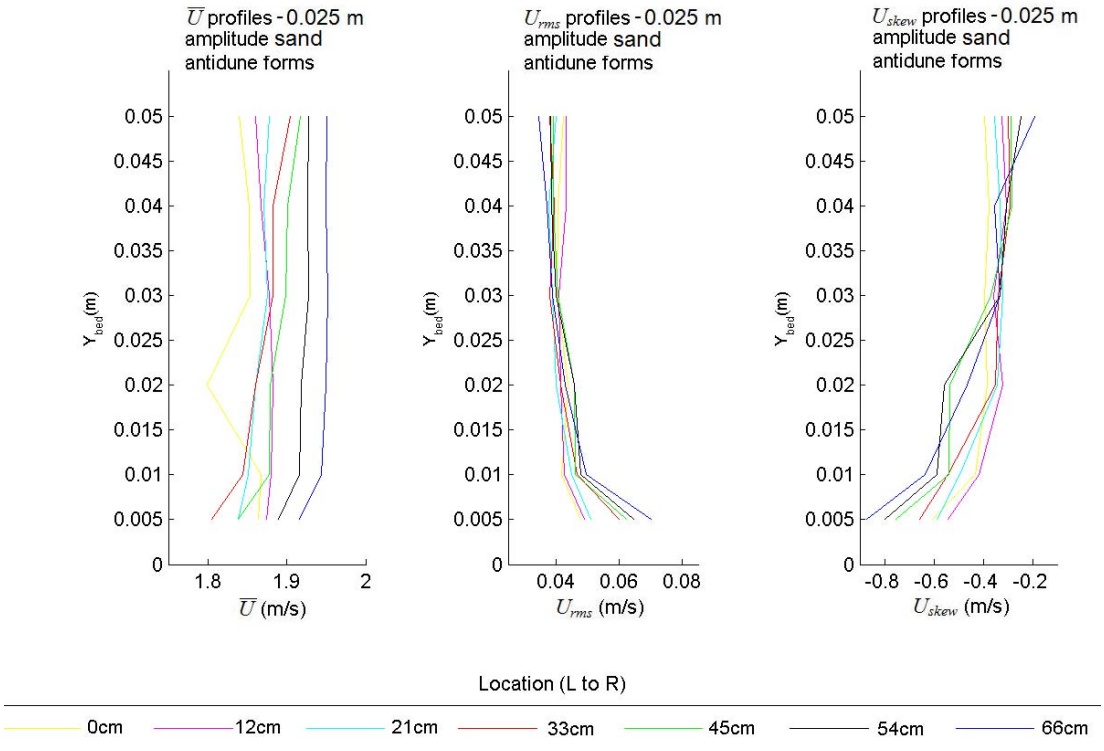

Figure 4.57 Profiles of $\overline{U}$, U_{rms} and U_{skew} for 0.025 m Amplitude Sand Antidune Bedform (ADV: 25 Hz)

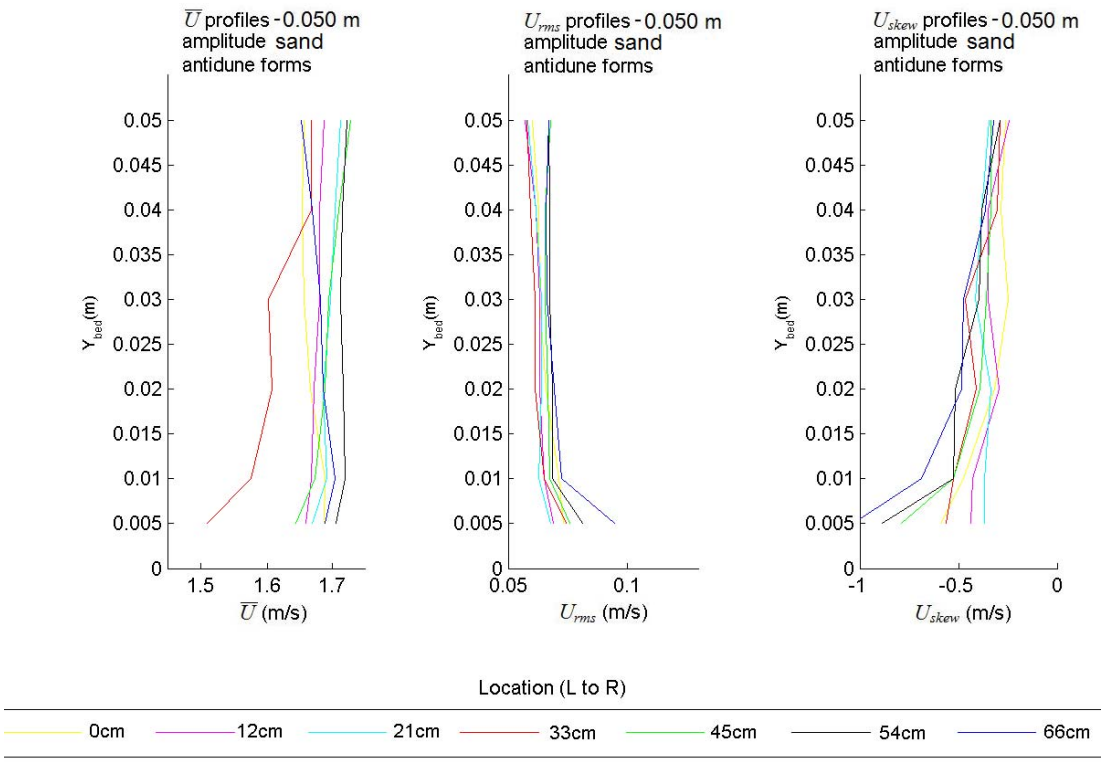

Figure 4.58 Profiles of $\overline{U}$, U_{rms} and U_{skew} for 0.050 m Amplitude Sand Antidune Bedform (ADV: 25 Hz)

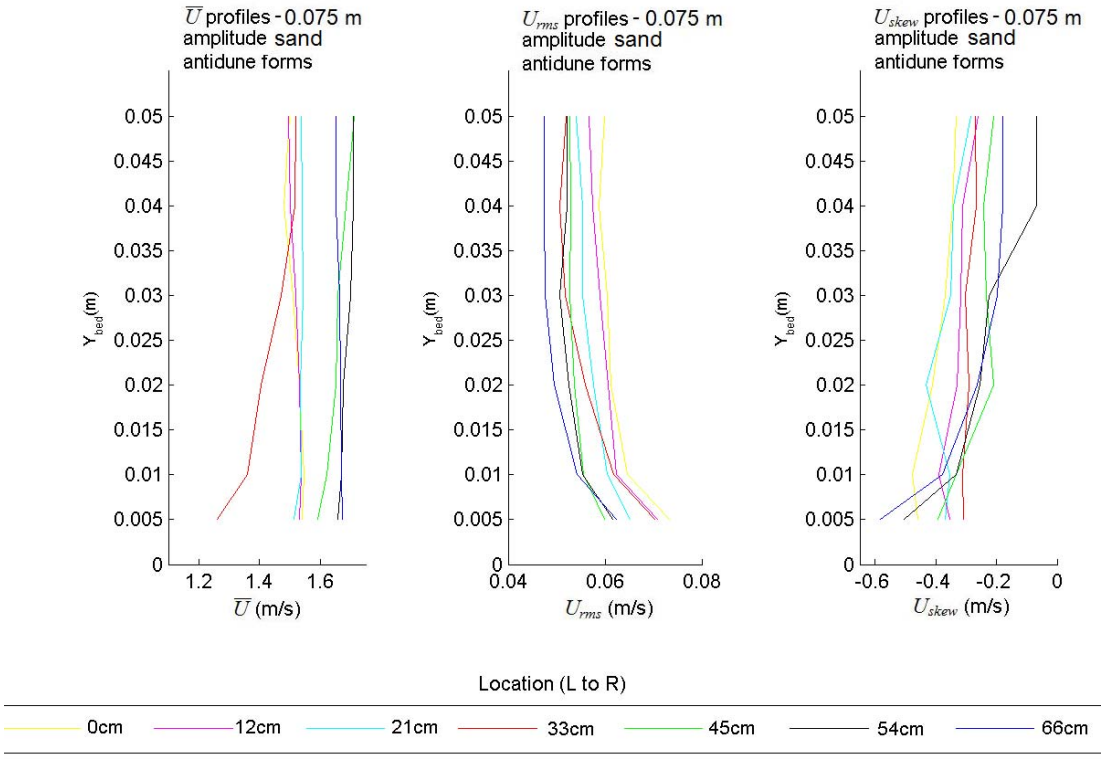

Figure 4.59 Profiles of $\overline{U}$, U_{rms} and U_{skew} for 0.075 m Amplitude Sand Antidune Bedform (ADV: 25 Hz)

4.3.2 $\overline{V}$, V_{rms} and V_{skew} for 0.025, 0.050 and 0.075 m Amplitude Sand Antidune Bedforms

For the vertical velocity element, (Figures 4.60 – 4.62) $\overline{V}$ tends towards positive (away from the bed) in the flow immediately above the bed of the upstream antidunes crest and downstream flank, and in the upper parts of the flow above the downstream antidunes upstream facing flank. Velocity tends towards negative (towards the bed) in the upper parts of the flow above the upstream antidunes flank and trough. As the amplitude increases, $\overline{V}$ values become increasingly negative in the upper parts of the flow on the downstream flank of the upstream antidune, and positive adjacent to the bed. As for U_{rms}, V_{rms} is highest near the bed, due to the variability of instantaneous velocities in the boundary layer above the antidune bedforms. The high values in the upper parts of the flow for 0.050 m sand antidunes are interpreted as a water surface effect. Likewise, V_{skew} tends to be most negatively skewed in the lower parts of the flow and with limited, or a slight positive skew in the upper parts of the flow. This indicates the occurrence of generally high instantaneous velocities in the upper parts of the flow with occasional very high instantaneous velocities, and generally high instantaneous velocities with some very low instantaneous velocities in the lower parts of the flow. The skews intensify from 0.025 m to 0.050 m amplitude antidunes, although for 0.075 m amplitude antidunes there is no clear trend. The line plots of $\overline{V}$, V_{rms} and V_{skew}, in Figures 4.63 – 4.65 further illustrate these trends. The change from more vertically symmetric, to vertically asymmetric flow can be seen toward the trough region, the flow becoming increasingly vertically asymmetric as antidune amplitude increases.

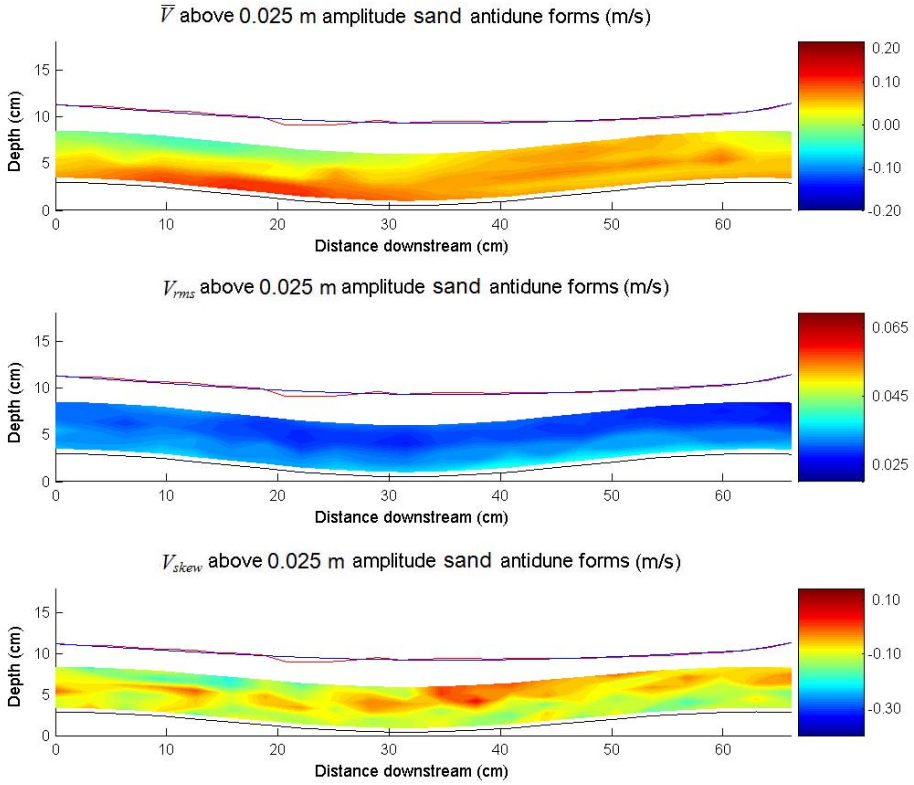

Figure 4.60 $\overline{V}$, V_{rms} and V_{skew} above a 0.025 m Amplitude Sand Antidune Bedform (ADV: 25 Hz)

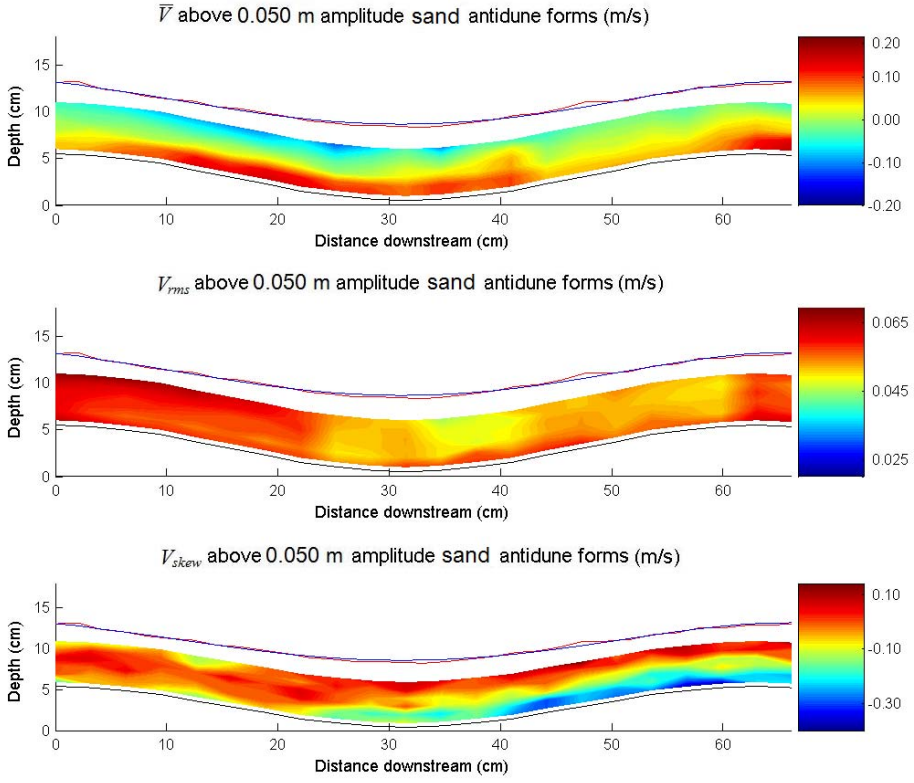

Figure 4.61 $\overline{V}$, V_{rms} and V_{skew} above a 0.050 m Amplitude Sand Antidune Bedform (ADV: 25 Hz)

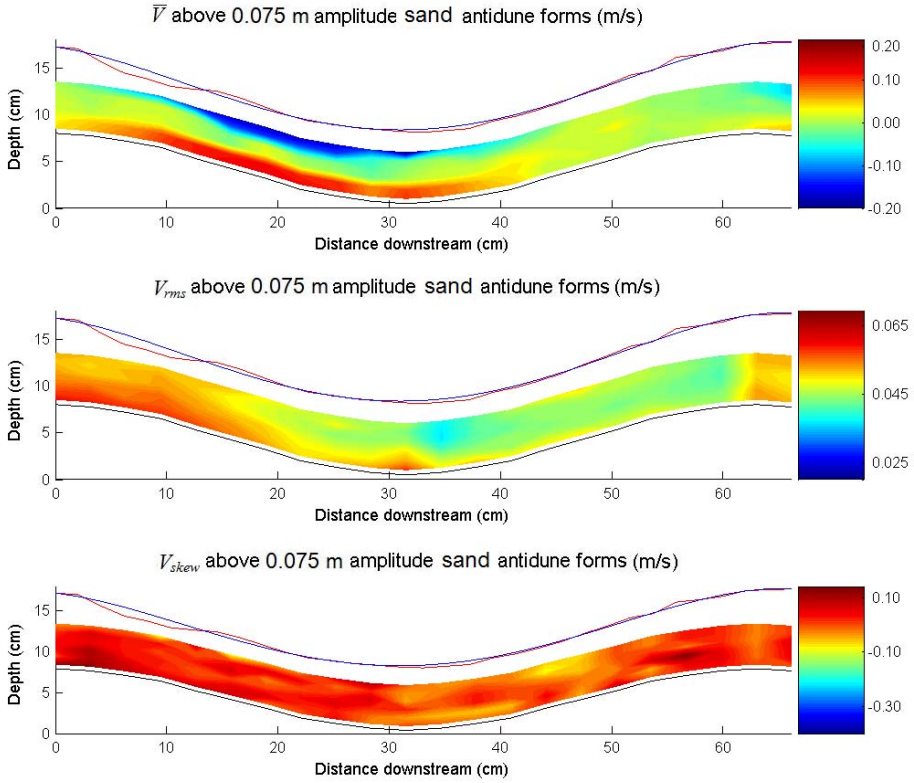

Figure 4.62 $\overline{V}$, V_{rms} and V_{skew} above a 0.075 m Amplitude Sand Antidune Bedform (ADV: 25 Hz)

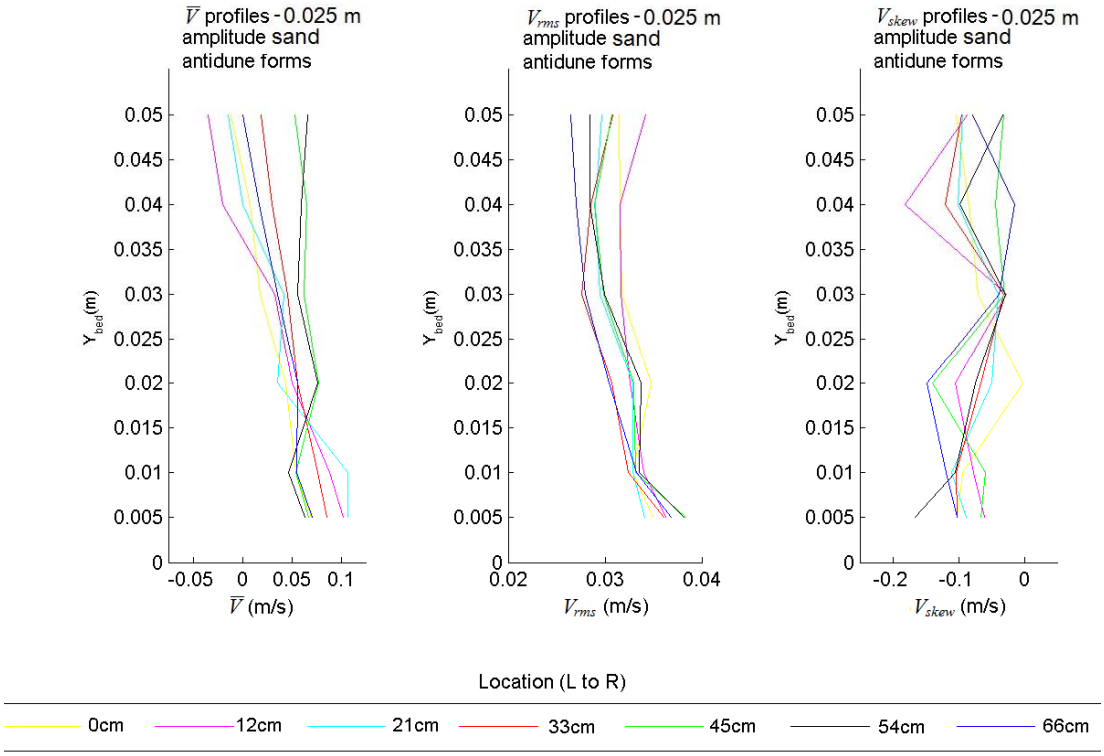

Figure 4.63 Profiles of $\overline{V}$, V_{rms} and V_{skew} for Flow above a 0.025 m Amplitude Sand Antidune Bedform (ADV: 25 Hz)

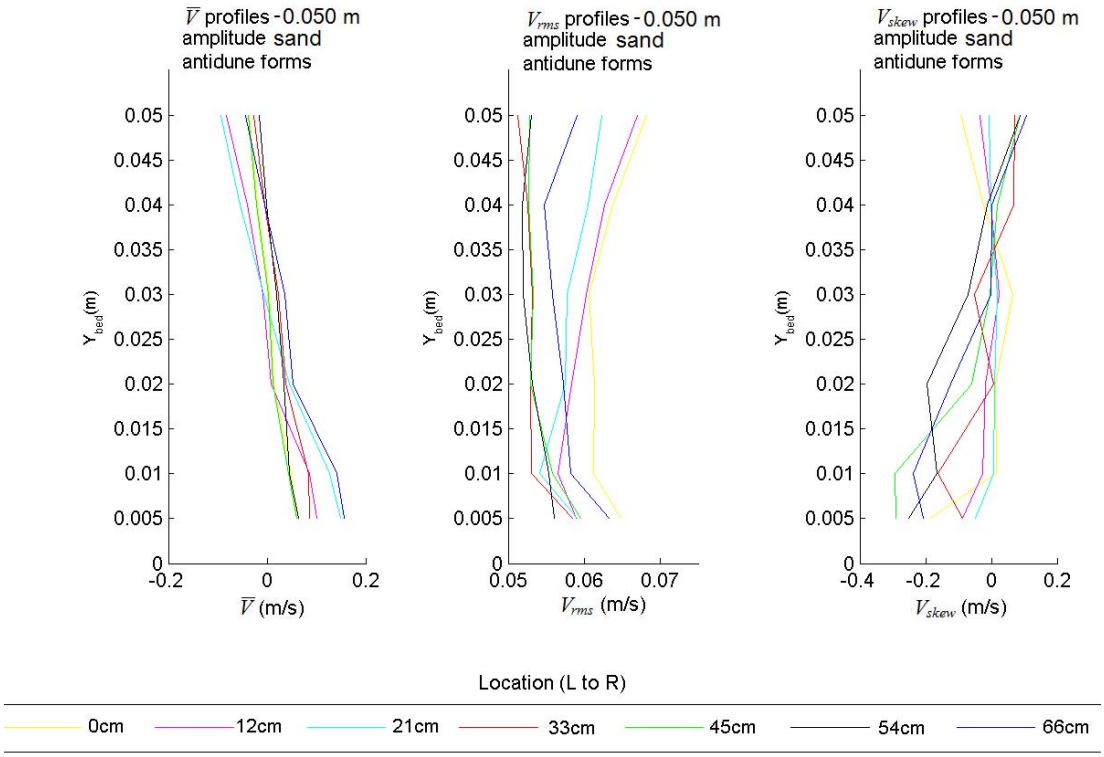

Figure 4.64 Profiles of $\overline{V}$, V_{rms} and V_{skew} for Flow above a 0.050 m Amplitude Sand Antidune Bedform (ADV: 25 Hz)

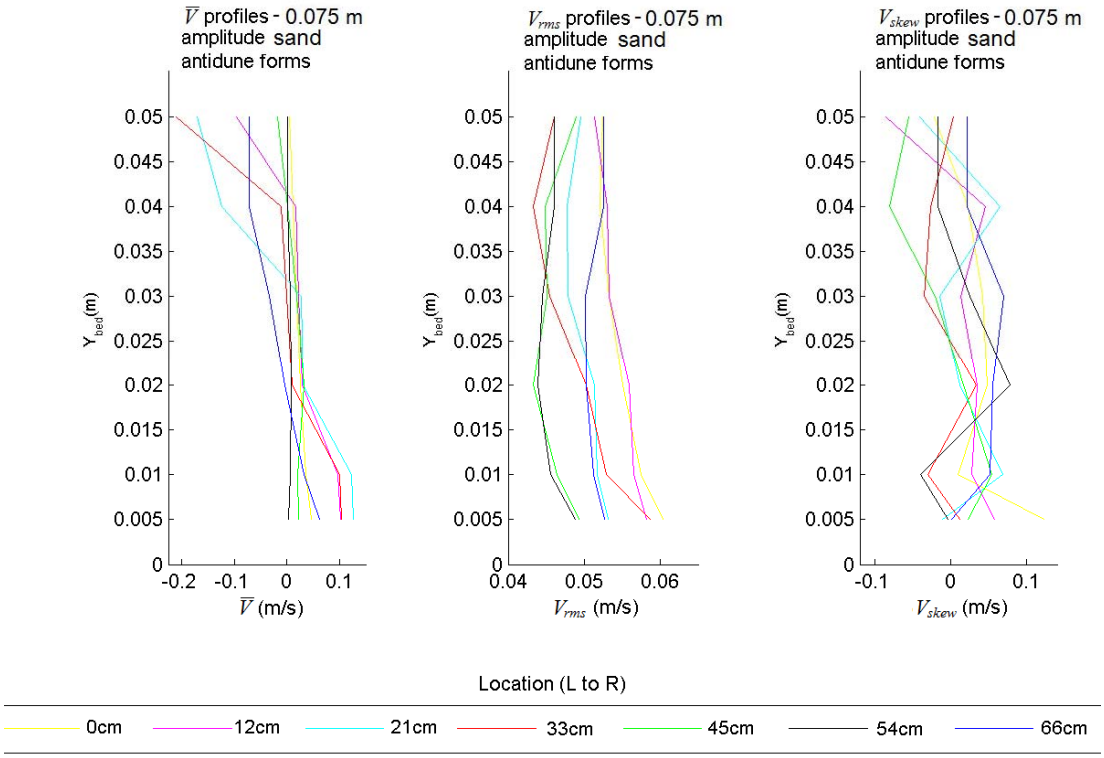

Figure 4.65 Profiles of $\overline{V}$, V_{rms} and V_{skew} for Flow above a 0.075 m Amplitude Sand Antidune Bedform (ADV: 25 Hz)

4.3.3 $\overline{W}$, W_{rms} and W_{skew} for 0.025, 0.050 and 0.075 m Amplitude Sand Antidune Bedforms

In terms of $\overline{W}$ (Figures 4.66 - 4.68) there is a clear, oscillating side to side secondary flow element in the flume, giving blocks of positive and negative $\overline{W}$. Trends in W_{rms} and W_{skew} values are more difficult to interpret, and appear to be heavily influenced by the secondary current.

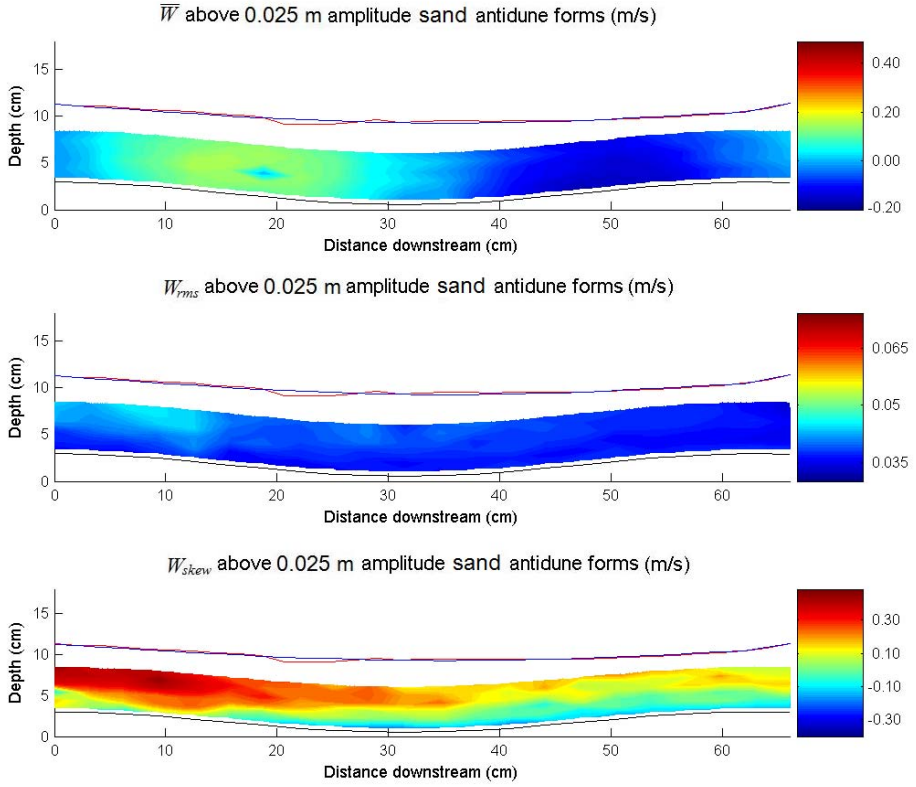

Figure 4.66 $\overline{W}$, W_{rms} and W_{skew} above a 0.025 m Amplitude Sand Antidune Bedform (ADV: 25 Hz)

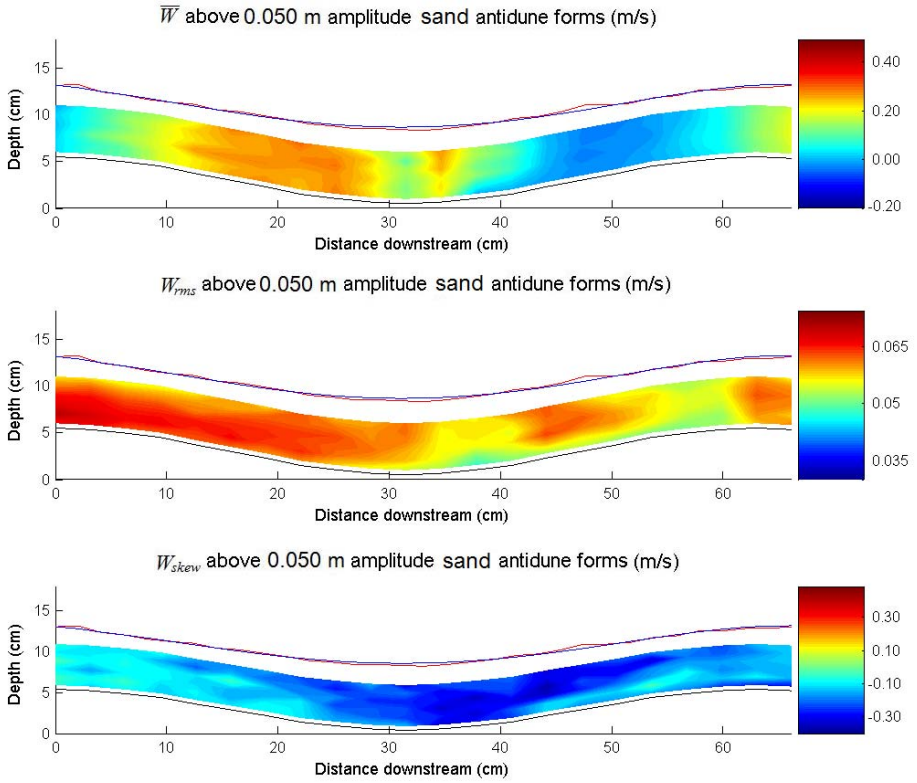

Figure 4.67 $\overline{W}$, W_{rms} and W_{skew} above a 0.050 m Amplitude Sand Antidune Bedform (ADV: 25 Hz)

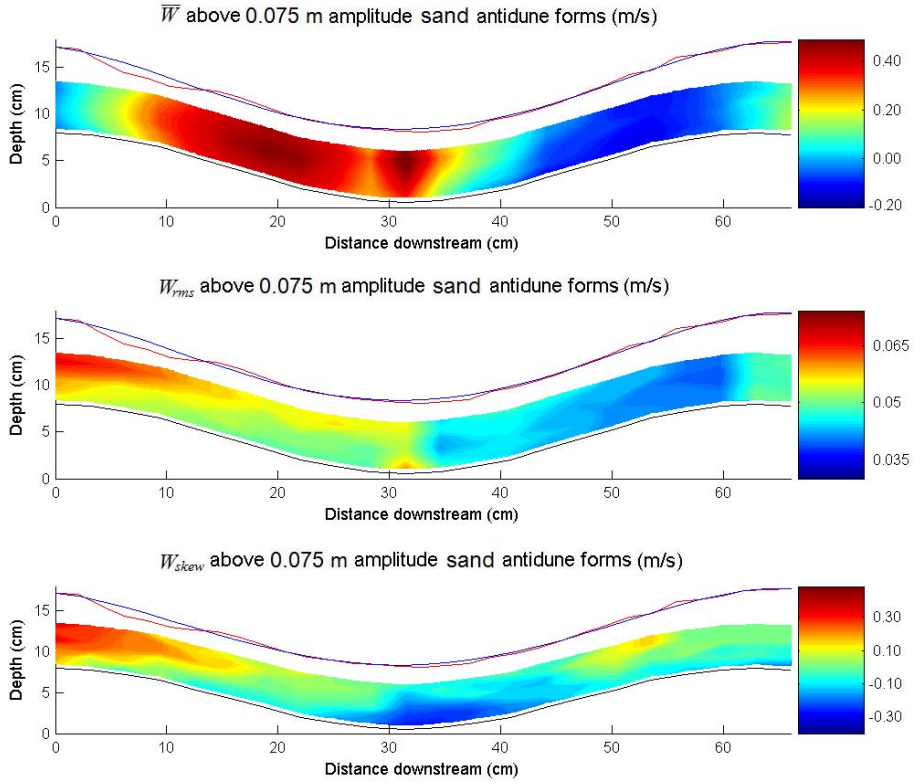

Figure 4.68 $\overline{W}$, W_{rms} and W_{skew} above a 0.075 m Amplitude Sand Antidune Bedform (ADV: 25 Hz)

4.3.4 TKE and τ_R for 0.025, 0.050 and 0.075 m Amplitude Sand Antidune Bedforms

Plots of TKE and τ_R (Figures 4.69 – 4.71) show close agreement, and indicate stresses are highest adjacent to the bed, especially on the upstream facing flank of the downstream antidune. An increase in TKE and τ_R can be seen with increasing amplitude from 0.025 to 0.050 m antidune. However, values are lower for 0.075 m antidunes, and stresses primarily concentrated in the trough region. The increases in τ_R towards the bed and particularly at the trough can be seen in the respective line plots in Figures 4.54c, 4.55c and 4.56c. The change from more vertically symmetric, to vertically asymmetric flow can be seen toward the trough region, flow becoming increasingly vertically asymmetric as antidune amplitude increases.

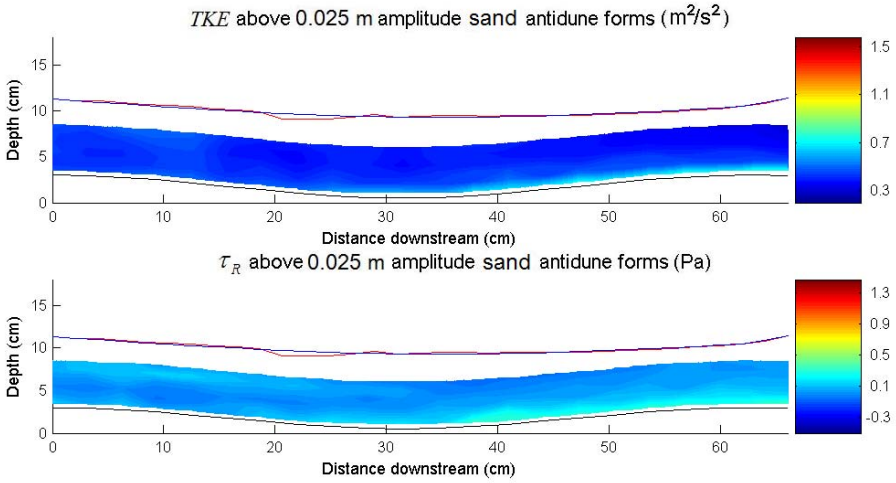

Figure 4.69 TKE **and** τ_R **above a 0.025 m Amplitude Sand Antidune Bedform (ADV: 25 Hz)**

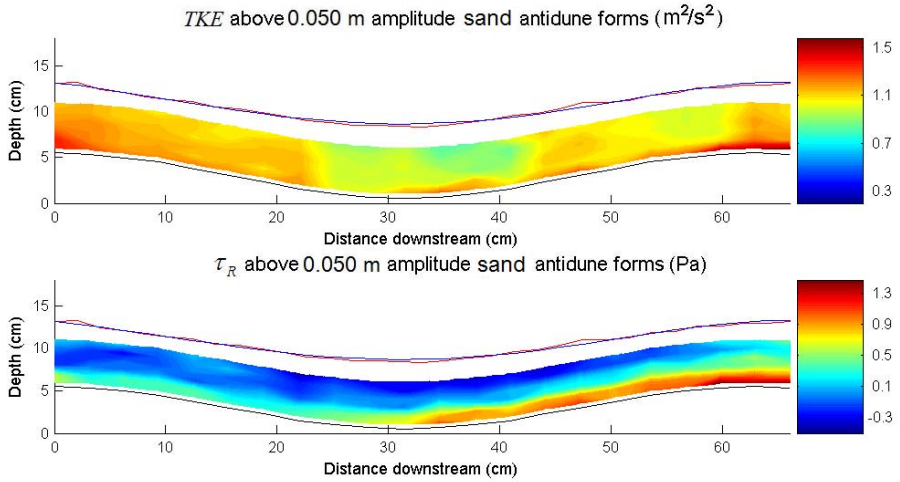

Figure 4.70 TKE **and** τ_R **above a 0.050 m Amplitude Sand Antidune Bedform (ADV: 25 Hz)**

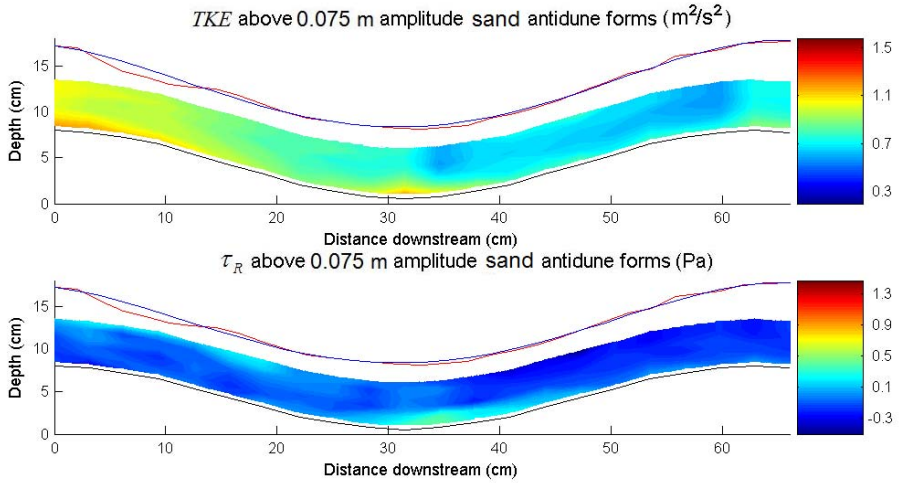

Figure 4.71 TKE **and** τ_R **above a 0.075 m Amplitude Sand Antidune Bedform (ADV: 25 Hz)**

4.3.5 Quadrant Analysis – Sand Antidune Bedforms 25 Hz

Proportion of Time Events above a Hole Size of 2 for 0.025, 0.050 and 0.075 m Amplitude Sand Antidune Bedforms

Quadrant Analysis (Figures 4.72 – 4.74) shows that the for all quadrants, the most events above the hole size occur in the upper parts of the flow. Significant events of sedimentological importance occur adjacent to the bed for between 0.3% and 3% of the velocity record.

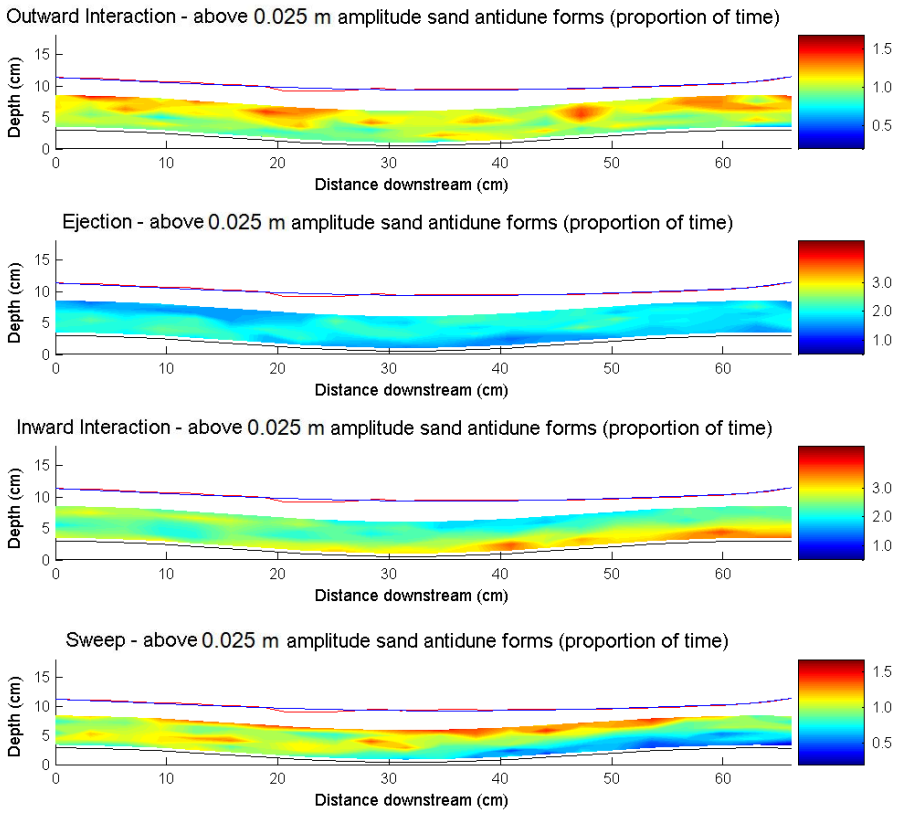

Figure 4.72 Quadrant Analysis of Turbulence above a 0.025 m Amplitude Sand Antidune Bedform (ADV: 25 Hz, Proportion of Time Events above Hole Size = 2)

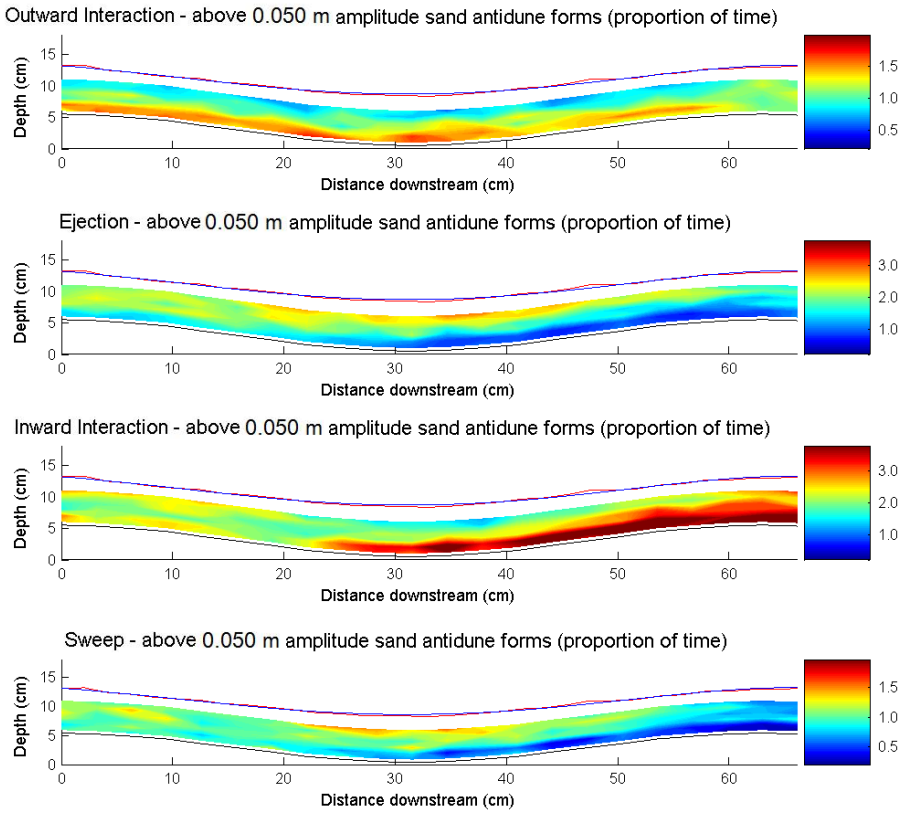

Figure 4.73 Quadrant Analysis of Turbulence above a 0.050 m Amplitude Sand Antidune Bedform (ADV: 25 Hz, Proportion of Time Events above Hole Size = 2)

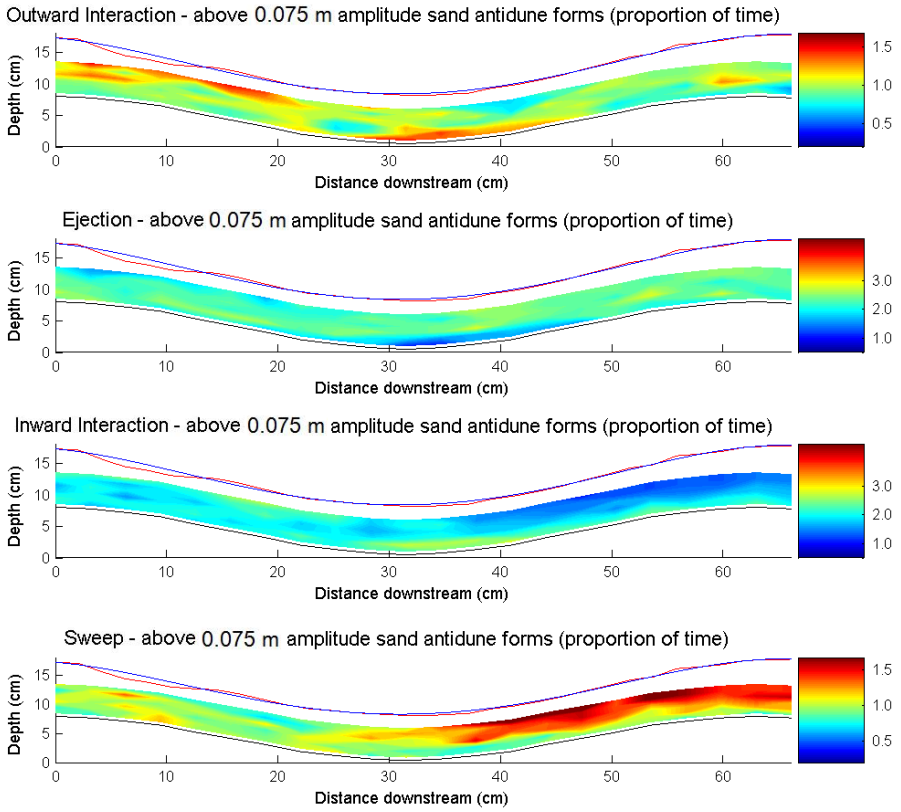

Figure 4.74 Quadrant Analysis of Turbulence above a 0.075 m Amplitude Sand Antidune Bedform (ADV: 25 Hz, Proportion of Time Events above Hole Size = 2)

Mean Stress for Events above a Hole Size of 2 for 0.025, 0.050 and 0.075 m Amplitude Sand Antidune Bedforms

Investigation of the average $|u'v'|$ stresses (Figures 4.75– 4.77) during these events indicates that the highest $|u'v'|$ stresses occur adjacent to the bed. The distribution of stresses is for the 0.025 m and 0.050 m amplitude cases spread out along the majority of the boundary layer, but in particular at the bed on the upstream facing flank of the downstream antidune. However for 0.075 m bedforms, highest stresses occur on the downstream facing flank of the upstream antidune. In particular, $|u'v'|$ values during ejections increase from only -0.0089 m/s for 0.025 m bedforms on the downstream antidunes upstream facing flank and crest, to -0.0189 m/s for 0.050 m bedforms on the downstream antidunes upstream facing flank and crest, and a slight decrease to -0.0149 m/s for 0.075 m bedforms, and located on the downstream facing flank of the upstream antidune. Likewise for sweeps, $|u'v'|$ values increase from -0.0069 m/s for 0.025 m bedforms on the downstream antidunes upstream facing flank and crest, to -0.0159 m/s for

0.050 m bedforms on the downstream antidunes upstream facing flank and crest, with a slight decrease to -0.012 m/s for 0.075 m bedforms, and located on the downstream facing flank of the upstream antidune.

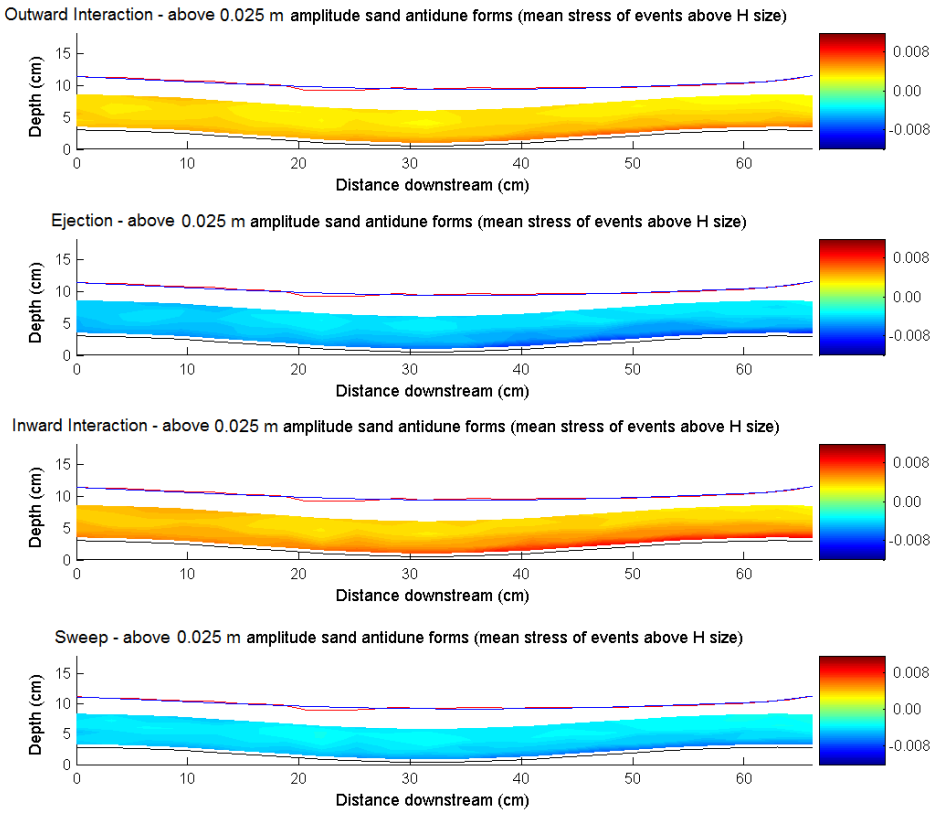

Figure 4.75 Quadrant Analysis of Turbulence above a 0.025 m Amplitude Sand Antidune Bedform (ADV: 25 Hz, Mean Stress for Events above Hole Size = 2)

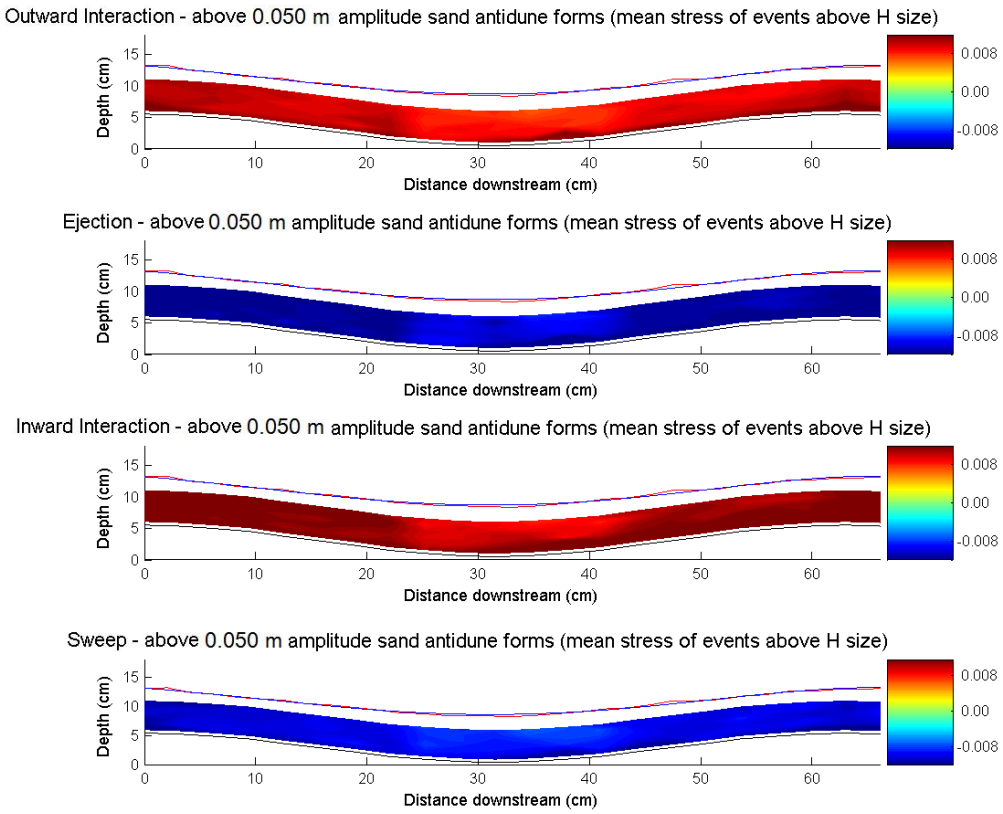

Figure 4.76 Quadrant Analysis of Turbulence above a 0.050 m Amplitude Sand Antidune Bedform (ADV: 25 Hz, Mean Stress for Events above Hole Size = 2)

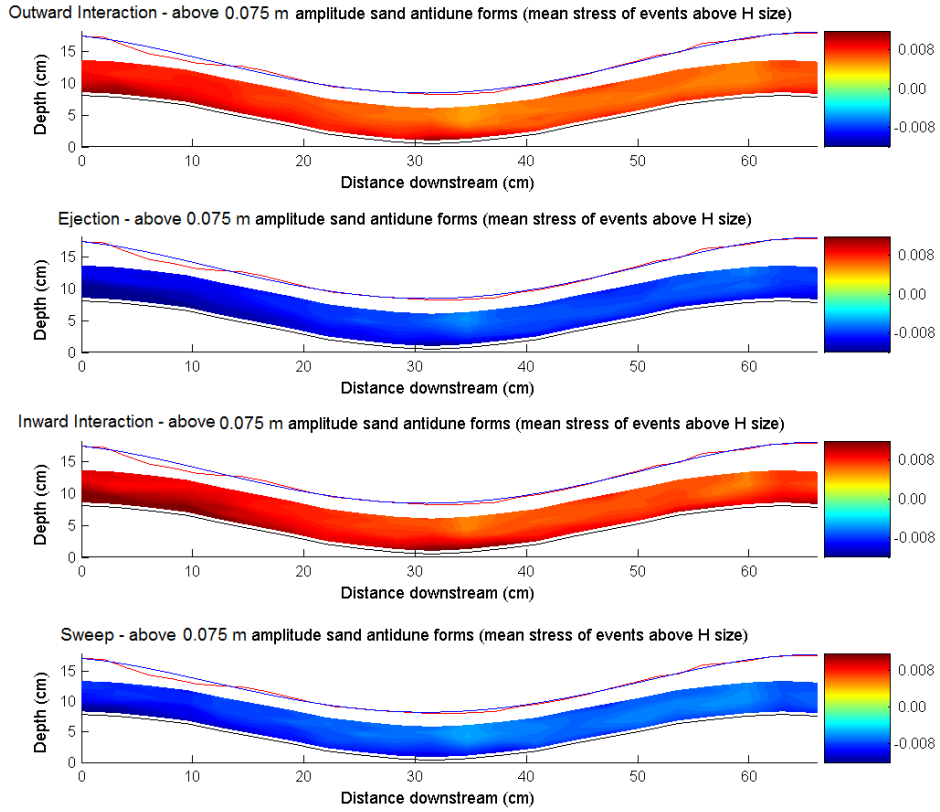

Figure 4.77 Quadrant Analysis of Turbulence above a 0.075 m Amplitude Sand Antidune Bedform (ADV: 25 Hz, Mean Stress for Events above Hole Size = 2)

4.3.6 P, R and TI for 0.025, 0.050 and 0.075 m Amplitude Sand Antidune Bedforms

Plots of P, R and TI (Figures 4.78 – 4.80), support the above results and interpretations. P is for the 0.025 and 0.050 m amplitude cases is concentrated at the bed on the upstream facing flank of the downstream antidune, with values of 0.14 and 0.5 respectively. For 0.075 m bedforms, levels drop back to 0.1, and become very concentrated in the trough region. R, a measure of the presence and integrity of any boundary layer, is relatively evenly distributed over 0.025 m (R: 0.1) and 0.050 m (R: 0.25) antidunes, indicating a constant, thin semi-developed boundary layer. However, for, the 0.075 m amplitude bedform high values of R (R: 0.1) occur primarily in the trough region. These values of R are perhaps on the low side, values of 0.3 – 0.5 having been found previously. As for P, TI is highest in the trough between each antidune for all three amplitudes of bedform. Values of TI increase from 0.035 to 0.055 between 0.025 m and 0.050 m amplitude bedforms, intensity being greatest between trough and crest of the downstream antidune. Values remain at 0.055 for 0.075 m bedforms, but are shifted to the downstream facing flank of the upstream antidune and trough region. The increases in TI towards the bed, and particularly at the trough can be seen in the respective line plots in Figures 4.54b, 4.55b and 4.56b.

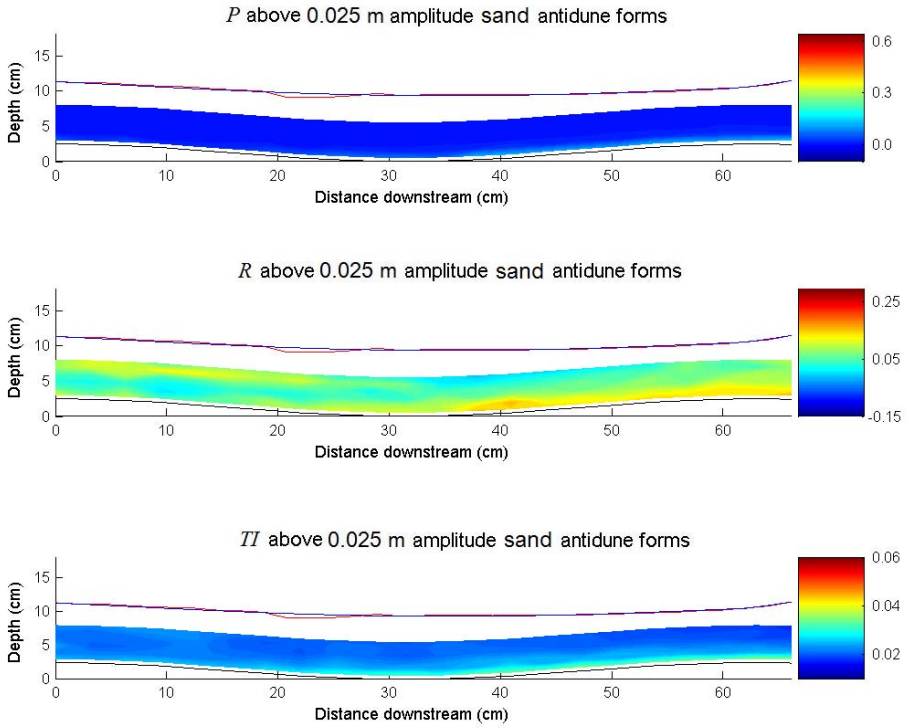

Figure 4.78 P, R and TI above a 0.025 m Amplitude Sand Antidune Bedform (ADV: 25 Hz)

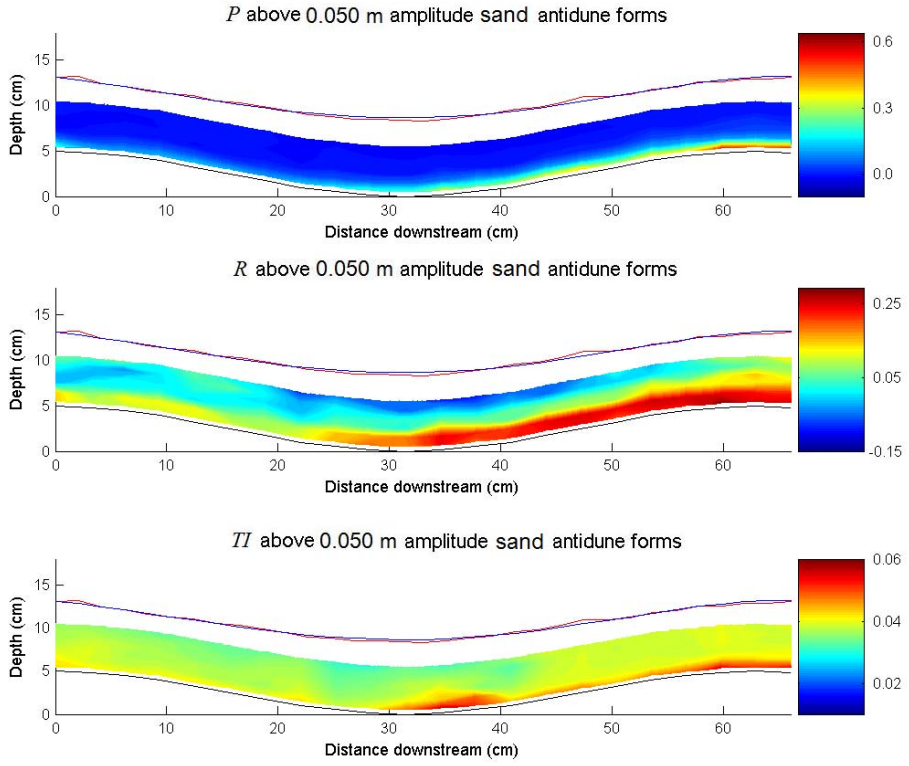

Figure 4.79 P, R and TI above a 0.050 m Amplitude Sand Antidune Bedform (ADV: 25 Hz)

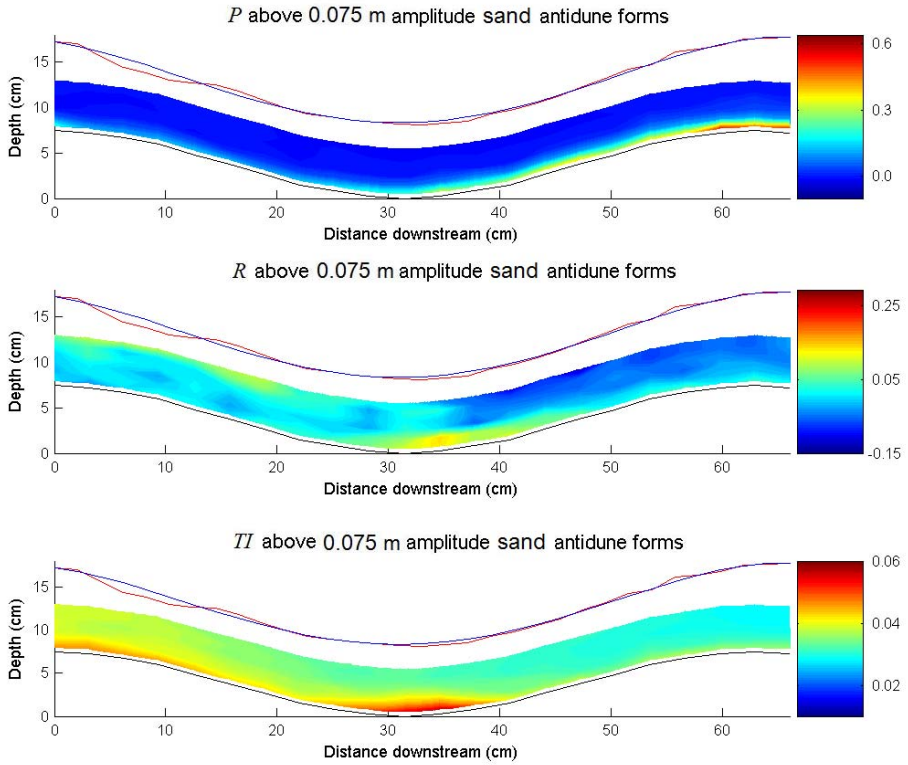

Figure 4.80 P, R and TI above a 0.075 m Amplitude Sand Antidune Bedform (ADV: 25 Hz)

Summary – Turbulence Structure over Sand Surfaced Antidunes

25 Hz ADV investigations show the same spatial distribution, as for gravel antidunes (Box 4.1 and 4.2), with the most intense turbulence occurring in the trough region. However, over sand surfaced antidunes spatial differences and turbulence intensities are much less pronounced than over gravel surfaced forms. In this lower trough region there are marked reductions in $\overline{U}$ values, and a corresponding increase in U_{rms} and V_{rms}. This difference between $\overline{U}$ values in the lower trough and upper parts of the flow increases (values of $\overline{U}$ in the lower trough being 95%, 92% and 78% of $\overline{U}$ values in the flow above for 0.025, 0.050 and 0.075 m amplitude forms respectively) as antidune amplitude increases. In the region between the downstream end of the trough and lower slope of the downstream antidune, values of turbulent stresses increase progressively from those over 0.025 to 0.050 m[1]: TI [0.0.35, 0.055 and 0.055], τ_R [0.35, 1.4 and 0.4], and TKE [0.7, 1.6 and 1.15], whilst Q2 (ejections) and Q4 (sweeps) become increasingly spatially concentrated into this region. It is unclear why a drop off occurs in values over 0.075 m amplitude forms. The magnitude of these values increases as the antidune amplitude increases. It is postulated that the intense turbulence associated with steepening antidunes, may lead to rapid erosion in the trough, steepening the downstream bedform, which causes the standing wave to collapse. Compared to gravel antidune forms (see Box

4.1, 4.2 and 4.4), the values for turbulence statistics over sand surfaced antidune bedforms are an order of magnitude smaller. Even accounting for the 25 Hz ADV used to measure flow, underestimating these turbulence statistics (see discussion in Section 3.3.1 and in Box 4.4) by up to 60%, turbulence levels are still significantly lower over sand surfaced antidune forms. This is discussed further in Section 7.1.3.

[1]Numbers in square brackets refer to values for 0.025, 0.050 and 0.075 m amplitude antidune bedforms respectively.

Box 4.3 Summary of Flow Profile and Turbulence over Sand Surfaced Antidunes (25 Hz)

4.4 Spatial Characteristics of Turbulence over Gravel Antidune Bedforms (ADV 25 Hz)

4.4.1 $\overline{U}$, U_{rms} and U_{skew} for 0.025, 0.050 and 0.075 m Amplitude Gravel Antidune Bedforms

With increasing amplitude, significant changes can be seen in the longitudinal distribution of $\overline{U}$ over the gravel surfaced antidune bedforms. Over 0.025 m amplitude forms (Figure 4.81) velocities are in the region of 1.64 – 1.8 m/s for the majority of the flow. A thin boundary layer is present near the bed, velocities at the crests drop to around 1.55 m/s, in the trough velocities drop to 1.31 m/s (0.76 of $\overline{U}$ in the upper parts of the flow). A relatively pronounced area of slower flow nearer the bed can be seen. Over 0.050 m amplitude forms (Figure 4.82) velocities are in the region of 1.1 – 1.4 m/s for the majority of the flow. A poorly developed boundary layer is present near the bed, velocities at the crests drop to 1.2 m/s. Velocities drop as low as 0.58m/s (0.46 of $\overline{U}$ in the upper parts of the flow), in the trough region. Over 0.075 m amplitude forms (Figure 4.83) velocities are in the region of 1.1 – 1.5 m/s for the majority of the flow. A poorly developed boundary layer is present near the bed concentrated in the trough region. Velocities at the crests drop to around 1.2 m/s, whilst velocities drop as low as 0.49 m/s (0.38 of $\overline{U}$ in the upper parts of the flow) in the trough region. The area of retarded flow in the trough area is increasingly pronounced, with an increasing divergence from velocities in the upper parts of the flow, which can be seen in the respective normalised velocity plots in Figures 4.84a, 4.85a and 4.86a.

As for the gravel or sand surface antidune bedform inserts and the openwork gravel antidune bedform inserts, for all amplitudes (Figures 4.81–4.83) the highest U_{rms} values occur adjacent to the bed. Similarly, for all three amplitudes U_{skew} is negative, meaning that whilst velocities are in general high, there is a notable amount of lower instantaneous velocities. For all three amplitudes, the lowest skew is present nearest the water surface (low friction, always high instantaneous velocities). Initially, a low skewness occurs adjacent to the bed (high friction, always small instantaneous velocities), more negative skewness being present in the middle parts of the flow. A cross-over effect can be seen developing for the 0.050 m, and then 0.075 m antidunes, as the most negative skew moves from the middle parts of the flow on the upstream antidune flank, to the bed on the downstream antidune. This is interpreted as being caused by the exposure of the downstream antidunes upstream facing flank to high velocity flow, the negative skew being caused by intermittent low instantaneous velocities attributable to the roughness of the adjacent bed. The line plots of $\overline{U}$, U_{rms} and U_{skew}, in Figures 4.87 – 4.89 further illustrate these trends.

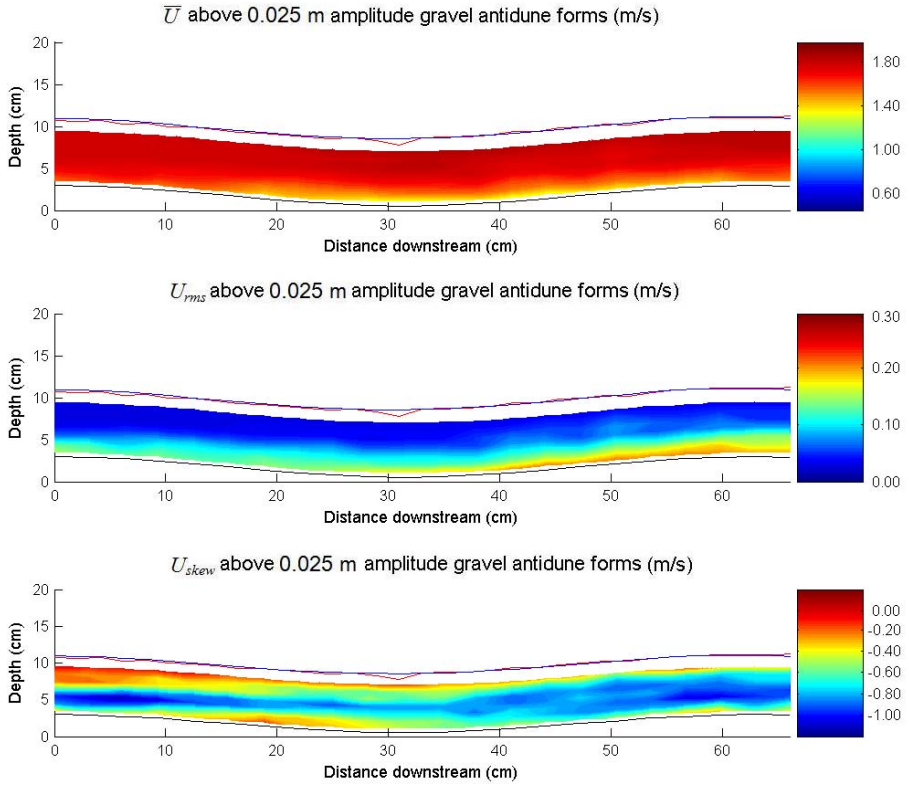

Figure 4.81 $\overline{U}$, U_{rms} and U_{skew} above a 0.025 m Amplitude Gravel Antidune Bedform (ADV: 25 Hz)

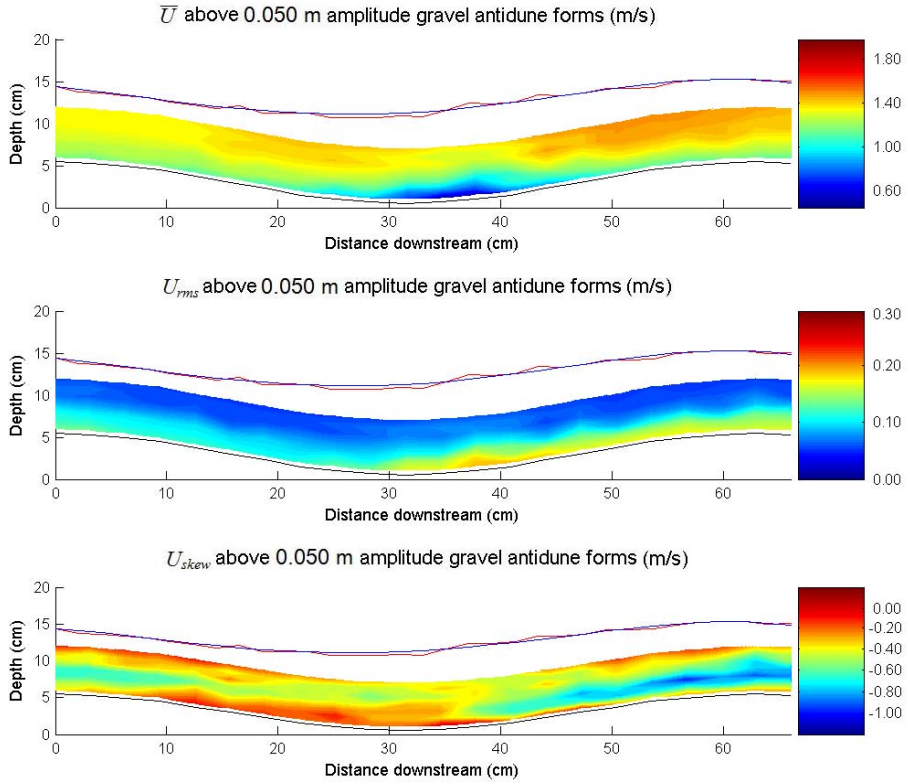

Figure 4.82 $\overline{U}$, U_{rms} and U_{skew} above a 0.050 m Amplitude Gravel Antidune Bedform (ADV: 25 Hz)

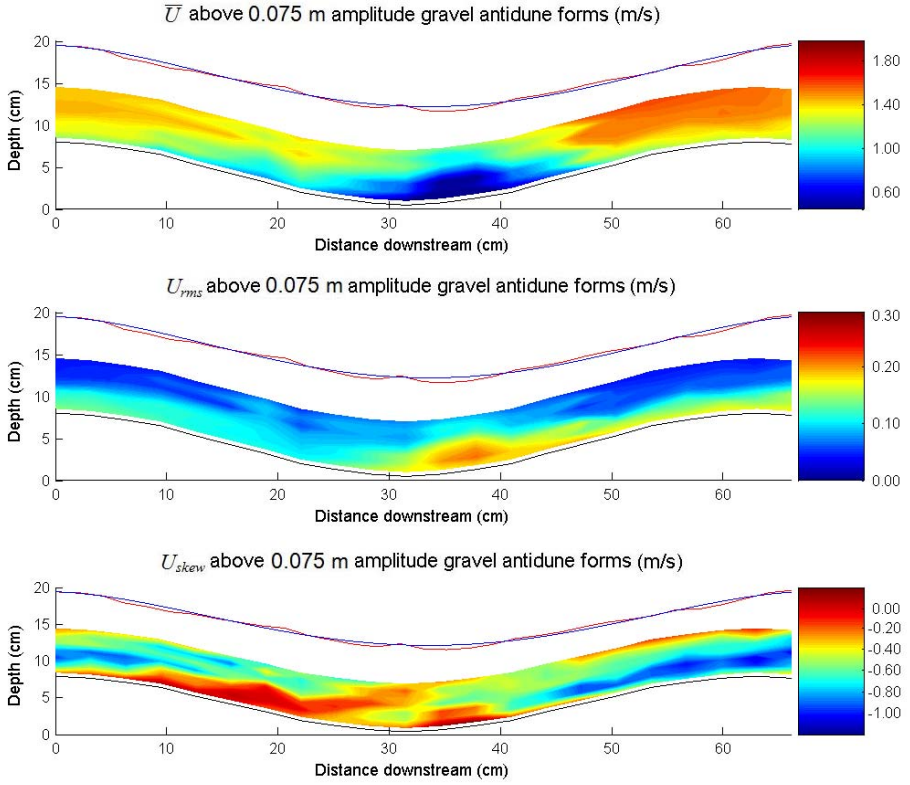

Figure 4.83 $\overline{U}$, U_{rms} and U_{skew} above a 0.075 m Amplitude Gravel Antidune Bedform (ADV: 25 Hz)

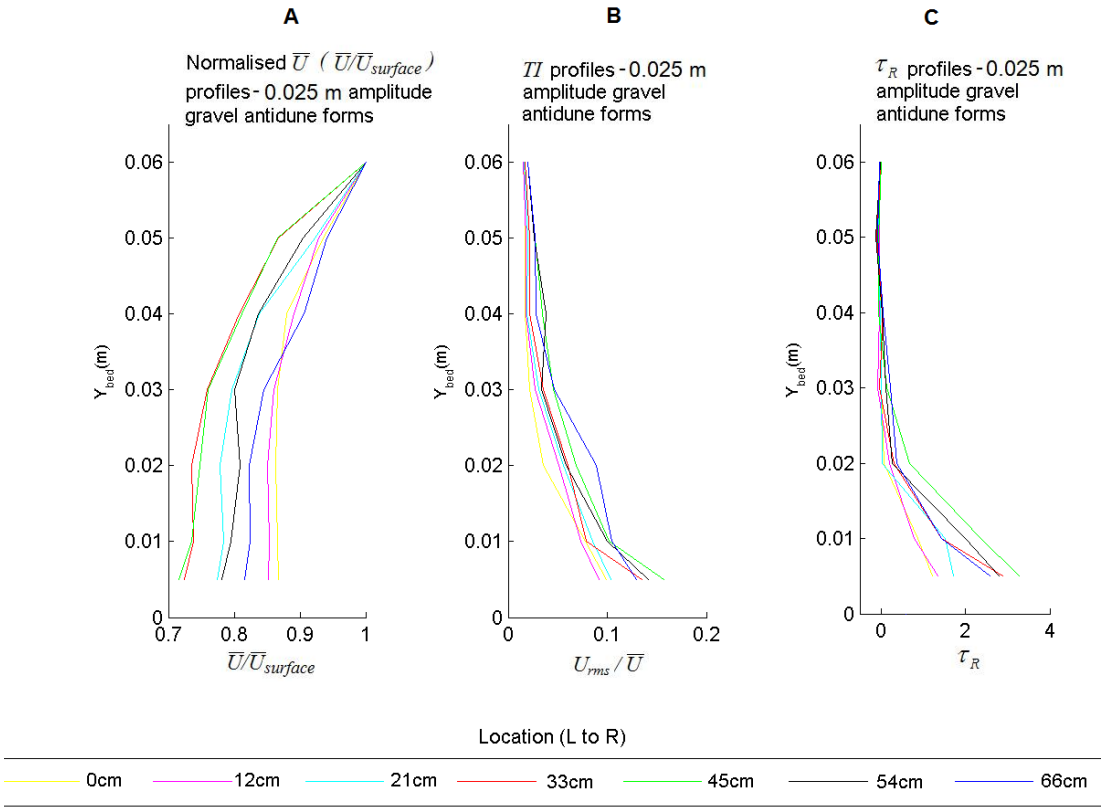

Figure 4.84 $\overline{U}$ *(normalised)*, TI and τ_R Profiles for Flow above a 0.025 m Amplitude Gravel Antidune Bedform (ADV: 25 Hz)

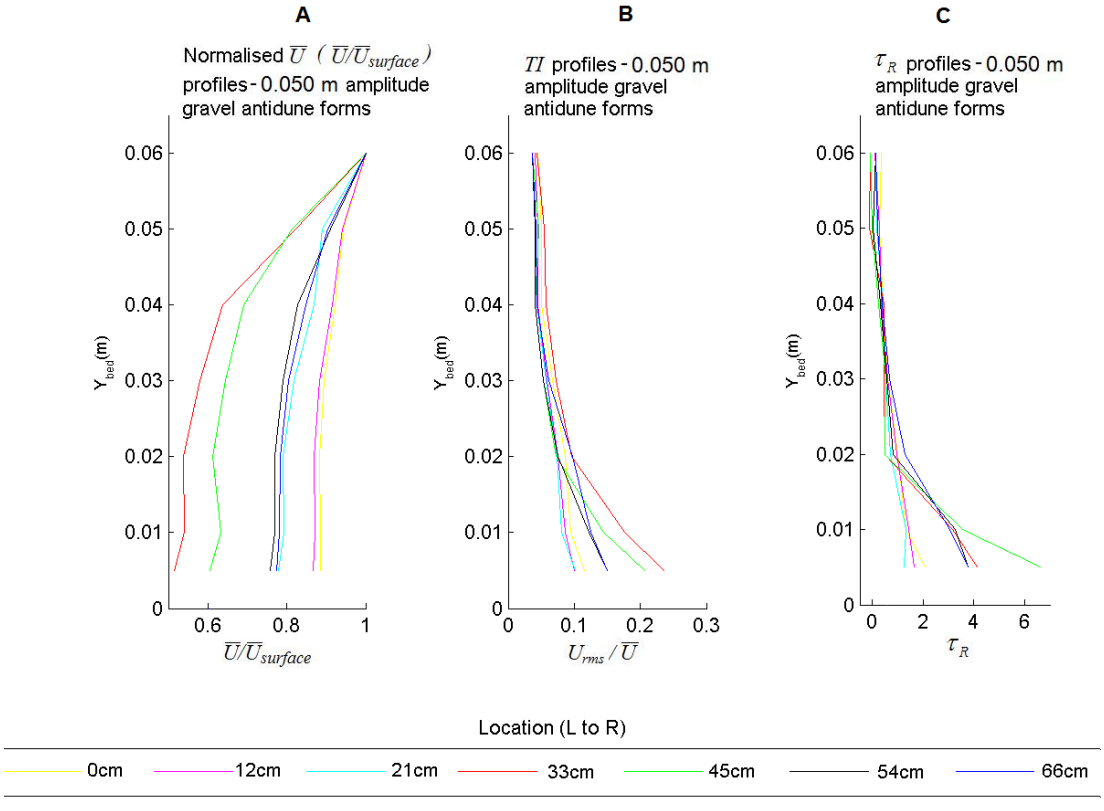

Figure 4.85 $\overline{U}$ *(normalised)*, TI and τ_R Profiles for Flow above a 0.050 m Amplitude Gravel Antidune Bedform (ADV: 25 Hz)

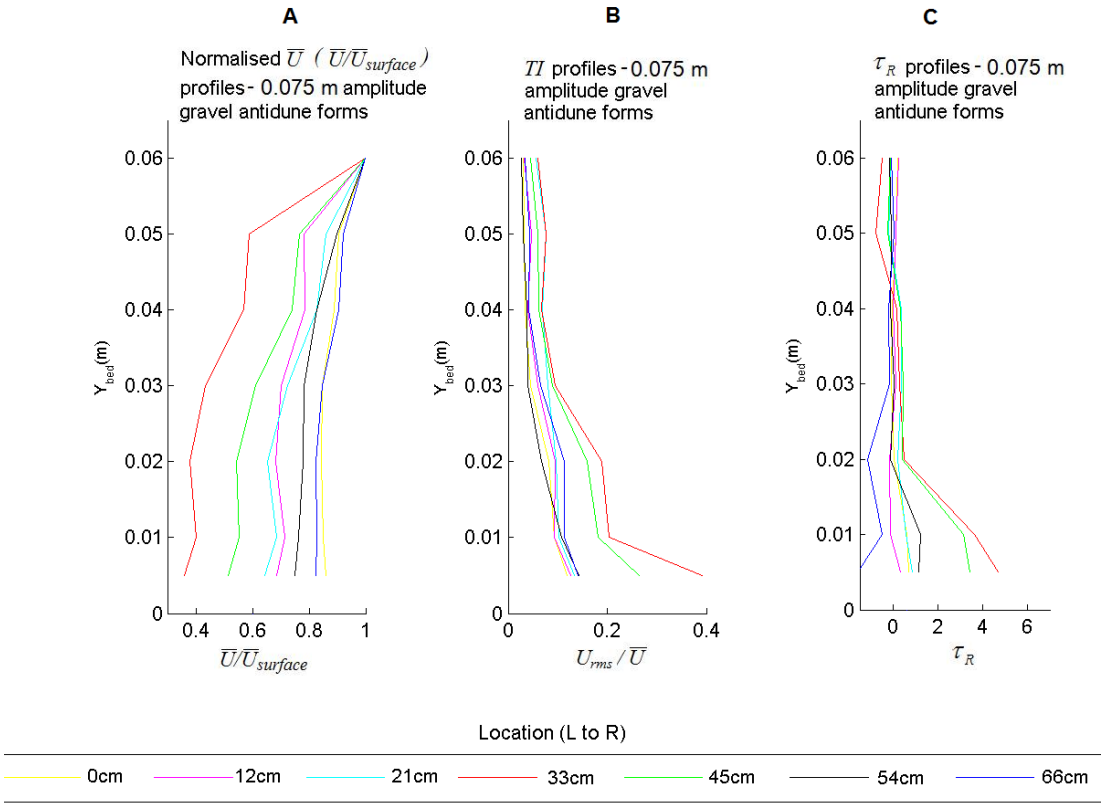

Figure 4.86 $\overline{U}$ *(normalised)*, TI and τ_R Profiles for Flow above a 0.075 m Amplitude Gravel Antidune Bedform (ADV: 25 Hz)

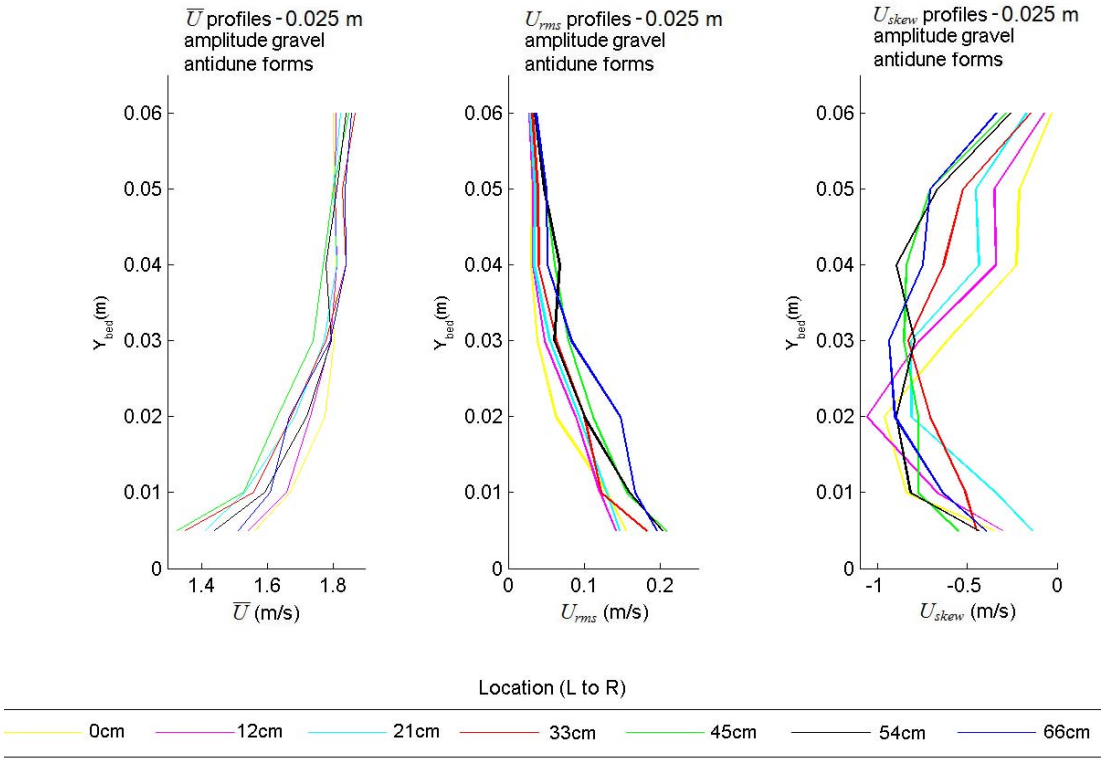

Figure 4.87 Profiles of $\overline{U}$, U_{rms} and U_{skew} for Flow above a 0.025 m Amplitude Gravel Antidune Bedform (ADV: 25 Hz)

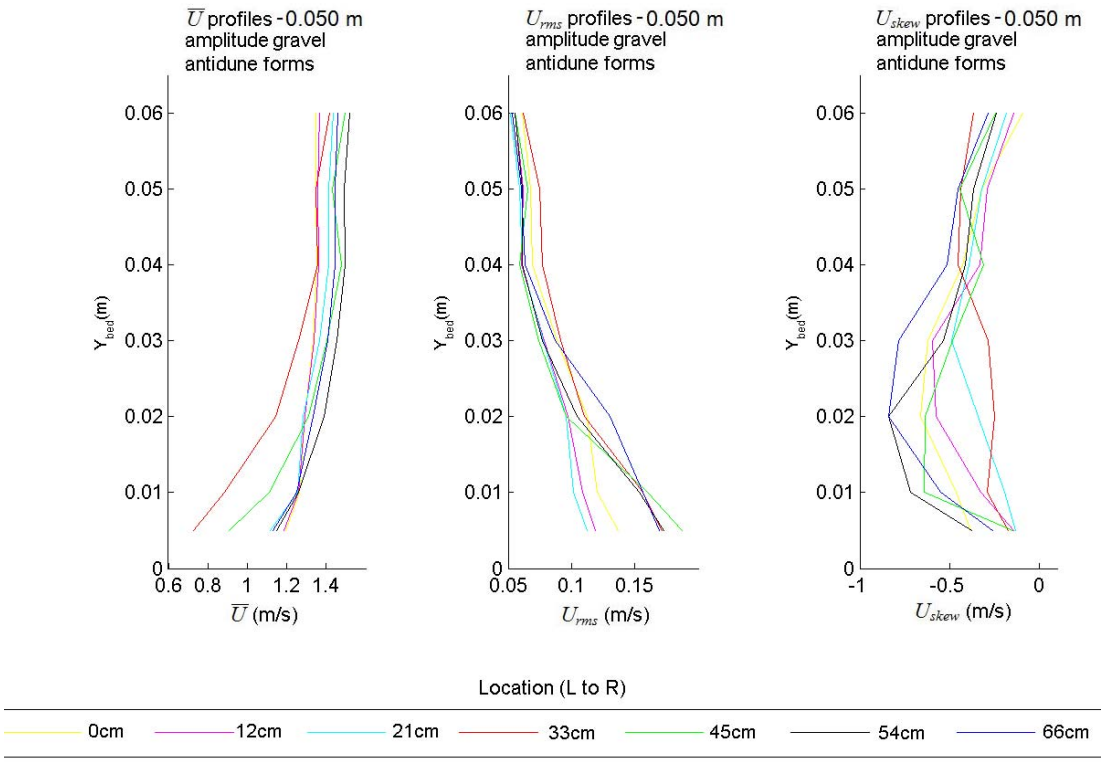

Figure 4.88 Profiles of $\overline{U}$, U_{rms} and U_{skew} for Flow above a 0.050 m Amplitude Gravel Antidune Bedform (ADV: 25 Hz)

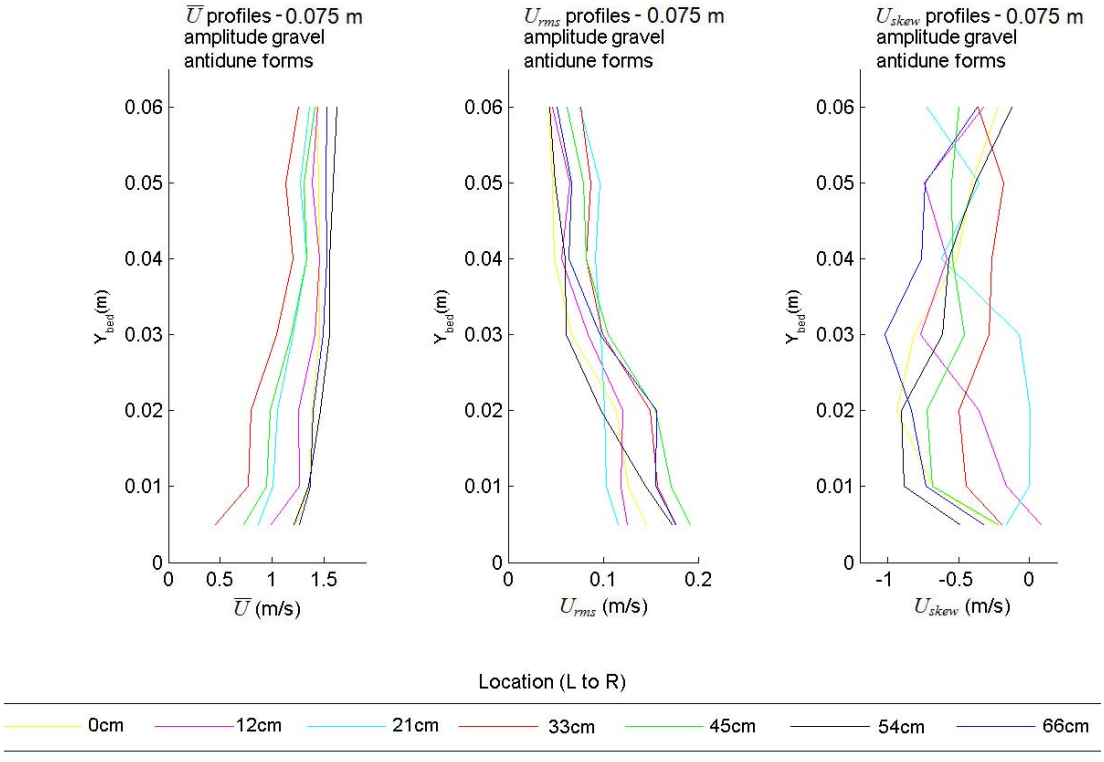

Figure 4.89 Profiles of $\overline{U}$, U_{rms} and U_{skew} for Flow above a 0.075 m Amplitude Gravel Antidune Bedform (ADV: 25 Hz)

4.4.2 $\overline{V}$, V_{rms} and V_{skew} for 0.025, 0.050 and 0.075 m Amplitude Gravel Antidune Bedforms

For the vertical velocity element, (Figures 4.90 – 4.92) $\overline{V}$ tends towards positive (away from the bed) in the flow immediately above the bed of the upstream antidunes crest and downstream flank, and in the upper parts of the flow above the downstream antidunes upstream facing flank. Velocity tends towards negative (towards the bed) in the upper parts of the flow above the upstream antidunes flank and trough. As the amplitude increases, values of $\overline{V}$ become increasingly negative in the upper parts of the flow on the downstream flank of the upstream antidune, and positive adjacent to the bed. As for U_{rms}, V_{rms} is highest near the bed, due to the variability of instantaneous velocities in the boundary layer above the antidune bedforms, becoming increasingly concentrated in the trough for 0.075m amplitude bedforms. Likewise, V_{skew} tends to be most negatively skewed in the lower parts of the flow and with limited, or a slight positive skew in the upper parts of the flow; this indicates the occurrence of occasional very high instantaneous velocities in the upper parts of the flow, and frequent low instantaneous velocities in the lower parts of the flow. The skews intensify from 0.025 to 0.050 m amplitude antidunes; although for 0.075 m amplitude antidunes there is no clear trend. The line plots of $\overline{V}$, V_{rms} and V_{skew}, in Figures 4.93 – 4.95 further illustrate these trends. The change from more vertically symmetric, to vertically asymmetric flow can be seen toward the trough region, the flow becoming increasingly vertically asymmetric as antidune amplitude increases.

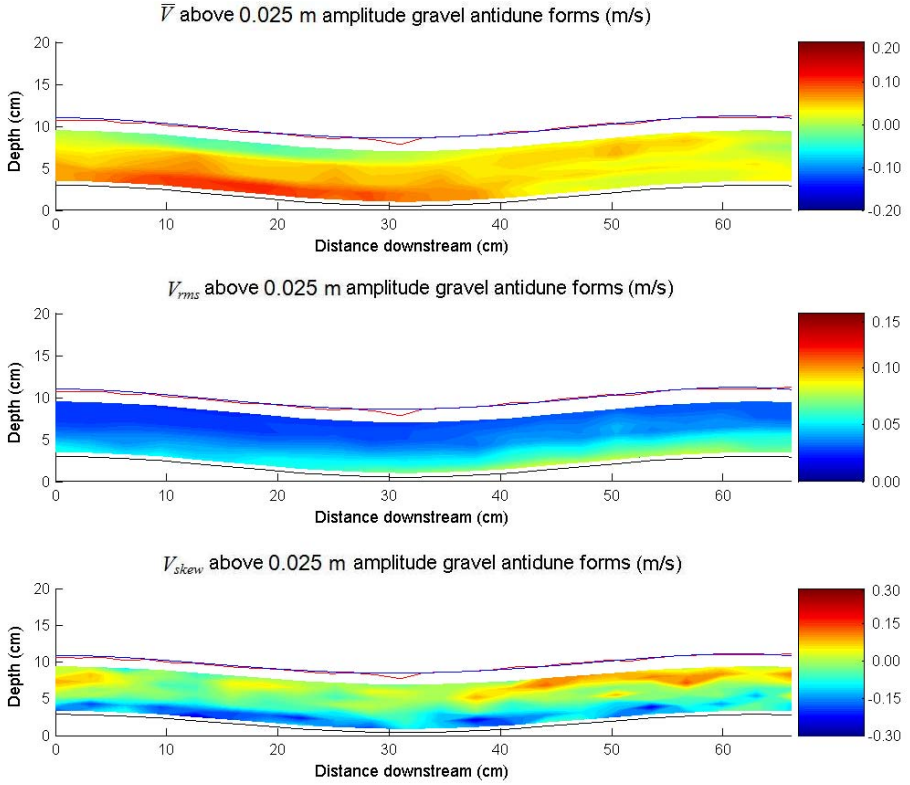

Figure 4.90 $\overline{V}$, V_{rms} and V_{skew} above a 0.025 m Amplitude Gravel Antidune Bedform (ADV: 25 Hz)

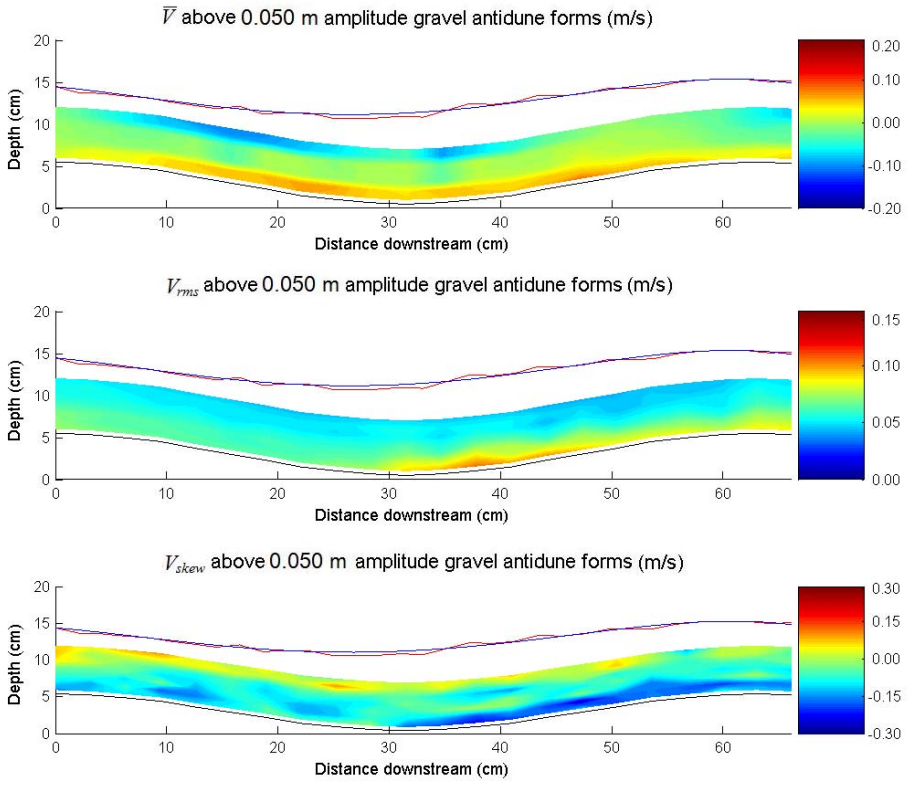

Figure 4.91 $\overline{V}$, V_{rms} and V_{skew} above a 0.050 m Amplitude Gravel Antidune Bedform (ADV: 25 Hz)

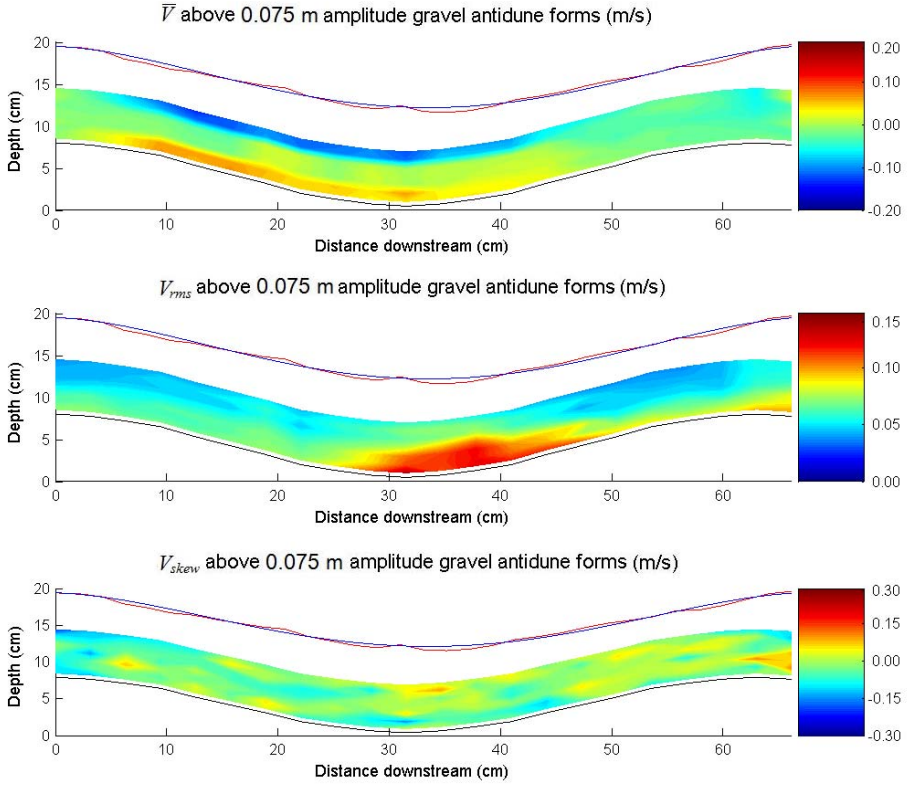

Figure 4.92 $\overline{V}$, V_{rms} and V_{skew} above a 0.075 m Amplitude Gravel Antidune Bedform (ADV: 25 Hz)

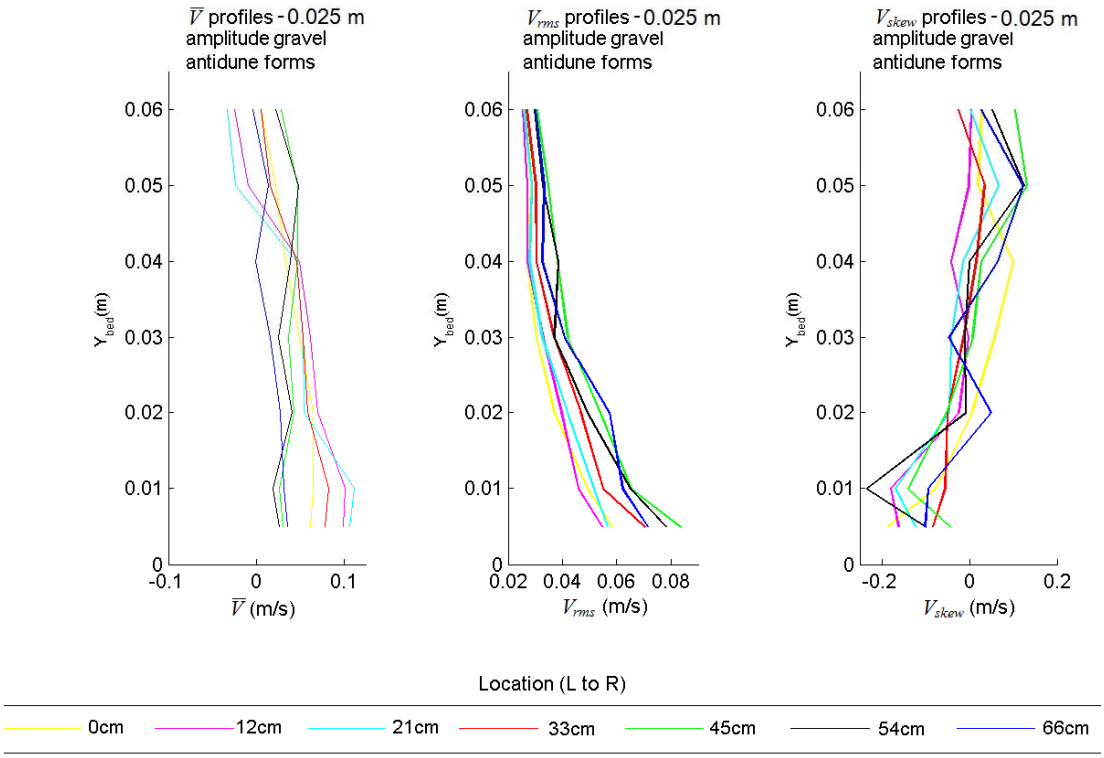

Figure 4.93 Profiles of $\overline{V}$, V_{rms} and V_{skew} for Flow above a 0.025 m Amplitude Gravel Antidune Bedform (ADV: 25 Hz)

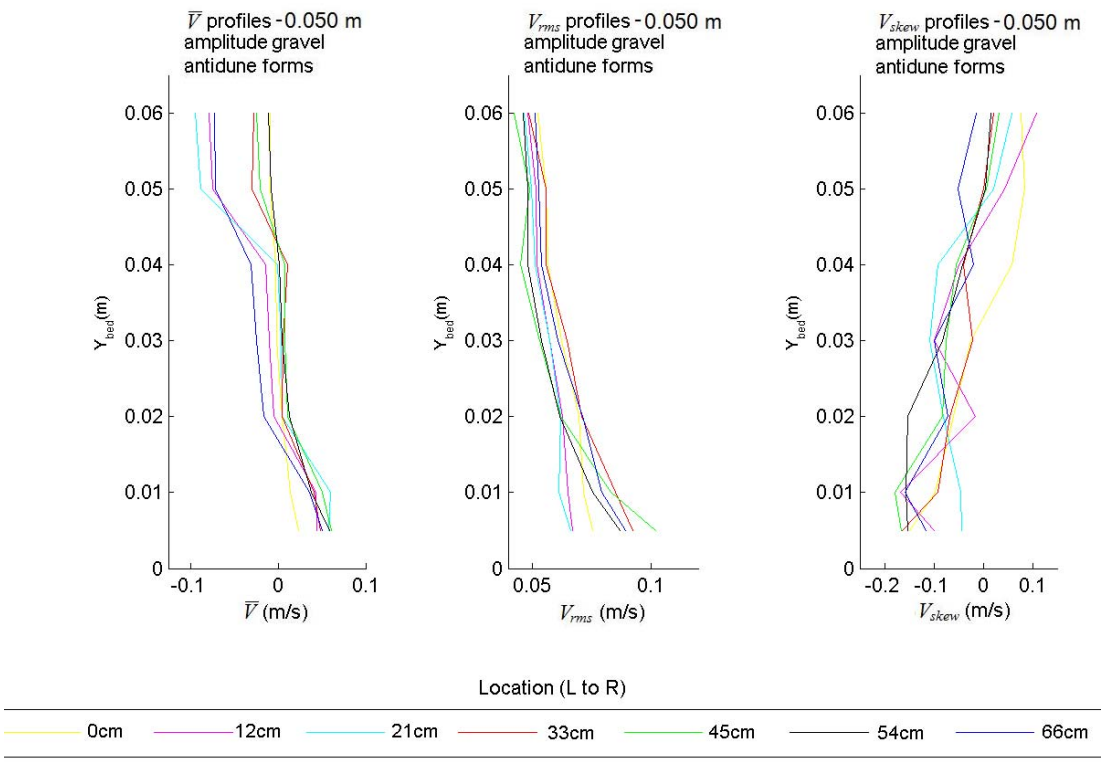

Figure 4.94 Profiles of $\overline{V}$, V_{rms} and V_{skew} for Flow above a 0.050 m Amplitude Gravel Antidune Bedform (ADV: 25 Hz)

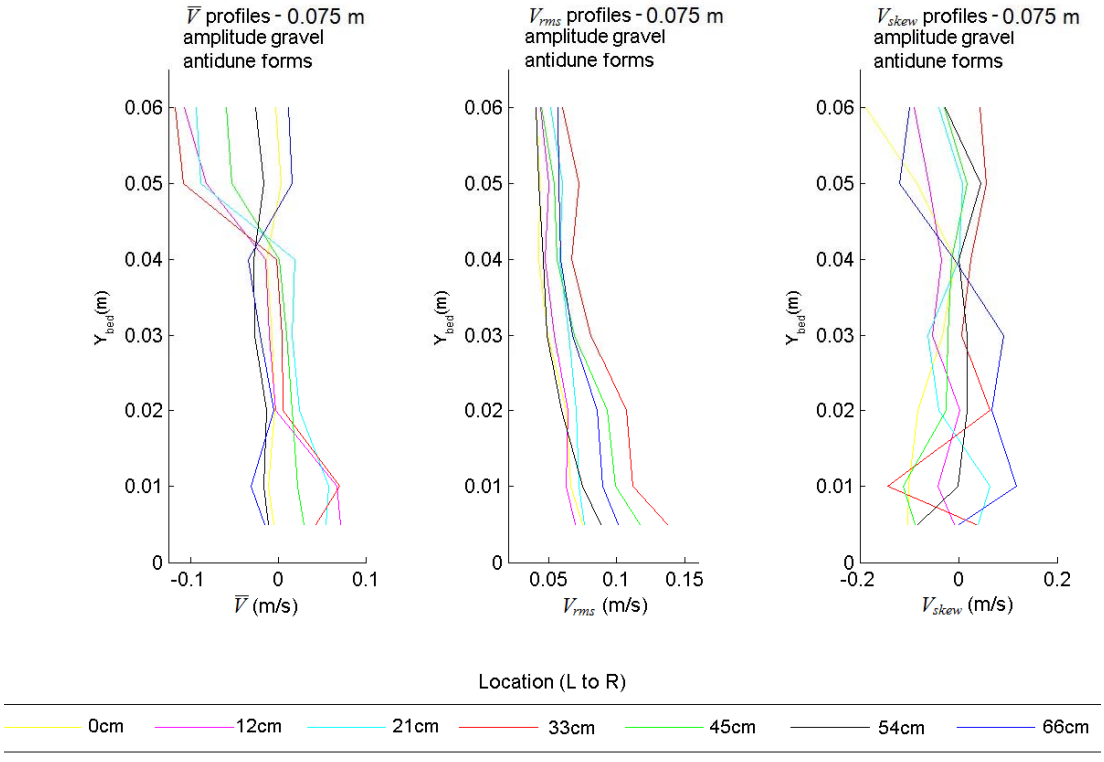

Figure 4.95 Profiles of $\overline{V}$, V_{rms} and V_{skew} for Flow above a 0.075 m Amplitude Gravel Antidune Bedform (ADV: 25 Hz)

4.4.3 $\overline{W}$, W_{rms} and W_{skew} for 0.025, 0.050 and 0.075 m Amplitude Gravel Antidune Bedforms

In terms of $\overline{W}$ (Figures 4.96 – 4.98) there is a clear, oscillating side to side secondary flow element in the flume, giving blocks of positive and negative $\overline{W}$. W_{rms} is highest nearest the bed, and becomes increasingly large in the trough region, whilst W_{skew} values are more difficult to interpret, and appear to be heavily influenced by the secondary current.

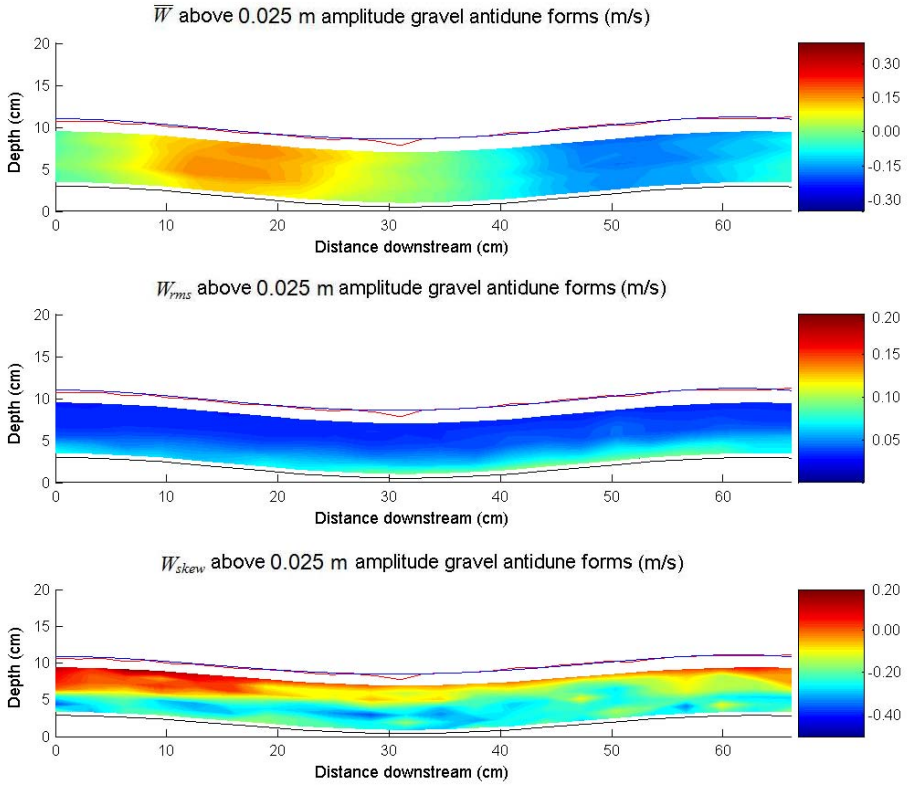

Figure 4.96 $\overline{W}$, W_{rms} and W_{skew} above a 0.025 m Amplitude Gravel Antidune Bedform (ADV: 25 Hz)

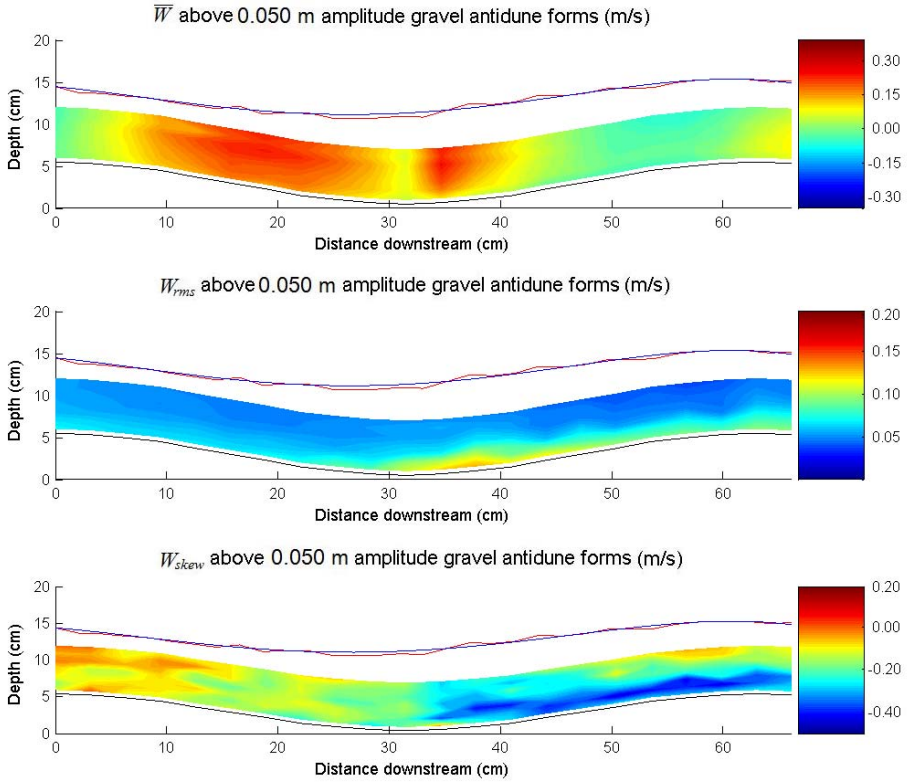

Figure 4.97 $\overline{W}$, W_{rms} and W_{skew} above a 0.050 m Amplitude Gravel Antidune Bedform (ADV: 25 Hz)

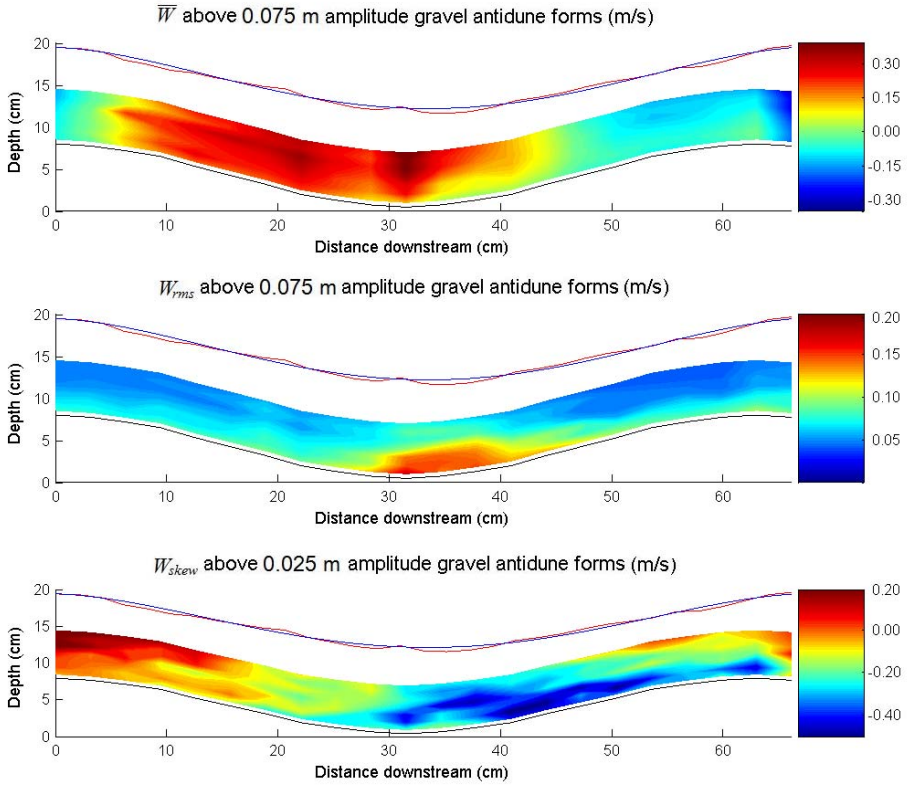

Figure 4.98 $\overline{W}$, W_{rms} and W_{skew} above a 0.075 m Amplitude Gravel Antidune Bedform (ADV: 25 Hz)

4.4.4 TKE and τ_R for 0.025, 0.050 and 0.075 m Amplitude Gravel Antidune Bedforms

Plots of TKE and τ_R (Figures 4.99 – 4.101) show close agreement, and indicate stresses are highest adjacent to the bed, especially on the upstream facing flank of the downstream antidune. An increase in TKE and τ_R can be seen with increasing amplitude from 0.025 m through to 0.075 m antidune. Although initially more spread along the upstream facing flank of the downstream antidune, stresses become increasingly concentrated in the trough region. The increases in τ_R towards the bed and particularly at the trough can be seen in the respective line plots in Figures 4.84c, 4.85c and 4.86c. The change from more vertically symmetric, to vertically asymmetric flow can be seen toward the trough region, the flow becoming increasingly vertically asymmetric as antidune amplitude increases.

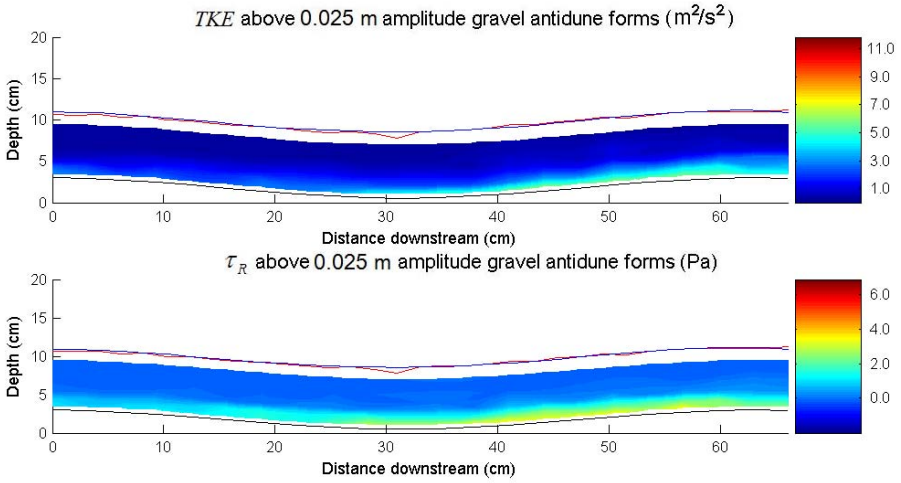

Figure 4.99 TKE and τ_R above a 0.025 m Amplitude Gravel Antidune Bedform (ADV: 25 Hz)

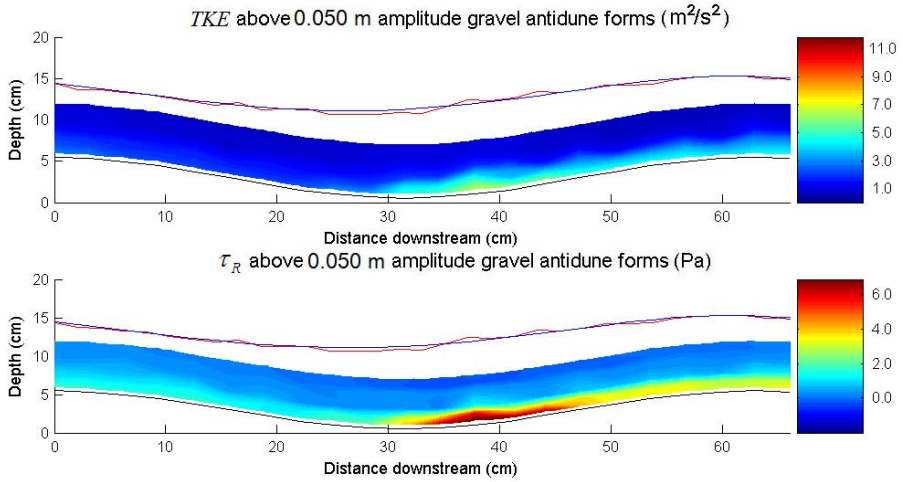

Figure 4.100 TKE **and** τ_R **above a 0.050 m Amplitude Gravel Antidune Bedform (ADV: 25 Hz)**

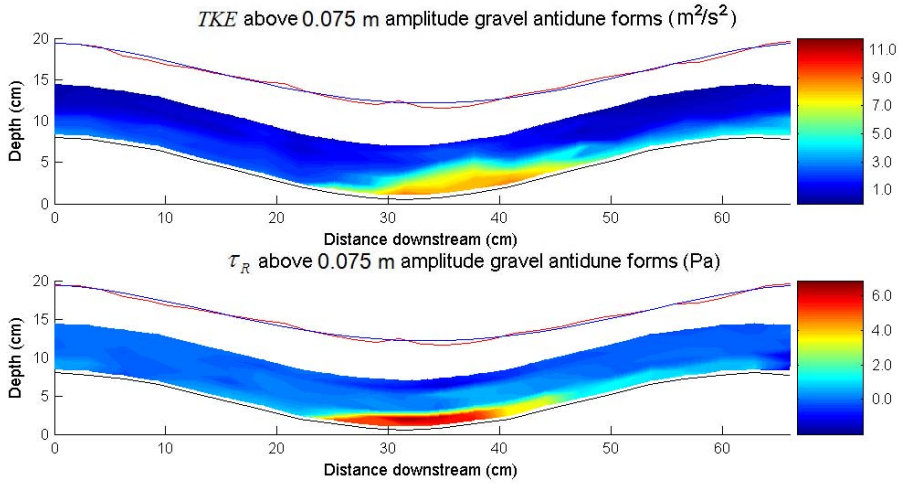

Figure 4.101 TKE **and** τ_R **above a 0.075 m Amplitude Gravel Antidune Bedform (ADV: 25 Hz)**

4.4.5 Quadrant Analysis – Gravel Antidune Bedforms 25 Hz

Proportion of Time Events above a Hole Size of 2 for 0.025, 0.050 and 0.075 m Amplitude Gravel Antidune Bedforms

Quadrant Analysis (Figures 4.102 – 4.104) shows that the for all quadrants, the most events above the hole size occur in the upper parts of the flow. Significant events of sedimentological importance occur adjacent to the bed for between 0.1% and 3.5% of the velocity record.

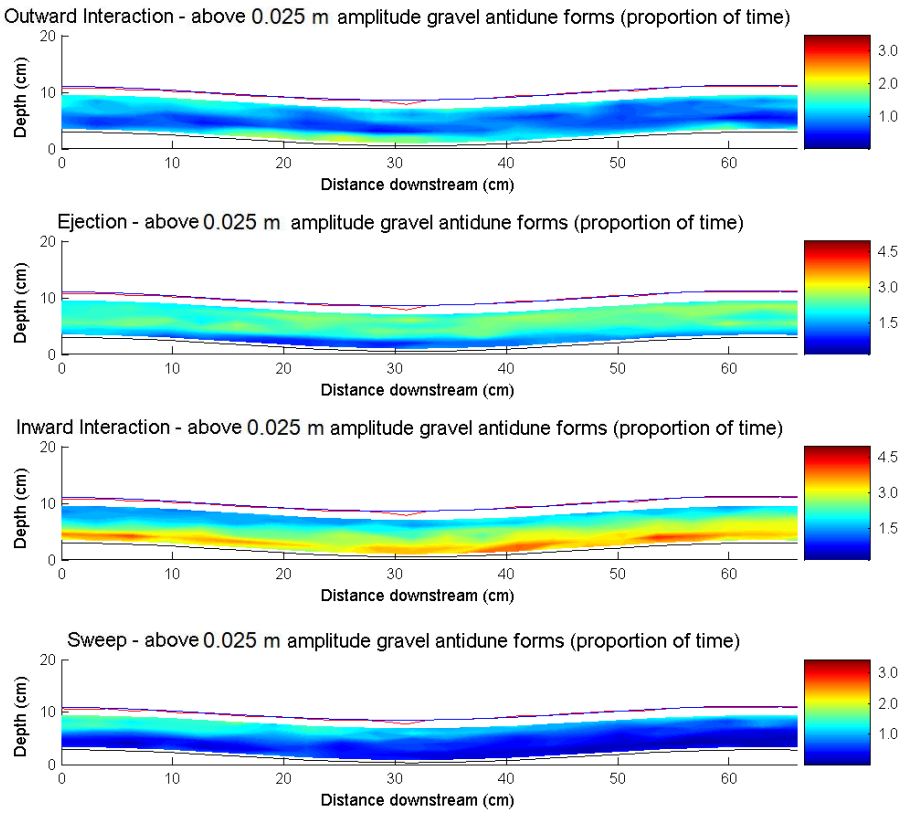

Figure 4.102 Quadrant Analysis of Turbulence above a 0.025 m Amplitude Gravel Antidune Bedform (ADV: 25 Hz, Proportion of Time Events above Hole Size = 2)

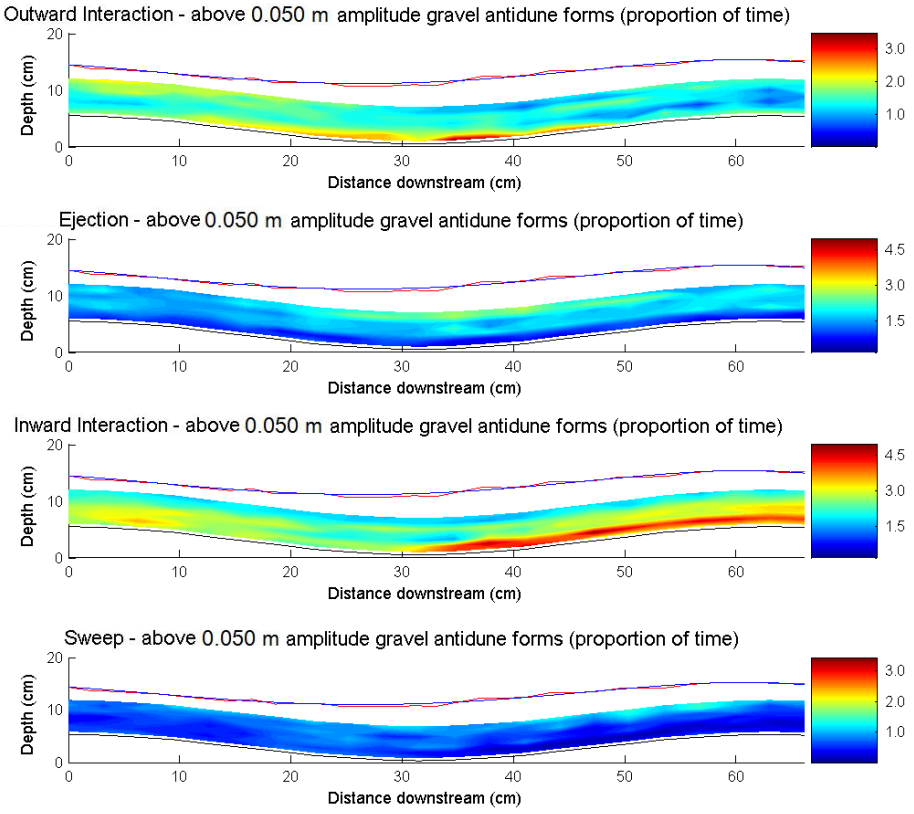

Figure 4.103 Quadrant Analysis of Turbulence above a 0.050 m Amplitude Gravel Antidune Bedform (ADV: 25 Hz, Proportion of Time Events above Hole Size = 2)

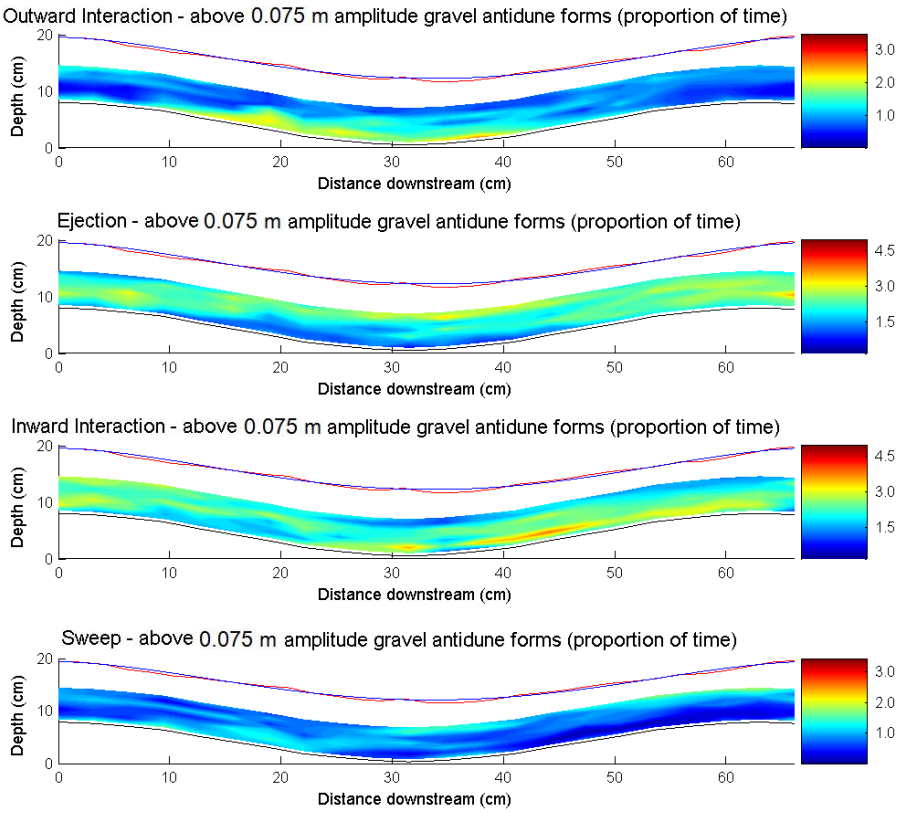

Figure 4.104 Quadrant Analysis of Turbulence above a 0.075 m Amplitude Gravel Antidune Bedform (ADV: 25 Hz, Proportion of Time Events above Hole Size = 2)

Mean Stress for Events above a Hole Size of 2 for 0.025, 0.050 and 0.075 m Amplitude Gravel Antidune Bedforms

Investigation of the average $|u'v'|$ stresses (Figures 4.105 – 4.107) during these events indicates that the highest $|u'v'|$ stresses occur adjacent to the bed. For the 0.025 and 0.050 m amplitude cases, the stresses are distributed at the bed along the majority of the boundary layer, but mostly the upstream facing flank of the downstream antidune, although for 0.075 m bedforms, highest stresses are more concentrated in the trough region. $|u'v'|$ values during ejections increase from -0.053 m/s for 0.025 m, to -0.056 m/s for 0.050 m and -0.073 m/s for 0.075 m bedforms. There is a change from stresses being distributed over the downstream antidunes upstream facing flank and crest for 0.025 m and 0.050 m bedforms, towards concentration in the trough region for 0.075 m bedforms. Likewise for sweeps, $|u'v'|$ values increase from -0.043 m/s for 0.025 m, to -0.058 m/s for 0.050 m bedforms

and -0.069 m/s for 0.075 m bedforms. A trend of increasing concentration of stresses towards the trough with increasing amplitude is evident.

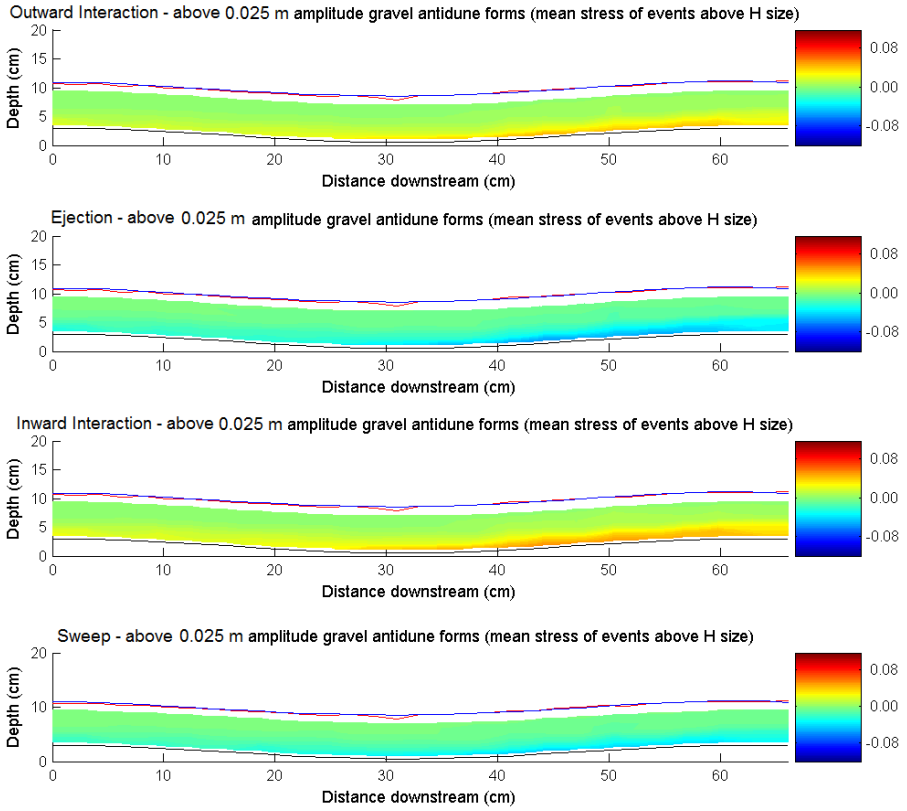

Figure 4.105 Quadrant Analysis of Turbulence above a 0.025 m Amplitude Gravel Antidune Bedform (ADV: 25 Hz, Mean Stress for Events above Hole Size = 2)

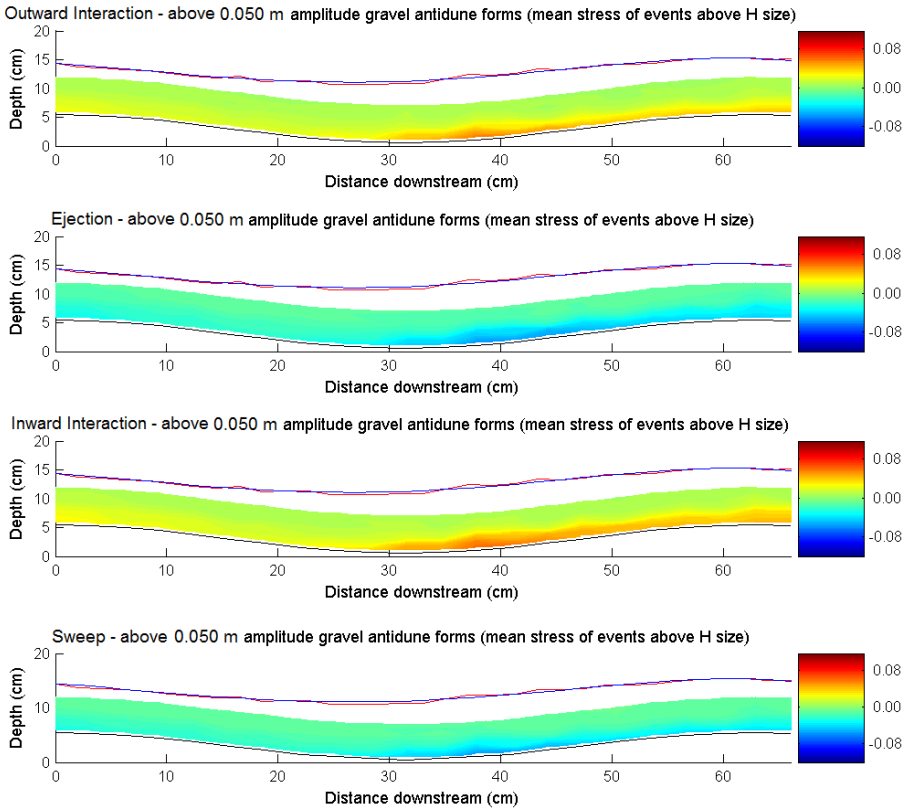

Figure 4.106 Quadrant Analysis of Turbulence above a 0.050 m Amplitude Gravel Antidune Bedform (ADV: 25 Hz, Mean Stress for Events above Hole Size = 2)

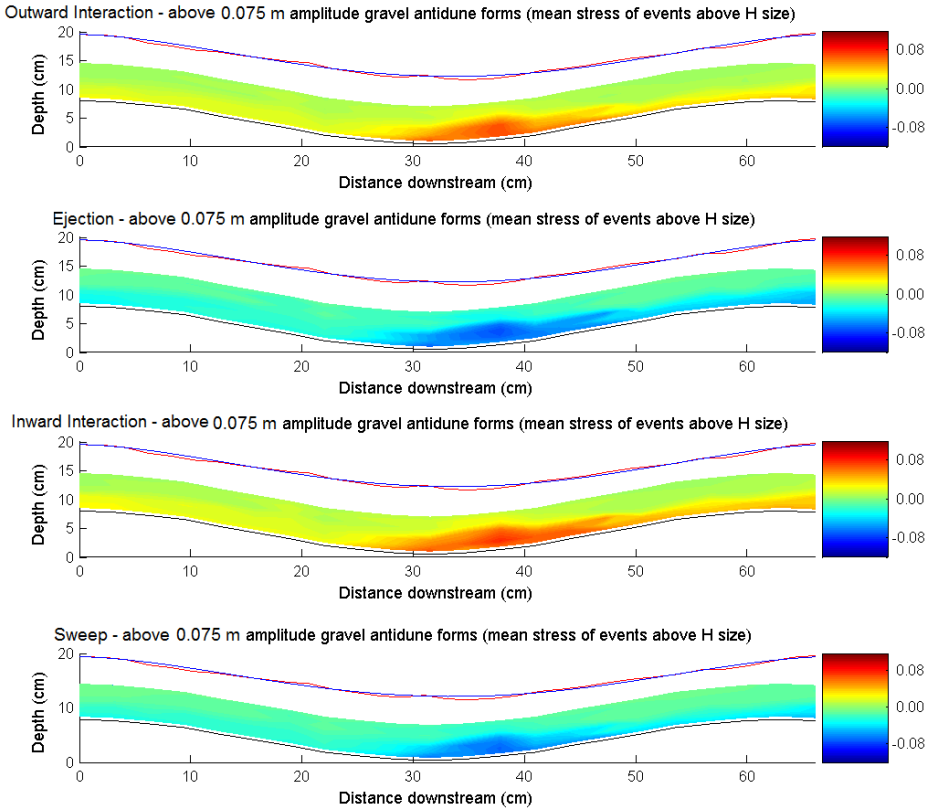

Figure 4.107 Quadrant Analysis of Turbulence above a 0.075 m Amplitude Gravel Antidune Bedform (ADV: 25 Hz, Mean Stress for Events above Hole Size = 2)

4.4.6 P, R and TI for 0.025, 0.050 and 0.075 m Amplitude Gravel Antidune Bedforms

Plots of P, R and TI (Figures 4.108 – 4.110), support the above results and interpretations. For the 0.025 m and 0.050 m amplitude cases P is concentrated at the bed along upstream facing flank of the downstream antidune, with values of around 1 for both amplitudes. For 0.075 m bedforms, levels drop back to 0.42, and become are concentrated in the trough region. R, a measure of the presence and integrity of any boundary layer, is relatively evenly distributed over 0.025 m antidunes (R: 0.2), indicating a constant, thin semi-developed boundary layer. However, for 0.050 m (R: 0.15 to 0.25) and especially 0.075 m amplitude bedforms (R: 0.00 to 0.15) high values of R occur primarily in the trough region. As for P, TI is highest in the trough between each antidune for all three amplitudes of bedform. Values of TI increase from 0.14, to 0.33 and 0.65 for 0.025 m, 0.050 m and 0.075 m amplitude bedforms, intensity being greatest between trough and crest of the downstream antidune for 0.025 m and 0.050 m bedforms, but concentrated in the trough area for 0.075 m bedforms. The increases in TI towards the bed, and particularly at the trough can be seen in the respective line plots in Figures 4.84b, 4.85b and 4.85c.

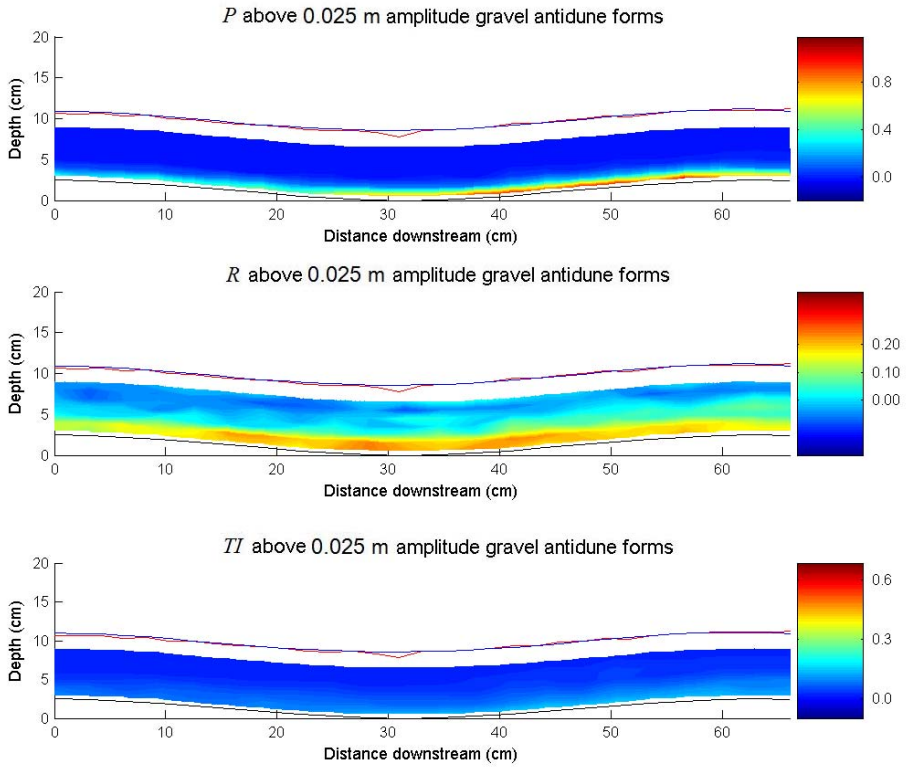

Figure 4.108 P, R and TI above a 0.025 m Amplitude Gravel Antidune Bedform (ADV: 25 Hz)

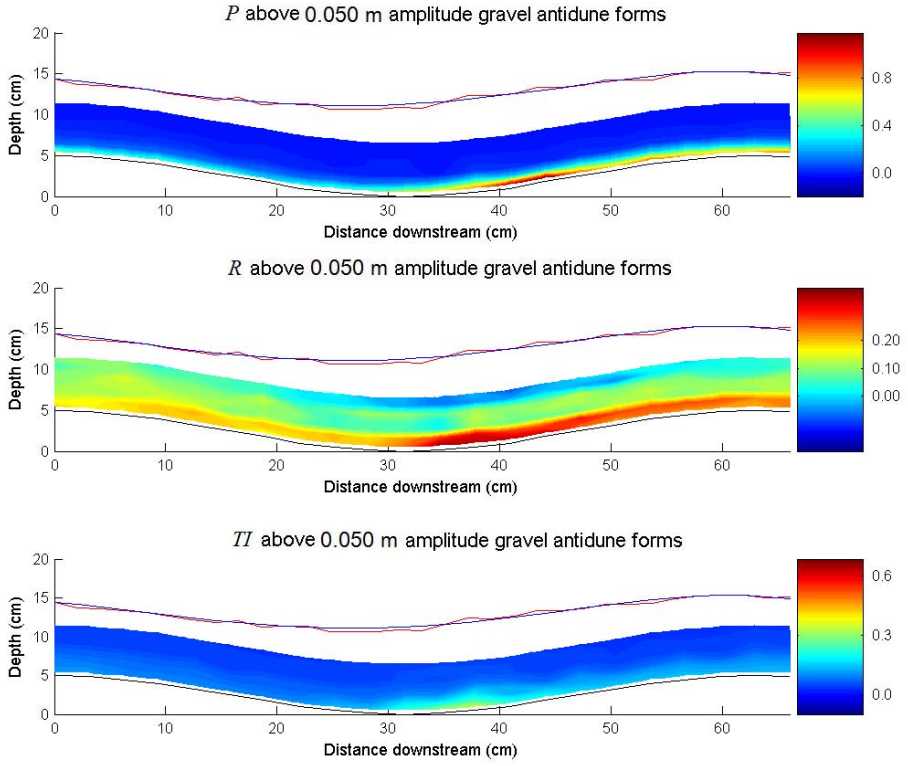

Figure 4.109 P, R and TI above a 0.050 m Amplitude Gravel Antidune Bedform (ADV: 25 Hz)

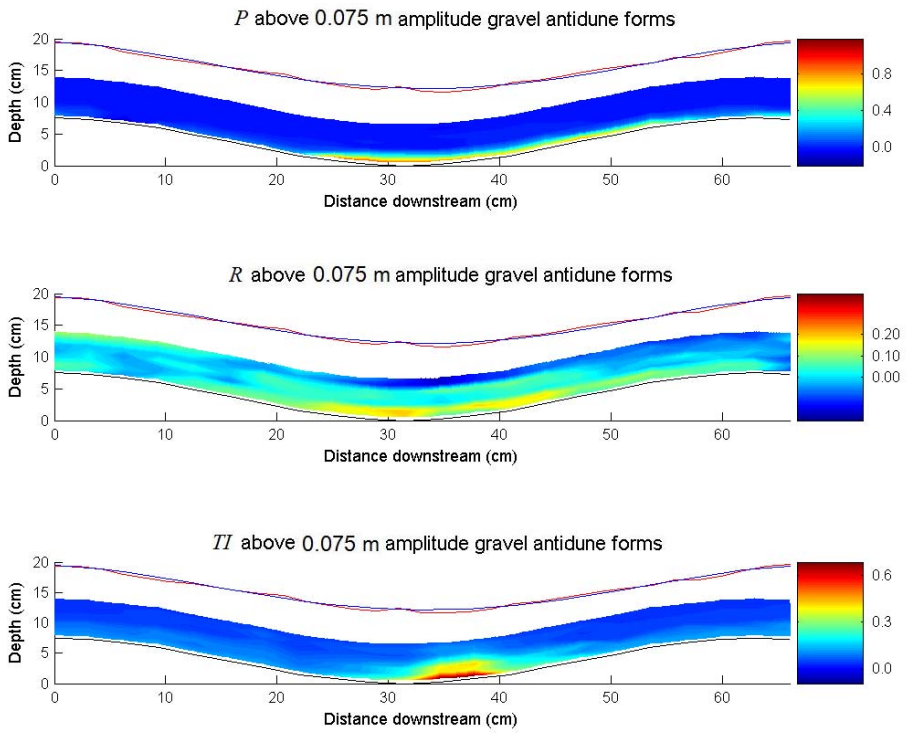

Figure 4.110 P, R and TI above a 0.075 m Amplitude Gravel Antidune Bedform (ADV: 25 Hz)

Summary – Turbulence Structure over Gravel Surfaced Antidunes

25 Hz ADV investigations show that the most intense turbulence occurs in the trough region. In this lower trough region there is a marked reduction in values of $\overline{U}$, and a corresponding increase in U_{rms} and V_{rms}. This difference in $\overline{U}$ values between the lower trough and upper parts of the flow increases (values of $\overline{U}$ in the lower trough being 76%, 46% and 38% of the $\overline{U}$ value in the flow above for 0.025, 0.050 and 0.075 m amplitude forms respectively) as antidune amplitude increases. In the region between the downstream end of the trough and lower slope of the downstream antidune, values of turbulent stresses increase progressively[1]: TI [0.14, 0.32 and 0.65], τ_R [3.2, 6.5 and 5], and TKE [5.5, 6 and 7.5], whilst Q2 (ejections) and Q4 (sweeps) become increasingly spatially concentrated into this region. The magnitude of these values increases as the antidune amplitude increases. It is postulated that the intense turbulence associated with steepening antidunes, may lead to rapid erosion in the trough, steepening the downstream bedform, which causes the standing wave to collapse.

Compared to solid gravel surfaced antidune forms at 100 Hz (see Box 4.1), the values for turbulence statistics over solid gravel surfaced antidune forms at 25 Hz are very similar – indicating a consistency between 100 Hz and 25 Hz ADV measurements. However, given that the 25 Hz ADV may have underestimated

these turbulence statistics (see discussion in Section 3.3.1), it is thought that turbulence is infact more intense (up to 60%) over these forms. Since the 100 Hz ADV may have underestimated these turbulence statistics (see discussion in Section 3.3.1), by up to 30% the close match remains. Importantly this lends veracity to the open-gravel and sand surfaced antidune measurements which were only collected at 25 Hz. This is discussed further in Section 7.1.1.

[1]Numbers in square brackets refer to values for 0.025, 0.050 and 0.075 m amplitude antidune bedforms respectively.

Box 4.4 Summary of Flow Profile and Turbulence over Gravel Surfaced Antidunes (25 Hz)

4.5 Spectral Analysis of ADV Turbulence Data

Spectral Analysis for gravel surfaced antidune bedforms (Figures 4.111 – 4.113) show that the turbulence spectra in the U and V dimensions follow Kolmogorov's -5/3 dissipation rate (larger less frequent eddies, dissipate into smaller more frequent perturbations). The inertial subrange for the U and V dimensions being clearly delineated by the -5/3 slope. Turbulence spectra in the W (spanwise) dimension appear to match the -5/3 dissipation rate comparatively poorly. From the unequal velocity spectras in Figures 4.111 to 4.113, it is clear that turbulence is nonisotropic. The levelling off of the spectras at high frequency represents the Doppler noise floor, which is a characteristic of Doppler based systems such as ADV at higher frequencies approaching the Nyquist frequency (Lohrmann *et al*., 1994). In the U and V domain dominant frequencies appear at around: 0.5, 0.7, 1.1, 1.3, 1.5 and 1.7 Hz, and further significant peaks at around 2.1, 2.9, 3.7, 4.6, 5.5 Hz. Shvidchenko and Pender (2001) noted a peak periodicity around ~2.5 Hz for their experiment (mean velocity 0.75 m/s), and in reviewed experiments (again 0.75m/s). In this experiment (~1.5 m/s) the higher frequencies observed compare well with the previously observed 2.5 Hz value. Best and Kostaschuk (2002) found that the higher frequency peaks were associated with turbulence generation near the bed. Lower frequencies were found to be more dominant in the flow further away from the bed, and were associated with eddy shedding associated with the separation zone between dunes. The spectral peaks observed are therefore thought to indicate that the full flow depth is dominated by high frequency turbulence shedding in the near bed zone. The lack of low frequency peaks is indicative of the lack of eddy shedding, due to the lack of zones of flow separation

For Gravel antidunes with a 25 Hz ADV, (Figures A1 – A3, Appendix A): dominant frequencies appear at: 0.5, 1.1, 1.5, 2.4 and 3 Hz. For Openwork-Gravel antidunes with a 25 Hz ADV, (Figures A4 – A5, Appendix A): dominant frequencies appear at: 0.7, 1.2, 1.4, 1.5, 1.7, 2.1, 2.3 and 2.7. For Sand antidunes with a 25 Hz ADV (Figures A6 – A8, Appendix A):

dominant frequencies appear at: 0.7, 1.1, 1.3, 1.6, 1.7, 2.1, 2.4, 2.8, 3.0 and 3.2. The same trends can be identified in the 25 Hz data as have been detailed above for the analysis of 100 Hz ADV data.

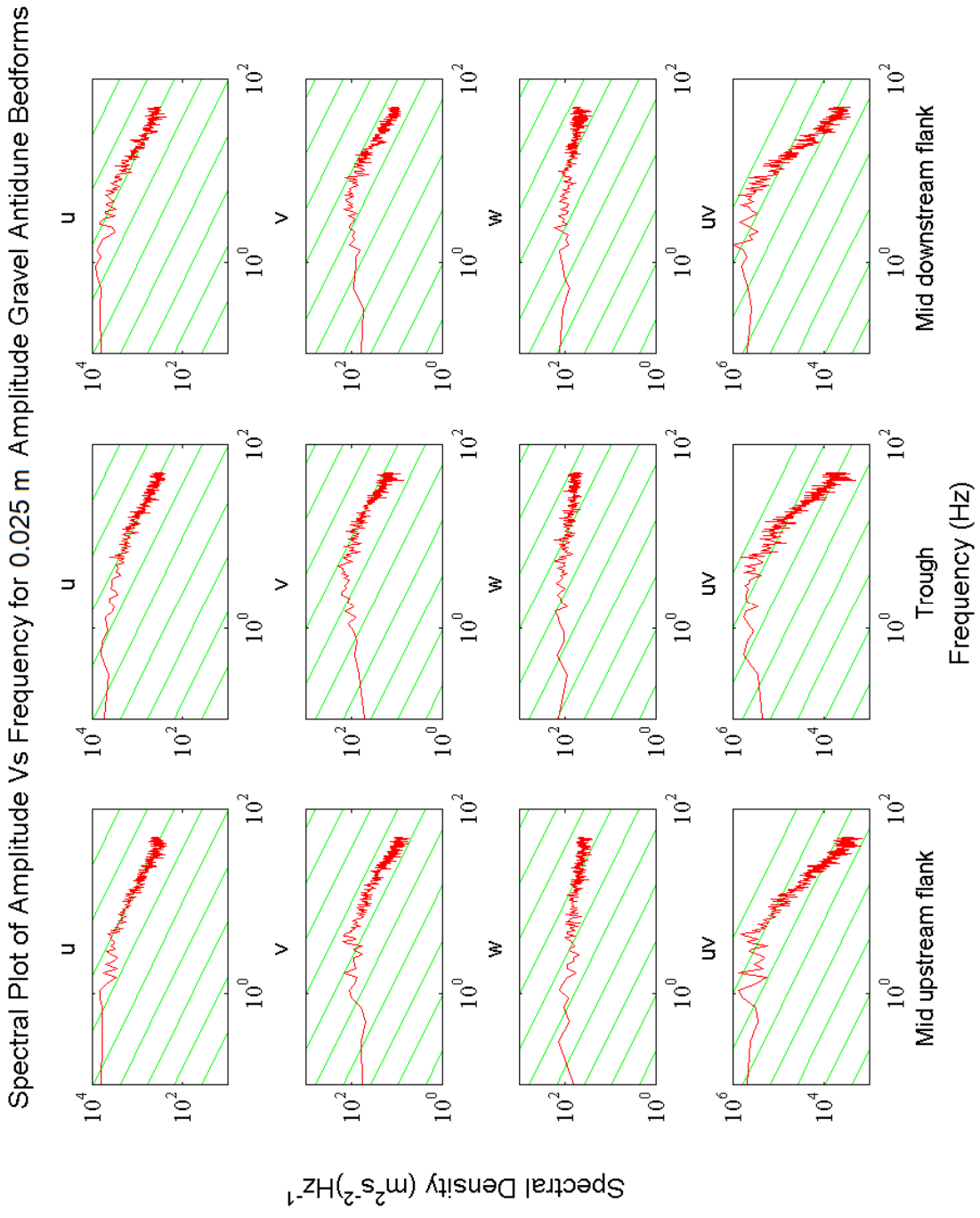

Figure 4.111 Spectral Plots for 0.025 m Amplitude Gravel Antidune, 180 s Record (ADV:100 Hz)

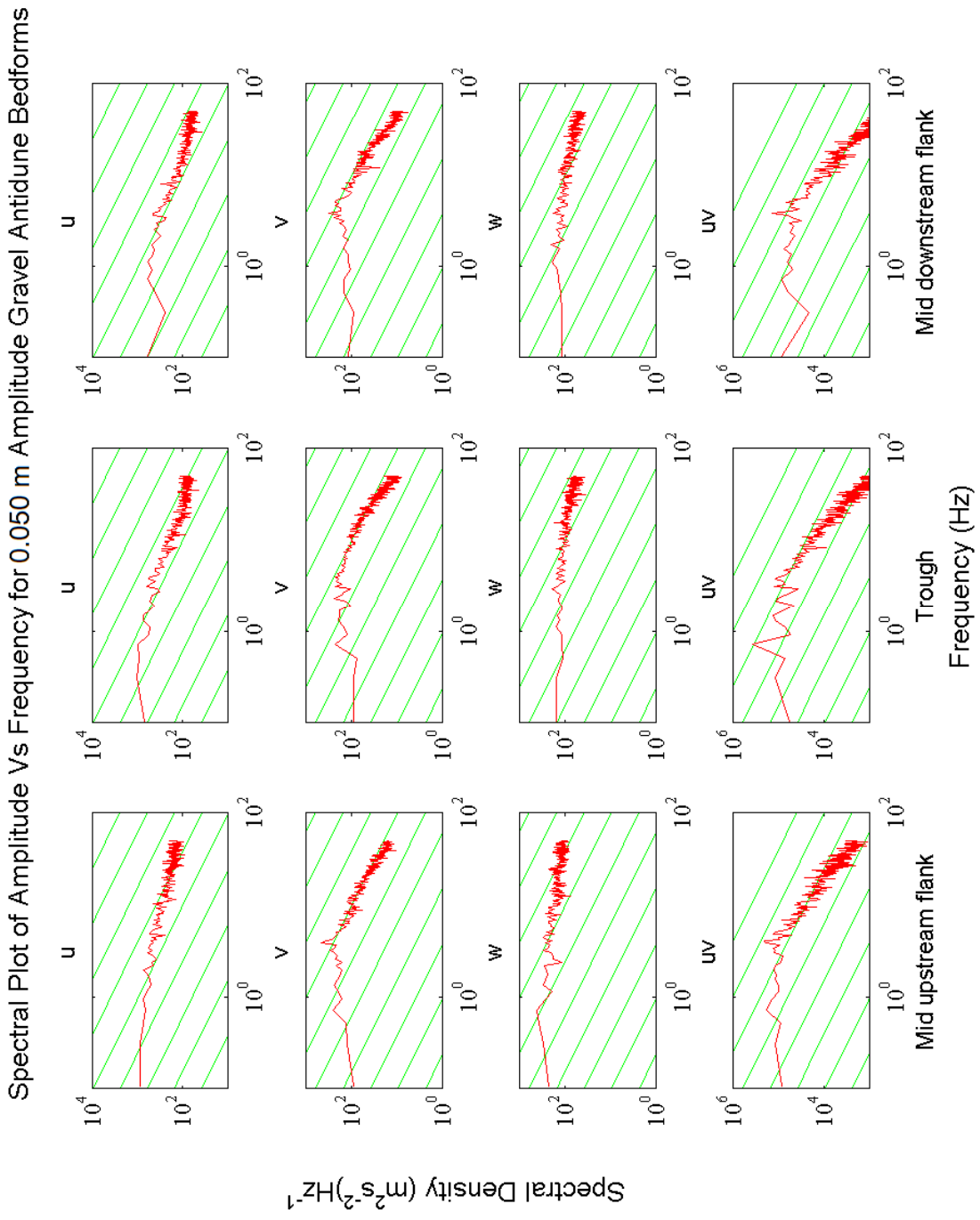

Figure 4.112 Spectral Plots for 0.050 m Amplitude Gravel Antidune, 180 s Record (ADV:100 Hz)

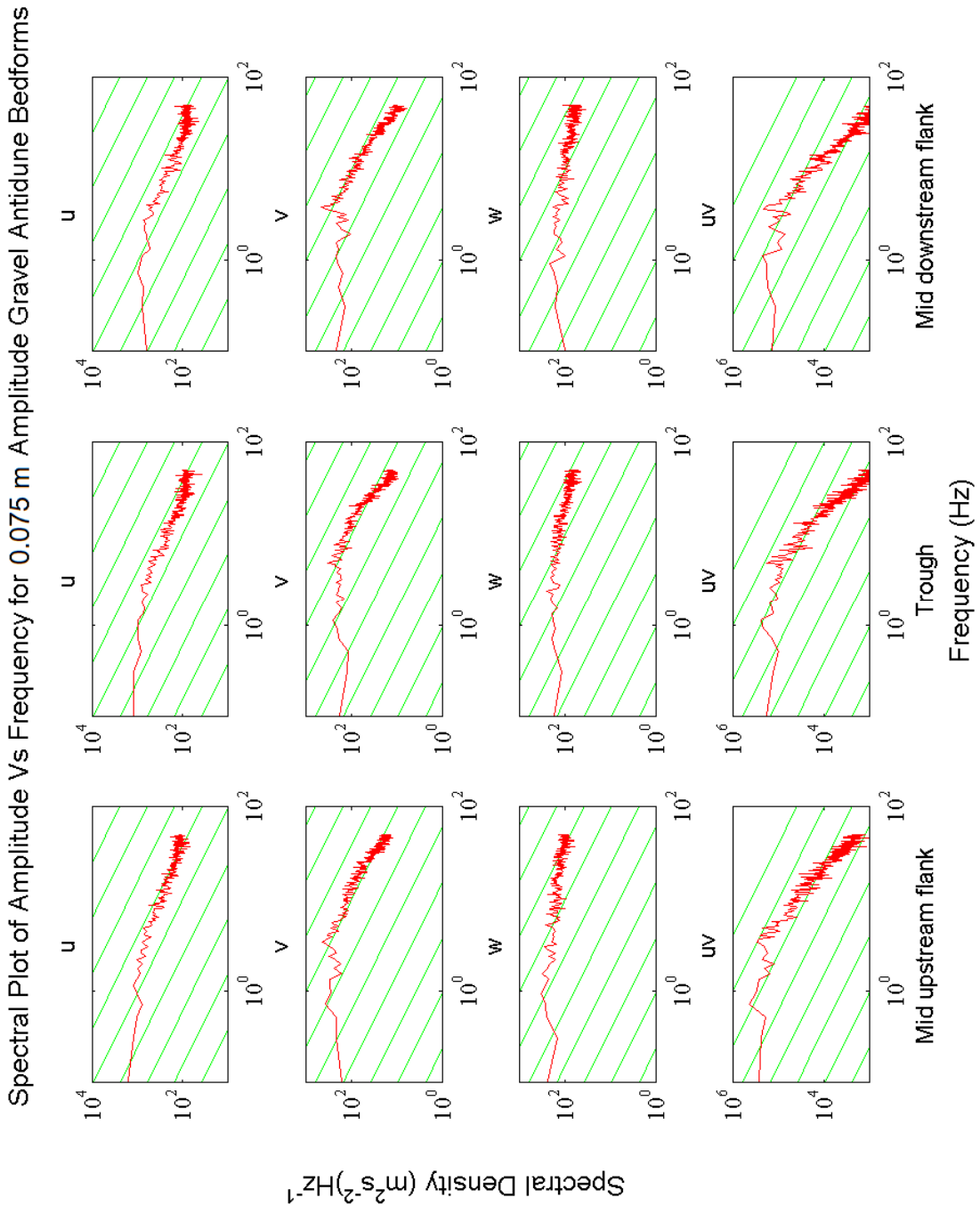

Figure 4.113 Spectral Plots for 0.075 m Amplitude Gravel Antidune, 180 s Record (ADV:100 Hz)

5 High Speed Video of Antidune Regime Flow – Results and Interpretation

5.1 Flow Conditions During Runs

The methods and techniques used in these experiments are outlined in the Methodology (**Chapter 3**).

5.2 High-Speed Video Stills

5.2.1 Observed Hydrodynamics

Composite still images of the flow extracted from the high-speed video imagery for gravel surfaced antidune bedforms (0.025, 0.050 and 0.075 m amplitudes) are shown in Figures 5.1 – 5.3, and sand surfaced antidune bedforms (0.025, 0.050 and 0.075 m amplitudes) in Figures 5.7 – 5.9. Individual frames for the gravel antidunes are shown in Figures 5.4 – 5.6. Flow is left to right in all images; yellow arrow annotations indicate typical observed particle streak lengths from play-back of the video at each location along the profile. The length of each yellow arrow is proportional to the length of streaks observed during video playback. In these images streaks are visible from the time a particle enters the frame from upstream, or from outside the light curtain, or the bed, to the time when they leave the downstream-side of frame or the light curtain. Within this period, the particle trajectory is sub-divided by the frame-speed of the camera into the streaks apparent in individual images. All tracer particles were moving downstream-wards as the streaks formed. The number of frames shown in each of the five parts of Figures 5.4, 5.5 and 5.6 (a, b, c, d and e) relate to the uniformity of observed tracer particle streaks. In sub-figures a and e the tracer streak lengths and trajectories were generally uniform, but in sub-figures b, c and d a greater variety of tracer particle streak lengths and trajectories were observed. For these latter sub-figures typical sequences of tracer streaks are presented over several frames.

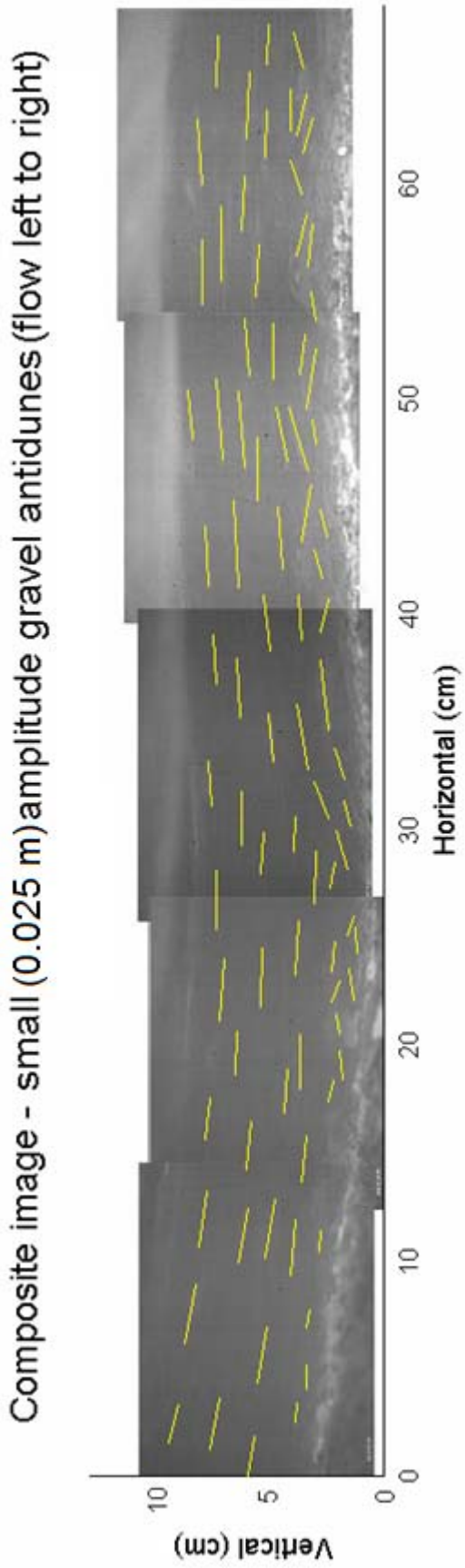

Figure 5.1 Annotation of Spatial Characteristics of Streaks over a 0.025 m Amplitude Gravel Antidune

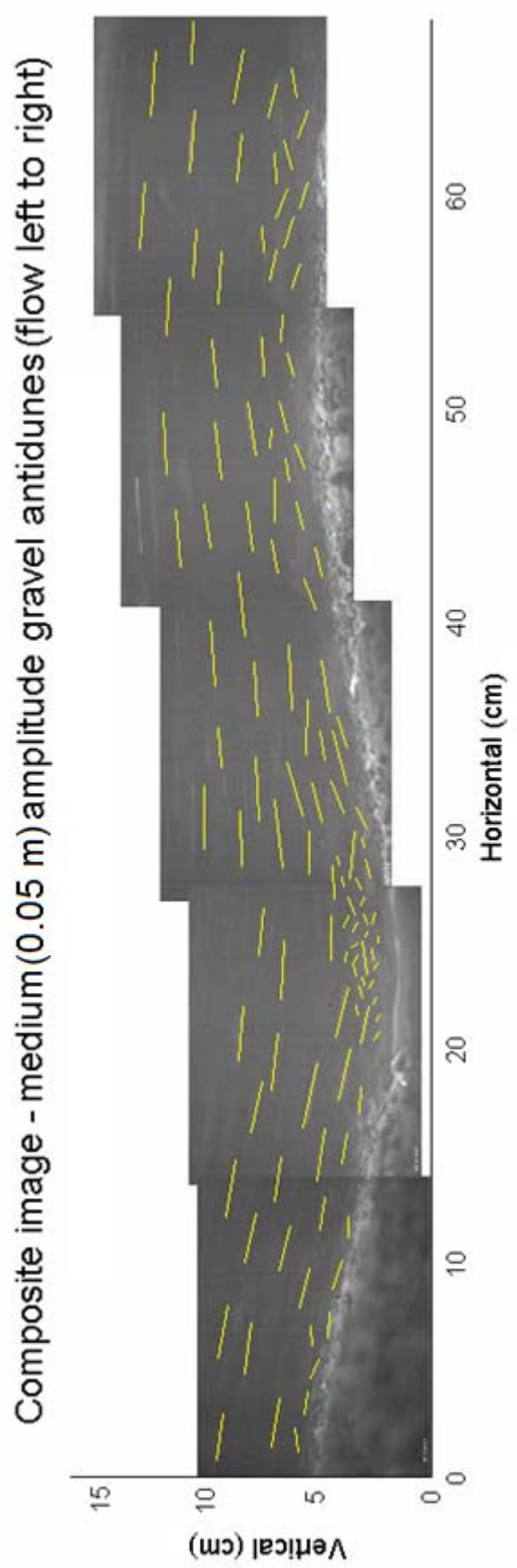

Figure 5.2 Annotation of Spatial Characteristics of Streaks over a 0.050 m Amplitude Gravel Antidune

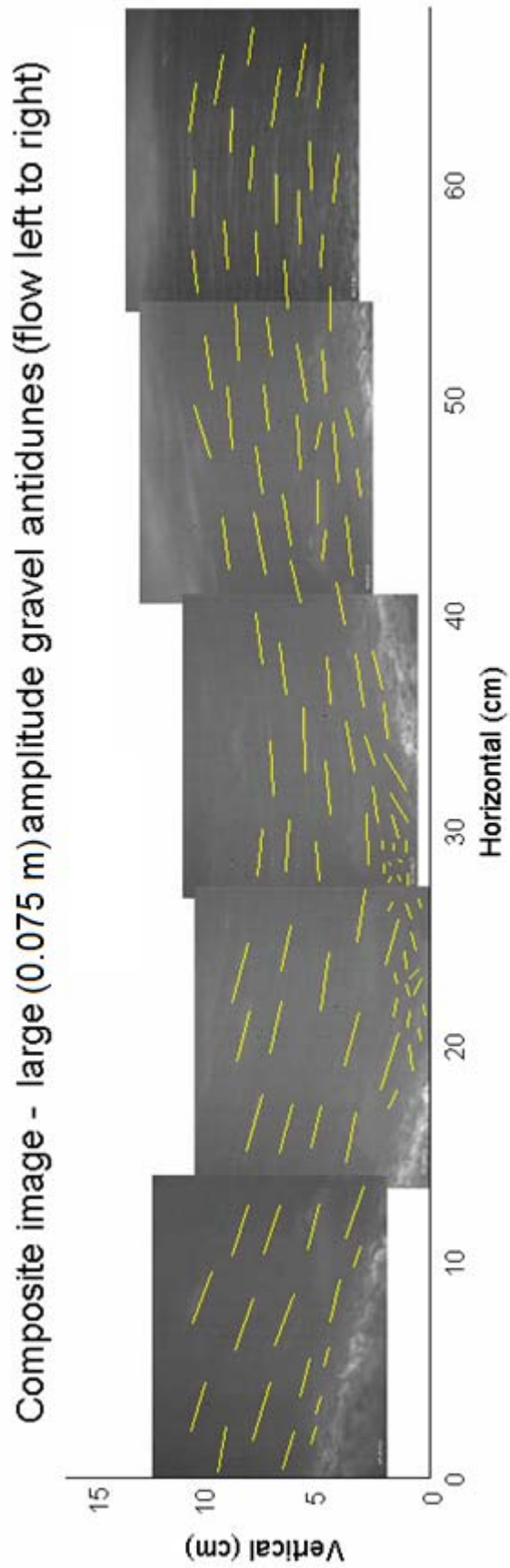

Figure 5.3 Annotation of Spatial Characteristics of Streaks over a 0.075 m Amplitude Gravel Antidune

Figure 5.4 Annotation of Temporal Distribution of Streaks over a 0.025 m Amplitude Gravel Antidune

Figure 5.4a - Part 1 of 5 (crest of upstream antidune bedform insert)

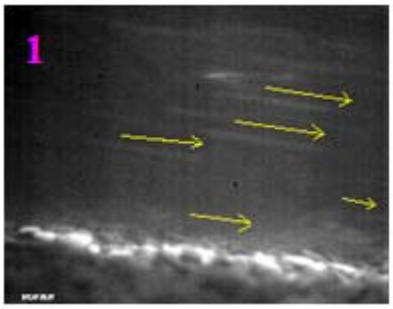

Figure 5.4b - Part 2 of 5 (downstream facing flank of upstream antidune bedform insert). Frames are 0.02 s apart.

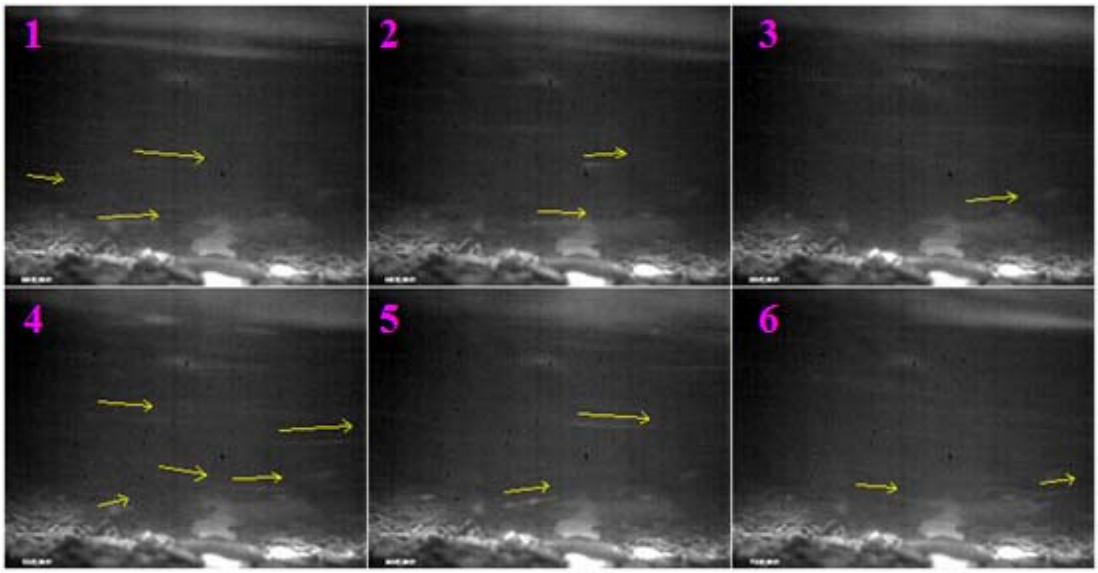

Figure 5.4c - Part 3 of 5 (trough between two bedform inserts). Frames are 0.02 s apart.

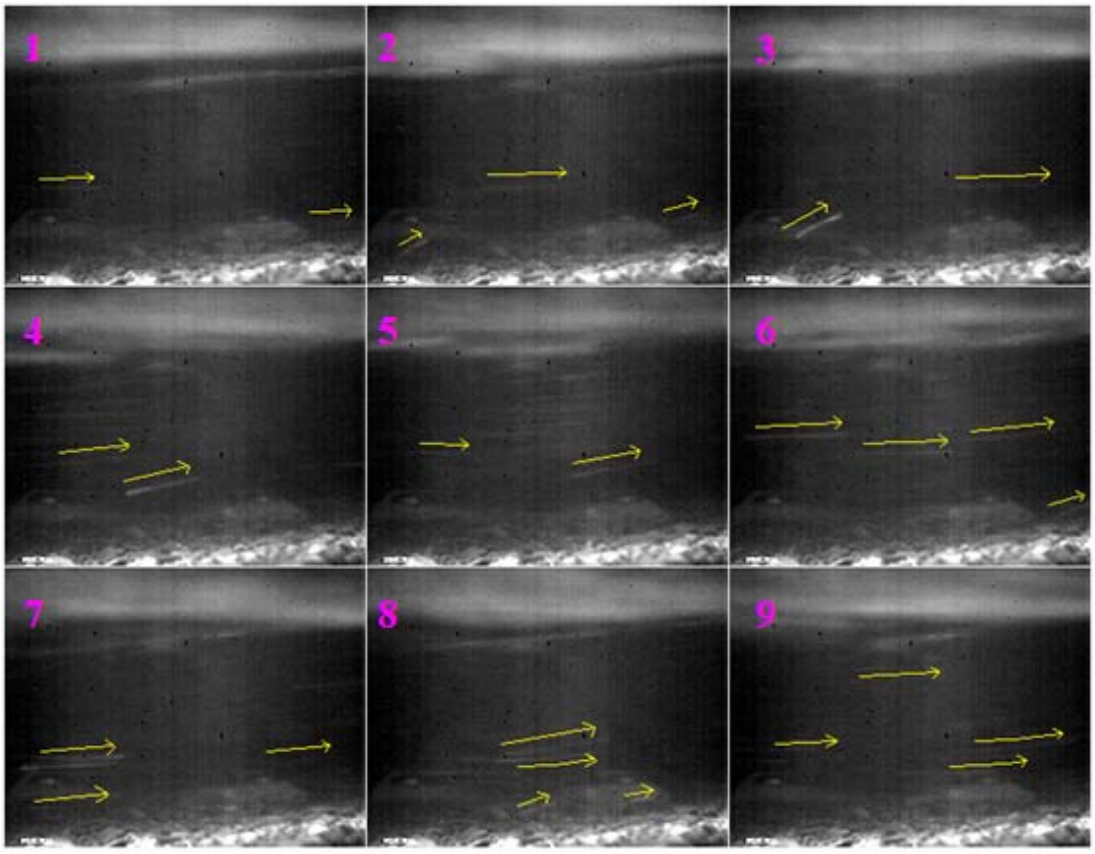

Figure 5.4d - Part 4 of 5 (upstream facing flank of downstream antidune bedform insert). Frames are 0.02 s apart.

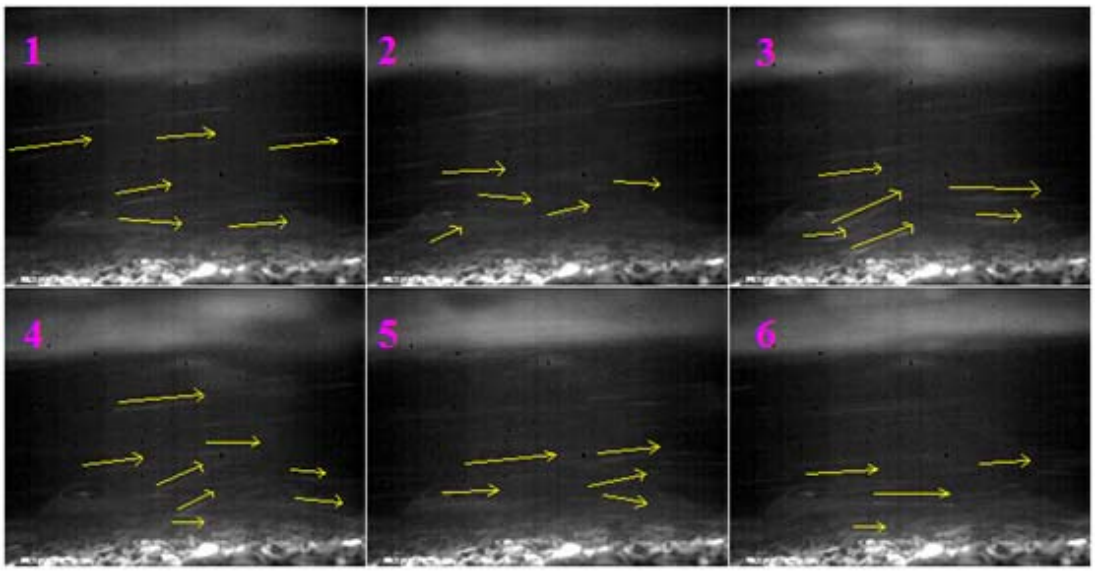

Figure 5.4e - Part 5 of 5 (crest of downstream antidune insert). Frames are 0.02 s apart.

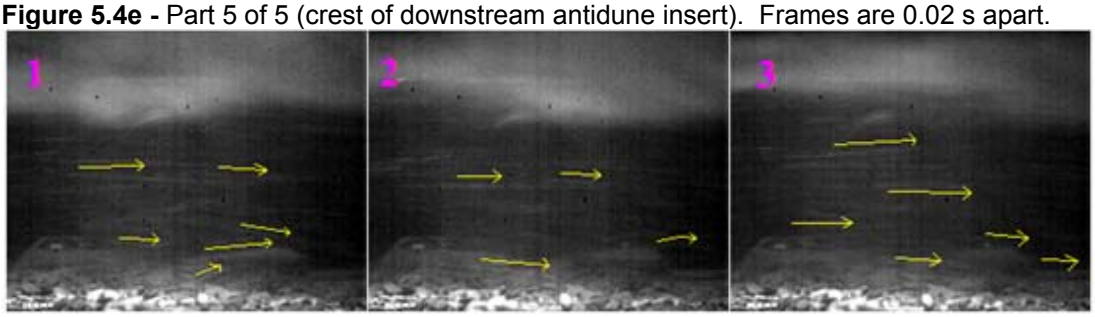

Figure 5.5 Annotation of Temporal Distribution of Streaks over a 0.050 m Amplitude Gravel Antidune

Figure 5.5a - Part 1 of 5 (crest of upstream antidune bedform insert)

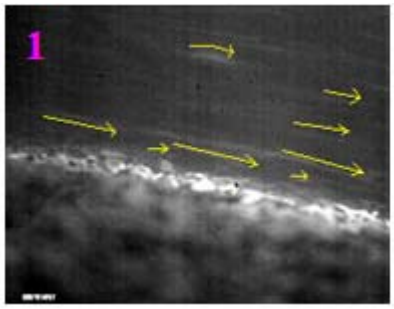

Figure 5.5b - Part 2 of 5 (downstream facing flank of upstream antidune bedform insert). Frames are 0.02 s apart. The grey area adjacent to the wall is the putty used to seal the bedform inserts against the side of the flume.

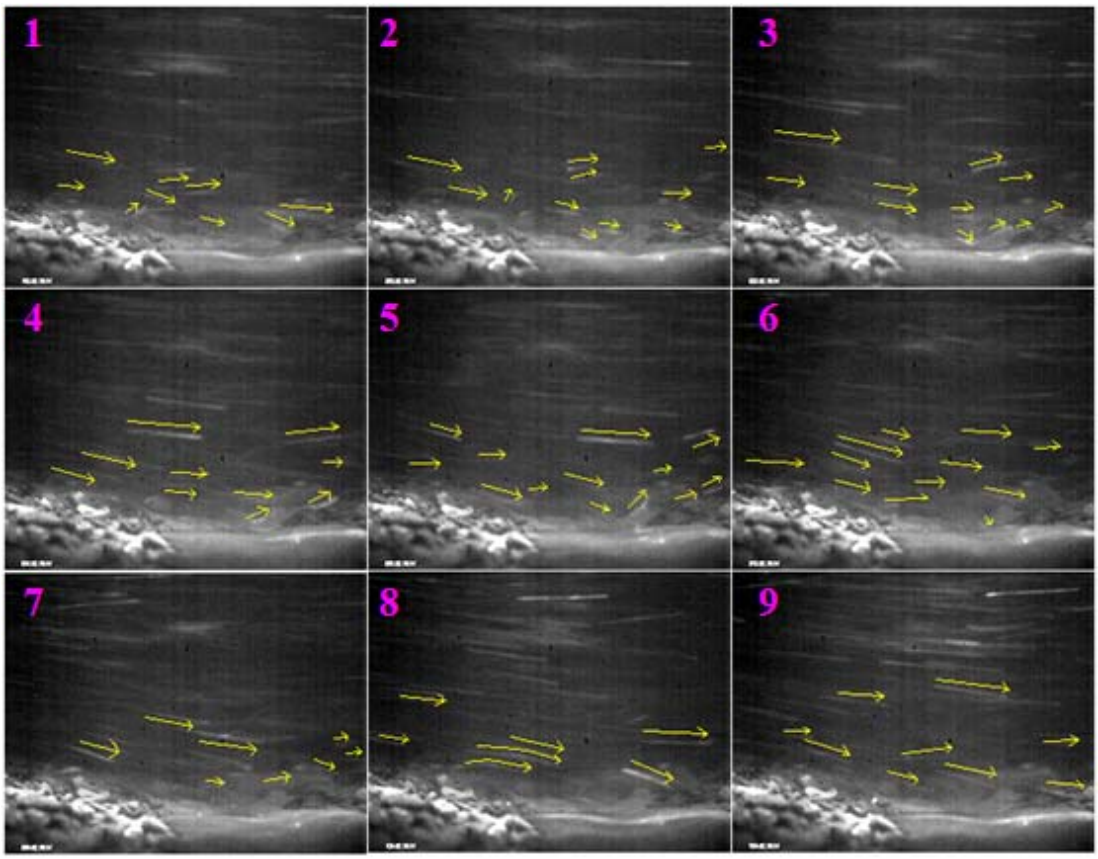

Figure 5.5c - Part 3 of 5 (trough between two bedform inserts). Frames are 0.02 s apart.

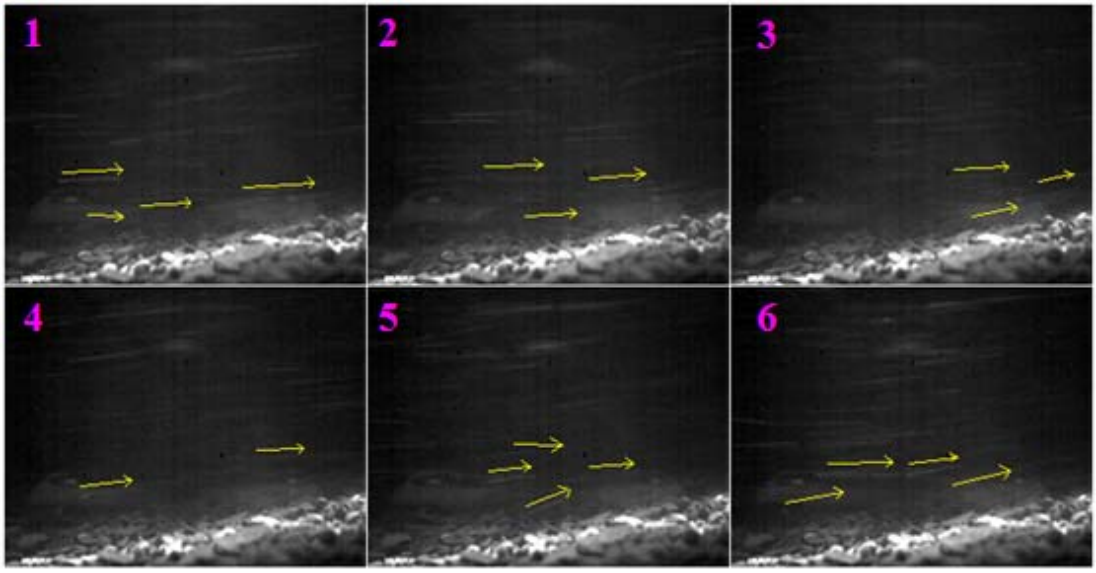

Figure 5.5d - Part 4 of 5 (upstream facing flank of downstream antidune bedform insert). Frames are 0.02 s apart.

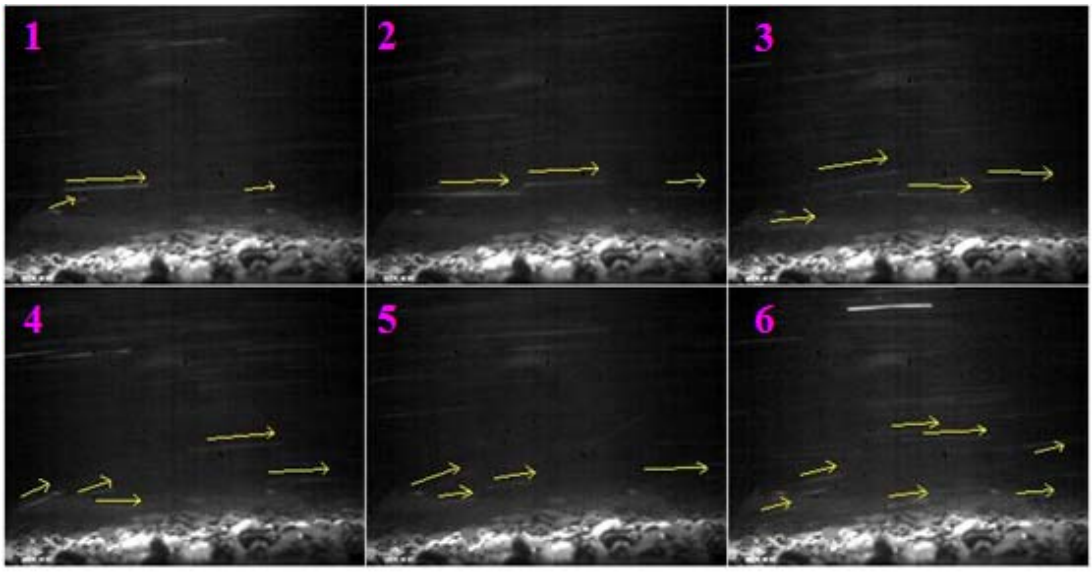

Figure 5.5e - Part 5 of 5 (crest of downstream antidune bedform insert). Frames are 0.02 s apart.

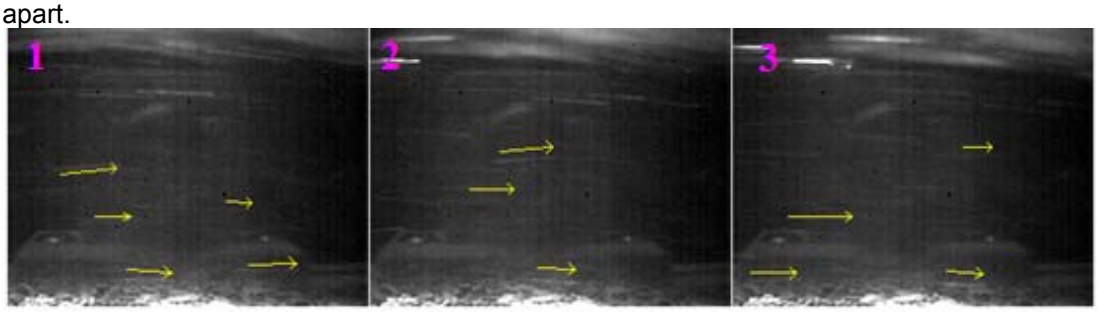

Figure 5.6 Annotation of Temporal Distribution of Streaks over a 0.075 m Amplitude Gravel Antidune

Figure 5.6a - Part 1 of 5 (crest of upstream antidune bedform insert)

Figure 5.6b - Part 2 of 5 (downstream facing flank of upstream antidune bedform insert). Frames are 0.02 s apart.

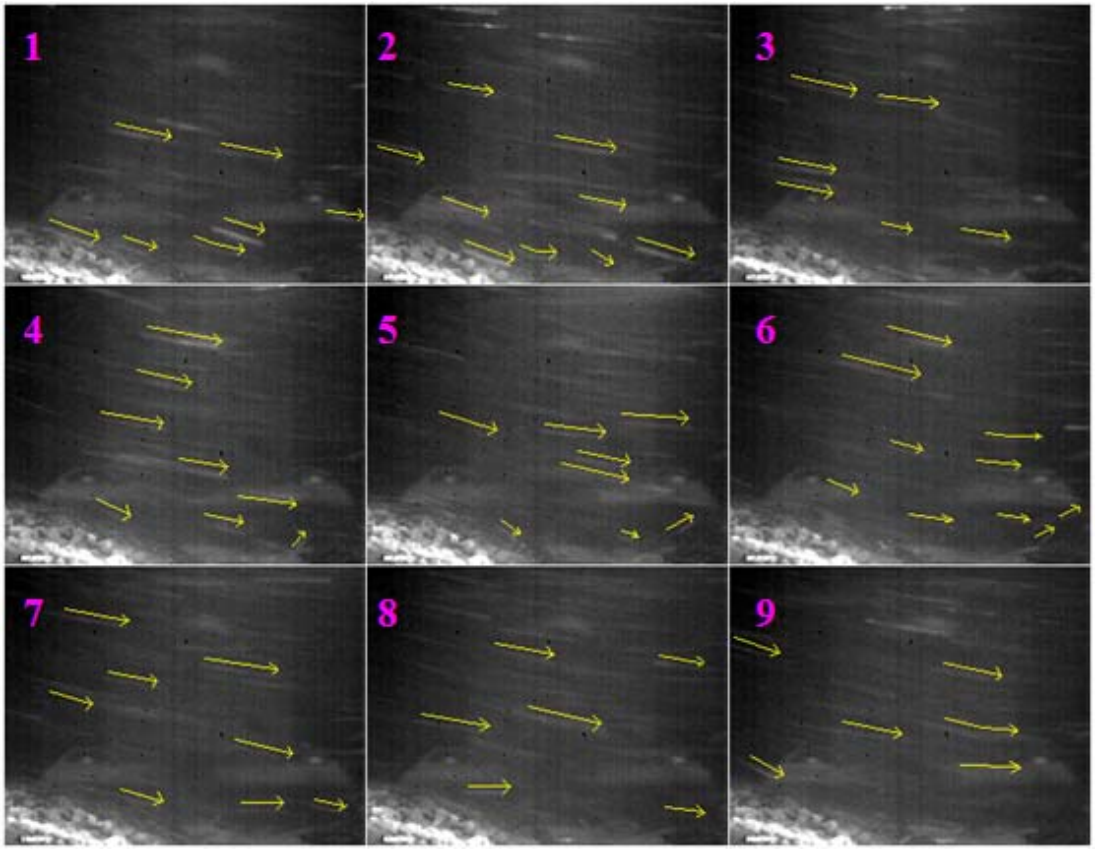

Figure 5.6c - Part 3 of 5 (trough between two bedform inserts). Frames are 0.02 s apart.

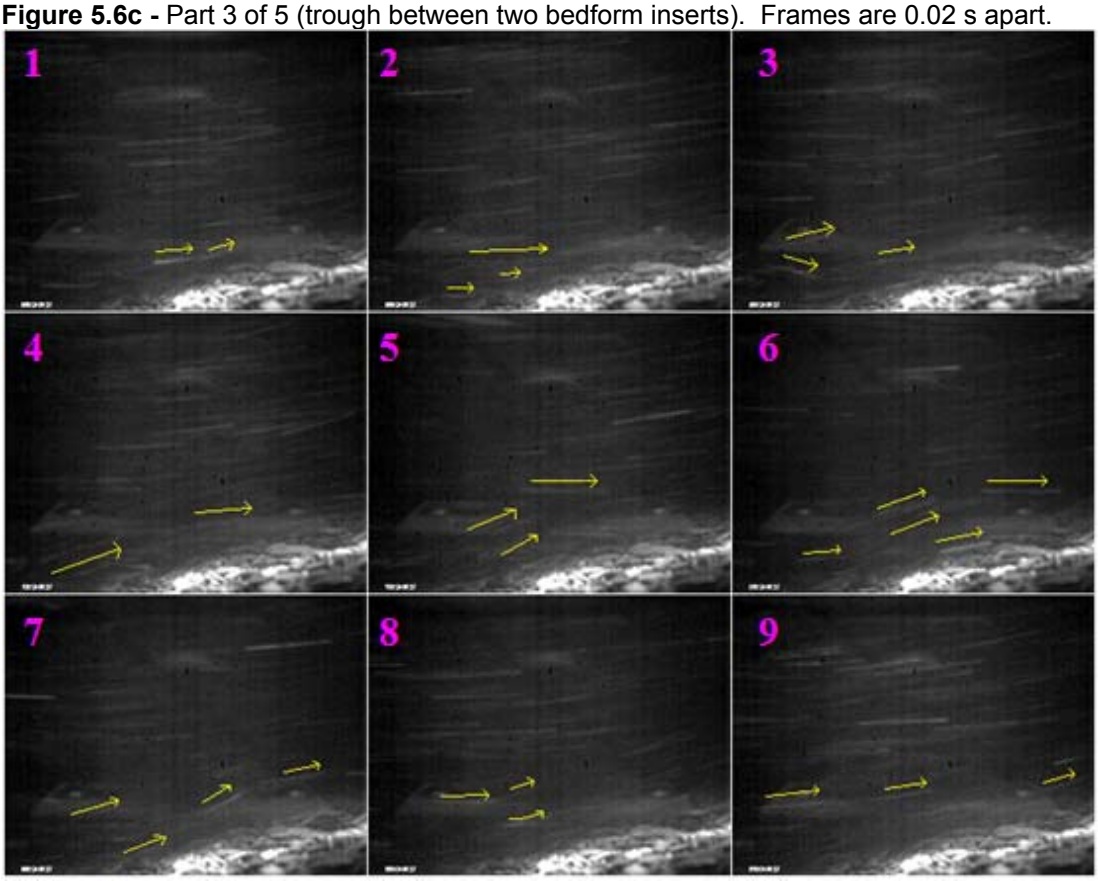

Figure 5.6d - Part 4 of 5 (upstream facing flank of downstream antidune bedform insert). Frames are 0.02 s apart.

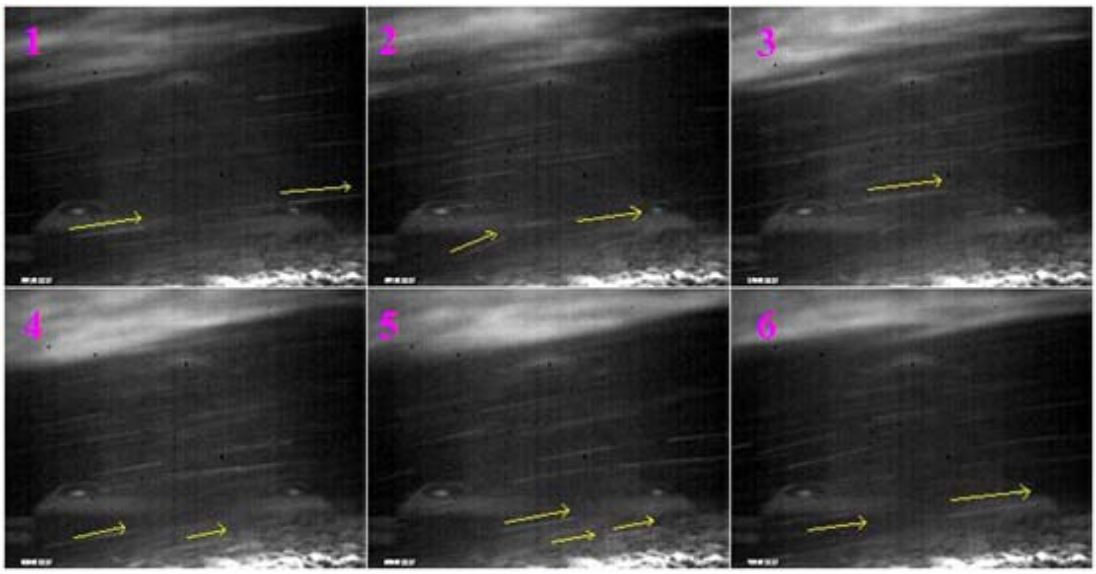

Figure 5.6e - Part 5 of 5 (crest of downstream antidune bedform insert). Frames are 0.02 s apart.

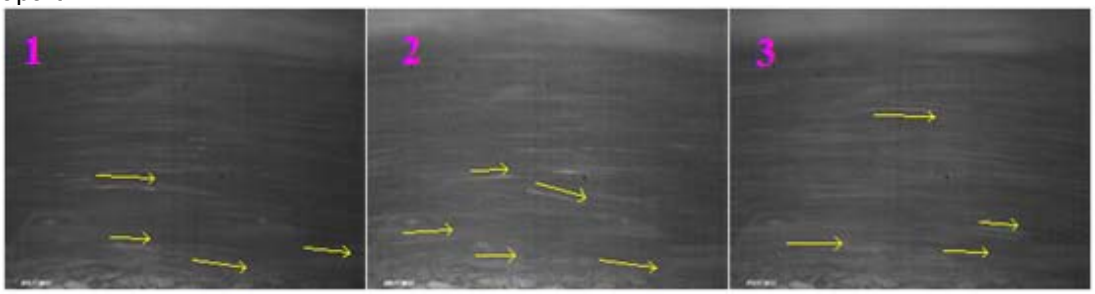

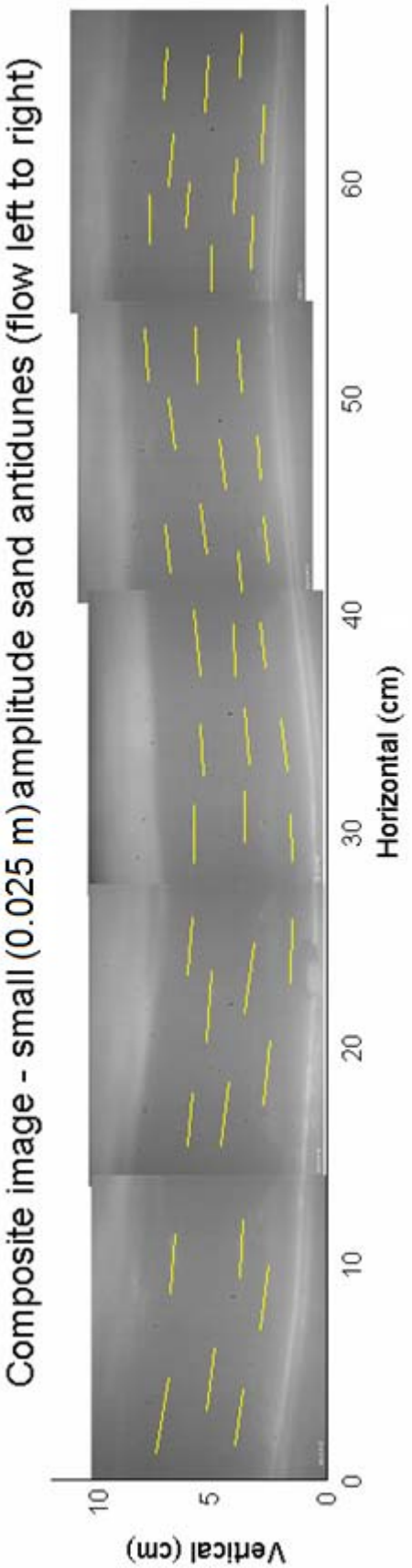

Figure 5.7 Annotation of Spatial Characteristics of Streaks over a 0.025 m Amplitude Sand Antidune

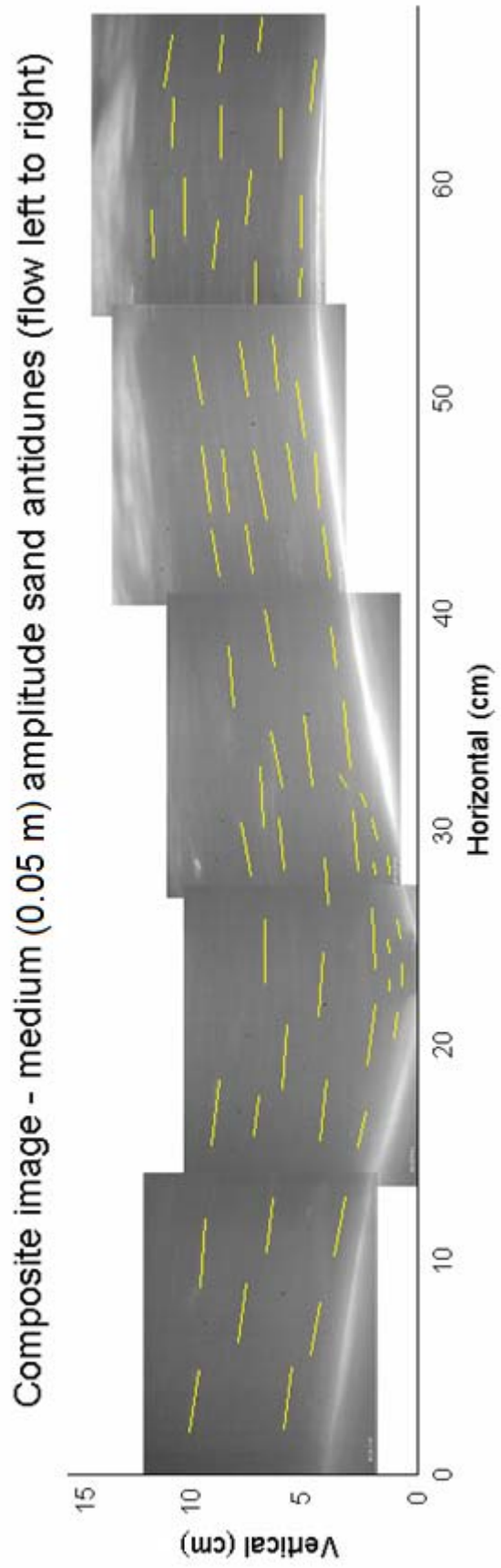

Figure 5.8 Annotation of Spatial Characteristics of Streaks over a 0.050 m Amplitude Sand Antidune

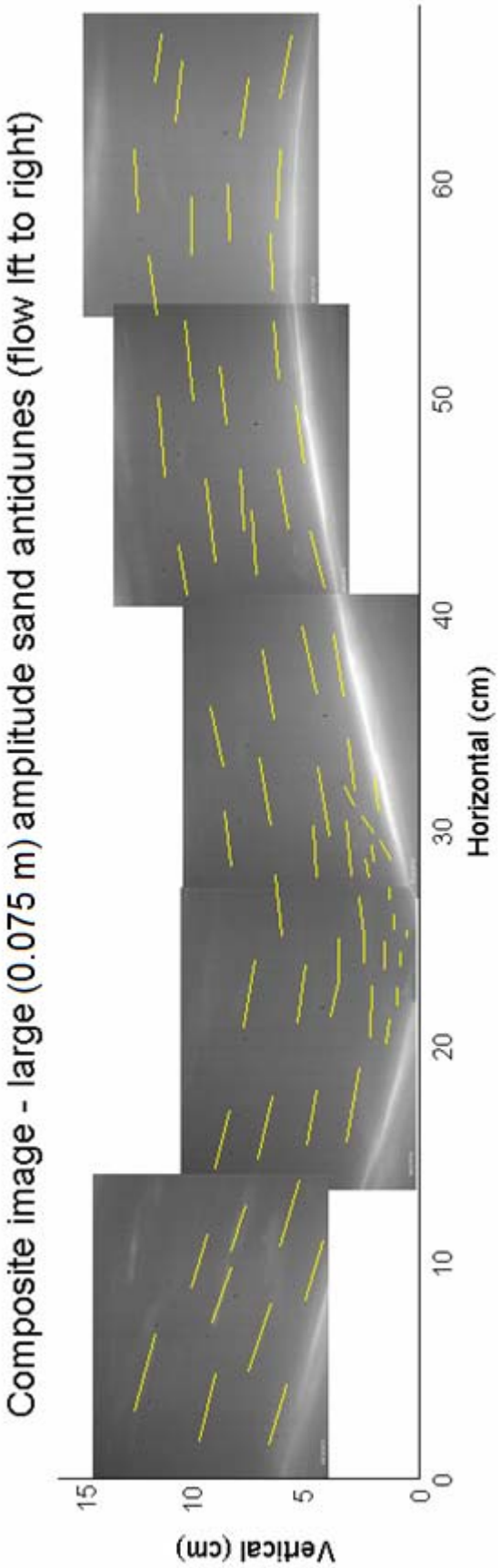

Figure 5.9 Annotation of Spatial Characteristics of Streaks over a 0.075 m Amplitude Sand Antidune

5.2.2 Interpretation of Images

The annotated images in Figures 5.1 – 5.9 show the typical streaks produced by neutrally-buoyant pumice particles (frame rate: 50fps) over fixed gravel antidunes. Figures 5.1 to 5.3 show for 0.025, 0.050 and 0.075 m amplitude gravel surface antidune bedforms, an array of individual frames concatenated to represent the flow pattern over one antidune, from crest to crest. Frames were chosen to highlight typical streaks produced by tracer particle movement. The annotation of these images is based on observations of the streaks seen in slow-motion playback of the recorded videos. Streaks are typically bed parallel across the antidunes and around 0.025 – 0.03 m long (equivalent velocity: 1.4 m/s). From the crest to the mid-flank of the three sizes of antidunes examined, high speed flow adjacent to the bed is indicated by the long streak lengths present adjacent to the bed on the downslope face. However, shorter streaks around 0.005 – 0.01 m in length (velocity: 0.35 – 0.7 m/s) that are either bed-parallel or upwards at up to 30˚ from the bed-parallel are present in the trough of the antidune. The orientations of streaks changes between these two states over irregular periods, in the order of 10 seconds. Changes in the structure of the flow can be seen as the antidune amplitude increases (through figures 5.1 - 5.3), this distinct area of retarded flow increases from 13% of flow depth, to 19% then to 25%, respectively. On the upslope flank of the 0.025 and 0.050 m amplitude antidunes (Figure 5.1 and 5.2), streaks adjacent to the bed extending away from the trough are less-regular in contrast to the bed-parallel streaks that occur higher in the flow. However, notably for 0.075 m antidunes on the upslope flank streaks are bed-parallel. This change towards bed parallel streaks is interpreted as perhaps indicting the transition from the growth phase; where sediment is being transported up the flanks of the antidune by turbulent motions (indicated by the varying streak orientations observed over the 0.025 m and 0.050 m antidunes), to the limiting case, where these turbulent motions no longer reach the crest. Instead, sediment transport occurs over the crest by the shearing action of this high-speed flow on the bed.

Figures 5.4 – 5.6 show sets of annotated individual stills of interest from the flow across 0.025, 0.050 and 0.075 m amplitude gravel surfaced antidune bedform inserts. Panels ('a', 'b', 'c', 'd' and 'e') are arranged left to right (i.e. 'a' would be the upstream frame and 'e', the right most downstream frame in the respective composite Figures 5.1 to 5.3). The number of panels shown depends on the relative amount of variability observed. Where a series of images is shown, images are consecutive (i.e. with a 0.02 second gap between frames). Figure 5.4a, 5.5a and 5.6a, show that on the downslope, immediately downstream of the crest, streaks throughout the flow profile are bed-parallel and distributed throughout the flow depth with limited temporal variation in trajectory. For the 0.025 m amplitude antidunes (Figure 5.4b), streaks in the upper flow profile are again bed-parallel with limited temporal variations. However, in the lower flow profile, not all streaks are bed-parallel, with some streaks orientated at 30˚ upwards from bed-parallel. At the same location over 0.050 m and 0.075 m amplitude antidunes (Figure 5.5b and 5.6b) variations in the lower flow profile are more notable. Generally streaks 'curve' over the trough region, but some higher velocity trajectories have downward trajectories, and enter the trough region, penetrating to the bed. Periodical low speed (short streak length) ejections occur, up away from the trough, with streaks orientated at around 30˚ upwards from bed-parallel, although alongside these ejections the majority of streaks elsewhere in the flow profile still have a bed parallel trajectory. This behaviour continues through Figure 5.4c, 5.5c and 5.6c, where in the upper flow profile, streaks are orientated bed-parallel with limited temporal variation in streak trajectory. However, in the lower flow profile the streaks are again bed-parallel with greater temporal variation of trajectories, with some streaks being orientated at 30˚ upwards from bed-parallel. Figure 5.4d, 5.5d and 5.6d show the upslope, below the crest, in the upper flow profile, streaks are bed-parallel with limited temporal variation. In the lower flow profile, streaks are also bed-parallel but with greater temporal variation of streak trajectory and some upwards, non bed-parallel trajectories. Figure 5.4e, 5.5e and 5.6e show the flow over the crest of the 0.025 m, 0.050 m and 0.075 m amplitude antidunes, streaks are bed-parallel away from the bed. However, closer to the bed above the 0.025 m antidunes, streaks are not bed-parallel but with

greater temporal variation of streak trajectory and some upwards, non bed-parallel trajectories. Near bed streaks become bed-parallel progressively, through 0.050 m amplitude antidunes, to the 0.075 m amplitude antidunes.

Figures 5.7 to 5.9 show for 0.025, 0.050 and 0.075 m amplitude fixed sand antidunes, an array of individual frames concatenated to represent the flow pattern over one antidune, from crest to crest. The figures show some of the same trends as noted for gravel surfaced fixed antidune forms, although trends are less pronounced. This is firstly due to faster moving particles (less exposure to light in frames which produces less contrast within the image and therefore making interpretation more difficult). Secondly, the lower bed roughness of the sand forms means that there is a more rapid transition (less than 5% of flow depth) from retarded flow at the bed due to friction with the bed, towards higher velocity flow above the bed. In contrast over gravel surfaced bedforms the lower 10 to 20% of the flow is retarded. An area of lower velocity flow representing the lower 15% of the flow profile is present in the troughs of the 0.050 and 0.075 m fixed sand antidune forms (see Figures 5.8 and 5.9), however this zone is less extensive (just 0.1 m in length), compared to 0.2 m for gravel antidunes. It appears that with sand antidunes, the lower bed friction, and presence of higher velocity flow close to the bed limits the extent to which an area of low velocity flow can develop in the trough between antidunes. At the downstream end of the trough between 0.075 m amplitude antidunes, streaks directed upwards at around 30˚, over bed-parallel were observed (Figure 5.9). Similar streaks were observed over the gravel forms; however these upward orientated streaks were much less common over the sand forms.

Summary – Streak Photography over Gravel and Sand Surfaced Antidunes

Interpretation of streak photography recorded over gravel and sand antidunes has supported the findings of the ADV investigation. Flow appears to be generally bed parallel over the majority of the antidune flow profile. However, there are notable slower streaks (and inferred slower velocities) in the trough region, compared to elsewhere in the flow profile. Streaks indicate that ejections of fluid occur from the

trough region, up into the flow at an angle of ~30˚. Contrasts between gravel and sand are evident, with the streak length being shorter (lower velocities) in the trough region over gravel antidunes. Additionally, more ejection movements of streaks were present in the trough region for gravel antidunes. The magnitude of these values increases as the antidune amplitude increases (0.025, 0.050 and 0.075 m amplitudes for both gravel and sand antidune bedforms). Therefore, as for the ADV work it is thought that for sand and gravel antidunes this intense turbulence associated with steepening antidunes, may lead to rapid erosion in the trough, steepening the downstream bedform, which causes the standing wave to collapse.

Box 5.1 Summary of Streak Photography Interpretation for Sand and Gravel Surfaced Antidunes

5.3 Particle Tracking from High Speed Video

5.3.1 Particle Tracking Velocities over Fixed Antidunes

The processed particle tracking data obtained from the high-speed video imagery for both the gravel and the sand fixed antidunes (0.025, 0.050 and 0.075 m amplitudes) is shown in Figures 5.10- 5.15.

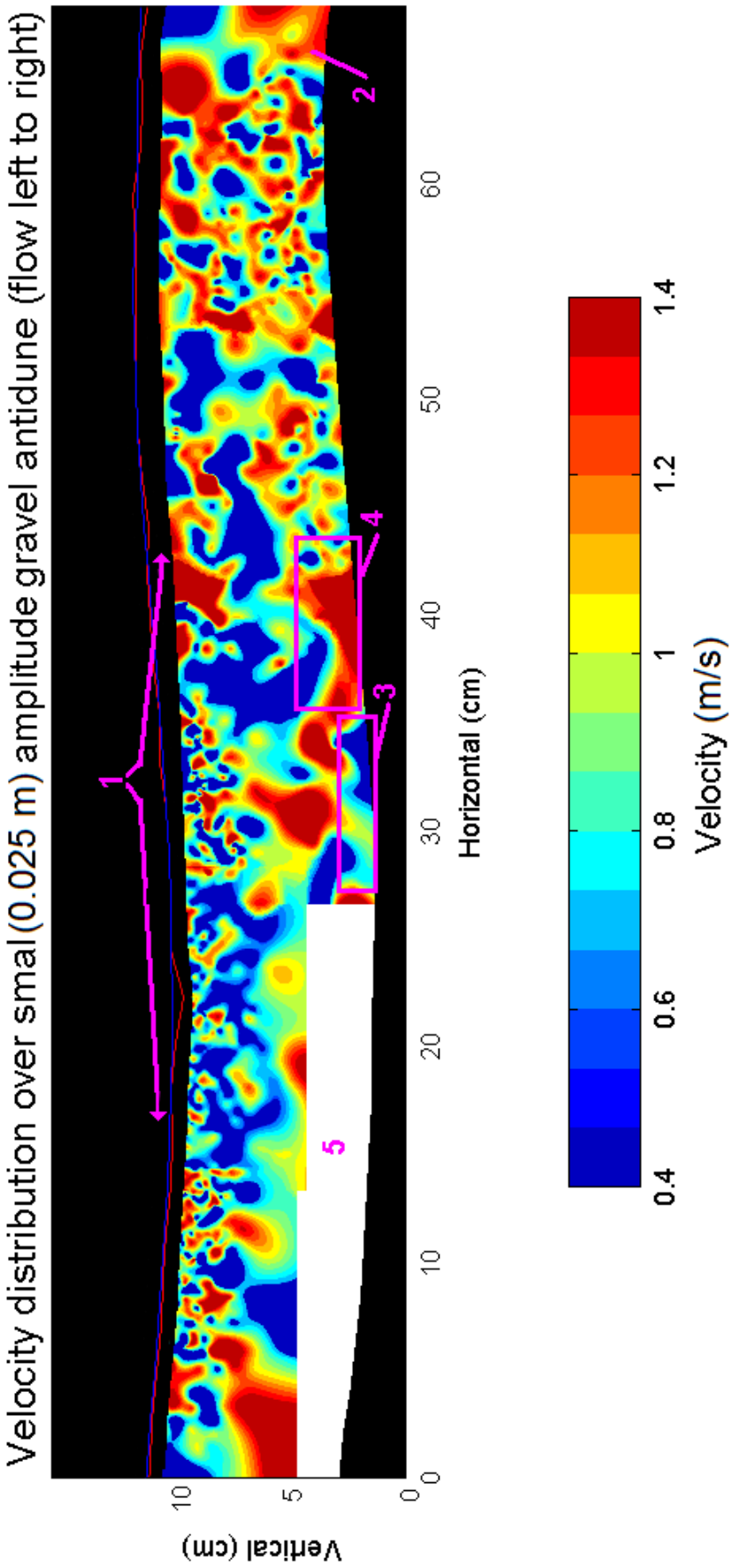

Figure 5.10 Velocity Distribution over a 0.025 m Amplitude Gravel Antidune

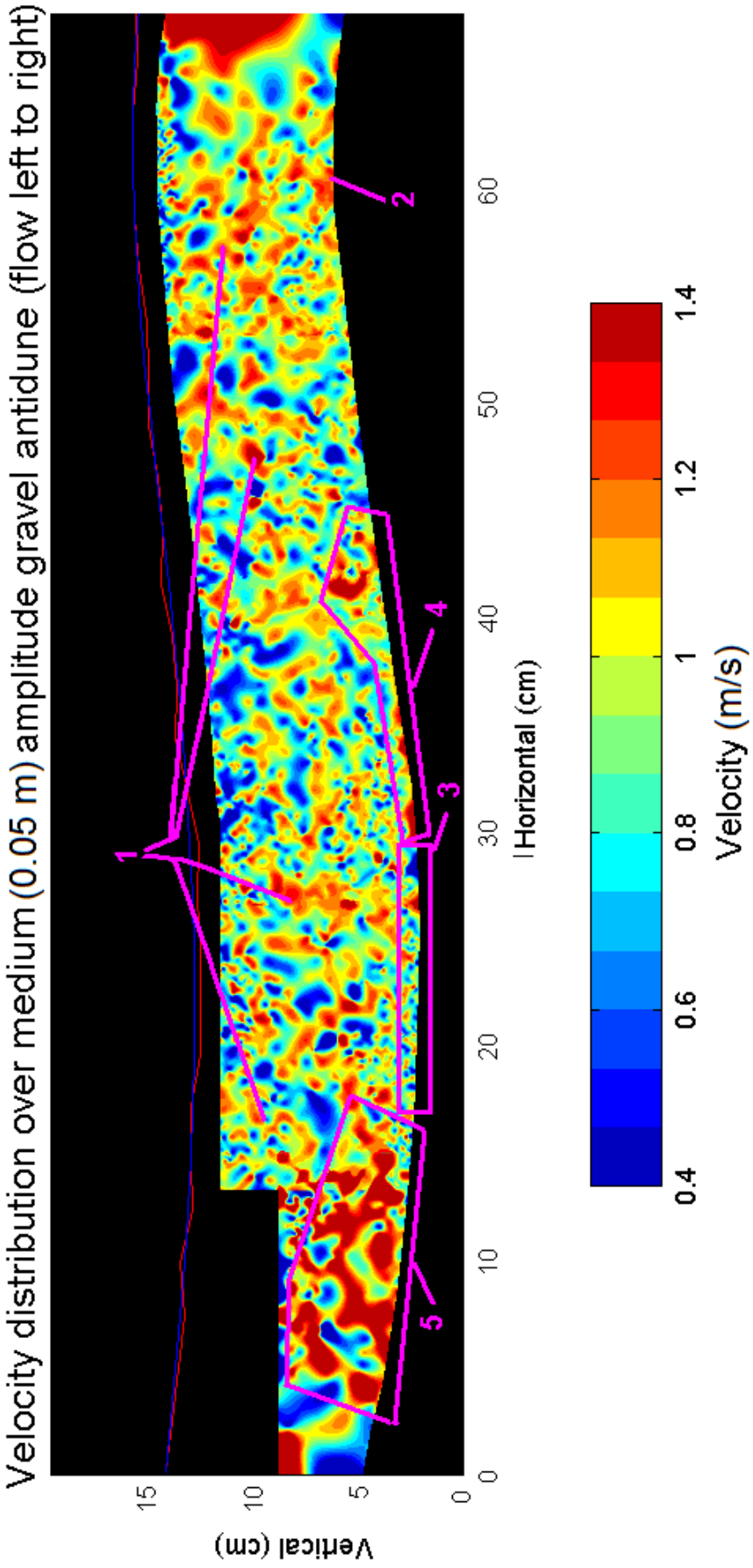

Figure 5.11 Velocity Distribution over a 0.050 m Amplitude Gravel Antidune

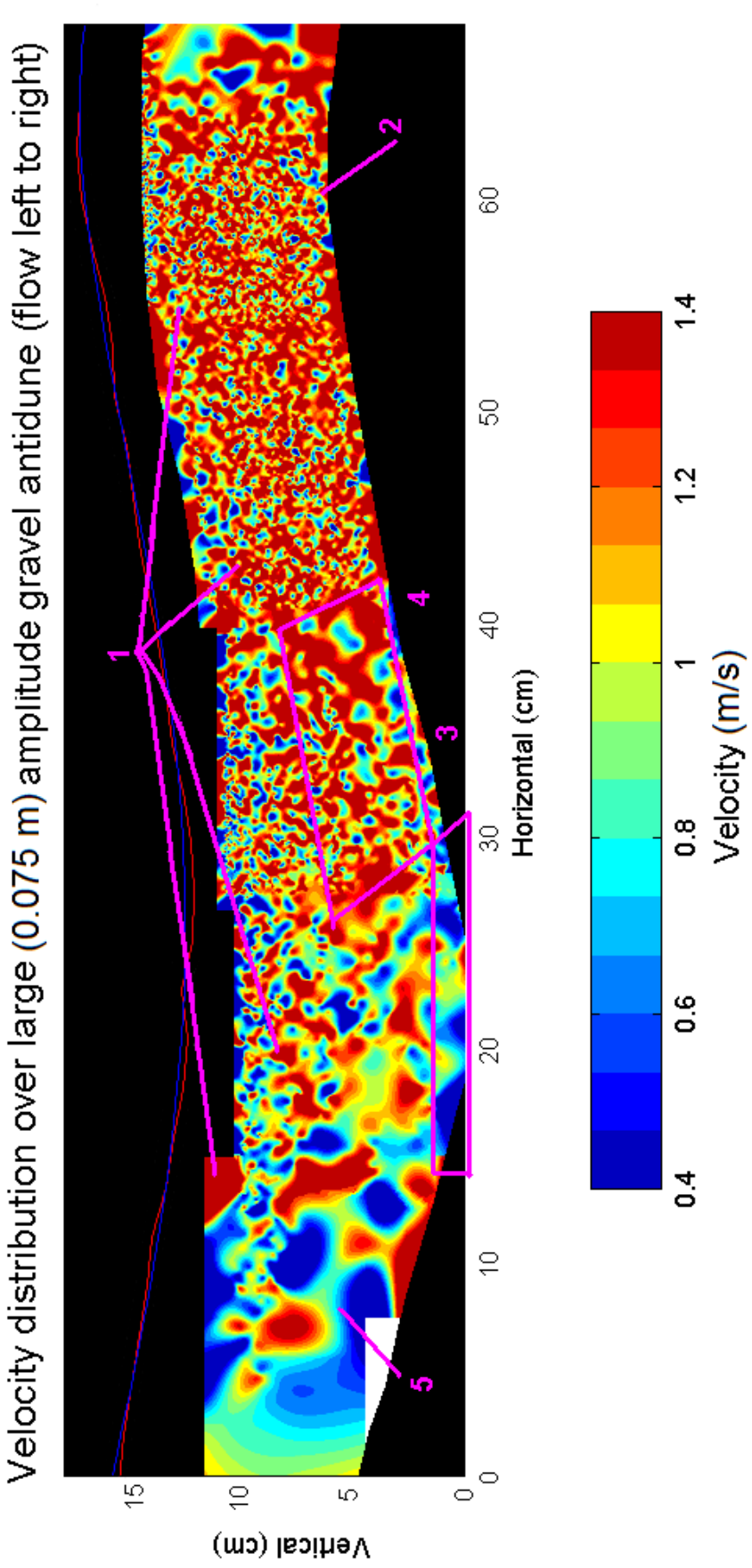

Figure 5.12 Velocity Distribution over a 0.075 m Amplitude Gravel Antidune

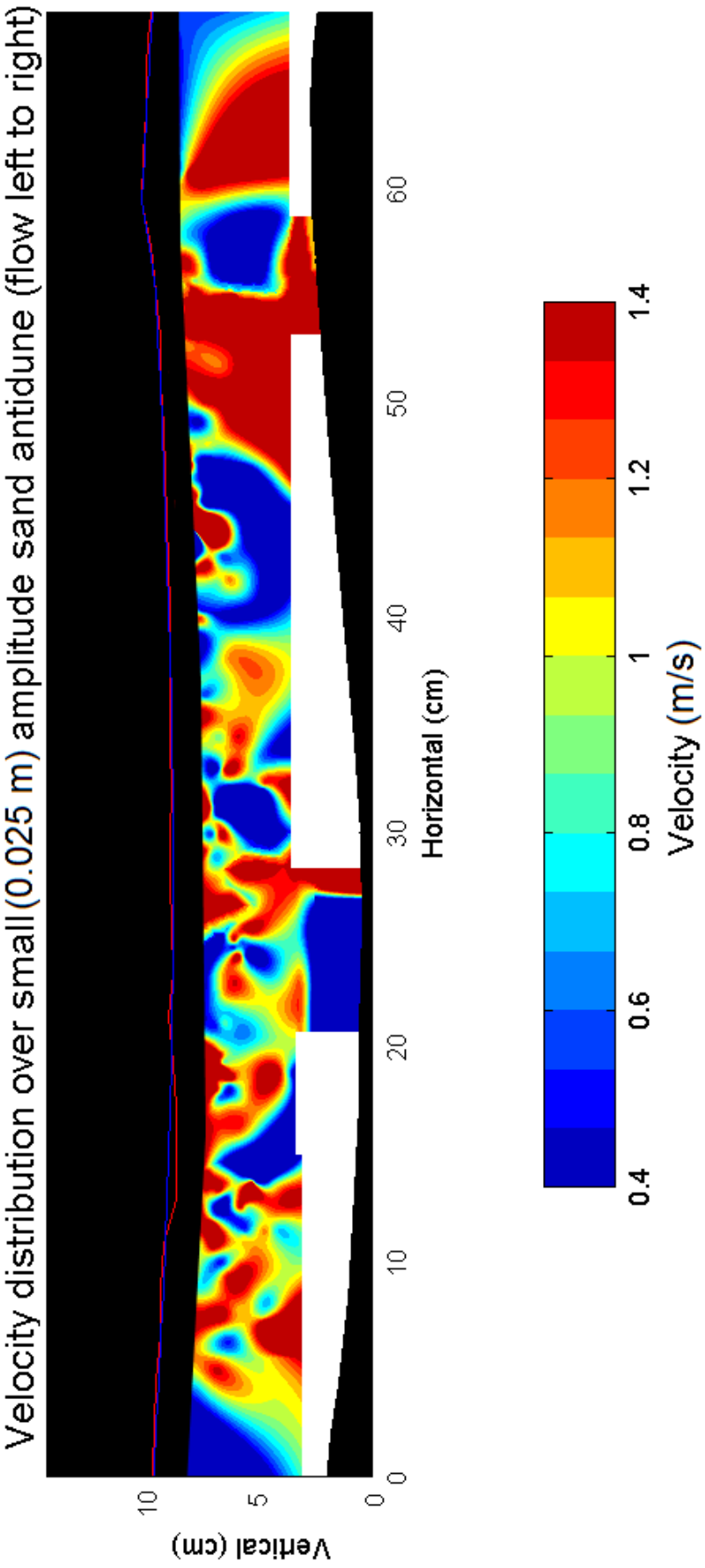

Figure 5.13 Velocity Distribution over a 0.025 m Amplitude Sand Antidune

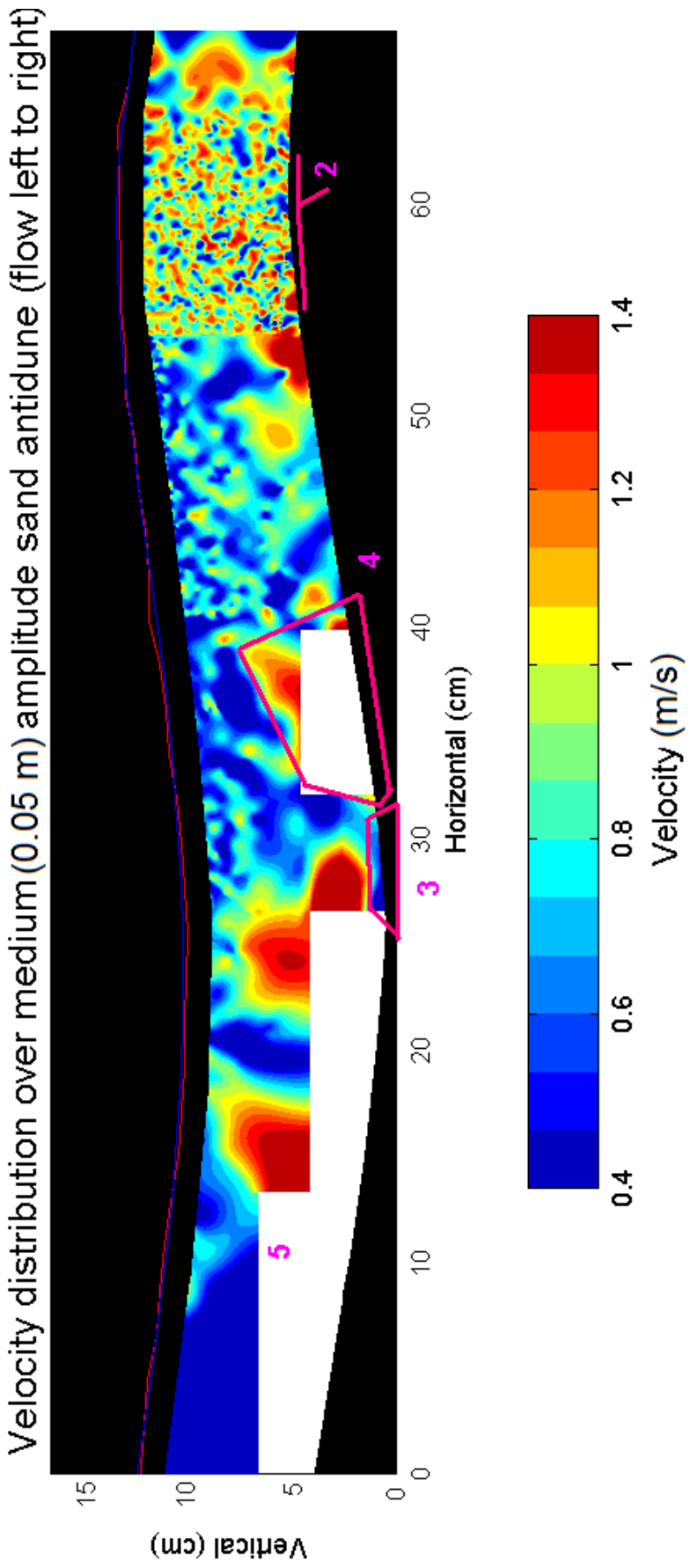

Figure 5.14 Velocity Distribution over a 0.050 m Amplitude Sand Antidune

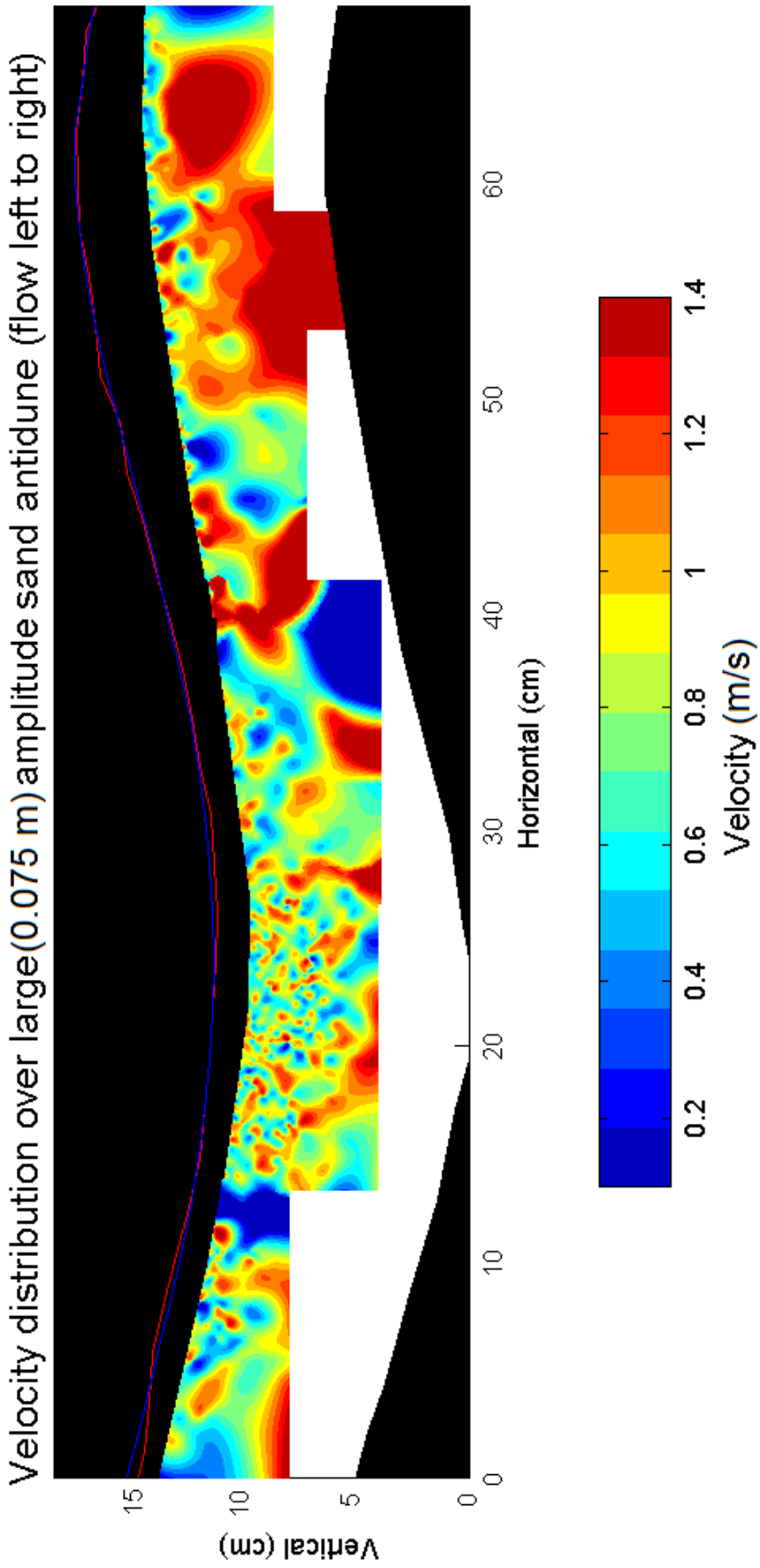

Figure 5.15 Velocity Distribution over a 0.075 m Amplitude Sand Antidune

5.3.2 Interpretation of Particle Tracking Experiments

Figures 5.10– 5.15 show the velocities detected by particle tracking over, 0.025, 0.050 and 0.075 m amplitude fixed antidunes with a gravel surface (Figures 5.10 – 5.12), and sand surface (Figures 5.13 – 5.15). The numbers in pink on these figures relate to the numbers in bold within the discussion below. Lines in blue represent the measured water surface levels and, in red, an moving average of measured levels. In all figures flow is left to right and the camera frame speed 200 fps (tracking method is described in Chapter 3). The black areas on the graph represent the solid bed, and the top portion of the flow (affected by a variable water surface due to the dynamic nature of antidune regime flow) and the air above. White areas are those where insufficient data were available from particle tracking analysis of the recorded images for the interpolation to produce data for the velocity slices seen in the figures. Some of the larger areas of constant colour within the figures, generally towards the edges (especially the top of the flow slice) and into corners are artefacts of the gridding process to produce contoured flow slices from the irregularly spaced tracked particle pairs, caused by limited data points used. It is felt that of all the experiments carried out in this thesis, the high speed particle-tracking experiments were the least successful. The use of higher-specification equipment to obtain higher quality results is discussed in Section 8.

For gravel surfaced antidune bedforms, Figure 5.10 indicates velocities tend to be high (1.4 m/s) in the upper areas of the flow profile over antidune bedforms ('**1**'). High velocities (1.2 – 1.4 m/s) are also present nearer the bed over the crests ('**2**'). An area of low-velocity (0.4 – 0.8 m/s) is indicated in the trough between antidune crests ('**3**'), followed by an area of high velocity (1.2 – 1.4 m/s) immediately downstream ('**4**'), located on the upslope face of the next antidune. Unfortunately, insufficient particles were tracked immediately above the bed on the downslope of the antidune in the left of the figure ('**5**'). Velocities adjacent to this area are relatively high; indeed the tracking of faster moving particles is more difficult as they tend to be less exposed in each frame. Potentially (comparing with behaviour in Figures 5.11 and 5.12) this would have been an area of higher velocity flow.

Figure 5.11 shows a similar pattern to Figure 5.10, but perhaps more clearly. High velocities (up to 1.4 m/s) can be seen in the upper portion of the flow profile ('**1**'), and at the crests high velocity (1.2 – 1.4 m/s) flow ('**2**') is present closer to the bed. An area of low-velocity (0.4 – 0.8 m/s) is indicated in the trough between antidune crests ('**3**'), followed by an area of high velocity (1.1 m/s – 1.3 m/s) immediately downstream ('**4**'), located on the upslope face of the next antidune. An area of high velocity (1.4 m/s) flow ('**5**') is present on the downslope of the antidune in the left of the figure.

Figure 5.12 shows a similar pattern to Figure 5.10 and 5.11. High velocities (1.2 – 1.4 m/s) can be seen in the upper portion of the flow profile ('**1**'), and at the crests high velocity (1.2 – 1.4 m/s) flow ('**2**') is present closer to the bed. It is unclear why the particle tracking has been more successful over the upslope of the antidune on the right of Figure 5.12, tracking many more particles. An area of low-velocity (0.4 – 0.8 m/s) is indicated in the trough between antidune crests ('**3**'), followed by an area of high velocity (1.2 – 1.4 m/s) immediately downstream ('**4**'), located on the upslope face of the next antidune. Unfortunately, insufficient particles were tracked immediately above the bed on the downslope of the antidune in the left of the figure ('**5**'). Reasons for this are discussed above for Figure 5.10, examination of individual frames from the high-speed video indicates that high velocity trajectories do occur at this location over gravel surfaced antidune bedforms, but are fainter and not being well identified by the software algorithms used to abstract particle tracing data.

The number of successful particle-pair trackings is detailed in Table 5.1. Each frame of the high speed video has an area of 0.0175 m^2, therefore, each flow slice has a total potential area of 0.0875 m^2. However, because typically 30% of each frame was masked (to remove image areas representing bed/air below/above the flow slice) the particles that were tracked occurred over an area of around 0.0600 m^2. Table 5.1 shows the number of particles detected in each of the six flow slices, and indicates that broadly maximum and median velocity decreases with antidune size. This data supports the interpretations discussed in Box 5.1 above. However, the limited quality of data makes it difficult to take the analysis further than outlined in Box 5.1.

Table 5.1 Quantity of Particle Pairs Tracked in Each Flow Slice

Fixed Antidune Form	Number of successful particle tracks	Particle pairs per cm^2	Maximum Velocity	Median Velocity
0.025 m Gravel	1619	2.6	1.77	1.11
0.050 m Gravel	8011	13.1	1.67	0.85
0.075 m Gravel	9271	15.1	1.34	0.82
0.025 m Sand	225	0.4	1.51	1.03
0.050 m Sand	5735	9.4	1.24	0.76
0.075 m Sand	2679	4.3	1.16	0.75

6 Antidune Sedimentology – Results and Interpretation

6.1 Flow Conditions During Runs

Methods and techniques used in these experiments are outlined in the Methodology (Chapter 3). The conditions during Run 1 (in the section of flume where antidunes were present and their sedimentary structures sampled) are plotted in Figures 6.1 and 6.2. Bed thickness increased steadily through the experiment and water depth was relatively constant. The decrease in water depth at 2.5 minutes in Figures 6.1 and 6.2 is due to the presence of an antidune trough adjacent to the point of measurement; there are corresponding increases in velocity and Fr.

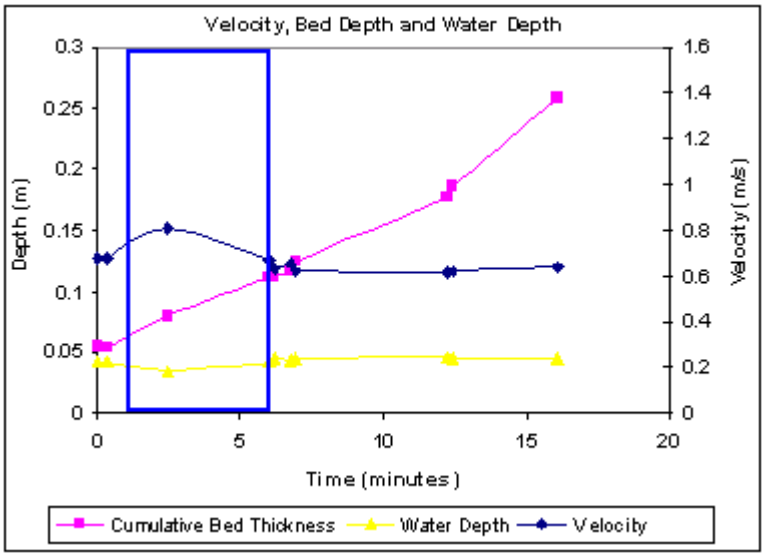

Figure 6.1 Graph of Velocity, Bed and Water Depth During Run 1.

The blue box indicates the time-window when antidunes were present in the flume. Bed level was measured by observing the depth of accumulated sediment at the location where antidunes formed against a scale on the flume wall in photos taken during the flume run. Unfortunately the scale was only visible adjacent to one photo of the antidunes that formed in Run 1, (for this reason video footage was taken in Run 2, which captured both scale and antidunes).

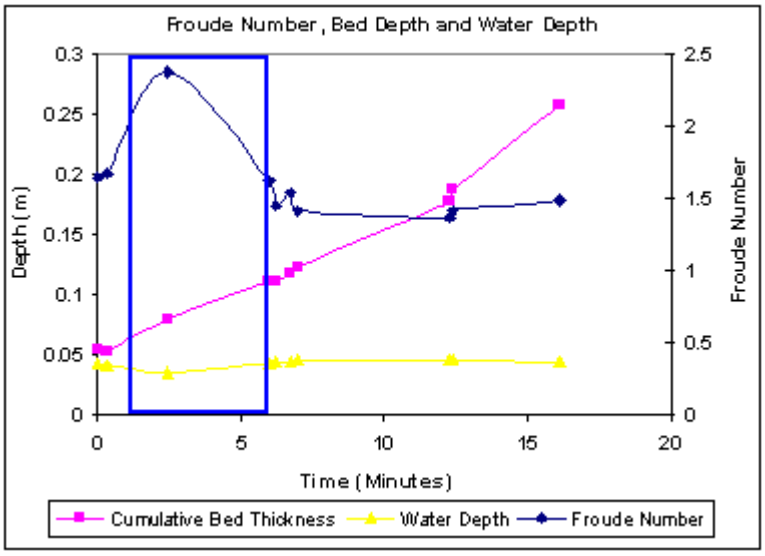

Figure 6.2 Graph of *Fr*, Bed and Water Depth During Run 1.

The blue box indicates the time-window when antidunes were present in the flume. Velocity was calculated based on the flume discharge (measured constantly during the run) divided by cross-sectional area (flume width X flow depth) to give the velocity. The *Fr* was calculated using this velocity and the depth of flow in each image, the *Fr* is therefore representative of the reach velocity, rather than local velocity within the actual standing wave.

The variation of conditions during Run 2 is plotted in Figures 6.3 and 6.4.

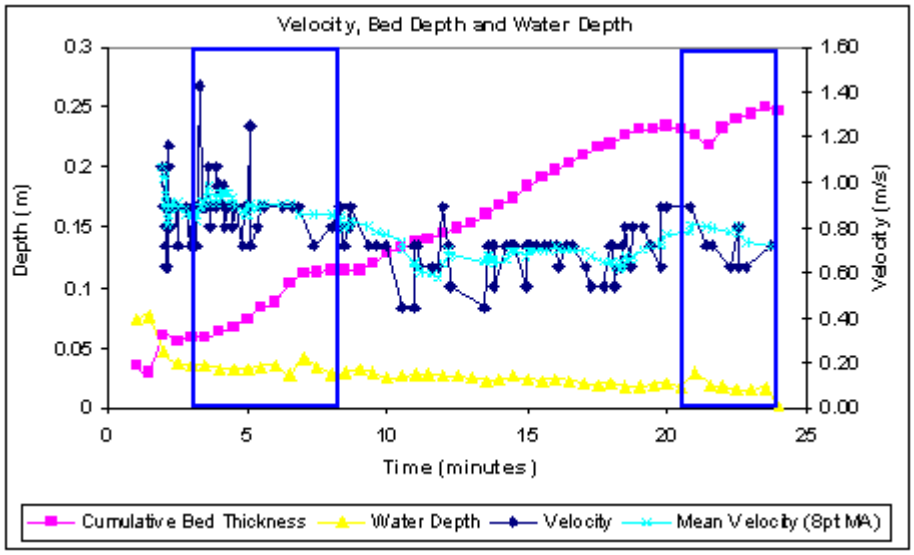

Figure 6.3 Graph of Velocity, Bed and Water Depth During Run 2.

The blue boxes indicate the time-windows when antidunes were present in the flume. Bed level was measured by observing the depth of accumulated sediment at the location where antidunes formed against a scale on the flume wall in stills from a video of the flume run.

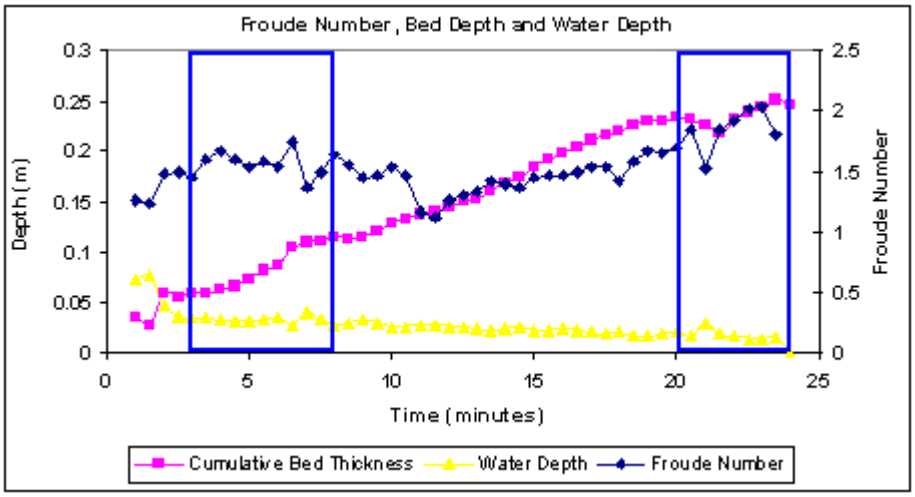

Figure 6.4 Graph of Fr, Bed and Water Depth During Run 2

The blue boxes indicate the time-windows when antidunes were present in the flume. Velocity was calculated based on the flume discharge (measured constantly during the run) divided by cross-sectional area (flume width X flow depth) to give the velocity. Since stills from a video of the flume run were used, values were calculated every 30 seconds. These calculations were verified against observations of particle movement between video stills. The Fr was calculated using this velocity and the depth of flow in each image, the Fr is therefore representative of the reach velocity, rather than local velocity within the actual standing wave.

Figures 6.3 and 6.4 show the greater variation in the rate of bed aggradation during antidune activity (periods indicated by the blue windows). The aggradation rate is initially lower at the beginning of the period, before increasing sharply towards the end of the periods of antidune activity. During the second period of antidune activity only limited cumulative bed aggradation occurs, with a period of net degradation. The USPB period which intervened between 8 and 20 minutes had an overall more consistent rate of aggradation, although aggradation rates were lower at the start of this USPB, and then tailed off again as antidune activity restarted. The rapid increase in bed thickness between 6 and 6 ½ minutes occurred between two periods of rooster tails, a sinusoidal bed (antidunes) remained, but when the rooster tails subsided net aggradation occurred. The decrease in bed thickness between 21 and 21 ½ minutes occurred due to the violent breaking of a standing wave (time 73 s to 91 s on Plates 6.5 – 6.6 and Figures 6.8 – 6.9). In both runs, antidune activity only occurred for a relatively short period of time, the antidunes are therefore not thought to be equilibrium forms. It is

unclear why antidunes were not more persistent, although it is thought that this may be linked to the sediment mixture being sand poor and gravel rich. Towards the end of Run 2 flow depth declined, whilst being indicative of declining pump discharge reasons were unclear, the pump having delivered constant discharge through all previous experiments (mobile bed experiments were undertaken after the ADV and video experiments). This was perhaps due to the lower head of water in the sump tank (water stored within the deposited sediment), and the higher head water had to be pumped up against (due to the depth of aggraded bed).

6.2 Description of Observed Hydrodynamics

In the text discussion, the still and cartoon timestamp is used to identify the precise frame being discussed. Flow is left to right on all images and SW is an abbreviation for Standing Wave.

6.2.1 Description of Run 1

Plate 6.1 shows a sequence of images with time stamps taken during antidune activity in run 1. First, a slowly upstream migrating SW and antidune pair (first row of images) formed in the flume. These forms then steepened, but remained relatively fixed (second row of images), the SW growing then becoming unstable (4m 49 s), but dissipating slightly instead of breaking (4m 58 s). The final two images indicate the SW and antidune dissipating. The bed was aggrading throughout these movements and because no breaking occurred (but pronounced SWs did occur), the resulting antidune sedimentary structures were preserved at depths between 0.04 and 0.1 m below the bed surface. Dimensions of the antidunes are shown in Table 6.2, the remainder of the run was characterised by USPB.

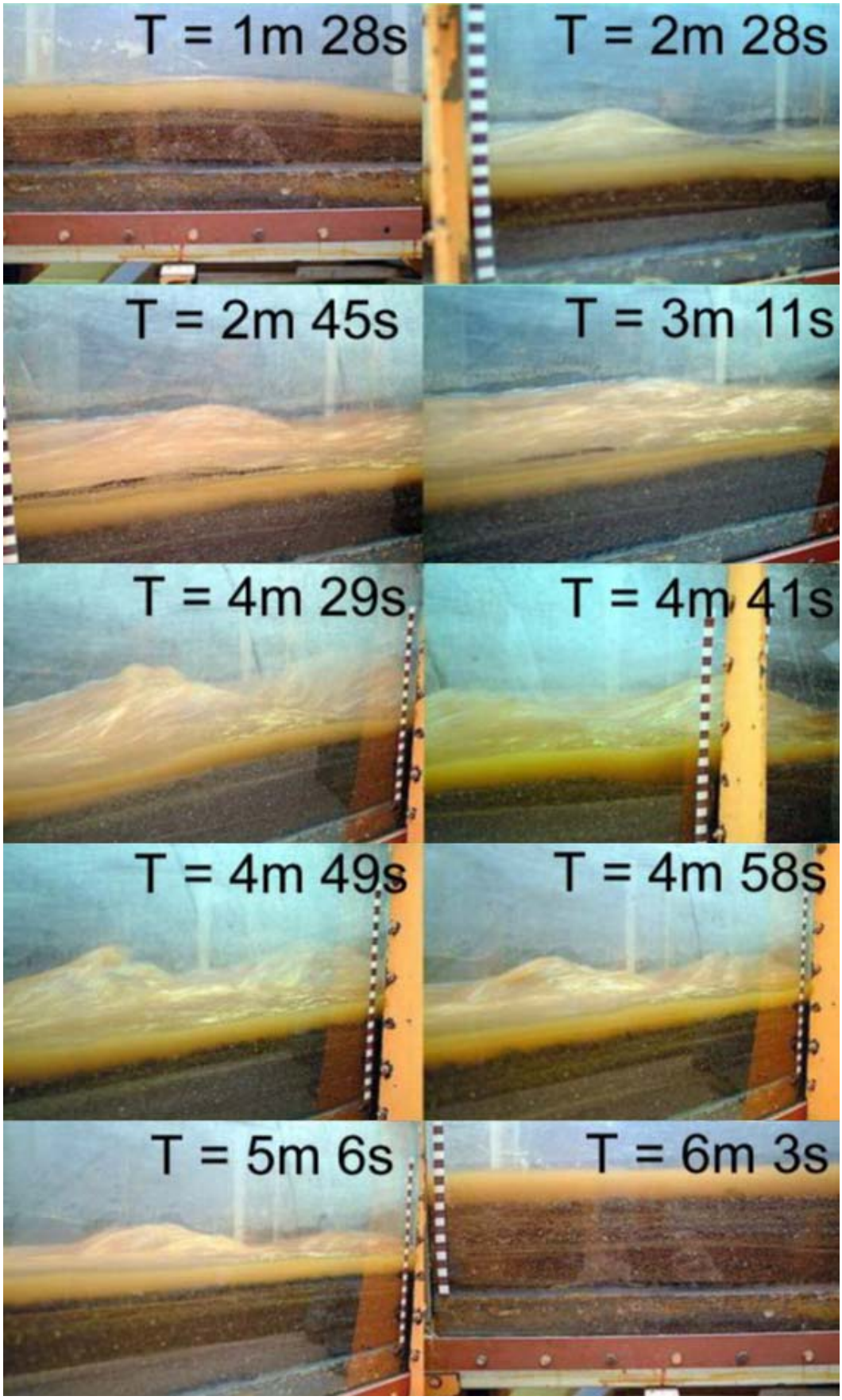

Plate 6.1 Still Photographs of Antidune Activity During Run 1

Black and white 1 cm graduations on scale. Time (T) indicated on frames.

6.2.2 Description of Run 2

Plates 6.2 – 6.7 and Figures 6.5 – 6.10 show stills from the video footage as described in Table 6.1 below. Antidunes occurred during two periods, at the beginning (Plates 6.2 – 6.4; Figures 6.5 – 6.7) and end (Plate 6.5 – 6.7; Figures 6.8 – 6.10) of the flume run.

Table 6.1 Details of Antidune Activity and Timing in Run 2

As Shown in the Following Figures.

Figure	Description	Shows	Timing
Plate 6.2	Composite A (s)	First set of stills/cartoons from antidune activity at the start of Run 2	From 3 m 20 s to 5 m 50 s (marked 000 s to 150 s)
Figure 6.5	Composite A (c)		
Plate 6.3	Composite B (s)	First set of stills/cartoons from antidune activity at the start of Run 2	From 6 m to 7 m 9 s (marked 167 s to 236 s)
Figure 6.6	Composite B (c)		
Plate 6.4	Composite C (s)	Second set of stills/cartoons from antidune activity at the start of Run 2	From 7 m 14 s to 8 m 2 s (marked 241 s to 289 s)
Figure 6.7	Composite C (c)		
Plate 6.5	Composite D (s)	First set of stills/cartoons from antidune activity at the end of Run 2	From 20 m 30 s to 21 m 43 s (marked 0 s to 73 s)
Figure 6.8	Composite D (c)		
Plate 6.6	Composite E (s)	Second set of stills/cartoons from antidune activity at the end of Run 2	From 21 m 48 s to 23 m 1 s (marked 78 s to 151 s)
Figure 6.9	Composite E (c)		
Plate 6.7	Composite F (s)	Third set of stills/cartoons from antidune activity at the end of Run 2	From 23 m 1 s to 23 m 21 s (marked 156 s to 171 s)
Figure 6.10	Composite F (c)		

Results in Figures 6.6 – 6.11

Plate 6.2 and Figure 6.5 show an antidune bedform (sometimes with a non-breaking SW) migrating slowly upstream as the bed aggrades. Plates 6.3 – 6.7 and Figures 6.6 – 6.10 mark a change in the type of antidune and SW behaviour observed near the beginning of Run 2. An initially low amplitude SW (0 s) migrates upstream (172 s, 177 s, 180 s), this wave then steepens, but remains relatively stationary (185 s and 188 s). The downstream edge of an upstream SW is just apparent on the left of frames 177 s to 196 s. Steepening and further movement of the SW upstream can be seen in frames 196 s to 221 s, before breaking and destruction of the SW and the antidune beneath, as the flow re-establishes (226 s to 231 s). An increase in flow depth due to dissipation of the SW and erosion of the bed can be on the downstream (right) side of 231 s and 236 s. By 241 s a new SW has established itself, and rapidly steepens upstreamwards (246 s, 251

s, 256 s and 261 s) with the upstream edge of a downstream SW becoming visible, these SWs however then gradually decrease in amplitude and dissipate (264 s through to 289 s), cutting down and levelling the bed and removing any sedimentary structures beneath the latter breaking SWs and for antidunes shown in Figures 6.8 to 6.11. The dimensions of these antidunes are presented in Table 6.2.

Results in Figures 6.12 – 6.17

Figures 6.12 – 6.17 represent the type of SW and antidune activity observed towards the end of Run 2. At 0 s an antidune and SW start to appear, moving upstream through 5 s, 10 s, 15 s and 20 s. At 25 s the SW steepens in the centre of the flume and a downstream SW appears, further steepening occurring at 35 s before the SW breaks and destroys the antidune at 38 s. The flow re-establishes in 43 s and 48 s, and SWs start to develop again at 53 s, 58 s, 63 s and 68 s before breaking again at 73 s and 78 s. The flow then again re-establishes at 82 s through to 91 s, this time however the antidune and SW pair that form have a much lower amplitude and their amplitude remains muted, these forms then migrate rapidly upstream (96 s – 111 s), followed by second pair (116 s to 126 s), a third pair (136 s – 151 s), and finally a fourth pair (156 s – 171 s).

Two types of UMA behaviour were observed in these figures: two upstream accreting antidunes that were rapidly formed and destroyed followed by four non-breaking migratory forms. Details of the antidune dimensions are presented in Table 6.2.

Table 6.2 Summary Details of Antidune Dimensions in Run 1 and Run 2.

	Antidune λ	**Observed Antidune *h***	**Predicted height (λ x 0.15)**	**Standing Wave**
Run 1	0.4 m	Up to 0.02 m at wall	0.06 m	Three-dimensional
Run 2 (start)	0.44 m	Up to 0.018 m at wall	0.066 m	Three-dimensional
Run 2 (end breaking)	0.55 and 0.62 m	0.045 m	0.08 and 0.093 m	Two-dimensional
Run 2 (end non-breaking)	0.62 m	0.045 m	0.093 m	Two-dimensional

For the three dimensional antidunes the bed in the centre of the flume under the SW is likely to have been higher than the bed at the wall, giving a taller antidune. Likewise the troughs in the centre of the flume would have scoured deeper than apparent from observations at the flume wall. This data supports the interpretations discussed in Box 5.1 above. However, the limited quality of data makes it difficult to take the analysis further than outlined in Box 5.1.

In Run 2 between the two periods of antidune activity and in Run 1 after the initial period of antidunes the formation of an USPB was observed. Plate 6.9 shows a still from the video footage of Run 2 showing two low-amplitude bedforms migrating downstream across the USPB, but in-phase with the water surface. Similar bedforms were identified by McBride *et al*. (1975) and Cheel (1990) in shallow supercritical flows.

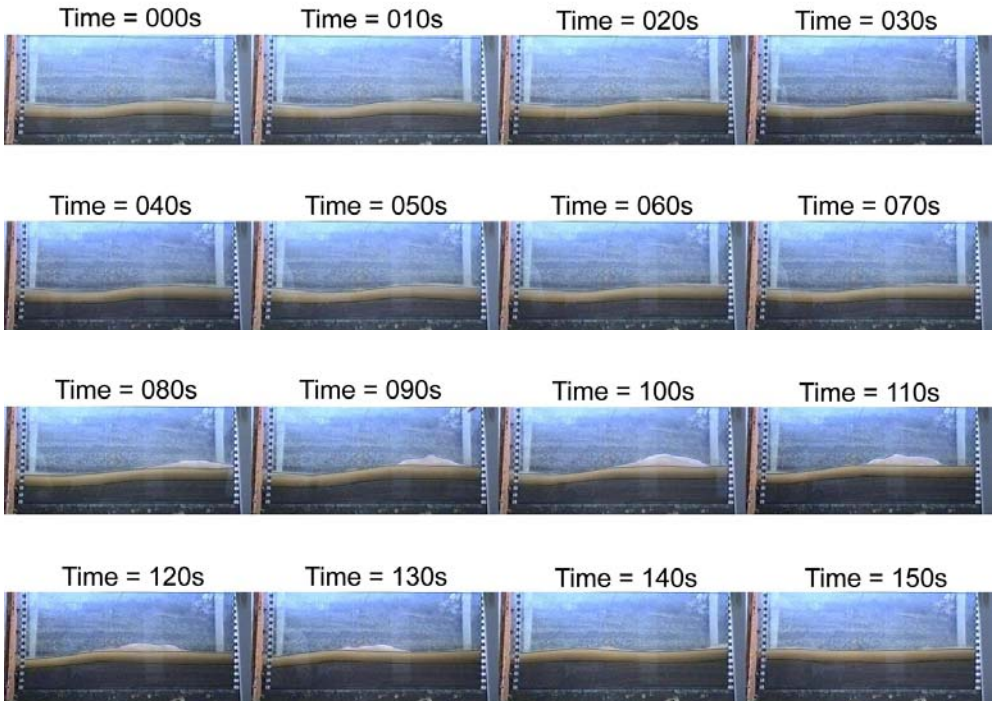

Plate 6.2 Composite A

(s) - beginning of Run 2, see Table 6.1 for details. Flow left to right, scale bars are in intervals of 0.01 m.

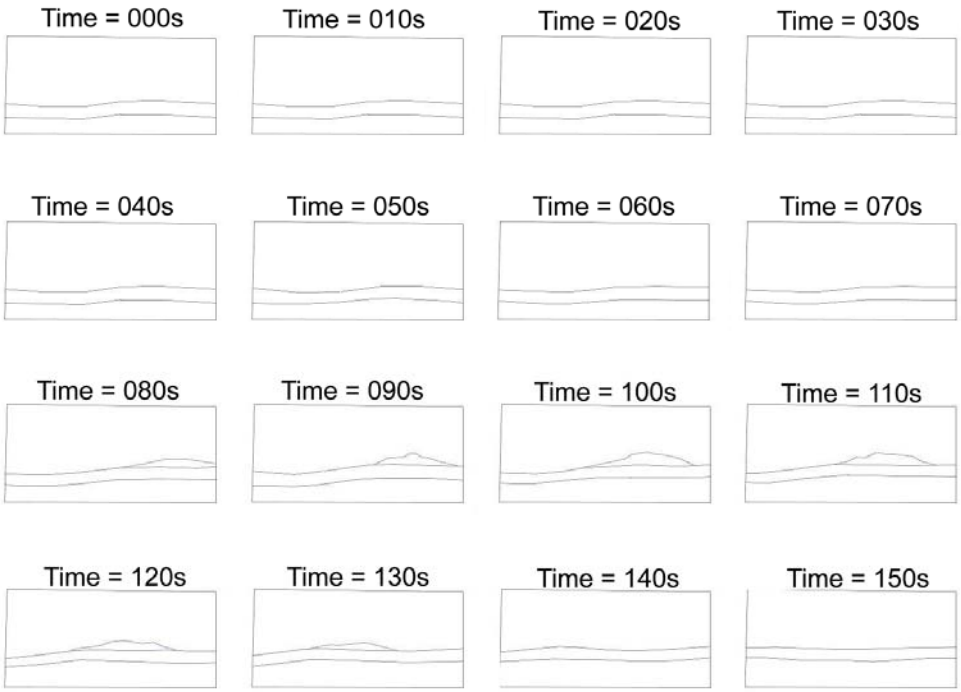

Figure 6.5 Composite A

(c) - beginning of Run 2, see Table 6.1 for details. Cartoon of Plate 6.2, flow left to right.

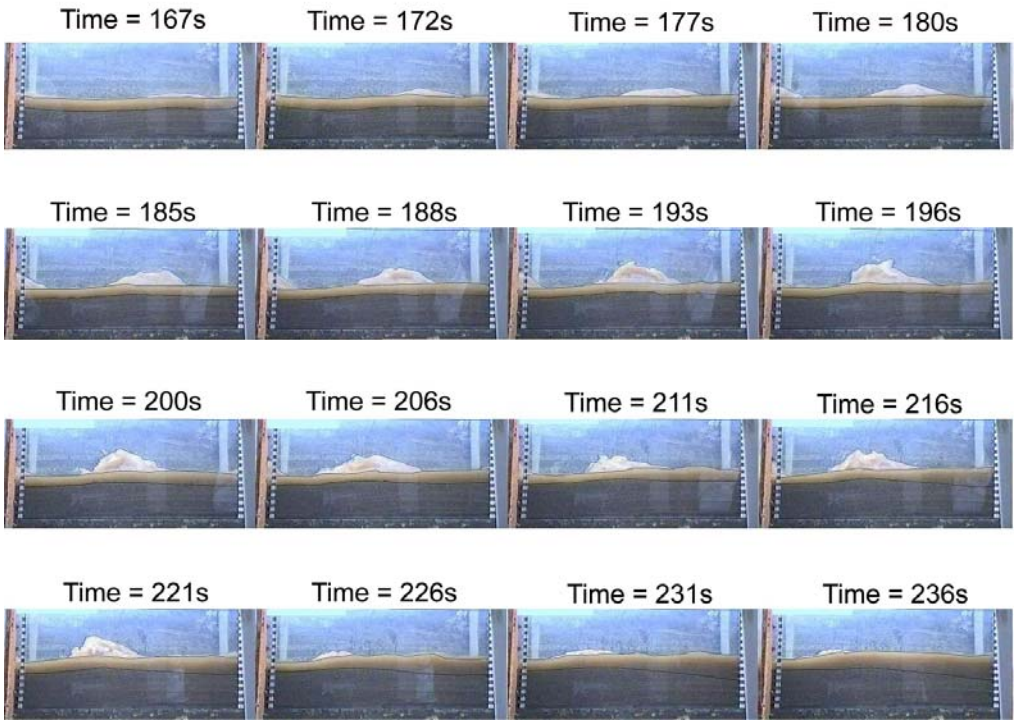

Plate 6.3 Composite B

(s) - beginning of Run 2, see Table 6.1 for details. Flow left to right, scale bars are in intervals of 0.01 m.

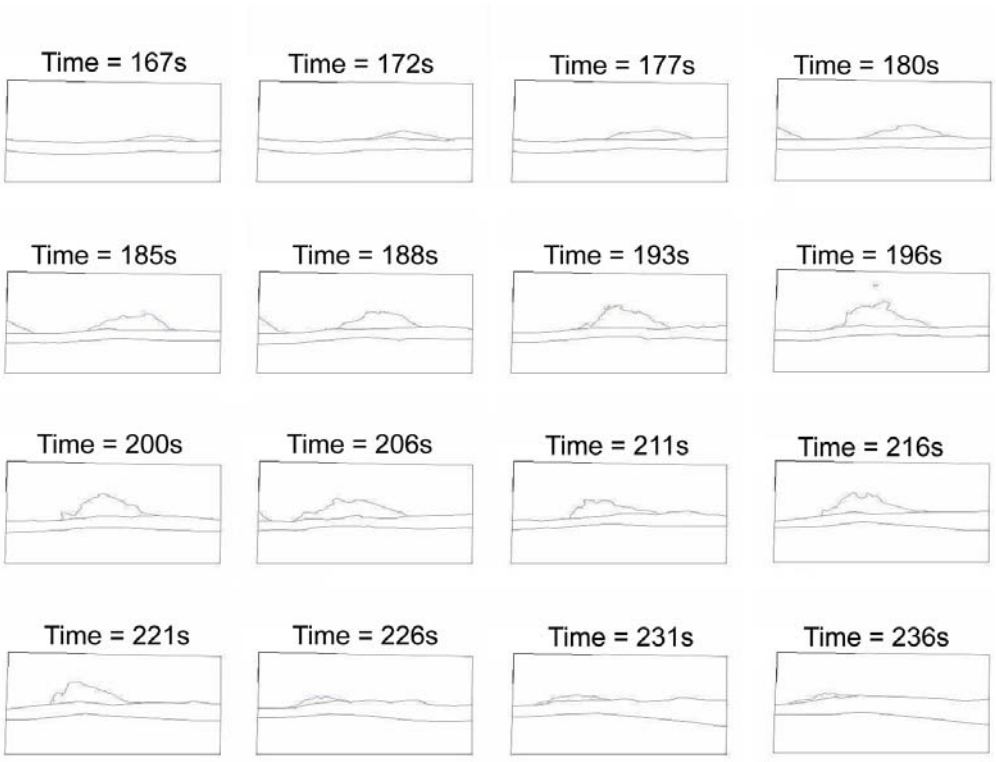

Figure 6.6 Composite B

(c) - beginning of Run 2, see Table 6.1 for details. Cartoon of Plate 6.3, flow left to right.

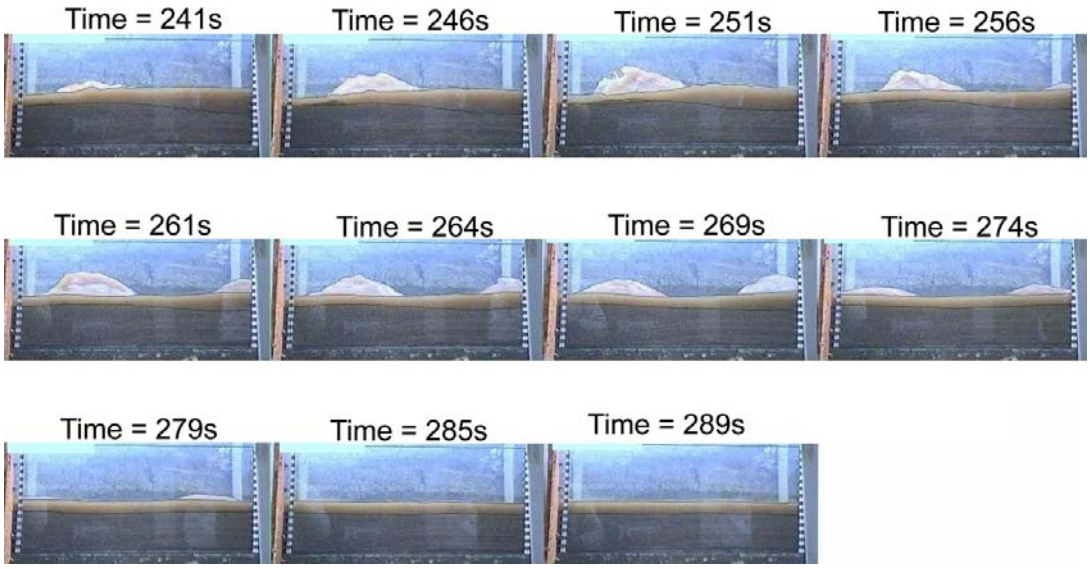

Plate 6.4 Composite C

(s) - beginning of Run 2, see Table 6.1 for details. Flow left to right, scale bars are in intervals of 0.01 m.

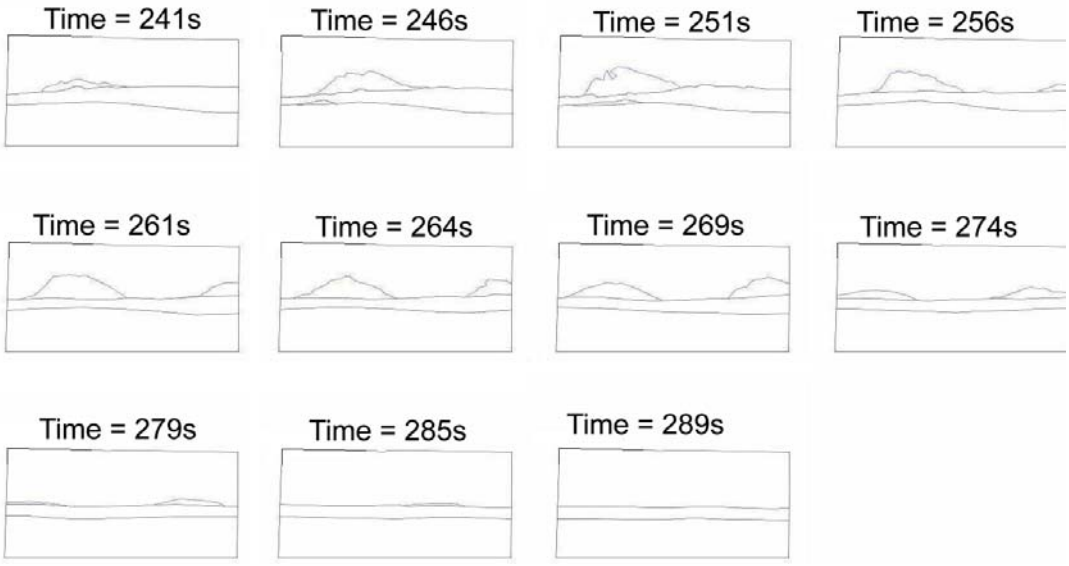

Figure 6.7 Composite C

(c) - beginning of Run 2, see Table 6.1 for details. Cartoon of Plate 6.4, flow left to right.

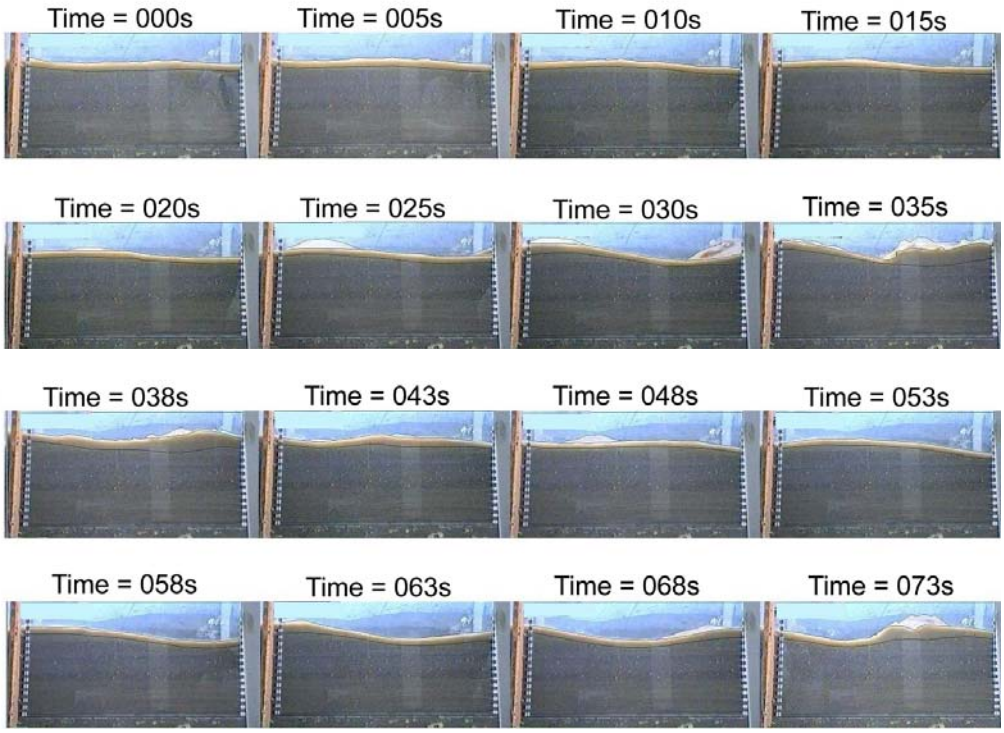

Plate 6.5 Composite D

(s) – towards the end of Run 2, see Table 6.1 for details. Flow left to right, scale bars are in intervals of 0.01 m.

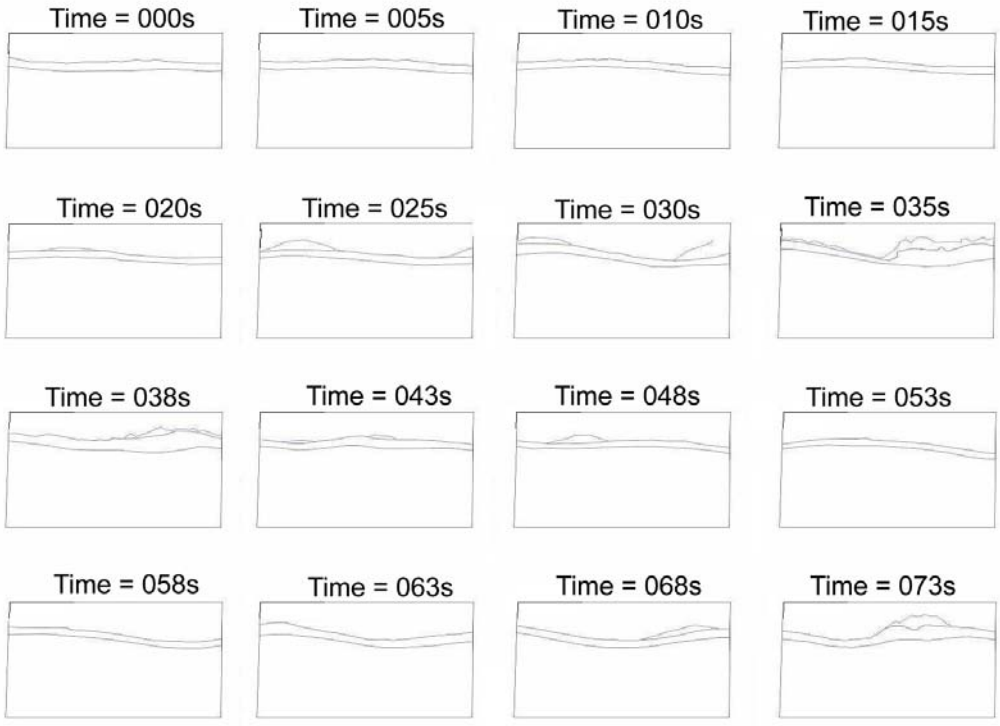

Figure 6.8 Composite D

(c) – towards the end of Run 2, see Table 6.1 for details. Cartoon of Plate 6.5, flow left to right.

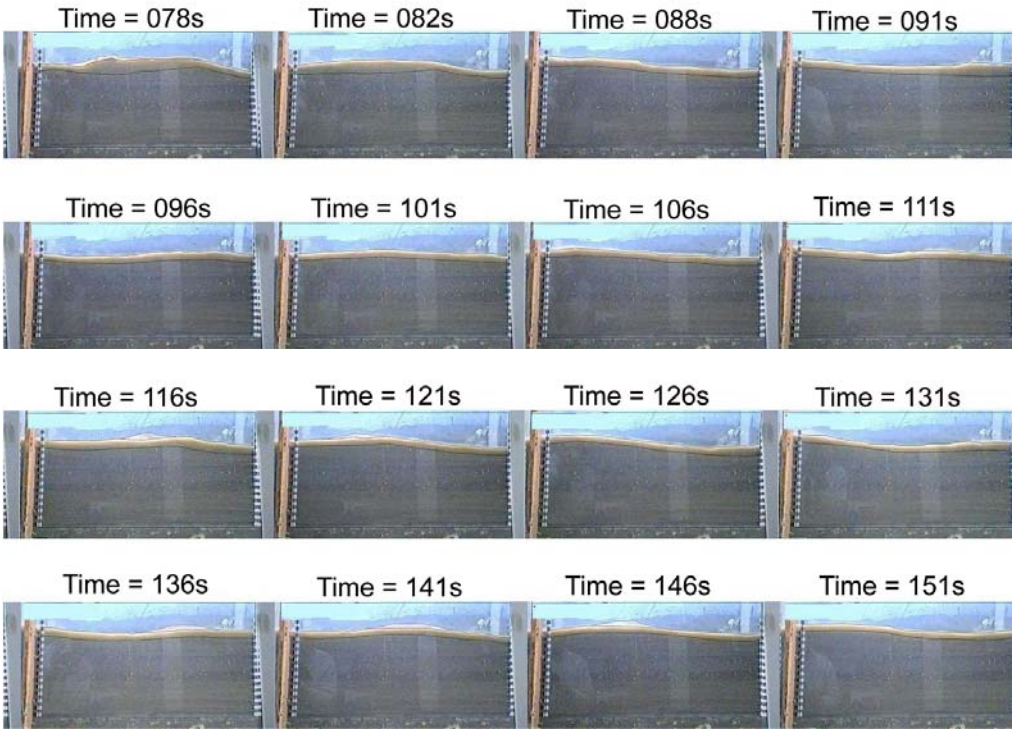

Plate 6.6 Composite E

(s) – towards the end of Run 2, see Table 6.1 for details. Flow left to right, scale bars are in intervals of 0.01 m.

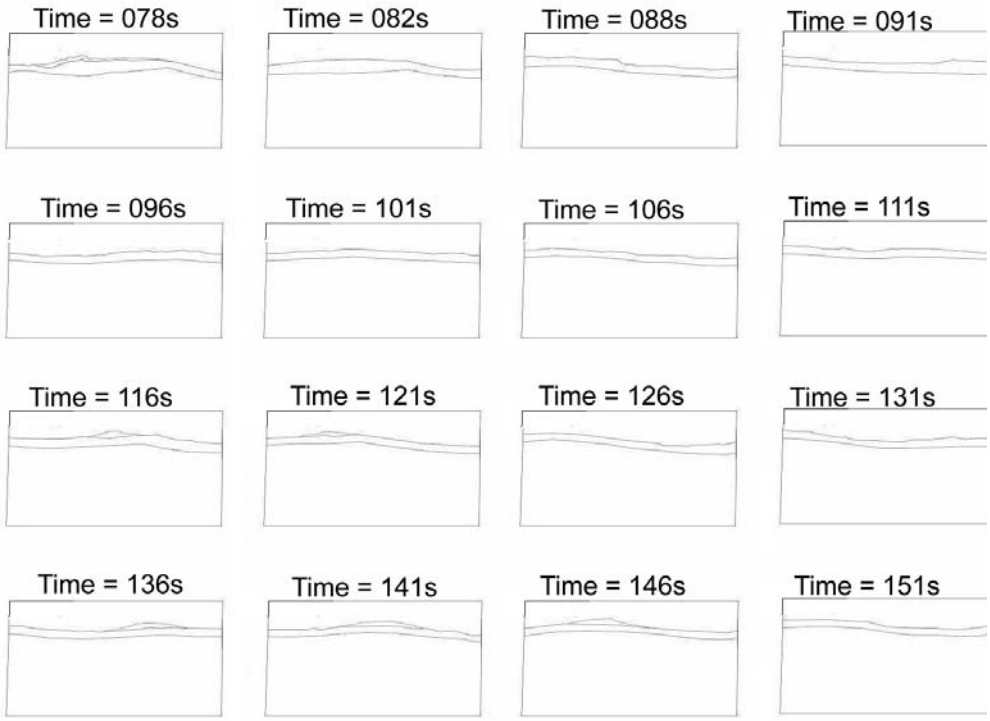

Figure 6.9 Composite E

(c) – towards the end of Run 2, see Table 6.1 for details. Cartoon of Plate 6.6, flow left to right.

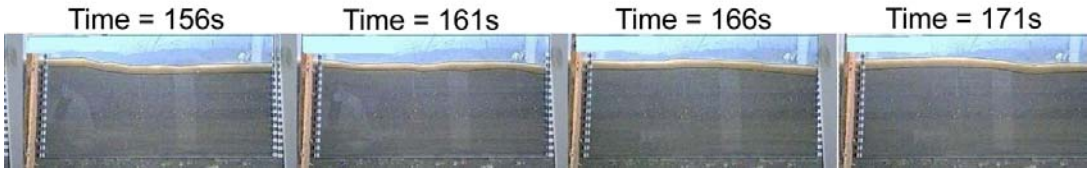

Plate 6.7 Composite F

(s) – towards the end of Run 2, see Table 6.1 for details. Flow left to right, scale bars are in intervals of 0.01 m.

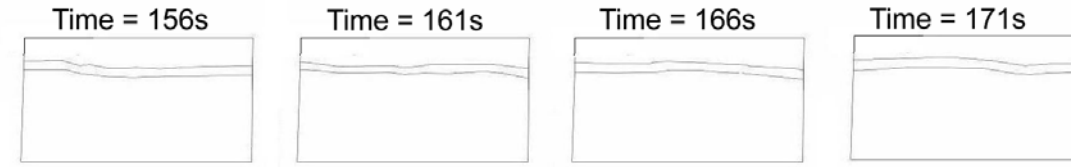

Figure 6.10 Composite F

(c) – towards the end of Run 2, see Table 6.1 for details. Cartoon of Plate 6.7, flow left to right.

6.3 Observed Sediment Transport Processes

During mobile bed runs sediment transport was observed to occur by suspension, saltation and traction. These processes broadly corresponded to particle size (Table 3.10 shows the sediment size parameters), with the sand to granule (approximately sub 2 mm) element in suspension, granule to small gravel particles (approximately 2 to 5 mm) moving by saltation, and the gravel fraction (approximately 5 to 20 mm) as a 0.005 – 0.015 m thick carpet of particles moving in the traction load (such as in Plate 6.8). Within this carpet, individual grains could be discerned as moving by rolling and sliding motions. The carpet was observed to move with frequent thicker pulses (discrete low amplitude bedwaves of ~0.015 m amplitude), these principally occurred leaving the trough region and moving up the flank of the next antidune. Sediment particles in the carpet, in particular sediment in the lower portion was seen to slow and stop on the upstream facing flank and crest of each antidune. Here, the majority of mobile grains within the carpet froze, with only grains near the bed surface continuing to move. Initially, occasional (at around 0.5 to 0.33 Hz) sediment ejection events from the downstream edge of the trough region were observed. However as antidunes built these sediment ejection events became increasingly frequent (at around 2 Hz, a frequency peak observed in spectral analysis of the ADV data), carrying sediment from the trough onto the lower to mid portions of the downstream antidunes flank. The larger particles entrained typically followed a curved trajectory, landing approximately 0.1 – 0.15 m downstream from the point of entrainment. Coarse clasts could be seen accumulating at the crest, before being buried or periodically entrained downstream. These observations are shown in Figure 6.11 which shows stills and accompanying line drawings of sediment transport events over several sequential stills. During the USPB phases that intervened between antidune phases, low amplitude bedload sheets were observed (see Plate 6.9).

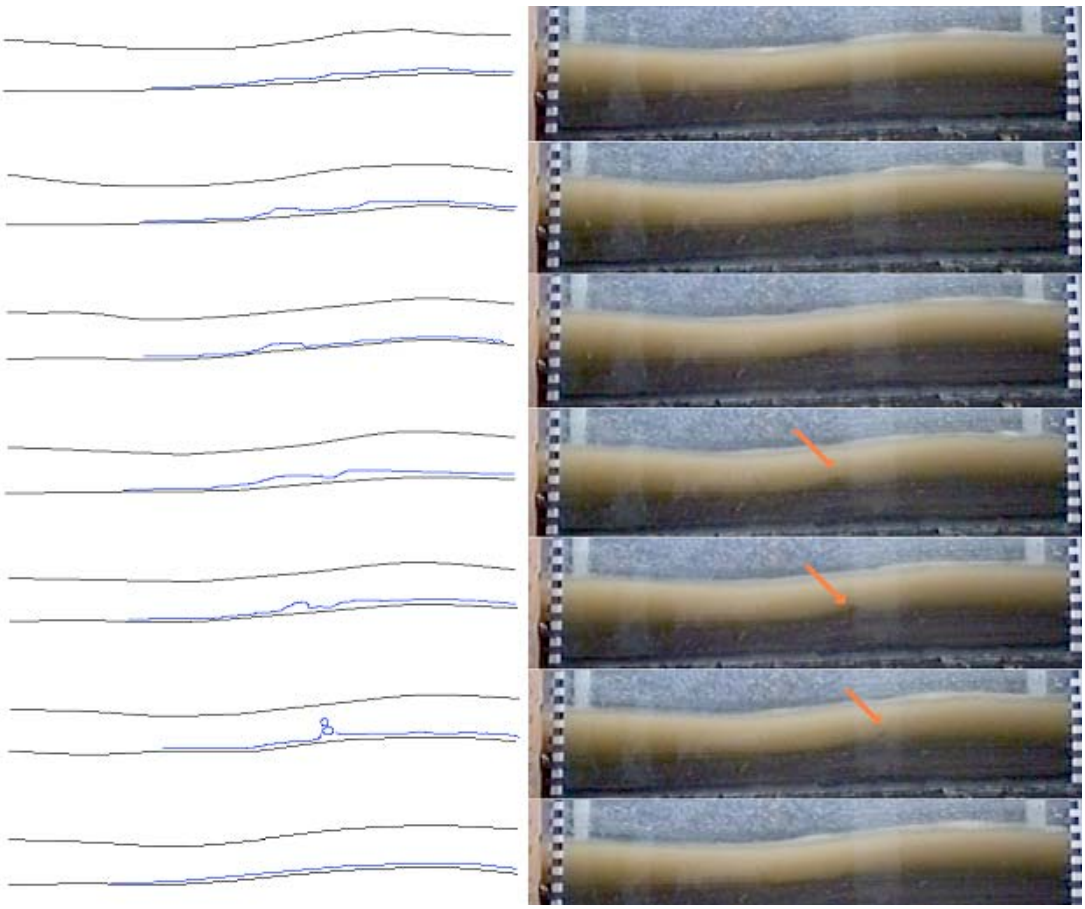

Figure 6.11 Stills and Line-Drawings of sediment Transport Processes

Stills with accompanying line drawings of sediment transport over antidune bedforms. Time of first frame (top) is 11 s; time between subsequent frames is 0.042 s. Pulses of sediment can be seen alongside an ejection event which lifts a large volume of sediment into suspension (ejection event frames have orange arrow). Scale bars are in 1 cm divisions.

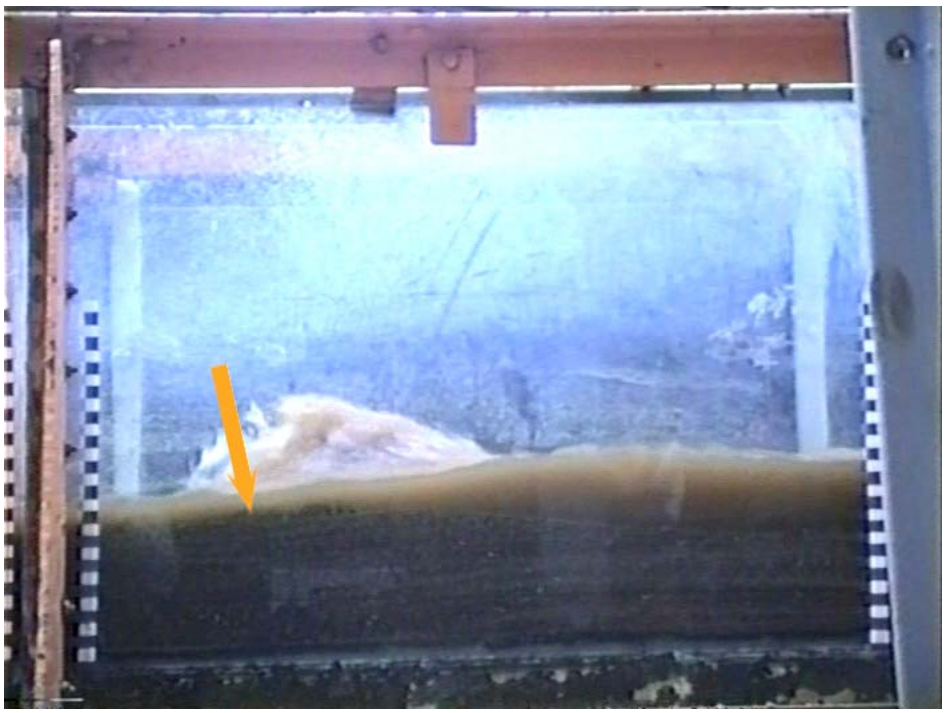

Plate 6.8 Coarse Bedload Accumulation

Coarse bedload (arrowed) accumulating on upstream side and crest of antidune (as per Alexander and Fielding 1997). Flow left to right, scale bars are in 0.01 m intervals. Low-angle upstream dipping beds can be clearly seen below standing wave. Still from 7 m 40 s into Run 2.

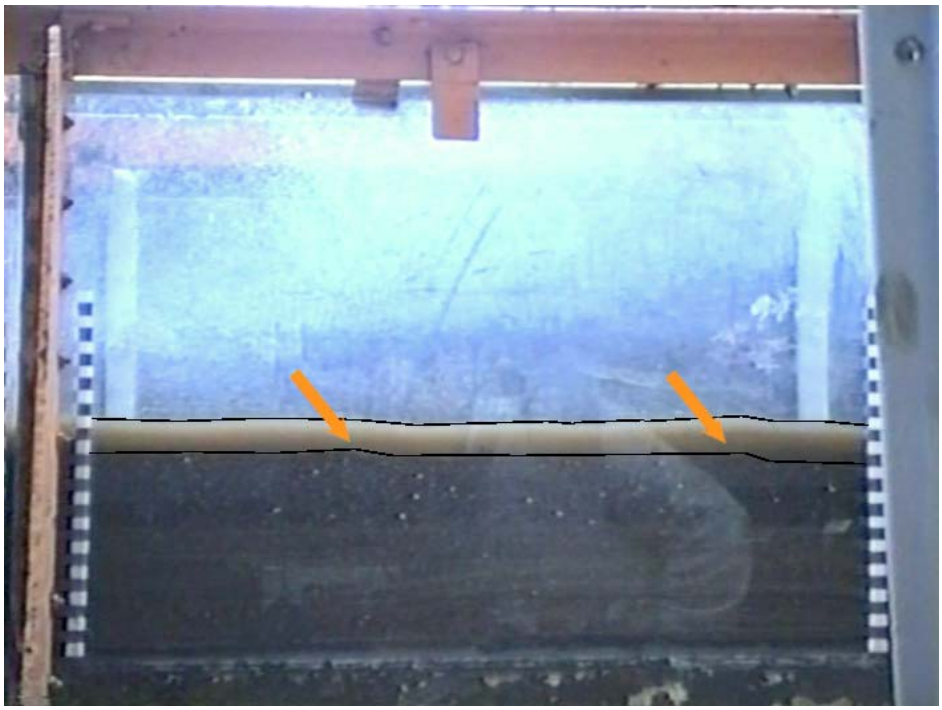

Plate 6.9 Low Amplitude In-Phase Bedwaves

View of two low-amplitude in-phase downstream migrating bedwaves (arrowed) during period of USPB bed deposition. Flow left to right, scale bars are in 0.01 m intervals. Still from 13 m 57 s into Run 2.

6.4 Sediment Peels from Run 1 and Run 2

Figures 3.5 and 3.6 show the layout of the sediment peels taken during Run 1 and Run 2. These peels are then shown in Figures 6.12 – 6.17.

6.4.1 Run 1 - Flow Parallel Peels

Description of Peel 2

Figure 6.12 shows the sets of deposits produced during Run 1 by the antidune activity shown in Plate 6.1. The set produced by antidune activity is coloured blue and occurs between 0.05 and 0.1 m from the base of the flume. This set has a concave erosional base ('**eb**') and overlies structureless sediment deposited at the beginning of the flume run. The top of the set of antidune deposits is gradational into the USPB set, which are coloured green. The top section of the peel (coloured red) is considered disturbed and is not evaluated here.

The base of the set of antidune deposits is sand-rich relative to other deposits in the peel. Within the set, the cross-strata are defined by low-angle upstream-dipping concave-upwards sets ('**ud**'), which downlap onto the erosional base of the set. Initially, these sets are sand-rich with lines of stringers – gravel clasts with their a-b planes parallel to the angle of dip. Later sets are increasingly sand poor, with increasingly limited amounts of sand differentiating the laminae; although the angle of gravel clasts a-b planes remains generally parallel to the angle of dip. Laminae are mostly concave upwards, and of varying thickness, from single clasts and 0.005 m of sand to several clasts thick (~0.005 m) and dip upstream at angles generally between 5.5˚ to 10.5˚ but up to 15˚ in places, with the base of laminae tending to dip at shallower angles (downlapping). These laminae are truncated by a downstream-dipping erosional surface ('**ds**'), above which a concave-upward downstream-dipping wedge of coarser sediment ('**dd**') is present. The gradational transition between antidune sets to the USPB set above is characterised by structureless sand-poor sediment ('**gt**'). The USPB set contains multiple, stacked planar laminae, alternating between sand-rich and sand-poor (marked '**sr**' and '**sp**' respectively).

Description of Peel 4

Figure 6.13 shows the sets of deposits produced during Run 1 downstream of the images shown in Plate 6.1 and sampled by Peel 2. The set produced by antidune activity is coloured blue, and is between 0.055 and 0.085 m from the base of the flume. This set has an almost planar erosional base ('**eb**') and overlies structureless sediment deposited at the beginning of the flume run. The top of the set of antidune deposits is gradational into the USPB set, which are coloured green. The top section of the peel (coloured red) is considered disturbed and is not evaluated here.

Peel 4 shows only a small set of strata preserved from the antidune activity in Run 1; at 0.03 m thick the set is half as thick as in Peel 2. The set has a concave lower boundary and a convex upper boundary. Internally, the set is sand-rich ('**sr**'), with a line of stringers ('**st**') one gravel clast thick dipping downstream at 2˚ with the clasts a-b planes orientated parallel. A layer of dark silicon carbide particles ('**sc**') is present at the upper boundary between antidune and USPB sets. The USPB sets contain multiple, stacked planar laminae, alternating between sand-rich and sand-poor (marked '**sr**' and '**sp**' respectively).

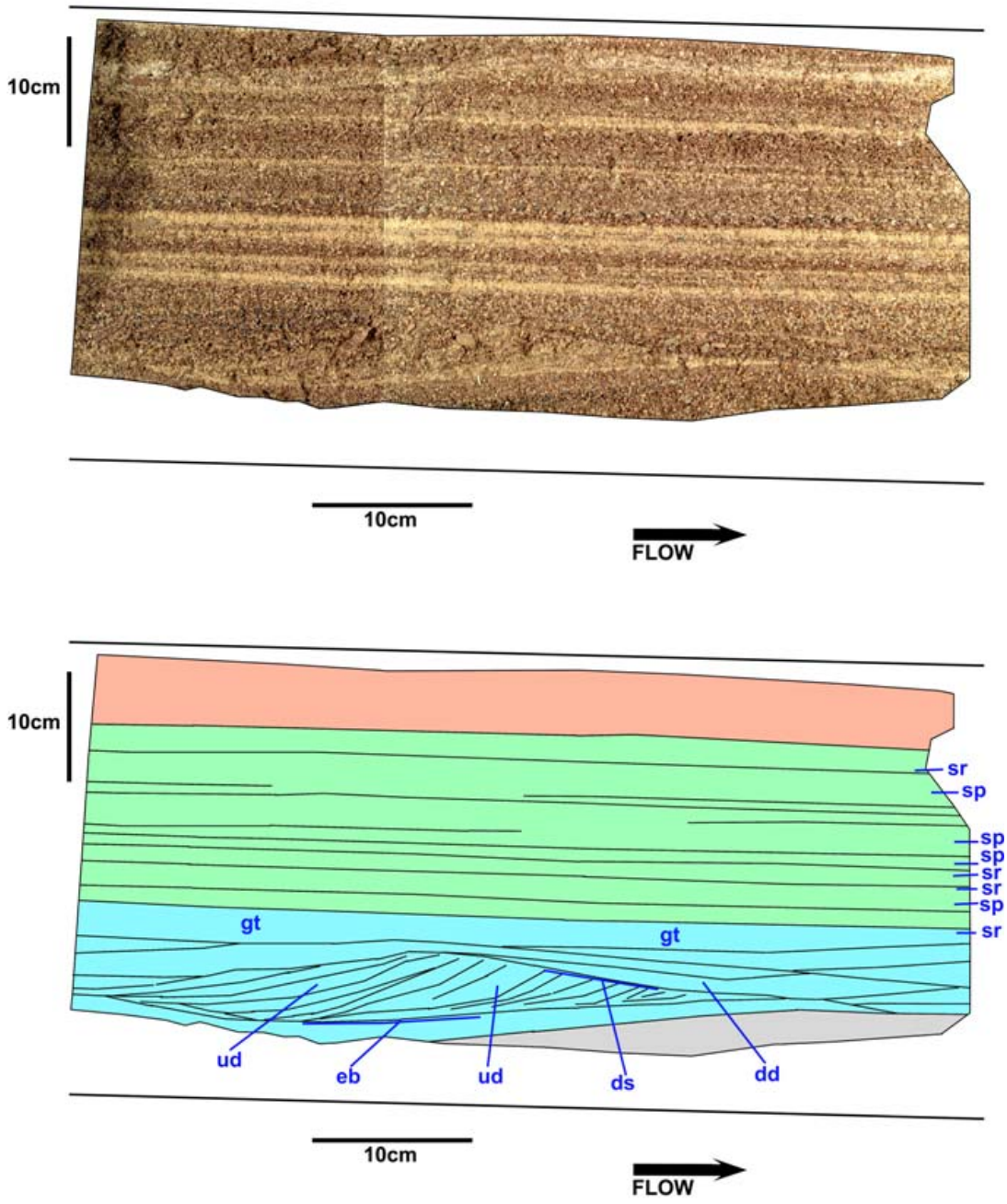

Figure 6.12 Peel 2 from Run 1

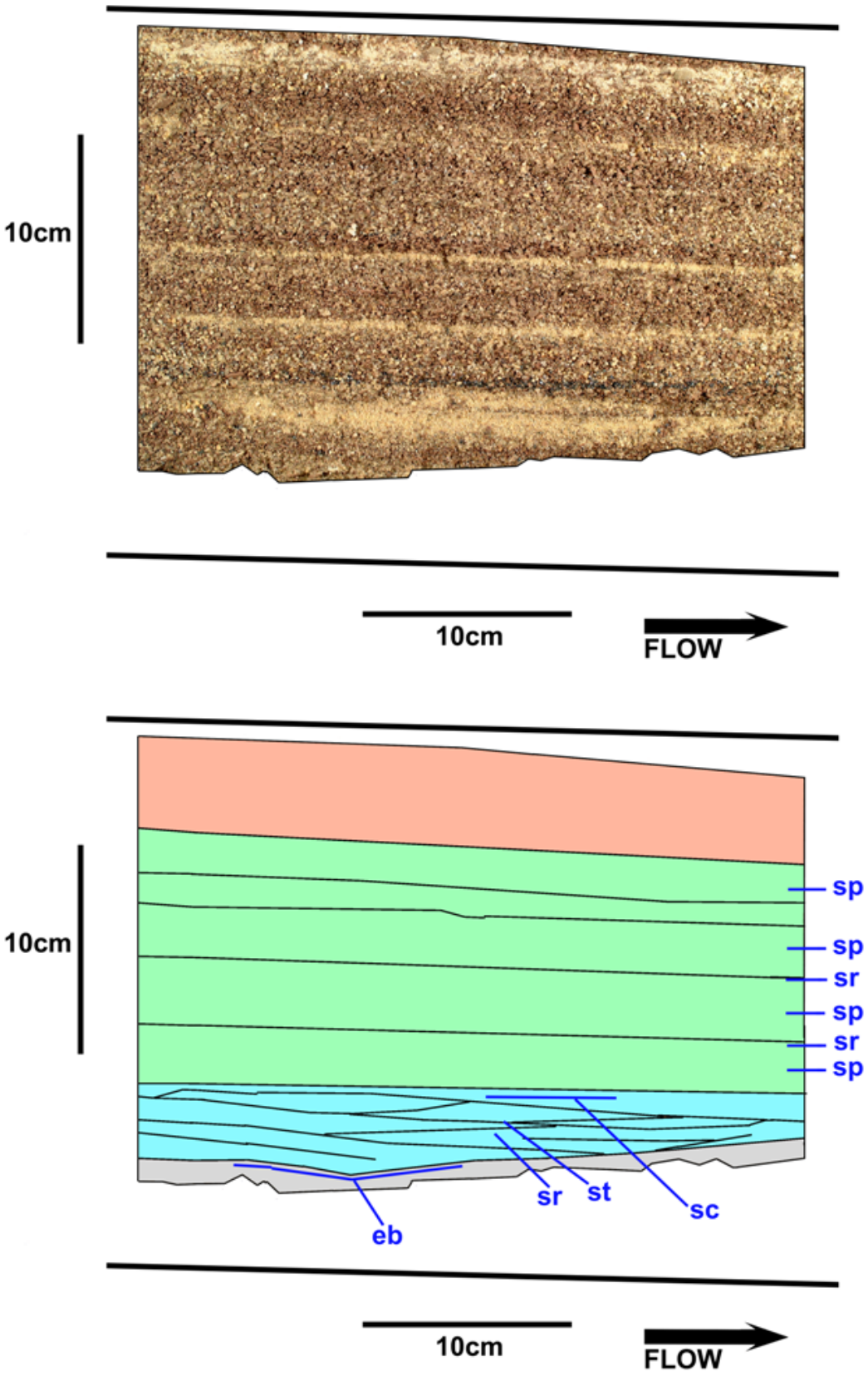

Figure 6.13 Peel 4 from Run 1

6.4.2 Run 1 - Flow Transverse Peels

Figures 6.14 and 6.15 show, transversely, the strata sets produced during Run 1, just upstream and downstream respectively of the activity shown in Plate 6.1 and sampled by Peel 2. The set produced by antidune activity is coloured blue, and is between 0.04 and 0.09 m from the base of the flume. This set has an almost concave erosional base ('**eb**') and overlies structureless sediment deposited at the beginning of the flume run. The top of the set of antidune deposits is gradational into the USPB set, which are coloured green. The top section of the peel (coloured red) is considered disturbed and is not evaluated here.

Description of Peel 1

The antidune set has an erosional base ('**eb**'), 0.04 to 0.06 m from the base of the flume. The antidune set appears gravel-rich and sand-poor, with some silicon carbide particles accumulated ('**sc**') in the sets base in the centre of the peel. The antidune set is asymmetric across the flume, with a 'wedge' of coarser sediment ('**we**') with some internal structures present on the right of Figure 6.14, and with a smaller less-well defined 'wedge' ('**we**') on the left of the figure. Above these wedges the remainder of the antidune set appears massive with no clear structures. The USPB set contains multiple, stacked planar laminae, alternating between sand-rich and sand-poor (marked '**sr**' and '**sp**' respectively).

Description of Peel 3

The antidune set has an erosional base ('**eb**'), 0.04 to 0.06 m from the base of the flume. The antidune set appears gravel-rich and sand-poor, with dark silicon carbide accumulations ('**sc**') in the sets base in the centre of the peel. The set is asymmetric across the flume, there being a 'wedge' of coarser sediment ('**we**') with some internal structures present on the left of Figure 6.15, with a smaller less-well defined 'wedge' ('**we**') on the right of the figure. Above these wedges the remainder of the antidune set appears massive with no clear structures. A thick silicon carbide-rich band marks the end of the antidune sedimentology, and was fed into the flume as the bed flattened out into USPB. The USPB set contains multiple, stacked planar

laminae, alternating between sand-rich and sand-poor (marked '**sr**' and '**sp**' respectively).

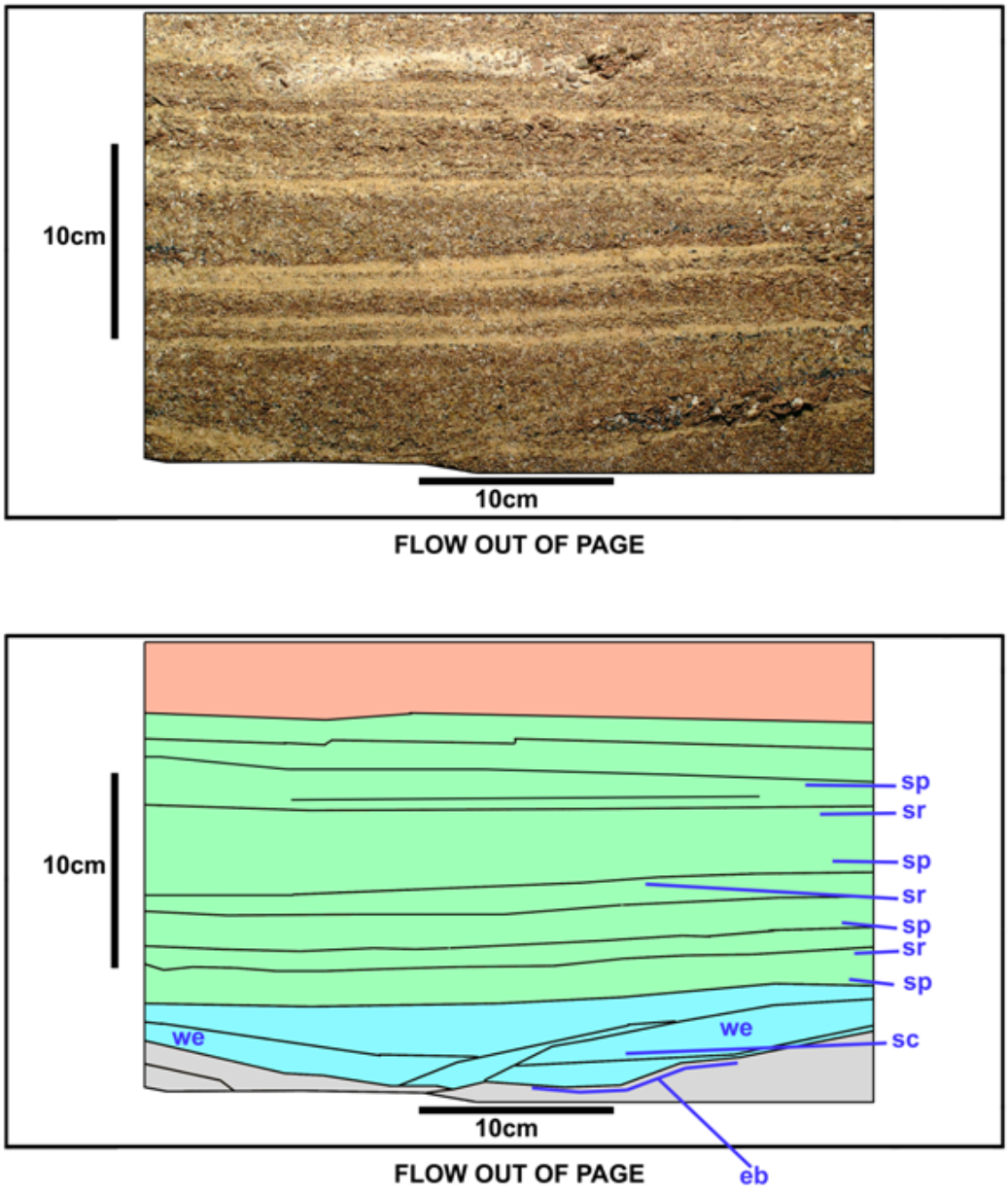

Figure 6.14 Peel 1 from Run 1

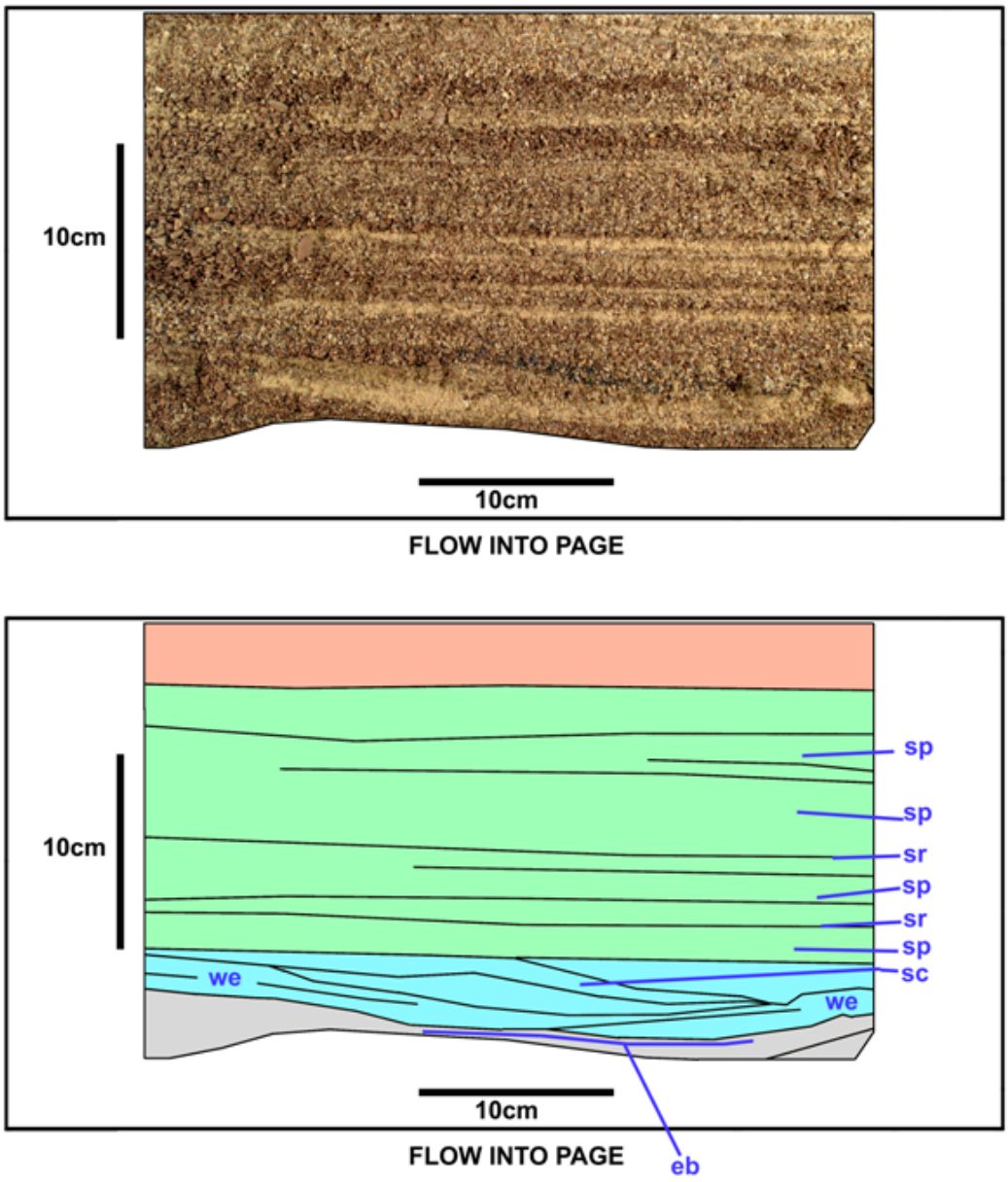

Figure 6.15 Peel 3 from Run 1

6.4.3 Run 2 - Flow Parallel Peels

Figures 6.16 and 6.17 (Peels 1 and 2 respectively) show the strata sets produced during Run 2 and represent an almost continuous stretch of flume, including the section shown in Plates 6.2 – 6.7; and Figures 6.5 to 6.10. The right hand edge of Peel 1 almost fits against the left hand edge of Peel 2, apart from a 0.04 m gap; hence they are not displayed as one section. Only the antidune activity that occurred towards the end of Run 2 is present in Peel 1 (the lower part of Peel 1 synchronous with the antidune activity preserved in Peel 2, formed through deposition from an USPB). In Peel 2, two antidune sets (coloured blue) are present with a USPB set (coloured green) intervening; the antidune sets occur between 0.04 and 0.085 m and then 0.155 and 0.23 m from the bed. The first antidune set overlies structureless sediment deposited at the beginning of the flume run. The first antidune set is gradational into the USPB set, whilst the second set has an erosional base cutting into the underlying USPB set. The top section of the peel (coloured red) is considered disturbed and is not evaluated here.

Description of Peels

The first antidune set is linked to antidune activity observed between 2 to 8 minutes into the run; and the second antidune set to activity observed between 20 and 23 minutes into the run. The first antidune set (Figure 6.17) contains three downstream-dipping erosional surfaces ('**es**') that are gravel-rich and sand-poor; these surfaces are initially level before becoming downstream-dipping, at an angle of 11˚ to 12˚. Beneath the three '**es**' erosional surfaces, faint upstream dipping laminae ('**ud**') (upstream dip 7˚ – 16˚) and multiple gravel clasts ('**gc**') are imbricated with their a-b planes dipping steeper than the laminae, dipping upstream at angles of between 20˚ to 45˚. There is only limited variation in the sand and gravel content to mark laminae boundaries, but the clast imbrications are sub-parallel to the expected geometry of laminae and are consistent throughout. The USPB set (Figure 6.16 and 6.17) contains multiple, stacked planar laminae, parallel to the flume bed and alternating between sand-rich and sand-poor (marked '**sr**' and '**sp**' respectively).

At the base of the second antidune set (Figure 6.17) there are two trough shaped internal structures ('**tr**') with erosional bases cutting into the

underlying USPB. Additionally, some further fainter internal structures ('**is**') are visible in the peel above these troughs. In Figure 6.16 and 6.17 above the USPB set, a close series of five stacked gently downstream-dipping (at an angle of 1.5˚ to 3.3˚) bipartite (sand-rich base grading upwards to gravel-rich) laminae ('**bl**') are present.

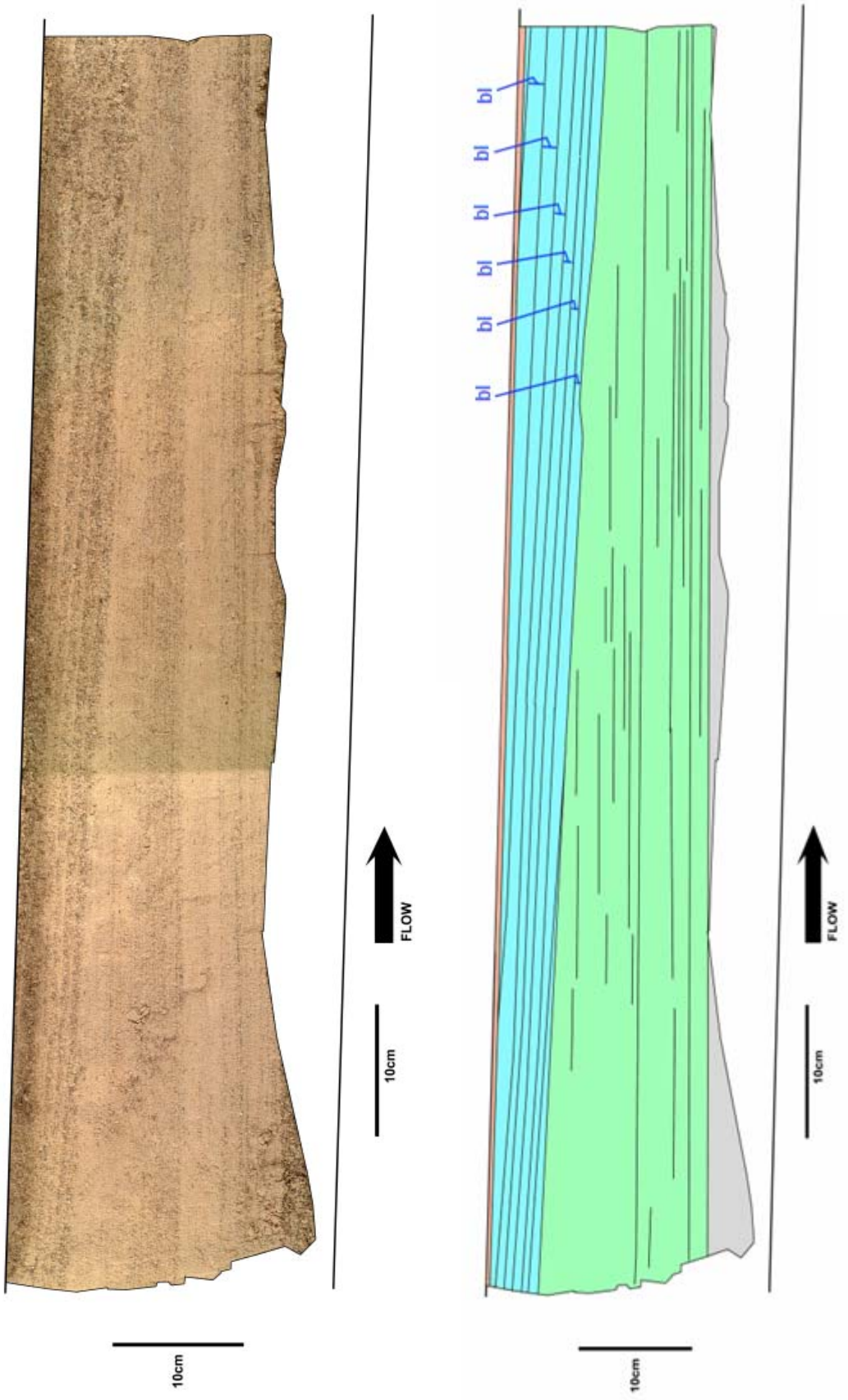

Figure 6.16 Peel 1 from Run 2

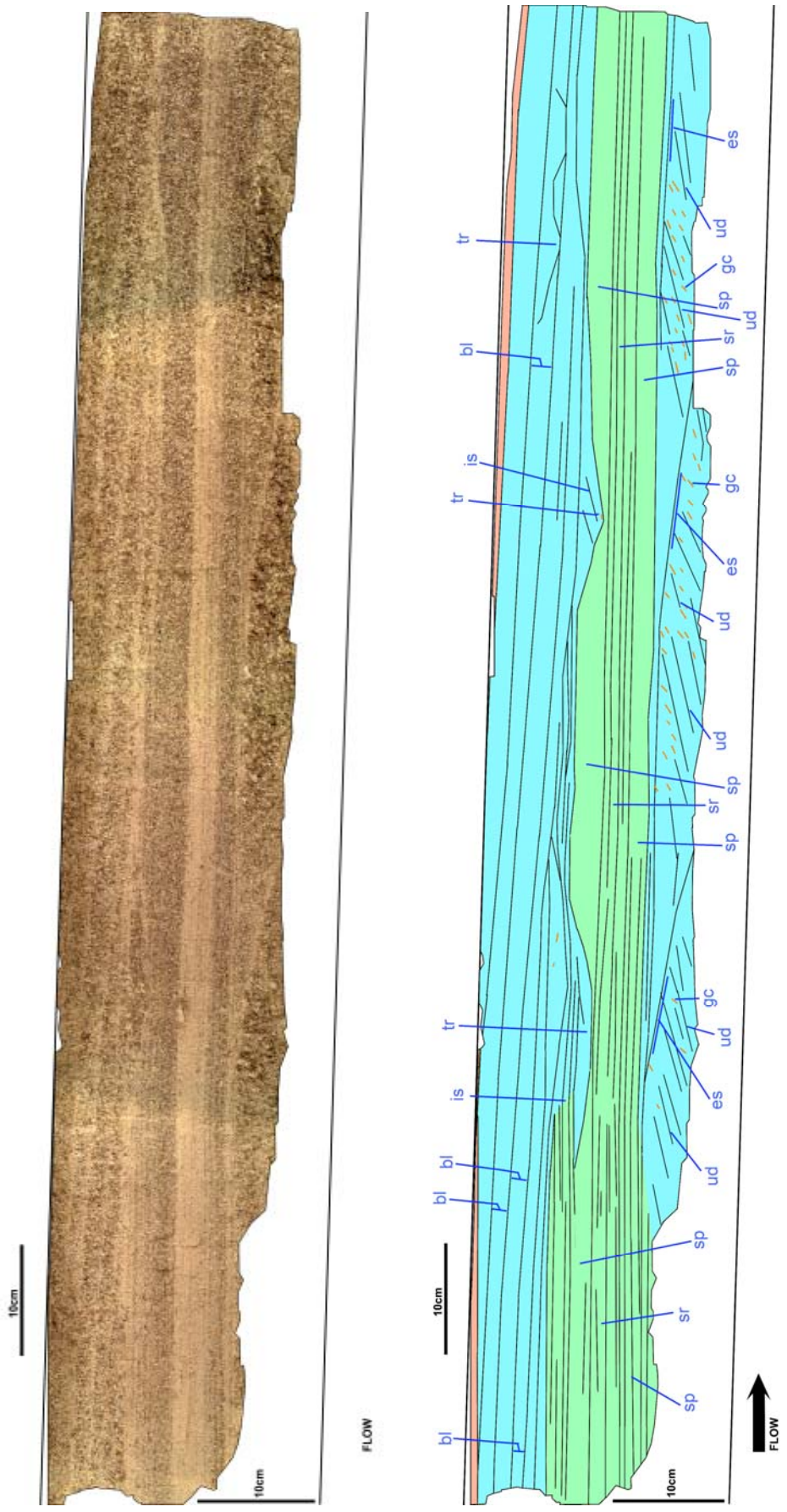

Figure 6.17 Peel 2 from Run 2

7 Discussion

7.1 Bulk Flow Structure and Detailed Investigation of Turbulence over Antidune Bedforms - ADV Investigations

Sections 4.1 – 4.4 detail the results from ADV measurements undertaken over the types of antidune bedform described in Tables 3.1 and 3.2. Key differences and common trends are now examined, and key findings discussed and related to relevant literature. Sections 7.1.1, 7.1.2 and 7.1.3 each compare data from two separate flume runs. However, the flume set up and the amplitude of the antidune inserts was identical in each of the flume runs compared. Ideally all runs would have utilised the 100 Hz ADV recording rate, but the special computer to run the ADV at this rate was only available during one flume run. For this reason, only flow over the gravel surfaced antidune bedforms was measured using an ADV recording at 100 Hz. However, flow measurements over the sand surfaced antidune bedforms and openwork-gravel antidune bedforms runs was undertaken using an ADV recording at 25 Hz. Therefore, an additional re-run measuring the flow over the gravel surfaced antidune bedforms but with the ADV recording at 25 Hz was undertaken to assist comparisons between the three types of antidune bedform insert. In this latter case (detailed in 7.1.1), since the antidune bedforms used in each run are wholly identical (i.e. gravel surfaced inserts in both runs), the measurement differences are due solely to the two different frequencies the of ADV data recording.

7.1.1 Comparison One – Flow Over Gravel Surfaced Antidune Bedform Inserts Measured With an ADV Recording at 100 Hz Compared to Flow Over Gravel Surfaced Antidune Bedform Inserts Measured With an ADV Recording at 25 Hz

A comparison of Figures 4.1 – 4.3 with Figures 4.81– 4.83, shows that $\overline{U}$ values when measured at both 100 Hz and 25 Hz are very similar. However, for ADV measurements recorded at 25 Hz, there was likely an underestimation of instantaneous velocities, due to the limited temporal resolution of the 25 Hz ADV, (for further discussion see Section 3.1.1 and

Garcia *et al*., 2005). The underestimation is most pronounced in the trough region, the lower correlation values for 25 Hz data are indicative of difficulties in distinguishing between noisy data and turbulence due to the lower frequency of measurement. Consequently some high-instantaneous velocity values will have been removed during data filtering, creating a bias towards lower mean velocities in the processed 25 Hz data. However there is still a remarkable similarity in the distribution of velocities when comparing 25 Hz and 100 Hz ADV data. Since filtering of 25 Hz data will have removed some genuine high instantaneous velocities due to their low correlations, U_{rms} values are lower than for the 100 Hz data. However, values of U_{skew} are similar when comparing each pair of runs with the same amplitude of bedform insert, regardless of whether flow was measured using the ADV recording at 100 or 25 Hz. Comparison of vertical velocities (Figures 4.10 – 4.12 compared with Figures 4.90 – 4.92) shows that $\overline{V}$ distributions are similar in general, although slightly less negative, and up to 0.05 m/s more positive. V_{rms} and V_{skew} show similar distributions and ranges for all amplitudes when comparing the 100Hz and 25 Hz datasets. For the spanwise velocity component (Figures 4.16 – 4.18 compared with Figures 4.96 – 4.98) $\overline{W}$, W_{rms} and W_{skew} values are broadly similar as are the distributions of values at both 100 Hz and 25 Hz. Comparison of TKE values (Figures 4.19 – 4.21 compared with Figures 4.99 – 4.101), shows that at 25 Hz, values are underestimated by around 25% for 0.025 m, 40% for 0.050 m and 25% for 0.075 m amplitude bedforms. Likewise for comparison of τ_R values (Figures 4.19 – 4.21 compared with Figures 4.99 – 4.101), shows that at 25 Hz, values are underestimated by around 25% for 0.025 m, 0% for 0.050 m and 25% for 0.075 m amplitude bedforms. At both 25 Hz and 100 Hz distributions of values for TKE and τ_R are similar for all amplitudes. In terms of percentage time in each quadrant (Figures 4.22 – 4.24 compared with Figures 4.102 – 4.104), distributions of values are similar although for the 100 Hz data quadrant events above the hole size occur for a larger proportion of the time. At 25 Hz, quadrant event $|u'v'|$ stresses (Figures 4.25 – 4.27 compared with Figures 4.105 – 4.107) are underestimated by between 30 and 50%. These differences are within the potential 15 – 50% underestimation for 100 Hz data and potential 30 – 60% underestimation for

25 Hz data described in Section 3.3.2. For P, R, and TI (Figures 4.28 – 4.30 compared with Figures 4.108 - 4.110), value ranges and distributions are similar at 25 Hz and 100 Hz. Overall, a comparison of the plots produced with 100 Hz ADV data with plots produced using 25 Hz ADV data, shows a very close match. This comparability exemplifies the repeatability of the flume experiments.

7.1.2 Comparison Two - Flow Over Openwork-Gravel Antidune Bedform Inserts Measured With an ADV Recording at 25 Hz Compared to Flow Over Gravel Surfaced Antidune Bedform Inserts Measured With an ADV Recording at 25 Hz

A comparison of Figures 4.31 – 4.32 with Figures 4.81 – 4.82, shows that $\overline{U}$, U_{rms} and U_{skew} values are all broadly similar for 0.025 m amplitude forms. For 0.050 m amplitude forms lower velocities are present in the trough region of 0.050 m openwork-gravel bedforms compared to solid gravel surfaced forms. Further for 0.050 m openwork-gravel bedforms values of U_{rms} are higher on the upstream facing slope compared to solid gravel surfaced forms. Compared to the solid gravel surfaced forms, openwork gravel bedforms have a larger area of the upstream facing flank with high U_{rms}, V_{rms} and W_{rms} values. For example, for U_{rms} over 0.050 m amplitude forms, high rms values occur for around 1/3 of flow depth as opposed to 1/4, and extend for 0.15 m up slope from the trough rather than 0.1 m over the openwork-gravel bedforms and gravel bedforms respectively. Values of U_{skew} remain similar over both openwork and solid bedforms. Comparison of vertical velocities (Figures 4.37 – 4.38 compared with Figures 4.90 – 4.91) again shows that $\overline{V}$ distributions are lower over the openwork-gravel forms. Over solid gravel surfaced forms, values of $\overline{V}$ are relatively evenly distributed, reaching a maximum of 0.07 m/s on the 0.050 m amplitude form. However, over openwork gravel forms, values of $\overline{V}$ are subdued at the bed on the downstream facing slope, and elevated on the upstream facing slope, reaching a maximum of 0.1 m/s on the 0.050 m amplitude form, an effect interpreted as flow entering or egressing from the bed respectively. The blocky distribution of $\overline{V}$ over 0.025 m amplitude openwork gravel forms (Figure 4.37) is attributed to the strong $\overline{W}$ (Figure 4.41) component in this

run. The distribution and ranges of V_{rms} values are similar for the 0025 m case of both forms (openwork or solid) and the 0.050 m amplitude case of both forms. An increase in values near the base of upstream facing slope can be seen for 0.050 m amplitude forms, when compared to 0.025 m amplitude forms. For the spanwise velocity component (Figures 4.41 – 4.42 compared with Figures 4.96 – 4.97) $\overline{W}$, W_{rms} values are broadly similar as are the distributions of values. The distribution and range of V_{skew} and W_{skew} magnitudes are similar for each amplitude when comparing between openwork and solid gravel bedforms.

Values of TKE (Figures 4.43 – 4.44 compared with Figures 4.99 – 4.100) are very similar, but for openwork-gravel bedforms, high values of TKE are present for around 1/4 of the flow depth on the upstream facing slope, compared to 1/5 of depth on solid forms. Values of τ_R (Figures 4.43 – 4.44 compared with Figures 4.99 – 4.100) are similar, with high values present for around 1/4 of the flow depth on the upstream facing slope of openwork forms, compared to 1/5 of depth on solid forms. Compared to the solid surfaced bedforms, over open-work gravel forms, there is a greater tendency for high τ_R values to be concentrated in the trough region. Looking at the 0.050 m amplitude forms, for openwork-gravel forms high TKE values extend for 0.2 m along the bed of the upstream facing slope, but for only 0.050 m for solid gravel surfaced forms. In terms of percentage time in each quadrant (Figures 4.45 – 4.46 compared with Figures 4.102 – 4.103), distributions of values are similar although over the openwork-gravel forms quadrant events above the hole size occur for a larger proportion of the time.

For Quadrant event $|u'v'|$ stresses (Figures 4.47 – 4.48 compared with Figures 4.105 – 4.106) , 0.025 m amplitude forms the range of mean $|u'v'|$ values are similar between solid gravel surfaced and openwork-gravel forms, however over 0.050 m amplitude forms the maximum values are around 130% higher for the openwork-gravel forms. In addition the zone of high $|u'v'|$ is thicker, reaching up to 1/3 of the flow depth on the upstream facing slope (compared to around 1/4 for solid gravel surfaced forms). These values of TKE, τ_R and Quadrants, measured with a 25 Hz ADV are subject to a potential 30 – 60% underestimation. This underestimation is due to the

limited temporal resolution of the 25 Hz ADV, and subsequent removal of high velocity data with low correlation scores, producing a bias in the filtered data. This bias is more fully discussed in Section 3.3.2.

For P, R, and TI (Figures 4.49 – 4.50 compared with Figures 4.108 – 4.109), value ranges and distributions are similar. On 0.050 m openwork-gravel forms P occurs along the whole of the upstream facing slope, rather than just the lower portion on solid gravel surfaced forms. However, there is a lower R for 0.050 m openwork-gravel forms than for the solid gravel surfaced forms, indicating a less developed boundary layer. On 0.050 m openwork-gravel forms TI occurs along a 0.25 m stretch of the bed in the trough region and is around 130% of the values for solid gravel surfaced forms, for which high values only occur along 0.1 m of bed in the trough.

7.1.3 Comparison Three - Flow Over Gravel Surfaced Antidune Bedform Inserts Measured With an ADV Recording at 25 Hz Compared to Flow Over Sand Surfaced Antidune Bedform Inserts Measured With an ADV Recording at 25 Hz

A comparison of Figures 4.51 – 4.53 with Figures 4.81 – 4.83, shows some significant differences in the distribution of $\overline{U}$ over sand and gravel surfaced forms. Maximum $\overline{U}$ values for sand are around 125% of those over gravel surfaced bedforms and minimum $\overline{U}$ values for sand are around 250% of those over gravel surfaced bedforms, indicating that for sand surfaced forms there is a much lesser degree of flow retardation in the trough region and a much lower contrast between extremes of $\overline{U}$. In the trough region of gravel surfaced forms the area of flow retardation is more extensive, covering a longer area of bed and a large proportion of the flow depth. Over sand forms, high values of U_{rms} and the lowest values of U_{skew} occur in a limited region along the bed on the upstream facing slope, elsewhere, values are relatively homogenous. The prevalence of homogenous values over large areas of the flow profile is thought to be due to the limited roughness of the sand bed surface, which allows high values of $\overline{U}$ to extend to the bed. Comparison of vertical velocities (Figures 4.60 – 4.62 compared with Figures 4.90 – 4.92) again shows some significant differences in the distribution of $\overline{V}$ over sand and gravel surfaced forms. Values of $\overline{V}$ are notably higher adjacent to the bed over sand surfaced forms, which is thought to relate to

the higher values of $\overline{U}$ near the bed, rather than any turbulence phenomena. There are significant differences in values of V_{rms} for all amplitudes of both sand and gravel surfaced forms. The higher V_{rms} values over gravel surfaced forms are interpreted as a function of the higher bed roughness. Reasons for the high V_{rms} in the upper flow profile above the downstream facing flank of the sand surfaced upstream antidune are unclear (i.e. as shown in Figures 4.61 and 4.62). The most likely explanation is that the high values are an artefact due to the significant values of $\overline{W}$ observed in this region. For the spanwise velocity component (Figures 4.66 – 4.68 compared with Figures 4.96 – 4.98) $\overline{W}$, W_{rms} values are greater in the 100 Hz case, but with broadly similar distributions of values. The lower values of U_{rms}, V_{rms} and W_{rms} over the sand surfaced forms are due to the lower roughness of the sand bed creating less turbulence and having less of an effect on retarding the flow in the bed-trough region.

Values of TKE (Figures 4.69 – 4.71 compared with Figures 4.99 – 4.101) are much lower over sand surfaced forms compared to gravel surfaced forms – with values just 10% for 0.025 m, 20% for 0.050 m and 10% for 0.075 m amplitude bedforms. Values of τ_R (Figures 4.69 – 4.71 compared with Figures 4.99 – 4.101) are again much lower over sand surfaced forms compared to gravel surfaced forms – with values just 6% for 0.025 m, 12% for 0.050 m and 4% for 0.075 m amplitude bedforms. For both TKE and τ_R, distributions are similar, although for sand forms there is less of an intensity of TKE and τ_R in the trough, with values being more spread out up the upstream facing antidune bedform slope. In terms of percentage time in each quadrant (Figures 4.72 – 4.74 compared with Figures 4.102 – 4.104), distributions of values are similar although over the sand surfaced forms quadrant events above the hole size occur for a smaller proportion of the time..

Quadrant event $|u'v'|$ stresses (Figures 4.75 – 4.77 compared with Figures 4.105 – 4.107) show that for 0.025 m bedforms ejection/sweep values are only 10% of those over gravel surfaced forms. For 0.050 m bedforms ejection/sweep values are only 20/25% of those over gravel surfaced forms, and for 0.075 m bedforms ejection/sweep values are only 10% of those over gravel surfaced forms. Given that Comparison One

(Section 7.1.1) showed that the 25 Hz ADV data underestimate $|u'v'|$ stresses by between 30 and 50%, the actual reduction is likely to be even more significant. Additionally, the near bed zone of high $|u'v'|$ stresses is much slimmer (around 20% to 25% of total flow depth for sand surfaced forms, compared to up to 33% over the solid gravel surfaced forms).

For P, R, and TI (Figure 4.78 – 4.80 compared with Figures 4.108 – 4.110), value ranges and distributions are generally similar. However, for the sand surfaced bedforms values of TI drop to only 20%, 20% and 10% (0.025, 0.050 and 0.075 m amplitudes respectively) of those for gravel surface bedforms.

7.1.4 Synthesis of Turbulence Investigations by ADV

Over fixed sand dune bedforms, Bennett and Best (1995) found the highest values of rms occurred in the lee of each dune, specifically the separation zone and in particular along the top of the separation zone and at the reattachment point. For antidunes, the rms values are similarly highest in the lee of each bedform, (i.e. in Figure 4.3 and Figure 4.12), although there is no separation zone, these high rms values occur along the bed and are associated with the areas of retarded flow in the lower trough region. Likewise, Bennett and Best (1995), found negative U_{skew} and V_{skew} values along the bed over dune bedforms, with the most negative values in the trough area, and the degree of skew reducing towards the downstream dune crest. A similar distribution of U_{skew} and V_{skew} values near the bed for antidunes has been found in this thesis. McLean *et al*. (1994) noted that the wake region present downstream of dunes, had positive values of U_{skew} and negative values of V_{skew}. A similar change towards less negative values of U_{skew} and more negative values of V_{skew} can be seen on the downstream facing flank of antidunes (Figures 4.1 – 4.3), which is perhaps a limited bedform wake effect.

From Quadrant Analysis of ADV data it appears that there is a degree of spatial structure to the turbulence flow field above the fixed antidunes in this thesis, including the presence of ejections (Q2 events). This is particularly pronounced for gravel surfaced forms, but much less pronounced for sand surfaced forms. Given that suspended sediment load will dominate

any localised contributions from turbulent ejections over real antidunes formed in sand, the suggestion of Jackson (1976), (see Section 2.3.2) that for antidunes in fine sands the ejection cycle is 'unlikely to be recognisable or relevant' holds. Gravel surfaced fixed antidunes in slightly deeper flows (such as in this thesis) appear to have a more stable spatial flow structure with more well developed turbulence phenomena. This more detailed flow structure lends support to the supposition of Saunderson and Lockett (1983) that transitional antidune forms, especially in coarser bed materials have a fully developed turbulence spatial structure.

The results of ADV investigations indicate that as for dunes, the highest TI values over antidune bedforms are found in the trough region, where flow is most retarded compared to velocities elsewhere over antidune forms. Nelson *et al*. (1993) and Venditti and Bauer (2005) found, for sand dunes (fixed in the flume and in the field respectively) that the highest values of TKE were concentrated in the separation zone region downstream of dune crests, the values being greatest with stronger flow separation. The same distribution was observed for τ_R values by Nelson *et al*. (1993); McLean *et al*. (1994); Bennett and Best (1995) and Venditti and Bauer (2005). Venditti and Bauer (2005) found the lowest TKE values (6-10 m^2s^2) occurred at the bed on the stoss and crest slope, the highest values (up to 23 m^2s^2) occurred over the downstream flow separation cell. For an undulating sand surfaced bed with supercritical flow, Chanson (2000) observed the bed shear stresses to be 10% greater in the trough region compared to the crest. Measurements from this thesis indicate values of between 0.1 and 1.2 m^2s^2 (highest values in the trough region) for sand surfaced bedforms and between 2 and 11 m^2s^2 (highest values in the trough region) for gravel surfaced bedforms.

In terms of R, the values obtained appear on the low side compared to the values of 0.3 – 0.5 obtained by Hinze (1975), McLean *et al*. (1994) and Best and Kostachuk (2002) perhaps indicating issues with insufficient flume length between the flume inlet and ADV measurement location to allow flow establishment.

It appears that the instantaneous flow measurements and turbulence statistics are broadly comparable over the solid gravel surfaced forms at 100 Hz and 25 Hz, and also the openwork-gravel at 25 Hz, however instantaneous flow measurements and turbulence statistics are much lower

over sand surfaced antidunes. For these sand-surfaced antidune forms, the limited resistance at the bed and the tight in-phase nature of bed and surface water waves, mean that high velocities are present close to the bed (i.e. compare values of $\overline{U}$ for sand surfaced forms in Figures 4.51 – 4.53 with gravel surfaced in Figures 4.81 – 4.83). It is thought that the lower bed roughness is responsible for the lower values of turbulence statistics over sand forms.

TKE and τ_R values are higher over gravel because the rougher surface provides both exposed clasts for eddy development, and a thicker zone of retarded near-bed flow, where turbulence can develop without being rapidly advected downstream. In terms of Quadrant Analysis, the results indicate that there appears to be no bias towards either ejections or sweeps, which Nelson *et al*. (1995) interpreted as an indication of no flow separation. This supports the observations herein of a zone of retarded flow with no flow separation. Interpretation of the Quadrant Analysis results indicates that the majority of $|u'v'|$ stresses occur during the rarer short-duration quasi-periodical quadrant events above the hole size threshold. It is likely that these are key events in the transport of sediment in antidune regime flow.

These detailed turbulence investigations have confirmed that in antidune regime flow, near-wall production of turbulence in the trough region is the main source of turbulence production over antidune bedforms. The ejection-sweep events are intermittent and quasi-periodic (as noted previously by Grass, 1971 Grass, 1982 and Grass and Mansour-Tehrani, 1996), and are associated with incursions of high velocity flow into a region of retarded flow in the trough region. Turbulence statistics are subdued in the upper flow profile, which is dominated by the high velocity bulk flow. In the upper flow profile there is a much lower longitudinal variation in $\overline{U}$ compared to the near-bed region.

Robinson (1991) defined a coherent structure as a: "*three dimensional region of the flow over which at least one fundamental flow variable exhibits significant correlation with itself or with another variable over a range of space and/or time that is significantly larger than the smallest scales of the flow*". On this basis, the detailed turbulence investigations presented within this thesis have quantified and clarified the spatial distribution of turbulence

over antidune bedforms. Turbulence statistics have been mapped in detail to show the coherent nature of the turbulence field throughout the flow profile. However, there appear to be significant differences between the turbulence environment over sand surfaced antidune bedforms, and the environment occurring over gravel versions. Over sand, the degree of flow retardation in the trough region and the intensity and duration of turbulent events are more limited. Given that turbulence is produced in the region of sharp velocity gradient at the bed (Nelson, *et al*. 1995); the differences in turbulence signatures are thought to primarily relate to the greater magnitude of turbulence production over rougher gravel beds compared to sand beds. No evidence of flow separation was found in these fixed bed experiments, however it should be noted that flow over the amplitudes investigated did not approach breaking point. More detailed investigation of antidune bedforms near breaking may yield data on intermittent flow separation before standing wave breaking, as was observed by Alexander *et al*. (2001). Figure 7.1 shows a synthesis of information gathered by ADV on the spatial structure of turbulence over fixed antidune bedforms. Based on these observations the conceptual model has been extended to show how the flow characteristics observed using an ADV could influence the critical case (0.100m amplitude for the fixed bedform λ used here) where the standing wave becomes unstable.

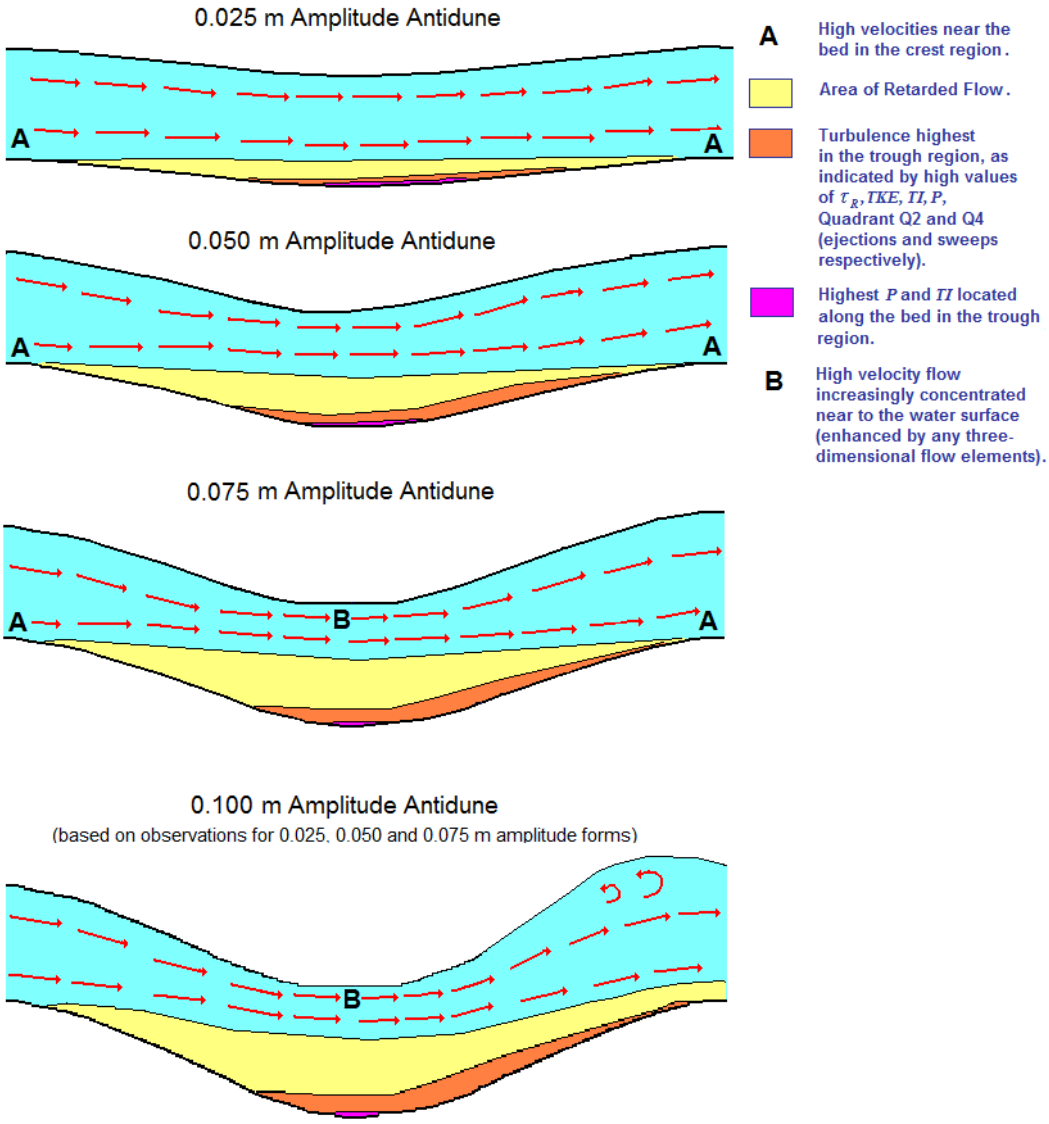

Figure 7.1 Synthesis of Turbulence Investigations Using ADV

The top three diagrams show the flow structure over 0.025, 0.050 and 0.075 m amplitude bedforms based on the ADV data presented in Section 4. The bottom diagram for the 0.100 m amplitude bedform is a supposition (based on the three examined amplitudes) of the flow state at the point where the standing wave breaks. The red arrows indicating the key flow paths are based on areas in the flow profile shown to have consistently high $\overline{U}$ however, it should be noted that in reality these are complex three dimensional flows. A zone of retarded flow develops in the trough region and increases in size as the antidune amplitude increases. The highest P and TI occur in a narrow zone along the bed at the base of the trough. High values of rms, TI and Quadrants 2 and 4 (ejections and sweeps) occur in a wider area adjacent to the bed, but extending up the upstream facing face of the downstream antidune. The size of the zone of retarded flow, and the magnitude of these turbulence parameters was observed to increase as bedform amplitude increased. Thus, it is thought that as the antidune's amplitude increases further towards the standing wave's breaking point, the size of the zone of retarded flow and the values of these variables further increase. If the zone of retarded flow extended to the

crest, then it may aid the separation of the flow from the bed at the antidunes crest, and hence contribute to collapse of the standing wave. At this critical point the standing wave becomes unstable, and collapses causing the partial or whole destruction of the antidune beneath (N.B. this diagram is for UMAs).

7.2 Bulk Flow Structure and Turbulence over Antidune Bedforms - Flow Visualisation Investigations

Over the fixed gravel antidunes, a general conceptual flow model can be produced, whereby:

1. High-speed flow (1.4 m/s) occurs through the upper 95% of the flow profile on the downslope of the upstream antidune flank. There appears to be an area of retarded flow in the trough region (indicated by shorter streak lengths). The high-speed flow flowing down the downslope appears to flow above the area of retarded flow; however occasional longer streak lengths occur in the trough region. This phenomenon may represent the incursion of high speed flow into the trough;
2. Upon reaching the trough, the flow remains bed-parallel, becoming horizontal. The vertical extent of high-velocity flow is reduced (it is thought the velocity increases slightly to ensure flow continuity), due to an increasing thickness of retarded flow (0.35 m/s) near the bed in the trough; increasing from 13% through 19% to 25% of flow depth from 0.025 m antidunes through to 0.075 m antidunes;
3. Flow trajectories near the bed in the trough between antidunes are less regular, being represented by shorter streak lengths with more varied and not always flow parallel streaks, compared to longer and flow parallel streaks in the upper flow profile. Further, regular ejections of flow occur, away from the bed into the flow towards the upslope of the downstream antidune. These ejections can be seen in Figure 5.5b – panels 3, 4 and 5; and figure 5.6b – panels 4, 5 and 6. These streaks are interpreted as representing turbulent ejections; they occur intermittently, with streaks beginning at the bed, and moving upward into the flow at angles of 30˚ to bed-parallel. The streaks merge with the bed-parallel flow as they leave the zone of retarded flow in the lower flow profile;

4. The occurrence of ejections of flow from near the bed continue up the upslope flank of the antidune, in 0.025 m amplitude antidunes persisting towards the crest, whereas for 0.075 m amplitude antidunes the behaviour stops approximately half way along the upslope, with high-speed (1.4 m/s) flow occurring very close to the bed;
5. At the crest, high-speed flow is again present near the bed.

The ejection motion of streaks noted here appears comparable to the flow-ejections identified by Garcia *et al.* (1996) as being responsible for particle entrainment into suspension. The temporal motion of particle trajectories during ejections in Figure 5.5b, panels 2 and 5 and Figure 5.6b, panels 4 to 6 matches the observed motions in the experiment of Garcia and colleagues wherein they observed that *"as a consequence of momentum transfer from the flow to the particle, velocity tends to increase as the particle is lifted away from the channel bottom and gets accelerated as it is being dragged by fluid of increasing momentum"*. This description fits well with the motion of particles seen in these panels. The comparatively rapid vertical transition from low near-bed streamwise velocity to higher streamwise velocities immediately above the antidune crests, in contrast to the more gradual vertical transition through the flow profile above the trough, seen in these experiments is similar to that measured by Nelson *et al.* (1993) and Best and Kostachuk (2002) for fixed, low angle, two-dimensional bedforms (without slip-faces or leeside separation) at lower velocity (0.21 m/s) flows. Further, the observed 'ejection' motions of the neutrally buoyant tracking particle trajectories occur between the trough and the mid-upslope of the downstream antidune, in the same region (trough up to mid-lee slope) as for these low-angle dunes, adjacent to the re-attachment point.

Synthesising this information for gravel antidunes (Figure 5.10 – 5.12) several key trends can be seen:

1. Higher velocities (up to 1.4 m/s) are present throughout the flow-profile on the downstream flank of the antidunes (where the flow is accelerating);

2. Velocities in the troughs drop as low as 0.4 m/s compared to velocities generally nearer 1.4 m/s higher up in the flow profile. This area of low velocity flow in the trough is around 0.2 m in length and occupies the bottom 10% of the flow profile;
3. An area (0.1 m long, occupying the bottom 20 – 30% of the flow profile) of high-velocity flow (1.4 m/s) occurs immediately above the bed downstream of the trough, on the upslope of the next antidune;
4. Through the sequence of 0.025 m, 0.050 m and 0.075 m antidunes, higher velocity flow is present increasingly close to the bed at the crest of the antidune; and
5. Inferred speeds from tracked particles vary rapidly over small distances through the flow profile.

These key points are developed into the conceptual model illustrated in Figure 7.2. Based on these observations with a high-speed camera, the conceptual model has been extended to show how the flow characteristics observed influence the critical case (0.100m amplitude for the bedform λ used here) where the standing wave becomes unstable.

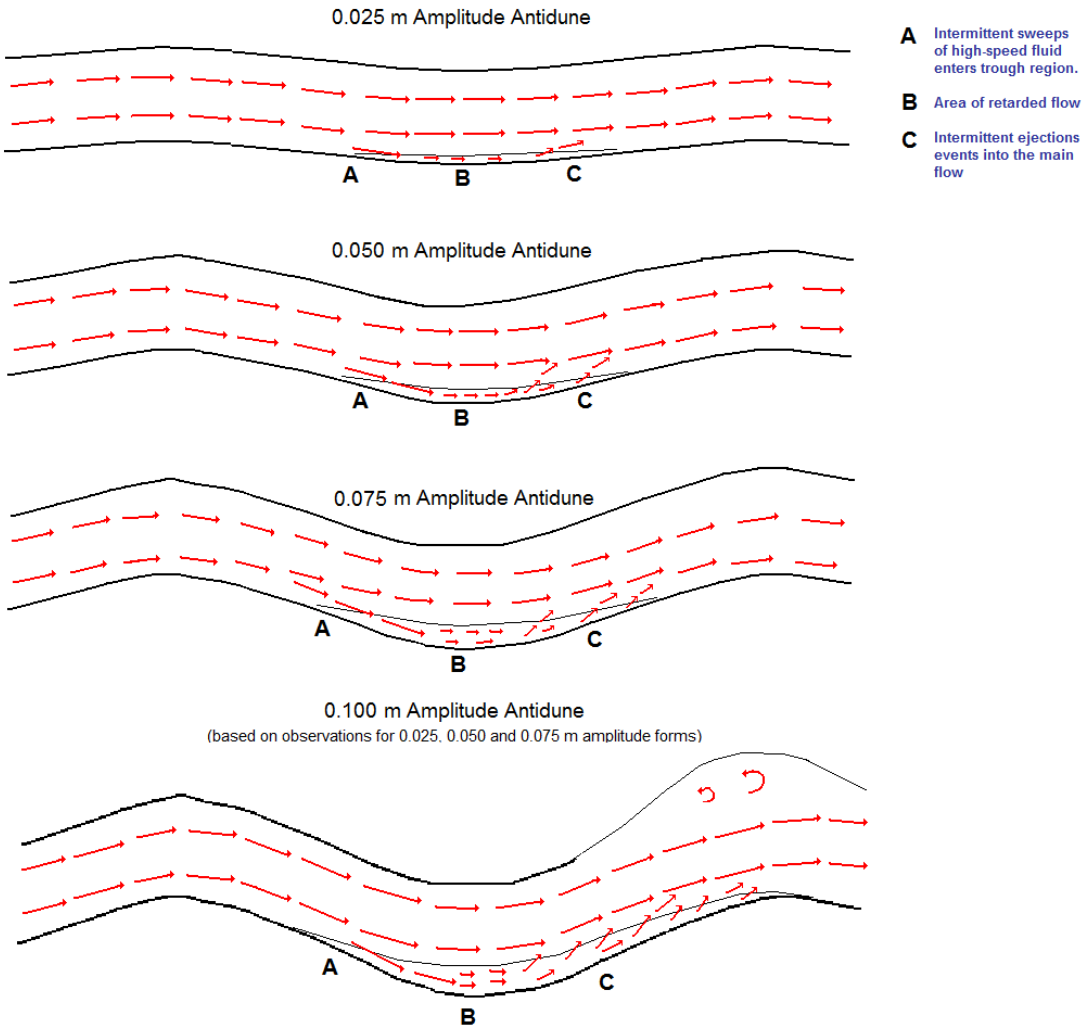

Figure 7.2 Conceptual Model of Flow Structure in Antidune Phase Flow

The top three diagrams show the flow structure over 0.025, 0.050 and 0.075 m amplitude bedforms based on the high-speed camera data presented in Section 5. The bottom diagram for the 0.100 m amplitude bedform is a supposition (based on the three examined amplitudes) of the flow state at the point where the standing wave breaks. Flow visualisation experiments over 0.025, 0.50 and 0.075m amplitude antidune bedforms show particle streaks with trajectories that are generally bed parallel. Within the trough region streaks are less common, shorter and their vectors more variable. Occasional relatively high-velocity streaks can be seen entering the trough region (sweeps) and relatively high-velocity streaks leaving the trough region (ejections). The intensity of these sweeps and ejections was observed to increase as bedform amplitude increases. It is thought that as the antidune's amplitude increases, the intensity of turbulence in the trough region further increases, excavating deeper into the trough and transporting more sediment downstream onto the upstream facing flank of the adjacent antidune. At a critical point where the standing wave becomes unstable, it collapses causing the partial or whole destruction of the antidune beneath (N.B. this diagram is for UMAs).

Sand antidunes (Figures 5.13 – 5.15) show similar features to those for gravel antidunes. However, it is more difficult to interpret the 'sand' images as the streak lengths are longer and less well exposed due to higher flow velocities over the sand surfaced antidune forms; however, ADV data helps support interpretations made from the streak data. Only limited data have been captured from the processing of images which contributed to the data presented in Figure 5.13 (0.025 m sand surface fixed antidune), making interpretation difficult. However for Figure 5.14 some interpretation is possible, at the crests higher velocity flow ('**2**') is present closer to the bed. An area of low-velocity is indicated in the trough between antidune crests ('**3**'), followed, possibly, by an area of higher velocity immediately downstream ('**4**'), located on the upslope face of the next antidune. Unfortunately, insufficient particles were tracked immediately above the bed on the downslope of the antidune in the left of the figure ('**5**'). For Figure 5.15, interpretation is again difficult, with limited data being captured for key areas of the flow slice. High-velocity flow further away from the bed and immediately above the crests can be seen. From the available data, it appears that the broad pattern of flow observed over sand antidunes is similar to that for gravel antidunes but levels of turbulence are much lower. It appears that with sand antidunes, the lower bed friction and presence of higher velocity flow close to the bed limits the extent to which an area of low velocity flow can develop in the trough between antidunes.

The particle tracking method used in this experiment appears to have been less successful at recording and/or identifying large quantities of particles with which to estimate the velocity distribution over the sand surfaced forms. It is thought this reflects the higher velocities experienced over these forms, particles moved further during each individual frame of the high-speed video recording and were less exposed. A faster frame speed was not possible due to limitations of data rates and writing to computer memory, in addition it would require more intense lighting to ensure adequate exposure during the shorter frame times.

7.3 Mobile Bed Experiments

7.3.1 Run 1 - Interpretation of Peel 2

The set in Peel 2 between 0.04 and 0.1 m from the flume base was observed to form during antidune activity during flume-bed aggradation as detailed in Section 6.2.1 and Plate 6.1. It is thought the sand-rich zone above the set's erosional base formed due to the infusing of sand into the gravel bed exposed upstream of the migrating antidune. This sand-rich zone having been subsequently buried by the upstream prograding antidune. The low-angle upstream-dipping laminae '**ud**' formed on the upstream side of the antidune under the non-breaking standing wave shown in the centre of the individual frames in Plate 6.1. The mechanism that formed these could not always be observed directly from the flume wall; however low amplitude bedwaves (see Plate 6.9) and sediment ejection events (Figure 6.11) were observed alongside momentary fluctuation of the standing wave up and downstream. The variation in sand content within the laminae is interpreted as a function of their speed of deposition: sand-rich upstream-dipping laminae match temporally with the initial lower amplitude standing wave and the later gravel-rich upstream-dipping laminae match with a higher amplitude standing wave. The growing antidune may increasingly capture coarser gravel clasts as velocity progressively reduces, and the slope steepens. The downstream dipping erosional surface '**ds**' is interpreted as being produced by the progressive upstream movement of the trough immediately downstream of this antidune. The concave-upward downstream-dipping wedge of coarser sediment '**dd**' is interpreted as being produced by the near-collapse of the standing wave above the antidune indicated in Plate 6.1, Section 6.2.1. The gradational transition '**gt**' between antidune and USPB sets was then produced as the bed aggraded through the transition between the waning standing wave and USPB conditions.

7.3.2 Run 1 - Interpretation of Peel 4

The smaller thickness of the antidune set in Peel 4 compared to Peel 2 is due to the more limited antidune activity seen here, which produced only limited low-angle upstream-dipping laminae. The predominantly sand rich set ('**sr**') is thought to indicate slower bed aggradation at this location, giving

more time for sand to infiltrate the gravel bed. The gradual flattening of the angle of each upstream dipping laminae seen in Peel 4 represents the relatively low-energy transition to USPB and accounts for the degree of antidune sedimentary structures preserved.

7.3.3 Run 1 - Comparison of Peels 2 and 4 with the Literature

Symmetrical low-angle upstream-dipping concave-upwards laminae ('**7**' in Figure 2.18) have been previously interpreted as the typical stratigraphy of UMAs by Middleton (1965), Harms and Fahnestock (1965), Panin and Panin (1967), Hand *et al*. (1969), Barwis and Hayes (1985) – '*low-inclination upflow dipping cross laminae'*, Yokokawa *et al*. (2000) and Alexander *et al.* 2001), and the lenticular bedsets of Duller *et al*. (in press). As found here, Yokokawa *et al*. (2000) and Alexander *et al*. (2001) observed that internally some of the sets are structureless. The concentration of finer sediment in the troughs and erosional bases below laminae, as in Peels 2 and 4, has been previously noted by Yokokawa *et al*. (2000) and Alexander *et al*. (2001). There are two key differences between the deposits examined in this thesis and those examined previously. Firstly, the rapid aggradation rate (12.9 mm/minute) in this run compared to the lower rates used by previous researchers is thought to be responsible for the relatively steep (up to 15°) angle of upstream dip of the deposits in Figure 6.12. For example, Alexander et al. (2001) used rates of 0 mm/minute (non-aggrading runs) and 0.6 mm/minute (aggradational runs), whilst Kennedy (1961) and Middleton (1965) used a recirculating flume with no net aggradation. Secondly, antidunes were present for a single period before the bed reverted to USPB; whilst during this period upstream bedform migration occurred, no truncation of antidune deposits by further cycles of antidune activity occurred. These two factors are thought to be responsible for the differences in appearance when comparing the appearance of the antidune laminae in Figure 6.12 herein with those of Alexander *et al*. (2001) and Yokokawa *et al*. (2000) which are shown in Figures 2.18 and 2.19 respectively. In these two studies multiple cycles of antidune activity produced superimposed and truncated sets of antidune deposits. The downstream dipping laminae found in the peels of Middleton (1965) and Alexander *et al*. (2001) were also observed in

the peels taken from Run 1 deposits. Located downstream and superimposed on lenticular sets of upstream dipping laminae (i.e. in Figure 6.12). It is unclear whether these formed in response to the standing wave breaking or due to a temporary downstream shift in the location of the standing wave above the antidune bedform during deposition. The antidune that produced the deposits in Figure 6.12 had a wavelength of approximately 0.4 m and amplitude of 0.05 m; whilst internally laminae were approximately 0.2 m in length and 0.01 m thick. This gives a laminae length to bedform length ratio of 0.5, in agreement with the findings of Barwis and Hayes (1985), Langford and Bracken (1987) and Alexander *et al*. (2001). The ratio of set thickness to formative antidune amplitude is approximately 0.9, markedly higher than the value of 0.4 observed by Alexander *et al*. (2001). This difference between these ratios is attributed to the much higher sediment feed rate and the favourable preservation of the sets in Figure 6.12, since these occurred at the end of the period of antidune activity, and were not destroyed during the smooth transition to USPB.

The angle of clast dip identified for gravel clasts in Section 6 is in accordance with previous studies but tends towards the steeper end. Hand *et al*. (1969) observed a steepening trend for backset dip in coarsening sands perhaps accounting for the higher angle of dip of these structures in fine gravel. The layout of the internal strata of the antidune sets presented matches the descriptions given in Cheel (1990), as they are analogous to his *"antidune backset cross-laminae"* (see Figure 2.20). However, Cheel's figure is a characterisation, based on literature of the expected sedimentary structures for USPB in fine sand, rather than direct interpretation of experimentally produced facies. The style of antidune set and internal structure in Peel 2 resembles the deposits examined by Blair (1999) shown in Figure 2.19. The relatively high angle of upstream dip seen in Blair's deposits may be related to the rapid sedimentation rate in these deposits which formed during a flash flood on a desert outwash fan. For example the backsets examined by Blair dipped upstream at 8˚ – 22˚, which further agrees with the dips observed in Peel 2, Run 1. Examination of the imbrication of clasts indicates it to be consistent throughout each antidune as proposed by Yagishita and Taira (1989) thus, the consistent imbrication style

as an indicator of unidirectional flow is a diagnostic criterion for deposits with an antidune origin.

The wedge of sediment ('**dd**') is interpreted as the product of standing wave collapse/dissipation and scour, causing some levelling and filling of the bed; similar deposits were observed by Alexander *et al*. (2001) as downstream dipping foresets formed by '*migration of asymmetrical bedwaves after wave breaking'* and *'poorly defined'* or '*trough fill'* (Yokokawa *et al.,* 2000 and Langford and Bracken,1987) – termed *'concave upward subhorizontal bed of washout phase'*; whilst, Blair (1999) noted similar wedges of sediment (see Figure 2.19). Yokokawa *et al*. (2000) and Alexander *et al*. (2001) attribute the formation of the '**ud**' laminae to low-amplitude bedforms or unsteady movement of the standing wave. Alternatively, the features observed here may be the granule analogues of the low-amplitude bedwaves observed by Hand (1974), McBride *et al*. (1975), Cheel (1990) and Alexander *et al*. (2001) in sand beds. The difference in appearance of the antidune sets presented here compared to those of Alexander *et al*. (2001) is thought to relate to the number of superpositioned stacks of packets of antidune laminae in Alexander *et al*.'s peels due to the more continuous and prolonged antidune activity in their flume runs. In contrast, the sedimentary structures presented herein are a product of relatively short isolated periods of intervening antidune activity during rapid bed aggradation occurring between periods of USPB deposition.

7.3.4 Run 1 - Interpretation of Peels 1 and 3

The total depth of the antidune sets in Peels 1 and 3 are consistent with the time period (between 1 to 6 minutes) during which antidunes were observed during the flume run. The erosional base to the antidune sets indicates that scour was deepest in the centre of the flume (where rooster tails were highest – see Plate 6.1). The internal structures present within the wedges in Peel 3 are interpreted as representing upstream-dipping laminae, cut through transversely. No video footage was recorded during this run, but during Run 2 a similar process occurred (between 5 and 6 minutes) and is shown in Figure 6.8. A concentration of larger coarse clasts silicon carbide granules (lower-right of Figure 6.14) is present in what was the trough region.

These clasts and heavy mineral granules represent a lag deposit, formed by the removal of more easily transported particles by sediment transport.

7.3.5 Run 1 - Comparison of Peels 1 and 3 with the Literature

To the author's knowledge the only other example of flow transverse peels taken from sedimentary deposits produced by observed in-flume antidunes was that of Alexander *et al*. (2001). In comparison, Peels 1 and 3 in this thesis show a more pronounced cross-flume variation, with the trough region clearly having cut down more deeply into the bed in the centre of the flume. This supports observations during the run, where the standing wave was three-dimensional (being clearly taller in the centre of the flume) and observations in the ADV data of a notable lateral flow component (i.e. Figures 4.16 to 4.18). The use of a longer, wider flume to reduce side-wall effects and any inlet effects would likely reduce these artefacts in these peels. The deposits show no sub-parallel horizontal laminae, as found by Alexander *et al*. (2001) since Peels 1 and 3 were located in the trough region between two antidunes. As the antidunes in this run were only present for a limited period before the bed reverted to USPB, stacked sets of antidune laminae (as shown in the flow transverse peels in Alexander *et al*., 2001) are not found in these peels.

7.3.6 Run 2 - Interpretation of Peels

The sloping part of the erosional surfaces ('**es**') within the first antidune set are interpreted as translational strata (Figure 2.24) formed by the migration of antidunes upstream, over an aggrading bed, the level boundary surface which they grade into is interpreted as the product of the final antidune collapse shown between 231 s and 279 s in Figure 6.6 - 6.7 and Plate 6.3 – 6.4, all of the lower antidune deposits in Peel 2 (Figure 6.17) thus relate to this last antidune-SW set, rather than the initial SWs shown in Figures 6.5 - 6.9. The upstream facing flank of the antidunes ('**ud**') is not clear due to the depositional environment on the upstream flank, which could not produce observable grain segregation. The collapse of the standing waves above the first set of observed antidunes (between 167 s and 226 s in Plate 6.3 and Figure 6.6) appears to have destroyed a proportion of the antidune stratigraphy deposited at the very start of Run 2. The levelling of

the translational strata was produced when the growth and migration of surface waves subsided (between 264 s and 279 s in Plate 6.4 and Figure 6.7). This levelling gradually reduced antidune amplitude and angle of climb, before the bed regime transformed gradually into USPB regime. This gradual transition allowed the preservation of antidune sedimentary structures. The concentration of larger clasts in the translational strata may have been produced as smaller, lighter clasts were preferentially entrained as the trough progressively moved upstream. The upstream dipping structures ('**ud**') and imbricated gravel clasts in this set are thought to represent the laminae of the UMAs. Whilst superficially similar to Peel 2 of Run 1; the upstream-dipping gravel clasts identified as marking laminae dip at an angle steeper than the upstream dip of the laminae evident in Run 1.

7.3.7 Run 1 and 2 - USPB

The USPBs are interpreted as having formed by the migration of low-amplitude bedwaves (as observed during Run 1 and Run 2 and shown in Plate 6.9) beneath in-phase water surface waves similar to those observed by McBride *et al*. (1975). However there are notable differences, whilst being in-phase the waves are asymmetric and primarily comprise the coarser fraction of the sediment fed into the flume (McBride's bedwaves were composed of the *finer* fraction of the sediment mix). This observation is interpreted as representing the relative availability of coarser sediment in the flume runs carried out here, with sand filling pores in the bed surface in advance of each bedwaves migration downstream. At less than a centimetre tall the migrating bedwaves did not produce foresets.

7.3.8 Run 2 – Interpretation of Peels

The antidune set from the second period of antidune activity contains two different sections of deposition: firstly, the sediments produced between 0 s and 82 s in Figures 6.8 – 6.9 and Plates 6.5 – 6.6 where large antidunes and standing waves formed and broke violently; secondly, the sediments produced between 82s and 171s in Figures 6.9– 6.10 and Plates 6.6 – 6.7 where antidunes and standing waves formed, but rapidly migrated upstream. The bipartite laminae identified '**bl**' were deposited by this second behaviour

of antidunes, the rapid upstream migration of antidunes on an aggrading bed with increased sediment supply (see Table 3.12). The two contrasting styles of sedimentation evident in this set were produced by two periods of antidune activity where differing behaviour of the observed antidunes occurred due to differences in the flow conditions (see Figure 6.3).

7.3.9 Run 2 - Comparison of Peels with the Literature

During this run the aggradation rate (approximately 8.8 mm/minute) was particularly rapid compared to the aggradation rates during experiments by previous researchers (see Section 7.3.2). Whilst antidune activity was more extensive, the two periods of antidune activity were separated by a period of USPB, and the characteristics of deposits formed during each period were quite different. The rapid bed aggradation rate is thought to be responsible for the relatively steep (up to 15°) angle of upstream dip of the deposits in the lower part of Figure 6.17. Secondly, as for Run 1, the antidunes here were present for a short period before the bed reverted to USPB. Whilst upstream bedform migration occurred during this period, no truncation of antidune deposits appears to have occurred due to standing wave collapse, and also since the reversion of the bed to USPB meant antidune deposits were not subsequently reworked by further cycles of antidune activity. The period of upstream migration was however much longer hence the preservation of more laterally extensive sets, with longer erosional bases ('**es**'). These two factors are thought to be responsible for the differences in appearance when comparing the appearance of the antidune laminae in Figure 6.17 herein with those of Alexander *et al*. (2001) and Yokokawa *et al*. (2000) which are shown in Figures 2.18 and 2.19 respectively. The downstream dipping laminae found in the peels of Middleton (1965) and Alexander *et al*. (2001) were not however observed in the peels taken from Run 2 deposits. Since downstream dipping laminae were present in the deposits produced during Run 1 it is not clear why they are not present in the deposits from Run 2. It is though thought most likely that the upstream migration of the three sets of antidune laminae shown in the lower portions of Figure 6.17 is responsible for the removal of any downstream dipping deposits that may have formed during bed aggradation during antidune growth and migration. As in Run 1, the antidune deposits in

Run 2 (Figure 6.17) have a wavelength of approximately 0.4 m and amplitude of 0.05 m; internally laminae are approximately 0.2 m in length and 0.01 m thick. This gives a laminae length to bedform length ratio of 0.5, in agreement with the findings of Barwis and Hayes (1985), Langford and Bracken (1987) and Alexander *et al*. (2001). As for Run 1, in Run 2 the ratio of set thickness to formative antidune amplitude is approximately 0.9, markedly higher than the value of 0.4 observed by Alexander *et al*. (2001). As for Run 1 this is attributed to the relatively smooth transition from antidunes to USPB. .

The erosional surfaces '**es**', are synonymous with the translational strata (Table 2.8 and Figures 2.23 – 2.24) identified by Clifton (1990). Similar translational strata (to '**es**') were termed Type I laminae by Clifton (1990), with rarer, fainter internal structures termed Type II laminae. The fainter bedding ('**ud**' and '**is**') observed in the first set of antidune strata matches these Type II strata, and are similar to the lenticular bedsets observed by Duller *et al*. (in press). Similar high angles of upflow a-b dip were noted for upstream dipping cross-sets by Yagishita and Taira (1989), Alexander and Fielding (1997) and Blair (1999). Dips of 20˚ to 30˚ were identified by Yagishita and Taira (1989) on antidunes with flanks sloping at 6-8˚, whilst Blair (1999) observed clasts with a-b angles dipping upstream at around 22˚ for sheetflood antidune deposits. The consistent angle of dip was also observed by Yagishita and Taira (1989) who noted its potential use as a diagnostic criterion for deposits of antidune origin.

The USPB sets presented here resemble those presented by McBride *et al*. (1975) – his figure 3. They are unlike deposits produced by antidunes, because they irregularly alternate between '**sr**' and '**sp**' and are parallel to the flume bed; the couplets ('**bl**') produced by antidune flow consisting of regular alternating sand and gravel rich layers which are inclined downstream.

The downstream-dipping bipartite laminae - couplets ('**bl**') located in the upper part of the peels in figure 6.16 and 6.17 formed after the sediment feed rate was increased from 0.8 kg/s to 1.1 kg/s. These deposits appear similar to the deposits detailed for sheetfloods with violently breaking standing waves by Blair (1999). Figure 2.23 show how Blair's couplets formed by rapid re-deposition of sediment in the antidune after standing-

wave breaking, similar deposits are shown by Clifton (1990). These downstream dipping ('**bl**') deposits coarsen upwards (inverse grading) as was observed for stable antidunes by Clifton (1990). However, in the case of these deposits formed in Run 2, breaking standing waves were not observed to produce these forms, instead rapidly upstream migrating bed and surface perturbations were seen. These bedforms may then be a new type of structure produced by sediment sorting associated with the rapid upstream migration of a low amplitude bedform on an aggrading bed. Whilst similar to the deposits described by McBride *et al*. (1974), the deposits produced by these researchers were produced by downstream migrating bedforms (in different runs by in phase bed and surface waves and by out of phase bed and surface waves). It is thought that the deposits that formed during Run 2 represent the upstream migrating case in a continuum of bedform morphologies. The similarity with the deposits of McBride *et al*. (1974) is further supported by the feed rate of 2 to 4 mm/minute used by these researchers, which approaches the rate used here. The couplet deposits described by Blair (1999) did though dip downstream at 3˚ as for the couplets ('**bl**') identified here. The division into sand rich and gravel rich is thought to be analogous to the sand-gravel couplets described by Blair (1999); with the shallow flow in this experiment accounting for the lesser degree of sorting into couplets. The bedding marked by the couplets '**bl**', is synonymous with the translational strata (Table 2.8 and Figures 2.23 – 2.24) identified by Clifton (1990).

Whilst having many similarities (as discussed above) to examples in the literature the deposits found here do appear substantially different to the deposits found in sand, such as by Barwis and Hayes (1985), Langford and Bracken (1987) and Alexander *et al*. (2001). Since the majority of previous flume studies of antidune bedding structures considered sand, it is perhaps not surprising that the majority of field examples of putative antidune bedding are examples from sandy environments. Thus potential antidune structures in gravel may have been overlooked. Direct comparisons of antidune regime flow and the resulting deposits here have elucidated the types of antidune sedimentary structure in gravel and the potential origin of the grain segregation responsible. It is clear that both upstream and downstream dipping strata can be produced by antidunes in gravel, in a similar manner to

the upstream and downstream dipping laminae often reported in the literature for sand beds.

7.3.10 Synthesis of Labile Bed Antidune Sedimentology

Based on the sediment transport observations in Section 6, a model (Figure 7.3) can be developed, illustrating the changing nature of sediment transport over antidunes as they grow and are ultimately partially or totally washed out by collapse of the standing wave above the bedform.

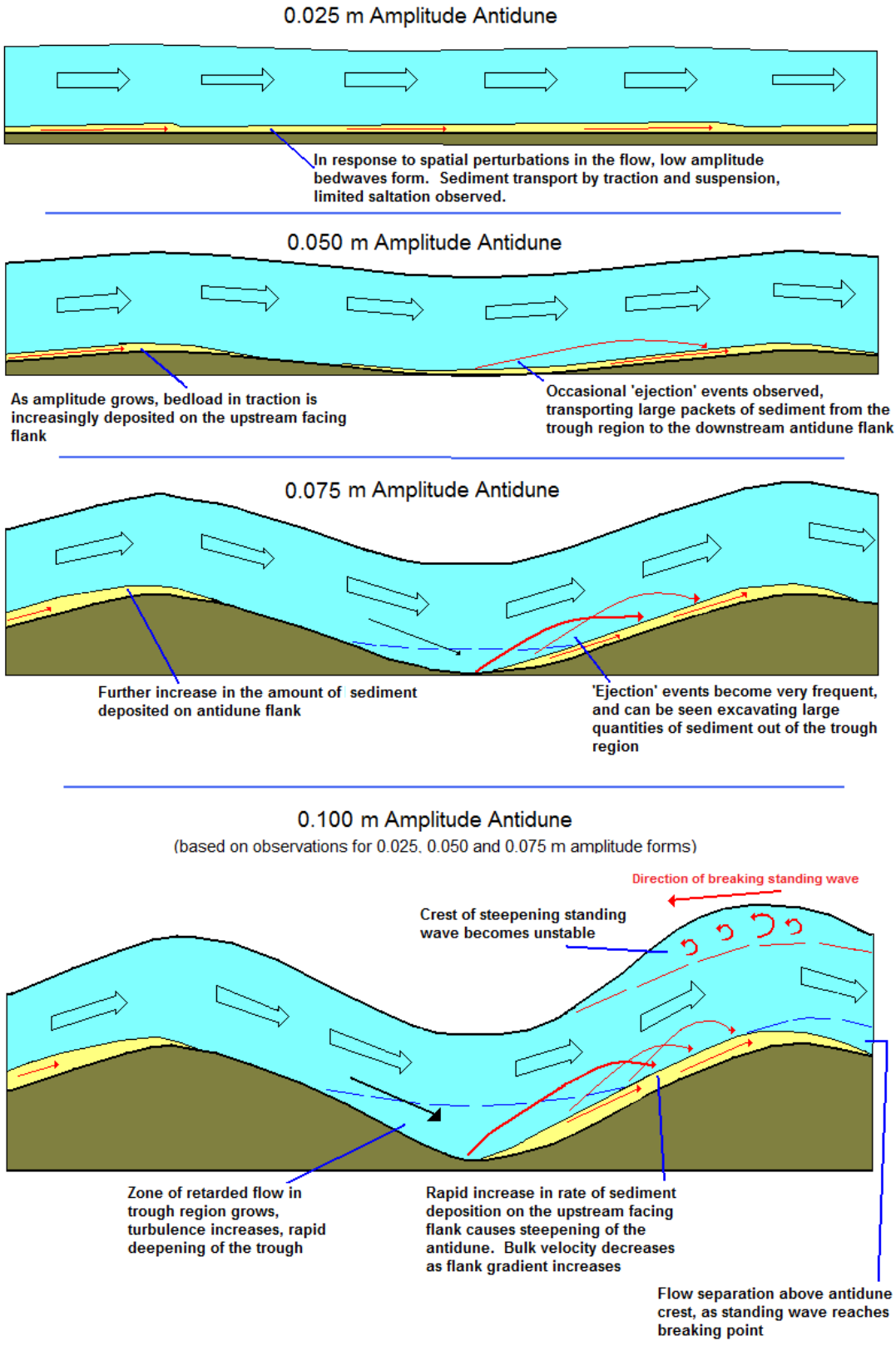

Figure 7.3 Summary of Observations of Antidune Phase Sediment Dynamics

Cartoons illustrating the changes in sediment transport dynamics observed (0.025, 0.050 and 0.075 m amplitude forms) following the transformation from a flat bed to increasingly tall antidunes. An initial bed irregularity forms in response to perturbations in the flow, and alters the local spatial structure of turbulence, causing more particles to accumulate; as the bedform grows it exerts increasingly influences

the spatial distribution turbulent phenomena. The steeper antidune becomes increasingly able to capture sediment in transport, and rapidly steepens. A cartoon is also provided for the critical case (0.100 m amplitude for this λ) showing the author's suppositions for this case. It is thought that the increasing magnitude of turbulence in the trough region leads to a rapid excavation of sediment and its subsequent deposition on the upstream facing flank of the downstream antidune. As the antidune rapidly steepens the flow may separate from the bed at the antidune crest, further contributing to the instability of the steepening standing wave. Once the standing wave oversteepens, it collapses, Fr falls below critical and a degree of erosion occurs, truncating the laminae within the antidune bedform.

For the UMAs observed, initially the traction-carpet of gravel moving across the bed becomes organised into a series of discrete low-amplitude bedwaves. This process is perhaps due to action of periodic perturbations in the unsteady supercritical flow on the bed, and the subsequent amplification of deformities such as might be induced by large or slow moving clasts causing sediment accumulation and the turbulent flow above. The amplitude of these bedwaves gradually increases as sediment is progressively captured on the upstream facing side. As the amplitude increases the proportion of material captured rapidly increases, creating a feedback process that allows the antidune to grow more rapidly and capture further sediment. As steepness increases and more sediment is caught on the upstream flank of each antidune deeper scour occurs in the troughs between, material being ejected from the trough between antidunes. The standing wave breaks when sediment transport processes cause the bedwave to be sufficiently steep that flow slows and becomes subcritical on the upstream facing slope.

Based on the amplitudes examined here, it is possible to extrapolate a relationship between antidune amplitude at standing wave breaking and bed roughness (Figure 7.4). From the cases examined it appears that for gravel antidunes higher levels of turbulence are present along the bed and in the trough region in particular. Further, for the openwork gravel forms, the standing wave above the 0.075 m amplitude bedform insert was not stable, despite the standing wave being stable over the 0.075 m amplitude gravel surfaced bedform insert. This suggests that the additional form roughness associated with an antidune bedform with interstitial flow has a notable impact on antidune stability. It is thought, that for the antidune wavelength examined in this thesis, the bed roughness places a limit on antidune

amplitude, with the standing wave above antidunes breaking at smaller amplitudes over rougher beds.

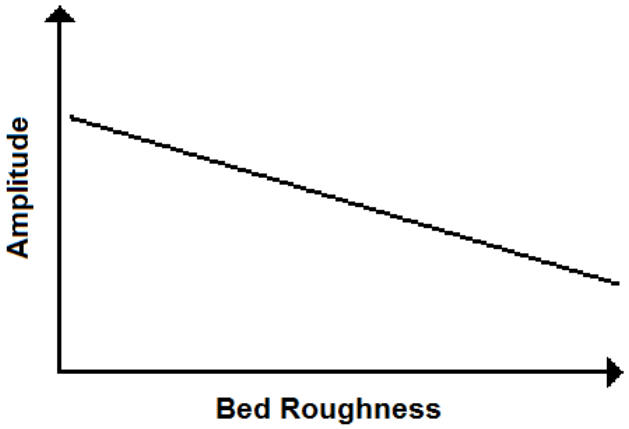

Figure 7.4 Antidune Amplitude and Bed Roughness Relationship

Based on investigations of the turbulence structure above sand surfaced, gravel surfaced and openwork gravel antidune bedform inserts used in this thesis and observations of standing wave stability a relationship can be elucidated between bed roughness and antidune amplitude at the point of standing wave breaking. For a given wavelength the amplitude at which the standing wave above an antidune collapses is lower for rougher beds (gravel) than for less rough beds (sand).

7.4 Overall Discussion and Synthesis

Experimental investigations in flumes are only representations – models - of hydraulic phenomena, and are only as accurate as the accuracy of the re-creation of field conditions or the measuring techniques used allow. However, these results provide a novel and useful characterisation of the bulk flow and basic turbulence structure of the flow profile during the antidune regime. No evidence of the downstream advecting large-scale macro-turbulence (i.e. as per investigations of Shvidchenko and Pender, 2001) has been found, and this is thought to be indicative that coherent turbulent structures are quickly dissipated into the flow above. This lack of detection could though be an artefact of the fixed bed used in the ADV and high-speed video runs. It is thought that a longer flume with better stabilised flow, monitored with a high-speed system and associated higher-intensity synchronised lighting could yield further information on the presence of large-scale turbulent structures over antidune bedforms.

Detailed turbulence investigations by ADV though have provided quantitative support to visual observations from both high-speed video of

particles and standard video of mobile bed flow. The turbulence investigation using ADV indicated that the highest intensity of ejection and sweep events occur at the downstream side of the trough region, an area where particles and sediment have been observed as erupting from the bed into the flow. There is thus a clear link between the turbulent environment and sediment transport. However, it appears that these events also occur alongside deposition via a carpet of bed particles moving in the traction load. The increase in ejection frequency as the antidune bedform steepens suggests they may be related to incursions of high instantaneous velocities into the trough region, which is characterised by generally low instantaneous velocities. This supposition is supported by the high rms, TKE, τ_R and Q2 and Q4 values in the trough region. The occurrence of these quasi-periodical ejections of high speed flow right to the bed then causes these sediment suspension events. Similarly for dunes McLean *et al*. (1994) and Bennett and Best (1995), found that sediment transport was not related to the mean flow velocity but to the non-uniform boundary layer and in particular regions of intense turbulence. These experiments have indicated that the boundary layer is non-uniform over antidunes and that there is a degree of spatial organisation of turbulence which is associated with sediment transport events. This turbulent environment evolves and increases in intensity with increasing antidune amplitude. Sediment transport also occurs via low-amplitude bedwaves and it is thought that these are related more to the mean flow velocity than quasi-periodical turbulent events. The observation of flow parallel orientation of clasts on antidune crests (i.e. Alexander and Fielding, 1997) is compatible with observations of the processed ADV data of low turbulence but high velocity flow at antidune crests. This causes more easily transported material to be removed and the remaining coarser clasts to be orientated flow-parallel. In Section 6 of this thesis, clasts in antidune laminae were found to have a-b planes parallel to the flow direction. During labile bed experiments, only upstream migrating antidunes occurred; stationary or downstream migrating forms were not observed. In terms of antidune sedimentology three sets of deposits were created:

1. Run 1 - Upstream dipping laminae (Type II laminae), deposited on an erosional base and grading into USPB. Some limited indication of

Type I laminae along the erosive base and truncating these. A downstream dipping laminae were observed in situ with these upstream dipping laminae.

2. Run 2 - Downstream dipping erosion surface – translational strata (Type I laminae). These truncate underlying upstream dipping laminae (Type II laminae), which occur above an erosional base. These were produced by more slowly migrating antidunes, which transformed into USPB regime deposition.
3. Run 2 - Bipartite laminae were observed in the deposits produced by more rapidly migrating and occasionally violently breaking antidunes in shallow, high Fr flow.

These processes are shown below in Figure 7.5.

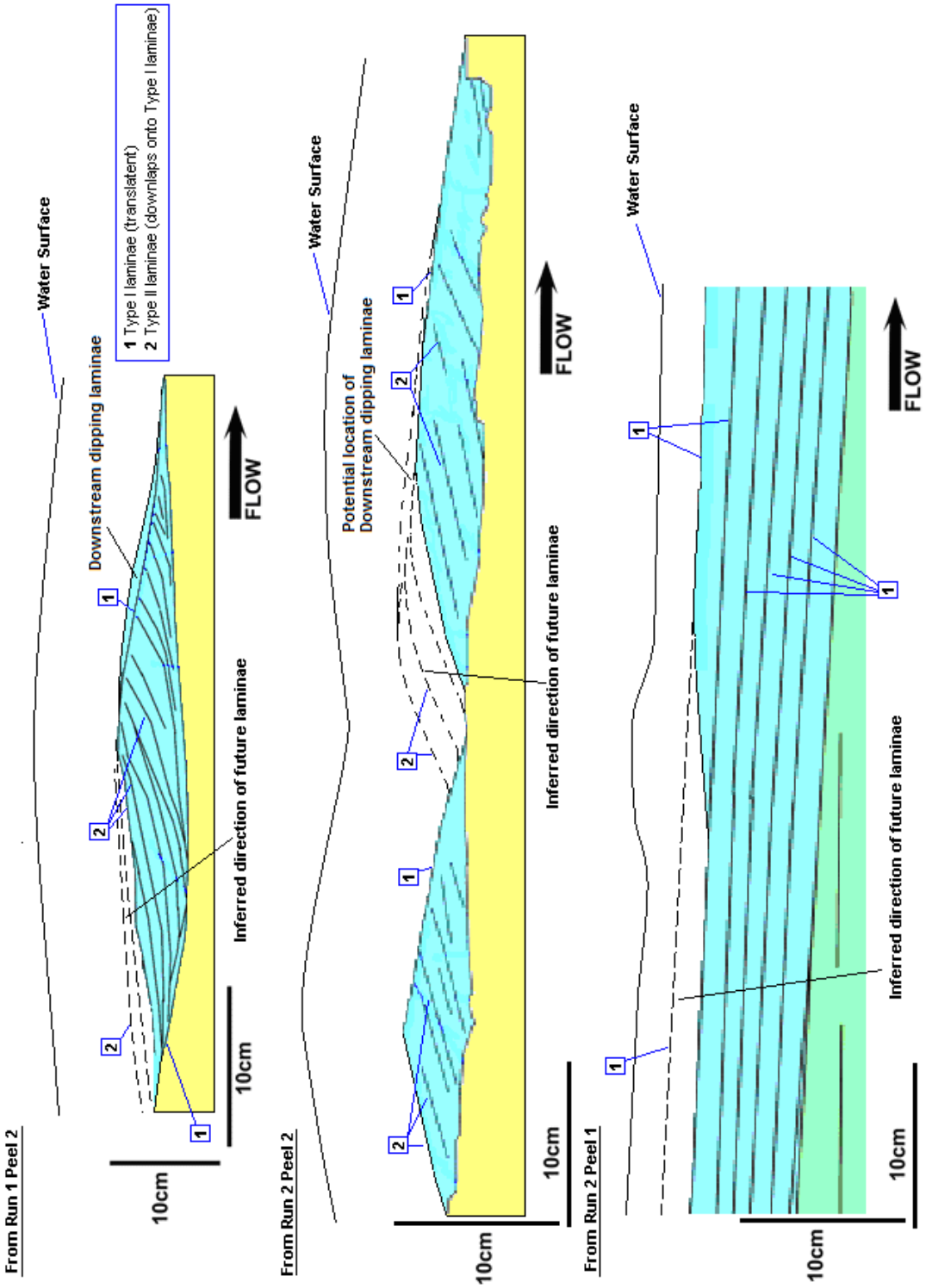

Figure 7.5 Observed Processes of Antidune Laminae Formation

Details of the three process of antidune laminae formation observed during labile bed experiments. Two cases of the production of Type I and Type II laminae were observed, the first case, in Run 1, antidunes gradually dissipated, with laminae decreased in steepness, before transforming into USPB. Downstream dipping deposits were observed overlying the truncated upstream dipping laminae, parallel to the erosional surface that would have formed the antidunes downstream facing flank. The upstream dipping laminae formed as the bedforms migrated upstream, with the downstream dipping laminae forming during the dissipation of the standing wave and

reversion to USPB. At the beginning of Run 2, antidunes with violent breaking standing waves occurred, and the remains of steeper Type I and Type II laminae sets were preserved. No downstream dipping laminae were observed in this peel. Finally, at the end of Run 2, in very shallow flow a different type of bipartite deposit was produced constantly beneath a standing wave. This contrasts with Blair (2000) who observed similar deposits and attributed them to formation during the collapsing phase of standing waves.

It is thought that deposits of Runs 1 and 2 were produced in the same hydrodynamic environment, the translational strata present in deposit 2 being produced by the longer period of antidune upstream migration. These deposits are therefore considered together. Deposit 3 (bipartite laminae) is thought to be have formed via a different mechanism to that described by Blair (1999). Based on video observations, the bipartite laminae appear to form during a two stage flow process, first coarser particles accumulating at the upstream facing base of the couplet, and then finer particles in suspension diffuse into the this coarser base-layer. In this way the bipartite laminae is extended upstreamwards with the migration of the standing wave. Given that the observed dimensions of the labile bed antidunes were broadly comparable to the fixed forms:

- λ 0.4 – 0.44m (62% of the λ of fixed bedforms);
- h ~0.05m; and
- Fr of 1.6 (between 75% and 125% of the values over fixed bedforms).

a combined synthesis is therefore thought appropriate. The upstream dipping laminae (1 and 2) are postulated to form due to deposition from low-amplitude bedwaves and/or the subsequent deposition of material on the antidunes upstream facing slope that were suspended into the flow in the trough region. However, due to the turbidity of the depositional environment, whether traction or ejection and suspension dominate remains unclear. Observations, of the region adjacent to the flume wall show that sediment in traction in low-amplitude bedwaves appears to provide the majority of sediment which is deposited on the upstream facing face of the UMAs. Previously, Section 2.5 discussed the potential mechanisms for antidune sedimentation - interpretations which the results of this thesis support. The degree of differentiation in sediment size, shape and density controls the potential for preferential separation of different grain sizes in order to mark

sedimentary structures. It is thought that kinematic sorting in the carpet of particles moving in the traction load allowed heavier more spherical particles to accumulate in the trough region (further discussion in section 2.5). Supporting this sediment transport process, is the observation that platey particles were found primarily deposited near the flume exit, with relatively few incorporated in the antidune bedding. In kinematic sorting, these are the particles that rise to the surface of a moving carpet of particles in the traction load and would be the least likely to be deposited.

8 Conclusions

In Section 2.6.2, four aims and four hypotheses were set out; these are now reviewed in light of the investigations, results and discussion.

8.1 Aims

1. This thesis has shown that using currently available equipment it is possible to collect detailed turbulent data of the flow over fixed antidune bedforms. Data have been collected, analysed and interpreted and have shown that there is a spatial organisation to the bulk flow structure and a coherent turbulent environment. These patterns have been interpreted with reference to their sedimentological importance. Turbulence statistics are typically an order of magnitude greater over gravel surfaced antidune bedforms than over sand surfaced antidune bedforms.

2. Areas of retarded flow were identified in the troughs between antidune bedforms. For the 0.025 m amplitude fixed antidunes used in this thesis, only a limited area of retarded flow was identified, overall flow remained similar to what might be expected over an USPB. This amplitude of bedform may therefore be more representative of conditions before antidunes are actively growing from a plane bed. In terms of bulk flow, as antidune amplitude increases, the area of retarded flow increases, and velocities in this region further decrease compared to flow elsewhere in the flow profile. Detailed examination of the turbulence structure (see Boxes 4.1, 4.2, 4.3 and 4.4 for summary information) of the flow (based on ADV data) shows that turbulent stresses are greatest at the bed in the trough and at the base of the flank of the downstream antidune. High-speed video imagery shows that whilst neutrally-buoyant particles in this area are indicative of relatively low velocities, occasional high velocity motions do occur, associated with high speed flow descending into the trough from the upstream antidune, and ejections of flow from the bed in the downstream region of the trough. Observations of video recordings of mobile bed runs, show regular eruptions of sediment from the trough

region, supplying sediment which then moves up and is deposited on the antidunes upstream flank, causing upstream migration.

3. During antidune regime flow, turbulence is spatially organised, in a similarly systematic manner to that found in dune-regime flow. Feedback exists between increasing bedform amplitude and increasing turbulence stresses (TKE, τ_R and TI). For the low-amplitude case (almost USPB) turbulence stresses and intensities are relatively low, and distributed relatively evenly along the bed at the base of the boundary layer. However, as the antidune amplitude increases turbulence becomes increasingly spatially varied. Values of $\overline{U}$ are markedly reduce in the trough region, with higher $\overline{U}$ values occurring closer to the bedform crests. For dunes the turbulence environment is dominated by eddy-shedding from the dune crest and reversing flow in the trough region. For the antidune regime the trough remains the key focus for turbulence although, instead of a separation zone the turbulence environment is dominated by high magnitude instantaneous velocities associated with periodic intrusions of higher velocity flow into the area of retarded flow in the trough region. Stresses in this region cause rapid erosion, excavating and mobilising sediment which is moved and deposited onto the antidunes upstream facing flank (causing the bedform to migrate upstream). Erosion occurs on the downstream facing flank, which has a limited sediment supply and is trimmed back progressively by erosion in the trough.

4. Upstream Migrating Antidune sedimentary deposits were produced in a sand-granule-fine gravel mixture. Within these deposits three types of sedimentary structure boundary were observed – Type II laminations (*sensu* Clifton, 1990) represent the deposition of material on the antidunes upstream facing flank, and above, but cutting through these, Type I laminations (*sensu* Clifton, 1990) represent the erosional base formed by antidune migration and collapse, above which further antidune sedimentary sequences may occur. Type I laminae are formed by an erosional surface cutting into the sedimentary structures

below and are delineated by lag-sediments that represent the coarser or denser fraction of the sediment mixture preferentially left behind by sediment erosion and transport processes (details in Section 7.3.9). As found previously by Alexander *et al*. (2001) downstream dipping laminae were also present in one peel adjacent to upstream dipping laminae (Type II) and parallel to Type I laminae. However, the formation of Type II laminations is not so clear, as these laminations mark individual packets of laminae, superimposed on each other over migrating antidunes a process operating during the antidune growth and migration process must be responsible for their formation. Based on observations of low-amplitude bedwaves and turbulent ejections of bed material from the trough onto the upstream facing flank, it is thought that these laminae represent the transport sorting of this sediment (such as the processes identified in Plates 6.8 and 6.9 and Figure 6.11). The kinematic sorting of material in the bedwave and the settling of the material in each ejection allow structured laminae to form. The findings of this thesis are in support of the potential mechanisms for antidune sedimentation discussed in Section 2.5. A key difference between these deposits and those of previous researchers is the relatively high bed aggradation rate (between 8.8 and 12.9 mm/minute) used in these runs. It is thought that this is responsible for the relatively steep dip (up to 15°) of the upstream dipping laminae. The short periods of antidune activity between otherwise rapidly aggrading USPB appears to have allowed preservation of whole antidune laminaesets with little reworking producing deposits without the complicated truncation of earlier deposits by later deposits and tightly packed adjacent upstream and downstream dipping laminae. It is thought that this accounts for the set thickness to formative antidune ratio of 0.9 (compared to the value of 0.4 observed by Alexander *et al*. (2001)). However, good agreement was found with regards to the ratio of laminae length to formative antidune wavelength, the value of 0.5 being in agreement with the ratio observed previously by Barwis and Hayes (1985), Langford and Bracken (1987) and Alexander *et al*. (2001). In terms of the bipartite deposits produced at the end of Run 2, the bedforms

observed may represent a new type of structure produced by sediment sorting associated with the rapid upstream migration of a low amplitude bedform on an aggrading bed. The similarity with the deposits produced by downstream migrating low amplitude bedforms of McBride *et al*. (1974) is further supported by the feed rate of 2 to 4 mm/minute used by these researchers (similar to the rate used here). The bipartite deposits observed at the end of Run 2 may represent the upstream migrating case in a continuum of bedform morphologies.

8.2 Hypotheses

1. It has been confirmed that there is a coherent structure to the turbulent flow above antidune bedforms. This flow structure can be measured using Acoustic Doppler Velocimetry, and observed using high-speed video recording. Data collected by ADV can be treated and described statistically in a similar manner to turbulence data from other sedimentological environments. The spatial distribution and temporal properties of the turbulence environment have been linked to the sedimentological behaviour of antidunes.

2. Linking observations of sediment transport during mobile bed experiments with the distribution of turbulence recorded quantitatively during ADV experiments and during high-speed camera runs has allowed the identification of the mechanisms responsible for erosion and deposition over antidunes. The key to antidune sedimentology is the increasing magnitude of instantaneous velocities in the trough region, which progressively increase in intensity as antidune amplitude increases. These erode and excavate sediment from the trough and redistribute it onto the downstream antidune flank, where turbulence subsides and deposition occurs as this volume of sediment transport can no longer be sustained. It is postulated that an antidune collapses when the flow stalls, as the trough becomes overdeepened and the flow and sediment cannot pass over the steepened downstream antidune. Individual turbulent ejections are responsible for the Type II laminae, the periodicity of these and the heterogeneity of sediment controlling the clarity of the laminations produced.

3. It is considered that two types of antidune laminae are produced – Type I and Type II, the former marking the erosional base formed translationally by antidune migrations, and also by the collapsing antidune phase, and the latter (Type II laminae) by the sorting of material removed from the trough between antidunes by low-amplitude bedwaves and turbulent ejections. Type II laminae were found to dip upstream at angles between 7˚ and 16˚ and, internal to these, clasts dipped upstream at angles between 20˚ and 45˚. Type I (translational) laminae dipped at between 11 and 12˚ downstream. Bipartite laminae dipped at between 1.5˚ and 3.3˚ downstream.

4. In the mobile bed experiments, distinctive deposits were produced by antidune deposition. Although deposits formed readily during experiments, only a fraction of the structures deposited by individual antidunes survived in rapidly aggrading conditions owing to reworking by migrating standing waves. However, the detailed laminations and structures within the deposits were similar to features previously identified for fluvial antidunes both in the flume (Middleton, 1965; Yagishita and Taira, 1989; Yokokawa *et al*., 2000; Alexander *et al*., 2001), in the field (Barwis and Hayes, 1985; Langford and Bracken, 1987; Clifton, 1990; Alexander and Fielding, 1997; Blair, 1999 and 2000; and Duller *et al*., in press) and in the geological record (Barwis and Tankard, 1983; Nakayama and Yoshikawa, 1997).

8.3 Application to Field Geology

The collected examples described and discussed in the literature review indicate that antidune regime deposits are perhaps less rare than is commonly thought. This thesis therefore reiterates the views of Clifton (1990) and Fielding (2006) that antidune regime deposits do occur with reasonable frequency in the sedimentological record. However, the truncation of upstream dipping (Type II) laminae, or even the total destruction and replacement by bipartite laminae means that a variety of sedimentary structures may have an antidune origin. The previous studies on antidunes in the flume, field and geological record summarised in Table 2.6, Table 2.7

and Table 2.10 respectively provide a guide to antidune morphology and sedimentary structures largely in sandy sediments, which may be of use to the field geologist. The observations of and resulting sedimentary structures from the labile bed experiments (Sections 6, 7 and 8) of sandy-gravels will provide a valuable framework to support postulated antidune origins of field deposits, recent or from the geological record exhibiting similar sedimentological features both in sandy deposits and importantly within sandy-gravel beds.

8.4 Recommendations for Future Investigations

1. The collected ADV data reported here contained a large degree of noise which required pre-processing and filtering. In addition, low correlation coefficients were present in measurements taken near the bed, especially in the trough region. The use of an instrument operating at a higher temporal resolution (200 Hz, as opposed to the maximum of 100 Hz used here) would provide much more refined data. Higher temporal resolution data would reduce the level of any potential biases towards lower velocities in the data caused by the removal of apparently 'noisy' high instantaneous velocity data and therefore the potential underestimation of turbulent statistics. This supposition pertains because, higher frequency data will lead to higher correlation values between adjacent instantaneous velocities, so genuinely high instantaneous velocities will not be removed when filtering by correlation. An ADV with a faster measurement rate would allow more detailed temporal measurements, with much reduced uncertainties. Similarly, wavelet processing of ADV data may aid the identification of genuine turbulence data and allow the more effective removal of signal noise. Alternatively a Laser Doppler Velocimeter (LDV) could be used to provide non-flow-intrusive estimations of velocities and turbulence. These measurements would allow a more detailed assessment of the coherency of turbulent structures in antidune regime flow.

2. In terms of high-speed video, particle tracking experiments were probably the least successful set of experiments undertaken as part of

this thesis. The use of a setup with a dedicated synchronised flash laser light sheet would allow high-quality images to be obtained at a much higher frame rate. Commercial algorithms alongside an improved quality of data collected with this equipment may aid the identification and tracking of tracer particles recorded in frames. This setup would allow a much more detailed, (higher temporal resolution) whole-field flow measurements to be collected and interpreted to illustrate bulk flow motions, and with further processing provide more information of the turbulent flow structure. Potentially a more sophisticated high-speed video setup would allow the detection of any large-scale macro-turbulence, such as during standing wave breaking.

3. Collecting data over the centreline of a set of *three* antidunes would provide a better understanding of the spatial changes which occur over a series of bedforms. This approach would provide a better means for generalising the flow structure over antidunes, by highlighting any abnormalities, introduced artificially by flume wall effects such as oscillating side-to-side flow.

4. In order to ensure more robust experimental conditions, a wider and longer flume would have allowed sidewall effects and entrance and exit effects to have been reduced. Additionally, more effective flow straightening may have aided the reduction in the side-to-side velocity element evident in the ADV experiments. This side-to-side component $\overline{W}$ was most pronounced for the 0.075 m amplitude forms (compare $\overline{U}$ between crests in Figures 4.1, 4.2 and 4.3), suggesting that with increasing antidune bedform insert amplitude the flows sensitivity to any non-uniformities in the flow increases. A wider flume would also reduce the impact of any possible boundary reflections on ADV data quality obtained along the centreline of the flume.

5. The use of a flume capable of recirculating sediment alongside the sediment feed would have may have allowed a more natural sediment transport – bed equilibrium to have been established.

6. It would also be worthwhile investigating the design of the antidune bedform inserts so that that the joints were moved from trough to crest, in order to entirely rule out the effect of the joint on the turbulence observed there.

7. Using an LDV would reduce any vibration effects, since it could be mounted independently of the flume, rather than to a carriage attached to the flume. An LDV should also provide more precise measurements of turbulence due to the smaller measurement volume, and the lack of an adjacent probe head (as is the case for ADV, although the measuring volume is located away from the ADV probe).

8. A wider variety of sedimentological hydrodynamic investigations are required to focus on the DMA and stationary antidune regimes, the hydrodynamics of which are not yet sufficiently clear. It would be beneficial if a proportion of these further experiments used coarse sediment mixtures because information on antidune bedforms and their sedimentary structures is particularly sparse in coarser sediments. Starting with medium sand as used by previous researchers and to then gradually increasing the gravel content would allow the impact of gravel content on the ability of antidunes to form from an USPB to be investigated. From the experiments carried out here, it appears that antidunes initiate less readily from a gravel bed compared to a sand bed.

9. Further investigation should be undertaken to determine the existence of DMAs. Currently it is unclear whether these bedforms do exist in their own right, or whether they form around dune (or even UMA) cores in response to waning flow.

9 Glossary

ADV	Acoustic Doppler Velocimetry
bi	bipartite laminae
BLCCR	Boundary Layer Correlation Coefficient
CMOS	Complementary Metal Oxide Semiconductor
COR	Correlation Coefficient
CU	Coarsening Upwards
dd	downstream dipping
DMA	Downstream Migrating Antidune
DN	Digital Number
ds	downstream dipping erosional surface
eb	erosional base
ECM	Electromagnetic Current Meter
fps	frames per second
FOV	Field of View
Fr	Froude Number
FU	Fining Upwards
GB	Gigabyte
gc	gravel clasts
gt	gradational transition
HCS	Hummocky Cross Stratification
HDPE	High Density PolyEthene
Hz	Hertz
is	internal structures
LDV	Laser Doppler Velocimetry
LSPB	Lower Stage Plane Bed
NaN	Not-a-Number
NDV	Nortek Doppler Velocimeter
PFT	Potential Flow Theory
rms	Root Mean Squared
SCS	Swaley Cross stratification
SNR	Signal to noise ratio
sc	silicon carbide
sp	sand poor
sr	sand rich
st	stringers
STR	Sediment Transport Rate
SW	Standing Wave
TDA	Three Dimensional Antidunes
TKE	Turbulent Kinetic Energy
tr	trough shaped
TRs	Transverse Ribs
ud	upstream dipping
UMA	Upstream Migrating Antidune
USPB	Upper Stage Plane Bed
we	wedge of sediment

10 References

Alexander, J. and Fielding, C. (1997) Gravel antidunes in the tropical Burdekin River, Queensland, Australia. *Sedimentology*, 44, 327-337.

Alexander, J., Bridge, J.S., Cheel, R.J., LeClair, S.F. (2001) Bedforms and associated sedimentary structures formed under supercritical water flows over aggrading sand beds. *Sedimentology*, 48, 133-152.

Allan, A., and Frostick, L.E., (1999) Framework dilation, winnowing and matrix particle size: the behaviour of some sand-gravel mixtures in a laboratory flume. *Journal of Sedimentary Research 1*, 69, 21-26.

Allen, J.R.L. (1966) On bedforms and palaeocurrents. *Sedimentology*, 6, 153-190.

Allen J.R.L. (1969a) The path of grains through wave-like bedforms. *Geologie en Mijnbouw*, 48, 3-8.

Allen, J.R.L. (1969b), On the geometry of current ripples in relation to stability of fluid flow, *Geografiska Annaler,* Ser. A, 51, 61– 96

Allen, J.R.L. (1982) *Sedimentary Structures*, Vol. 2, Elsevier, Amsterdam, Netherlands.

Allen J.R.L. (1983) River bedforms: progress and problems. In: *Modern and Ancient Fluvial Systems* (Ed. by Collinson, J. and Lewin, J.), pp. 5-18. Blackwell Scientific Publications, Oxford, UK.

Allen, J.R.L. (1984) *Sedimentary Structures: Their Character and Physical Basis*. Elsevier, Amsterdam, Netherlands.

Allen, J.R.L. (1985) *Principles of Physical Sedimentology*. George Allen & Unwin, London, UK.

Allen, J.R.L. and Leeder, M. R. (1980). Criteria for the instability of upper-stage plane beds. *Sedimentology*, 27, 209–217.

Anderson, A. (1953) The characteristics of sediment waves formed by flow in open channels, pp379 – 395. In: *Proceedings of the Third Midwestern Conference on Fluid Mechanics, 23 - 25 March 1953*. University of Minnesota, Institute of Technology

Araya, T. and Masuda, F. (2001) Sedimentary structures of antidunes: An overview. *Journal of the Sedimentological Society of Japan*, 53, 1-15.

Ashley, S. (1990) Classification of large-scale subaqueous bedforms: A new look at an old problem. *Journal of Sedimentary Petrology,* 60, 160-172.

Ashmore, P. (1982) Laboratory modelling of gravel braided stream morphology. *Earth Surface Processes and Landforms*, 7, 201-225.

Ashworth, P., Best, J., Leddy, J.O. and Geehan G.W. (1994) The physical modelling of braided rivers and the deposition of fine grained sediment. In: *Process Models and Theoretical Geomorphology* (Ed. by Kirkby, M.), John Wiley & Sons Ltd, Chichester, UK.

Bartsch-Winkler, S. and Schmoll, H.R. (1984) Bedding types in Holocene tidal channel sequences, Kink Arm, Upper Cook Inlet, Alaska. *Journal of Sedimentary Petrology*, 54, 1239-1250.

Barwis, J.H. and Hayes, M. (1985) Antidunes on modern and ancient washover fans. *Journal of Sedimentary Petrology*, 55, 907-916.

Barwis and Tankard (1983) Pleistocene shoreline deposition and sea-level history at Swartklip, South Africa. *Journal of Sedimentary Petrology*, 53, 1281-1294.

Batchelor, G.K. (1960) Scientific Papers of Sir Geoffrey Ingram Taylor. Volume 2, Meteorology, Oceanography and Turbulent Flow. Cambridge University Press, Cambridge, UK.

Beeson, D.L., Self, S. and McPherson, J.G. (1984) Mega cross-bedding in pyroclastic flow deposits: A product of high energy, aggradation deposition on steep slopes. *AAPG Bulletin*, 68, 4, 453.

Bennett, S.J. and Best, J.L. (1995) Mean flow and turbulence structure over fixed, two-dimensional dunes: implications for sediment transport and bedform stability. *Sedimentology*, 42, 491–513.

Bennett, S.J. and Bridge, J.S. (1995) An experimental study of flow, bedload transport and bed topography under conditions of erosion and deposition and comparison with theoretical models. *Sedimentology*, 42, 117-146.

Best, J.L. and Bridge, J.S. (1992) The morphology and dynamics of low amplitude bedwaves upon upper stage plane beds and the preservation of planar laminae. *Sedimentology*, 39, 737-752.

Best, J.L. (1993) On the interactions between turbulent flow structure, sediment transport and bedform development : some considerations from recent experimental research. In: *Turbulence : perspectives on flow and sediment transport* (Ed. By Clifford, N., French, J.R., Hardisty, J.), pp. 61-92. Wiley and Sons, Chichester, UK.

Best, J.L. and Kostachuk, R.A. (2002) An experimental study of turbulent flow over a low-angle dune. *Journal of Geophysical Research*, 107, 18-1-18-19.

Billi, P., D'Agostino, V., Lenzi, M.A., and Marchi, L. (1998) Bedload, slope and channel processes in a high-altitude Alpine torrent. Proceeding of the 4th International Gravel-Bed Rivers Workshop (GBR-IV) held at Gold Bar, Washington, August 20-26, 1995.

Blair, T.C. (1987) Sedimentary processes, vertical stratification sequences, and geomorphology of the Roaring River alluvial fan, Rocky Mountains National Park, Colorado. *Journal of Sedimentary Petrology*, 57, 1-18.

Blair, T.C. and McPherson, J.G. (1999) Alluvial fans and their natural distinction from rivers. *Journal of Sedimentary Research*, A64, 3, 450-489.

Blair, T.C. (1999) Sedimentary processes and facies of the waterlaid Anvil Spring Canyon fan, Death valley, California. *Sedimentology*, 46, 913-940.

Blair, T.C. (2000) Sedimentology and progressive tectonic unconformities of the sheetflood-dominated Hell's Gate alluvial fan, Death Valley, California. *Sedimentary Geology*, 132, 233-262.

Boothroyd, J.C. (1970) Recent Braided-Stream Sedimentation, South-Central Alaska. *AAPG Bulletin*, 54, 5, 836.

Boothroyd, J.C. and Ashley, G. (1975) Processes, bar morphology and sedimentary structures on braided outwash fans, north-eastern gulf of Alaska, pp. 193-222. In: *Glaciofluvial and Glaciolaucustrine sedimentation* - SEPM special publication 23 (Ed. by Jopling A. and McDonald, B.). Society of Economic Palaeontologists and Mineralologists, Tulsa, Oklahoma, USA.

Bornhold, B.D. and Prior, D.B. (1990) Morphology and sedimentary processes on subaqueous Noeik River Delta, British Columbia, Canada. In: *Coarse Grained Deltas* - Special Publication 10 of the IAS (Ed. by Colella, A. and Prior, D.B.), pp. 169-181. Blackwell Scientific Publications, Oxford, UK.

Boudon, G. and Lajoie, J. (1989) The 1902 Peléean deposits in Fort Cemetery of St. Pierre, Martinique: a model for the accumulation of turbulent nuées ardentes. *Journal of Volcanology and Geothermal Research,* 38, 113-129.

Boyer, C. and Roy, A.G. (1991) Bed morphology around an obstacle in shallow flow. *Geographie Physique et Quaternaire*, 45, 91-99.

Brown, R.J. and Branney, M.J. (2004) Event-stratigraphy of a caldera-forming ignimbrite eruption on Tenerife: the 273 ka Poris Formation. *Bulletin of Volcanology*, 66, 392-416.

Brennand, T. (1994) Macroforms, large bedforms and rhythmic sedimentary sequences in subglacial eskers, south-central Ontario: implications for esker genesis and meltwater regime. *Sedimentary Geology*, 91, 9-55.

Bridge, J.S. and Bennett, S.J. (1992) A model for the entrainment and transport of sediment grains of mixed sizes, shapes and densities. *Water Resources Research*, 28, 337-363.

Bridge, J.S. and Best, J.L. (1988) Flow, sediment transport and bedform dynamics over the transition from dunes to Upper-Stage Plane Beds:

implications for the formation of planar laminae. *Sedimentology*, 35, 753-763.

Bridge, J.S. and Best, J.L. (1997) Preservation of planar laminae due to migration of low-relief bed waves over aggrading upper stage plane beds: comparison of experimental data with theory. *Sedimentology*, 44, 253-262.

Bridge, J.S. (2003) *Rivers and floodplains: forms, processes, and sedimentary record*. Blackwell Science, Oxford, UK.

Buffin-Bélanger, T. and Roy, A.G. (1998) Effects of pebble cluster on the turbulent structure of a depth-limited flow in a gravel-bed river. *Geomorphology*, 25, 249-267.

Buffin-Bélanger T., Roy, A.G. and Kirkbride, A. (2000) On large-scale flow structures in a gravel-bed river. *Geomorphology,* 32, 417-435.

Buffin-Bélanger, T. and Roy, A.G. (2005) 1 min in the life of a river: selecting the optimal record length for measurement of turbulence in fluvial boundary layers. *Geomorphology*, 68, 77-94.

Cantwell, B.J. (1981) Organized motion in turbulent fluid. *Annual Review of Fluid Mechanics,* 13, 457-515.

Carling, P.A. (1999) Subaqueous gravel dunes. *Journal of Sedimentary Research*, 69, 534-545.

Carling, P. A. and Shvidchenko, A. B. (2002) A consideration of the dune: antidune transition in fine gravel. *Sedimentology,* 49, 1269-1282.

Carling, P.A. and Breakspear, R.M.D. (2006) Placer formation in gravel-bedded rivers: a review. *Ore Geology Reviews*, 28, 377-401.

Carling, P.A., Radecki-Pawlik, A., Williams, J.J., Rumble, B., Meshkova, L., Bell, P. and Breakspear, R. (2005) The morphodynamics and internal structure of intertidal fine-gravel dunes: Hills Flats, Severn Estuary, UK. *Sedimentary Geology*, 183, (3-4), 159-179.

Cassidy, N.J., Russell, A.J., Marren, P.M., Fay, H., Knudsen, Ó., Rushmer, E.L. and Van Dijk, T.A.G.P. (2003) GPR derived architecture of November 1996 jökulhlaup deposits, Skeiðarásandur, Iceland. In: *Ground Penetrating Radar in Sediments.* Eds: Bristow, C.S. and Jol, H.M. Geological Society, London. Special Publications, 211, 153-166.

Chakraborty, C. and Bose, P. (1992) Ripple/dune to upper plane bed transition: some observations from the ancient record. *Geological Journal*, 27, 349-359.

Chanson, H. (1999) *The hydraulics of open channel flow: an introduction*. Arnold, London, UK.

Chanson, H. (2000) Boundary shear stress measurements in undular flows: Application to standing wave bedforms. *Water Resources Research*, 36, 3063-3076.

Chanson, H., Trevethan, M. and Koch, C. (2007) Discussion of "Turbulence Measurements with Acoustic Doppler Velocimeters" by Carlos M. García, Mariano I. Cantero, Yarko Niño, and Marcelo H. García. *Journal of Hydraulic Engineering*, 131, 1062-1073. *Journal of Hydraulic Engineering*, 133, 1283-1292.

Charland, A. and Lajoie, J. (1989) Characteristics of pyroclastic deposits at the margin of Fond Canonville, Martinique, and implications for the transport of the 1902 nuées ardentes of Mount Pelée. *Journal of Volcanology and Geothermal Research,* 38, 97-112.

Chartrand, S.M. and Whiting, P.J. (2000) Alluvial architecture in headwater streams with special emphasis on step-pool topography. *Earth Surface Processes and Landforms*, 25, 583-600.

Cheel, R.J. (1984) Heavy mineral shadows, a new sedimentary structure formed under upper-flow-regime conditions: its directional and hydraulic significance. *Journal of Sedimentary Petrology* 54, 1175-1182.

Cheel, R.J. and Middleton, G.V. (1986) Horizontal Laminae formed under upper flow regime plane bed conditions. *Journal of Geology* 94, 489-504.

Cheel, R.J. (1990) Horizontal lamination and the sequence of bed phases and stratification under upper flow regime conditions. *Sedimentology*, 37, 517-529.

Chin, A. (1999) On the origin of step-pool sequences in mountain streams. *Geophysical Research Letters*, 26, 231-234.

Clifford, N.J. and French, J.R. (1993) Monitoring and Modelling Turbulent Flow: Historical and Contemporary Perspectives. In: *Turbulence: Perspectives on Flow and sediment Transport* (ed by Clifford, N.J., French, J.R. and Hardisty, J.), 1-33 John Wiley, Chichester, UK.

Clifton, A.E., Phillips, R.L. and Hunter, R.E. (1973) Depositional structures and processes in the mouths of small coastal streams, south-western Oregon. In: *Coastal Geomorphology: A proceedings volume of the 3rd annual geomorphology symposia series held at Binghampton, New York Sept. 28-30, 1972.,* Ed: Coastes, D.R. State University of New York, New York, USA.

Clifton, T. R. (1990) Sedimentology of antidune flow; controls on sediment transport and stratification. PhD Thesis, University of California, Santa Cruz, CA, United States.

Cole, P.D. (1991) Migration direction of sand-wave structures in pyroclastic surge deposits: implications for depositional processes. *Geology*, 19, 1108-1111.

Cole, P.D. and Scarpati, C. (1993) A facies interpretation of the eruption and emplacement mechanisms of the upper part of the Neapolitan Yellow Tuff, Campi Fregrei, southern Italy. Bulletin of Volcanology, 55, 311-326.

Coleman, S.E. and Fenton, J.D. (2000) Potential-flow theory and alluvial stream bed forms. *Journal of Fluid Mechanics*, 418, 101-117.

Collinson, J. (1966) Antidune bedding in the Namurian of Derbyshire, England. *Geologie en Mijnbouw*, 45e, 262-264.

Collinson, J. and Thompson, D. (1982) *Sedimentary Structures*. George Allen & Unwin, London, UK.

Colombini, M. (2004) Revisiting the linear theory of sand dune formation. *Journal of Fluid Mechanics*, 502, 1-16.

Cornish, V. On Kumatology: the study of waves & wave structures of the atmosphere, hydrosphere & lithosphere. *Geophysical Journal* 13, 624-628. 1899.

Cotter, E. and Graham, J.R. (1991) Coastal plain sedimentation in the late Devonian of Southern Ireland; hummocky cross-stratification in fluvial deposits? *Sedimentary Geology*, 72, 201-224.

Crowe, B.M. and Fisher, R.V. (1973) Sedimentary structures in base-surge deposits with special reference to cross-bedding, Ubehebe Craters, Death Valley, California. *Geological Society of America Bulletin*, 84, 663-682.

Curran, J.C. and Wilcock, P.R. (2005) Characteristic dimensions of the step-pool bed configuration: An experimental study. *Water Resources Research*, 41, W02030, doi:10.1029/2004WR003568.

Davis Jnr, R. (1985) *Coastal Sedimentary Environments*. Springer-Verlag, Berlin.

Deigaard, R. (2006) Breaking antidunes: cyclic behaviour due to hysteresis. *Journal of Hydraulic Engineering*, 132, 620-623.

Delaney, C. (2002) Sedimentology of a Glaciofluvial landsystem, Lough Ree area, Central Ireland: implications for ice margin characteristics during Devensian deglaciation. *Sedimentary Geology*, 149, 111-126.

Dittrich, A., Nestmann, F. and Ergenzinger, P. (1996) Ratio of lift and shear forces over rough surfaces, pp. 125-146. In: *Coherent Flow Structures in Open Channels* (Ed. by Ashworth, P.J., Bennett, S.J., Best, J.L., McLelland, S.J.). John Wiley & Sons, Chichester.

Duller, R.A., Mountney, N.P., Russell, A.J. and Cassidy, N.C. (in press) Architectural Analysis of a Volcanistic Jökulhlaup Deposit, Southern Iceland: Sedimentary Evidence for Supercritical Flow. *Sedimentology*.

Einsele, G. (2000) *Sedimentary Basins: Evolution, Facies and Sediment Budget*. Springer-Verlag, Berlin, Germany.

Einsele, G. and Seilacher, A. (1991) Distinction of Tempestites and Turbidites. In: *Cycles and Events in Stratigraphy* (eds Einsele, G., Ricken, W. and Seilacher, A.). Springer-Verlag, Berlin Heidelberg, Germany.

Engelund, F. and Hansen, E. (1966) Investigations of flow in alluvial streams. Civil Engineering and Building Construction Series No. 35. Acta Polytechnica Scandinavica, Copenhagen, Denmark.

Engelund, F. and Fredsøe, J. (1982) Flow over sinusoidal bed with large amplitude. Progress Report 36, 21-26. Institute of hydrodynamics and hydraulic engineering, Technical University of Denmark.

Fahnestock, R.K. (1963) Morphology and Hydrology of a Glacial stream – White River, Mount Rainer Washington. USGS Professional Paper 422-A.

Falk, P. and Dorsey, R. (1998) Rapid development of gravelly high-density turbidity currents in marine Gilbert-type fan deltas, Loreto Basin, Baja California Sur, Mexico. *Sedimentology*, 45, 331-349.

Fay, H. (2002) Formation of ice-block obstacle marks during the November 1996 glacier-outburst flood (jökulhlaup), Skeidarársandur, southern Iceland. In: *Floods and Megaflood Processes and Deposits: Recent and Ancient Examples* (Ed. By Martini, I.P., Baker, V.R., Garzón, G), pp. 85-97. Blackwell Science, Oxford, UK.

Ferro, V. (2003) ADV measurements of velocity distributions in a gravel-bed flume. *Earth Surface Processes and Landforms*, 28, 707-722.

Fielding, C.R. and Webb, J.A. (1996) Facies and cyclicity of the Late Permian Bainmedart Coal Measures in the Northern Prince Charles Mountains, MacRobertson Land, Antarctica, *Sedimentology*, 43, 295-322.

Fielding, C.R. (2006) Upper flow regime sheets, lenses and scour fills: extending the range of architectural elements for fluvial sediment bodies. *Sedimentary Geology*, 190, 227-240.

Fildani, A., Normark, W.R., Kostic, S. and Parker, G. (2006) Channel formation by flow stripping: large-scale scour features along the Monterey East Channel and their relation to sediment waves. *Sedimentology*, 53, 1265-1287.

Fisher, R.V. and Waters, A.C. (1969) Bed forms in base-surge deposits; lunar implications. *Science*, 165, 1349-1352.

Fisher, R.V. and Waters, A.C. (1970) Base surge bed-forms in Maar Volcanoes. *American Journal of Science*, 268, 157-180.

Fisher, R.V. (1990) Transport and deposition of a pyroclastic surge across an area of high relief: The 18 May 1980 eruption of Mount St. Helens, Washington. *Geological Society of America Bulletin*, 102, 1038-1054.

Foley, M. (1977) Gravel lens formation in antidune regime flow - a quantitative hydrodynamic indicator. *Journal of Sedimentary Petrology*, 47, 738-746.

Foley, M. (1978) Scour and fill in steep, sand-bed ephemeral streams. *Geological Society of America Bulletin*, 89, 559-570.

Foley, M., Vessell, R., Bonis, S., and Davis, D. (1978) Bed-load transport mechanism during flash floods. In: Preprint volume from "*Conference on hydrometeorological aspects of flash floods*", Los Angeles, California, USA.

Fox, P.J., Heezen, B.C. and Harian, A.M. (1968) Abyssal Anti-dunes. *Nature*, 220, 470-472.

Fralick, P. (1999) Paleohydraulics of chute-and-pool structures in a Paleoproterozoic fluvial sandstone. *Sedimentary Geology*, 125, 129-134.

Fredsøe, J. (1974) The formation of sediment waves in closed channels. Progress Report 32, 29-36. Institute of Hydrodynamic and Hydraulic Engineering, Technical University of Denmark.

Fukuoka, S., Okutsu, K., Yamasaka, M. (1982) Dynamic and kinematic features of sand waves in upper regime. *Japanese Society of Civil Engineers*, 323, 77-89.

Galli, G. (1990) Origins of event beds in the Jurassic 'Calcari Grigi' formation, Venetian Alps, Italy. *Geologie en Mijnbouw*, 69, 375-390.

Garde, R. and Ranga-Raju, K. (1977) *Mechanics of Sediment Transportation and Alluvial stream Problems*. Wiley Eastern Ltd, New Delhi, India.

García, M., Niño, Y. and López, F. (1996) Laboratory Observations of Particle Entrainment into Suspension by Turbulent Bursting, pp 63-86. In: *Coherent Flow Structures in Open Channels* (Ed. by Ashworth, P.J., Bennett, S.J., Best, J.L., McLelland, S.J.). John Wiley & Sons, Chichester, UK.

García, C.M., Cantero, M.I., Niso, Y. and García, M. H. (2005) Turbulence measurements with acoustic Doppler velocimeters. *Journal of Hydraulic Engineering*, 131, 1062–1073.

Gevrek, A.I. and Kazanci, N. (2000) A Pleistocene, pyroclastic-poor maar from central Anatolia, Turkey: influence of a local fault on a phreatomagmatic eruption. *Journal of Volcanology and Geothermal Research*, 95, 309-317.

Giannetti, B. and de Casa, G. (2000) Stratigraphy, chronology, and sedimentology of ignimbrites from the white trachytic tuff,

Roccamonfina Volcano, Italy. *Journal of Volcanology and Geothermal Research*, 95, 243-295.

Gilbert, G.K. (1914) Transportation of debris by running water. *U.S. Geological* Survey, Professional Paper, 86.

Gordon, L. (2000) Surf zone observations with a Nortek vector velocimeter and Sontek ADVO. Technical Report Number 014, Nortek.

Goring, D.G. and Nikora, V.I. (2002) Despiking Acoustic Doppler Velocimeter Data. *Journal of Hydraulic Engineering,* 128, 117-126.

Gorrell, G. and Shaw, J. (1991) Deposition in an esker, bead and fan complex, Lanark, Ontario, Canada. *Sedimentary Geology*, 72, 285 – 314.

Grachev, N.R. (1980) Stopped waves and channel process. *Soviet Hydrology*, 19, 64-68.

Gradowczyk, M. (1968) Wave propagation and boundary instability in erodible-bed channels. *Journal of Fluid Mechanics*, 33, 93-112.

Grant, G.E., Swanson, F.J. and Wolman, M.G. (1990) Pattern and origin of stepped-bed morphology in high-gradient streams, Western Cascades, Oregon. *Geological Society of America Bulletin*, 102, 340-352.

Grant, G.E. and Mizuyama, T. (1992) Origin of step-pool sequences in high-gradient streams: a flume experiment. In: *Proceedings of the Japan-U.S. Symposium on Snow Avalanche, Landslide, and Debris Flow Prediction and Control* (Ed. by Tominaga, M.). Tsukuba, Japan, Sept 30-Oct.3, 1991, p. 523-532.

Grant, G. (1997) Critical flow constrains flow hydraulics in mobile-bed streams: A new hypothesis. *Water Resources Research*, 33, 349-358.

Grass, A.J., (1970) Initial instability of Fine Bed Sand, *Journal of the Hydraulic Division ASCE*, 96, 619-632.

Grass, A.J. (1971) Structural features of turbulent flow over smooth and rough boundaries. *Journal of Fluid Mechanics*, 50, 233-255.

Grass, A.J. (1982) The Influence of Boundary Layer Turbulence on the Mechanics of Sediment Transport. In: *Euromech 156: Mechanics of Sediment Transport*, Istanbul, Turkey.

Grass, A.J. and Mansour-Tehrani, A. (1996) Generalized Scaling or coherent Bursting Structures in the Near-wall Region of Turbulent Flow over Smooth and Rough Boundaries, pp. 41-61. In: *Coherent flow structures in Open Channels* (Ed. by Ashworth, P.J., Bennett, S.J., Best, J.L., McLelland, S.J.). John Wiley and Sons Ltd, Chichester, UK.

Gustavson, T. (1974) Sedimentation on gravel outwash fans, Malaspina Glacier foreland, Alaska. *Journal of Sedimentary Petrology*, 44, 374-389.

Guy, H.P., Simons, D.B., Richardson, E.V. (1966) Summary of alluvial data from flume experiments 1956-61. *U.S. Geological Survey Professional Paper, 462-I*

Gyr, A. and Müller, A. (1996) The role of coherent structures in developing bedforms during sediment transport pp. 227-236. In: *Coherent Flow Structures in Open Channels* (Ed. by Ashworth, P.J., Bennett, S.J., Best, J.L., McLelland, S.J.). John Wiley & Sons, Chichester, UK.

Hand, B. Wessel, J.M., Hayes, M.O. (1969) Antidunes in the Mount Toby Conglomerate (Triassic), Massachusetts. *Journal of Sedimentary Petrology*, 39, 1310-1316.

Hand, B., Middleton, G.V., Skipper, K. (1972) Discussion: Antidune cross-stratification in a turbidite sequence, Cloridorme, Gaspe, Quebec. *Sedimentology*, 18, 135-138.

Hand, B. (1974) Supercritical flow in density currents. *Journal of Sedimentary Petrology*, 44, 637-648.

Harms, J. and Fahnestock, R. (1965) Stratification, bedforms, and flow phenomena (with an example from the Rio Grande), pp. 84-115. In: *Primary Sedimentary structures and their hydrodynamic interpretation*, Society of Economic Palaeontologists and Mineralogists, Special Publication 12 (Ed. by Middleton, G.V.).

Hayashi, T. (1970) Formation of dunes and antidunes in open channels. *Journal of the Hydraulics Division, ASCE*, 96, 357-365.

Heathershaw, A.D. and Thorne, P.D. (1985) Sea-bed noises reveal role of turbulent bursting phenomenon in sediment transport by tidal currents. *Nature*, 316, 339-342.

Hinze, J.O. (1975) *Turbulence*. McGraw-Hill Publishing, New York, USA.

Ho, R. and Gelhar, L. (1983) Turbulent flow over undular permeable boundaries. *Journal of the Hydraulics Division, ASCE*, 109, 741-756.

Hogg, A.J., Dade, W.B., Huppert, H.E., and Soulsby, R.L. (1996) A Model of an Impinging Jet on a Granular Bed, with Application to Turbulent, Event-driven Bedload Transport. In: *Coherent Flow Structures in Open Channels* (Ed. by Ashworth, P.J., Bennett, S.J., Best, J.L., McLelland, S.J.), pp. 101-124. John Wiley and Sons, Chichester, UK.

Hornung, J.J., Asprion, U. and Winsemann, J. (2007) Jet-afflux of a subaqueous ice-contact fan, glacial Lake Rinteln, northwestern, Germany. *Sedimentary Geology*, 193, 167-192.

Huang, L. and Chiang, Y. (2001) The formation of dunes, antidunes and rapidly damping waves in alluvial channels. *International Journal for Numerical and Analytical Methods in Geomechanics*, 25, 675-690.

Hubbell, D.W. and Ali, K.A. (1961) Qualitative effects of temperature on flow phenomena in alluvial channels. *U.S. Geological Survey Professional Paper*, 424-D, D-21-D-23.

Hughes Clarke, J.E., Shor, A.N., Piper, D.J.W., Mayer, L.A. (1990) Large scale current induced erosion and deposition in the path of the 1929 Grand Banks turbidity current. *Sedimentology*, 37, 613-629.

Hunzicker, A.A. (1930) A laboratorical study of antidune traction and the transportation and deposition of ellipsoidal and disk-shaped pebbles. *MA Thesis, University of Wisconsin, USA.*

Jackson, R. (1976) Sedimentological and fluid-dynamic implications of the turbulent bursting phenomenon in geophysical flows. *Journal of Fluid Mechanics*, 77, 531-560.

Jopling, A. and Richardson, E.V. (1966) Backset bedding developed in shooting flow in laboratory experiments. *Journal of Sedimentary Petrology*, 36, 821-825.

Kennedy, J.F.K. (1961) Stationary waves and antidunes in alluvial channels. California Institute of Technology, W.M. Keck laboratory of Hydraulics and Water Resources, Pasadena 146.

Kennedy, J.F.K. (1963) The mechanics of dunes and antidunes in erodible-bed channels. *Journal of Fluid Mechanics*, 16, 521-546.

Kennedy, J.F.K. (1969) The formation of sediment ripples, dunes and antidunes. *Annual Review of Fluid Mechanics*, 1, 147-168.

Kjær, K.H., Sultan, L., Krüger, J. and Schomacker, A. (2004) Architecture and sedimentation of outwash fans in front of the Mýrdalsjökull ice cap, Iceland. *Sedimentary Geology*, 172, 139-163.

Klaven, A.B. and Kopaliana, Z.D. (1974) On the Relationship between the length of dunes with longitudinal dimensions of large-scale turbulence components. *Transactions State Hydrology Institute*, 216, 19-24.

Kline, S.J., Reynolds, W.C., Schraub, F.A. and Runstadler, P.W. (1967) The structure of turbulent boundary layers. *Journal of Fluid Mechanics*, 30, 741–773.

Kolmogorov, A.N. (1941) Dissipation of energy in a locally isotropic turbulence. Doklady Akad. Nauk USSR, 32, 141. (English translation in: American Mathematical Society Translations 1958, 2, 8, 87, Providence R.I)

Kostaschuk, R. and Villard, P. (1996) Flow and sediment transport over large subaqueous dunes: Fraser River, Canada. *Sedimentology*, 43, 849-863.

Koster, E. (1978) Transverse ribs: their characteristics, origin and paleohydraulic significance. In: *Fluvial Sedimentology* (Memoir 5) (Ed. by Miall, A.), pp. 161-186. Society of Petroleum Geologists, Calgary, Alberta.

Kubo, Y. and Nakajima, T. (2002) Laboratory experiments and numerical simulation of sediment-wave formation by turbidity currents. *Marine Geology*, 192, 105-121.

Kubo, Y. and Yokokawa, M. (2001) Theoretical study of breaking of waves on antidunes. In: *Particulate Gravity Currents* (Ed. by Special Publication IAS), pp. 65-70. Blackwell, Oxford, UK.

Lamb, H. (1932) *Hydrodynamics*. Cambridge, Cambridge University Press, Cambridge, UK.

Lane, S.N., Biron, P.M., Bradbrook, K.F., Butler, J.B., Chandler, J.H., Crowell, M.D., McLelland, S.J., Richards, K.S., Roy, A.G. (1998) Three-Dimensional measurement of river channel flow processes using Acoustic Doppler Velocimetry. *Earth Surface Processes and Landforms*, 23, 1247-1267.

Langford, R. and Bracken, B. (1987) Medano Creek, Colorado, A model for upper-Regime fluvial deposition. *Journal of Sedimentary Petrology*, 57, 863-870.

Lapointe, M.F. (1992) Frequency spectra and intermittency of the turbulent suspension process in a sand-bed river. *Sedimentology*, 43, 439-449.

Lapointe, M.F., De Serres, B., Biron, P. and Roy, A.G. (1996) Using spectral analysis to detect sensor noise and correct turbulence intensity and shear stress estimates from EMCM flow records. *Earth Surface Processes and Landforms*, 21, 195-203.

Le Couturier, M.N., Grochowski, N.T., Heathershaw, A., Oikonomou, E. and Collins, M.B. (2000) Turbulent and Macro-turbulent Structures developed in the Benthic Boundary Layer Downstream of Topographic Features. *Estuarine Coastal and Shelf Science*, 50, 817-833.

Leclair, S.F. (2002) Preservation of cross-strata due to the migration of subaqueous dunes: An experimental investigation. *Sedimentology*, 49, 1157-1180.

Lee, A.J. and Ferguson, R.I. (2002) Velocity and flow resistance in step-pool streams. *Geomorphology*, 46, 59-71.

Lee, K. (2004) A Note on Camas Prairie, Or, More Unusual Currents in Glacial Lake Missoula. Field Guide, www.mines.edu/academic/geology/faculty/klee/CamasPrairie.pdf

Leeder, M. (1983) On the interactions between turbulent flow, sediment transport and bedform mechanics in channelised flows. In: *Modern and ancient fluvial systems* (Ed. by Collinson, J. and Lewin, J.), pp. 5-18. Blackwell Scientific Publications, Oxford, UK.

Leeder, M.R. (1999) *Sedimentology and Sedimentary basins: from turbulence to tectonics*. Blackwells, Oxford, UK.

Lenzi, M.A. (2001) Step Pool evolution in the Rio Cordon, northeastern Italy. *Earth Surface Processs and Landforms*, 26, 991-1008.

Leys, C.A. (1983) Volcanic and sedimentary processes during formation of the Saefell tuff-ring, Iceland. *Transactions of the Royal Society of Edinburgh: Earth sciences*, 74, 15-22.

Lister, J.C. (1981) The sedimentology of Camas Prairie Basin and its significance to the Lake Missoula floods Sanders County, Montana. *M.S. Thesis, University of Montana, USA.*

Lohrmann, A., Cabrera, R. and Kraus, M. (1994) Acoustic Doppler Velocimeter (ADV) for Laboratory use. In: *Hydraulic Measurements and Experimentation Proceedings,* Sponsored by the Hydraulic Division/ASCE Held August 1-5, 1994 Buffalo, New York, USA pp 551-365.

Lu, S.S. and Wilmarth, W.W. (1973) Measurements of the structure of the Reynolds stress in a turbulent boundary layer. *Journal of Fluid Mechanics*, 60, 481-511.

Lunt, I.A. and Bridge, J.S. (2004) Evolution and deposits of a gravelly braid bar, Sagavanirktok River, Alaska. *Sedimentology*, 51, 415–432.

Mack, G. McIntosh, W.C., Leeder, M.R., Monger, H.C. (1996) Plio-Pleistocene pumice floods in the ancestral Rio Grande, southern Rio Grande rift, USA. *Sedimentary Geology*, 103, 1-8.

Maddux, T.B. McLean, S.R., Nelson, J.M. (2003) Turbulent flow over three-dimensional dunes: 2. Fluid and bed stresses. *Journal of Geophysical Research*, 108, 11-1-11-17.

Malinverno, A., Ryan, W.B.F., Auffret, G.A., Pautot, G. (1988) Sonar images of the path of recent failure events on the continental margin off Nice, France. *Special Paper - Geological Society of America*, 229, 59-75.

Manville, V., Segschneider, B., White, J.D.L. (2002) Hydrodynamic behaviour of Taupo 1800a pumice: Implications for the sedimentology of remobilized pyroclasts. *Sedimentology*, 49, 955-976.

Martin, V., Fisher, T.S.R., Millar, R.G. and Quick, M.C. (2002) ADV Data Analysis for Turbulent Flows: Low Correlation Problem. In: *Hydraulic Measurement and Experiment Methods 2002*, Proceedings of the Speciality Conference (Eds. Wahl, T.L., Pugh, C.A., Oberg, K.A. and Vermeyen, T.B.), ASCE, Reston, VA.

Massari, F. (1996) Upper-regime stratification types on steep-face, coarse-grained, Gilbert-type progradational wedges (Pleistocene, Southern Italy). *Journal of Sedimentary Research*, 66, 364-375.

Massari, F. and D'Alessandro, A. (2000) Tsunami-related scour-and-drape undulations in Middle Pliocene restricted-bay carbonate deposits (Salento, south Italy). *Sedimentary Geology*, 135, 265-281.

Masuda, F., Yokokawa, M. and Sakamoto, T. (1993) HCS mimics in Pleistocene, tidal deposits of the Shimosa Group and flood deposits of the Osaka Group, Japan. *Journal of the sedimentological Society of Japan*, 39, 27-34.

Mattson, P.H. and Alvarez, W. (1973) Base surge Deposits in pleistocene volcanic ash near Rome. *Bulletin Volcanlogique*, 37, 553-572.

McBride, E.F., Shepard, R.G. and Crawley, R.A. (1975) Origin of parallel, near-horizontal laminae by migration of bed forms in a small flume. *Journal of Sedimentary Petrology*, 45, 132-139.

McConnico, T.S. and Bassett, K.N. (2004) Well preserved 'antidune' deposits and backset beds associated with slumping on the foresets of a gravelly Gilbert-style fan delta, New Zealand. *Geological Society of America: 2004 Denver Annual Meeting*, Paper No. 138-17.

McCracken, W.A. (1969) Sedimentary structures and paleocurrent analysis of Sespe Formation, Ventura Basin, California. *AAPG Bulletin*, 53, 463.

McDonald, B.C. and Banerjee, I. (1971) Sediments and bedforms on a braided outwash plain. *Canadian Journal of Earth Sciences*, 8, 1282-1301.

McDonald, B.C. and Vincent, J.S. (1972) Fluvial Sedimentary Structures formed experimentally in a pipe, and their implications for interpretation of subglacial sedimentary environments. *Geological Survey of Canada*, 72-27, 30pp.

McDonald, B.C. and Day, T.J. (1978) An experimental flume study on the formation of transverse ribs. *Geological Survey of Canada*, 78-1-A, 441-451.

McLean, S.R., Nelson, J.M., Wolfe, S.R. (1994) Turbulence structure over two-dimensional bedforms: Implications for sediment transport. Journal of Geophysical Research, 99, 12729-12747.

McLelland, S.J. and Nicholas, A. (2000) A new method for evaluating errors in high-frequency ADV measurements. *Hydrological Processes*, 14, 366.

Mehrotra, S. (1983) Antidune Movement. *Journal of the Hydraulics Division, ASCE*, 109, 302-304.

Merzkirch, W. (1974) *Flow Visualization*. Academic Press, London, UK.

Middleton, G. (1965) Antidune cross-bedding in a large flume. *Journal of Sedimentary Petrology*, 35, 922-927.

Migeon, S., Savoye, B., Zanella, E., Mulder, T., Faugères, J.C. and Weber, O. (2001) Detailed seismic-reflection and sedimentary study of turbidite sediment waves on the Var Sedimentary Ridge (SE France): significance for sediment transport and deposition and the mechanisms of sediment-wave construction. *Marine and Petroleum Geology,* 18, 179-208.

Morris, S.A., Kenyon, N.H., Limonov, A.F., Alexander, J. (1998) Downstream changes of large-scale bedforms in turbidites around the Valencia channel mouth, north-west Mediterranean: implications for palaeoflow reconstruction. *Sedimentology*, 45, 365-377.

Moscariello, A., Marchi, L., Maraga, F. and Mortara, G. (2002) Alluvial fans in the Italian Alps: sedimentary facies and processes. In: *Flood and megaflood processes and deposits: recent and ancient examples.* Eds: Martini, P., Baker, V.R. and Garzón, G. Special Publication, IAS, 32, 17-35.

Moss, A.J., Walker, P.H. and Hutka, J. (1980) Movement of loose, sandy detritus by shallow water flows: an experimental study. *Sedimentary Geology*, 25, 43-66.

Nakagawa, H. and Tsujimoto, T (1980) Sand bed instability due to bedload motion. *Journal of the Hydraulics Division, ASCE*, HY12, 2029-2051.

Nakayama, K. and Yoshikawa, S. (1997) Depositional processes of primary to reworked volcaniclastics on an alluvial plain; an example from the Lower Pliocene Ohta tephra bed of the Tokai Group, central Japan. *Sedimentary Geology*, 107, 211-229.

Nelson, J., McLean, S.R. and Wolfe, S.R. (1993) Mean flow and turbulence fields over Two-dimensional bed forms. *Water Resources Research*, 29, 3935-3953.

Nelson, J., Shreve, R.L., McLean, S.R., Drake, T.G. (1995) Role of near-bed turbulence structure in bed load transport and bed form mechanics. *Water Resources Research*, *31*, 8, 2086.

Nemec, W. (1990) Aspects of sediment movement on steep delta slopes. In: *Coarse Grained Deltas,* Eds: Colella, A. and Prior, D.B. *Special Publication IAS,* 10, 29-73.

Nicholas, A.P. (2005) Computational fluid dynamics modelling of boundary roughness in gravel-bed rivers: an investigation of the effects of random variability in bed elevation. *Earth Surface Processes and Landforms* 26, 345 –362.

Nikora, V. and Goring, D. (1998) ADV measurements of turbulence: Can we improve their interpretation? *Journal of Hydraulic Engineering*, 124, 630-634.

Nordin, C.F. (1963) A preliminary study of sediment transport parameters Rio Puerco near Bernardo, New Mexico. *U.S. Geological Survey Professional Paper,* 462-C, p. C1-C21.

Normark, W.R., Hess, G.R., Stow, D.A.V. and Bowen, A.J. (1980) Sediment waves on the Monterrey Fan Levee: A preliminary physical interpretation. *Marine Geology*, 37, 1-18.

Nezu, I. and Nakagawa, H. (1993) Turbulence in Open-channel flows. IAHR monograph, A.A. Balkema, Rotterdam, Netherlands.

Ohtsu, I. Yasuda, Y. and Gotoh, H. (2003) Flow conditions of undular Hydraulic jumps in horizontal rectangular channels. *Journal of Hydraulic Engineering, ASCE*, 129, 948-955.

Owens, J. (1908) Experiments of the transporting power of sea currents. *Geological Journal*, 31, 424.

Paiement-Paradis, G., Buffin-Bélanger, T. and Roy, A.G. *(*2003) Scalings for large turbulent structures in gravel-bed rivers. *Geophysical Research Letters*, 30, 1773-1777.

Panin, N and Panin, ST. (1967) Regressive sand waves on the Black Sea shore. *Marine Geology*, 5, 221-226.

Paola, C. Wiele, S.M. and Reinhart, M.A. (1989) Upper-regime parallel lamination as the result of turbulent sediment transport and low-amplitude bed forms. *Sedimentology*, 36, 47-59.

Papanicolaou, A.N. (2000) The Role of Near-Bed Turbulence in the Inception of Particle Motion. *International Journal of Fluid Dynamics*, 4, online: http://elecpress.monash.edu.au/ijfd/2000_vol4/paper2/paper.html .

Paphitis, D. and Collins, M.B. (2001) The 5m long recirculating flume at the SOES, University of Southampton Part II: Flow characteristics. Internal Document No. 68, 76pp. SOES, University of Southampton, UK.

Parker, G. (1975) Sediment inertia as a cause of river antidunes. *Journal of the Hydraulics Division, ASCE*, 101, 211-221.

Peakall, J., Ashworth, P.J., and Best, J.L. (1996) Physical modelling in fluvial geomorphology: Principles, applications and unresolved issues. In: *The Scientific Nature of Geomorphology: Proceedings of the 27th Binghampton Symposium in Geomorphology* (Ed. by Rhoads, B. and Thorn, C.), pp. 221-253. John Wiley & Sons Ltd, Chichester, UK.

Pickering, K.T. and Hiscott, R.N. (1985) Contained (reflected) turbidity currents from the Middle Ordovician Cloridorme Formation, Quebec, Canada: an alternative to the antidune hypothesis. *Sedimentology*, 32, 373-394.

Pickering, K.T. (1995) Are enigmatic erosional sandy wave-like bedforms in Jurassic Bridport Sands, Dorset, due to standing waves? *Journal of the Geological Society, London*, 152, 481-485.

Pickering, K.T., Hodgson, D.M., Platzman, E., Clark, J.D., Stephens, C. (2001) A new type of bedform produced by backfilling process in a

submarine channel, Late Miocene, Tabernas-Sorbas Basin, SE Spain. *Journal of Sedimentary Research*, A71, 692-704.

Pierson, T.C. and Scott, K.M. (1985) Downstream dilution of a Lahar: Transition from debris flow to a hyperconcentrated streamflow. *Water Resources Research*, 21, 1511-1524.

Piper, D.J.W. and Kontopoulos, N. (1994) Bed forms in submarine channels: comparison of ancient examples from Greece with studies of recent turbidite systems. *Journal of Sedimentary Research*, A64, 247-252.

Power, W.R. (1961) Backset beds in the coso formation, Inyo County, California. *Journal of sedimentary Petrology*, 31, 603-607.

Prave, A. (1990) Clarification of some misconceptions about antidune geometry and flow character. *Sedimentology*, 37, 1019-1052.

Prave, A. and Duke, W. (1990) Small-scale hummocky cross-stratification in turbidites: a form of antidune stratification. *Sedimentology*, 37, 531-539.

Prinos, P. (1995) Bed-suction effects on structure of turbulent open-channel flow. *Journal of Hydraulic Engineering*, 121, 404-412.

Raudkivi, A.J. (1966) Bedforms in alluvial channels. *Journal of Fluid Mechanics*, 26, 15-33.

Raudkivi, A.J. and Witte, H.H. (1990) Development of bed features. *Journal of Hydraulic Engineering*, 116, 1063-1079.

Reinheck, H. and Singh, I.B. (1973) *Depositional Sedimentary Environments*. Springer-Verlag, Berlin, Germany.

Reynolds, A. (1965) Waves on the erodible bed of an open channel. *Journal of Fluid Mechanics*, 22, 113-133.

Rice, J.W., Parker, T.J., Russell, A.J. and Knudson, O. (2002) Morphology of fresh outflow channels on Mars. 33rd Lunar and Planatary Science Conference, March 11th – 15th 2002, Pasadena, California, USA.

Richards, K.J. (1980) The formation of ripples and dunes on an erodible bed. *Journal of Fluid Mechanics*, 99, 597-618.

Robillard L. (1965) Free surface flow over a wavy bed. Unpub. MSc Thesis, MIT, USA.

Robillard L. and Kennedy, J.F. (1967) Some experimental observations on free surface flow over a wavy boundary. In: Proceedings 12th Conference IAHR, Vol. 1, pp. 41-48. Fort Collins, Colorado, USA.

Robinson, S.K. (1991) Coherent motions in the turbulent boundary layer. *Annual Review of Fluid Mechanics*, 23, 601-639.

Rowley, P.D., MacLeod, N.S., Kuntz, M.A and Kaplan, A.M. (1985) Proximal bedded deposits related to pyroclastic flows of May, 1980, Mount St. Helens, Washington. Geological Society of America Bulletin, 96, 1373-1383.

Roy, A.G., Buffin-Bélanger, T., and Deland, S. (1996) Scales of Turbulent Coherent Flow Structures in a Gravel-bed River. In: *Coherent Flow Structures in Open Channels* (Ed. by Ashworth, P.J., Bennett, S.J., Best, J.L., McLelland, S.J.), pp. 147-183. John Wiley and Sons, Chichester, UK.

Roy, A.G., Buffin-Bélanger, T., Lamarre, H., and Kirkbride, A.D. (2004) Size, shape and dynamics of large-scale turbulent flow structures in a gravel-bed river. *Journal of Fluid Mechanics,* 500, 1-27.

Russell, A.J. (2005) The geomorphological and sedimentary impact of jökulhlaups skeiðarársandur. In: *Rekonstrukcja Procesow Glacjalnych W Wybranych Strefach Marginalnych Lodowcow Islandii – Formy I Osady Islandia* (*Reconstruction of glacial processes in the chosen marginal zones of the Icelandic glacial deposits*), 14-28 Sierpnia 2005. Toruñ, Poland: Instytut Geografi UMK, 2005, pp73-96 (In English).

Russell, A.J., Tweed, F.S., Harris, T., Marren, P.M., Roberts, M.J. Fay, H. and Mountney, N.P. (2002) Icelandic Glaciers: Expedition Report 2002, University of Newcastle, UK.

Russell, A.J., Tweed, F.S., Harris, T., Marren, P.M., Roberts, M.J. and Cassidy, N.J. (2003) Icelandic Glaciers: Expedition Report 2003, University of Newcastle, UK.

Russell, H.A.J. and Arnott, R.W.C. (2003) Hydraulic Jump and Hyperconcentrated Flow Deposits of a Glacigenic Subaqueous Fan: Oak Ridges Moraine, Southern Ontario. *Journal of Sedimentary Research*, 73, 887-905.

Rust, B. R. and Gostin, V.A. (1981) Fossil transverse Ribs in Holocene alluvial fan deposits, Depot Creek, Australia. *Journal of Sedimentary Petrology,* 51, 441-444.

Rust, B. R. and Gibling, M.R. (1990) Three-dimensional antidunes as HCS mimics in a fluvial sandstone: The Pennsylvanian South Bar formation near Sydney, Nova Scotia. *Journal of Sedimentary Petrology,* 60, 540-548.

Saunderson, H. and Lockett, F. (1983) Flume experiments on bedforms and structures at the dune-plane bed transition. In: *International. Association of Sedimentologists: Special Publication 6 Modern and Ancient Fluvial Systems,* Eds. Collinson, J.D. and Lewin, J. pp. 49-58.

Schminke, H., Fisher, R.V., Waters, A.C. (1973) Antidune and chute and pool structures in the base surge deposits of the Laacher See area, Germany. *Sedimentology*, 20, 553-574.

Schwartz, R.K. (1982) Bedform and stratification characteristics of some modern small-scale washover sand bodies. *Sedimentology*, 29, 835-849.

Segschneider, B., Landis, C.A., Manville, V., White, J.D.L. and Wilson, C.J.N. (2002) Environmental response to a large, explosive rhyolite eruption: sedimentology of post-1.8 ka pumice-rich Taupo volcaniclastics in the Hawke's Bay region, New Zealand. *Sedimentary Geology*, 150, 275-299.

Shaw, J. and Kellerhals, R. (1977) Paleohydraulic interpretation of antidune bedforms with applications to antidunes in gravel. *Journal of Sedimentary Petrology*, 47, 257-266.

Shiki, T. and Yamazaki, T. (1996) Tsunami-induced conglomerates in Miocene upper bathyal deposits, Chita Peninsula, central Japan. *Sedimentary Geology*, 104, 175-188.

Shvidchenko, A.B. and Pender, G. (2001) Macroturbulent structure of open-channel flow over gravel beds. *Water Resources Research*, 37, 709-719.

Simon, A. and Hardison, J.H. (1994) Critical and supercritical flows in two unstable mountain rivers, Toutle River System, Washington. In: *Hydraulic Engineering '94: Proceedings of the 1994 Conference of the Hydraulics Division*, (Eds Cotroneo, G. V. and Rumer, R. R.), 742–746, American Society of Civil Engineers, New York, USA, 1994.

Simons, D.B., Richardson, E.V., and Albertson, M.L. (1961) Flume studies using medium sand (0.45mm): Studies of flow in Alluvial channels: A comprehensive study of fluvial hydraulics. *U.S. Geological Survey Water-Supply paper*, 1498-A.

Simons, D.B. and Richardson, E.V. (1963) Forms of bed roughness in alluvial channels. *Transactions of the ASCE*, 128, 284-323.

Simons, D.B., Richardson, E.V. and Nordin, Jr. C.F. (1965) Sedimentary structures generated by flow in alluvial channels. In Middleton, G.V., ed., Primary Sedimentary Structures and their Hydrodynamic Interpretation: *SEPM Special Publication* 12, p. 34-52.

Simons, D.B. and Richardson, E.V. (1971) *River Mechanics: Flow in Alluvial Sand Channels*. Privately Published, Fort Collins, Colorado, USA.

Skipper, K. (1971) Antidune cross-stratification in a turbidite sequence, Cloridorme formation, Gaspe, Quebec. *Sedimentology*, 17, 51-68.

Skipper, J.A., Ward, D.J. and Johnson, A. (1998) A rapid, lightweight sediment peel technique using polyurethane foam. *Journal of Sedimentary Research*, 68, 516–518.

Smit, A.J. and Lim, T.T. (1997) *Flow Visualization: techniques and examples*. Imperial College Press, London, UK.

Smith, C.R. (1996) Coherent Flow Structures in Smooth-wall Turbulent Boundary layers: Facts, Mechanisms and speculation. In: Coherent Flow Structures in Open Channels (Ed. by Ashworth, P.J., Bennett, S.J., Best, J.L., McLelland, S.J.), pp. 1-39. John Wiley and Sons, Chichester, UK.

Southard, J.B. and Boguchwal, L.A. (1990) Bed configurations in steady unidirectional water flows. Part 2: synthesis of Flume Data. *Journal of Sedimentary Petrology*, 60, 658-679.

Southard, J.B. (1971) Representations of bedforms in depth-velocity-size diagrams. *Journal of Sedimentary Petrology*, 41, 903-915.

Strom, K.B. and Papanicolaou, A.N. (2007) ADV Measurements around a Cluster Microform in a Shallow Mountain Stream. *Journal of Hydraulic Engineering*, 133, 1379-1389.

Sukhodolov, A., Thiele, M. and Bungartz, H. (1998) Turbulence structure in a river reach with sand bed. *Water Resources Research*, 34, 1317-1334.

Thompson, C.E.L. Amos, C.L., Jones, T.E.R., Chaplin, J. (2003) The manifestation of Fluid-transmitted Bed Shear Stress in a Smooth Annular Flume - a Comparison of Methods. *Journal of Coastal Research*, 19, 1094-1103.

Twenhofel, W. (1950) *Principles of Sedimentation* . McGraw-Hill, New York, USA.

Venditti, J.G. and Bauer, B.O. (2005) Turbulent flow over a dune: Green River, Colorado. *Earth Surface Processes and Landforms*, 30, 289-304.

Venditti, J.G., Church, M. and Bennett, S.J. (2005) On the transition between 2D and 3D dunes. *Sedimentology*, 52, 1343-1359.

Voulgaris, G. and Trowbridge, J. (1998) Evaluation of the Acoustic Doppler Velocimeter (ADV) for Turbulence measurements. *Journal of Atmospheric and Oceanic Technology*, 15, 272-289.

Wahl, T.L. (2000) Analysing ADV Data using WinADV. In: *2000 Joint Conference on Water Resources Engineering and Water Resources Planning & Management, July 30th – August 2nd 2000*. Minneapolis, Minnesota, USA.

Wahl, T.L. (2003) Discussion of "Despiking Acoustic Doppler Velocimeter Data" by Derek G. Goring and Vladimir I. Nikora (2002), *Journal of Hydraulic Engineering,* 128, 117-126. *Journal of Hydraulic Engineering,* 129, 484-488.

Walker, R. (1967) Upper flow regime bed forms in turbidites of the Hatch Formation, Devonian of New York State. *Journal of Sedimentary Petrology*, 37, 1052-1058.

Whittaker, J. and Jaeggi, M. (1982) Origin of Step-Pool systems in mountain streams. *Journal of the Hydraulics Division, ASCE*, 108, 758-773.

Wieprecht, S. (2000) Development and Behaviour of Bed Forms of Coarse Bed Material. University of Federal Armed Forces, Institute of Hydraulics, Vol. 74. Oldenbourg Verlag, 153 pp (in German).

Wilcock, P.R. (1993) critical shear stress of natural sediments. *Journal of Hydraulic Engineering*, 119, 491-505.

Wilcock, P. (2000) The flow, the bed, and the transport: Interaction in flume and field. In: *Gravel-bed Rivers V* (Ed. by Mosley, M.), pp. 183-219. New Zealand Hydrological Society, Wellington, New Zealand.

Wilcock, P., Kenworthy, S.T., Crowe, J.C. (2001) Experimental study of the transport of mixed sand and gravel. *Water Resources Research*, 37, 3349-3358.

Wilcox, A.C. and Wohl, E.E. (2007) Field measurements of three-dimensional hydraulics in a step-pool channel. *Geomorphology*, 83, 215-231.

Williams, G.P. (1970) Flume width and water depth effects in sediment-transport experiments. *U.S. Geological Survey Professional Paper*, 562-H.

Williams, J.J. Thorne, P.D.; Heathershaw, A.D. (1989) Measurements of turbulence in the benthic boundary layer over a gravel bed. *Sedimentology*, 36, 959-971.

Williams, J.J. (1996) Turbulent flow in rivers. In: *Advances in fluvial dynamics and stratigraphy* (Ed. by Carling, P.A. and Dawson, M.R.), pp. 1-32. John Wiley and Sons, Chichester, UK.

Wilmarth, W.W. and Lu, S.S. (1972) Structure of the Reynolds stress near the wall. *Journal of Fluid Mechanics*, 54, 39–48.

Wooldridge, C.L. and Hicken, E.J. (2002) Step-pool and Cascade morphology, Mosquito Creek, British Colombia: a test of four analytical techniques. *Canadian Journal of Earth Sciences*, 39, 493-503.

Wren, D.G., Bennett, S.J., Barkdoll, B.D. and Kuhnle, R.A. (2005) Distributions of velocity, turbulence, and suspended sediment over low-relief antidunes. *Journal of Hydraulic research*, 43, 3-11.

Wunderlich, F. (1972) Georgia Coastal Region, Sapelo Island, U.S.A.: Sedimentology and Biology. *Senckenbergiana Maritima*, 4, 15-45.

Wynn, R.B., Weaver, P.E., Ercilla, G., Stow, D.A.V. and Masson, D.G. (2000) Sedimentary processes in the Selvage sediment-wave field, NE Atlantic: new insights into the formation of sediment waves by turbidity currents. *Sedimentology*, 47, 1181-1197.

Wynn, R.B., Piper, D.J.W. and Gee, J.R. (2002) Classification and characterisation of deep-water sediment waves. *Marine Geology*, 192, 7-22.

Wynn, R.B. and Stow, D.A.V. (2002) Classification and characterisation of deep-water sediment waves. *Marine Geology*, 192, 59-78.

Yagishita, K. and Taira, A. (1989) Grain fabric of a laboratory antidune. *Sedimentology*, 36, 1001-1005.

Yagishita, K. (1994) Antidunes and traction-carpet deposits in deep-water channel sandstones, Cretaceous, British Columbia, Canada. *Journal of Sedimentary Research*, A64, 1, 34-41.

Yagishita, K. (1995) Antidunes in a small gorge on the beach sand, the Sanriku Coast, northeast Japan. *Journal of the sedimentological Society of Japan*, 42, 21-28.

Yagishita, K., Arakawa, S. and Taira, A. (2004) Grain fabric of hummocky and swaley cross-stratification. *Sedimentary Geology*, 78, 181–189.

Yalin, M.S. (1972) *Mechanics of sediment transport*. Pergamon, Oxford, UK.

Yalin, M.S. (1992) *River Mechanics*. Pergamon, Oxford, UK.

Yokokawa, M., Masuda, F., Sakai, T., Endo, N., Kubo, Y. (2000) Sedimentary structures and Grain Fabric of antidune cross-stratification in an experimental flume with sediment supply: the origin of HCS mimics. Unpublished Manuscript.

Zielinski, T. (1982) Contemporary high-energy flows, their deposits and reference to outwash depositional model. Prace Naukowe Uniwersytetu Slaskiego NR519, Geologia, 6, 98-110 (In Polish).

Zimmermann, A. and Church, M. (2001) Channel morphology, gradient profiles and bed stress during flood in a step-pool channel. *Geomorphology*, 40, 311-327.

Appendix A

A.1 Spectral Plots for 0.025, 0.050 and 0.075 m amplitude Gravel Antidune bedforms (25 Hz)

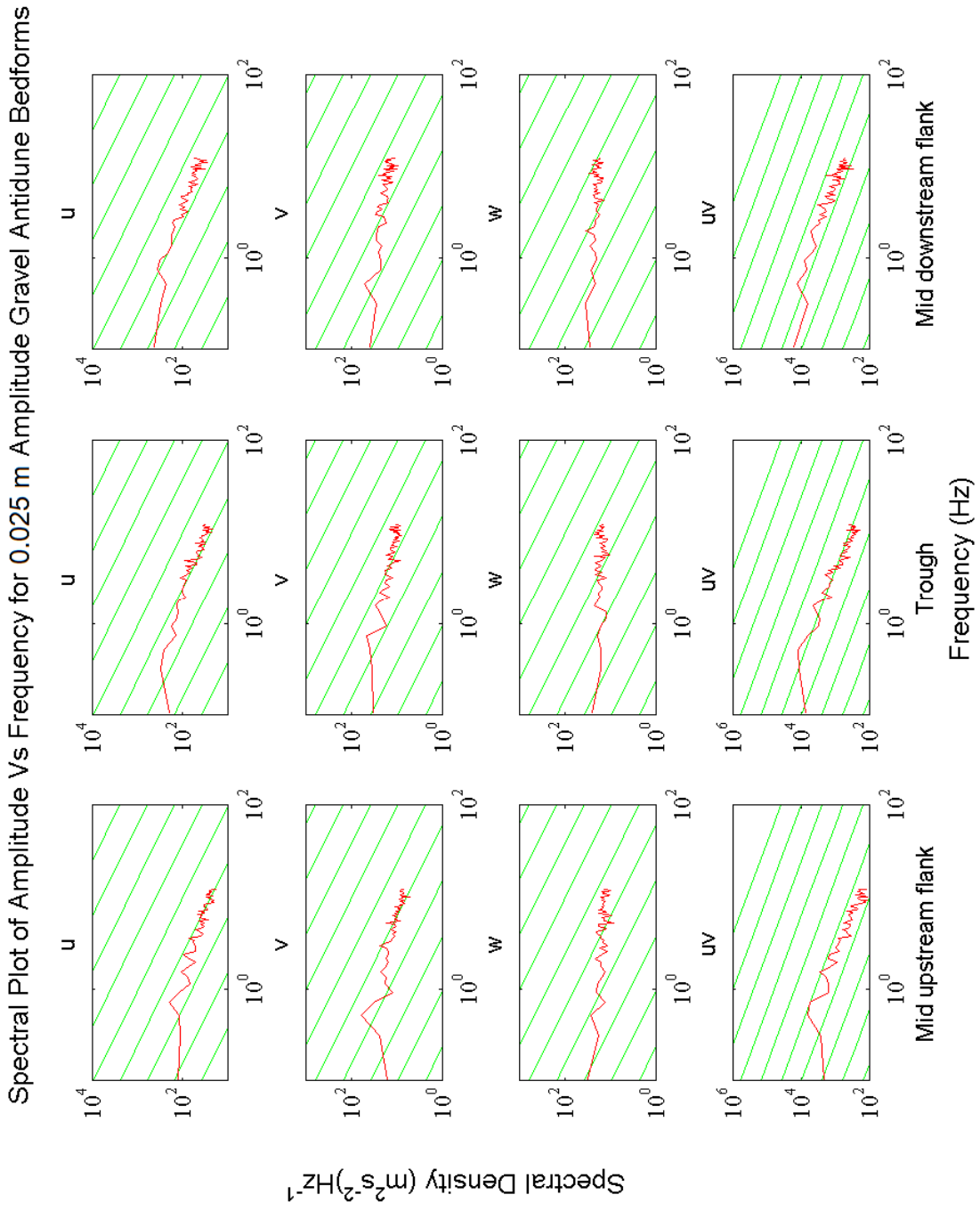

Figure A.1 Spectral Plots for 0.025 m Amplitude Gravel Antidune, 180 s Record (ADV:25 Hz)

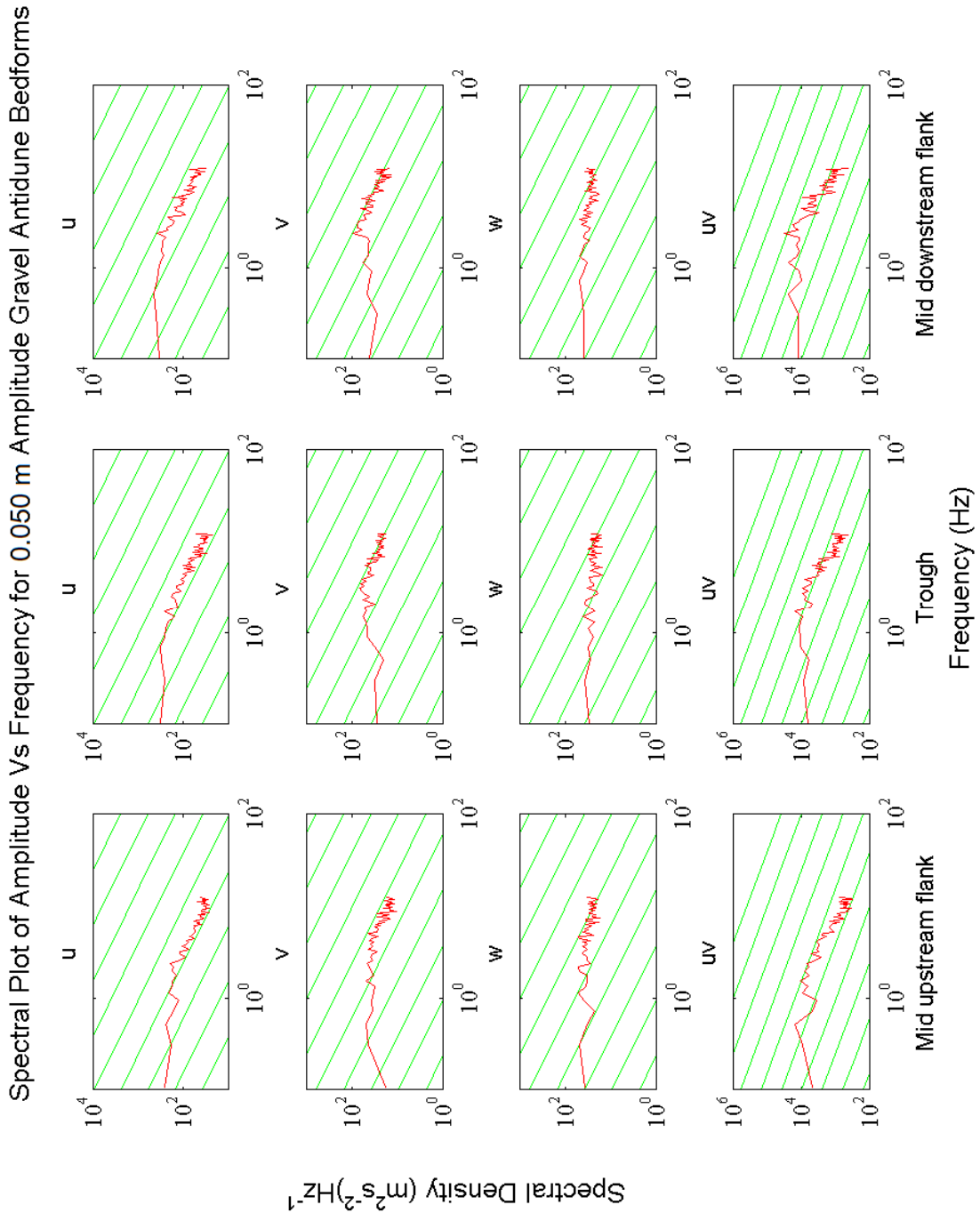

Figure A.2 Spectral Plots for 0.050 m Amplitude Gravel Antidune, 180 s Record (ADV:25 Hz)

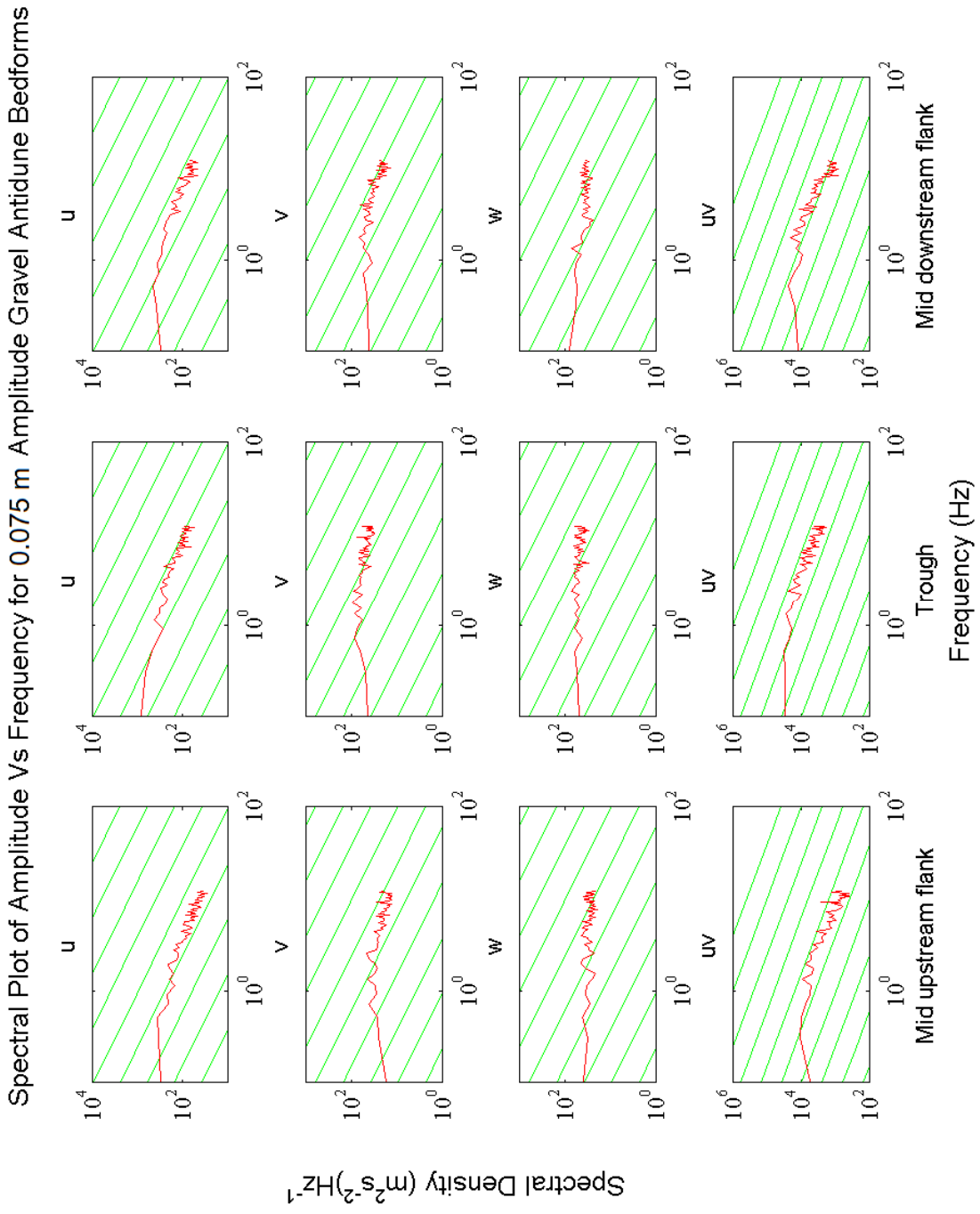

Figure A.3 Spectral Plots for 0.075 m Amplitude Gravel Antidune, 180 s Record (ADV:25 Hz)

A.2 Spectral Plots for 0.025 and 0.050 m Amplitude Openwork-Gravel Antidune Bedforms (25 Hz)

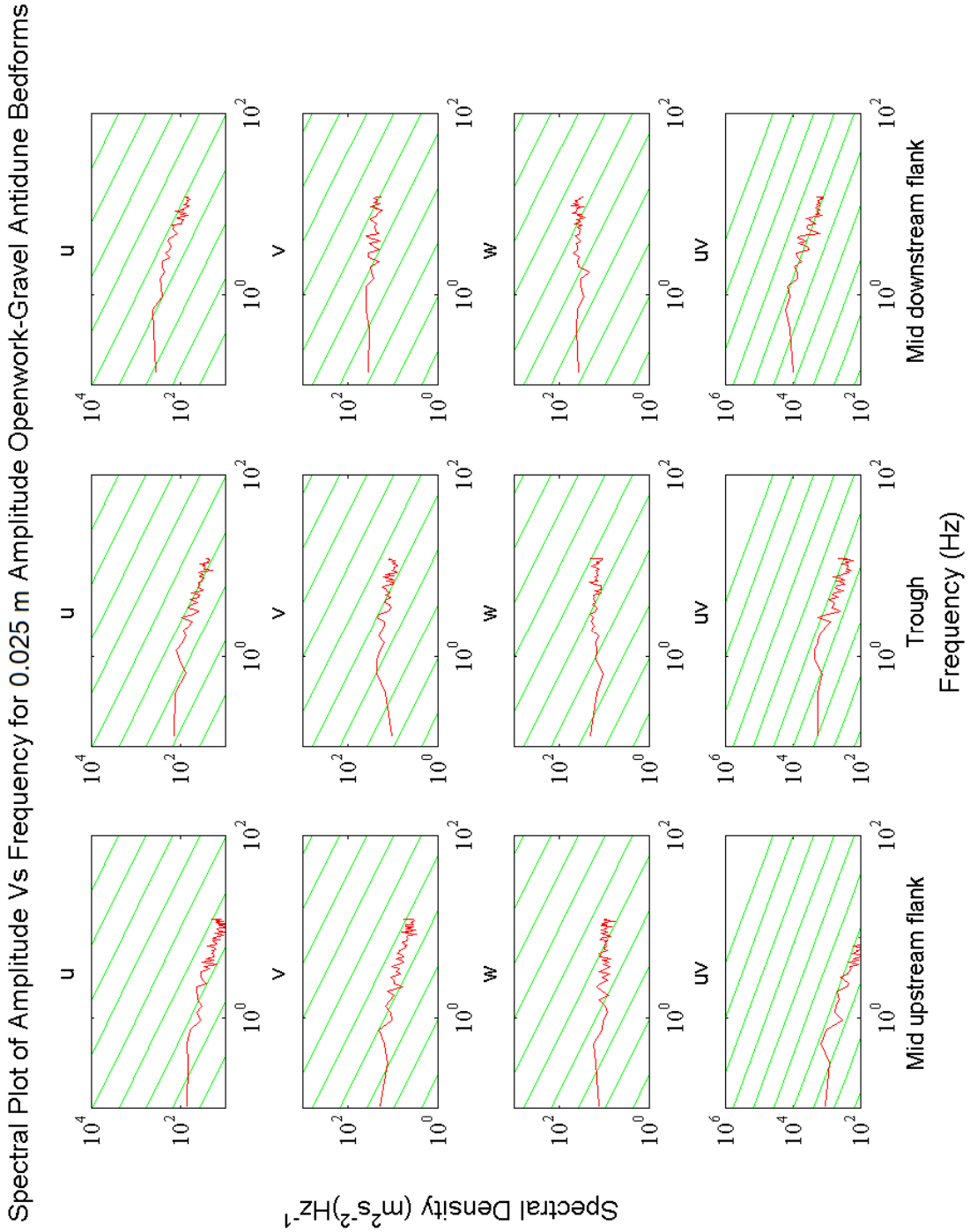

Figure A.4 Spectral Plots for 0.025 m Amplitude Openwork-Gravel Antidune, 180 s Record (ADV:25 Hz)

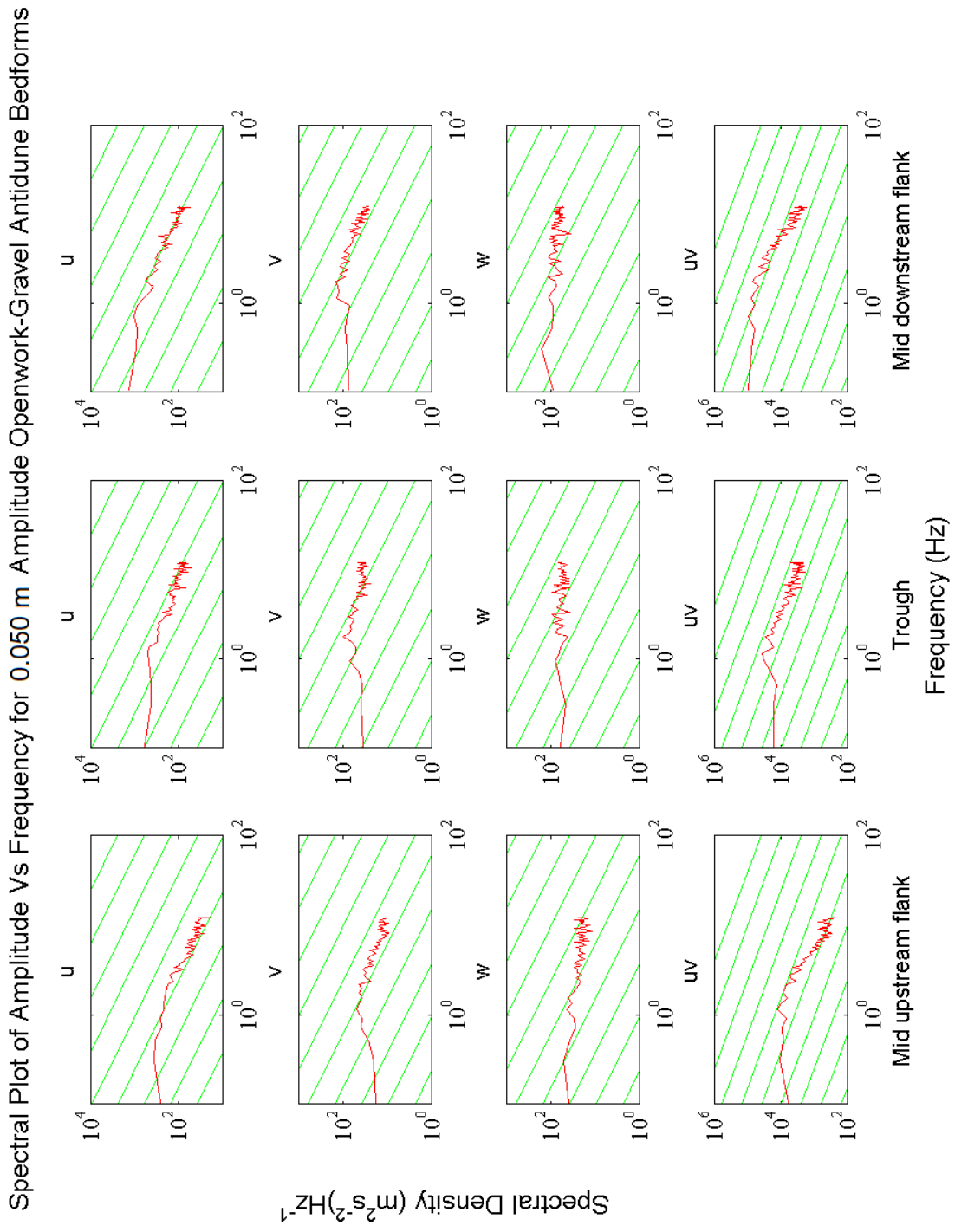

Figure A.5 Spectral Plots for 0.050 m Amplitude Openwork-Gravel Antidune, 180 s Record (ADV:25 Hz)

A.3 Spectral Plots for 0.025, 0.050 and 0.075 m Amplitude Sand Antidune Bedforms (25 Hz)

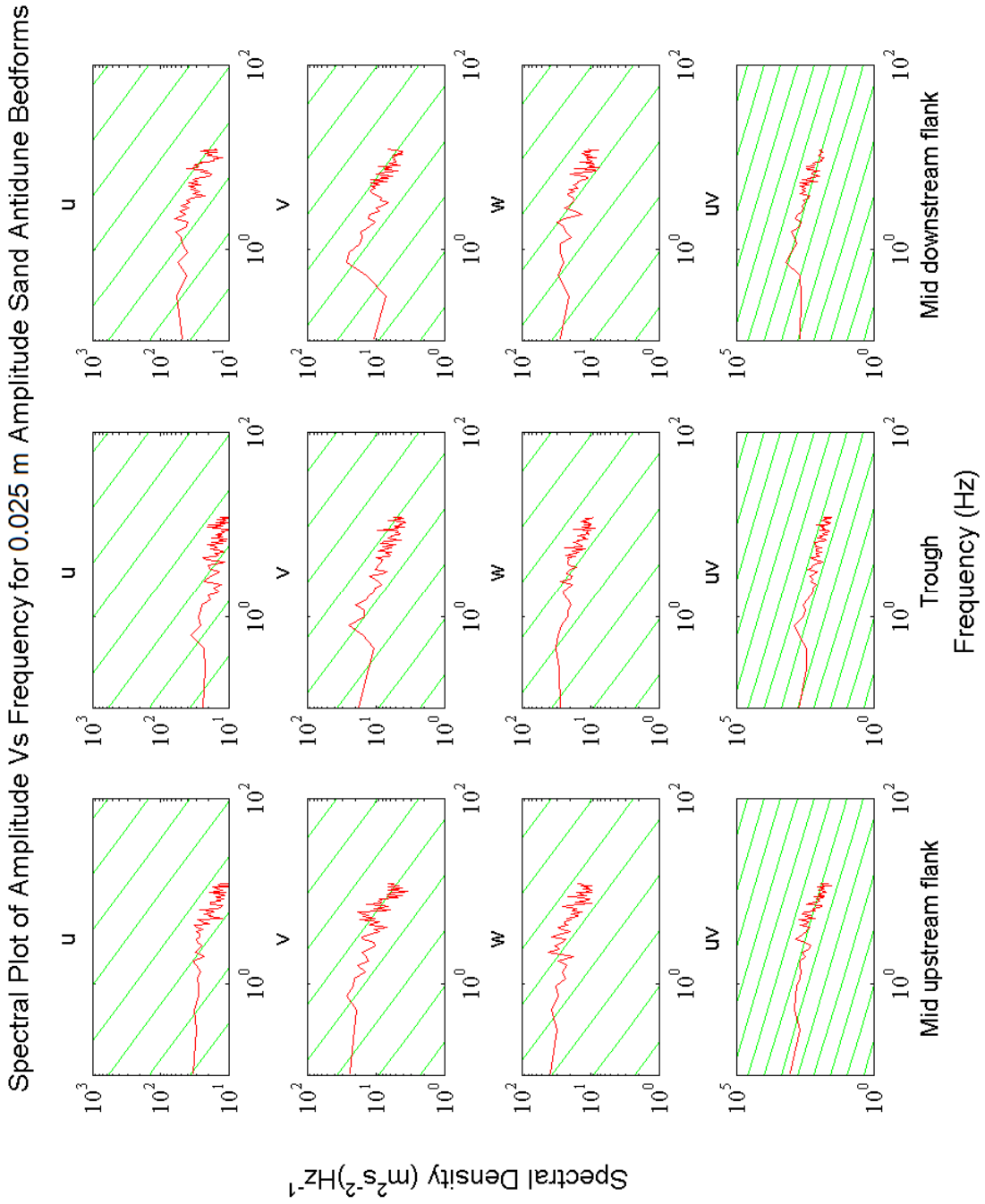

Figure A.6 Spectral Plots for 0.025 m Amplitude Sand Antidune, 180 s Record (ADV:25 Hz)

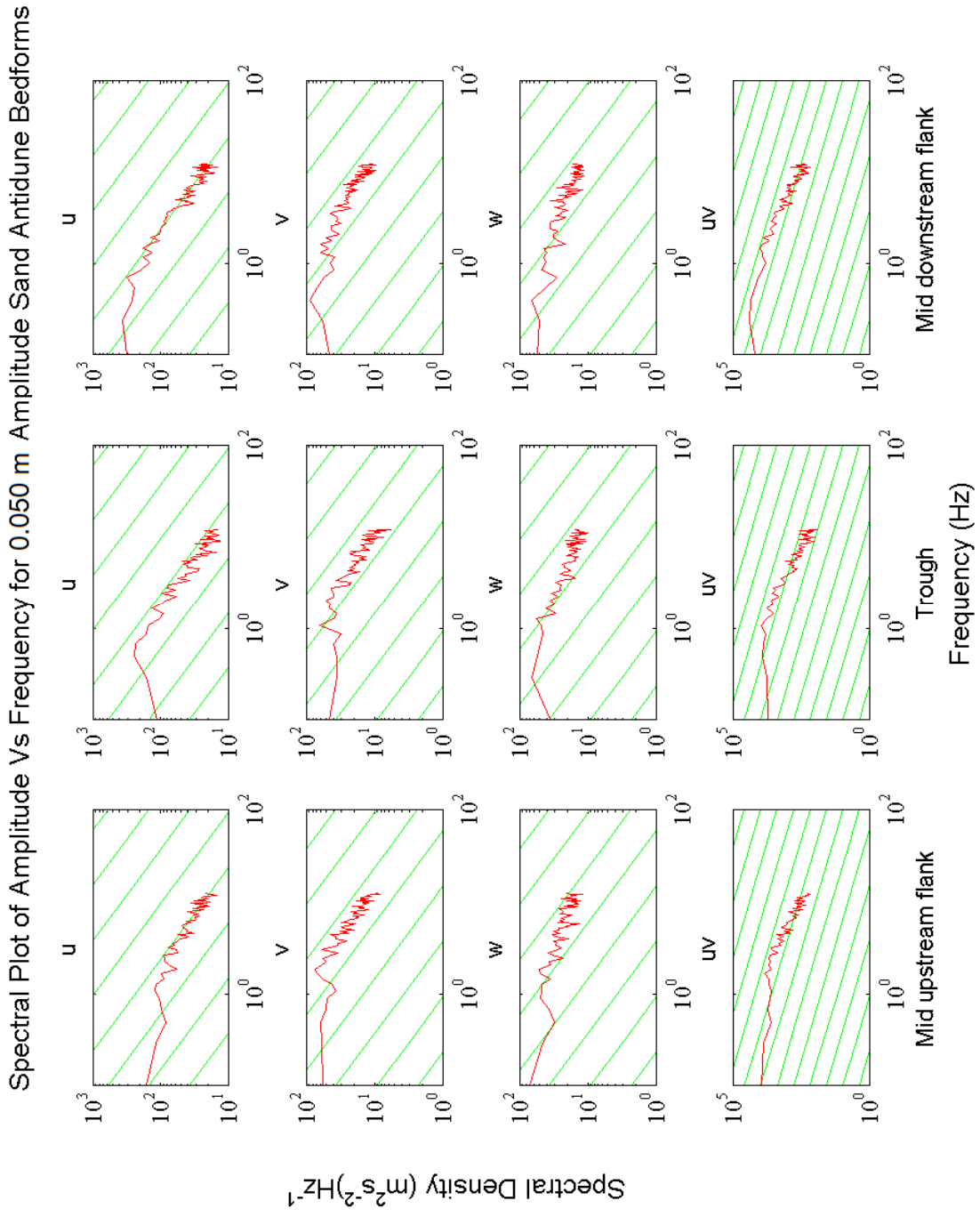

Figure A.7 Spectral Plots for 0.050 m Amplitude Sand Antidune, 180 s Record (ADV:25 Hz)

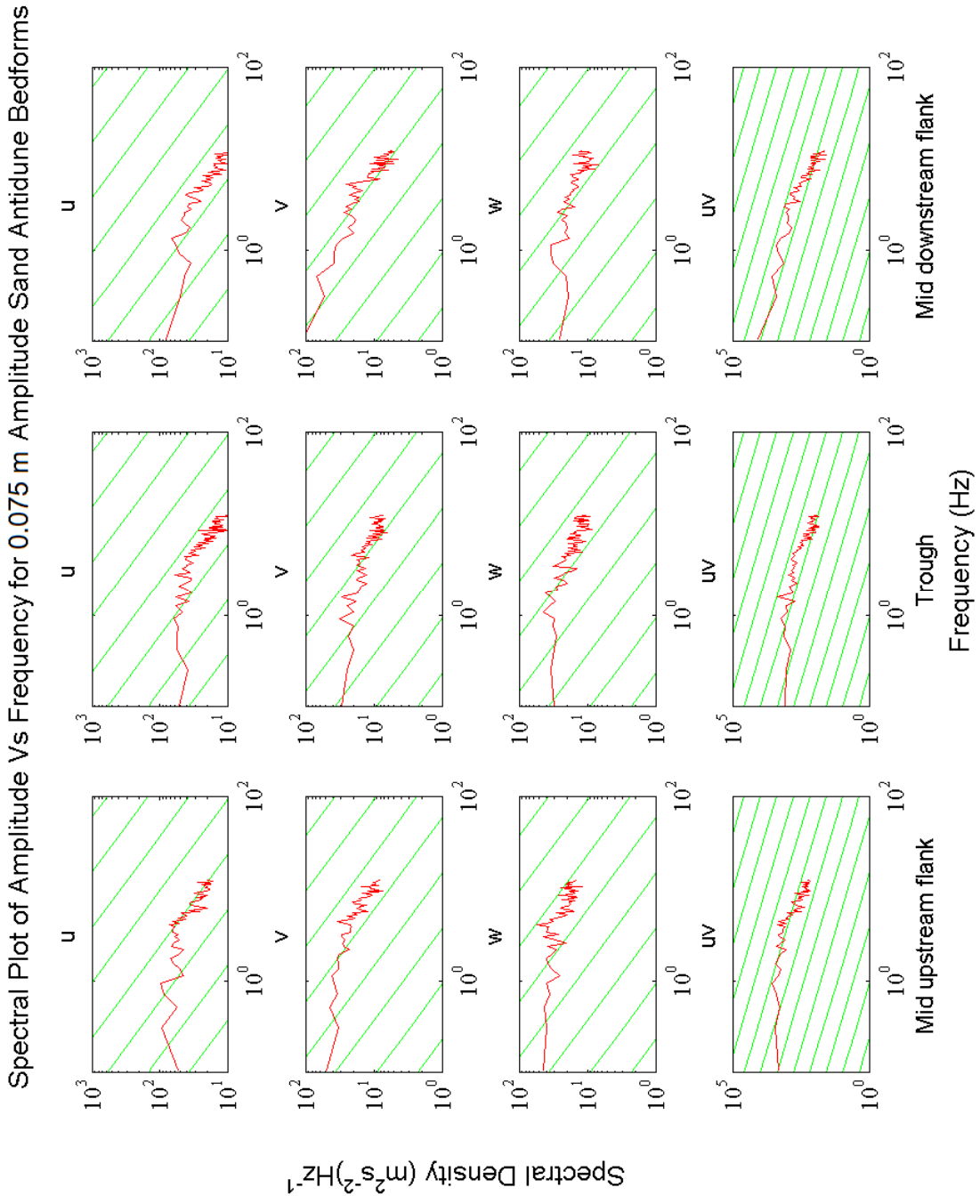

Figure A.8 Spectral Plots for 0.075 m Amplitude Sand Antidune, 180 s Record (ADV:25 Hz)

Appendix B

Appendix for Section 6 [DVD of Run 2 Labile bed run in insert inside back cover]

Table B.1 Observations from Footage of Flume Experiment

Time	Observation
00.14	Video starts, small standing waves are visible on concrete bedform
00.41	Vibratory feeder turned on, initially the depth is not obvious, and the water surface fluctuates.
01.00	Sediment starts appearing in footage, the standing wave becomes smoother and moves downstream a little.
02.01	Deposition becomes apparent with large particles moving along the bed, the standing wave starts moving.
02.12	Depth is an even 0.04 m, flow becomes smoother
02.14	An antidune starts forming; 'jerky' wedges of sediment can be seen moving across the upstream side.
03.48	[flow 0.04 m deep]
04.13	Antidune starts to aggrade faster and moves upstream slowly.
04.48	A raised standing wave appears.
05.55	Initial antidune has moved upstream and disappears off-shot. A second antidune appears on far left.
06.16	There are two standing waves in the picture frame as antidunes continue to move upstream.
06.25	Rapid gain in each antidune's and standing wave's h.
06.29	Antidunes rapidly move upstream and further increase in h.
06.32	Antidune becomes much steeper, standing waves become almost angular.
06.38	Standing wave becomes much more angular, can see sediment pushed out of trough upstream, and up onto flanks of downstream antidune crest.
06.44	Lots of splashing from standing waves.
06.57	Water around steep standing wave in centre very jerky.
07.12	The second remaining standing wave flattens out.
07.31	Both antidunes have moved up to right, one completely off screen, and one at 3/4 of the way to right.
07.33	Suddenly the (stationary) standing wave steepens up again.
07.36	Very sudden steepening of standing wave.
07.43	Standing wave and antidune stationary clear deposition on upstream flank.
07.46	Third antidune starts to appear on far left of screen.
08.02	Bed is flattening out as is water surface, but still with two large steep standing waves in the centre of the screen.
08.13	Flat USPB and openwork gravel are being deposited.
08.16	Water surface and bed surface are level.
08.22	Magnetite added.
08.32	More magnetite added.
09.16	Flat USPB conditions, gravel appears to be much more openwork now.
10.09	[0.02 m of openwork gravel, flow appears to be 0.03 m deep]
11.09	[0.03 m of openwork gravel, flow appears to be 0.03 m deep]
12.59	[0.04 m of openwork gravel, flow appears to be 0.025 m deep]
13.44	Feedrate upped from 25% to 35% (calibrated)

14.13	[0.065 m of openwork gravel]
15.06	Magnetite added.
15.16	Magnetite added.
15.34	Magnetite added.
17.17	[0.11 m of openwork gravel, flow appears to be 0.025 m deep]
18.51	[0.125 m of openwork gravel, flow appears to be 0.025 m deep]
19.28	Water depth decreasing still.
20.14	Water depth/velocity re-established.
20.24	Bed and water surfaces start to undulate again.
20.36	Antidunes start to form.
20.43	Aggrading on upstream side is clear, moving upstream slowly
20.59	More pronounced standing waves starts to appear. One on the left, one on right the right of screen.
21.04	Antidunes moving upstream at 0.06 m in 10 s.
21.05	Standing waves become very pronounced.
21.08	Standing wave on left breaks.
21.09	Wave has broken, water surface flat but turbulent.
21.17	Upstream standing wave had broken too, Bed and water surface flatten out.
21.25	Erosion on left hand side.
21.29	Erosion on right hand side.
21.38	Standing wave starts to appear on right hand side, standing wave and trough moving upstream.
21.40	Standing wave and antidune appear on the left, migrating upstream.
21.48	Standing wave on antidune that's just moved into view from left starts to steepen.
21.50	Standing wave progressively steepens.
21.51	Standing wave breaks upstreamwards.
21.52	Standing Wave fully broken, considerable erosion to the bed.
21.59	Rapid erosion and flattening of the bed.
22.19	Rapid bed aggradation.
22.35	Standing wave starts to appear on left and right of screen.
22.40	Standing waves move upstream, leaving just one in view.
22.49	Standing waves move upstream, another comes into view from left.
23.03	Further movement upstream.
23.07	Messy (antidune?) flow some deposition.
23.45	Pump turned off, flow decreases gradually.
24.00	Flow stops.
24.14	[sound of flume sump overfilling and spilling with excess water from flume]
24.19	End of video.